

# U.S. DEPARTMENT OF COMMERCE

National Oceanic and Atmospheric Administration

# COLLECTED REPRINTS-1975 Volume I

ATLANTIC OCEANOGRAPHIC AND METEOROLOGICAL LABORATORIES

AU NO. DOC FILE COPY.

DISTRIBUTION STATEMENT A

Approved for public release; Distribution Unlimited



U.S. DEPARTMENT OF COMMERCE Juanita M. Kreps, Secretary

NATIONAL OCEANIC AND ATMOSPHERIC ADMINISTRATION
Robert M. White, Administrator
ENVIRONMENTAL RESEARCH LABORATORIES
Wilmot N. Hess, Director

# Collected Reprints-1975. Volume T

# ATLANTIC OCEANOGRAPHIC AND METEOROLOGICAL LABORATORIES

ISSUED FEBRUARY 1977 Boulder, Colorado



Approved for public release;
Distribution Unlimited

Atlantic Oceanographic and Meteorological Laboratories Miami, Florida 33149

For sale by the Superintendent of Documents, U. S. Government Printing Office, Washington, D. C. 20402

# 4.25

406366

Inec

### FOREWORD

This is the tenth annual publication of the collected reprints of NOAA's Atlantic Oceanographic and Meteorological Laboratories. It brings together our research results published during 1975 in a wide range of scientific and technical journals as well as in some internal NOAA publications. Although the generation of new knowledge is of itself satisfying to the researcher who does it, the usefulness to others is largely a function of how well the knowledge is disseminated. For this reason, our collected reprints receive a wide distribution to the libraries of universities, research institutions, and government agencies in this country and abroad.

The Atlantic Oceanographic and Meteorological Laboratories conduct research on the physical, chemical, and geological characteristics and processes of the ocean waters, the seafloor, and the overlying atmosphere. During 1975, these research efforts were carried out by four major groups:

Physical Oceanography Laboratory Volume 2 continue Marine Geology and Geophysics Laboratory

Sea-Air Interaction Laboratory

Ocean Remote Sensing Laboratory

The reprints in this volume are arranged alphabetically by the last name of the first author within each of these groups.

Harris B. Stewart, Jr. Director, AOML

Atlantic Oceanographic and Meteorological Laboratories 15 Rickenbacker Causeway Virginia Key Miami, Florida 33149, U.S.A.

NTIS	White Cocion
200	Buff Section
HEBBARD	
JUSTIFICAT	104
)T	
DY	TION /AVAILABILITY COORS
DY DISTRIBU	TION AVAILABILITY COORS

## CONTENTS

### VOLUME I

	GENERAL	Page No.
1.	Stewart, H. B., Jr.	
	Bologna Workshop on Marine Science-Concluding Observations. Report of the Marine Science Workshop held by the Johns Hopkins University, Bologna, Italy, October 15-19, 1973, Annex D, 73-78.	1
2.	Stewart, H. B., Jr.	
	Book Review: Handbook of Marine Science, Volume I and II. Sea Frontiers 21, No. 1, 58.	7
3.	Stewart, H. B. Jr.	
	The National Oceanic and Atmospheric Administration and the Outer Continental Shelf. Proc. of the Estuarine Research Federation, OCS Conference and Workshop, Marine Environmental Implications of Offshore Oil and Gas Development in the Baltimore Canyon Region of the Mid-Atlantic Coast, VIMS, Wachapreague, Virginia, 27-38.	
	PHYSICAL OCEANOGRAPHY LABORATORY	
4.	Beardsley, R. C., W. C. Boicourt, and D. V. Hansen.	
	Physical Oceanography of the Middle Atlantic Bight. Proc.of Special Symposium, "The Middle Atlantic Continental Shelf and the New York Bight," American Museum of Natural History, New York City, 3-4-5 November 1975, 1 p.	20
5.	Brown, W., W. Munk, F. Snodgrass, H. Mofjeld, and B. Zetler.	
	MODE Bottom Experiment. Journal of Physical Oceanography 5, No. 1, 75-85.	21
6.	Charnell, R. L. (Editor), D. A. Mayer, D. V. Hansen, D. Swift, A. Cok, D. Drake, G. Freeland, W. Lavelle, T. McKinney, T. Nelson R. Permenter, W. Stubblefield, D. Segar, P. Hatcher, G. Berberian L. Kiester, M. Weiselberg.	
	Assessment of Offshore Dumping in the New York Bight, Technical Background: Physical Oceanography, Geological Oceanography, Chemical Oceanography. NOAA Technical Report ERL 332-MESA 3, 83 p.	32

/.	Charnett, R. L., and D. A. Mayer.	
	Water Movement Within the Apex of the New York Bight During Summer and Fall of 1973. NOAA Technical Memorandum ERL MESA-3, 32 p.	122
8.	Chew, F.	
	The Interaction Between Curvature and Lateral Shear Vorticities in a Mean and an Instantaneous Florida Current, A Comparison. <i>Tellus XXVII</i> , No. 6, 606-618.	154
9.	Gordon, H. R. and W. R. McCluney.	
	Estimation of the Depth of Sunlight Penetration in the Sea for Remote Sensing. <i>Applied Optics 14</i> , 413-416.	167
10.	Hansen, D. V.	
	Review of: Progress in Oceanography, Volume 6. Edited by B. A. Warren, Pergamon Press, New York. Bulletin of the American Meteorological Society 56, No. 9, 997-998.	171
11.	Hazelworth, J. B., B. L. Kolitz, R. B. Starr, R. L. Charnell, G. A. Berberian, and M. A. Weiselberg.	
	New York Bight Project, Water Column Sampling Cruises #6-8 of the NOAA Ship FERREL, April-June 1974. NOAA Data Report MESA-1, 177 pages. *	172
12.	Hazelworth, J. B., and R. B. Starr.	
	Oceanographic Conditions in the Caribbean Sea During the Summer of 1971. NOAA Technical Report ERL 344-AOML 20, 144 p.	200
13.	Hazelworth, J. B., B. L. Kolitz, R. B. Starr, R. L. Charnell, G. A. Berberian, and M. A. Weiselberg.	
	New York Bight Project, Water Column Sampling Cruises 9-12 of the NOAA Ship FERREL, July-November 1974. NOAA Data Report ERL MESA-3, 234 p.**	347
14.	Kirwan, A. D., Jr., G. McNally, M. S. Chang, and R. Molinari.	
	The Effect of Wind and Surface Currents on Drifters. Journal of Physical Oceanography 5, No. 2, 361-368.	348

<sup>\*</sup>Text only; pp. 26-177 are station data. \*\*Abstract only; complete text on microfiche.

15.	Maul, G. A.	
	Circulation of the Eastern Gulf of Mexico and Its Possible Relation to Red Tides. Proc. of the Florida Red Tide Conference, Florida Marine Research Publication, Florida Department of Natural Resources, Marine Research Laboratory, Sarasota, Florida, October 10-12, No. 8, 9-10.	356
16.	Maul, G. A.	
	An Evaluation of the Use of the Earth Resources Technology Satellite for Observing Ocean Current Boundaries in the Gulf Stream System. NOAA Technical Report ERL 335-AOML 18, 125 p.	357
17.	Maul, G. A. and S. R. Baig.	
	A New Technique for Observing Mid-Latitude Ocean Currents from Space. Proc. of the American Society of Photogrammetry, 41st Annual Meeting, Washington, D. C., March 9-14 1975, 713-716.	485
18.	Maul, G. A. and H. R. Gordon.	
	On the Use of the Earth Resources Technology Satellite (LANDSAT-1) in Optical Oceanography. Remote Sensing of Environment 4, No. 2, 95-128.	489
19.	Mayer, D. A.	
	Examination of Water Movement in Massachusetts Bay. NOAA Technical Report ERL 328-AOML 17, 46 p.	523
20.	Mayer, D. A. and D. V. Hansen	
	Observations of Currents and Temperatures in the Southeast Florida Coastal Zone During 1971-1972. NOAA Technical Report ERL 346-AOML 21, 36 p.	572
21.	Mofjeld, H. O. and M. Rattray, Jr.	
	Barotropic Rossby Waves in a Zonal Current: Effects of Lateral Viscosity. Journal of Physical Oceanography 5, No. 3, 421-429.	611
22.	Mofjeld, H. O.	
	Empirical Model for Tides in the Western North Atlantic Ocean. NOAA Technical Report ERL 340-AOML 19, 24 p.	620
23.	Molinari, R. L.	
	A Comparison of Observed and Numerically Simulated Circulation in the Cayman Sea. <i>Journal of Physical Oceanography 5</i> , No. 1, 51-62.	647

647

24.	Molinari, R. L. and A. D. Kirwan, Jr.	
	Calculations of Differential Kinematic Properties from Lagrangian Observations in the Western Caribbean Sea. <i>Journal of Physical Oceanography</i> 5, No. 3, 483-491.	659
25.	Segar, D. A. and A. Y. Cantillo.	
	Direct Determination of Trace Metals in Seawater by Flameless Atomic Absorption Spectrophotometry. Advances in Chemistry Series, Number 147, Analytical Methods in Oceanography, 56-81.	668
26.	Segar, D. A. and G. A. Berberian.	
	Trace Metal Contamination by Oceanographic Samplers. A Comparison of Various Niskin Samplers and a Pumping System. Advances in Chemistry Series, Number 147, Analytical Methods in Oceanography, 9-15.	694
27.	Zetler, B., W. Munk, H. Mofjeld, W. Brown, and F. Dormer.	
	MODE Tides. Journal Physical Oceanography 5, No. 3, 430-441.	701
	VOLUME II	
	MARINE GEOLOGY AND GEOPHYSICS LABORATORY	
28.	Ballard, R. D., W. B. Bryan, J. R. Heirtzler, G. Keller, J. G. Moore, and T. van Andel.	
	Manned Submersible Observations in the FAMOUS Area: Mid-Atlantic Ridge. Science 190, 103-108.	713
29.	Dietz, R. S., J. F. McHone, and N. M. Short.	
	Oman Ring: Suspected Astrobleme. Meteoritics 10, No. 4, 393.	719
30.	Freeland, G. L. and D. J. P. Swift.	
	New York Alternative Dumpsite Assessment-Reconnaissance Study of Surficial Sediments. IX International Congress of Sedimentology; Nice, France, Theme 10, 13-18. Also appeared in Offshore Technology Conference, Paper #OTC 2385, 505-511.	720
31.	Freeland, G. L., D. J. P. Swift, W. L. Stubblefield, and A. E. Cok.	

32.	Gadd, P. E., J. W. Lavelle, and D. J. P. Swift.	
	Calculations of Sand Transport on the New York Shelf Using Near-Bottom Current Meter Observations. American Geophysical Union, Fall Annual Meeting 56, No. 12, 1003.	729
33.	Hatcher, P. G. and L. E. Keister.	
	Carbohydrates and Organic Carbon in the New York Bight Sediments as Possible Indicators of Sewage Contamination. Mid-Atlantic Shelf/New York Bight ASLO Symposium, 31-33.	730
34.	Hatcher, P. G., B. R. Simoneit, and S. M. Gerchakov.	
	Mangrove Lake, Bermuda; Its Sapropelic Sedimentary Environment. Seventh International Meeting on Organic Geochemistry, Madrid, Spain, 61.	733
35.	Hulbert, M. H. and R. H. Bennett.	
	Electrostatic Cleaning Technique for Fabric SEM Samples. Clays and Clay Minerals 23, 331-335.	734
36.	Kearey, P., G. Peter, and G. K. Westbrook.	
	Geophysical Maps of the Eastern Caribbean. Journal of the Geological Society 131, 311-321.	739
37.	Keller, G. H.	
	Sedimentary Processes in Submarine Canyons off Northeastern United States. IX International Congress of Sedimentology, Nice, France, Theme 6, 77-80.	750
38.	Keller, G. H.	
	Book Review: The Ocean Basins and Margins - Volume 2: The North Atlantic. Edited by A.E.M. Nairn and F.G. Stehli, Plenum Publ., New York. <i>Marine Geotechnology 1</i> , No. 1, 159-161.	757
39.	Keller, G. H. and L. L. Minter.	
	Cariaco Trench - Sediment Geotechnical Properties. Journal of Sedimentary Petrology 45, No. 1, 292-294.	760
40.	Keller, G. H., S. H. Anderson, and J. W. Lavelle.	
	Near-Bottom Currents in the Mid-Atlantic Ridge Rift Valley. Canadian Journal of Earth Science 12, No. 4, 703-710.	763

41.	Lavelle, J. W., G. H. Keller, and T. L. Clarke.	
	Possible Bottom Current Response to Surface Winds in the Hudson Shelf Channel. <i>Journal of Geophysical Research 80</i> , No. 15, 1953-1956.	771
42.	Lavelle, J. W., D. J. P. Swift, H. R. Brashear, and F. N. Case.	
	Tracer Observations of Sand Transport on the Long Island Inner Shelf. American Geophysical Union, Fall Annual Meeting 56, No. 12, 1003.	775
43.	McGregor, B. A. and P. A. Rona.	
	Crest of the Mid-Atlantic Ridge at 26° N. Journal of Geophysical Research 80, No. 23, 3307-3314.	776
44.	McGregor, B. A., G. H. Keller, and R. H. Bennett.	
	Seismic Profiles Along the U.S. Northeast Coast Continental Margin. $EOS$ 56, No. 6, 382.	784
45.	McHone, J. F., Jr. and R. S. Dietz.	
	Impact Structures on LANDSAT Imagery (Abstract). Geological Society of America Annual Meetings, Abstracts with Programs 7, No. 7, 1196.	785
46.	Maupomé, L., R. Alvarez, S. W. Kieffer, and R. S. Dietz.	
	On the Terrestrial Origin of the Tepexitl Crater, Mexico. <i>Meteoritics</i> 10, No. 3, 209-214.	786
47.	Maupomé, L., R. Alvarez, S. W. Kieffer, and R. S. Dietz.	
	Tepexitl Crater, Mexico: Not Meteoritic (Abstract).  Meteoritics 10, No. 4. 454-455	792
48.	Minter, L. L., G. H. Keller, and T. E. Pyle.	
	Morphology and Sedimentary Processes in and Around Tortugas and Agassiz Sea Valleys, Southern Straits of Florida. <i>Marine Geology 18</i> , 47-69.	793
49.	Permenter, R. W., W. L. Stubblefield, and D. J. P. Swift.	
	Substrate Mapping by Sidescan Sonar. Florida Scientist 38, Supplement 1, 13-14.	816

50.	Richards, A. F., K. Oien, G. H. Keller, and J. V. Lai.	
	Differential Piezometer Probe for an In Situ Measurement of Sea-Floor Pore-Pressure. <i>Geotechnique</i> 25, No. 2, 229-238.	817
51.	Rona, P. A.	
	Book Review: Sonographs of the Sea Floor. Journal of Geology 83, No. 4, 536.	827
52.	Rona, P. A.	
	Letters to the Editors: Minerals and Plate Tectomics. Science 190, No. 4213, 422.	828
53.	Rona, P. A.	
	Relation of Offshore and Onshore Mineral Resources to Plate Tectonics. Proc. Offshore Technology Conference, Paper No. OTC 2317, 713-715.	829
54.	Rona, P. A.	
	Salt Deposits of the Eastern and Western Atlantic (Abstract). Proc. International Symposium on Continental Margins of Atlantic Type, Brazil, 1-15.	833
55.	Rona, P. A.	
	Viewpoint. Encounter with the Earth, edited by L. F. Laporte, Canfield Press, San Francisco, CA, 83-86.	834
56.	Rona, P. A., B. A. McGregor, P. R. Betzer, G. W. Bolger, and D. C. Krause.	
	Anomalous Water Temperatures Over Mid-Atlantic Ridge Crest at 26° North Latitude. Deep-Sea Research 22, 611-618.	838
57.	Scott, R. B., J. Malpas, G. Udintsev, and P. A. Rona.	
	Submarine Hydrothermal Activity and Seafloor Spreading at 26° N, MAR. Geological Society of America, Abstracts with Programs 7, No. 7, 1263.	846
58.	Stubblefield, W. L. and R. W. Permenter.	
	Temporal and Spatial Substrate Variation in the New York Bight Apex. Geological Society of America, Abstracts with Programs 7, No. 7, 1285-1286.	847

59.	Stubblefield, W. L., J. W. Lavelle, D. J. P. Swift, and T. F. McKinney.	
	Sediment Response to the Present Hydraulic Regime on the Central New Jersey Shelf. <i>Journal of Sedimentary Petrology</i> 45, No. 1, 337-358.	848
60.	Swift, D. J. P.	
	Barrier-Island Genesis: Evidence From the Central Atlantic Shelf, Eastern U.S.A. Sedimentary Geology 14, 1-43	870
61.	Swift, D. J. P.	
	Response of the Shelf Floor to Geostrophic Storm Currents, Middle Atlantic Bight of North America. Sedimentary Mechanics, IX International Congress of Sedimentology, Nice, France, Theme VI, 193-198.	913
62.	Swift, D. J. P.	
	Tidal Sand Ridges and Shoal-Retreat Massifs. Marine Geology 18, 105-134.	921
63.	Swift, D. J. P., G. L. Freeland, P. E. Gadd, J. W. Lavelle, and W. L. Stubblefield.	
	Morphologic Evolution and Sand Transport in the New York Bight. Mid-Atlantic Shelf/New York Bight ASLO Symposium, 65-66.	950
	SEA-AIR INTERACTION LABORATORY	
64.	McLeish, W. L. and G. E. Putland.	
	The Initial Water Circulation and Waves Induced by an Airflow. NOAA Technical Report ERL 316-AOML 16, 45 p.	952
65.	McLeish, W. and G. E. Putland.	
	Measurements of Wind-Driven Flow Profiles in the Top Millimeter of Water. Journal of Physical Oceanography 5, No. 3, 516-518.	999
66.	Ostapoff, F., J. Proni and R. Sellers.	
	Preliminary Analysis of Ocean Internal Wave Observations by Acoustic Soundings. Preliminary Scientific Results of the GARP Atlantic Tropical Experiment, prepared by the International Scientific and Management Group (ISMG) of the World Meteorological Organization, Volume II, GATE Report No. 14, 392-397.	1002

67.	Ross, D.	
	A Comparison of SKYLAB S-193 and Aircraft Views of Surface Roughness and a Look Toward SEASAT. Proceedings of the NASA Earth Resources Survey Symposium, Houston, Texas, June 1975, Vol. 1-C, 1911-1936.	1008
68.	Stegen, G. R., K. Bryan, J. L. Held, and F. Ostapoff.	
	Dropped Horizontal Coherence Based on Temperature Profiles in the Upper Thermocline. <i>Journal of Geophysical Research 80</i> , No. 27, 3841-3847.	1034
	OCEAN REMOTE SENSING LABORATORY	
69.	Apel, J. R.	
	Seasat: A Spacecraft Views the Marine Environment with Microwave Sensors. Remote Sensing: Energy-Related Problems, edited by Dr. T. Veziroglu, J. Wiley & Sons, 47-60.	1041
70.	Apel, J. R., H. M. Byrne, J. R. Proni, and R. L. Charnell.	
	Observations of Oceanic Internal and Surface Waves from the Earth Resources Technology Satellite. <i>Journal of Geophysical Research</i> 80, No. 6, 865-881.	1055
71.	Apel, J. R., J. R. Proni, H. M. Byrne, and R. L. Sellers.	
	Near-Simultaneous Observations of Intermittent Internal Waves on the Continental Shelf from Ship and Spacecraft. Geophysical Research Letters 2, No. 4, 128-131.	1072
72.	Proni, J. R., and J. R. Apel.	
	On the Use of High-frequency Acoustics for the Study of Internal Waves and Microstructure. <i>Journal of Geophysical Research 80</i> , No. 9, 1147-1151.	1076
73	Proni 1 P D C Pona C A lauter 1r and P I Sellers	

1081

Acoustic Observations of Suspended Particulate Matter in the Ocean. Nature 254, No. 5499, 413-415.

Reprinted from: Report of the Marine Science Workshop held by the Johns Hopkins University, Bologna, Italy, October 15-19, 1973, Annex D, 73-78.

Annex D - Page 73

# BOLOGNA WORKSHOP ON MARINE SCIENCE CONCLUDING OBSERVATIONS

Harris B. Stewart, Jr.\*

This has been a most interesting--even exciting--week at The Johns Hopkins University Bologna Center. I have enjoyed it. I have met some old friends and made some new ones. I have eaten too much of this delicious Bologna food, slept too little--thanks to the jet-lag problems with my biological clock--and have heard a good many ideas, some of them very good new ideas, proposed and discussed. How, then, do you summarize a meeting such as this one where representatives from twenty-two different nations at varying levels of development have expressed their own ideas on the why, what, and how of support for programs in marine science? At the reception last evening, I proposed to Dr. Hollick that it could be nicely summarized by "Send money, people, and equipment," but she seemed to feel that a somewhat more detailed summary was required.

What, then, are the results and conclusions from this week-long workshop? Certainly one of the results is the establishment of strong personal ties among the individual scientists of twenty-two different countries. You can learn a lot over a two-hour lunch! In the years ahead, these person-to-person ties will allow free communication among the countries and at a considerably faster rate and more effectively than on a government-to-government basis. Keep the list of our addresses you received today and use them to exchange reprints of published papers and ideas, and we should use them to initiate plans and programs among ourselves. Each of us now has a fellow marine scientist as a contact in at least twenty-one other countries. Use them.

Several points were repeatedly made during the week, and I feel these should be singled out for special emphasis. Not everyone concurred in all of these ideas, but they seemed to have the agreement of the majority:

- 1. The development of a viable national marine science capability is not accomplished instantaneously. It is a long, slow process, but it can be considerably speeded up by capitalizing on the experience and capability of nations which have been involved in marine science longer and have advanced further down the road toward an independence in their ability to deal effectively with the ocean and its resources.
- 2. "The Lord helps those who help themselves" is the way one speaker expressed the idea that a nation cannot sit back and wait for an outsider to solve its marine science problems. Each nation must

<sup>\*</sup>Director, NOAA Atlantic Oceanographic and Meteorological Laboratories, Miami, Florida, U.S.A.

- Annex D Page 74
  initiate its own efforts, establish national goals and priorities,
  hopefully obtain a national commitment to learning about its
  ocean and the resources it contains, and be willing, as a nation,
  to commit a portion of its own manpower and funding to this effort.
  - 3. The marine science and technology needs of each coastal nation wanting to move ahead in this field must be carefully studied, evaluated, and documented. The international agencies may be the best means for accomplishing this, but the present marine scientists of the country must be involved in the elaboration of these national needs. Future requests for assistance must be relevant to meeting these national needs.
  - 4. The universities in each nation, as the traditional fountainheads of knowledge, must be heavily involved in the national marine science program, for the role of the university is not only the importing of knowledge but, in fact, the generation of new knowledge. Marine science also provides an intellectual stimulus and challenge that, if properly met, can provide the intellectual outlet that man as a reasoning being demands.
  - 5. Although intellectual stimulation is an admirable national goal, for many countries it ranks, on the list of national priorities, well below those of adequate animal protein for a growing population, optimum utilization of marine resources, and improvement of the national economic base and gross national product. The development of a sound scientific basis for meeting these needs must rest in the universities, and it is essential that they be a viable element of any national program in marine science.
  - 6. The development of a marine science capability and the increase in the effective recovery of a nation's marine resources must go hand in hand, must proceed cooperatively together. This was not a unanimously agreed upon concept by any means. Those who disagreed felt, "Give us the fish and the oil, and we will worry about the science later." The general feeling, however, and examples were cited, was that any project involving offshore resources-be they living or nonliving-involved the accumulation of data that could contribute to the overall understanding of the systems and regimes that impact the resource. Developing understanding is the business of research, so the two are natural allies and should proceed together--resource development and management and research.
  - 7. Numerous programs in the past between developed and developing countries as well as programs of international agencies carried our in developing countries have, upon their termination, left nothing behind. There was a complete consensus that local marine scientists and technicians must be heavily involved in any assistance program, to the extent that they can carry on the work when the formal project is completed.

- 8. No global solutions are possible, but rather each nation must be considered as a separate case with unique national needs, present capabilities, degree of national commitment, abundance of offshore resources, and desire for assistance. These must all be considered in any plan for assistance.
- 9. Cooperation nationally among the university researchers in marine science and the nonuniversity groups involved in oceanic affairs (navy, industry, fisheries agency, geological survey, weather bureau, foreign office, etc.) is essential if a firm basis for the receipt of bilateral or UN agency assistance is to be developed.
- 10. Means must be found for generating a marine enthusiasm among the students who are attracted to science and technology as their life work. Visiting lecturers and berths on visiting research ships can contribute to this kindling of an occanic interest.
- 11. National mechanisms must be developed whereby the leading marine scientists have a meaningful input into the formulation of national policies affecting the ocean and marine resources.
- 12. The major marine science need of developing countries appears to be the development of an adequate critical mass of manpower adequately educated and trained in technology to provide the base for intelligent resource management and recovery.
- 13. Although fisheries received the major attention among the possible recoverable marine resources, it was pointed out repeatedly that there are other reasons for nations to learn about the sea. These include mineral resources (oil, gas, sand and gravel, the minerals in manganese nodules, phosphorite, and dissolved minerals), the disposal of man's wastes (radioactive and others), weather forecasting, commerce, national defense, recreation, and the providing of an outlet for man's innate curiosity about the seas around him.
- 14. The results of any experiment or study offshore by any nation must be integrated into the local framework. This entails the providing of results in the form of data and/or published results as well as specimens for the local reference collection.
- 15. In general, assistance is more welcome from UN agencies than from bilateral arrangements because the receiving nation is part of the agency itself and the level of trust is higher than for bilateral arrangements in which there may be some degree of mistrust of the motives of the more developed country.

- Annex D Page 76
  However, bilateral arrangements are often preferable where
  there are social or political ties or where a particular and
  perhaps unique capability is desired.
  - 16. Sophisticated and expensive equipment should be shared on a regional basis with the most advanced nation acting as the overseer.
  - 17. Developing countries should be accorded the chance and provided with the ability to make their own decisions.
  - 18. Developing countries do not need to start out with the sophisticated equipment in use in the more developed countries. If the degree of accuracy of a measurement is known, the degree of precision is less important.
  - 19. Data <u>per se</u> are useful only as they contribute--through scientific endeavor--to knowledge. This reinforces the need for good university departments in marine science.
  - 20. High priority should be accorded the development of human resources, and this should probably be the first rather than nearly the last of this series of items on which there appeared to be general agreement.
  - 21. Visiting "experts" must be carefully selected. Even though a developing country can benefit from a visit of even short duration, it is desirable to have these experts remain in the country for two to three years if maximum benefits are to be realized.
  - 22. For the more developed countries that have some expertise, it is often more desirable to develop cooperative bilateral arrangements whereby they can carry out joint projects to the material benefit of both nations.

These 22 concepts are ones that were generally agreed upon either in the full meetings or in the working groups or in smaller luncheon groups. There is plenty of room for discussion, so if you do not agree with these concepts, I urge that you let me know.

During the smaller working group sessions, there were some interesting ideas that surfaced, and even though they were not all brought up for general discussion, I have selected four of them to be noted in a summary such as this one.

1. We appear to be concentrating heavily on the methods and techniques of obtaining assistance from the larger developed countries and UN agencies when, in fact, we can do a great

Annex D - Page 77 deal to help ourselves on a regional basis. No two countries have developed their marine science capabilities in exactly the same manner or to the same degree. So each nation in a region should identify its own strongest areas in marine science and those of its neighbors and mutually arrange the exchanges or other mechanisms to insure the maximum effective transfer of those capabilities among the region. For example, Chile and Peru need not go to the United States for help in developing a seismology program when Colombia has a well-developed effort in this field, and, in addition, is more familiar with the South American area and has no language barriers.

- 2. Mutual assistance projects on an institute-to-institute basis developed through personal scientist-to-scientist contacts can be particularly useful and have the added advantage of avoiding the delays and constraints often associated with the usual negotiations between governments or with the international agencies.
- 3. If any of the developing countries find themselves in the almost enviable position of having overproduced marine scientists—that is, having more new PhD's than its own marine science community can absorb—every effort should be made to see that funding is provided so that these recent graduates can work for an extended period in the developing countries. Probably a UN agency such as UNESCO should act as the manager for any such program to insure that national needs are matched to available personnel and to avoid the mistrust or feeling that ulterior motives are involved on the part of the assisting nation. Use of this possible manpower source through bilateral arrangements, however, should not be ruled out.
- 4. Senior scientists in other countries who are willing to assist foreign graduate students should be identified and put in correspondence with students working in their field of specialization. This would augment local university capabilities and would upgrade the research and thesis levels of graduate students through the providing of guidance by a recognized authority in the field, the providing of reprints and literature references, and the assurance that the research is scientifically meaningful. Particularly attractive is the fact that little or no funding is required.

In conclusion, I would like--on behalf of all of--to thank Dr. Serfaty and the Bologna Center for their great hospitality and highly effective staff support for this workshop. You have a fine group, and we wish you continuing success. Most of all we are indebted to The Johns Hopkins University School of Advanced International Studies, which brought us together and provided the opportunity to express our own

Annex D - Page 78 ideas on the important role that marine science has to play in the developing countries. To Dr. Hollick, Jim Zimmerman, and all the others who made it all possible we say a sincere "Thank you."

Finally, on behalf of the ocean itself, I would urge that each of us, upon his return to his own country, see that the ideas we have generated here are widely disseminated--particularly to the decision makers in our governments. If this week is to be useful for the greater understanding of the magnificent complexity of the global sea and for our ability to recover and manage its resources intelligently for the general betterment of all mankind, it is our responsibility to see that these ideas do not stop as a report but are used as weapons in the continuing battle to understand and utilize the ocean as one of the greatest resources we have on earth.

### HANDBOOK OF MARINE SCIENCE Volumes I and II

Volume 1—F. G. WALTON SMITH, Ed. 1974, 627 pp. \$43.95. Volume II—F. G. WALTON SMITH and F. A. KALBER, Eds. 1974, 390 pp. \$36.50. CRC Press, 18901 Cranwood Parkway, Cleveland, Ohio 44128. (No discount. Order direct

from publisher.)

Traditionally marine scientists and the broad range of ocean practitioners have had to rely on a veritable 5-foot shelf of reference works, handbooks, journals, and reprints to insure the availability of the tables, constants, and properties that the editors have brought together in these fine volumes. They and the several individual authors have in these volumes provided a badly needed service to oceanography and ocean engineering.

The oceans encompass many sciences, and so the ocean scientist has been forced to go to the handbooks of many disciplines to find the numbers he needs in his work. These volumes remove this annoyance nicely by pulling together a most complete compendium of the tables, constants, etc., that ocean people need.

The first volume consists of tabulated data on chemical oceanography, physical oceanography, meteorology, marine geology, ocean engineering, and general tables. The second volume includes sections on primary productivity, phytoplankton, zooplankton, and the size, distribution and catches of the commercial fishery stocks of the world.

These volumes are a must for the practicing marine scientist and engineer. It is suggested that each have his own, for the library copies are sure to be in use elsewhere, H.B.S., Jr.

Reprinted from: Proc. of the Estuarine Research Federation, OCS Conference and Workshop, Marine Environmental Implications of Offshore Oil and Gas Development in the Baltimore Canyon Region of the Mid-Atlantic Coast.

THE NATIONAL OCEANIC AND ATMOSPHERIC ADMINISTRATION AND THE OUTER CONTINENTAL SHELF

Harris B. Stewart, Jr.
NOAA Atlantic Oceanographic and
Meteorological Laboratories

Frank Hebard of NOAA Headquarters was scheduled to give NOAA's views relevant to the Outer Continental Shelf, but he is unable to make it and asked me to do it for him. One of the nice things about being a substitute speaker is that you can throw out what the other man has prepared and say what you want, and he has relatively little recourse. This is just what I have done with the exception of a bit of boiler plate that I asked NOAA Headquarters for. I did ask Frank to provide me with some information on the relevant authority and legislation for NOAA's involvement on the Outer Continental Shelf. That, after all, is that this session with presentations by the Federal agencies is supposed to be all about, so I felt it should be included. I will, however, keep this to an absolute minimum and then get on to things that I consider to be somewhat more interesting.

Briefly, the legislative responsibilities of NOAA which are related to the impact of OCS oil and gas development are included in four

pieces of legislation:

- 1. Coastal Zone Management Act--Section 303 of the 1972 Coastal Zone Management Act, which is administered by U.S. Department of Commerce, states that "it is the national policy . . . to preserve, protect, develop, and where possible, to restore or enhance, the resources of the nation's coastal zone for this and succeeding generations." The same section also states that "it is the national policy . . . to achieve wise use of the land and water resources of the coastal zone giving full consideration to ecological, cultural, historic, and aesthetic values as well as needs for economic development." The best hope for incorporating this national policy into coastal zone management programs is the environmental impact statement process under the National Environmental Policy Act. The requirement for the EIS by the Bureau of Land Management prior to the granting of exploration and development leases is then in direct compliance with the National Environmental Policy Act and furthers the national policy enunciated in the Coastal Zone Management Act.
- 2. Marine Protection, Research and Sanctuaries Act, approved on October 23, 1972, assigned the Secretary of Commerce in Title II responsibility for initiating a comprehensive and continuing program of research with respect to long range effects of pollution, overfishing, and man-induced changes of ocean ecosystem. Title III

provides that the Secretary of Commerce in consultation with other Foderal officials, may designate marine sanctuaries as far seaward as the outer edge of the Continental Shelf to preserve or restore such areas for conservation, recreational, ecological, or aesthetic values.

3. Reorganization Plan No. 4 of 1970, Executive Order 11564 of October 6, 1970, vests in the Secretary of Commerce functions which include the gathering, processing, analyzing and interpreting of data and the performance of relevant research which insures the safety and welfare of the public, and furthers the nation's interests and activities with respect to the protection of public health against environmental pollution, the protection and management of the nation's biological, mineral and water resources, the maintenance of environmental quality, fisheries, industry, transportation, and the preservation of the nation's recreation areas.

4. Under 16 U.S.C. 742d, NOAA is authorized to conduct investigations and other activities regarding, among other things, the availability and abundance and the biological requirements of the fish and wildlife resources. 16 U.S.C. 742f(a) (4) authorizes NOAA to take such steps as may be required for the development, advancement, management, conservation, and protection of the fisheries resources.

That briefly covers NOAA's statutory responsibilities in the OCS area. Technically I have now covered what was expected, and I could sit down. However, all of us are here to accomplish a job for the Bureau of Land Management, and I feel that NOAA's contribution to this objective can be considerably more than a sterile listing of our legislative and executive responsibilities in the OCS. Therefore, for the remainder of the NOAA pitch I plan to cover two points. The first of these is a brief summary of what we are now doing in the northern part of the Baltimore Canyon Trough area in our New York Bight Marine Ecosystems Analysis (MESA) program, and the second is a summary of the thinking that NOAA has already done regarding what we feel BLM should undertake regarding the environmental assessment of oil and gas development in the Baltimore Canyon Trough area.

But let me digress a moment. As a former member of the Advisory Committee on Undersea Features of the U.S. Board on Geographic Names, I object to the term Baltimore Canyon Trough. I know how it came about: there is a trough in the basement at the outer edge of the Continental Shelf filled with something between five and six kilometers of consolidated sediment. The nearest surficial topographic feature is the Baltimore Canyon, so in order to identify both the trough itself and its nearest topographic feature in the name, someone came up with Baltimore Canyon Trough as the name for this structure. Personally I object to seeing "canyon" and "trough" in the same name, so I would propose the term Mid-Atlantic Shelf Area for the area under discussion during

these workshops.

Whatever you want to call it, NOAA in our MESA Program is even now conducting a fairly intensive study of the northernmost portion of the area under consideration, and I feel that it is important for this group to

have a quick overview of what we are doing in the area called the New York Bight. For the complete details, I refer you to the MESA Annual Report now in the final stages of preparation. It should be available from the MESA Project Office (Marine Sciences Research Center, SUNY, Stony Brook, New York 11794) in a month or so. Briefly, MESA is directed towards providing the environmental framework required by those concerned with making decisions on the use of some 15,000 square miles of ocean and seafloor lying south of Long Island and east of New Jersey.

Working with the results of surface and seabed drifters, anchored arrays of current meters, free-drifting drogues, ERTS images, and contributing results from the chemical, biological, and sediment studies, we are beginning to get a feel for the circulation in the area and something of the variations with time. We have worked with the suspended sediments and studied in detail the interrelationship of the bottom sediments and the dynamics of the bottom of the water column. We have studied the distribution of hydrocarbons, total organic carbon, carbohydrates, and heavy metals. We have collected and studied the benthic organisms in the area, and we have sampled, photographed, side-scansonared (if there is such a word), dived on with SCUBA and submersibles, plotted, and contoured the bottom. We have discovered the topographic effects of 35 years of dumping cellar dirt and debris, we have used the by-products of acid waste dumping to trace the routes this material takes, we have seen the effects of offshore dumping on the organisms in the area, and we have evaluated potential alternate dumpsites. We have used radioisotopes to trace the movement of bottom sediments and have planted current meters in the Hudson Valley and the Hudson Canyon to measure water movements. When I say "we", I mean the MESA Project, and there are a good many involved other than NOAA. To date, for example, some 17 university groups have been involved running the alphabetical gamut from Adelphi to Yale, and at least 13 other agencies -- federal, state, and local -- have also been involved.

MESA is a complex study of the total ecology that can be accomplished only when biologists, geologists, chemists, physical oceanographers, fisheries specialists, data processers, ship operators, project managers, and a whole raft of others can be pulled together into a team effort. It is an exciting concept both scientifically and managerially, and—I am pleased to say—it seems to be working. It is just this sort of multidisciplinary cooperative effort that must be brought to bear on the Baltimore Canyon Trough area, so I strongly suggest that whoever ends up managing the BCT Project plan to sit down with NOAA's MESA people and learn where we have succeeded, where we have had problems, and benefit from our experience.

We anticipate our MESA activities in the New York Bight area to continue for at least three more years and feel that it will make a considerable contribution to the overall understanding of the Baltimore Canyon Trough area. Any BCT-OCS studies should be coordinated with

NOAA's MESA activities in the northern part of the proposed study area.

The second point that I want to cover is NOAA's thoughts to date on just what BLM should know about the area in order to meet their responsibilities for environmental assessment relative to the leasing of offshore acreage for oil and gas development. We in NOAA began thinking seriously about this problem last spring. We were goaded into action by two developments. The first of these was the realization that the MAFLA exercise in St. Petersburg last winter was really just the first of several comparable exercises and that Interior apparently was serious about moving ahead with the leasing of large acreages on the Outer Continental Shelf. If there were OCS environmental assessments to be made, we felt that NOAA, of all the Federal agencies was the logical group to carry them out. Since then, we have been given the management responsibility for several of the Alaskan areas, and this work is even now under way. The second development that spurred our thinking relative to OCS development was the rider on the Energy Research and Development Bill that provided the funds to reactivate three NOAA ships that had been laid up, the DISCOVERER, SURVEYOR, and the MILLER FREEMAN but with the proviso that these ships be used for energy related work at sea.

Early last summer, NOAA brought together biologists, fisheries experts, geologists, physical oceanographers, marme chemists, meteorologists, and data management specialists from NOAA facilities on both coasts for a solid week of discussions and planning. These sessions came up with a rough draft document detailing the environmental information we felt that BLM should have for the BCT area. It was strictly an internal document, and it has gone through several iterations since then. My own personal feeling is that a batch of good scientists have given the problem a good deal of serious thought and that we in NOAA should make our thinking to date available to this session so that you can mull over our ideas and throw them out or adopt them as you see fit. We will have about one day or less available for the actual workshops, so if we can assist in making these as effective as possible, we want to do so. I have talked to Gene Cronin, and he has agreed to have duplicated from our draft document the sections on physical oceanography, chemistry, geology, and biology for the use of the Chairman of each of the workshops to be held during this meeting.

In the time remaining to me here, I would like to highlight some of NOAA's thinking about the environmental assessment of OCS development in the Mid-Atlantic Shelf. Perhaps what follows can be used as a straw man during your workshops on Tuesday evening and Wednesday.

Our feeling is that there are a goodly number of really interesting scientific problems in the area under consideration that it would be nice to work on with BLM funding. I am sure that many of you here feel the same way. However, the era of unfettered marine research on someone else's money appears to be on the way out, and we as marine scientists have been forced to focus our attention on those marine problems which

someone has money to have solved. In this case, the Bureau of Land Management must have information on the potential environmental impact of oil and gas development on the Outer Continental Shelf. I am sure that they would like to support a big program of basic oceanographic research if they could; but they have regainements, and we had better tailor our workshop recommendations to their requirements. If we can get some good science out of the exercise, so much the better for us, but that is not BLM's purpose. With this as background, I would like to give you a quick summary of the results of our thinking on what a program for BLM on the BCT Outer Continental Shelf might entail.

### ISSUES OF CONCERN

There are six main issues that we feel that BLM should be concerned about, and these are directly related to the possible environmental consequences of the proposed oil and gas activities on the Outer Continental Shelf in the BCT area.

1. What are those aspects of the environment most subject to change as a result of the anticipated activity?

Some changes may result in environmental modifications considered as "good", e.g., the development of ecological niches around production platforms where fish congregate in at least sport fishing quantities, or "bad" modifications such as those to be expected to result from the accidental introduction of hydrocarbons or heavy metals into the environment. Efforts in the first 12 to 18 months will include studies to identify and understand the role of those elements most susceptible to the expected environmental impact of petroleum activities.

2. What is the probable occurrence of hurricanes and other severe storms, high waves, earthquakes, and other natural environmental hazards which could result in the accidental discharge of oil or other contaminants into the environment?

Not only is this information needed to obtain some feel for the frequency and intensity of natural phenomena that might result in deleterious environmental impacts, but it is also needed to assist in developing design criteria for the construction of the drilling, production, and transportation facilities required to obtain petroleum from the area and deliver it to the coast for processing.

The first phase study would be an evaluation based on the available historical data, and subsequent studies should provide improved estimates related to specific lease areas. In particular, surface wave data, now almost totally lacking from the Baltimore Canyon Trough area, will have to be developed through a field program in those phases subsequent to the 12-18 months of the initial study.

3. What are--and how effective are--the physical transport mechanisms which will govern the distribution of contaminants?

This is perhaps the single most basic element of the study in that it will permit predictions of the trajectories and dastal arrival areas of oil spills or of other introduced contaminants at I enable these to be related to possibly environmentally sensitive areas as well as providing information leading to an understanding of the distribution of such free-floating biological elements as phytoplankton, larvae, fish eggs, etc. In addition better knowledge of the physical transport mechanism will assist in the intelligent location of long-term environmental monitoring stations within the area. The study during the first 12-18 months will produce a general description of the circulation patterns within the Baltimore Canyon Trough area and will include the initiation of the field measurement program which over the longer period will produce the more detailed picture of the circulation pattern and its variations with time. These data are essential inputs to a realistic trajectory and landfall prediction model which will be initiated during the first phase and refined as the additional data become available. Initial studies of sediment types and distribution will provide a preliminary estimate of transport or accumulation of contaminants in the sediments, whereas continuing studies of the dynamic processes operating at the bottom will provide the more complete understanding of the source-flux-sink system which will determine the ultimate fate of contaminants which become part of the bottom sedimentary regime.

4. What are the background levels of oil and selected heavy metals in the environment and the sources and sinks of these materials?

With the large volume of heavy metals and petroleum products introduced into the Baltimore Canyon Trough study area through coastal runoff from the heavily industrialized region bordering the area, offshore dumping, heavy shipping, the introduction of airborne contaminants, and the possibility of natural oil and gas seeps, the first 12-18 months can provide no more than a preliminary evaluation of the levels of these contaminants in the water column and the sediments at a few selected sites. However, this information is essential in the establishment of "baseline levels' against which future measurements will be compared. During the remainder of the study period, additional sampling will provide a better understanding of the pre-drilling areal and temporal variations in these contaminant concentrations, and the study will be extended to include concentrations within the biota. Special studies aimed at determining specific indicator elements, compounds, or organisms especially indicative of or susceptible to introduced contaminants will--if successful--enable subsequent post-drilling estimates of the environmental effects of these OCS activities.

Monitoring on a continuing basis should commence just prior to the initiation of drilling activities in the Baltimore Canyon Trough area.

5. What is the natural abundance and distribution within the Baltimore Canyon Trough area of selected elements of the biota important from the point of view of sport and commercial fisheries resources, of importance within the overall food web, or important as indicator species?

Required is information on the acute mortality of selected organisms and such long-term sublethal effects as reduced rates of reproduction and survival and interference with migration routes.

The first 12-18 months of effort will be directed towards the evaluation of existing data from the Baltimore Canyon Trough area, experimental design, and preparation of facilities for the more detailed effort. For the remaining period it is probable that only preliminary results can be expected from the studies of sublethal effects, but the groundwork will have been laid for continuing research on this aspect. On the other hand, the study's results should be accurate and complete enough at the end of the 3 to 5 year period to provide a reasonable predictive capability for acute toxicity response in selected organisms.

6. What physical interference with fishing or other human activities will result from oil and gas development in the Baltimore Canyon Trough area?

This aspect of the study will allow estimates to be made as to the extent to which OCS development will interfere substantially with commercial fishing through fouling nets or impeding trawling operations or with commercial shipping through introducing navigational hazards in areas of shipping activity.

These aspects should be determined in the first 12-18 months by determining the nature and extent of commercial fishing operations and shipping activity within the Baltimore Canyon Trough area and by correlating these findings with results observed in other offshore areas where oil and gas production is already under way.

But enough of the glowing generalities, what are the specifics that should be incorporated in any plan for the environmental assessment of the proposed leasing activities? Again, I would go back to the work that NOAA has already done in thinking about this. As I said earlier, the details are being provided to the Workshop Chairmen for consideration, but I would like briefly to hit the highlights of each major discipline.

### PHYSICAL OCEANOGRAPHY

The proposed OCS activities will have little effect on the physical oceanography of the area. The one possible exception is the optical properties. These may very possibly be modified by suspended material in the water resulting from the disposal of formation water, well cuttings. and drilling muds. Therefore, baseline studies on turbidity measured in situ by a spectral irradience meter should be carried out.

A historical summary of the marine climatology should be made. and much of this information has already been compiled and is available. Sea state forecasts should be improved, and a spectral wave model for hurricanes and winter storms should be developed. A pre-drilling survey of the occurrence of sea slicks should be carried out, and NOAA has learned that the Coast Guard through the Pollution Prevention and Enforcement Branch of their Marine Environmental Protection Division has for several years been running slick surveillance flights at the rate of two per week. They have also agreed to make these data available, so no additional work on this aspect needs to be planned.

The most important aspect of physical oceanography, however, is its role in predicting the routes and possible landfalls of environmental contaminants introduced into the environment as the result of an accidental oil spill. We envision a combination of at least monthly STD observations at repeat stations, a minimum set of two cross-shelf lines of three or four current meter stations each with four meters on each string to run at least one full year, and monthly plants of free-drifting telemetering buoys which will move through the current meter array providing at least position data--probably via a satellite such as NIMBUS-F. Don Hansen of NOAA's Atlantic Oceanographic and Meteorological Laboratories in Miami has come up with a very nice scheme to determine the appropriate dispersion tensor coefficients using a combination of these Eulerian and Lagrangian current measurements. These he would use as inputs to an advanced predictive model for the trajectory of a contaminant introduced at any point within the BCT area. His concept is an interesting one, and I have had a copy of his formulation made for the Chairman of the Physical Oceanography Workshop.

### CHEMICAL OCEANOGRAPHY

In considering the chemical aspects of the problem, we see five major objectives:

1. To describe the baseline concentrations of those chemicals which may be released into the environment from offshore oil and gas development, and we consider hydrocarbons and metal compounds as the most important. Studies should include dissolved and suspended chemicals in the water column, in selected organisms, and in the bottom sediments...

15

- 2. To develop the ability to determine the source of hydrocarbon pollution, whether it be crude oil, refined oil products, or naturally occurring hydrocarbons. The reliability of using selected specific hydrocarbons as "indicators" of offshore oil pollution should be investigated.
- 3. To determine the inputs, transport pathways, and sinks for selected hydrocarbons and trace metals by studies carried out in cooperation with the biological, physical, and sedimentological projects.
- 4. To establish a monitoring system so that possible environmental effects from offshore oil and gas development can be evaluated.
- 5. To maintain a research, development, test, and evaluation program so that sampling procedures, monitoring, and analytical techniques will be of the highest quality.

More specifically, as proposed by Doug Segar of my labs in Miami, water column assessment during the baseline phase should be carried out along two to five lines of cross-shelf stations, and these should be the same stations at which physical measurements are made and samples taken for biological and sedimentological studies. At each station, measurements should be made of salinity, temperature, depth, dissolved oxygen, total hydrocarbons, individual hydrocarbons, dissolved and particulate total organic carbon, and the trace metals, Fe, Ni, Cd, Cu, Pb, V, Ba, and Cr. The suspended matter should also be examined physically and chemically for hydrocarbons (if possible), total organic carbon, Ca, Si, Fe, Cd, Ni, Cu, Pb, and Ba. Sediments and organisms should also be analyzed for hydrocarbons and trace metals with only slight variations in the lists as given for the water column. Segar's evaluation of the problem and his proposed solution go into much more detail than I can give here, but I would add that particular care must be taken in the sampling, shipping, and analysis of the hydrocarbons and that special attention should be paid to having some method for standardizing analytical techniques so that analyses made by different laboratories can be intercompared. Bum techniques give bum results, and this work must be good. Segar's recommendations in toto have been provided to the Chairman of the Chemistry Workshop as a straw man for his consideration.

Since Don Swift who put together the geology section of NOAA's ideas on all of this is giving an invited paper tomorrow, and because Jack Pearce of NOAA's Sandy Hook NMFS Laboratory who generated most of the biology and fisheries part of our thinking to date is also giving an invited paper, and more importantly because I am running out of my allotted time, I must give an undeserved short shrift to the geology and biology portions of this paper. I apologize to them and to you for this, but I don't feel too badly knowing that their respective

Workshop Chairmen have received their thoughts on paper and that both Don Swift and Jack Pearce will attend these workshops in person.

### GEOLOGICAL OCEANOGRAPHY

Briefly, the objective here is to assess those aspects of the substrate--bottom sediments--relevant to the impact of the development of oil and gas resources on the Outer Continental Shelf in the BCT area. What, for example, becomes of drilling muds and hydrocarbons that find their way into the sediments? What processes move them about? Will single-incident contaminants be buried by subsequent sedimentation or will they be resuspended and moved elsewhere? Are some areas more likely than others to become sinks for contaminants? Can sediment type be used as an indicator of a specific benthic community of organisms, or must all organisms be sampled throughout the entire area? What is the fate of the finer grained contaminants that become part of and move with the suspended sediments? Is the calm-weather sedimentary regime or the occasional storm regime more effective in modifying the bottom? These are the sorts of questions that the sedimentological portion of the geological oceanography program must answer.

The USGS-Woods Hole Oceanographic Institution efforts have already done the reconnaissance sampling of the surficial sediments of the area, but more detailed sampling is needed for the present project. Blanket sampling of the whole area is out of the question, so a nested or stratified sampling program in "critical" areas is called for. A good deal of sediment work has already been accomplished in the BCT area by a broad spectrum of investigators including NOAA, USGS, Woods Hole, VIMS, EPA, University of Delaware, and others, and these results must be considered in planning for any additional work.

The bathymetric maps of Stearns and of Stearns and Garrison cover the northern half of the area, and the work of VIMS covers the southern half. However, these two efforts are at different resolutions, and NOAA's National Ocean Survey is even now undertaking the compilation of these two works and their own into a series of 1:125,000 bathymetric maps of the area.

The area under consideration is one consisting primarily of a sheet of sand. Thus the dynamic interactions of the lower water column and the sand sheet are of prime importance. Through study of these interactions, one should be able to predict the fate of contaminants that become part of the bottom sediments. Swift talks of substrate monitoring, suspended sediment monitoring, and the monitoring of sand transport, and we in NOAA feel that these all are aspects that should be considered.

### BIOLOGY AND FISHERIES OCEANOGRAPHY

The biological aspects of the BCT project are of prime importance because the socio-economic concerns about the possible effects of oil and gas development usually center around the impacts on the living resources of the area. Of particular importance in the area of demersal fish and shellfish is an effort to regroup the available data on abundances and distributions for the area. The fin fish, for example, have for a good number of years been monitored by the Middle Atlantic Coastal Fisheries Center of NOAA's National Marine Fisheries Service at Sandy Hook, New Jersey. These data together with those of the Woods Hole NMFS Laboratory should be prepared for computer analysis, retrieval, and the preparation of summary reports, and it is NOAA's feeling that no additional sampling for demersal fish and shellfish in the BCT area is required.

The planktonic organisms present a very real problem that I would like to present to you for possible resolution during the Plankton Workshop on Wednesday. The NOAA biologists that have studied the available data on planktonic distributions and abundances in the BCT

available data on planktonic distributions and abundances in the BCT area feel that there is so little known at this point and the variations are so large that within the time and funds expected to be available there is no chance that a sufficiently meaningful background or baseline framework can be established against which changes that might be due to oil and gas development can be measured. I have seen the recent work of El-Sayed of Texas A & M University from which he concludes that offshore drilling in the Gulf of Mexico has had no deleterious effects on the phytoplankton communities in the Louisiana offshore areas, and my cohorts at Scripps say that comparable results have been obtained for the Santa Barbara Channel following the big spill there. Thus, the question I would pose for your workshop is do you feel that planktonic studies are required for the Bureau of Land Management to make an assessment of the environmental impact of oil and gas development on the Outer Continental Shelf in the BCT

area. As a marine geologist, I do not know and must leave this up

to you.

Within the plankton, however, are fish eggs and larvae, and these, we feel, are important. We feel that pre-drilling studies should locate areas of high standing stocks of the eggs and larvae of the more important commercial and sport species and that their areal and temporal distributions should be related to water circulation patterns and properties. Benthic organisms are probably the best to use as pollution indicators because they are generally sessile and therefore subject to long-term pollution effects. These organisms in the BCT area should be sampled within the baseline framework to (1) assess those areas containing benthic assemblages most likely to be damaged by OCS development, (2) identify key indicator organisms likely to reflect environmental change, (3) establish quarterly (seasonal) baselines against which future changes can be compared, and (4) provide information useful in

18

modeling the potential impact of oil related activities on the marine benthic communities and related living resources.

Sea birds and mammals within the BCT area have been described in detail, and we feel that little if any additional work on this aspect of the biology can be justified. Although the NOAA people considering the BCT area did not include a microbiologist, we did feel that a baseline study of the occurrence and distribution of petroleum degrading microorganisms should be made in the BCT area and at control stations, and we further felt that changes in species composition and abundance should be monitored during both the exploration and drilling phases.

As with the other portions of the NOAA thoughts on this, I have made a copy of our ideas to date on the biological and fisheries aspects of OCS development available in written form to the Chairman of the Biology Workshop. Knowing Jack Pearce will be in attendance, I'll

not worry further about this one.

In planning for this talk, I felt that a rather dull recital of NOAA's statutory responsibilities in the BCT area or a lengthy discussion of what various arms of the NOAA octopus have been doing in the area in the past would be something less than stimulating. Since we have put in considerable thought as to what BLM will need to know, I felt it would be much more useful to pass some of these ideas along to you to mull over, accept, or reject in your workshops. The whole project has very real relevance to the critical energy crisis. But at the same time it provides some fine opportunities to push back the barriers of ignorance on our Continental Shelf. If we can learn something new while at the same time providing the Bureau of Land Management with the information it needs we have served both BLM and marine science—an end greatly to be desired.

Reprinted from: Proc. of Special Symposium, "The Middle Atlantic Continental Shelf and the New York Bight," American Museum of Natural History, New York City, 3-4-5 November 1975, 1 p.

R.C. Beardsley, WIOI, Woods Hole, MA; W.C. Boicourt, CBI, JHU, Balto. MD; D.V. Hansen, ACML, NOAA, Miami, FL

# PHYSICAL OCEANOGRAPHY OF THE MIDDLE ATLANTIC BIGHT

Recent work has also shed light on the exchange processes between the shelf and the slope water, which are diffinary results from the National Oceanic and Atmospheric Administration MESA program, the National Sciknowledge of circulation patterns and hydrographic structure in the Middle Atlantic Bight. Prelimimechanisms which govern the lower frequency (subtidal) variability of water motion have been identishore water motion and the distribution of mean transport along and across the shelf. The physical ence Foundation sponsored shelf programs, and other investigations reveal details of the mean long-Historical information in combination with recent physical observations provide a first-order fied and estimates can now be made of their contribution to the longshore mass transport. cult to observe properly because of their small spatial scales and their time dependency.

topographic influences on local circulations in the New York Bight apex and in the Hudson shelf valley. Modern techniques of direct current measurement and temperature and salinity sensing have allowed shelf water and the slope water usually occurs as a sharp front. Both extrusions ("bubbles") of shelf major part of the shelf-slope exchange. Attention has been focused also on the dynamics of the front longer time-series records and greater spatial coverage and resolution. Physical oceanographers are the nearshore region is the centrel that estuaries exert on the nearby shelf waters. Another is the water off the shelf and intrusions of slope water have been observed and are likely to constitute a now able to pursue their interests in the local, smaller scale processes. One specific interest in In the offshore region, interests focus on the shelf break region where the transition between the itself -- its movements, velocity shears and mixing processes.

### MODE Bottom Experiment 1

Wendell Brown,<sup>2</sup> Walter Munk,<sup>2</sup> Frank Snodgrass,<sup>2</sup> Harold Mofjeld<sup>3</sup> and Bernard Zetler<sup>2</sup>

(Manuscript received 2 July 1974, in revised form 9 September 1974)

### ABSTRACT

Pressure fluctuations on the deep seafloor at frequencies below inertial and tidal have been measured. Between 0.1 and 1 cycle per day the variance is about 2 mb², spectra diminish with increasing frequency as  $\omega^{-n}$ , n=1.5 to 2, and a signal-to-instrument noise ratio of 10 dB is achieved. Fluctuations are in phase and highly coherent within the MODE area (>0.95 at 200 km) and even with inferred (atmosphere plus sea level) Bermuda subsurface pressures (0.8 at 700 km). Station differences (to which MODE-sized eddies would make the principal contribution) are relatively small. The large horizontal scale of the recorded bottom pressure fluctuations resembles that of atmospheric pressure, yet the coherence locally between atmospheric and bottom pressure is slight; the recorded fluctuations may be related to a barotropic ocean response to a variable wind stress on the subtropical gyre. Bottom temperature records show "sudden" (1 day) changes of order 30 millidegrees Celcius separated by long intervals (20 days) of uniform temperatures. The changes are much larger than have been observed in the Pacific. They are correlated at horizontal separations of 2 km, but uncorrelated to bottom pressure and to temperatures 1 km above the seafloor.

### 1. Introduction

Measurements of atmospheric surface pressure go back to the very beginnings of meteorology. When these measurements are referred to some standard level (sea level), it is found that surface winds are directed approximately along isobars with a speed proportional to the horizontal pressure gradient. "Geostrophy" is the term applied to this idealization in the relation (sea level or aloft) between wind and pressure fields.

The corresponding practice (or malpractice) of inferring currents from the pressure field is equally embedded in oceanography, yet an experiment to test the geostrophic "law" using direct pressure measurements has not been previously attempted. Accordingly, the Bottom Experiment Subcommittee (J. Baker, Chairman) of the Mid-Ocean Dynamics Experiment (MODE) planned for an array of bottom pressure recorders, to be closely coordinated with measurements of currents and the density field. There was never any question of referring pressures to some common level (following meteorological practice); differences in the elevation of the various instruments are not known to anywhere near the required precision. The goal was to measure variations in the pressure differences between

stations, for comparison with corresponding variations in currents.<sup>4</sup>

The experiment was considered marginal from the outset. Surface atmospheric pressure can vary by a few percent; geostrophic bottom fluctuations by some millibars represent a fractional change of only a few parts in 10<sup>6</sup>. The geostrophic fluctuations are small compared to the tidal variations at higher frequency (the reverse holds for surface atmospheric pressure). The chief difficulty, however, is not a lack of instrument sensitivity, nor the removal of high-frequency tidal components (nor even the relative remoteness of the seafloor), but rather the instrumental noise at low frequencies, i.e., drift. In this connection the longer oceanic time scales (months compared to days) adds to the difficulties.

With the very reality of signals in doubt, emphasis was placed on redundancy rather than spatial coverage. And this was indeed a wise choice. It demonstrated that we did, in fact, succeed in measuring geostrophic (subinertial) bottom pressure fluctuations, but that the relatively small station differences were only marginally above instrument noise level and not adequate to test "geostrophy." The results are not those we anticipated

<sup>&</sup>lt;sup>1</sup> MODE Contribution No. 15.

<sup>&</sup>lt;sup>2</sup> Institute of Geophysics and Planetary Physics, Scripps Institution of Oceanography, University of California, La Jolla 92037

<sup>&</sup>lt;sup>3</sup> Atlantic Oceanographic and Meteorological Laboratories, NOAA, Miami, Fla. 33124

<sup>&</sup>lt;sup>4</sup> As stated succinctly by a reviewer, if we write  $A = \rho^{-1}\partial p/\partial x$ -fv = 0, classical oceanography considers  $\partial A/\partial z$ , while the present experiment is concerned with  $\partial A/\partial t$ .

<sup>&</sup>lt;sup>5</sup> Throughout this paper, "geostrophic fluctuation" refers to any fluctuation at frequencies small compared to the inertial frequency.

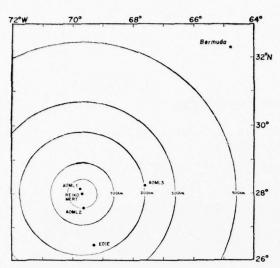


Fig. 1. MODE bottom pressure stations: AOML (1, 2, 3) and IGPP (EDIE, MERT, REIKO). REIKO and MERT were 2 km from the central mooring (28°00′ N, 69°40′ W).

(as is so often the case in an oceanographic experiment), but that does not make them any less interesting.

### 2. Measurements

The AOML<sup>6</sup> deployment consisted of three stations (Fig. 1) of which AOML 1 and AOML 3 produced useful time series of bottom pressure. Each station involved the deployment and recovery of a Gulf/GA pressure gauge by the NOAA ship *Researcher*. The Filloux Bourdon tube transducer in each gauge experienced creep, resulting in an apparent instrumental drift in pressure of about 430 mb. This drift, rapid at first and then slowing with time, follows a logarithmic law and has been removed from the AOML pressure records.

The IGPP deployment consisted of three cruises: installation, monitoring and repair, and recall. Prior to the MODE deployment, there had been extensive laboratory tests and a series of Pacific drops. All this is discussed in gruesome detail by Snodgrass et al. (1975). For the present purpose we note that there is no attempt to remove drift; after the initial day or two this is small (of the order 1 mb per month), but still the limiting factor for measuring pressure differences between stations. Pressures and temperatures were both measured by crystal gauges, and pressure records were corrected for temperature (corrections are only of the order 0.1 mb). But the temperature series are of some independent interest, and we shall describe them briefly.

### 3. Bottom temperatures

The principal results are summarized in Figs. 2 and 3. Records are characterized by "sudden" (1-day) changes of the order of 30 millidegrees Celcius (m°C) separated by long intervals (20 days) of uniform temperatures (within 5 m°C). The corresponding instrumental noise is of order 1 m°C (Snodgrass *et al.*, 1975).

Month-to-month changes cannot be detected, as they are less than instrumental drift (0.5 m°C in two months). Measurements at REIKO and MERT (Fig. 1) (separated by 2 km at the central mooring) exhibit reproducible features, with lags of the order of 1 day. There is no correlation with EDIE 180 km to the south. The fluctuations are larger by a factor of 10 than those we measured in the Pacific, and almost certainly related to the presence of Antarctic Bottom Water.

There is no resemblance to bottom pressure, nor to temperatures measured 1 km above the sea bottom. The latter are the result of vertical displacement (by several hundred meters!) from internal waves and geostrophic fluctuations (Brown, 1975).

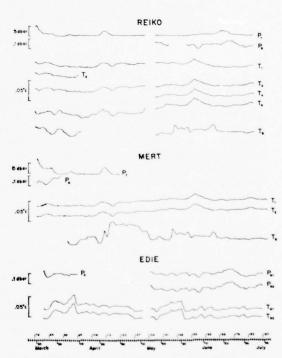


Fig. 2. Summary of low-passed 1973 IGPP MODE pressure and temperature records plotted at 20 h intervals [see Snodgrass et al. (1975) for the "raw" records].  $P_B$  and  $T_B$  refer to bottom pressures and temperatures,  $P_T$  to pressure at the top of a 1 km cable (an indication of cable tilt), and  $T_1$ ,  $T_2$ , ..., refer to temperatures at the upper end of the cable. EDIE has duplicate pressure and temperature instrumentation on the sea bottom, none aloft;  $P_C$  is a composite of  $P_{B1}$  and  $P_{B2}$  (both of which were noisy). REIKO and EDIE were recovered, repaired and relaunched in mid-May. All temperatures are plotted to the same scale.

<sup>&</sup>lt;sup>6</sup> The following abbreviations are used throughout: AOML, Atlantic Oceanographic and Meteorological Laboratories; IGPP, Institute of Geophysics and Planetary Physics; NOAA, National Oceanographic and Atmospheric Administration.

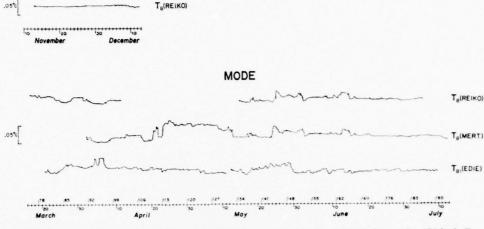


Fig. 3. Bottom temperatures at REIKO and MERT (separation 2 km) and EDIE (separation 170 km). For comparison, a typical Pacific record (REIKO 250 SW; Snodgrass et al., 1975) is shown on the same scale. In contrast to Fig. 2, the records have not been low-passed, and are plotted at 24-min intervals.

#### 4. Bottom pressures

Tides were removed by subtracting the "response predicted" deep-sea tides, with Bermuda-predicted tides taken as reference (Zetler et al., 1975). There is no significant tidal residual in the "detailed" records. For good measure, the detided time series of 45 s averages were low-passed with a 40 dB reduction at 1 cycle per day (cpd) (Fig. 4), and plotted at 24 h intervals (Fig. 5).

Three instruments within 15 km of the central mooring, AOML 1 (a Filloux Bourdon tube), MERT and REIKO (quartz crystals), show a strong resemblance during times of overlapping records. Pressure changes are larger and more sudden than we had suspected; they can amount to 5 mb in a few days. An unexpected result is the resemblance with the distant MODE stations EDIE and AOML 3. Evidently the bottom pressure fluctuations have larger horizontal scales than typical MODE eddies.

We have also plotted atmospheric pressures in the MODE and Bermuda areas,<sup>7</sup> and these are clearly coherent. In order to learn whether bottom pressures in the two areas are similarly related, we define the "subsurface pressure" (at a fixed point)

$$SSP = p_{atm} + \rho g \eta,$$

where  $\eta$  is the recorded sea level (detided). For a homogeneous ocean the subsurface and bottom pressure

<sup>7</sup> Mr. Frank Marks, Dept. of Meteorology, MIT, compiled the series of daily atmospheric pressures in the MODE area from weather maps and MODE ships' microbarograph data. Hourly values of atmospheric pressure were provided by the Environmental Data Service, NOAA, Ashville, N. C.; values of Bermuda sea level were provided by the National Ocean Survey, NOAA, Rockville, Md.

should be the same, and this is nearly the case for the barotropic response of a stratified ocean (see Appendix). For baroclinic waves of odd order, including the gravest mode, subsurface and bottom pressures (aside from atmospheric effects) are of equal amplitude but in antiphase. We regard the resemblance between Bermuda subsurface and MODE bottom pressures as an indication for a predominantly barotropic response. Further, island interference is evidently not a major consideration. As we shall find, the SSP emerges as a useful index whose interpretation is quite distinct from that of its two components, atmospheric pressure and sea level.

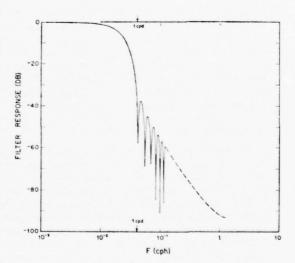


Fig. 4. Low-pass filter applied to MODE records. The energy rejection at 1 cpd is 40 dB.

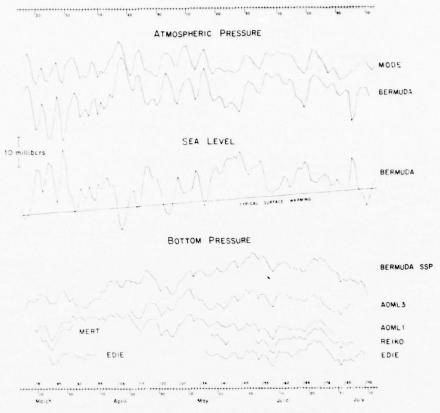


Fig. 5. Atmospheric pressure at Bermuda and in the MODE area, Bermuda sea level (detided, and in equivalent pressure units), Bermuda subsurface pressure (atmospheric plus equivalent sea level), and various MODE recorded bottom pressures. All plots to the same scale. Dates and year days are indicated. Tick marks are Greenwich midnight.

To a good approximation the components cancel in accordance with the "inverted barometer" response.

A superimposed upward drift in  $\rho g \eta$  and hence SSP, which is not found in the MODE bottom pressures, can reasonably be ascribed to thermal expansion from seasonal warming of Bermuda surface waters; if so, this would not be associated with any change in the mass per unit area, or resulting bottom pressure.

# 5. Spectral estimates

We now attempt to lend these qualitative remarks some semblance of the magnitudes involved. Spectra of Bermuda subsurface and observed MODE bottom pressures are in accord (Fig. 6). The rise centered at 0.35 cpd is consistent with the behavior of atmospheric pressure spectra (Fig. 7). Atmospheric pressure spectra are higher by a factor of 5 than those on the seafloor.

MODE bottom spectra are significantly coherent (except at the lowest frequency) among one another (Fig. 8), and with respect to Bermuda subsurface pressure. MODE and Bermuda atmospheric pressures

are highly coherent, as expected (Fig. 9). MODE bottom pressures somewhat lag Bermuda subsurface pressures, whereas the opposite holds for atmospheric pressure. Bermuda sea level and atmospheric pressure are highly coherent and out of phase (Fig. 10). On the other hand, bottom and local atmospheric pressures are barely coherent, and show no fixed phase relation. A summary of the statistical analyses is presented schematically in Fig. 11. All of the evidence points toward something other than local atmospheric pressure for the source of the bottom pressure fluctuations. This inference will be examined in the light of a simple model.

#### 6. Model

We follow the analysis by Munk and Bullard (1963). Let

$$p_1 = a \cos(\omega t + \alpha)$$

$$p_2 = ra \cos(\omega t + \alpha) + sa \sin(\omega t + \alpha) + x(t) = \bar{\rho}g\eta$$

$$p_3 = p_1 + p_2 = (1 + r)a \cos(\omega t + \alpha) + sa \sin(\omega t + \alpha) + x(t)$$

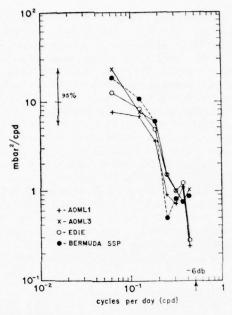


Fig. 6. Spectra of bottom pressure fluctuations for MODE (solid) and Bermuda (dashed) (16 degrees of freedom). Frequencies above those plotted are significantly reduced by numerical filtering (-6 dB at 0.5 cpd).

designate atmospheric, sea-level and bottom pressures within a narrow frequency band centered on  $\omega$ ; a(t) and  $\alpha(t)$  are slowly varying (compared to  $\omega$ ) amplitude and

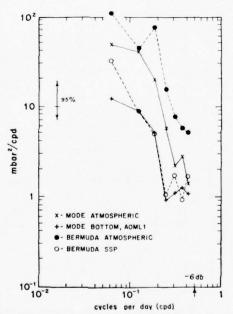


Fig. 7. Comparative spectra of atmospheric and bottom pressures (34 degrees of freedom) for MODE (solid) and Bermuda (dashed).

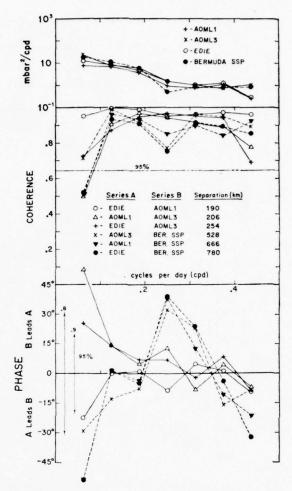


Fig. 8. Cross spectra for MODE pressures and Bermuda subsurface pressures (all spectra and cross spectra involving Bermuda are dashed). Degrees of freedom are 16; the 95% significance level for coherence (not squared), and the 95% phase uncertainties for 0.8 and 0.9 coherences are indicated.

phase. We interpret  $\langle \frac{1}{2}a^2 \rangle$  as the spectral energy in the band  $\omega \pm \frac{1}{2}\delta\omega$ . x(t) is that portion of  $p_2$  and  $p_3$  which is uncorrelated to  $p_1$ , i.e.,

$$\langle p_1(t)x(t-\tau)\rangle = 0.$$

Then by performing the appropriate lagged covariances and Fourier transforms, it follows that

$$S_{11} = \langle \frac{1}{2}a^2 \rangle$$

$$S_{22} = [r^2 + s^2]S_{11} + S$$

$$S_{33} = [(1+r)^2 + s^2]S_{11} + S$$

$$C_{12} = rS_{11}, \qquad Q_{12} = sS_{11}$$

$$C_{13} = (1+r)S_{11}, \qquad Q_{13} = sS_{11}$$

are the spectra, co- and quadrature spectra, respectively, with  $S(\omega)$  the spectrum of x(t).  $S_{22}$  and  $S_{33}$  are

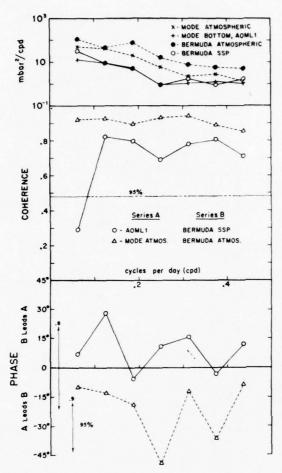


FIG. 9. Cross spectra of MODE vs Bermuda atmospheric pressure (dashed) and MODE vs Bermuda subsurface pressures (34 degrees of freedom). The 95% phase uncertainties are drawn for 0.8 and 0.9 coherences.

written as the sum of two terms: the first is coherent with atmospheric pressure, the second (S) is incoherent. For an inverted barometer's response<sup>8</sup>

$$r=-1$$
,  $s=0$ :  $S_{22}=S_{11}+S$ ,  $S_{33}=S$ .

In terms of coherence  $R_{ij}$  and phase  $\phi_{ij}$ ,

$$\binom{C_{ij}}{Q_{ij}} = (S_{ii}S_{jj})^{\frac{1}{2}}R_{ij}\binom{\cos\phi_{ij}}{\sin\phi_{ij}},$$

$$r = R_{12} \cos \phi_{12} (S_{22}/S_{11})^{\frac{1}{2}}, \quad s = R_{12} \sin \phi_{12} (S_{22}/S_{11})^{\frac{1}{2}},$$

$$S = (1 - R_{12}^2)S_{22}, S_{33} = S_{22} + (2r + 1)S_{11}.$$

These formulas permit the calculation of r, s, S,  $S_{33}$  from the measured  $S_{11}$ ,  $S_{22}$ ,  $R_{12}$ ,  $\phi_{12}$  (the cross spectrum of atmospheric pressure and sea level). Fig. 12 has been

so constructed, leaning on Wunsch's (1972) Bermuda analysis for the low frequencies, and the MODE observations at the central and high frequencies.

With regard to  $S_{22}$  at the central frequencies, this nearly equals  $(r^2+s^2)S_{11}$ , the contribution coherent with atmospheric pressure. Since the inverted barometer (IB) condition nearly holds,  $S_{22} \approx S_{11}$ . (See Appendix for a discussion of the IB condition.) The incoherent contribution S is smaller by an order of magnitude. This is not the case at very high and low frequencies, where  $S \gg S_{11}$  and  $S_{22} \rightarrow S_{33}$ . Evidently the predominance of  $S_{22}$  over  $S_{33}$  at central frequencies is related to a change in slope of the  $S_{11}$  spectrum.

With regard to  $S_{33}$  the situation is different, and the principal contribution comes from S at all frequencies. We will not attempt here to identify the incoherent spectrum S with any specific geophysical process; the large horizontal scale suggests an atmospheric process, and the coherence found by Wunsch between Bermuda

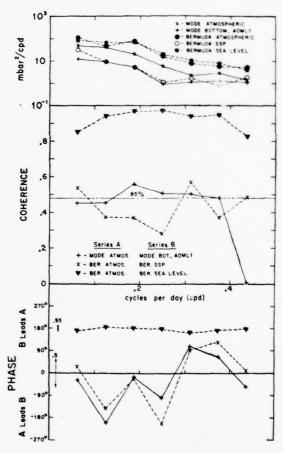


Fig. 10. Cross spectra of bottom pressures and Bermuda sea level vs local atmospheric pressures (34 degrees of freedom). Bermuda spectra are dashed. Phase uncertainties are shown for 0.95 and 0.5 coherences.

<sup>&</sup>lt;sup>8</sup> This interpretation has to be qualified if winds make a significant contribution that is coherent with atmospheric pressure.

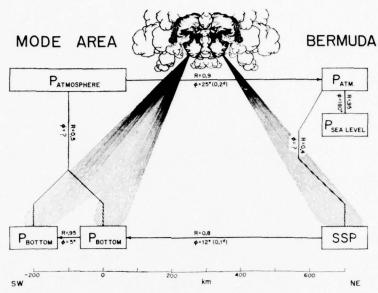


Fig. 11. Schematic presentation of coherences R and phases  $\phi$  (in direction of arrows) in the 0.1–0.5 cpd frequency band. Atmospheric pressures (or SSP) are highly coherent over the MODE area and between MODE and Bermuda, as are MODE bottom pressures and MODE bottom pressure with Bermuda SSP; but the local coherences between atmospheric and bottom pressure (or SSP) are very low. Some common and unknown source of the MODE and Bermuda bottom pressures is indicated.

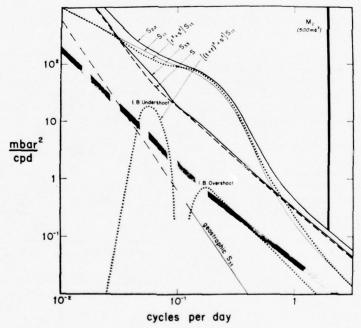


Fig. 12. Idealized spectra of atmospheric pressure  $(S_{11})$ , sea level  $(S_{22}$ , in equivalent pressure units) and bottom pressure  $(S_{32})$ .  $[r^2+s^2]S_{11}$  and  $[(1+r)^2+s^2]S_{11}$  are the contributions to  $S_{22}$  and  $S_{33}$ , respectively, that are coherent with atmospheric pressure; S is the noncoherent contribution to both  $S_{22}$  and  $S_{33}$ . Bottom pressures inferred from MODE bottom velocity measurements are designated "geostrophic  $S_{33}$ ," and lie below the noise spectrum of bottom pressure transducers (inferred from duplicate instrumentation); extrapolation from 0.1 to 0.01 cpd is uncertain.

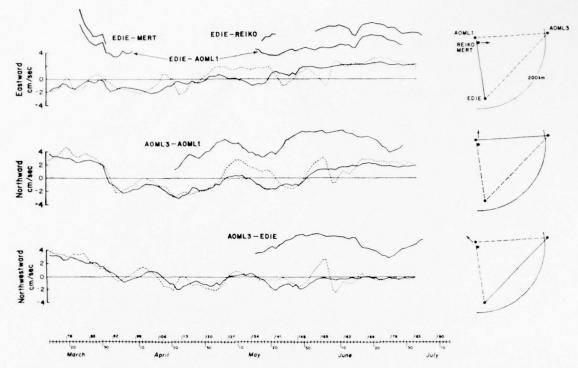


Fig. 13. Components of measured bottom currents (depth 5356 m, dashed) and deep currents (3963 m, solid) at central mooring. For comparison, fluctuations in currents inferred geostrophically from pressure differences between stations are plotted to the same scale, but with arbitrary zero offset.

sea level and local winds (Figs. 8 and 10 of Wunsch, 1972) is certainly suggestive. The analysis by Phillips (1966) leads to a reasonable magnitude: rms(p<sub>3</sub>)  $=(L/h) \operatorname{rms}(\tau)$ , where  $p_3$  and  $\tau$  are bottom pressure and surface stress, and L/h = 5000 km/5 km is the ratio of the horizontal stress scale to ocean depth (Appendix). For  $\tau = 1$  dyn cm<sup>-2</sup>,  $p_3 = 10^3$  dyn cm<sup>-2</sup> = 1 mb.

At 0.1 cpd the IB condition is taken to be exactly fulfilled, and S is the sole contribution to  $S_{33}$ ; at other frequencies there is an additional slight  $[(1+r)^2+s^2]S_{11}$ contribution to  $S_{33}$  because of the departure from the IB condition: an IB undershoot below 0.1 cpd, an IB overshoot above 0.1 cpd. If we take 1+r, s and  $1-R_{12}$ as small and all of order  $\epsilon$ , then the relative magnitude in the coherent and incoherent (with atmospheric pressure) contributions to sea level and sea bottom spectra is as follows:

	Coherent	Incoherent	
Sea level	1	•	
Sea bottom	$\epsilon^2$	•	

# 7. Discussion

Bottom and deep currents at the MODE central mooring9 are plotted in Fig. 13, together with the

geostrophic currents computed from station differences. There is a resemblance in the northward components at low frequencies (currents 1400 m above the seafloor are better correlated than bottom currents). The "geostrophic" spectrum in bottom pressure has been estimated from the bottom velocity spectrum, using a factor

$$\langle p_3^2 \rangle / \langle v^2 \rangle = (10^{-3} \rho f/k)^2 = (0.4 \text{ mb cm}^{-1} \text{ s}^{-1})^2$$

for typical MODE eddies  $(k=2\pi/\lambda=2\pi/350 \text{ km})$ ,  $f = 6.8 \times 10^{-5} \text{ s}^{-1}$ ). This lies far beneath the observed  $S_{33}$ , and also below the instrumental noise figure by Snodgrass et al. (1975), except perhaps at very low frequencies (Fig. 12). This is related to the fact that the difference between two instruments placed side by side is of the same order as the station difference (Fig. 14).

Bottom pressure and velocity fluctuations (rms) can now be estimated as follows:

		0.01 to 0.1 cpd	0.1 to 1 cpd
MODE eddies	$(\lambda/2\pi = 50 \text{ km})$	2 mb 5 cm s <sup>-1</sup>	0.2 mb 0.5 cm s <sup>-1</sup>
Large-scale fluctuations	$(\lambda/2\pi = 1000 \text{ km})$	8 mb 1 cm s <sup>-1</sup>	1.5 mb 0.2 cm s <sup>-1</sup>

We are grateful to the Woods Hole Oceanographic Institution for having made the records available.

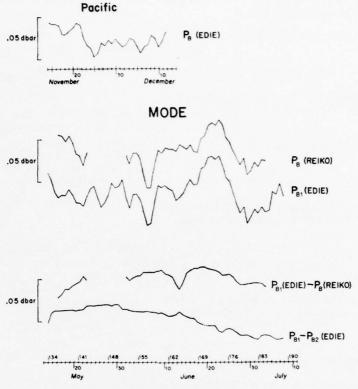


Fig. 14. Some bottom pressures and pressure differences during the latter half of the MODE experiment. The difference  $P_{B1}-P_{B2}$  between two pressure sensors on EDIE capsule is of the same order as the difference between capsules EDIE and REIKO separated by 170 km [the negative spike in  $P_{B1}(\text{EDIE})-P_{B}(\text{REIKO})$  on 13 June occurs during a period of excessive instrument noise (Snodgrass et al., 1975)]. For comparison, a Pacific record taken in 1972 is plotted to the same scale.

The large-scale fluctuations have larger pressure variations than the MODE eddies, but because of their much larger horizontal scale, the associated current velocities are relatively small. (On hindsight, this situation might

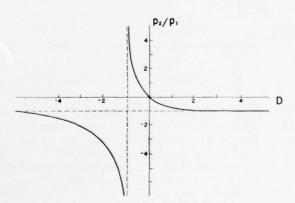


Fig. 15. Response of sea level to atmospheric pressure:  $p_2/p_1 = -1$  for inverted barometer response.

have been anticipated from an extrapolation of Wunsch's results.) Consequently, the observed bottom pressures are related primarily to the large-scale fluctuations, whereas the observed bottom currents are related mostly to MODE eddies. (Pressure differences between stations would be dominated by MODE eddies, but are only marginally above noise level.) We have succeeded in measuring geostrophic bottom pressures, but failed in testing geostrophy.

Acknowledgments. IGPP work was supported by the Office of Naval Research (Contract N00014-69-A-0200-6008) and the National Science Foundation (Grant NSF-GX-29052). The AOML work was supported under the National Science Foundation agreement AG-253 for NOAA participation in the International Decade of Ocean Exploration.

### APPENDIX

#### Subsurface Pressure

For a free progressive wave in a rotating ocean of constant Väisälä frequency N and depth h, the ratio of

subsurface pressure  $\rho_0 g_\eta$  to bottom pressure is given by (Munk and Phillips, 1968, p. 450)

$$SSP/p_b = cos(Nh/C)$$
,

with

$$\tan(Nh/C) = CN/g$$

serving as a definition for C (the phase speed in a non-rotating system). For barotropic waves,  $Nh/C\ll 1$ ; hence

$$C = \sqrt{gh}(1+\epsilon^2/6)$$
, SSP/ $p_b = 1-\frac{1}{2}\epsilon^2$ ,

where

$$\epsilon^2 = N^2 h/g = O(\Delta \rho/\rho)$$

is a small number. Subsurface and bottom pressures are nearly the same. For baroclinic waves,  $(Nh/C - r\pi) \ll 1$ ,  $r = 1, 2, \cdots$ .

$$C = \frac{Nh}{r\pi} \left( 1 - \frac{\epsilon^2}{r^2 \pi^2} \right), \quad SSP/p_b = (-1)r \left( 1 - \frac{\epsilon^4}{2r^2 \pi^2} \right).$$

Thus, subsurface and bottom pressures are of very nearly the same amplitude, but out of phase for odd modes.

#### Inverted Barometer Problem

Let u,v designate eastward and northward velocity components,  $\eta$  the surface elevation, and  $p_1 = \rho g \xi$  surface atmospheric pressure. We then have for an ocean of constant depth h and density  $\rho$ 

$$\begin{cases} \frac{\partial u}{\partial t} - fv = -g \frac{\partial}{\partial x} (\xi + \eta) \\ \frac{\partial v}{\partial t} + fu = -g \frac{\partial}{\partial y} (\xi + \eta) \\ \frac{\partial \eta}{\partial t} = -h \left( \frac{\partial u}{\partial x} + \frac{\partial v}{\partial y} \right) \end{cases},$$

which can be combined into

$$\frac{\partial^2 u}{\partial v \partial t} - \frac{\partial^2 v}{\partial x \partial t} - \beta v + f h^{-1} \frac{\partial \eta}{\partial t} = 0,$$

where  $\beta = df/dy$ , and f the Coriolis frequency. For frequencies  $\omega$  small compared to f, we neglect  $\partial(u,v)/\partial t$ , and

$$\lambda^{2} \frac{\partial}{\partial t} \nabla^{2}(\xi + \eta) + \beta \frac{\partial}{\partial x} (\xi + \eta) = \frac{\partial \eta}{\partial t},$$

where

$$\lambda = (gh)^{\frac{1}{2}}/f$$

is the Rossby radius of deformation. Assuming cellular oscillations of the type

$$\cos ly \cos(kx - \omega t)$$
,

we obtain

$$\frac{p_2}{p_1} = \frac{\eta}{\xi} = -\frac{D}{1+D}, \quad D = \lambda^2 (k^2 + l^2 + \beta k/\omega).$$

In the limit of large-scale disturbances,  $k, l \rightarrow 0$  and  $D \rightarrow 0$ ,  $\eta \rightarrow 0$  (frozen surface), and the atmospheric pressure is geostrophically balanced. In the low-frequency limit of eastward/westward waves,  $\omega \rightarrow \pm 0$  and  $D \rightarrow \pm \infty$ ,  $p_2/p_1 \rightarrow -1$  (inverted barometer), and u, v = 0. For D = -1,

$$\frac{\omega}{k} = -\frac{\beta}{\lambda^{-2} + k^2 + l^2},$$

which is the (westward) phase velocity of free Rossby waves, and so  $\eta \to \pm \infty$  because of resonance.

The scaling

$$\hat{k}, \hat{l} = \lambda(k,l), \quad \hat{\omega} = \omega/f,$$

is convenient, leading to

$$D = \hat{k}^2 + \hat{l}^2 + (\hat{k}/\hat{\omega})\nu^{-\frac{1}{2}}$$

with

$$\nu^{\frac{1}{2}} = 2\Omega a/(gh)^{\frac{1}{2}}$$

a parameter [O(1)] familiar from tidal theory. Setting  $\lambda = 3000$  km,  $\hat{k}$ ,  $\hat{l} = 5$ ,  $\hat{\omega} = \pm 0.1$ ,  $\nu^{\frac{1}{2}} = 2.15$  gives  $D = 50 \pm 23$ , and we expect  $p_2/p_1$  to be within a few percent of unity.

The foregoing analysis applies to an infinite ocean of constant depth. For the "real" ocean one may have to replace  $\beta = df/dy$  by a "topographic"  $\beta$  arising from the gross slope and small-scale topography.

#### Wind Stress

According to Phillips (1966), a variable eastward wind stress

$$\tau_x = \tau_0 \sin(\pi y/L)e^{i\omega t}, \quad -\frac{1}{2}L \leqslant y \leqslant \frac{1}{2}L,$$

generates a meridional component of barotropic flow

$$v = \frac{2\tau_0}{\rho h \beta L} \cos\left(\frac{\pi y}{L}\right) e^{i\omega t} V(\xi, \mu),$$

where L=5000 km is the distance between the trade winds and westerlies. V is a complicated function of the distance  $\xi = x/L$  from the coast, and of frequency  $\mu = \omega/\omega_{\rm max}$ , with  $\omega_{\rm max} = \beta L/2\pi = 2\pi/(5.71 {
m days})$ . V exhibits a series of resonant peaks, but their contributions to  $\langle v^2 \rangle$  are secondary in the interval  $\mu = 0.2$  to  $\mu = 1$  (0.02 to 0.2 cpd), and  $V \approx V_0 \mu^{-1}$ ,  $V_0 \approx [\pi^2(1+2\xi)^2+4]^{\dagger} \approx 5$  for  $\xi = 0.2$ . The wavelength  $\mu L = \mu \cdot 5000$  km is consistent with the observed scale of pressure coherence.

To obtain rms pressures, multiply by  $\rho f/k$  with  $k = 2\pi/\mu L$ , and replace  $\cos(\pi \mu/L)e^{i\omega t}$  by its rms value  $\frac{1}{2}$ :

$$\mathrm{rms}(p_3) = \frac{V_0}{2\pi} \frac{f}{\beta L} \frac{L}{h} \mathrm{rms}(\tau_0).$$

Accordingly, the seafloor pressure spectrum is proportional to the  $\tau_0$  spectrum. Numerically,  $V_0/2\pi\approx 1$ ,  $f/\beta L\approx 1$  and  $L/h\approx 10^3$ . Thus rms pressures (mb) are roughly equal to rms stresses (dyn cm<sup>-2</sup>).

#### REFERENCES

Brown, W. S., 1975: MODE internal waves. J. Phys. Oceanogr. (in preparation).

Munk, W. H., and E. C. Bullard, 1963: Patching the long-wave spectrum across the tides. J. Geophys. Res., 68, 3627-3634.
—, and N. Phillips, 1968: Coherence and band structure of inertial motion in the sea. Rev. Geophys., 6, 447-472.

Phillips, N., 1966: Large-scale eddy motion in the western Atlantic. J. Geophys. Res., 71, 3883-3891.

Snodgrass, F. E., W. S. Brown and W. H. Munk, 1975: MODE: IGPP measurements of pressure and temperature. J. Phys. Oceanogr., 5, 63-74.

Wunsch, C., 1972: Bermuda sea level in relation to tides, weather and barcclinic fluctuations. Rev. Geophys. Space Phys., 10, 1-40

Zetler, B. D., W. H. Munk, H. Mofjeld, W. S. Brown and F. O. Dormer, 1975: MODE tides. Submitted to J. Phys. Oceanogr.



U.S. DEPARTMENT OF COMMERCE Rogers C. B. Morton, Secretary

NATIONAL OCEANIC AND ATMOSPHERIC ADMINISTRATION
Robert M. White, Administrator
ENVIRONMENTAL RESEARCH LABORATORIES
Wilmot N. Hess, Director

# NOAA TECHNICAL REPORT ERL 332-MESA 3

Assessment of Offshore Dumping in the New York Bight, Technical Background: Physical Oceanography Geological Oceanography Chemical Oceanography

ROBERT L. CHARNELL, Editor

Atlantic Oceanographic and Meteorogical Laboratories Miami, Florida

BOULDER, COLO April 1975

#### DISCLAIMER

The NOAA Environmental Research Laboratories do not approve, recommend, or endorse any proprietary product or proprietary material mentioned in this publication. No reference shall be made to the NOAA Environmental Research Laboratories, or to this publication furnished by the NOAA Environmental Research Laboratories, in any advertising or sales promotion which would indicate or imply that the NOAA Environmental Research Laboratories approve, recommend, or endorse any proprietary product or proprietary material mentioned herein, or which has as its purpose an intent to cause directly or indirectly the advertised product to be used or purchased because of this NOAA Environmental Research Laboratories publication.

## PREFACE

In late 1973 and early 1974, attention in the scientific community was focused on consequences of sewage sludge dumping in the apex of the New York Bight. Newly acquired data seemed to indicate a change was occurring in the movement and distribution of sludge material in bottom sediments. To some university scientists, it appeared that increases in the rate of disposal had produced a quantity of sludge that could no longer be assimilated by the environment; the alarm was sounded that if the dumping continued at the same rate, irreversible contamination would occur to the beaches of Long Island within a few years. A call for immediate relocation of the present dumpsites was made.

Early in August 1974, United States Senator James L. Buckley convened the Subcommittee on Environmental Pollution of the Senate Public Works Committee for a public hearing on the sewage sludge dumping issue. The subcommittee was eliciting facts in the matter, in order to make an informed recommendation regarding dumpsite relocation.

The National Oceanic and Atmospheric Administration (NOAA) was asked to provide testimony at this hearing. Since 1973, NOAA had been conducting a large scale examination of the New York Bight marine ecosystem and had been collecting relevant data in the apex that could shed light on the suggested irreversible degradation of the environment. NOAA's Atlantic Oceanographic and Meteorological Laboratories (AOML) had been collecting data for the Marine Ecoystems Analysis (MESA) Program in the apex since July 1973; with these and historic data, a picture of the present conditions and reasons for and rates of change were beginning to emerge.

This report is a summary of AOML analyses of the apex ecosystem as we understood it at the end of July 1974. The three parts represent three different single-discipline views of a complex ecosystem. Because our research has not been completed, conclusions of this report must be considered tentative; they are nevertheless immediately useful in preliminary assessments of the environmental significance of sewage sludge dumping in the New York Bight apex.

Robert L. Charnell November 1974 Technical Report ERL 332-MESA 3 supersedes Technical Memorandum ERL MESA-1.

# CONTENTS

				page
1.		ICAL OC YORK BI	CEANOGRAPHY; WATER MOVEMENT WITHIN THE APEX OF THE	1
	1.1	Introd	uction	1
	1.2	Lagran 1969	gian Measurements Using Surface and Seabed Drifters-	2
		1.2.1	Temporal Variations	2
		1.2.2	Spatial Structure of Seabed Drifter Returns	4
		1.2.3	Spatial Structure of Surface Drifter Returns	6
	1.3	Direct	Current Measurements in the Bight Apex	7
		1.3.1	Temporal Variability of Flow	7
		1.3.2	Phase I Average Flow	9
		1.3.3	Phase II Flow Character	11
		1.3.4	Speed of Flow Near Long Island	13
	1.4	Infere	nce of Surface Flow from ERTS Data	14
			OCEANOGRAPHY; SEDIMENTATION IN THE NEW YORK BIGHT PLICATION TO PROBLEMS OF WASTE DISPOSAL	16
	2.1	Introd	uction	16
	2.2	Physic	al Nature of the Sea Floor	18
		2.2.1	Topography, Shallow Structure, and Geologic History	18
		2.2.2	Distribution and Micro-topography of Surficial Sediments	19
	2.3	Sedime	nt Transport in the Bight Apex	37
		2.3.1	Modes of Sediment Transport	37
		2.3.2	Suspended Sediment Transport: General Concepts	37

				page
		2.3.3	Suspended Sediment Transport in the Bight Apex	39
		2.3.4	Suspended Sediment Transport and the Deposition of Bottom Muds	48
		2.3.5	Coarse Sediment Transport: General Concepts	50
		2.3.6	Coarse Sediment Transport in the Bight Apex	54
	2.4		ation of Sediment Transport Data to the Problem of Sludge Disposal	57
		2.4.1	Pattern of Waste Dispersal	57
		2.4.2	Bottom Muds Versus Sewage Sludge Beds	58
	2.5	Refere	nces	60
3.			D GEOCHEMICAL OCEANOGRAPHY OF THE NEW YORK BIGHT APEX T PERTAINS TO THE PROBLEM OF SEWAGE SLUDGE DISPOSAL	62
	3.1	Introd	uction	62
	3.2	Waste	Disposal	62
		3.2.1	Contaminants Introduced into the New York Bight	62
		3.2.2	Composition of Sewage Sludge	62
		3.2.3	Fate of Sewage Sludge After Dumping into the Ocean	63
		3.2.4	Methods for Identification of Sewage Sludge in Marine Sediments	64
	3.3	Prelim	inary Results of the MESA Program	67
		3.3.1	Water Column Chemistry	67
		3.3.2	Sediment Chemistry	72
	3 /	Poforo	200	82

#### ABSTRACT

Physical Oceanography: Analysis of historic and MESA data shows two distinct circulation regimes. 1) Near the harbor mouth and along the New Jersey coast, New York Harbor discharge flows southward parallel to the New Jersey coast; at depth, there is a return flow of external water into the estuary. In spite of its importance in the oceanographic and ecological systems of the region, this superposed flow system is recognized in measurements as only a slight imbalance of much stronger ebb and flood tidal currents. 2) Outside the region of strongest influence from river discharge, a persistent clockwise circulation or eddy appears to exist. In the eddy's most inshore portion, flow is toward the north and east, counter to the general flow over the continental shelf adjacent to this part of the coast. Details of its horizontal extent, its vertical structure, and its persistence are imperfectly known at present.

Geological Oceanography: Fine-grained waste dumped in New York Bight is entrained in a clockwise circulation pattern and is dispersed to the north. A significant portion is deposited in the low area (Christiaensen Basin) immediately northwest of the dumpsites. The fraction of finer dredge spoils and the bulk of sewage sludge is widely dispersed through the Bight apex in highly dilute form. There are no "pure" sludge beds; there has been no detectable aggradation of the sewage sludge site since 1936. However, the Christiaensen Basin, a natural zone of mud deposition, appears to be significantly contaminated with sewage sludge. Near Long Island beaches, there are scattered, thin, small patches of mud, physically indistinguishable from natural mud patches on similar, less populous coasts. Microscopic examination of samples indicates that less than 3 percent of the resolvable particles in these patches are of artificial origin, the lowest contamination level detected by microscopic technique in the Bight apex. No evidence for a front of sewage sludge approaching the Long Island shore was observed.

Chemical Oceanography: Data from water sampling show that nutrient (nitrates, nitrites, silicates, and phosphates) distributions are dominated by the lower New York Bay outflow, with dumped sewage sludge contributing very small amounts. Bottom grab samples were analyzed for total organic carbon and total carbohydrates. The carbohydrate/TOC ratio indicates that the whole Bight contains some sewage-derived materials with the greatest concentration in the Hudson Shelf Valley, in the Christiaensen Basin, and north of the geographical sewage sludge dumpsite. This is consistent with the distribution expected if sewage sludge were disseminated throughout the apex by the hypothesized current pattern (gyre). Although carbohydrate/TOC ratios in sediments throughout the area close to Long Island suggest the presence of sewage-derived material, low TOC values found in all but isolated pockets demonstrate that contaminant material comprises only a small fraction of the sediments.

# 1. PHYSICAL OCEANOGRAPHY; WATER MOVEMENT WITHIN THE APEX OF THE NEW YORK BIGHT

Robert L. Charnell, Dennis A. Mayer, Donald V. Hansen

#### 1.1 INTRODUCTION

The Marine Ecosystems Analysis (MESA) New York Bight Project is in the field phase of a program to evaluate changes in the water quality of the region. The physical oceanographic part of the effort is oriented to supplying information that will lead to understanding the mechanisms of water movement and material dispersion and eventually result in predictive models for coastal zone planners and managers.

MESA measurements in the apex were begun in mid 1973 and at the time of this writing only preliminary analyses of these data have been completed. Heretofore only scattered direct measurements of currents had been made and these dominantly were in the apex. Data from these measurements were inadequate to describe temporal and spatial structure of flow, but were useful in designing the MESA measurement program.

Present interest in the structure of water movement around the apex dumpsites southeast of Ambrose Light Station required an evaluation of what is known about flow in this area. At present the picture can only be general, with a quantitative description to be supplied as analysis of MESA data progresses. This summary report is based on two data sources: the historic data from a seabed and surface drifter program conducted by the National Marine Fisheries Service Sandy Hook Laboratory in 1969 and from the two measurement efforts conducted for the MESA program in the last half of 1973.

The general movement of water over the continental shelf off southern New England and the Middle Atlantic States is to the west and south, parallel to the continental margin. The net current is, however, masked by high spatial and temporal variability. Structure of the spatial variability in currents of the Bight apex has been a prime focus of the MESA project; temporal variability is the principal impediment to its rapid elucidation. The major features of the spatial structure of circulation that relate to disposal of waste materials in shelf waters of the New York Bight are as follows:

a. In the immediate vicinity of the entrance to the Hudson and Raritan Rivers estuary, the oceanographic regime is dominated by influence of discharges from these rivers. As in all such estuaries, there is a seaward flow of brackish water in surficial layers. At sea, this discharge turns to flow southward, paralleling the New Jersey shoreline. Lower in the water column, there is return flow of Bight water into the estuaries.

This two-layer flow appears in measurements only as a slight imbalance of the much stronger ebb and flood tidal currents in the respective layers.

b. There is strong evidence from recent MESA results that outside the region of strongest influence from river discharges, there is a persistent clockwise circulation or eddy. In the eddy's most inshore portion, off New Jersey and Long Island, flow runs counter to the general flow over the continental shelf adjacent to this part of the coast. Details of the seaward extent and vertical structure of the eddy are imprefectly known.

The evidence on which these statements are based is developed in sequel.

# 1.2 LAGRANGIAN MEASUREMENTS USING SURFACE AND SEABED DRIFTERS-1969

Data from the Sandy Hook Laboratory's 1969 study most relevant to movement of materials by currents in the New York Bight resulted from deployment of Lagrangian drifters which measure water movement at the surface and bottom of the water column. Reaction of these drifters to water movement approximates that of other small movable objects at the surface and near the seabed. Their behavior thus provides a direct estimate of the effect of water movement on the transport and dispersal of sewage sludge and dredging spoils. The seabed drifter is a positively buoyant plastic saucer (18 cm diameter) fastened to a small diameter stem 54 cm long. The free end of this stem is weighted so that the whole drifter has slight negative buoyancy. Surface drifters used for the study were small bottles, ballasted to float vertically and to present a low above-surface profile to minimize wind effects. Drifter movement in the marine environment is effected by advective and dispersive processes, each with many time and space scales. Recovery data represent a time and space integral of these processes, about which little structural information is available.

### 1.2.1 Temporal Variations

During 1969, drifters were deposited along a grid of 23 stations on approximately a monthly basis. Of the 1886 surface drifters released, 497 or about 26% were recovered by the public and returned to the project office. Of the 2190 seabed drifters released, 710 or about 32% were returned. This represents the total release and recovery for all stations during 1969 without regard to temporal variations. These rates of return are very high for this type of sampling. Data on the rate of return for all stations as a function of time are presented in figure 1.1.

The central portion of the figure shows rate of return for surface drifters released at times indicated by dots while the bottom portion

shows rate of return for seabed drifters released at times also indicated by dots. The uppermost part of the figure shows the weekly mean wind vectors at Ambrose Light Station during 1969. Winds showed a dramatic shift in mean direction from northerly to southerly during March and April. Winds continued to be from the south and weaker until near the end of September when another shift to northerlies occurred. During spring and summer the winds exhibited a diurnal periodicity in the north component.

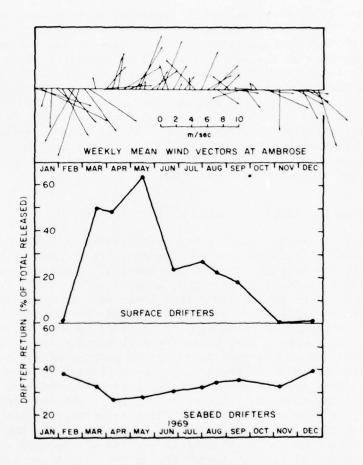


Figure 1.1 Time history of drifter returns compared with wind at Ambrose Light Station.

It is apparent from the surface drifter returns that wind-induced effects tended to dominate surface circulation. In the early part of the year when winds were from the north-northwest, virtually no surface

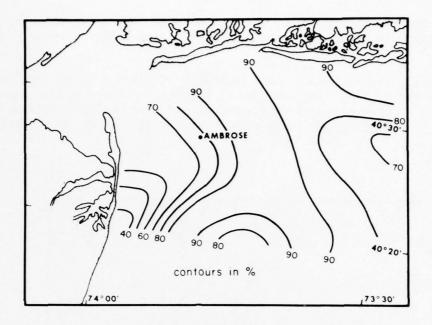
drifters were recovered; they undoubtedly were swept out to sea. Conversely, during spring and summer, winds pushed surface water, and hence drifters, in toward the Long Island beaches. Then during late summer and fall, recoveries decreased as the winds became variable and ultimately switched toward the southeast. It is not likely that decreased beach traffic in winter months accounted for the decline of surface drifter returns since returns of bottom drifters had a slight maximum for this period.

In general, however, return of seabed drifters showed only slight seasonality. There was a slight decrease below the annual average during the period of high surface return. This suggests that during the spring when river outflow at the surface and return of bottom water into the harbor mouth due to estuarine circulation processes are the strongest, more seabed drifters return up into the Hudson estuary. Once inside the estuary, they tend to be lost because few areas are suitable for beaching and recovery of drifters. Recoveries from within the estuary tend to show a slightly different picture; for just two months, August and September, recoveries were much higher than for any other two month segment. This higher rate is nearly three times the recovery rate for the more nearly average months of April and May.

# 1.2.2 Spatial Structure of Seabed Drifter Returns

In addition to the tendency for bottom water to flow northwest into the Hudson mouth, there is a marked tendency for northward flow with only a slight tendency for flow to the west; 477 drifters were recovered along the south coast of Long Island, whereas 127 drifters beached along the eastern coast of the mainland from Sandy Hook to Cape May. To examine the tendency for flow toward Long Island the drifter data have been organized by normalizing recoveries of drifters on Long Island to the total number recovered. This ratio for each station in the apex grid has been presented (as percentage) in the lower portion of figure 1.2. The data indicate that most drifters recovered on Long Island beaches originated at stations east of the Hudson Shelf Channel, while very few originated west of the channel. This is not strictly the case for drifters released within 8 km of Long Island; their recoveries dominantly show a dependence of recovery only on distance from shore. The high rate of relative return from the south central portion of the apex suggests that dominant long period flow is toward the north. The general impression conveyed by this year of bottom drifter data leads to the hypothesis of general clockwise circulation in the Bight.

This picture is consistent with the rates of return of seabed drifters released near the existing sewage sludge dumpsite. Return rate for those drifters was slightly lower (24%) than the overall return rate of seabed drifters (30-40%), but still relatively high. Two-thirds of recoveries for drifters released near the dumpsite were on Long Island. The drifters did not move rapidly across the 19 km to the beach.



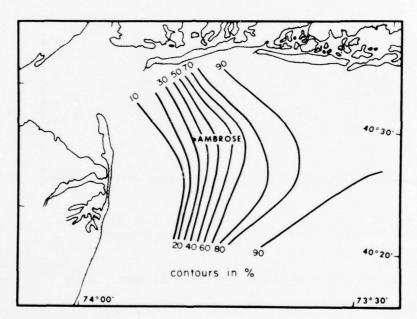


Figure 1.2 Origin of drifters recovered on Long Island.
Contours are of total recovered on Long Island as percent
of all returns from individual stations. Upper panel:
Surface drifters. Lower panel: Seabed drifters.

Although the earliest recovery was made only 13 days after release, the average time in the water was 88 days, with some drifters being found as much as 1 year after release.

Data for the bottom drifters recovered within the harbor are presented in figure 1.3. The contours of percent return provide a measure of the region most strongly influenced by the near bottom estuarine flow. This effect apparently does not extend east of the Hudson Shelf Valley.

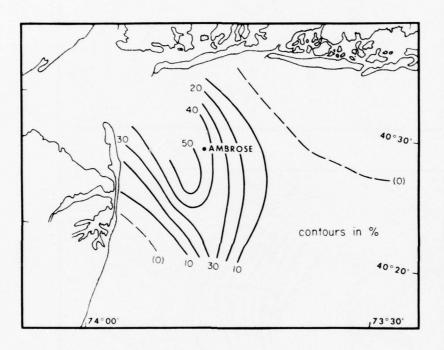


Figure 1.3. Origin of seabed drifters recovered within the Hudson Estuary.

# 1.2.3 Spatial Structure of Surface Drifter Returns

Flow implied by surface drifter returns is much more uncertain due to a higher degree of variability induced by the winds. However, it is clear from the data that drifters released closest to Long Island's south shore had the greatest incidence of shore recovery. In a manner similar to that used to show the seabed drifter recoveries, the origin of release for the 406 drifters collected on the south shore of Long Island is shown in the upper segment of figure 1.2. There is a ridge of

high rate of return to the north shore from the center of the apex with areas of low return on either side. This ridge is due to the incidence of summer winds which move the drifters to the northward and ground them on Long Island. At least for 1969, the predominant character of non-winter surface flow is inferred to be northward.

For surface drifters released near the sewage sludge dumpsite, only 17% of all those released were recovered, but over 90% of those recovered were found on Long Island beaches. The apparent low recovery rate is due to the tendency, for nearly one-half the year, for wind to blow surface water (and drifters) out of the apex to the southeast.

### 1.3 DIRECT CURRENT MEASUREMENTS IN THE BIGHT APEX

During the first field year of the MESA New York Bight Project, a major effort was made to collect data on water movement in the apex. Measurements were made to provide data on mean currents as well as temporal and spatial variations in circulation in the region surrounding the dumpsites. One objective of the current meter array was to provide data to test the hypothesis of clockwise circulation in the apex. The main placement of recording current meters was in two transects perpendicular to the New York and New Jersey shores. Meters were also placed at stations in the New Jersey-Rockaway transect, adjacent to Long Island, east of the main set of stations, and about 56 km southeast of the harbor mouth.

The array of stations was occupied twice during the last half of 1973: Phase I: August-September, and Phase II: October-December. Maximum period of sampling for each phase was about 45 days. Near the end of Phase I, a current meter station was placed near the sewage sludge dumpsite and obtained a concurrent two-week record. Results from preliminary analysis of data from these measurements are discussed in the following subsections.

# 1.3.1 Temporal Variability of Flow

One of the more difficult oceanographic concepts to convey to other than professional oceanographers is that of temporal variability, especially low frequency variability, on ocean currents. A useful technique for displaying amount and type of flow variability is the spectrum function for energy of the flow. Two such spectrum functions are shown in figure 1.4. The curves, denoting energy in the east component of flow at station F for Phase I and II, are typical of nearshore current measurements in the Bight. The major features of these functions are the peaks that occur near periods of 12 hours, 19 to 25 hours, and at the left-hand limit. Respectively, these peaks are associated with the

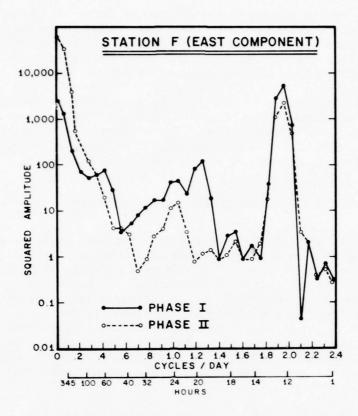


Figure 1.4 Energy spectra for east component of current meter data from Station F during Phases I and II.

semidaily tides, a mixture of inertial currents and daily tides, and irregular variations of time scales amounting to several days. Each time scale plays a particular role in the movement of water-borne materials. In general terms, the effect of energetic currents of high frequency is to create turbulence and to maintain materials in suspension, but not necessarily to transport or disperse them over long distances. Advective transport is effected by low frequency processes. A period of 40 hours is commonly used to distinguish between high and low frequency processes in the ocean. For the Station F spectra shown in figure 1.4, about 75% of the current variance occurred at periods less than 40 hours during Phase I. However, during Phase II these higher frequencies accounted for only 36% of the current variance. During Phase II a similar frequency distribution of current energy was found at the nearshore Station K.

However at Station A, further offshore, the high frequency portion of current energy is only 28% for Phase I, then drops to about 10% for Phase II. By comparative measure, the ratio of variance energy to energy of the mean flow, a ratio that is the prime interest in discussions of pollutant advection, shows a value at Station F of about 13 for Phase I which drops to 3 for Phase II.

# 1.3.2 Phase I Average Flow

Phase I measurements were made during the period of the year when strong stratification exists in apex. Accompanying salinity-temperature-depth (STD) data show that during most of the period a strong pycnocline existed about midway in the water column, although the structure changed from one of a multilayer to one of marked two layers during the period of measurement. The bulk of current meter data was obtained from the lower portion of the water column.

Figure 1.5 shows the mean current vectors for Phase I. The vectors represent the net movement in the lower portion of the water column over the 50 days the current meters were in operation. Locations in the water column of meters used in this compilation and that of figure 1.6 are shown in table 1.1.

Table 1.1 Level of Current Meter Observations

Station	Water Depth (m)	Distance of Meter above Bottom (m)	Percent of Water Column
A	45	15	33
D	10	1	10
E	16	8	46
F	24	9	38
G	38	15	41
K	20	9	44
ST-4	28	11	39

Station ST-4 is the dumpsite station whose period of observation was 14 days. Data from all stations show estuarine circulation into the Raritan Bay and support the hypothesis of clockwise gyral circulation in the apex.

Data from station D are dominated by strong tidal motions. There is a net bottom water flow into the harbor of about 3 cm  $\sec^{-1}$ . This flow is consistent with estuarine circulation concepts.

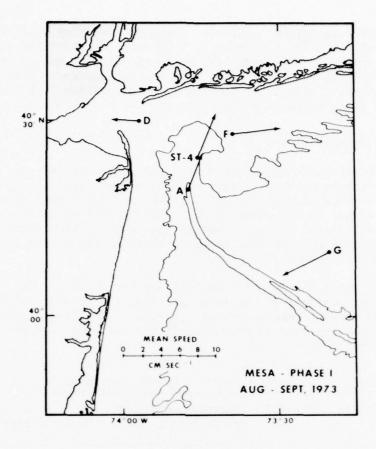


Figure 1.5 Mean current vectors for selected stations during Phase I.

Mean speed at all other stations is a reasonably consistent 4-6 cm sec<sup>-1</sup>. This speed is substantially below the instantaneous speeds characteristic for this period. The data records exhibit a high degree of variability due primarily to tides, but with winds dominating flow for significant portions of the records. Characteristically, at Station F maximum speeds are about 50 cm sec<sup>-1</sup>, nearly ten times the long term mean.

Data from a station (H, not shown) to the east, adjacent to Long Island, show a weak mean speed (3 cm  $\sec^{-1}$ ) and a direction of flow

toward the southwest. This direction is consistent with shelf flow reflected by Station G but represents a reversal of the inshore counterflow at Station F. During Phase I this Long Island station appears to occupy a position outside of the apex gyre. Station G data may not indicate the position of the southeast limb of the gyre but they do indicate that general long term movement on the shelf is toward the southwest.

# 1.3.3 Phase II Flow Character

The second phase of current measurement was begun in late October and completed in early December 1973. Several stations were added to the original array to increase measurement density in the sections perpendicular to New York and New Jersey and in the Sandy Hook to Rockaway transect.

During Phase II the water had become nearly homogeneous in temperature and salinity. Historical data suggest this transition occurs sometime in October and continues through January. Data from STD casts made while the current meters were operating show a homogeneous water column that was gradually cooling for the entire operation period.

A preliminary examination of records from several levels at selected stations suggests that the effect of stratification on currents is significant. When a layered density structure exists (Phase I), flow in various layers generally has different speeds and directions; during non-stratified conditions, measurements at various levels on a single station generally show flow to be more uniform top to bottom. The effect of stratification may be significant in relation to the competence of the flow to erode or suspend particulate material in Bight waters.

Direction of long term mean flow during Phase II is not significantly different from that observed during Phase I. Speeds are generally higher owing to the higher level of wind energy input to the water column. Figure 1.6 shows a summary of the direction data for each station at the level approximately 30-40% of the way up the water column. The data were subjected to a low pass filter to remove variations with periods less than 2 hours. The polar histograms of figure 1.6 show the frequency distribution of currents partitioned into 10-degree increments, where the length of each line represents the percentage of the total record occupying that direction segment. As in Phase I, data taken from the transect denoted by Station A and K show that flow is generally northward; for the Long Island transect (Stations E, F) flow is predominantly eastward.

Comparison of data from Stations E and F indicates that at stations further offshore, low frequency flow has a greater frequency of crosscontour flow than at the inner stations. The strong directionality of the data from Station A is due to the major depth change associated with the Hudson Shelf Channel where Station A is located.

Although the station at the sewage sludge dumpsite was not reoccupied during Phase II, these data have been included for comparison. Favored flow directions here are to the northeast, in conformance to the counterflow, and to the northwest, perhaps associated with the estuarine bottom flow into the mouth of the Hudson estuary. Estuarine return flow is still indicated at Station D, but it is evident that there is great variability in this confined region.

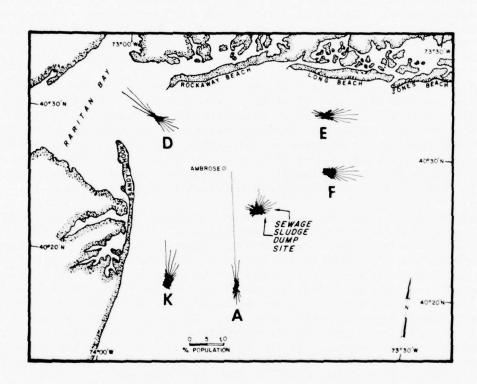


Figure 1.6 Polar histograms of direction frequency for stations of Phase II.

# 1.3.4 Speed of Flow Near Long Island

The direction roses of figure 1.6 show only the tendency for the direction of flow. A speed rose, constructed in a similar manner but using average speed in each direction component shows little directionality in speed. This suggests that figure 1.6 can be used to indicate general magnitude of transport during Phase II.

A more direct manner to exhibit current speed data is to present the current vectors as a sequence in time. Such a presentation of vector time series for Station E is shown in figure 1.7. Here the data

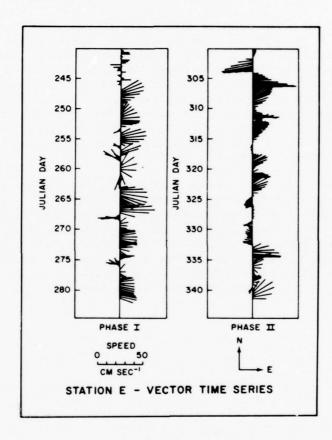


Figure 1.7 Vector time series of data from Station E during Phases I and II.

were subjected to a 40-hour low-pass filter to remove the high frequency (tidal) component and then resampled every 6 hours. The data for both Phase I and II are presented with time increasing toward the bottom of the page. In general, direction is more consistent in Phase II, but both data sets show a dominance of eastward flow. Speed of flow is comparable for each phase with speeds of 20-30 cm sec<sup>-1</sup> characteristic. A speed of 50 cm sec<sup>-1</sup> occurred abruptly during Phase II near day 305 following a reversal in flow. This reversal and high speed were observed in conjunction with passage of a major storm front through the area.

#### 1.4 INFERENCE OF SURFACE FLOW FROM ERTS DATA

In the foregoing discussion of direct current measurements no mention was made of the surface circulation. During the first year of the MESA field effort no near surface current measurements were made. Drifter data suggest some seasonal changes in the surface flow and also indicate the tendency for surface material deposited in the western portion of the Bight apex to remain in that sector and preferentially move toward the New Jersey shore. Historic density data show that flow in the western portion of the apex tends to be dominated by the outflow from the Hudson River, and this flow during spring and summer is generally to the south along the New Jersey coast.

These data have been supported with remotely sensed data from the Earth Resources Technology Satellite (ERTS-1). Figure 1.8 is an example of the output from an ERTS overpass of the New York Bight. The figure shows a portion of the apex approximately 48 km x 48 km. Outflow from the Hudson is clearly visible in the left side of the frame and appears to hug the New Jersey coast. Data from subsequent overflights during spring and summer show much the same picture. Material visible in the center of the picture is residue from waste dumps.



Figure 1.8 ERTS-1 data (0.6-0.7µm) for overflight of New York Bight apex on 16 August 1972.

2. GEOLOGICAL OCEANOGRAPHY; SEDIMENTATION IN THE NEW YORK BIGHT APEX AND APPLICATION TO PROBLEMS OF WASTE DISPOSAL.

Donald Swift, Anthony Cok (Adelphi University), David Drake George Freeland, William Lavelle, Thomas McKinney (Vassar College) Terry Nelsen, Richard Permenter, William Stubblefield

#### 2.1. INTRODUCTION

The New York Bight apex is a major depository for the disposal of waste, including waste acid, dredge spoil, cellar dirt, and sewage sludge. Waste disposal at the sewage sludge dumpsite presently occurs at a rate of approximately 4.5 million  $m^3/yr$ . Of this volume approximately 6% or 270,000 tons is solid material (based on percent solid estimates by Gross, 1972). This dumping (at ever increasing rates) has been taking place for 45 years (Dewling, 1974). The following calculation gives some idea of the maximum volume of solid material dumped during the 45 years: If we use the present-day rate of dumping over the 45-year periods, then complete retention of the sewage sludge solids in a 5 x 5 km area would result in a pure sludge bed about 50 cm (approximately 1.5 ft) thick. This would produce an insignificant depth change at the dumpsite. The obvious conclusion is that, while sewage sludge may be dispersed from the dumpsite area, it is not because the dumpsite depression has filled and is now overflowing.

Because Manhattan, Brooklyn, and Staten Island discharge raw sewage directly to New York Harbor, Hudson River, and East River at the rates of 1840 million liters/day, it is estimated that about 1.7 million m³/yr of sewage sludge (containing 100,000 tons of solids) are deposited in New York Harbor. This material subsequently is dredged (along with natural mud) and disposed of at the dredge spoil (mud) dumpsite on the west side of Hudson Shelf Channel (Environmental Protection Agency (EPA), 1973). In fact, the quantity of total solids dumped at the mud site each year is at least 10 times greater than that dumped at the sewage sludge site. Sediment and chemical analyses by Gross (1972) suggest that, in terms of the ecology of the New York Bight, the dredge spoil (mud) dumpsite may be more significant.

Prior to 1972, 32 municipal waste treatment plants along the New Jersey coast discharged about 157 million liters/day of effluent to the Atlantic via outfall pipelines (most of this was primary treated, disinfected effluent). During November through March of each year the accumulated sewage sludge was pumped through the pipelines to the nearshore New Jersey shelf (EPA, 1973). Federal action stopped this practice in 1972 and the sludge is now barged to the offshore dumpsite.

Gross (1972), using data from 1964-1968, pointed out that total ocean dumping off New York including dredge spoil, sewage sludge, waste acid, and cellar dirt amounted to approximately 4.6 million tons/yr of

solids (see table 2.1). This amount of sediment is roughly equivalent to the natural sediment load of all rivers between Connecticut and Cape Hatteras, North Carolina.

Recent advances in our understanding of ocean currents over continental shelves have shown that landward residual transport near the bottom commonly occurs within 10 to 50 km of the shore (Bumpus, 1965; Gross et al., 1969). Onshore bottom water flow is especially evident off major coastal estuaries. This type of circulation tends to trap both coarse and fine-grained sediments in the estuaries, coastal wetlands, and inner shelf areas (Meade, 1972).

This potential feedback of some of the wastes dumped offshore and the demonstrated environmental deterioration in the immediate dumpsite areas are among the important reasons for a thorough assessment of man's effects on New York Bight ecology.

Table 2.1. Waste Disposal New York Bight Apex Dumpsites

	Volume $(10^6 \text{ m}^3/\text{yr})$	Solids (10 <sup>6</sup> tons/yr)
Sewage Sludge	3.8 to 4.5	0.23 to 0.27*
Dredge Spoils	5.6 to 5.8	3.5t
Cellar Dirt	0.54	0.59++
Acid Wastes	2.3 to 3.5	0.23 to 0.35**
Average totals:	13.3	4.6

<sup>\*</sup> Average solid content of 6% (Gross, 1972).

Recently public concern has been aroused relative to the deleterious effects of waste disposal in the Bight apex, and in particular, relative to the effects of sewage sludge disposal on the safety of the beaches of the Long Island South Shore.

This report summarizes relevant data acquired by the geological oceanography program of the MESA New York Bight Project. The program has been concerned with (1) the physical nature of the substrate of the Bight apex; its topography, surficial sediment distribution, and distribution of sediment with depth, and (2) the dynamic system of sediment erosion, transport, and deposition within the Bight apex. Data collection and analysis for this program are far from complete. Even when complete the data must be carefully integrated with data from the biological, chemical, and physical oceanography programs, before they can be

<sup>†</sup> Based on bulk densities of 1.3 tons/m³ (Gross, 1972; EPA, 1973).

<sup>††</sup> From Gross (1972).

<sup>\*\*</sup> From Gross (1972) and EPA (1973).

applied to problems of ocean dumping. However, because of the urgency of the public problem, available data are set forth in this report.

# 2.2 PHYSICAL NATURE OF THE SEA FLOOR

# 2.2.1 Topography, Shallow Structure, and Geologic History

The main topography elements of the floor of the Bight apex (fig. 2.1) are the Hudson Shelf Valley, the Christiaensen Basin (Veatch and Smith, 1939), Cholera Bank, and the New Jersey Platform. The origin of these features must be sought in the geologic history of the Bight apex during the past 15,000 years.

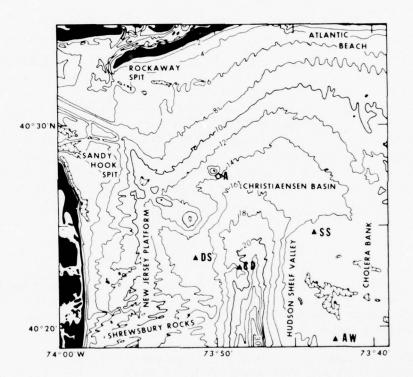


Figure 2.1. Bathymetry of the New York Bight apex from ESSA bathymetric map 0808N55, and names used in the text. "A" is Ambrose Light; "SS", sewage sludge dumpsite; "DS", dredge spoil dump site; "CD", cellar dirt dumpsite; "AW", acid waste dumpsite.

Approximately 15,000 years ago, during the period of the last major ice advance of the Pleistocene Ice Age, so much sea water was locked up in the continental ice sheets that sea level was lowered more than 125 m (Milliman and Emery, 1968). The New York--New Jersey shoreline withdrew to the edge of the continental shelf, over 200 km to the east. The Hudson Shelf Valley was incised at this time by the Hudson River flowing east over the extended coastal plain to the distant shoreline.

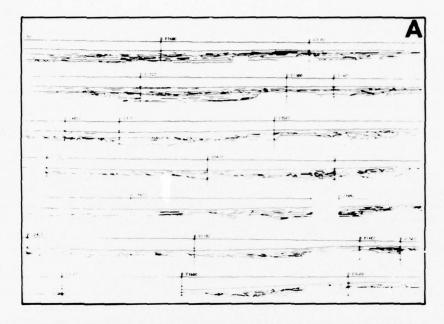
As the ice sheets melted, the shoreline advanced to its present position. Low coasts of sand and clay, such as the coast of the New York Bight, tend to have a characteristic submarine profile, maintained by wave and wind-driven currents. The profile consists of a relatively steep shoreface (gradient 1:10 to 1:200) which descends to a depth of 15 to 20 m, 2 to 5 km from shore, and which is followed in a seaward direction by a more gently sloping (gradient greater than 1:200) inner shelf floor. During the post-glacial rise in sea level, this profile retreated landwards by a process of erosional shoreface retreat due to scour of the shoreface by wind and wave driven currents (Swift et al., 1972). The sediment eroded from the retreating shoreface was deposited as a blanket of relatively clean sand over the shelf floor. As the Long Island shoreline retreated, sand moving southward in the breaker-driven littoral current tended to pile up on the north side of the ancestral Hudson Estuary mouth in the form of tide-molded shoals. The landward movement of the shoal zone as the estuary mouth retreated has resulted in a raised north rim of the shelf valley (Cholera Bank). South moving littoral drift from the retreating shoreline and sediment swept south after the passage of the shoreline by storm currents have resulted in appreciable filling in the east side of the shelf valley and in the Christiaensen Basin (figs. 2.2 and 2.3).

Approximately 4,000 to 7,000 years ago, the rate of sea level rise decreased. Since this decrease, the coastline of the Bight apex has assumed its present form. Within this relatively recent period Sandy Hook spit has grown into the harbor mouth, and within the historical period, Rockaway spit has done so (Shepard and Wanless, 1972, p. 73-74; Taney, 1961).

Comparison of a recent NOAA bathymetry survey (August, 1973, unpublished) with the 1936 bathymetry (fig. 2.1) indicates a change of less than 2 m throughout the area, except in the vicinity of the dredge spoil dumpsite, where shoaling up to 12 m has occurred.

# 2.2.2 Distribution and Micro-topography of Surficial Sediments

Figure 2.4 presents the net of stations at which samples of surficial sediments were collected by means of a Shipek grab sampler. During this sampling operation, accomplished between June 1972 and July 1974, navigation was provided by Loran A and radar in some sectors, and by Raydist in others.



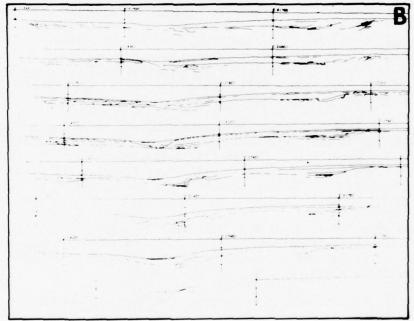


Figure 2.2. Seismic profiles of the Bight apex, collected with a 3.5 KHz profiling system. Scale indicators are 2,000 m apart. Each tick is 20 m sec. Total depth of penetration is about 50 m.

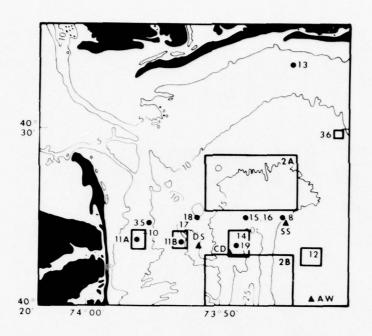


Figure 2.3. Index map for illustrations in this report.

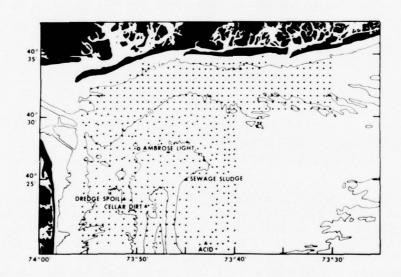


Figure 2.4. Net of Shipek grab samples in the Bight apex. Sample interval is approximately 0.9 km.

Figure 2.5 presents the distribution of surficial sediment on the floor of the Bight apex. The map is based on macroscopic comparison of samples with standards, but does not significantly differ from a grain size map based on precision settling techniques (in preparation).

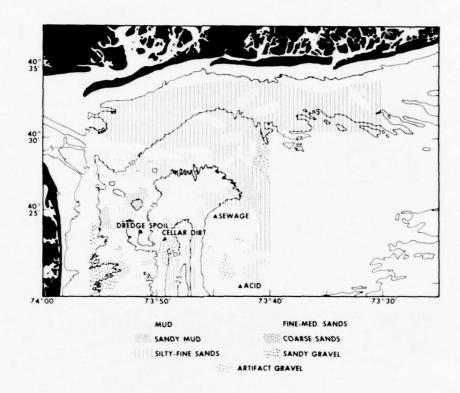


Figure 2.5. Distribution of surficial sediment types in the Bight apex, based on visual examination of samples.

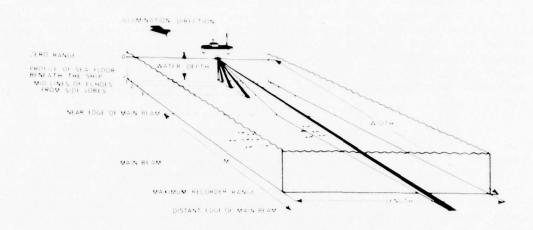
Distribution of surficial sediments in the Bight apex is quite systematic. Grain size is primarily a function of depth. Mud occurs in low areas, namely in the axis of the shelf valley, in the Christiaensen Basin, and in the extension of the Hudson Shelf Valley toward the mouth of outer New York Harbor. Small patches of mud also occur in shallower water, near the Long Island shore. The New Jersey Platform and Cholera Bank are floored with sand. The coarsest sand and sandy gravel occur in the shallower northern Cholera Bank and Shrewsbury Rock areas. However, artifact gravel (brick, cement, plaster, stone, wood, metal) occurs on sea floor highs of artificial origin, and on Cholera Bank.

Considerable additional information concerning the distribution of surficial sediments is available from sidescan sonar records. Sidescan sonar is a profiling system that sends overlapping beams of sound obliquely outwards from a transducer towed by the survey ship to the sea floor on either side, and that records sound reflected back to the transducer. The result is analogous to an oblique aerial photograph of the sea floor on either side of the ship (fig. 2.6). Coarse sediment is a better acoustic reflector than fine sediment and shows up on the sidescan record as a dark zone.

The Bight apex has been surveyed by means of sidescan sonar, according to a regular survey pattern (fig. 2.7). As a result, it has been possible to map microtopography, or bottom roughness provinces. Such bottom roughness is induced by interaction between the loose sediment of the sea floor and the overlying flow. One of the simplest and most widespread forms of bottom roughness so induced is ripples, a response of the sandy sea floor to the reversing surge generated by the passage of surface waves. Ripples are rarely more than a few centimeters high and a few tens of centimeters apart (fig. 2.8) and are generally too small to be detected by the sidescan sonar. However, larger bedforms induced by fluid flow occur. Six bedform patterns were recorded.

On the shoreward end of Cholera Bank, and again along the New Jersey shore, sand ribbons were observed (figs. 2.9-2.11). These are straight to sinuous, irregular, or branching strips of medium sand overlying a coarser sand or sandy gravel of subequal width. The sand ribbons are responses to peak flow events when the bottom boundary layer of the flow field is organized into alternating zones of convergent and divergent flow. Sand is swept into ribbons elongated in the flow direction.

More narrowly spaced and more regular streaks of dark on sidescan records (5 to 50 m wide) are interpreted as sand waves, or large-scale current-induced ripples (figs. 2.9, 2.12, 2.13). The pattern is locally asymmetrical in that the light bands (finer sand of the sand wave crests) have sharp western boundaries against the alternating dark bands on the western sides but have gradiational boundaries on the eastern sides. This asymmetry and the fact that some of the features occur very near the Long Island shore in a shore-normal position, suggest that they are sand waves (current-transverse bedforms) rather than sand ribbons (current parallel bedforms). The asymmetry is most commonly weak to absent, however, and the features, unlike true sand waves, rarely have appreciable relief. Hence, it is believed that they were formed as sand waves during peak flow events associated with winter storms, and by the period of observation had been degraded by bottom wave surge and by the activity of burrowing organisms. The sand-wave-like features occur on the north margin of the Christiaensen Basin, and on the seaward portion of Cholera Bank. Their probability of formation is increased over that of sand ribbons where the substrate consists of deep medium-to-fine grained sand, rather than a thin layer of medium sand over a coarser substrate.



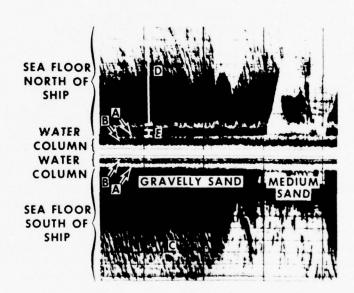


Figure 2.6. Above: Diagrammatic representation of sidescan sonar system. (The transducer used for the work described by this report was towed behind the ship, rather than fixed beneath it.) A similar beam of sound extends from the far side of the transducer. [From Belderson et al., 1972.] Below: Anatomy of a sidescan record. A. Bottom of sea floor. B. Turbulence in water column due to ship's wake. C. Zig-zag pattern due to refraction of sound in density-stratified water. D. Portion of record due to reflection of side lobe (see above). E. Portion of record due to reflection of main beam.

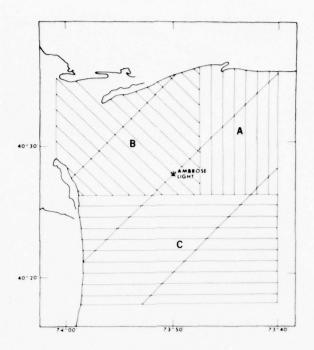


Figure 2.7. Pattern of tracklines for electronic survey of New York Bight apex. Every fifth line is shown. Sidescan sonar records were obtained from every second line. Selected transects are reoccupied on a quarterly basis.



Figure 2.8. Sea floor photograph of fine rippled sand from the Bight apex. See figure 2.3 for location.

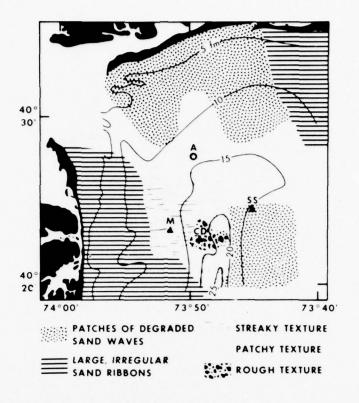


Figure 2.9. Distribution of bottom roughness patterns in the New York Bight apex.

Two other patterns are associated with fine-grained bottoms (fine silty sand to mud). A patchy texture (figs. 2.9, 2.14, 2.15, 2.16) appears to be the result of the deposition of a thin discontinuous blanket of mud or silt (light pattern) over a slightly coarser substrate (dark pattern). The patches are up to 20 m in diameter, and tend to be elongated in the predominant flow direction. The few cores collected to date suggest that the patchy layers are a few cm or less thick, and that in areas whose surface is characterized by this pattern the underlying sediment consists of stacked sequences of sand and mud layers. On the margin of the cellar dirt dumpsite, however, the light pattern appears to fill lows on a surface of dumped rubble.

On the New Jersey Platform a more streaky pattern is seen on the surface of the pocket of mud that fills the extension of the Hudson Shelf Valley towards the New York Harbor mouth, perhaps because of the more intense semidiurnal tidal flow experienced by the sea floor in this area (figs. 2.9, 2.11, 2.17).

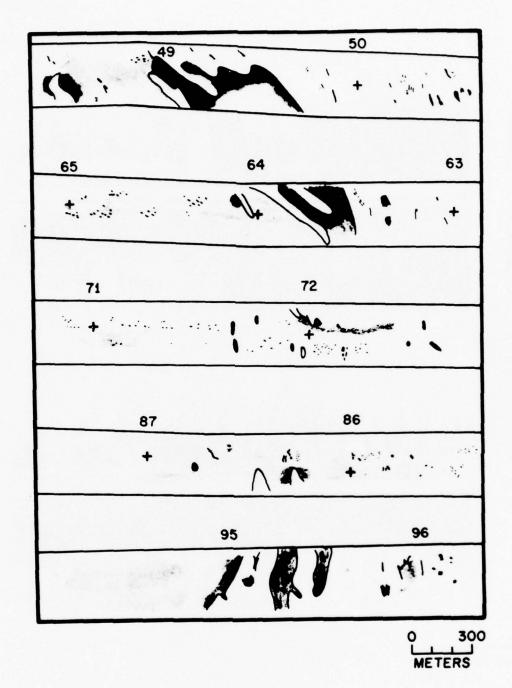


Figure 2.10. Reproduction of sidescan sonar records showing large, irregular sand ribbon pattern. Recorded strips are 366 m wide. See figure 2.3 for location.

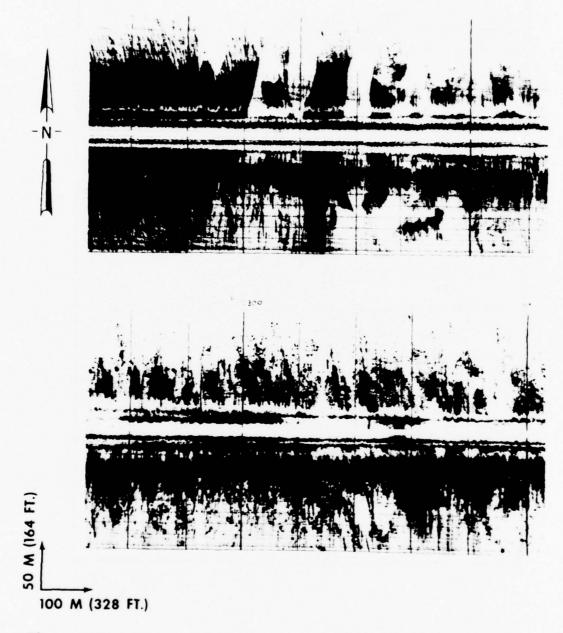


Figure 2.11. Above: Sidescan sonar record of large, irregular sand ribbons. Below: Sidescan sonar record of small scale ribbon-like features (streaky texture). Blocky objects with dark sides towards sound source are boulders protruding through sediment cover.

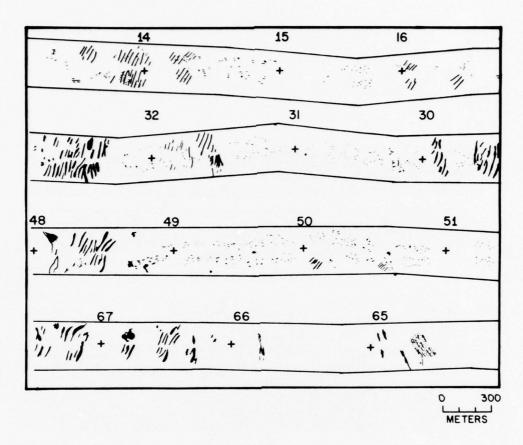


Figure 2.12. Reproduction of sidescan sonar records showing sand-wave-like features on Cholera Bank. Recorded strips are 366 m wide. See figure 2.3 for location.

Finally a characteristic dark, rubbly texture is seen in the vicinity of the cellar dirt dumpsite (figs. 2.9, 2.14, 2.18, 2.19). Individual blocks of stone or concrete may be occasionally discerned.

Figure 2.20 is a running average of the directions of bedform trends, constructed by placing a 4 n mi grid over a sidescan mosaic drawn with angular correction from the original records. Mean trends within grid squares were estimated. The dashed line encircles the zone where the bedforms are believed to be dominantly current-parallel, rather than current-transverse. Except in zones of patchy texture (fig. 2.9), grain size distribution within the Bight apex appears stable with time (fig. 2.21).

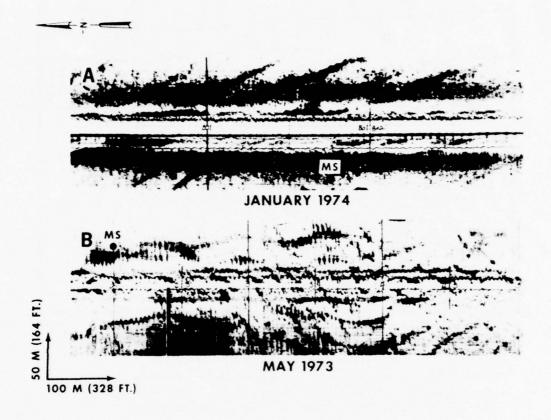


Figure 2.13. Two sidescan sonar records taken in the same small area off the Long Island south shore. Apparent degraded sand waves visible in January as light (medium sand) streaks between dark (coarse gravelly sand) streaks have been largely obliterated by a poorly defined sinuous pattern by May 1974. Dots labelled MS are the locations of medium sand samples. Positioning error on the sample is  $^{\pm}$  15 m. See figure 2.3 for location.

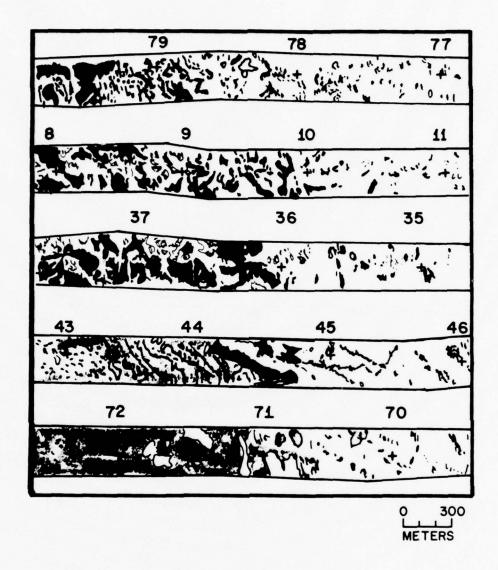
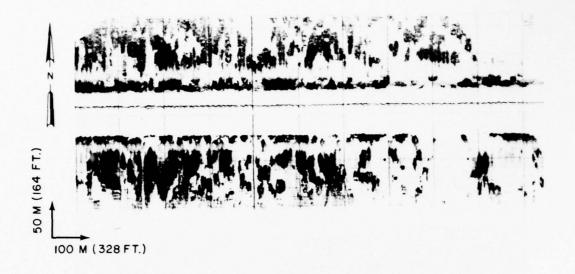


Figure 2.14. Reproduction of sidescan sonar records showing smooth bottom in northeast, grading into patchy texture in center, and into rubbly texture in southwest corner (cellar dirt dumpsite). Recorded strips are 366 m wide. See figure 2.3 for location.



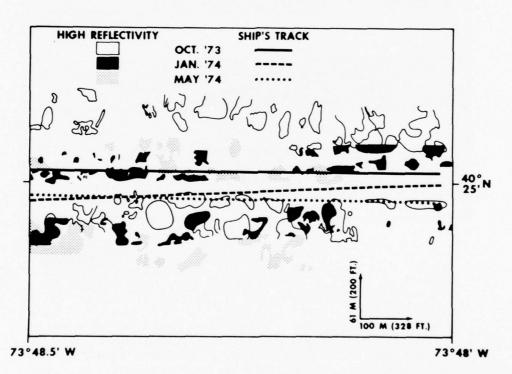


Figure 2.15. Above: Patchy texture from near cellar dirt dumpsite.

Below: Schematic of three sidescan sonar records of the same area on three successive occasions, illustrating patchy texture, and the temporal variation of the pattern. Probable error of Raydist positioning system: ± 15 m.

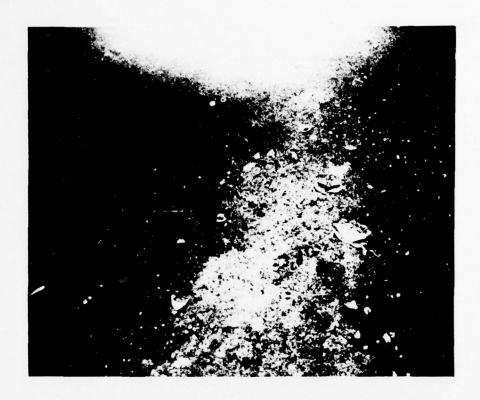


Figure 2.16. Sea floor photo of patchy texture. Fine sand on right; muddy, silty, very fine sand on left.

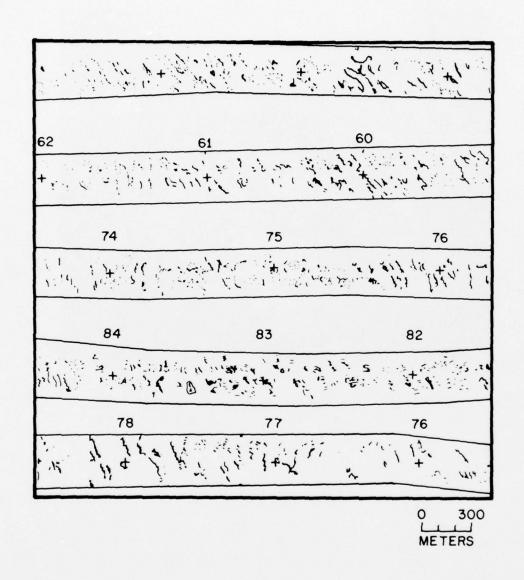


Figure 2.17. Reproduction of sidescan sonar records showing streaky texture. Recorded strips are 366 m wide. See figure 2.3 for location.



Figure 2.18. Sidescan sonar record showing rubbly texture. Vertical streaking is an artifact due to rolling of transducer in heavy sea. See figure 2.3 for location.



Figure 2.19. Sea floor photo from zone of rubbly texture.

See figure 2.3 for location.

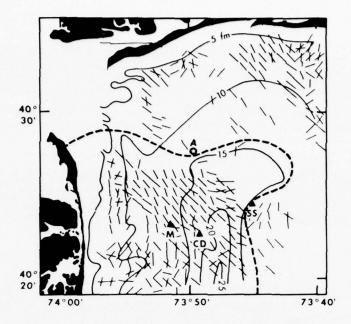


Figure 2.20. Trends of linear bedforms as revealed by sidescan sonar records. Bedforms are inferred to be primarily current-parallel within the dashed area, current-transverse elsewhere.

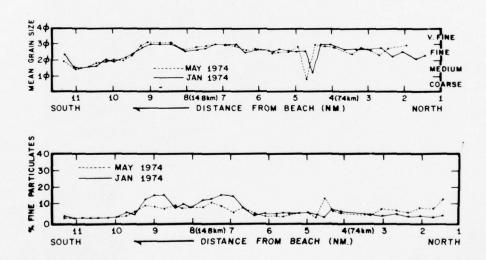


Figure 2.21. Above: Mean grain diameters from two surveys of north-south transect from sewage sludge dumpsite to Long Island shore. Below: Percent fine particulate matter for same surveys.

#### 2.3 SEDIMENT TRANSPORT IN THE BIGHT APEX

## 2.3.1 Modes of Sediment Transport

Sedimentary processes in the New York Bight apex fall into two basic categories. Coarse sediment (mainly sand) is entrained and transported only by intense flows. Sand moves nearly continuously in the intense, coast-parallel, wave-generated current in the zone of breaking waves near the beach. It is also moved by intense tidal flows at the mouth of New York Harbor. On the floor of the Bight apex, however, flows sufficiently intense to entrain sand (approximately 30 to 40 cm sec<sup>-1</sup> at 100 cm above the bottom) occur only intermittently, mainly during winter storms, when strong winds can generate strong surface flows of water, and when the water column is unstratified, so that the downward turbulent transfer of momentum can entrain layers of water as far downward as the sea floor. During such periods of strong winds, bottom wave surge, whose peak velocities may be several times as intense as mean flow velocity, increases the discharge of sand, by an unknown but probably great amount, by suspending sand grains in the mean flow.

Suspended fine sediment (mud) is also entrained by the action of bottom wave surge during periods of strong winds, and is transported by peak flow events. However, the minute clay mineral particles when resuspended from the ocean floor tend to form low density, high surface-area agglomerates. These composite particles are loosely bound, in part by electrostatic charges, but probably mainly by the binding action of such organic materials as algal mucus and bacterial slime. Such particles may consist largely of degraded organic matter and diatom frustules, with only minor quantities of embedded clay mineral grains. Pelletization by mud-feeding invertebrates results in denser aggregates. During periods of plankton blooms, the bulk of the suspended material may be living, consisting of diatoms, foraminifera, algae, and other plankton. Settling velocities of these composite particles are low and they may remain in suspension for days or weeks after entrainment, during which periods they may be transported for distances of many tens of kilometers by the slow, tide-modulated fair-weather circulation pattern. Thus the pattern of mud transport and also the coastal mud budget is markedly different than the transport pattern and budget of sand.

### 2.3.2 Suspended Sediment Transport: General Concepts

Detailed studies of fine sediment transport in other coastal areas have shown that the coastal mud budget is not simply a matter of the seaward movement of river derived particles. All of the clay mineral particles that comprise the mud deposits of the New York Bight apex must have been transported down the Hudson or Connecticut Rivers at some time, but in many cases, this must have happened in the distant geologic past. Suspended fine sediment is presently being introduced into the Bight apex from the mouth of the Hudson River, but the volume of throughput is

probably small relative to the traffic on the numerous feedback loops of the transport system (fig. 2.22).

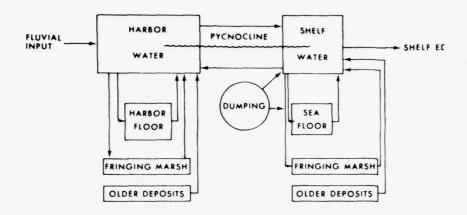


Figure 2.22. Schematic representation of suspended fine sediment transport system of New York Bight apex. Pycnocline is zone of rapid vertical change in water density between lighter (warmer, fresher) upper water and denser (cooler, saltier) lower water.

The basic feedback loop is driven by the two-layered (estuarine) circulation, whereby the less saline upper water, flowing seaward over more saline bottom water, entrains bottom water. More bottom water must therefore slowly flow into the river mouth to replace the water thus consumed. Suspended sediment agglomerates may enter the zone of maximum thermohaline stratification either from the up-river side, with the turbid, brackish surface water, or from the sea, with the turbid, saline bottom water. In either case, the agglomerates tend to become caught in a closed loop, whereby they rain out of the seaward-flowing upper water, into the landward-flowing bottom water, only to be re-entrained again in the surface water. Other feedback loops are formed by exchange of mud between the water column on one hand, and sea floor and coastal (lagoonal, salt marsh) mud deposits on the other. The net result of this multicycle, fine-sediment transport system is to maintain relatively high concentrations of suspended fine sediment in the Hudson River estuary and in

the coastal waters of the Bight apex. These concentrations are markedly higher than those in the river landward of the salt water intrusion, or on the shelf seaward of the zone of two-layer (thermohaline) circulation.

This picture of coastal suspended sediment circulation has these significant implications for the problems of pollution in the New York Bight apex. First, coastal waters adjacent to such estuarine systems tend to be turbid and brown whether there is human activity in the area or not. Bight apex waters may conceivably have been as brown when visited by Henry Hudson as they are now. Second, the transport system is very nearly an "ergodic" one. In probabilistic terminology this means that it doesn't matter greatly where in the system the fine waste materials are dumped; they will cycle through the system until they reach naturally determined reservoirs of long-term storage, or sinks of permanent storage (estuary floor or shelf floor mud deposits; lagoon floor deposits; fringing marsh deposits). Third, the distinction between natural fine sediment and dumped sediment tends to become blurred subsequent to the introduction of the waste, as it cycles through the feedback loops. Unstable organic compounds break down into more stable ones, which are similar to the stable residues derived from the decay of planktonic life forms, with which they mingle. Inorganic particles are sorted for size, and are mixed with organic particles of similar size. In the more distant parts of the system, increasingly obscure chemical and biologic "signatures" must be sought in order to identify the degree of contamination, including those which are signatures of materials that are significant in terms of environmental quality such as toxic trace metals and pathogenic micro-organisms.

The preceeding analysis suggests that dredge spoil or sewage sludge dumped in the New York Bight apex may ultimately be deposited, albeit in highly dilute form and with altered composition, in areas as far apart as the upper meter of marsh muds in the Hackensack Marshes, or in the upper meter of lagoon floor muds in Great South Bay. Some degree of quantification of the coastal mud budget of the Bight apex may be a final product of the MESA project. The data collected to date, while extensive, do not begin to permit quantification. The most salient elements of the data are presented below. For details, the reader is referred to Drake (1974).

### 2.3.3 Suspended Sediment Transport in the Bight Apex

Figure 2.23 presents the average suspended particulate matter concentration in the Bight apex during the fall of 1973, as determined by Niskin bottle sampling and filtration (see Drake, 1974, for methods). The pattern clearly reflects the mean circulation pattern as deduced by the physical oceanography program (see sec. 1).

Surface water flowing out of the Hudson Estuary turns to the south and forms an easily distinguishable turbid current flowing along the New

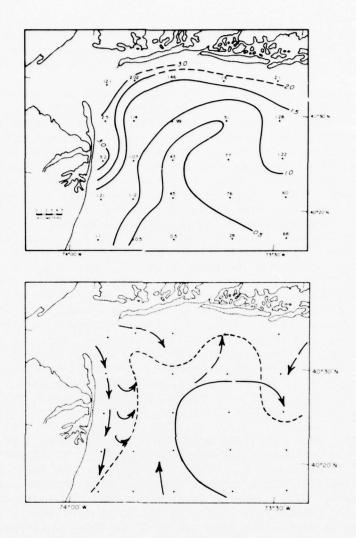


Figure 2.23. Above: Total suspended load in mg/liter, at 10 meters depth, November 1973. Below: Generalized circulation pattern of the New York Bight apex as inferred from the distribution of suspended sediments during fall, 1973. Dashed line is mean position of boundary between more turbid coastal water and less turbid offshore water. Turbid, brackish surface effluent of harbor flows down New Jersey shore. Clockwise gyre is driven by southwesterly drift of offshore shelf water and, on bottom, by the influx of saline water into the harbor. Solid arrows are currents that appear to be persistent.

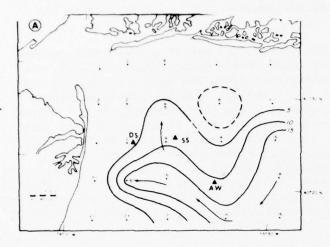
Jersey coast. If a suspended particulate matter concentration of > 1.0  $\,\mathrm{mg/l}$  is used to arbitrarily mark the seaward width of this current the average width is 4 to 6 km.

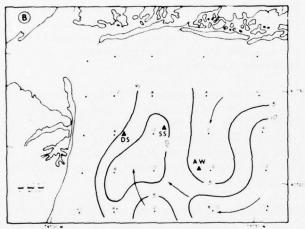
A sharp decline in suspended particulate matter and a marked compositional change are observed to the east of the Hudson Plume; in fact, the lowest suspended particulate concentrations in the area are observed over the north-south trending Hudson Shelf Valley. Samples above the valley contain the abundant diatom population which is characteristic of central shelf water, and chemical analysis indicates that these samples are rich in high protein phytoplankton. In addition, water in the channel is often colder than water at the same depth elsewhere in the area. These data demonstrate a northward (upslope) flow of water from offshore along the Hudson Shelf Valley that is in part channelized by the valley. When meteorological conditions are appropriate (strong westerly or northwesterly winds) this current reaches the sea surface and may extend to within at least 5 km of Long Island.

Figure 2.23 shows that the Hudson Shelf Valley current turns to the northeast as it approaches the Long Island shore, and that it becomes coupled with, or entrained by a turbid plume extending south along the eastern margin of Cholera Bank. The plume is easily recognizable in ERTS-1 images, and resembles an enormous rip current.

Iron oxide particles generated at the acid waste dumpsite provide an excellent tracer of the circulation pattern (fig. 2.24). The particles range in size from colloidal, yellow filter coatings to sand sizes (> 62 microns) as orange and red aggregates having the appearance of floccules. X-ray defractograms show no evidence of crystal structure, and there is reason to believe that the grains are a mixture of hydrated iron oxide and iron stained plankton debris.

Characteristic vertical distributions of suspended sediment are presented in figures 2.25, 2.26, and 2.27. Figures 2.26 and 2.27 present representative examples of the vertical distribution of suspended particulate material through the fall of 1973. The vertical profiles reflect the seasonal breakdown of temperature and salinity stratification. In early September, both temperature and salinity contribute to a stable stratification with a distinct, steep, gradient pycnocline between 15 and 25 m (fig. 2.25). The pycnocline during this period tends to shoal toward shore, suggesting a slow upwelling of deeper shelf water. In nearshore areas (within 5 to 7 km of the coastline) flow of relatively low salinity water from the Hudson estuary and Long Island inlets produces a 5 to 10 m thick, low density, high turbidity surface layer (fig. 2.26).





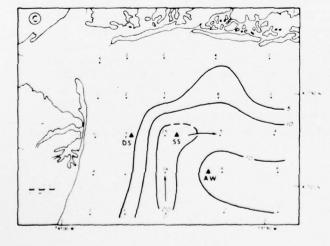


Figure 2.24. Distribution of iron oxide particles in late November 1973, in terms of number of grains (x 10³) per liter of water. At the surface the distribution reflects (A) the surface gyre, but with increasing depth it reflects (B) the influence of the shelf valley, and (C) the acceleration of flow due to the saline bottom water indraught of the harbor.

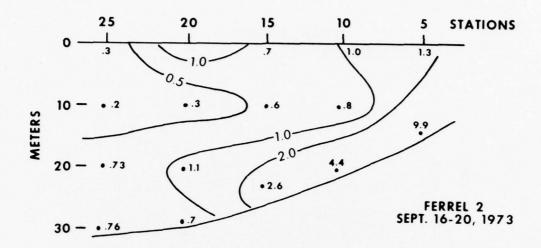


Figure 2.25. Vertical distribution of total suspended load in mg/liter. The cross section extends south from Long Island. The distribution, showing high values near the surface and very high values near the sea floor, is typical of shelf areas. The near bottom turbid layer has been termed the "nepheloid layer" and it is expected that this layer will contain and transport much of the New York Bight contaminants.

Suspended particulate matter is stratified in response to this density layering. Three layers typically present nearshore (fig. 2.25) are a turbid surface layer, a relatively clear mid-water zone located within or below the shallow pycnocline, and a turbid layer near the sea floor, resulting from wave resuspension of bottom materials. Further seaward the surface turbid layer becomes less distinct as the shallow pycnocline breaks down. The small maxima at the surface in the offshore parts of the area can be attributed to plankton production. However, the significant near-bottom increase in suspended particulate matter appears to be a permanent feature of all portions of the Bight apex. The near bottom ash content of this material ranges between 40 and 84 percent of the total weight, and most of this material is probably resuspended inorganic clay and silt.

By late November of 1973, surface water cooling, convective mixing, and the effects of increasingly frequent storms had produced a nearly homogeneous surface layer ranging from 10 to 30 m in thickness (fig. 2.27). The vertical distribution of suspended particulate matter reflected the weak or no stratification, with essentially uniform concentrations from the surface to the top of the bottom turbid layer at many stations. During the period of stratification, throughout the period of study, the

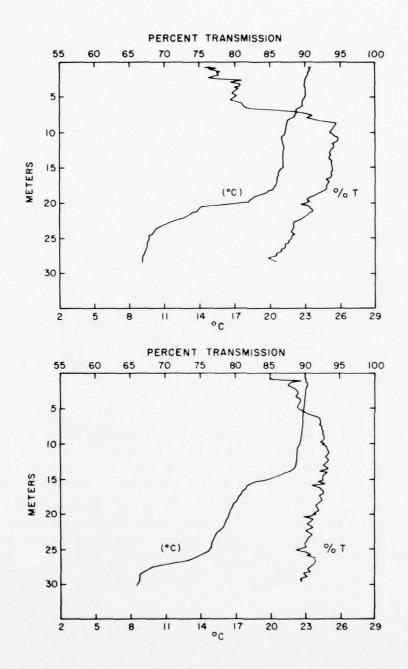


Figure 2.26. Vertical profiles of light beam transmission and temperature at stations 8 (above) and 18 during August 27-30, 1973. Data from Hazelworth et al. (1974).

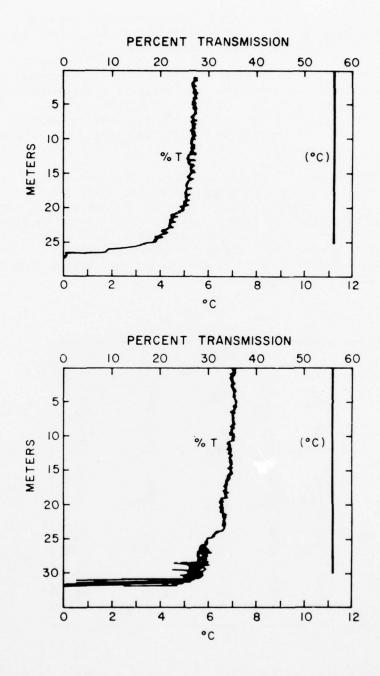


Figure 2.27. Vertical profiles of light beam transmission and temperature at stations 8 (above) and 18 during November 26-29, 1973.

highest concentrations of suspended particulate material were observed in the wave-surge generated bottom turbid layer, and it is in this layer that the bulk of the suspended material is transported.

Grain size analysis of suspended mineral grains sheds further light on the nature of particle resuspension and transport. Inorganic mineral grains typically make up 25 to 50 percent by volume of the total suspended matter close to shore and near the bottom. In the seaward portions of the Bight apex and within clear water from the central shelf, the mineral content is below 5 to 10 percent.

During the September 1973 cruise, surface suspended sediment was predominantly fine silt and clay with 1 percent of the particles larger than 16 microns (fig. 2.28). The material counted as > 16 microns consisted, in nearly all cases, of aggregates of many smaller grains bound together by amorphous organic matter. The coarsest particles were found nearest to shore. During the November 1973 cruise, surface particles were significantly coarser than in September (fig. 2.29), and near bottom samples were the coarsest of all samples studied.

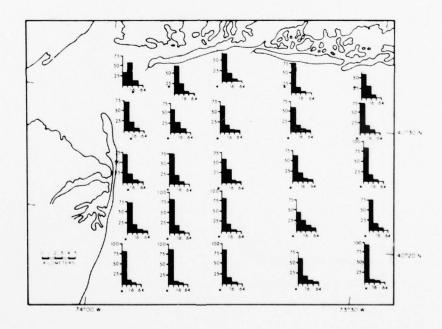
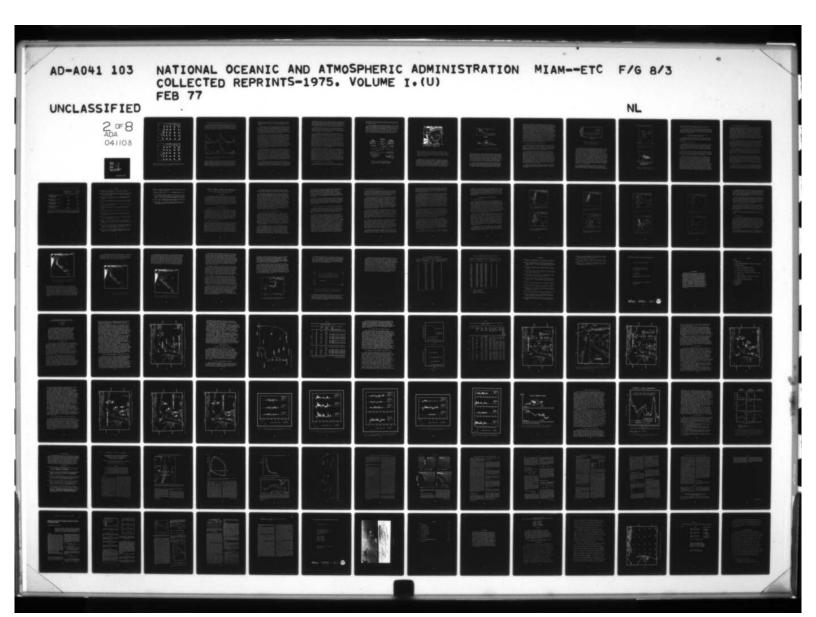
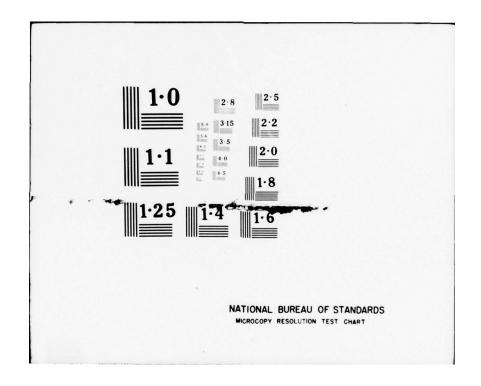
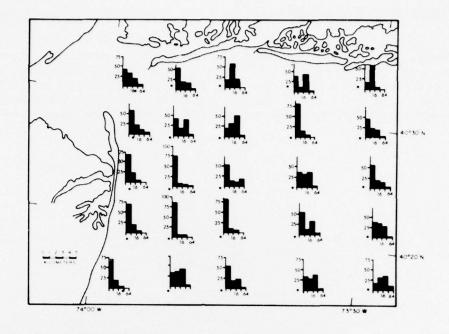


Figure 2.28. Size distributions of mineral grains suspended in surface waters during September 16-19, 1973. The arguments of the histograms are volume percent (vertical axis) and mean diameter in microns (horizontal axis).







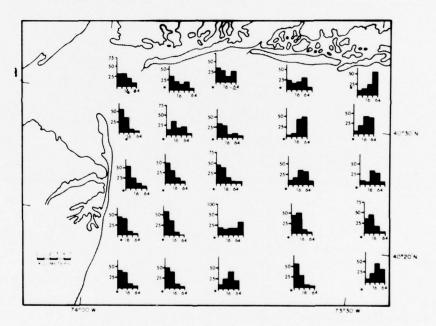


Figure 2.29. Size distributions of mineral grains suspended in surface waters (above) and 2 m off the bottom (below) during November 26-29, 1973. Axes of histograms as in Fig. 2.28.

## 2.3.4 Suspended Sediment Transport and the Deposition of Bottom Muds

The pattern of bottom mud deposits as represented by figure 2.5 becomes explicable when the controls of fine sediment deposition are considered. As noted by McCave (1972) the balance between deposition and resuspension of bottom muds, resulting in net aggradation or erosion of the bottom, is a function of the concentration of suspended sediment and the intensity of flow near the bottom (fig. 2.30). Both factors tend to

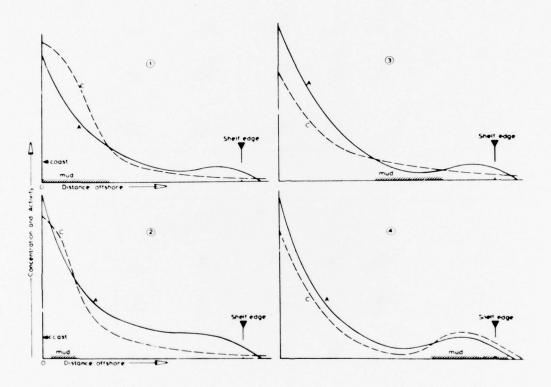


Figure 2.30. Deposition of shelf mud as a function of the hydraulic "activity" of the mud (A) and the concentration of suspended sediment (C) (from McCave, 1972).

increase exponentially towards shore current intensity increases because of the increasing release of wave surge energy as the sea floor shoals. Suspended sediment concentration increases because of the two-layer estuarine circulation mechanism which tends to concentrate suspended sediment near the shore (see sec. 2.3.2). Very near the beach a further circulation mechanism transpires, whereby the landward asymmetry of

bottom wave surge causes bottom water to move towards the beach, while surface rip currents flow seaward to relieve the pressure head. This hydraulic system also results in a closed loop of suspended particulate transport.

Muds accumulate on the floor of the Bight apex in deeper areas such as the Hudson Shelf Valley, and the Christiaensen Basin, where the energy of bottom wave surge available for the resuspension of fine sediment is less intense. However, thin patches of mud also tend to accumulate on the shoreface, in less than 20 m of water. Here wave surge is intense, but the suspended sediment concentration is exceedingly high, because of the two-layer, wave-driven circulation. This circulation tends to recycle suspended particulate matter in a zone near the beach.

The initiation of a mud patch in this wave-agitated zone probably requires a period of calm sea, when mud can be deposited on the turn of the tide, in the slight depressions associated with degraded sand waves or sand ribbons. Such a mud film will rapidly compact under its own weight, expel pore water, and will undergo a marked increase in cohesiveness, perhaps sufficient to insure its survival through the next period of intense wave activity. Once initiated, the growth of a mud patch tends to be self sustaining. With the initiation of such a mud layer, the hydraulic microclimate in the lowest layer of water changes. The flat, microscopic clay particles do not protrude through the laminar sublayer of the bottom boundary layer of wave-induced flow, and additional clay particles that settle into this laminar sub-layer will tend to adhere to the bottom rather than be resuspended. The cloud of turbid water immediately over the mud patch tends to extend beyond the patch, and causes its edges to grow.

Clay patches on bottoms suitable for their development do not migrate, but do wax and wane in areal extent in response to periods of mild and intense hydraulic activity. The scale of change is such that sidescan profiles reoccupied on a quarterly basis in zones of patchy bottom show almost no continuity of pattern (fig. 2.15). In the nearshore zone, such mud patches tend to be small in extent (usually less than 10 m in diameter and less than 15 cm thick). Systematic SCUBA dives performed during early July 1974, seaward of the surf off Long Beach, Long Island, suggest that such small mud patches are very abundant in terms of absolute numbers, although still occupying much less than 10 percent of the bottom. The sample pattern of figure 2.5 is too coarse to clearly resolve the distribution of mud patches which are both more abundant and smaller than shown in figure 2.5.

A parenthetic note concerning the color of shelf floor muds is in order here. Shelf floor muds are invariably enriched in organic matter, as a consequence of hydraulic sorting processes, which tend to group finely divided clay particles with comminuted organic matter. Clays also characteristically contain about 5 percent by weight of iron oxide. These two

components are responsible for the color of shelf mud. Characteristically a shelf mud is veneered by a thin, oxidized "brown layer" pigmented by  ${\rm Fe}_2{\rm O}_3$ . Depletion of oxygen by decaying organic matter several millimeters below the water-sediment interface results in a black color which is due to carbonaceous organic material. This color pattern is characteristic of muds on totally unpopulated coasts as well as highly populated ones.

Mud patches on the Long Island coast may or may not be highly contaminated with sewage sludge, but gross color and texture are no guides. Terms such as "sludge", "black greasy stuff", "like black mayonnaise" do not indicate whether the organic admixture consists of degraded planktonic material of natural origin, or of human waste.

It is possible to make some order-of-magnitude calculations with respect to the vexing problem alluded to earlier, namely the relative roles of natural materials and introduced materials in the fine sediment dispersal system of the Bight apex (Drake, 1974), based on the data collected in the fall of 1973. The calculations attempt to determine the amount of fine sediment entrained during the storm of November 26 to 27. They assume that the concentrations of suspended material observed from the beginning of September through November 9 were characteristic of the fair weather regime. It is further assumed that contribution of "new" material from land and plankton production were constants. This is unlikely. However, microscope analysis of filters indicates that the plankton standing crops in September-October were higher than in November; hence the "excess" turbidity measured in late November is underestimated rather than overestimated. The late November storm involved high velocity winds (20 to 30 knots) but no coastal precipitation; hence a constant discharge from the Hudson estuary may be assumed.

Using all data for the fall surveys (Drake, 1974), the mean difference in suspended particulate matter for the apex water volume between the first four surveys and the survey of November 26 to 30 is approximately 0.5 mg/l. This omits the poorly known concentrations in the near bottom zone (0 to 5 m above the bottom), and therefore is a conservative estimate. The volume of the Bight apex included within our station grid is roughly 20 km³, which yields a suspended solids "excess" of the poststorm period over the pre-storm period of about 10,000 metric tons, assuming a particle density of 2.0 g/cm³. This figure may be compared with the estimated average daily input of sewage solids of 750 metric tons. In other words, the late November period of heightened hydraulic activity increased the suspended particulate concentration from an apparent steady state condition to a more intense concentration level equivalent to the addition of 12 days worth of barge dumping.

# 2.3.5 Coarse Sediment Transport: General Concepts

In the previous section it was pointed out that the fine sediment transport pattern of the Bight apex is not simply a matter of turbid river

water flowing out to sea, but instead a much more complex system in which the traffic on numerous feedback loops may be much more voluminous than the throughput volume.

The fluvial throughput model of sediment transport is yet less applicable to the sand budget of the Bight apex. Most estuaries serve as sand sinks rather than sand sources for the coastal sand budget, and the morphology of the Hudson estuary mouth suggests that it is no exception. The littoral drift discharge of both the northern New Jersey and Long Island coastal compartments converges on the estuary mouth (figs. 2.31, 2.32). Here the sand accumulates in a massive sand shoal filling the estuary mouth. Such estuary mouth shoals tend to be stabilized by the interdigitation of ebb-dominated and flood-dominated paths of tidal flow.

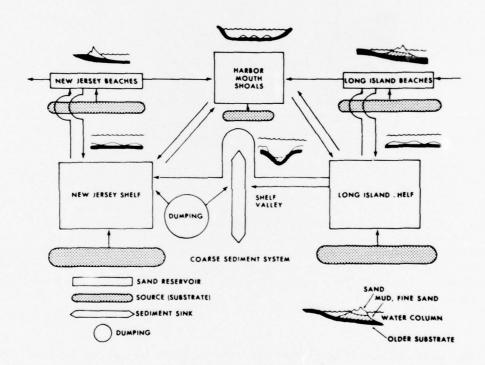
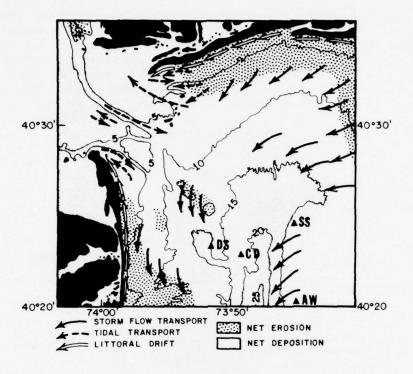


Figure 2.31. Schematic representation of probable pattern of coarse sediment exchange in New York Bight apex. Compare with figure 2.22.



rigure 2.32. Probable sense of net coarse sediment transport, as inferred from topography (fig. 2.1), (including detailed maps of harbor mouth), from grain size distribution (fig. 2.5), and from bedform patterns (fig. 2.20). Coarse sediment transport is storm-driven, and the inferred pattern differs markedly from that for fine sediment transport. (Compare with fig. 2.23.)

The main source of sand for the coastal sand budget is instead the eroding shoreface and inner shelf surface. This surface is presumably attempting to develop the ideal, concave up, exponentially curved surface in response to the present hydraulic regime. However, the ideal surface toward which the actual shelf surface is trending is not a stationary one, but one which is slowly translating upwards and landwards in response to the slow post-glacial rise in sea level (fig. 2.33). The actual surface, in attempting to follow this ideal surface, must release sand by

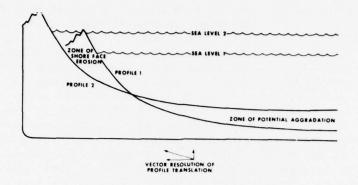




Figure 2.33. Erosional retreat of the inner shelf profile, and resulting coarse sediment dispersal.

shoreface erosion during storm flows and redistribute the sand over the adjacent shelf surface. Although no direct evidence is yet available, such redistribution must occur during periods of intense easterly winds. During such periods water is driven against the coast. The excess pressure head may be relieved by means of a downwelling coastal jet whose bottom water sweeps sand down coast and seaward. Circumstantial evidence for such flows occurs in the form of patches of sand-waves (figs. 2.9, 2.13), oriented oblique to the coast, which are most clearly defined in early spring, and which tend to be obliterated by the end of summer.

During such peak flow events the Bight apex gyre probably does not function, and the flow trends instead west and south through the apex. This spasmodic, high intensity flow field rather than the fair weather flow field is probably responsible for the bedform patterns of figure 2.9, which may constitute a time-averaged response to such flows. It is

probably also responsible for the distribution of sand grain sizes of figure 2.5. The coarse, gravelly sands of inner Cholera Bank and the New Jersey Platform may be lag concentrates beneath zones of flow constriction and acceleration during storms, where finer sands may be swept away to be deposited in such probable zones of flow expansion and deceleration as the shelf valley and the Christiaensen Basin. Circumstantial evidence for such a sand dispersal pattern may be seen in the sub-bottom profiles of figure 2.2. These clearly indicate that the ancestral subaerial valley has undergone appreciable filling, and that the filling has been asymmetrical, occurring mainly on the east side. The highly sandy nature of the muds of the shelf valley and the Christiaensen Basin attest to the efficiency of these topographic features as sand traps. It must be recognized, however, that much of the infilling of these features may have been accomplished by the littoral sand discharge of the retreating Long Island coastline into the retreating Hudson estuary mouth. The persistence of these topographic features indicates that the rate of coast-wise sand flux has not been high enough relative to the rate of sea level rise to fill the lows completely in the millenia since transgression. The intense northward flows recorded in the shelf valley (see section 1) may have played a role in keeping the shelf valley open.

## 2.3.6 Coarse Sediment Transport in the Bight Apex

An intensive program of computations is underway to convert current meter data into estimates of rates and directions of sand flux in the Bight apex. The calculations will be calibrated by independent estimates attained at key points by the release of relatively long-lived (3-month working period) radioisotope tracers. The following is a preliminary statement of approach, together with some preliminary data.

The initiation of coarse sediment movement has been extensively studied in the last three decades, and the flow velocity requisite for varying grain densities, bed configurations, and water viscosities is generally understood. Figure 2.34, shows threshold velocities for a smooth bed of quartz sand, from information developed by Shields and published by Graf (1971) and subsequent workers. A band rather than a single line is presented because of uncertainties in resolving the velocity profile of the boundary layer that are beyond the scope of this report. A representative threshold curve is close to but slightly below the upper margin of the band. For a rippled bed whose corrugated surface has developed resistance to flow, the curve should be near or slightly above the upper margin of the band. In general, the minimum velocity threshold for grain motion is approximately 30 cm sec-1 for fine sand, and slightly higher for coarser grades.

In order to appreciate the significance of this number, the reader should review the velocity records described in section 1. During the fall of 1973, peak flows regularly attained velocities of 50 cm sec<sup>-1</sup> at mid-depth.

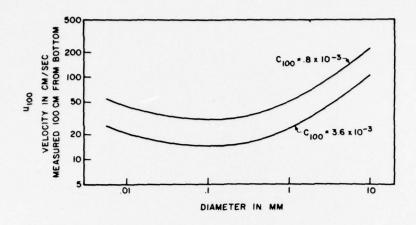


Figure 2.34. Curves for threshold of grain transport at different estimates of drag coefficient (C). Based on work of Shields (Graf, 1971).

The first attempt to independently measure coarse sediment flux by means of radioisotope tracers was undertaken in November 1973, using the radioisotope sand tracer (RIST) system developed by Oak Ridge National Laboratory and the Coastal Engineering Research Center (Duane, 1970). Sand from the Bight apex was impregnated with a radioisotope of gold, with an 8-day effective working period (approximately 3 half-lives). The experiment, undertaken 4 km off the New Jersey coast in 30 m of water, corroborated our estimate of threshold velocities and supported the hypothesis that sand transport occurs mainly under severe storm conditions. Bottom currents measured coincidentally with the experiment show a northnortheast residual current superimposed on a relatively strong tidal flow. Peak current velocities measured at 100 cm from the bottom were on the order of 35 cm  $\sec^{-1}$ , just sufficient to initiate sand transport, and insufficient to move appreciable quantities. Figure 2.35, shows contours of observed radiation on the final survey day. Caution must be used in interpretation of the figure because of the contouring algorithm employed. However, the lower left hand dispersal pattern displays a very limited dispersal to the north-northeast.

In April 1974, sand labeled with an isotope of Ruthenium (120-day effective working period) was released on the crest of Cholera Bank. Figure 2.36 presents the time development of the pattern through two surveys undertaken 3 weeks apart. Sand from the drop sites was transported

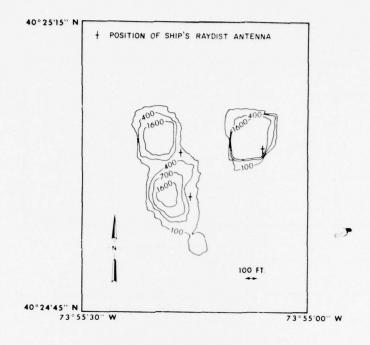


Figure 2.35. Dispersal pattern of goldlabeled tracer sand at end of November 19, 1974, experiment. See figure 2.3 for location.

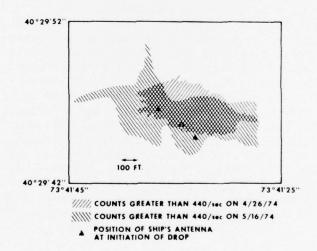


Figure 2.36. Dispersal patterns for two surveys, Ruthenium labeled sand of spring experiment. See figure 2.3 for location.

first to the east and then to the west, in response to coast parallel flow, modulated by tidal currents peaking at 30 to 40 cm  $\sec^{-1}$ .

The dispersal patterns of radioisotope deployment will serve as the basis for mass balance calculations, which will be compared with theoretical sand discharges calculated from current meter records. Simultaneous deployments of radioisotope tracers and current meters are planned for the winter months of peak water flow.

# 2.4 APPLICATION OF SEDIMENT TRANSPORT DATA TO THE PROBLEM OF SEWAGE SLUDGE DISPOSAL

The preceeding sections have described the natural system of sediment transport and deposition in the Bight apex. Although the data are incomplete and only partly processed, it is possible to draw the following inferences.

## 2.4.1 Pattern of Waste Dispersal

Suspended solids concentrations in the lower one-third of the water column surrounding the dredge spoil and sewage sludge dumpsites are 30 to 50 percent higher than would be expected if no dumping were occurring. Existing data do not permit distinguishing of dredge spoil from sewage sludge. Quantitative measurement of these components in natural suspended material requires identification of the chemical signature of sewage sludge.

The dispersal of easily identifiable red iron hydroxide particles from the acid waste dumpsite (figure 2.24) indicates entrainment of these particles in the clockwise circulation pattern (figure 2.23). There seems to be no question that material from all of the dumpsites is being transported by this clockwise gyre toward the Long Island shore.

Suspended solids concentrations (biogenic remains and mineral particles) are naturally high and quite variable within 10 km of both the Long Island and New Jersey shores (figure 2.23). This material is composed of both living and non-living plankton and terrigenous minerals that are supplied by the Hudson River estuary, by inner shelf currents moving westward along Long Island, by tidal exchange with the shallow lagoons behind Long Island's barrier islands, and by in situ plankton production. Microscopic analysis shows that suspended solids at all water depths within 15 km of Long Island during the fall of 1973 contained only trace amounts (much less than 1 percent by grain count) of processed cellulose (assumed to be disintegrated toilet paper) and the black soot particles that are characteristic of suspended solids samples collected from the near bottom water of the sewage sludge dumpsite. It is clear that the sewage-related materials that move in suspension are tremendously diluted by natural particles during transport northward toward Long Island.

## 2.4.2 Bottom Muds Versus Sewage Sludge Beds

A major conclusion derived from our initial data is that the entry of sewage-related materials into natural bottom deposits is a subtle process indeed. These materials are too fine and mobile to pile up and remain on the bottom at the dumpsite. It is significant that the sea floor at the dumpsite consists predominantly of bare sand. Patches of mud, whether natural or sewage-related are thin, small, and infrequent. The locus of organic-rich muds deposition appears to coincide precisely with the contours of the Christiaensen Basin. This basin lies between the designated dumpsite and the mouth of New York Harbor, and the high concentrations of organic carbon described in section 3 may be the consequence of short dumping. However, our analysis of the fine sediment transport system indicates that the bulk of the sewage sludge will wind up in this zone of natural fine sediment deposition no matter where it is dumped in the Bight apex.

To better define the distribution of sewage-derived particulate materials that are being deposited in the Bight apex, 13 bottom samples were separated into light and coarse fractions, filtered onto membrane filters, and microscopically examined for artificial contaminants. Three samples were from the Christiaensen Basin muds immediately northwest of the sewage sludge dumpsite; four were from mud patches within 5 km of the Long Island shore; four were from brown muds near the New Jersey coast, and two were from muds inside Jones Inlet. The results are presented in Table 2.2.

These data suggest the following conclusions. The muds off Long Island are predominantly natural in origin and contain at most only 2 to 3 percent of sewage-derived particles. Muds from other areas contain more solid material attributable to man than do the black muds from the Long Island shore. The relatively large amounts from the New Jersey Platform, for instance, are probably derived from the Hudson River outflow.

There is no material on the floor of the New York Bight apex that has been clearly identified as sewage sludge (predominantly sewage-derived material), although the muds of the Christiaensen Basin are probably significantly contaminated, and may locally contain more contaminant than natural materials. No front of sewage sludge, or of any other material was observed moving towards the Long Island shore. The dimensions of muddy areas, and the boundaries between sand areas and mud areas probably shift with the passage of the seasons. Nearshore mud patches appear and disappear

Microscopic examination of samples from nearshore mud patches do not reveal indicators of contamination in significant quantities. However, it is not possible to resolve toxic trace metals or pathogenic microorganisms by microscopic methods, and these materials are potentially more mobile and transportable than the observed cellulose fibers and soot particles.

Table 2.2 Particle Count Analysis of Contamination of Bight Apex Muds

	Natural Mineral and Biogenic Grains	Artificial* Grains	
	(% by grain counts per 2	!50 grains)	
Near Dumpsite Samples (3 samples)			
Coarse fraction	89%	11%	
Fine fraction	84%	16%	
Long Island Shore (4 samples)			
Coarse fraction	97.6%	2.4%	
Fine fraction	>99.0%	<1.0%	
New Jersey Platform (4 samples)			
Coarse fraction	96.8%	3.2%	
Fine fraction	96.7%	3.3%	
Jones Inlet Muds (2 samples)			
Coarse fraction	97.8%	2.2%	
Fine fraction	98.6%	1.4%	

<sup>\*</sup>Processed cellulose fibers (mainly toilet paper) and soot-like particles. The latter are a significant component of sediments on the northwest side of the dumpsite but may be derived from other waste dumping in the New York area.

#### 2.5 REFERENCES

- Belderson, R. H., N. H. Kenyon, A. H. Stride, and A. R. Stubbs, 1972. Sonographs of the Sea Floor. Elsevier, New York, 185 pp.
- Bumpus, D. F., 1965. Residual drift along the bottom on the continental shelf in the Middle Atlantic Bight area. Limnol. and Oceanogr., 10 (Redfield Vol.): R50-R53.
- Dewling, R. T., 1974. Ocean disposal. In Ocean dumping in the New York Bight. Environmental Protection Agency briefing report, p 19-29.
- Drake, D. E., 1974. Suspended particulate matter in the New York Bight Apex: September-November 1973. NOAA Tech. Rept. ERL 318-MESA 1, 56 pp.
- Duane, D. B., 1970. Synoptic observations of sand movement. Proc. 12th Coastal Eng. Conf., p 799-813.
- Environmental Protection Agency 1973. Ocean dumping in the New York
   Bight: facts and figures. Environmental Protection Agency,
   Region II.
- Graf, W. H., 1971. <u>Hydraulics of sediment transport</u>. McGraw-Hill, New York, 504 pp.
- Gross, M. G., 1972. Geologic aspects of waste solids and marine waste deposits New York metropolitan region. Bull. Geol. Soc. Amer., 83: 3163-3176.
- Gross, M. G., B. A. Morse, and C. A. Barnes, 1969. Movement of near-bottom waters on the continental shelf off the northwestern United States. J. Geophys. Res., 74: 7044-7047.
- Hazelworth, J. B., B. L. Kolitz, R. B. Starr, R. L. Charnell and G. A. Berberian, 1974. New York Bight Project, Water Column Sampling Cruises #1-5 of the NOAA Ship FERREL, August-November, 1973. MESA Report 74-2.
- McCave, I. N., 1972. Transport and escape of fine-grained sediment from shelf areas. In D. J. P. Swift, D. B. Duane, and O. H. Pilkey (editors), Shelf Sediment Transport: Process and Pattern. Dowden, Hutchinson and Ross, Stroudsburg, Pa., p 225-248.
- Meade, R. H., 1972. Transport and deposition of sediments in estuaries. In B. W. Nelson (ed.), Environmental Framework of Coastal Plain Estuaries. Geol. Soc. Amer. Mem., 133: 91-120.

- Milliman, J. D., and K. O. Emery, 1968. Sea levels during the past 35,000 years. Science, 162: 1121-1123.
- Shepard, F. P., and H. R. Wanless, 1972. Our Changing Coastlines. McGraw Hill, New York, 557 pp.
- Swift, D. J. P., 1972. Holocene evolution of the shelf surface, central and southern shelf of North America. In D. J. P. Swift, D. B. Duane, and O. H. Pilkey (editors), Shelf Sediment Transport: Process and Pattern. Dowden, Hutchinson and Ross, Stroudsburg, Pa., pp 499-574.
- Taney, N. B., 1961. Geomorphology of the south shore of Long Island, New York. Beach Erosion Board Tech. Memo. 128, 50 pp.
- Veatch, A. C., and P. A. Smith, 1939. Atlantic submarine valleys of the United States and the Congo Submarine Valley. Geol. Soc. Amer. Special Paper 7,101 pp.

3. CHEMICAL AND GEOCHEMICAL OCEANOGRAPHY OF THE NEW YORK BIGHT APEX REGION AS IT PERTAINS TO THE PROBLEM OF SEWAGE SLUDGE DISPOSAL

Douglas A. Segar, Patrick Hatcher, George A. Berberian Larry E. Keister, Maxine Weiselberg

#### 3.1 INTRODUCTION

The following is a summary of the New York Bight ecosystem chemistry as it relates to understanding the disposition of sewage sludge barged and dumped into the ocean about 16 km south of Long Island and 13 km east of New Jersey. Three basic questions are of concern: Is sewage-derived material approaching the Long Island beaches? Is the material reportedly found near the beaches derived from the barge-dumped sewage sludge? Does any such material exist at high concentrations so as to be a significant contaminant in the marine environment? Unequivocal answers are not possible at this time. However, the available evidence is reviewed in the context of these questions.

#### 3.2 WASTE DISPOSAL

## 3.2.1 Contaminants Introduced into the New York Bight

Sewage sludge is not the only contaminant being released into the New York Bight. Other materials such as dredge spoil and acid wastes are dumped at sites close to that of the sewage sludge dumping. Both of these materials can contain large amounts of trace metals. The dredge spoil often contains large quantities of organic matter, much of which is derived from sewage introduced directly into estuaries from which the spoil is removed. In addition, a multiplicity of point sources ranging from the Hudson estuary to the smallest drainage ditch introduce many contaminants into the Bight. Contaminants contained in such outfalls include a spectrum of organic compounds, trace metals, and suspended materials, including treated and untreated sewage.

#### 3.2.2 Composition of Sewage Sludge

Raw sewage reaching the treatment facility originates from a variety of sources, principally domestic human and kitchen wastes, industry, and commercial establishments. Primary sewage treatment involves degritting, grease and scum removal, and then clarification by sedimentation. The clarified waste water is then pumped off and the remaining thickened sludge disposed of by dumping. Secondary treatment usually consists of aeration of the clarified waste water from the primary treatment together with the addition of some of the sludge to supply biological activators. The resulting products are then disposed of as with primary treatment. Chlorination is frequently used at one or more stages of these processes. In New York the resulting sludge slurry is barged to the ocean disposal site.

Sewage sludge is an extremely heterogeneous material comprising amorphous organic aggregates but including such identifiable material as tomato and melon seeds, human hair, and fragments of rubber and plastic.

Organic matter in sewage sludge has not yet been, and probably never will be totally characterized; however, some major constituents have been identified (Hunter and Heukelekian, 1965; Gross, 1972; Walter, 1961). Total organic carbon usually accounts for 20% to 40% of the dry weight of solids. Proteins and carbohydrates compose around 20% and 10% of dry weight respectively. One constituent of the sludge is cellulose fibers originating primarily from paper products. Other minor components are amino sugars, soluble acids, fats, anionic detergents, hydrocarbons, and amides, all together composing less than 10% of the dry weight of solids. Recently Kolattukudy and Purdy (1973) identified a biopolymer called cutin as a significant component of sewage sludge. This biodegradation-resistant polymer is derived from the cuticle waxes of most staple vegetables. Also, associated with the solid sludge material are bacterial and fungal populations, and trace metals originating both in domestic and non-domestic wastes. Dissolved trace metals and organic compounds released into the sewage system may be at least partially scavenged from solution by the solid materials during the sewage transportation and treament process.

## 3.2.3 Fate of Sewage Sludge After Dumping into the Ocean

When sewage sludge is released into sea water, the new chemical environment causes rapid chemical alteration of the sludge. The nature and extent of such transformations have not been studied in detail. In addition, sludge material undergoes biological and physical changes. Certain microbial species in sewage experience a hostile environment and eventually die out. These are subsequently replaced by marine microbes. Physical fractionation occurs due to the wide range of densities and sizes of particles introduced to the water column. The range of particle sizes dumped changes as the electrolyte action of sea water permits the aggregation of small particles to form larger clumps. The physical separation of fractions of the sludge is important for determining both the initial sedimentation site and any subsequent resuspension, transport, and redeposition.

Physical transport of material in the New York Bight apex is discussed in more detail in sections 1 and 2. However, it is relevant to point out that different types of material may be deposited and transported in very different patterns. Therefore, it is not possible to delineate the ultimate distribution of sewage sludge per se from the observed distribution of any one of its component parts. For example, distributions of tomato seeds, hair, and cellulose particles may be totally different even though they are all derived from the same barge. This problem is further complicated by the fact that different fractions

of the sludge will be subjected to degradation and transformation to materials which may be physically indistinguishable from the naturally occurring sediments or dissolved components. Additionally, the different fractions may experience different rates of decomposition during the time they reside in the marine environment. For example, plastic particles may be transported great distances over long periods of time while more easily degradable materials will be assimilated by the ecosystem within a few days and before they can be transported far from the dumpsite.

The fate of sewage sludge dumped into the oceans is thus not easily understood nor simply described and is a complex function of the physical, geological, and particularly the biological and chemical forces working in different ways on different materials within the sludge. Ultimately all of the materials of the sludge will be converted into chemical forms which may be indistinguishable from those of naturally occurring compounds and solids.

## 3.2.4 Methods for Identification of Sewage Sludge in Marine Sediments

Methods for identification of sewage sludge in the sediments from natural waters are all dependent upon some physical or chemical property of sludge being traced to the site of deposition. However, as pointed out, the distribution of any one component of sewage in bottom sediments may not necessarily reflect the fate of the transported sludge as a whole.

Physical properties of sewage such as its "black, mayonnaisey consistency", and the presence of human hairs, plastic particles, and tomato seeds, have recently been used in attempts to define the boundaries of the so-called sludge bed resulting from ocean dumping in the New York Bight and other areas. Sediments that are black and sloppy in texture usually contain large quantities of organic matter which is fine grained and has a density not very different from that of water. Because of the fine grain and low density, such sediments are found to accumulate in topographic depressions or in areas of low wave and current energy. Also, because of these physical characteristics they are easily resuspended and transported by the overlying water. In coastal locations such sediments are often formed naturally from the detrital organic matter generated at the coastline and by shallow water plant communities. It is likely, therefore, that without any contribution from man, pockets of black mud-like sediments would occur naturally in the New York Bight, particularly close to the shore and to river and channel mouths. Presence of this type of sediment in pockets close to the Long Island shore is, therefore, not necessarily related to the dumping of sewage sludge offshore. This is particularly true when it is considered that a number of inlets along the Long Island shore are themselves probable

sources of sewage-derived organic detritus.

Slowly biodegradable constituents of sewage sludge such as tomato seeds and hair are not rendered unidentifiable in the marine environment until long after the other components of the sludge are oxidized and assimilated. They may, therefore, be transported beyond the area reached by the major proportion of the sludge and their distribution will not accurately define the area adversely affected by the sludge.

Several reports concerned with the New York Bight (Gross 1969, 1970 a, 1970 b, 1972; Carmody et al., 1973) have discussed the distribution of trace metal concentrations in the sediments. High trace metal concentrations have been observed at the sewage sludge dumpsite. The concentrations decrease with increasing distance from this area. Although sediments derived from sewage sludge contain high trace metal concentrations, it cannot be inferred that all fine sediments with high trace metal concentrations in the New York Bight contain sewage sludge. High trace metal concentrations (in some instances higher than the highest observed in the New York Bight) are found in many fine-grained sediments throughout the marine environment. Anomalously high local concentrations have been observed in areas where contaminant inputs do not include sewage (Segar & Pellenbarg 1973).

High organic carbon content of sediments would give an indication of the presence of sewage sludge, if the contribution of organic matter from other sources to the sediments were negligible. This in fact is not the case, particularly near the coastline. We have estimated that the total amount of organic matter dumped into the Bight as sewage sludge is less than one-half the organic matter produced in the region by marine plants. Therefore, organic carbon contents alone cannot be used to trace the sewage sludge influence, particularly at sites far from the dumpsite where organic carbon values are comparatively low and natural sources are significant.

Nevertheless, since sewage sludge is composed primarily of organic materials it seems logical to use some of these components as possible tracers. Whatever components are chosen as tracers must ideally be major components of sewage, only slowly biodegradable, and not found naturally in the dumping environment in any significant quantities. We are searching for specific compounds or groups of compounds to act as organic tracers and to enable us to delineate the transport patterns and fate of sewage sludge. Preliminary work has indicated that total carbohydrates normalized to total organic carbon may be used to obtain a crude estimate of the distribution of sewage-derived materials.

Carbohydrates derived from phytoplankton are generally those easily degraded in the marine environment. Glucose, fructose, mannose, and other monosaccharides constitute a substantial fraction of phytoplankton-derived organic matter (Parsons et al., 1961). As the organisms die and

settle to the sediments, these carbohydrates are preferentially oxidized or degraded as compared with more resistant cellulolytic carbohydrates which comprise a small fraction of phytoplankton carbohydrates. Carbohydrates are therefore rarely retained in recent sediments comprising mainly phytoplankton remains.

Terrigenous organic matter generally contains a substantial amount of carbohydrates, mainly structural carbohydrates such as cellulose and hemicellulose (Rogers 1965). If we define the carbohydrate/ $TOC \times 100$ ratio as R, then the expected R for these terrigenous substances is generally greater than 30. Sewage is considered a terrigenous substance and, therefore, possesses similar properties. The organic matter in soils derived from terrigenous substances undergoes extensive and rapid decomposition soon after it is deposited. The breakdown of cellulolytic carbohydrates is accelerated as compared with the marine environment, and R decreases rapidly to a value of generally less than 10. The major input of terrigenous organic matter to the near-shore areas is derived from the leaching of these low carbohydrate soils in the watershed. Since R of this leached material is generally low, and the contribution of terrigenous matter to the New York Bight is small (Meade 1969). sedimentary contribution of non-sewage terrigenous materials is expected to be low.

In non-polluted near-shore sediments R is generally less than 10, indicating that carbohydrates comprise only a small fraction of the organic matter (Degens et al., 1961). Even after substantial decomposition, this ratio remains low due to the fact that, although the labile carbohydrates have long disappeared, the resistant cellulolytic carbohydrates also undergo bacterial degradation. This process is slow but, nevertheless, more rapid than the breakdown of highly resistant non-carbohydrate materials which may account for more than 80% of the organic matter present. Under these circumstances, the C/TOC ratio would be expected to decrease with increasing age.

Sewage sludge contains a substantial amount of carbohydrate material (Walter, 1961), mostly in the form of cellulose and hemicellulose (Hunter and Heukelekian, 1965), both of which are resistant to biological degradation. After sludge is dumped in the ocean, it undergoes substantial microbial degradation, both before and after it reaches the sediments. The amount of organic matter thereby decreases. Cellulolytic carbohydrates, however, do not undergo the equivalent amount of decomposition in such a short time span as other more easily degradable organic constituents of sewage. Therefore the R would be expected to increase upon rapid biological degradation. Extremely high R ratios might therefore be characteristic of sewage-derived material that has been aged somewhat in the environment.

In sediments of the New York Bight, R is commonly greater than 20, indicating a high proportion of carbohydrates relative to organic matter

as compared with other similar areas. As sewage sludge contains large amounts of cellulose and other resistant carbohydrates (R=30), it seems likely that these cellulolytic carbohydrates have enriched the sediments of the New York Bight. The non-biodegradable nature of these cellulolytic carbohydrates over a short time span allows them to enrich the surficial sedimentary organic matter and, therefore, reflect a relatively high C/TOC ratio. The ratio may therefore be a crude tracer of sewage derived materials.

#### 3.3 PRELIMINARY RESULTS OF THE MESA PROGRAM

## 3.3.1 Water Column Chemistry

In the New York Bight apex, the nutrients, [nitrate  $(NO_3)$ , nitrite  $(NO_2)$ , silicate  $(SiO_3)$ , and phosphate  $(PO_4)$ ], have been measured at periodic intervals in conjunction with a water sampling and hydrographic program. Additionally, analyses of dissolved and suspended trace metals and of suspended organic matter have recently been initiated. Nutrients are released with most urban and industrial contaminants; their concentration distributions may, therefore, be related to the proximity of outfalls or dumpsites. Their concentrations are also intimately related to biological production and degradation in the water. The distribution and cycles of nutrients in an area such as the New York Bight are, therefore, complex and depend upon the water circulation patterns and various physical, chemical, and biological reactions between the diverse components of the outfalls and dumps and the sea water.

Sewage sludge is generally enriched in dissolved nutrients such as nitrates, nitrites, and phosphates (Weinberger, et al., 1966). Approximately 5 x  $10^{\circ}$  tons of sludge are being disposed of in the New York Bight annually. This equals  $1.5 \times 10^{4}$  tons daily, a locally large volume of liquid in the dump area. As this sludge is dumped, mixing occurs rapidly thereby diluting the concentrations of nutrients. In the immediate vicinity of a dump, the nutrient concentrations are expected to be high. However, as the sewage sludge liquids mix into an area comparable to the MESA water chemistry grid, the calculated concentrations of nutrients derived from sewage sludge decrease significantly to values which are below detectable levels. It is therefore not too surprising to find that nutrient concentrations in the Bight are not indicative of sewage sludge disposal.

Preliminary analyses of data from MESA Cruises 2 and 5 (September 16--20 and November 25--29, 1973), are presented here. These cruises were during periods of highly stratified, and well mixed conditions, respectively. Surface and bottom nitrate and silicate distributions are presented in figures 3.1 - 3.8.

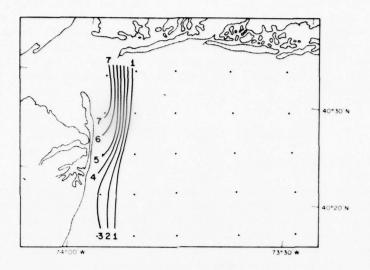


Figure 3.1 Distribution of surface nitrate ( $\mu g$ -at/ $\ell$ ) measured during MESA Cruise 2, September 16-20, 1973.

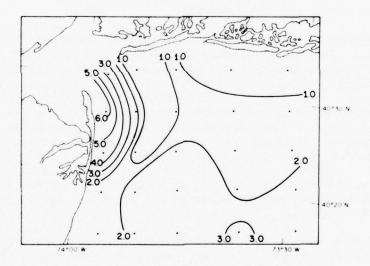


Figure 3.2 Distribution of bottom nitrate (µg-at/l) measured during MESA Cruise 2, September 16-20, 1973.

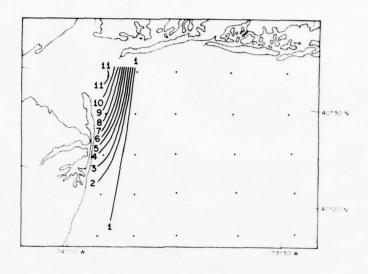


Figure 3.3 Distribution of surface silicate (µg-at/l) measured during MESA Cruise 2, September 16-20, 1973.

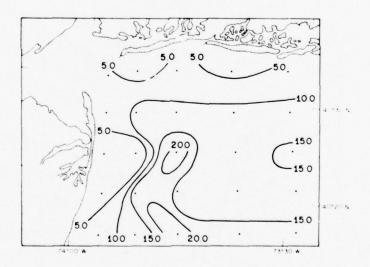


Figure 3.4 Distribution of bottom silicate (µg-at/l) measured during MESA Cruise 2, September 16-20, 1973.

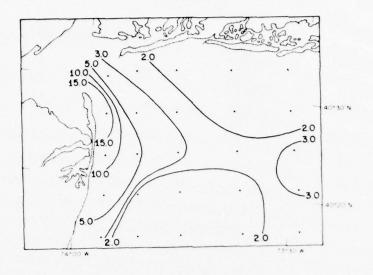


Figure 3.5 Distribution of surface nitrate (ug-at/l) measured during MESA Cruise 5, November 25-29, 1973.

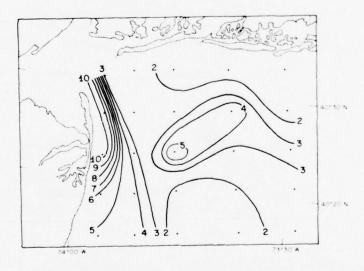


Figure 3.6 Distribution of bottom nitrate (ug-at/l) measured during MESA Cruise 5, November 25-29, 1973.

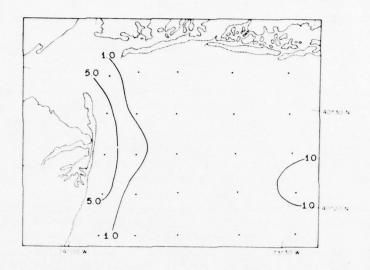


Figure 3.7 Distribution of surface silicate (µg-at/l) measured during MESA Cruise 5, November 25-29. 1973.

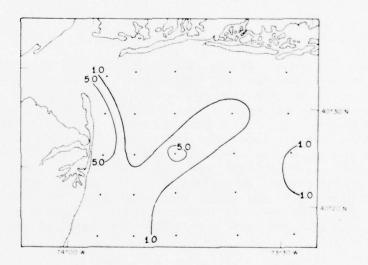


Figure 3.8 Distribution of bottom silicate (ug-at/l) measured during MESA Cruise 5, November 25-29, 1973.

A prominent feature of all the distributions is the high concentrations along the New Jersey coast. This is probably nutrient-rich lower New York Bay water flowing into the Bight, consistent with other observations that this estuarine output flows south along the New Jersey shore. Generally higher concentrations of the nutrients were found in the vicinity of the sewage sludge dumpsite that is located close to the central station of the sampling grid.

During Cruise 2, when the water was stratified, the bottom silica values were generally anomalously high but were highest at the station closest to the sewage sludge dumpsite. During Cruise 5, more normal low silica concentrations for these depths were observed but again the bottom concentrations near the sewage sludge dumpsite were somewhat high as were the nitrate concentrations. The distribution of the other nutrients was in agreement with these observations.

It is apparent from our data that the water close to Long Island normally has much lower concentrations of all the nutrients, both at the surface and the bottom, than water along the New Jersey shore. It appears that the nutrient distribution in the water column is influenced more by the outflow of water from lower New York Bay than by contamination from the dumpsite except perhaps for silica during highly stratified conditions.

The release of nutrients from the dumped sewage sludge does not appear to be a major additive to the normal nutrient level occurring in the area.

## 3.3.2 Sediment Chemistry

Bottom sediments of the New York Bight collected in the fall of 1973 have been analyzed for carbohydrates and for total organic carbon (TOC). Figure 3.9 shows that high concentrations of organic carbon are located primarily in topographic lows. This is consistent with the observation that coastal marine fine sediments that settle in topographic lows elsewhere are generally high in TOC (Froelich, et al., 1971). The highest concentrations of organic carbon in New York Bight sediments are in the Christiaensen Basin, the center of which is 8 km to the west of the designated sewage sludge dumpsite. The highest values encountered are approximately 5% dry weight TOC, which is in agreement with Gross (1970 b). This value is almost an order of magnitude less than that for sewage sludge taken directly from the municipal sewage treatment facility.

Previous workers have attempted to define the sludge bed extent using organic matter concentration distributions. This definition assumes that the only significant source of organic sedimentary material

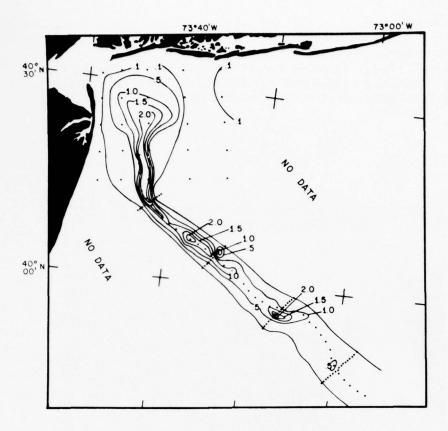


Figure 3.9 The total organic carbon (% dry weight) in sediments of the New York Bight collected during August-September 1973. The dots represent the sampling stations.

in the New York Bight is dumped sewage sludge. It ignores the terrigenous organic matter input, both natural and contaminant, and the material photosynthetically produced in the marine ecosystem itself. The latter has been estimated to be at least twice as large an input as the organic matter in dumped sewage sludge. Even in the absence of any input from man it is probable that the distribution pattern of TOC in the Bight sediments, although not the quantity, would be similar to that observed today. The distribution of TOC in sediments is inversely related to particle size (compare fig. 3.9 with fig. 2.5). Finer sediments contain more TOC than do the coarser sands. This relationship between TOC and particle size distributions is a normal feature of all coastal sediments.

The same sediments from the New York Bight, analyzed for TOC concentrations, have also been analyzed for total carbohydrates. The distribution pattern shown in figure 3.10, is similar to that of the TOC concentrations. [Thus, the same factors that influence the TOC distribution (particularly particle density and size distribution) appear also to be a major influence on the carbohydrate distribution.]

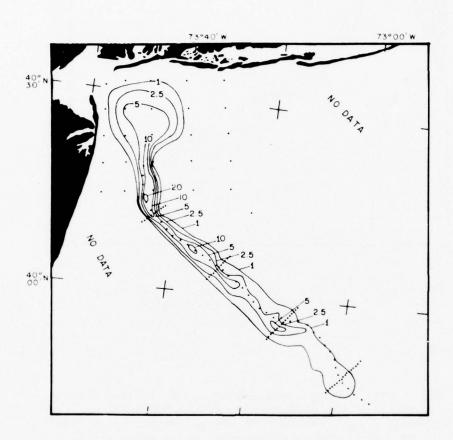


Figure 3.10 The distribution of total carbohydrates (% dry weight x 1000) in sediments of the New York Bight collected August-September 1973. The dots represent sampling stations.

The distribution of R, taking into account these changes, suggests that sewage derived materials are probably being entrained or transported within the hypothesized current gyre in the apex (see section I). The entrained particles would be successively deposited and resuspended by wave, tide, and current energy and would tend to accumulate in the topographic lows where such energy is at a minimum. There is such a topographic low at the head of the Hudson Shelf Valley where material with high R values is accumulating. The seaward extent of the current gyre is not well defined but R ratios indicate that sewage-derived materials are being transported to and accumulating in the Hudson Shelf Valley many miles offshore (fig. 3.11). It is not known how this material is

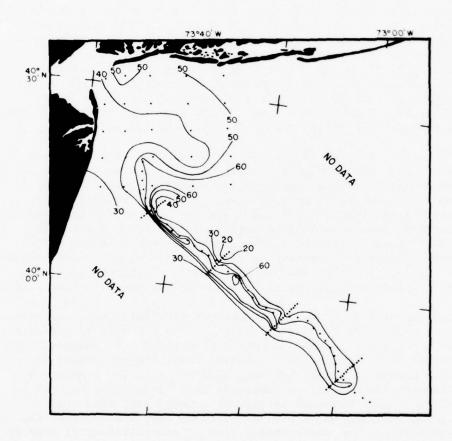


Figure 3.11 The carbohydrate/TOC ratio in sediments of the New York Bight, Aug-Sept, 1973. The dots represent sampling stations.

Sewage sludge is composed primarily of small particles of organic matter. If these particles accumulate in depressions or topographic lows, the resultant mud will be black and sludge-like and will have a high organic carbon and carbohydrate content despite dilution with naturally occurring fine grained sediment. Where these particles are mixed with sandy or other coarse inorganic sediments, the resultant mud may still be black, but will have lower organic carbon and carbohydrate concentrations. At high dilutions, these coarse sediments will no longer appear black and will not have high TOC concentrations even though they contain sewage-derived material. To determine whether or not the organic matter in each of these types of sediments is derived from sewage sludge we must establish a qualitative measure of this type of organic matter (e.g., high R).

As previously stated, it is reasonable to assume that the bulk of the carbohydrates in these sediments is oxidation-resistant cellulolytic material derived from sewage although not necessarily the barge-dumped sewage sludge. Figure 3.11 shows the distribution of R in the New York Bight and may be used to infer the relative contribution of sewage-derived material to the organic matter in sediments at any location. The whole apex area is enriched in carbohydrates relative to TOC with values of R ranging from 20-70 compared with normal coastal sediment values of about 10. The higher values (50 and above) are located in the axis of the Hudson Shelf Valley and toward the Long Island shore.

It is important to realize that a high R implies, only, that an appreciable fraction of the organic matter within a sediment sample is derived from sewage. If this same sample contains very little total organic matter then the total amount of sewage-derived material in it must be small. As is the case for sediments near the Long Island shore, the TOC or organic matter content is generally very low and R is high. Therefore, it follows that although the organic matter in these sediments is probably derived from sewage, the total amount of sewage-derived material is low. Only in isolated pockets, where the TOC is high, can the sediments contain an appreciable fraction of sewage-derived material.

We would expect R to increase somewhat as materials are transported further from the dumpsite because of the increased exposure to microbial degradation in the water column. Comparison of the R's in sewage sludge and in sediments of the Christiaensen Basin, whose organic matter is believed to be primarily sewage-derived, substantiates the previously stated speculation that the ratio increases upon biodegradation. In addition, if the sewage material settles in a sandy environment as opposed to a mud environment, R will probably be higher because of the more rapid degradation and preferential loss of non-cellulolytic organic matter from the oxygenated sands.

transported. The shelf valley may be acting as a conduit as suggested by the higher R values observed on the southern flank of the valley. Alternatively the fine material may simply be dispersing in a broad pattern offshore and accumulating in the topographic lows. Regardless of the mechanism involved the observed distribution strongly suggests that a significant proportion of the dumped sewage sludge is being transported away from the coastline into deeper water.

In addition to the data of figs. 3.9-3.11, samples from the MESA substrate monitoring program (locations shown in fig. 3.12) and recently collected samples from the south shore of Long Island (locations shown in fig. 3.13) have also been analyzed for TOC and carbohydrates. Preliminary results (Table 3.1 and 3.2) indicate that pockets of black mud, rich in TOC ( $^5$ %), do exist within  $1\frac{1}{2}$  miles of the Long Island beach. This TOC concentration is similar to that found close to the actual dumpsite. Within one-half mile of the beach other pockets of mud were found to contain sediments having a TOC concentration of approximately 2%. The more extensive sandy sediments in the immediate vicinity were observed to have a TOC varying from 0.04% to 0.3%.

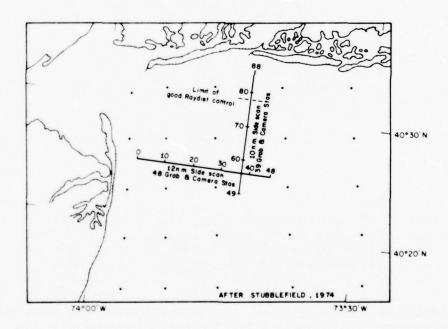


Figure 3.12 SUMP Cruise-2 track lines. The numbers on the lines designate station positions.

Generally, R is high for all of these samples; values range from 40 to 60, the same range observed for samples from the Christiaensen Basin. Thus, sediments close to the south shore of Long Island contain organic matter enriched in carbohydrate indicating a probable sewage source (either dumped sewage sludge or any other sewage discharge). This organic material has accumulated as thin layers in small pockets admixed with and covering silicate sands.

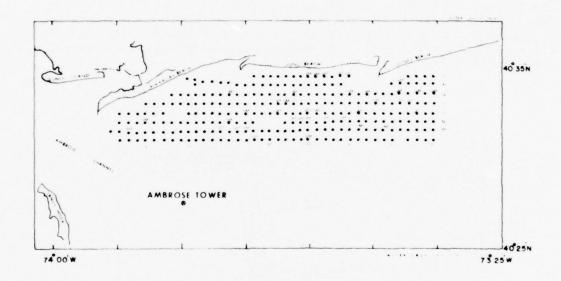


Figure 3.13 The approximate sampling sites for the recent SIS cruise off the Long Island Shore. The stations are defined by the grid and designated with letters (left) and numbers (below). SM indicates that the sample is a sandy mud.

Sediments from Rockaway Inlet, East Rockaway Inlet, and Jones Inlet were also analyzed for R (Table 3.2). The values are generally low (~20) within all the inlets despite some high organic carbon concentrations. This suggests that humic materials from the wetlands, other natural organic detritus, and possibly new sewage are major contributors to the organic matter in the sediments.

In summary, (1) The R ratio ir the Bight apex, indicates that nonbiodegradable carbohydrates, possibly derived from sewage, are significant contributors to the sedimentary organic matter. (2) The apex of the Bight seems to be enriched in carbohydrates (or sewage-derived materials) relative to the TOC as compared with the lower Hudson Shelf Valley and the New Jersey shore. (3) The dumped sewage sludge undergoes substantial alteration before and after settling to the sediment and/or admixture with natural nonorganic sediments. This is indicated by the large difference between the TOC concentrations of sewage sludge sediment in the Christiaensen Basin. (4) Isolated pockets of mud near the Long Island shore were found to have approximately the same TOC concentration and R as mud from the Christiaensen Basin, an indication that the Long Island mud is possibly derived in part from sewage. (5) It is not possible, using currently available techniques, to distinguish between sedimentary organic matter derived from barge-dumped sewage sludge or derived from other sources of treated or untreated sewage.

Table 3.1 The Organic Chemistry Data for Sediments Collected on the SUMP II Cruise

Station #	% Carbohydrates	% TOC	(Carbohydrates/TOC) x100
9	0.160	0.460	35
11	0.26	2.99	42
13	0.413	1.40	30
15	0.283	0.644	44
21	0.948	2.45	39
23	1.025	1.96	52
25	0.997	1.64	61
28	0.731	1.26	58
29	1.48	2.85	52
31	2.20	5.08	43
33	1.89	3.85	49
35	1.99	3.04	65
58	0.143	0.352	41
62	0.230	0.409	56
66	0.435	0.840	52
69	0.294	0.477	62
78	0.021	0.053	40
82	0.077	0.168	47
85	0.062	0.115	54
88	0.063	0.099	64

Table 3.2 Carbohydrates, TOC, and Carbohydrates/TOC in Sediment Samples Collected South of Long Island (SIS)

Station #	% Carboh	ydrates	% тос	(Carbohydra	tes/TOC) x 100
	1	2		<u>1</u>	2
§JI-1	0.0089	0.010	0.042	21	24
§JI-2	0.014	0.015	0.106	13	14
+ER	0.018	0.016	0.089	20	18
N-25	0.029	0.027	0.055	52	49
N-24	0.036	0.037	0.083	43	45
N-23	0.154	0.132	0.277	55	48
*N-22	0.043	0.044	0.080	54	55
*S-22	0.034	0.042	0.083	41	51
S-27	0.322	0.394	0.597	54	66
S-26	0.969	1.36	2.28	43	60
*S-24	0.029	0.033	0.070	41	47
S-30	0.127	0.142	0.211	60	67
N- 5	0.047	0.047	0.088	53	53
*R-24	0.844	0.808	1.49	57	54
R-36	2.26	2.17	4.56	50	48
M- 3	0.042	0.045	0.085	49	53
M-14	0.419	0.403	0.770	54	52
*M-19	0.086	0.086	0.152	57	57
M-31	0.392	0.421	0.712	55	59
M-34	0.088	0.107	0.226	39	47
0-26	0.479	0.464	1.20	40	39
P-21	0.896	1.28	2.31	39	55
P-23	2.288	2.45	5.21	44	47
Q-30	0.887	1.00	1.86	48	54
Q-36	0.083	0.068	0.181	46	38
Q-38	0.811	0.813	1.99	41	41

<sup>\* -</sup> samples from sandy areas

<sup>§ -</sup> Jones Inlet samples

<sup>+ -</sup> East Rockaway Inlet samples

#### 3.4 REFERENCES

- Carmody, D. J., J. B. Pearce, and W. E. Yasso, 1973. Trace metals in sediments of New York Bight. Mar. Poll. Bull., 4(9): 132-135.
- Degens, E. T., A. Prashnowsky, K. O. Emery, and J. Pimenta, 1961.
  Organic materials in recent and ancient sediments of Santa Barbara
  Basin, California. Neues Jahrb. Geol. Palaontol. Monatsh., 1961,
  413-426.
- Froelich, P., B. Golden, and O. H. Pilkey, 1971. Organic carbon in sediments of the North Carolina continental rise. S. E. Geology., 13: 91-97.
- Gross, M. G., 1969. New York City: A major source of marine sediment.
  Mar. Sci. Res. Center, SUNY Tech. Rept. No. 1, State University of
  New York, Stony Brook, New York.
- Gross, M. G., 1970 a. Preliminary analysis of urban wastes New York Metropolitan area. Mar. Sci. Res. Center, SUNY Tech. Rep. No. 5, State University of New York, Stony Brook, New York.
- Gross, M. G., 1970 b. Analysis of dredged wastes, fly ash and waste deposits, New York metropolitan region. Mar. Sci. Res. Center, SUNY Tech. Rep. No. 7, State University of New York, Stony Brook, New York.
- Gross, M. G., 1972. Geologic aspects of waste solids and marine waste deposits, New York metropolitan region. Am. Bull., 83: 3163-3176.
- Hunter, J. V., and H. Heukelekian, 1965. The composition of domestic sewage fractions. J. Water Poll. Control Fed., 37: 1142-1163.
- Kolattukudy, P. E., and R. E. Purdy, 1973. Identification of cutin, a lipid biopolymer, as significant component of sewage sludge. Envir. Sci. and Tech., 7: 619-622.
- Meade, R. H., 1969. Landward transport of bottom sediments in estuaries of the Atlantic Coastal Plain. J. Sed. Pet., 39: 222-234.
- Parsons, T. R., K. Stephens, and J. D. H. Strickland, 1961. On the Chemical composition of eleven species of marine phytoplankters. J. Fish. Res. Bd., Can., 18: 1011-1016.
- Rogers, M. A., 1965. Carbohydrates in aquatic plants and associated sediments from two Minnesota lakes. Geochim. Cosmochim. Acta, 29: 183-200.

- Segar, D. A., and R. E. Pellenbarg, 1973. Trace metals in carbonate/organic rich sediments. Effects of industrialization and urbanization. Mar. Poll. Bull., 4(9): 138-142.
- Walter, L., 1961. Composition of sewage and sewage effluents. Water and Sewage Works, Part 2. Scranton Pub. Co., Chicago, Ill., 478 pp.
- Weinberger, L. W., D. G. Stephen, and F. M. Middleton, 1966. Solving our water problems - Water Renovation and Reuse. <u>Annals of the</u> N. Y. Academy of Sciences, 136: art. 5, 131.

7 Reprinted from: NOAA Technical Memorandum ERL MESA-3, 32 p.

NOAA Technical Memorandum ERL MESA-3

WATER MOVEMENT WITHIN THE APEX
OF THE NEW YORK BIGHT DURING SUMMER
AND FALL OF 1973

R. L. Charnell D. A. Mayer

Physical Oceanography Laboratory, AOML Miami, Florida

Marine EcoSystems Analysis Program Office Boulder, Colorado April 1975

UNITED STATES
DEPARTMENT OF COMMERCE
Rogers C.B. Morton, Socretary

NATIONAL OCEANIC AND ATMOSPHERIC ADMINISTRATION Robert M. White, Administrator Environmental Research Laboratories Wilmot N. Hess. Director



#### DISCLAIMER

The NOAA Environmental Research Laboratories do not approve, recommend, or endorse any proprietary product or proprietary material mentioned in this publication. No reference shall be made to the NOAA Environmental Research Laboratories, or to this publication furnished by the NOAA Environmental Research Laboratories, in any advertising or sales promotion which would indicate or imply that the NOAA Environmental Research Laboratories approve, recommend, or endorse any proprietary product or proprietary material mentioned herein, or which has as its purpose an intent to cause directly or indirectly the advertised product to be used or purchased because of this NOAA Environmental Research Laboratories publication.

# CONTENTS

ABS	TRACT		Page 1		
1.	INTR	ODUCTION	1		
2.	DIRE	CT CURRENT MEASUREMENTS IN THE NEW YORK BIGHT APEX	2		
3.	CURR	ENT METER DATA	4		
	3.1	Phase I Environmental Conditions	4		
	3.2	Phase II Environmental Conditions	4		
	3.3	Initial Data Processing-Filtering	7		
	3.4	Character of Low Frequency Variations in Flow	7		
	3.5	Current Roses	13		
	3.6	Vector Time Series of 40-Hr Low-Pass Data	15		
	3.7	Temporal Variability of Flow	25		
	3.8	Coherence and Phase Estimates	25		
4.	RECA	PITULATION	27		
5.	ACKNOWLEDGMENTS				
6.	REFERENCES				

# WATER MOVEMENT WITHIN THE APEX OF THE NEW YORK BIGHT DURING SUMMER AND FALL OF 1973

R. L. Charnell and D. A. Mayer

An investigation of the water movement within the New York Bight Apex was made during the summer and fall of 1973. Observations from this study produced a fairly consistent picture of a general clockwise circulation for the mean and low frequency (periods greater than 40 hr) current motions. Additionally, the effects of stratification on the vertical structure of the flow showed the difference between the summer and late fall flow regimes. There also appeared to be, for low frequencies, excellent spatial coherence between stations in the apex area and a fairly strong relation between meteorological forcing and current motions; currents tended to lag wind by up to 18 hr.

#### 1. INTRODUCTION

The Marine Ecosystems Analysis (MESA) New York Bight Project is currently in the field phase of a program designed to evaluate changes in the water quality of the region. The physical oceanographic part of the effort is oriented to supplying information that will lead to understanding the mechanisms of water movement and material dispersion and eventually will result in a hierarchy of predictive models for use by coastal zone planners and managers.

Overall net movement of water on the continental shelf off southern New England and the Middle Atlantic States is to the west, southwest, and south, parallel to the continental margin (Bumpus, 1973). However, the complete picture is quite thoroughly masked by high spatial and temporal variability.

It is of considerable interest to understand the flow patterns within what is commonly called the apex of the New York Bight--the area within 50 km of the harbor mouth. The major dump sites of metropolitan New York-New Jersey are located in this zone. However, few field data exist with which to construct an adequate description of water movement in this coastal area. Most of what is presently known about the physical oceanography of the apex is based in part on historic data collected on behalf of the U.S. Army Corps of Engineers in 1969-70. Data include temperature and salinity values, recovery information of surface and seabed drifters, and current meter observations. Analysis of these data by

Charnell and Hansen (1974) suggests that the major features of the spatial structure of circulation that relate to disposal of waste materials in shelf waters of the New York

Bight are as follows:

(a). In the immediate vicinity of the entrance to the Hudson and Raritan Rivers estuary, the oceanographic regime is dominated by discharges from these rivers. As in all such estuaries, there is a seaward flow of brackish water in near-surface layers. At sea, this discharge turns to flow southward, paralleling the New Jersey shoreline. Lower in the water column, there is return flow of external water into the estuaries. In spite of its importance in the oceanographic and ecological systems of the estuaries and bight, this superposed flow system is to be recognized in measurements only as a slight imbalance of the much stronger ebb and flood tidal currents in the respective layers.

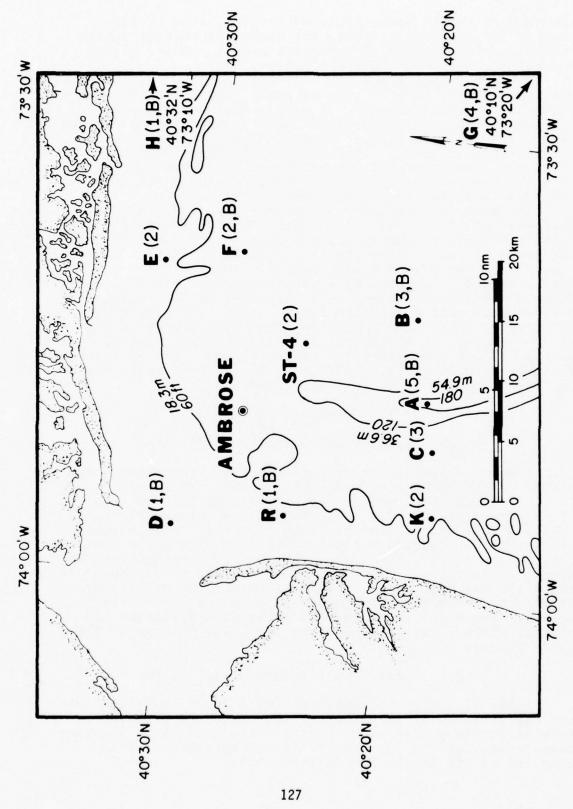
(b). There is strong evidence that outside the region of strongest influence of river effluent, there is persistent clockwise circulation. In its most inshore portion, off New Jersey and Long Island, this flow runs counter to the general flow over the continental shelf adjacent to this part of the coast. Although its existence in some areas of critical interest relative to ocean dumping is strongly supported by historic data, its horizontal extent and vertical

structure are imperfectly known at present.

This picture, which represents present understanding of apex water circulation, is inadequate. Consequently, first efforts of the MESA New York Bight Project were designed to supply data from fixed-level current meters to improve understanding of this aspect of the physical oceanography. Structure of spatial variability of the kinematics within the New York-New Jersey area has been the prime focus of the current observation; temporal variability seriously complicates this investigation. This report summarizes results obtained from the first two phases of the current meter measurements which were conducted from August through December 1973.

## 2. DIRECT CURRENT MEASUREMENTS IN NEW YORK BIGHT APEX

During the first field year of the MESA New York Bight Project, a major effort was made to collect background data on water movement in the apex. Measurements were made to provide data on mean currents as well as temporal and spatial variations in circulation in the region surrounding the dumpsites. One objective of the current meter array was to provide data to test the hypothesis of clockwise circulation in the apex. To meet these objectives, the main placement of recording current meters occurred in transects perpendicular to the New York and New Jersey shores. Current meter stations were also placed (a) in the Sandy Hook-Rockaway transect; (b) adjacent to Long Island, east of the main set of stations; and (c) about 55 km southeast of the harbor mouth. A summary of station locations and designations is given in figure 1.



Station locations for the MESA current meter measurement program conducted in August-December 1973. Figure 1.

The numbers within parenthesis adjacent to some of the station designations indicate the number of current meters placed at each station; B indicates a bottom meter placed

approximately 100 cm above the bottom.

Aanderaa model RCM-4, internally recording current meters, were used exclusively in this program. For these measurements, a 10-min sampling interval was used. With the exception of stations having a single current meter, the stations were of the taut-wire, subsurface-float design. A sketch of a typical mooring is in figure 2. On several stations, a current meter was placed so that the rotor was 1 m above the bottom. For this purpose a modified version of the standard Aanderaa,

called an inverted meter, was used.

The array of stations was occupied twice during the last half of 1973: Phase I. August-September; and Phase II. October-December. Maximum period of sampling for each phase was about 45 days. Near the end of Phase I, station ST-4 was placed near the sewage sludge dumpsite and obtained a 2-week record concurrent with the main array. Table I summarizes mooring information and record lengths for acceptable observations made during these two phases. Station R was deployed in support of a Radio Isotope Sand Tracer (RIST) study conducted in November. The RIST study, conducted by the Marine Geology and Geophysics Laboratory of AOML, is described elsewhere (Swift et al., 1975), but the current meter record has been included in the present analysis.

#### CURRENT METER DATA

### 3.1 Phase I Environmental Conditions

Phase I observations were made during late summer, a period during which apex water historically is strongly stratified (Charnell and Hansen, 1974). As part of this program, two cruises for collecting water column data at 25 stations were made while the Phase I stations were occupied. The salinity-temperature-depth (STD) data from these cruises (Hazelworth et al., 1974) show that a strong pycnocline, due primarily to thermal stratification, existed about midway in the water column; there was a progression from multilayer structure at the beginning of Phase I to two well-defined The majority of current meter data collected as part of Phase I was obtained from the lower portion of the water column.

### 3.2 Phase II Environmental Conditions

Phase II current measurements were begun in late October and completed early in December. For these observations, several stations were added to the Phase I array to increase measurement density in those transects perpendicular to Long Island and to the New Jersey coast.

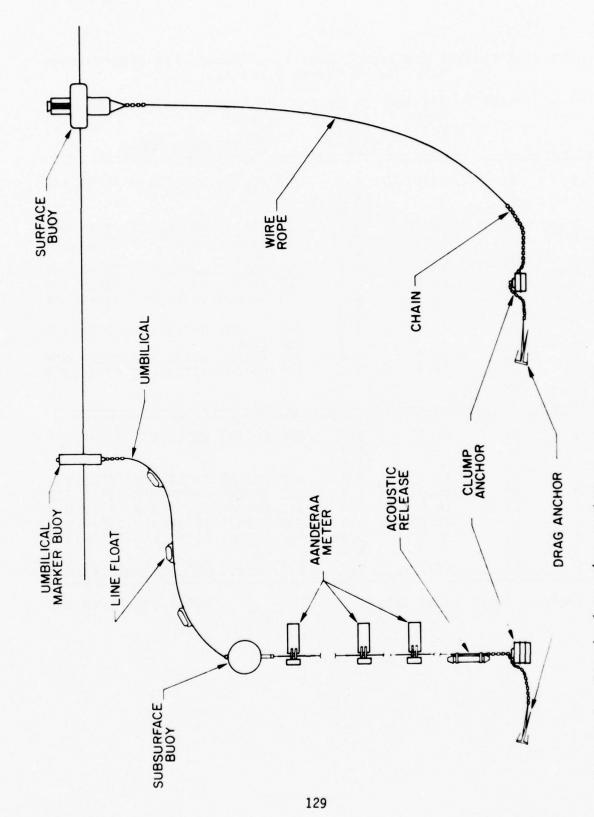


Figure 2. Standard mooring system.

Station	Meter #	Station depth (m)	Distance from bottom (m)		40-hr 1; start time (GMT)(J	p Coordina	
A	A1 A2 A3	44.9	8.9 14.9	239	(0000)	40°19.4'N	73°47.8'W
B C	B1 C1	25.9 23.8	25.0 8.9 2.7	239 240		40°20.0'N 40°18.4'N	73°43.5'W 73°51.5'W
Phase	C2 D1 E1 F1	10.0 16.5 23.5	8.6 0.9 7.6 0.9	246 247 247	(0000)	40°29.7'N 40°32.0'N 40°28.2'N	73°56.7'W 73°40.9'W 73°40.0'W
G	F 2 G 1 G 2	37.6	8.9 3.1 15.2	265 251	(0000) (0000)	40°10.2'N	73°24.8'W
H ST-4	H1 41 42	24.7	8.9 2.7 11.0	252 271		40°33.4'N 40°25.0'N	73°10.6'W 73°45.1'W
A	A1 A2	46.1	0.9	300	(0000)	40°19.0'N	73°48.0'W
D C D	A3 C1 D1	22.9 10.3	14.9 8.6 0.9	300 301	(0000)	40°18.4'N 40°29.7'N	73°50.9'W 73°56.7'W
Phase X 4 E E	E1 F1 K1	16.5 22.9 20.1	2.7 8.9 0.9	301 301 300	(0000) (0000) (0000)	40°32.0'N 40°28.4'N 40°18.0'N	73°41.0'W 73°40.0'W 73°55.0'W
R	K2 R1	13.7	8.9	319	(0000)	40°25.0'N	73°56.0'W

Ambrose Tower (wind data)

40°27.6'N 73°49.8'W

Observations made during Phase II occurred after the apex water had reached a nearly homogeneous condition, indicative of winter character. Historical data suggest this breakdown of stratification occurs early in October and homogeneous conditions exist until January with a gradual cooling. Data from STD casts made during Phase II (Hazelworth et al., 1974) show apex water to be conforming to these general conditions.

# 3.3 Initial Data Processing-Filtering

Data from both phases were filtered to remove noise and partition the series into three frequency bands. Three basic filters were used: 3-hr low-pass, 40-hr low-pass, and 40-hr high-pass. Figures 3a and 3b show the response for both 3-hr and 40-hr low-pass filters. It should be mentioned here that all useable data were included. Those stations excluded such as I and J (not discussed) were either too short (2 days or less), had a poor signal-to-noise ratio, and/or large gaps in the speed or direction data. The 3-hr low-pass filter was used to smooth the raw data and to resample the time series into a more convenient number of points; the filtered series were resampled every hour. In addition, the data were partitioned into low and high frequency time series, so that low and high frequency processes could be examined separately. A period of 40 hr can be used to distinguish conceptually between low and high frequency processes by excluding frequencies with periods less than 2 days. The 40-hr high-pass data include tidal and inertial frequencies by admitting frequencies with periods less than 2 days but longer than 3 hr. A summary of results from these filter operations is presented in table II.

# 3.4 Character of Low Frequency Variations in Flow

Figure 4 shows the mean current vectors for Phase I. The vectors represent net movement in the lower portion of the water column over the entire observational period. Record lengths and statistics associated with each station are given in table II. Figure 5 relates selected data from the inner stations to the offshore station G during Phase I. Figure 6 shows the mean current vectors for apex stations occupied during Phase II. These data support the hypothesis of anticyclonic circulation in the low frequency component for flow in the apex. Data for station D in both phases show a net bottom outflow, contrary to what might be expected from estuarine circulation principles. This result is probably due to the stations not being located in Ambrose channel but atop the shallower area to the southwest.

channel but atop the shallower area to the southwest.

Mean speeds for Phase I are a reasonably consistent 4 to 10 cm/s. This speed is substantially below the instantaneous speeds characteristic of this period. The data records exhibit a high degree of variability due primarily to tides, but with winds dominating flow for significant portions of the

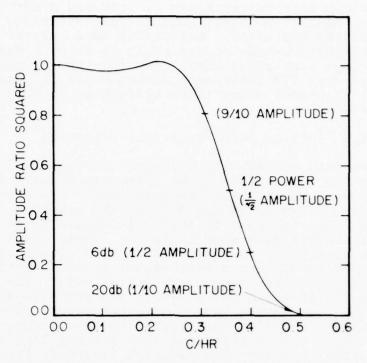


Figure 3a. Response of 3-hr low-pass filter.

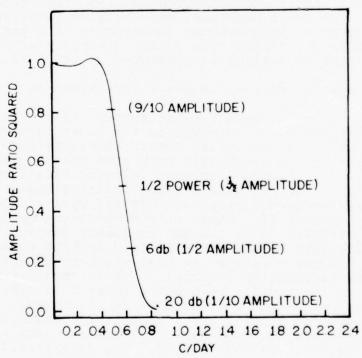


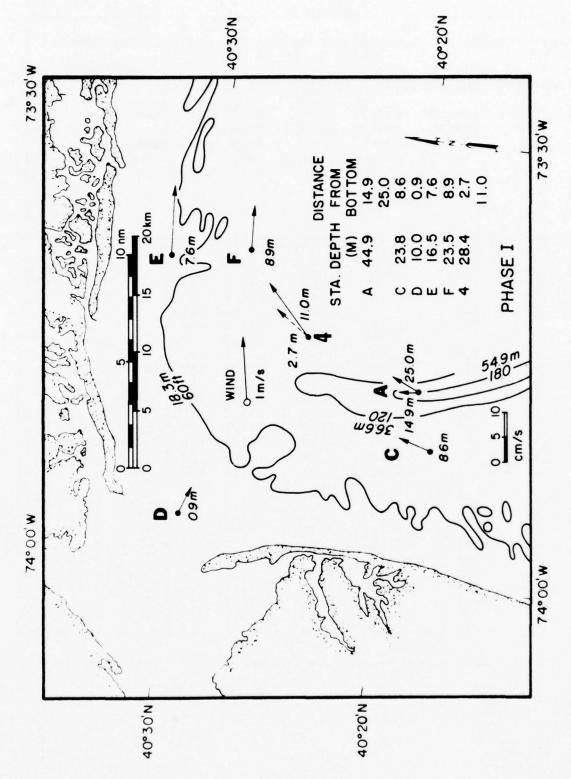
Figure 3D. Response of 40-hr low-pass filter.

Table II.

Record Lengths and Statistical Information for Each Station in Phases I and II.

Data below apply to 40-hr 1p and 40-hr hp series (  $\Delta t=1.0 \text{ hr}$ )

Sta.	Meter #	Record length # of pts.	cm/s mean com- ponen	com-	HPV high- pass vari- ance	LPV Squar- low- ed pass mean vari-speed ance	HPV: total vari- ance	
				Phase I				
A	A1	980	-0.33	-1.11	48.4	104.0 1.3	0.32	
	A2		1.88	0.26	59.3	119.5 3.6	0.33	49.7
	A3		4.22	1.75	104.9	67.4 21.0	0.61	8.2
В	B1	984		Distorted	by bad	data		
C	C1	956	-0.43	0.12	98.8	67.5 0.2	0.59	
	C2		5.49	1.55	214.9	115.2 32.5	0.65	10.2
D	D1	810	-1.03	3.93	540.8	17.9 16.5	0.97	33.8
E	E1	836	1.01	10.36	401.4	185.4 108.4	0.68	5.4
F	F1	837	0.34	0.86	33.8	13.3 0.9	0.72	55.8
	F2		0.44	6.40	383.2	168.4 41.2	0.69	13.4
G	G1	720	-0.90	-0.94	59.5	27.9 1.7	0.68	51.7
	G2	722	-3.99	-7.19	194.1	64.3 67.6	0.75	3.8
Н	Н1	694	-2.01	-0.18	381.6	116.6 4.1	0.77	
ST - 4	41	262	4.70	3.14	92.1	28.9 32.0	0.76	3.8
	42		6.62	6.94	297.6	106.9 92.0	0.74	4.4
		1000		Phase II		227 ( 27 0	0	
A	A1	1009	4.83	-0.77	32.5	223.6 23.9	0.13	10.7
	A2		7.06	-2.25	65.9	517.0 54.9	0.11	10.6
	A3	1011	16.76	-3.22	88.8	581.0291.3	0.13	2.3
C	C1	1011	9.22	-0.45	181.4	311.9 85.2	0.37	5.8
D	D1	911	-3.73	2.71	904.4	45.1 21.3	0.95	44.7
E	E1	980	2.10	7.24	139.6	221.1 56.8	0.39	6.4
F	F1	982	0.79	13.26	241.7	354.5176.5	0.41	3.4
K	K1	1011	2.70	-1.96	23.1	59.6 11.1	0.28	7.5
D	K2	100	7.74	1.67	189.6	297.8 62.7 23.0 61.5	0.39	7.8
R	R1	480	7.60	1.94	181.2	23.0 01.3	0.89	3.3



Mean current vectors for measurements during August-September 1973. Figure 4.

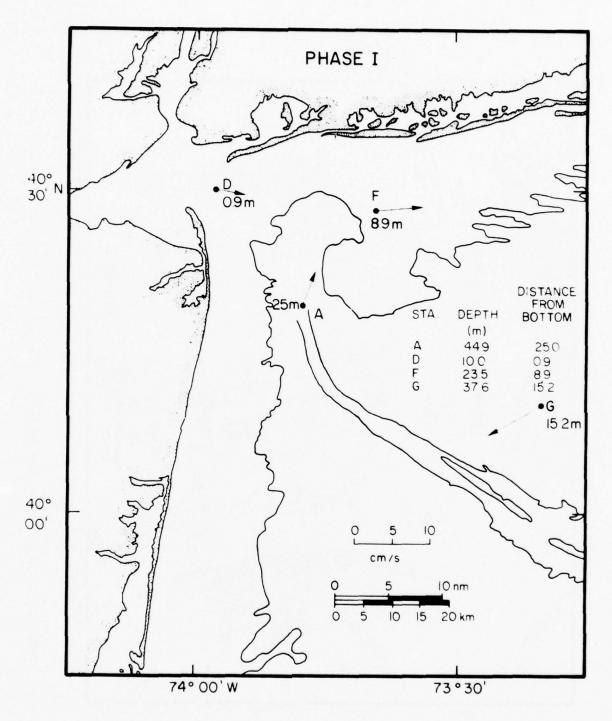
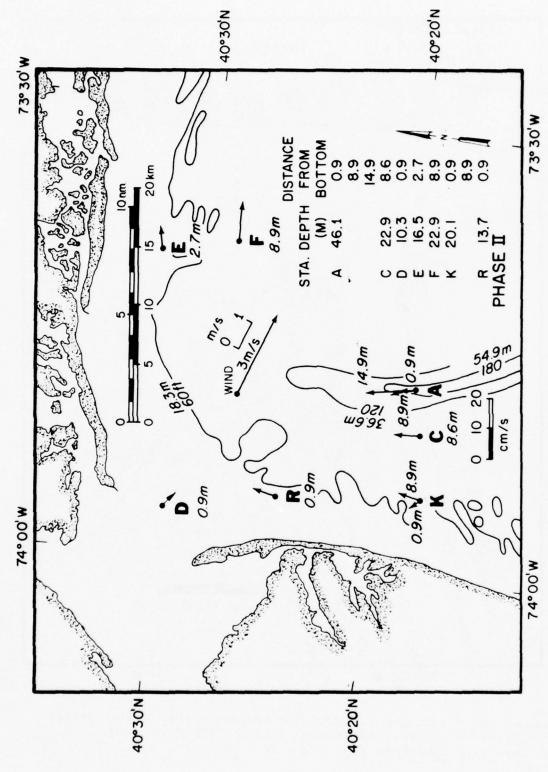


Figure 5. Mean current vectors for measurements during August-September 1973, relating outer station G data to data from selected apex stations (cf. fig. 4).



Mean current vectors for measurements during October-December 1973. Figure 6.

records. Characteristically, at station F, maximum speeds are about 50 cm/s, nearly an order of magnitude greater than the long-term mean.

Data from station H adjacent to Long Island show a weak mean speed (3 cm/s) and a direction of flow toward the southwest. This direction is consistent with shelf flow reflected by station G (fig. 5), but represents a reversal of the nearshore flow depicted by station F. During this measurement period, station H appears to occupy a position outside of the apex gyre. Station G data may not indicate the position of the southeast limb of the gyre, but do indicate that general long-term movement on the shelf is toward the southwest.

A preliminary examination of records from several levels at selected stations suggests that the effect of stratification on currents is significant. When a layered density structure exists (Phase I), the flow in various layers generally has different speeds and directions; during the nonstratified conditions, measurements at various levels on a single station generally show flow to be more uniform top to bottom. The mean vectors at station A for each phase show this quite clearly. This situation may be significant relative to competence of flow to erode or suspend particulate material in bight waters.

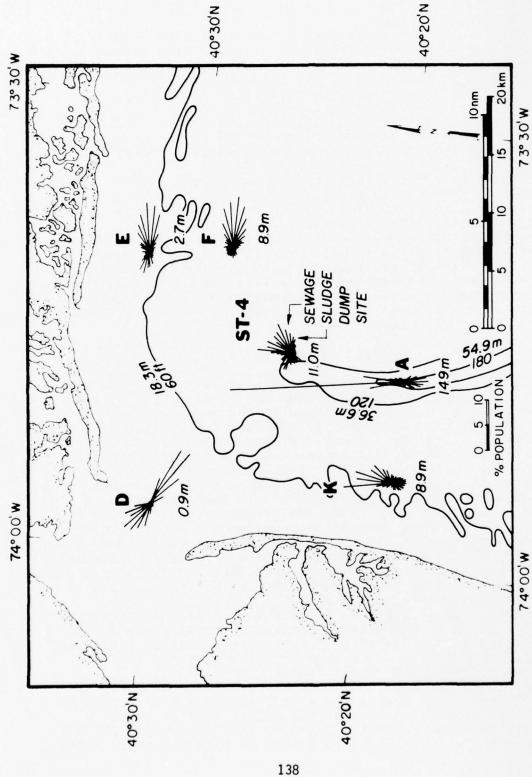
#### 3.5 Current Roses

While speeds representative of long-term mean flow are generally higher for Phase II than for Phase I, due to the higher level of wind energy input to the water column, direction for this component of the flow is not significantly different for the two periods. Figure 7 shows a summary of direction data for apex stations and is a composite of both phases; the number adjacent to each station indicates the height of the current meter above the bottom. These data include all periods greater than 3 hr. The histograms of figure 7, in polar form, show the frequency distribution of currents partitioned into 10-deg increments; the length of each line represents the percentage of the total record occupying that direction segment. Data taken from the transect denoted by stations A and K show that flow is generally northward, while for the Long Island transect (stations E and F) flow is predominantly eastward.

Comparison of stations E and F indicates that further offshore there is a greater tendency for cross-contour flow than at the inner stations. Strong directionality exhibited by data from station A can probably be attributed to its

location in the Hudson Shelf Channel.

Although the station at the sewage sludge dumpsite was not reoccupied during Phase II, its Phase I direction data have been included for comparison. This station exhibits bimodal direction character; favored flow directions at this site are to the northeast, in agreement with clockwise flow,



Data Direction histograms for apex stations during both Phases I and II. have been 3-hr low-pass filtered. Figure 7.

and to the northwest, perhaps associated with an estuarine bottom flow into the mouth of the Hudson Estuary.

Data presented in figure 7 have been 3-hr low-pass filtered, but otherwise reflect both low and high frequency processes. The roses tend to show a structure similar to that seen in the mean current vectors of figures 4 and 6. The high frequency component of flow can be examined in a display similar to figure 7, but using the high-pass component of each record. Figures 8, 9, and 10 summarize direction data for the high frequency processes; the figures display histograms for the 40-hr high-pass time series. There are two figures for Phase I; figure 8 shows roses for the current meters nearer the surface, and figure 9 displays the roses for the current meters nearest the bottom. Because low frequency direction data are not included in these current roses, each rose is basically symmetric about a major axis. By comparing figures 8 and 9, it can be seen that the frequency distributions of direction data exhibit a rotation of the major axis with depth. This feature occurred at a time when the water column was strongly stratified.

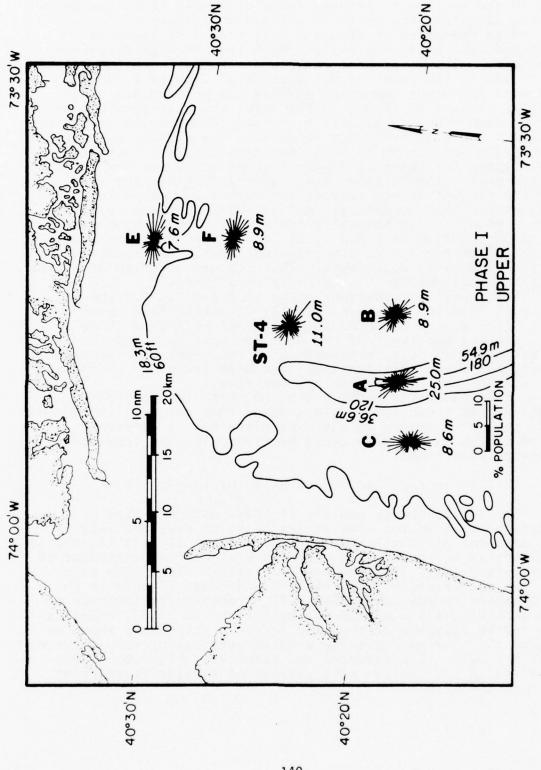
Frequency distributions shown in figure 10 for the Phase II data are not significantly different from Phase I data. There were a few additional stations during Phase II. By comparing the roses of the 3-hr low-pass data and the 40-hr high-pass data, orientation of the major axis appears to shift; for almost all stations, the high frequency component

has a stronger tendency for onshore flow.

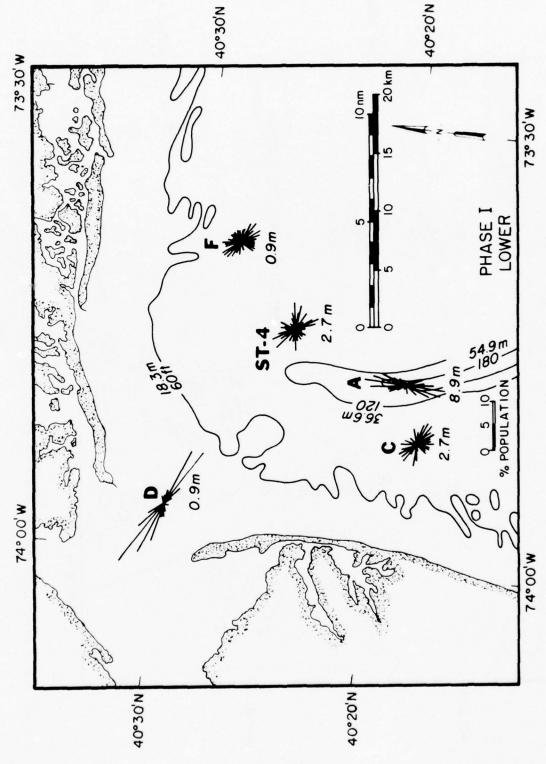
It should be noted also that no phase information is contained in these roses. This means that material introduced into the water column at the same place but at different times in the tidal cycle could be transported in completely opposite directions.

# 3.6 Vector Time Series of 40-Hr Low-Pass Data

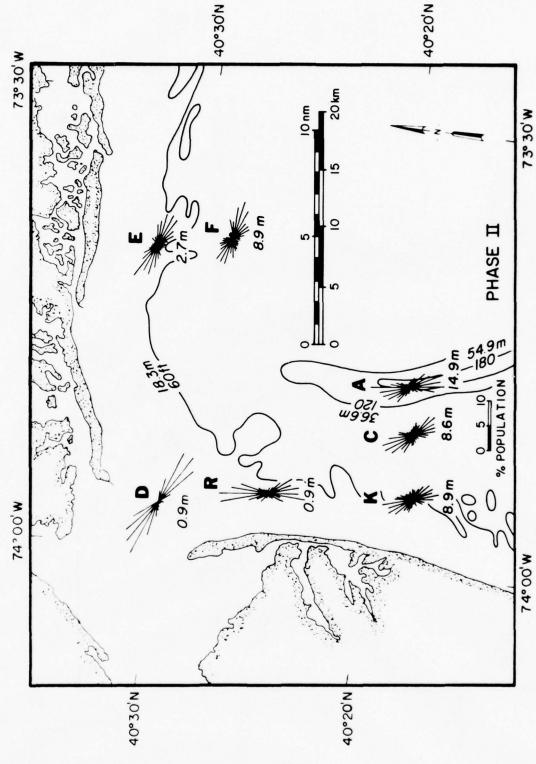
The low frequency content of these data can also be displayed as a vector time series or stick diagram. All of the stations off the New Jersey shore (fig. 11, 12, 13, and 14) show mostly northward flow, and the stations perpendicular to Long Island (fig. 15) show mostly eastward flow. The most obvious difference between Phase I and Phase II data is the much higher speeds during Phase II, probably attributable to the much higher windspeeds during the second phase, Progressive vector diagrams of the wind for both phases are shown in figure 16. During Phase II, a major reversal of flow occurred near Day 305. This reversal and associated high speed were observed in conjunction with passage of a major storm front through the area.



Direction histograms of 40-hr high-pass data for Phase I measurements in the upper portion of the water column.



Direction histograms of 40-hr high-pass data for Phase I measurements in the lower portion of the water column. Figure 9.



Direction histograms of 40-hr high-pass data for Phase II measurements. Figure 10.

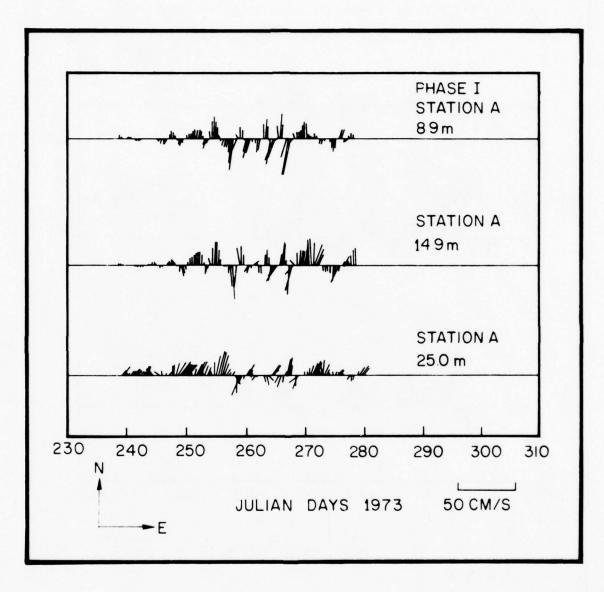


Figure 11. Vector time series of 40-hr low-pass data from station A during August-September 1973.

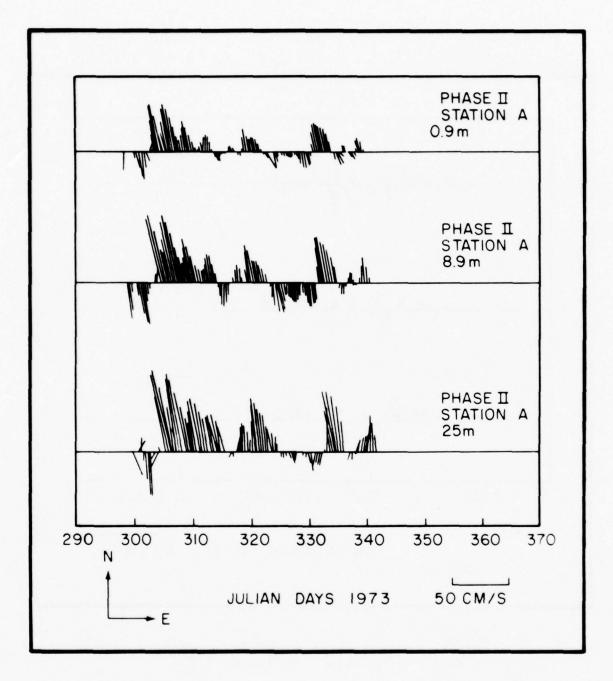


Figure 12. Vector time series of 40-hr low-pass data from station A during October-December 1973.

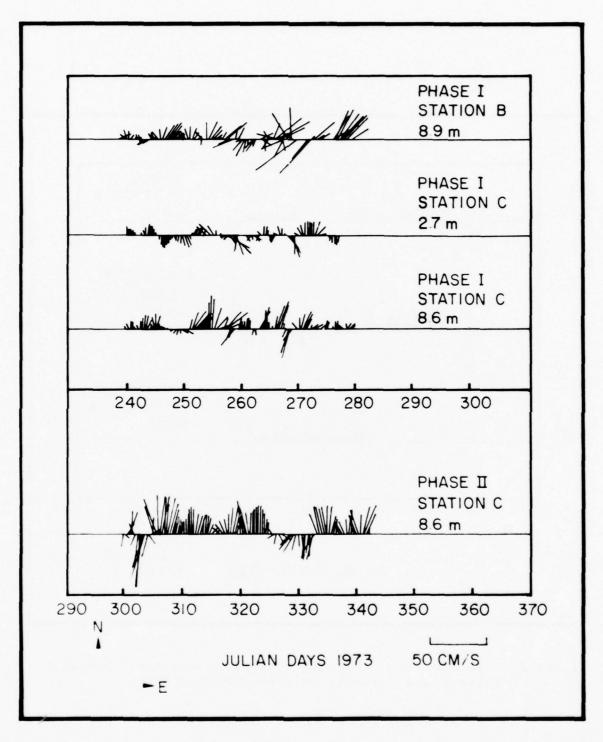


Figure 13. Vector time series of 40-hr low-pass data from stations B and C from August-September 1973 and from station C during October-December 1973.

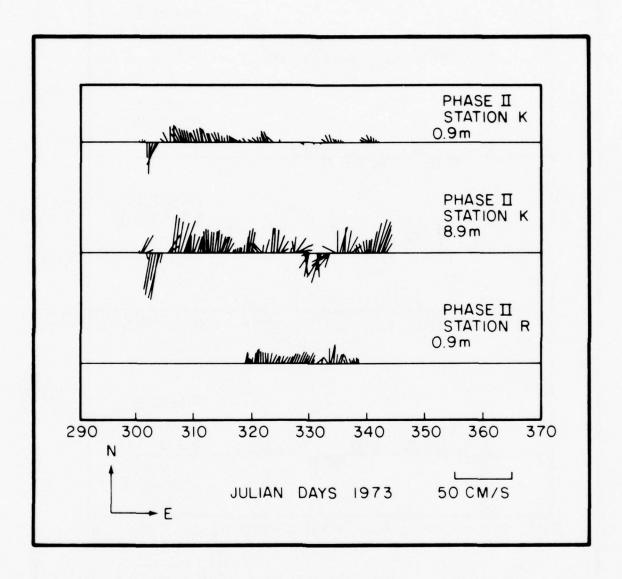


Figure 14. Vector time series of 40-hr low-pass data from stations K and R during October-December 1973.

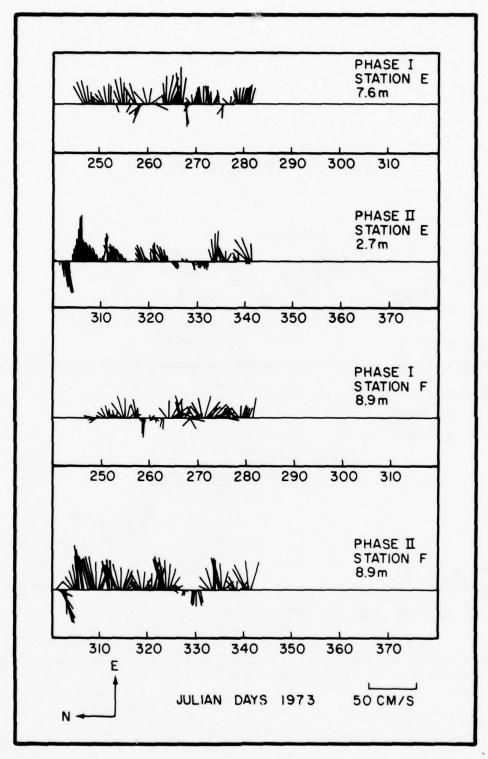
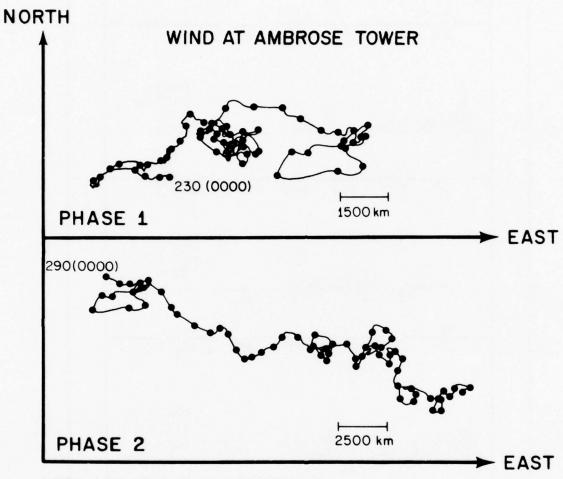


Figure 15. Vector time series of 40-hr low-pass data from stations E and F for both Phases I and II.



# DOTS ARE AT ONE DAY INTERVALS

Figure 16. Progressive vector diagrams of wind data taken at Ambrose Light Station during Phases I and II. Indicated start times are in Julian Days and Eastern Standard Time.

# 3.7 Temporal Variability of Flow

One of the more difficult oceanographic concepts to convey is the distribution of temporal variability in ocean currents. A useful technique for displaying amount and type of flow variability is the energy spectrum. An example of the energy spectrum for station F is shown in figure 17. The curves denoting energy in the east component of flow at station F for Phases I and II are typical of nearshore current measurements in the bight. The major features of these functions are the peaks that occur near periods of 12 hr, 19 to 25 hr, and at the left-hand limit. Respectively, these peaks are associated with semidally tides, a mixture of inertial currents and daily tides, and longer period variations normally associated with meteorological events amounting to several days. Each of these time scales plays a particular role in the movement of waterborne materials. In general terms, the effect of energetic currents of high frequency is to create turbulence and maintain materials in suspension, but not necessarily to transport or disperse them over long distances. Advective transport is affected by low frequency processes.

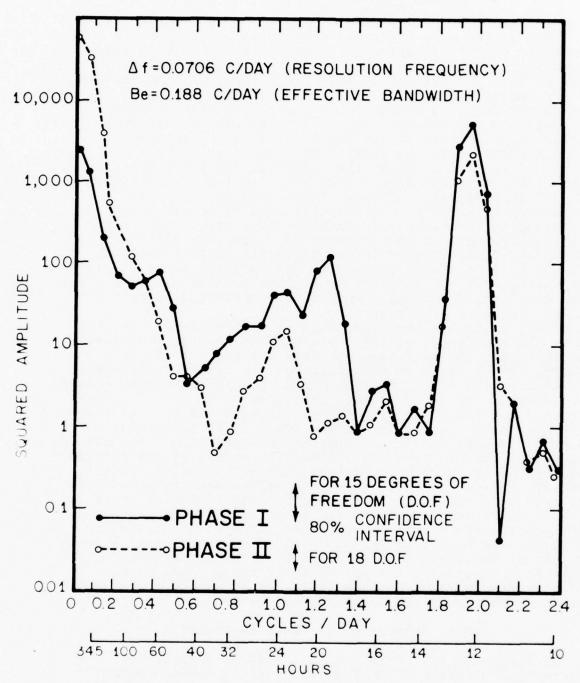
Variability of the water motions in the apex is reflected by the statistics of the current meter records, tabulated in table II. The variances computed are the sum of the squares of the standard deviations of the velocity components for each of the 40-hr low-pass and 40-hr high-pass time series. In addition, the ratio of high-passed variance (HPV) to total variance and the ratio of total variance to the squared mean speed are also given. The latter ratio is of particular interest in analyzing the dispersion of materials. For station F spectra shown in figure 17, about 70 percent of the current variance occurred at periods less than 40 hr during Phase I. However, during Phase II, these higher frequencies accounted for only 40 percent of the current variance. During Phase II, a similar frequency distribution of current energy was found at the nearshore station K. However, at station A, further offshore, the high frequency portion of current energy is only 30 percent for Phase I, then drops to about 10 percent for Phase II. Generally, for all of these data, there is a shift from high frequency dominance for nearshore stations to

# low frequency dominance for offshore stations.

## 3.8 Coherence and Phase Estimates

The apparent steady-state anticyclonic gyre poses interesting questions: What is the spatial coherence and phase of the low frequency motions in the gyre?; and what, if any, relation does the wind have to the dynamics of the apex circulation? To obtain a quantitative description of the low frequency kinematics in the apex, cross spectra, coherence, and phase were computed for the east component of wind and the selected stations A, K, and F. Wind data were

# STATION F (EAST COMPONENT)



INERTIAL PERIOD = 18.5 hr AT 40° 30' N f1 = 1 30 C/DAY

Figure 17. Energy spectra for east component of current measurements at station F for both Phases I and II.

obtained from the standard observations made at Ambrose Tower every 6 hr. Figure 18, summarizing these computations, shows that there are two important frequencies associated with wind forcing. The left-hand column in figure 18 shows the cross spectrum, cross phase, and coherence squared for the east component of wind and the north component of currents at station A during Phase I. The east component of wind is used for coherence and phase analysis because, for the Ambrose data, most wind energy is in the east component. There are two peaks in the cross spectrum; periods corresponding to these peaks are approximately 4 and 7 days. Motions at station A lag the wind by approximately 12 hr for the 7-day period and about 18 hr for the 4-day period. The most significant coherence is approximately 0.7 for the 4-day period. Coherence in the Phase I data suggests that water in the vicinity of station A responds to eastward winds with northward flow; in general, the gyral circulation within the apex seems to be a wind-induced phenomenon.

The center and right-hand columns of figure 18 show for Phase II the cross spectra, cross phase, and coherence squared between the north components of stations A and K and between the north component of K and east component of F, respectively. These data show coherence squared greater than 0.75 for periods greater than 5 days. Additionally, phase differences are negligible. These data indicate that, for the space scale of the apex array, Phase II motions are coherent for frequencies less than those near 0.2 cycles/day.

#### 4. RECAPITULATION

During the last half of 1973, direct current observations were made in the New York Bight Apex. These efforts produced 24 current meter records from in situ recording Aanderaa current meters. These records were partitioned into low and high frequency bands where each band was analyzed for temporal and spatial variability. These analysis produced the following observations:

(a) For the period August-December 1973, the mean flow within the apex consists of clockwise circulation with a

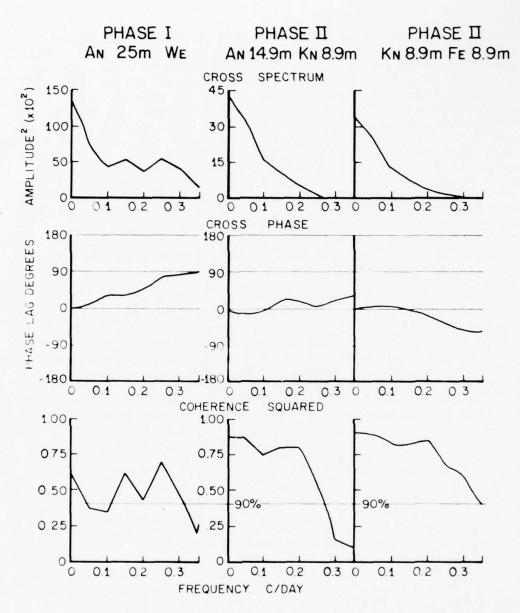
mean speed of approximately 4 to 10 cm/s.

(b) Low frequency component of flow is less depth dependent in the late fall when the water column is well mixed than during the summer when a well-developed two-layered system exists.

(c) Low frequency response of apex water to meteorological forcing is coherent over the apex with a phase lag of up to 18 hr. Coherence diminished markedly above 0.2

cycles/day.

(d) Spatial coherence over the study area (35 km) is high with negligible phase lag for frequencies less than 0.2 cycles/day.



BANDWIDTH = 0.067 C/DAY

DEGREES OF FREEDOM = 10.9 LAGS = 40.0

Δt = 6 HOURS

Figure 18. Cross spectra, phase, and coherence estimates for various combinations of wind and current data: (a) Left column: east component of wind and north component of current at station A during Phase I. (b) Center column: north components of currents at stations A and K during Phase II. (c) Right column: north component of current at station K and east component of current at station F during Phase II.

#### ACKNOWLEDGMENTS

Field operational aspects of this program were carried out in part by the officers and crew of the NOAA ship Ferrel. MESA was responsible for logistic and maintenance support; NOIC for calibration; EDL for mooring-design field testing and meter acceptance criteria; and NOS, Rockville, Md., for initial data conversion. Dave Brooks of the University of Miami assisted with time series calculations. This work was supported in part by the Environmental Research Laboratories and the Marine Ecosystems Analysis Program of the National Oceanic and Atmospheric Administration.

#### 6. REFERENCES

- Bumpus, D. F. (1973): A description of the circulation on the continental shelf of the east coast of the United States, in Progress in Oceanography, vol. 6, Pergamon Press, New York City, N. Y., 111-157.
- Charnell, R. L., ed. (1975): Assessment of offshore dumping; technical background, NOAA Technical Memorandum ERL MESA-1, Marine Ecosystems Analysis Program Office, Boulder, Colo., 83 pp.
- Charnell, R. L., and D. V. Hansen (1974): Summary and analysis of physical oceanography data collected in the New York Bight Apex during 1969-70, MESA Report No. 74-3, U. S. Govt. Print. Off., Washington, D. C., 44 pp.
- Hazelworth, J. B., B. L. Kolitz, R. B. Starr, R. L. Charnell, and G. A. Berberian (1974): New York Bight Project, water column sampling cruises #1-5 of the NOAA ship Ferrel, August-November 1973, MESA Report No. 74-2, U. S. Govt. Print. Off., Washington, D. C., 191 pp.
- Swift, D. J., A. Cok, D. Drake, G. Freeland, W. Lavelle, T. McKinney, T. Nelsen, R. Permenter, and W. Stubblefield (1975): Geological oceanography; sedimentation in the New York Bight Apex and application to problems of waste disposal, in Assessment of Offshore Dumping; Technical Background: NOAA Technical Memorandum ERL MESA-1, Marine Ecosystems Analysis Program Office, Boulder, Colo., 16-61.

# The interaction between curvature and lateral shear vorticities in a mean and an instantaneous Florida Current, a comparison

By FRANK CHEW, Atlantic Oceanographic and Meteorological Labs., Environmental Research Laboratories, NOAA, Miami, Florida 33149, USA

(Manuscript received March 12, 1974; in final form Jan. 9, 1975)

#### ABSTRACT

The question of how much of the dynamics of an instantaneous current is retained in the dynamics of a model derived from its mean structure is considered in terms of a comparison between two case studies of the Florida Current. In the mean model, fluid elements are restrained from crossing the speed axis. But in an observation of an instantaneous current there was an interaction between curvature and lateral shear vorticities accompanied by a systematic movement of fluid elements across the speed axis. This difference is considered from two points of view. The first is that of the equations governing the interaction process, particularly the banking mechanism that converts curvature vorticity to lateral shear vorticity and vice versa. The second is that of the dynamics of the geostrophic potential vorticity. It is concluded that, because of the imposed geostrophic constraint, the mean model does not retain the interaction process.

#### Introduction

The most concise statement of the dynamics of an adiabatic, inviscid flow is the law of conservation of potential vorticity. However, for diagnostic studies the relative vorticity equation is more useful because it brings out the mechanisms that change the relative vorticity. In this sense, the curvature and lateral shear vorticity equations derived by Chew (1974) are even more useful because they bring out the mechanisms that govern the individual change of curvature and lateral shear vorticities separately. One of these mechanisms induces interaction between the curvature and lateral shear vorticity. The purpose of this paper is to detail a manifestation of the interaction and to compare the manifestation in two studies of the Florida Current. One is the model of a mean current constructed by Schmitz (1969), and the other is an instantaneous current observed by Chew (1974).

In the special case of a fluid element situated initially in the instantaneous speed axis of a meandering current at the point of inflection, the process of interaction takes on a unique

form. An observer riding with the element will find the speed axis of the current alternately forming to his left and right depending on the sign of the flow curvature. Equivalently, an observer using the changing location of the speed axis as a reference will find the fluid element moving across the speed axis. This crossing of the axis is related to a characteristic cross-stream distribution of potential vorticity. Hence the comparison of the interaction process may be phrased in terms of potential vorticity conservation. But the mere satisfaction of the conservation law does not imply an identity or even a similarity in dynamics. For the law applies equally, e.g., to both linear and nonlinear regimes. Our consideration of the interaction process in the context of the conservation law will serve also to illustrate this point.

The mean model constructed by Schmitz was based on data collected over a 30-day period in 1965 in a segment of the Florida Current downstream of the segment observed by Chew in a 5-day period in 1971. These differences in time and place are assumed immaterial on the premise that the dynamics of the Florida Current remained unchanged.

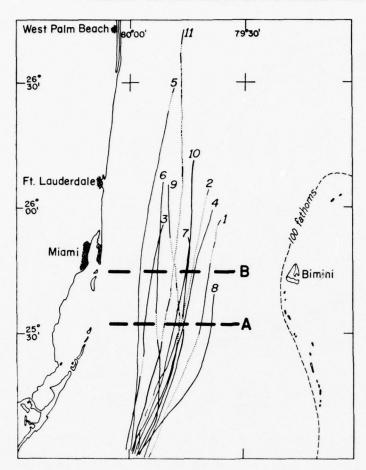


Fig. 1. The two dashed lines A and B mark the locations of velocity and density observations made by Schmitz in the period 24 May to 24 June, 1965. The curvilinear lines 1 to 11 mark the paths of shallow drifting drogues made by Chew & Berberian in the period 15 February to 9 March, 1969.

First the model of the mean current is summarized and the features of interest identified. Next, comparable features for the instantaneous current and their interpretation from the viewpoint of potential vorticity conservation are presented. To explain the dynamics involved, the formulation of the equations that govern the individual change of curvature and lateral shear vorticities separately are next reviewed. Finally, by use of these equations the limitations of the dynamics of the mean model are shown.

Tellus XXVII (1975), 6

# Potential vorticity in a mean Florida Current

From a series of velocity and density measurements taken along the two lines labelled A and B in Fig. 1, Schmitz constructed a model of a mean Florida Current in terms of a single moving layer whose thickness, H, he identified as equal to the thickness of the surface layer with a vertically averaged sigma-t of 25.0. Fig. 2 shows his cross-stream distribution of the thickness of the layer and its corresponding

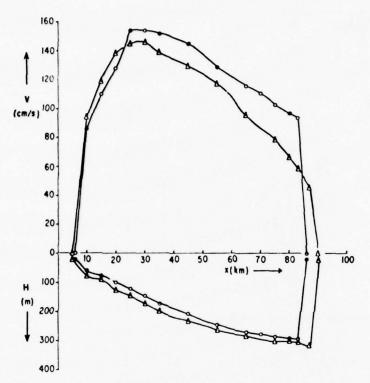


Fig. 2. Downstream speed (v) and layer depth (H) vs. cross-stream distance (x). Triangles for section A and circles for section B as shown in Fig. 1. Reproduced from Schmitz (1969).

downstream speed. The feature of direct interest is the locations of the speed axes between 25 and 30 km.

For the one-moving-layer model, the potential vorticity of an individual column is the ratio of its absolute vorticity to its thickness, H. The absolute vorticity is a sum of the vertical components of the planetary and relative vorticities. Because his data did not permit an adequate evaluation of the significance of the curvature vorticity, Schmitz made the assumption of equating the relative vorticity to the lateral shear vorticity alone. Using this assumption and the distribution of variables in Fig. 2, Schmitz computed the potential vorticity at different locations along the two lines to obtain the cross-stream distributions shown in Fig. 3, whose principal feature is that east of km 30, the distributions of potential vorticity are relatively uniform, but that to the west of km 30, in the regions of both the speed axes and the left flanks the distributions show a steep rise in potential vorticity. In a regime where potential vorticity is conserved, fluid elements with a given potential vorticity may move only to regions where the potential vorticity is the same. In the right flank east of km 30 in Fig. 3, if the small cross-stream variation in potential vorticity may be ignored, individual columns there can move laterally without constraint. However, in the regions of both the speed axis and the left flank, because of the large change in potential vorticity, individual columns in these regions are constrained to remain in their relative lateral positions. In consequence, there can be no flow across the speed axis. The comparison centers on the determination of whether or not this consequence holds also for an instantaneous Florida Current. The direct way to find out is to observe the lateral movements of individual parcels relative to the instantaneous speed axis.

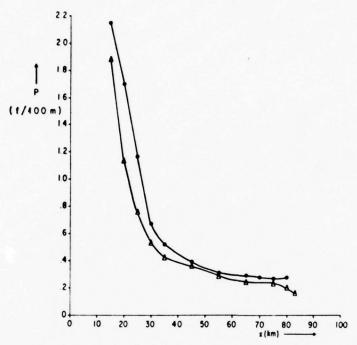


Fig. 3. Potential vorticity (P) vs. cross-stream distance (x). Triangles for section A and circles for section B as shown in Fig. 1. Reproduced from Schmitz (1969).

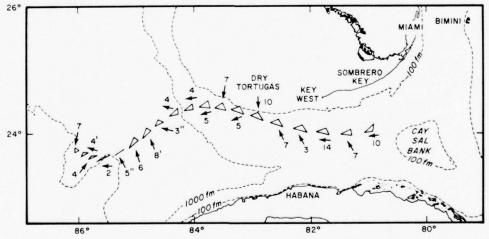


Fig. 4. Path of drogue formation and encountered winds in the observation of 1971. Individual drogues located at the vertices of the triangles spaced six hours apart. The time for the first triangle is 0000 hr (Universal Time), August 27. Arrows represent directions of winds as observed from the drogue-tracking ship, and numerals give wind strengths in knots, both corrected for ship drift. The time of each plotted wind corresponds to the time of the nearest plotted drogue formation, with the exception of four cases indicated by numerals with prime and double primes. The single prime cases are off the indicated time by one hour, the double primes cases two hours.

Tellus XXVII (1975), 6 39 – 752898

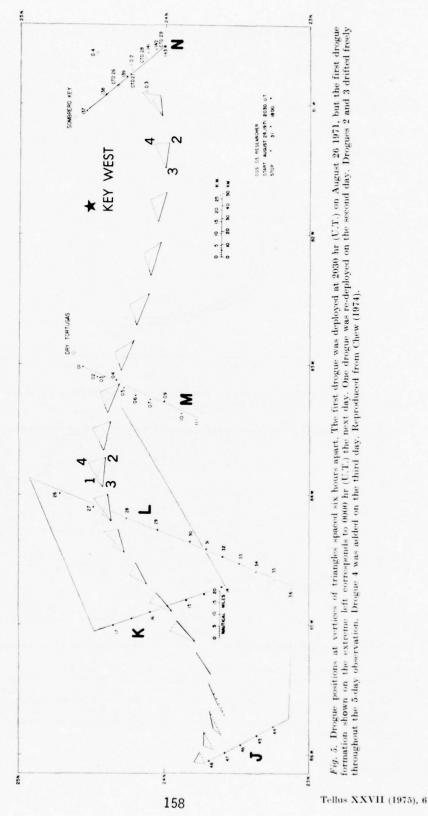


Fig. 5. Drogue positions at vertices of triangles spaced six hours apart. The first drogue was deployed at 2030 hr (U.T.) on August 26 1971, but the first drogue formation shown on the extreme left corresponds to 0000 hr (U.T.) the next day. One drogue was re-deployed on the second day. Drogues 2 and 3 drifted freely throughout the 5-day observation. Drogue 4 was added on the third day. Reproduced from Chew (1974).

However, we anticipate that measurement uncertainty and interference of other processes will render the observation imprecise, and that in conjunction with observation it is necessary as well to consider the general interaction process of which the crossing of the speed axis is but one manifestation. The observation is presented first.

## Observation of an instantaneous Florida Current

Figs. 4 and 5 summarize Chew's observation of the Florida Current by means of free-drifting drogues at a 40 m depth. Three drogues were initially deployed 200 km north of the Yucatan Strait as shown in Fig. 4, whose salient feature is the lack of significant downstream reduction in the meandering amplitude of the current in spite of large decreases in both the water depth and channel width. Shown in Fig. 5 for every six hours, are the drogue formations obtained by connecting simultaneous drogue positions with straight lines. Because all drogues presumably drifted at a constant depth, and because parcel motion is three-dimensional even in large-scale flow, the drogue formation did not track the same parcel throughout. But if the vertical advection is only a small part of the individual change, then the individual change is approximated well by the change in drogue formation. This is assumed; and in this context we shall refer to the tracking of a single parcel. The justification will be given later after the appropriate equations are presented. Moreover, the sign of the path curvature was observed, but according to Blaton's equation the observation also gives the sign of the stream-line curvature provided the current is quasi-steady. This is also assumed. In the reference frame of natural coordinates, with positive cross-stream direction to the left, the lateral shear is negative when, in a drogue formation, the drogues on the left lagged behind the drogues on the right; and the lateral shear is positive when the drogues on the right lagged behind the drogues on the left. Accordingly, in Fig. 5 where the curvatures were positive at the two cyclonic bends, the lateral shears were also positive, and where the curvature was negative at the anticyclonic bend the shear was also negative.1 Because these different sign combinations are

those of an individual parcel tracked by the drogue formation, the curvature and lateral shear of the parcel must turn zero somewhere between, say, the positive curvature and lateral shear at the cyclonic bend and the negative curvature and lateral shear at the downstream anticyclonic bend. Moreover, it is plausible that the curvature and the lateral shear both turned zero together. In Fig. 5 at the two inflection points near sections K and M where the curvatures were zero, the lack of significant change in the shape of the two successive six-hour drogue formations there indicates that the accompanying lateral shears were also zero. Hence the relationship is one of the sign of the lateral shear following the sign of the flow curvature.

Now, for simplicity, consider a meandering current with a single speed axis, a situation quite consistent with the temperature sections shown in Fig. 6 where cross-stream isothermal slopes are generally largest in the water columns supporting the drogue formations. In this case, negative lateral shear is confined to the left flank, and positive shear to the right flank. It follows that a drogue formation is in the speed axis when the shear is zero, in the left flank when the shear is negative, and in the right flank when the shear is positive. Accordingly, in following the movement of the parcel downstream from the inflection near section K in Fig. 5, we see that the parcel moved off the speed axis and entered the left flank on approaching the anticyclonic turn. Then on moving out of the anticyclonic turn, the parcel also moved laterally out of the left flank and re-entered the speed axis as the curvature of the path became zero at the inflection point downstream of section M. Finally, on approaching the cyclonic turn, the parcel again moved laterally off the speed axis, but this time into the right flank. Thus the parcel elements crossed the speed axis systematically. This is in sharp disagreement with the requirement contained in the model presented by Schmitz. Before explaining the disagreement, attention will be given first to the likely effects of local winds on the drift of the drogues and of the

<sup>&</sup>lt;sup>1</sup> In Fig. 20 in the paper by Chew (1974) the speed differences at the anticyclonic bend show a positive shear. This is discounted here, because errors in speed estimates are 10 cm/s, and there is also the possible presence of a local interfering phenomenon.

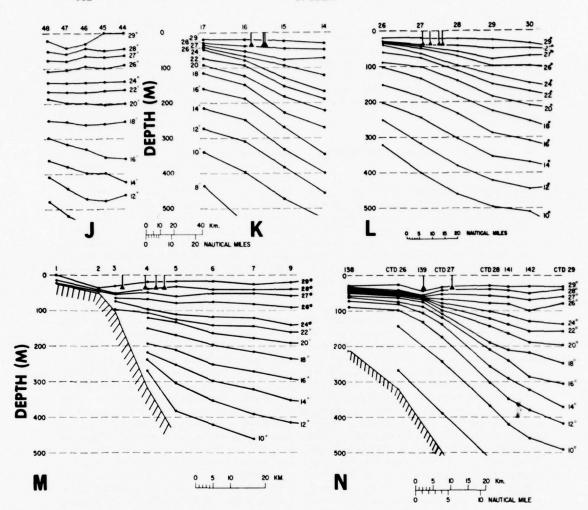


Fig. 6. Temperature distribution along sections J, K, L, M and N shown in Fig. 5. Adapted from Chew (1974).

downstream channel constriction off Miami on the interaction between curvature and lateral shear there.

#### Wind effect and channel constriction

Some of the local winds observed from the drogue-tracking ship while drifting with the current are shown in Fig. 4. The winds encountered were generally light. So light that in

a direct test of wind effect on drogue systems with different surface buoys, Chew (1974) found these winds to have essentially the same effects even though the sail areas of the buoys were much different. Strong and persistent winds can be an important source of error, but a typical wind strength in Fig. 4 is only 7 knots. According to a diagram given by Brown (1959), the approximate effect of a 7-knot wind is to drag the drogue system through the water at 1.7 cm/s. This is small compared with the

spend of the current. Moreover, since the wind directions were variable and bear no apparent relationship to the large systematic lateral movement of the drogues, the winds encountered may be dismissed as a significant factor in the observed interaction.

As shown in Fig. 1, there is a channel constriction in the region where Schmitz constructed his mean model. The question is, does the constriction effectively suppress the interaction between curvature and lateral shear, and hence the crossing of the speed axis? There is reproduced in Fig. 1 from the work of Chew & Berberian (1972), the mean paths of eleven lines of three drogues each. The lines, all starting from a common area, were each tracked for about one day in the order in which they are numbered in the figure. As successive lines were tracked, the curvatures took on different signs and magnitudes as in the passage of a meander train. Detailed in the original work, but not reproduced here, are the lateral shears accompanying the flow curvatures. But primarily because these lines are short, the sign of the flow curvature is sometimes in doubt. But where the curvature sign is clear cut, as for lines 5, 8, 10, and 11 in Fig. 1, the sign of the shear clearly follows the sign of the curvature. This agreement in signs suggests the probability that had each line been tracked for a longer period, the interaction between curvature and shear in general, and the crossing of the speed axis in particular would have been more clearly delineated. Hence it is concluded that it is not the channel constriction, but an artifact of the mean model that suppressed the interaction. To understand the artifact, it is necessary first to understand the mechanism responsible for the interaction. And to emphasize the relation of the interaction to the general process that maintains the conservation of potential vorticity, we consider first a condition imposed by the conservation.

#### An imposed condition

In a natural coordinate system with geometric height as vertical axis, let the components of a three-dimensional velocity be written  $\mathbf{V} = V\mathbf{s}$  for the horizontal, and  $w\mathbf{k}$  for the upward component;  $\mathbf{n} = \mathbf{k} \times \mathbf{s}$  is positive to the left of  $\mathbf{V}$ . Hence in natural coordinates

(s, n, z, t), the vertical component of relative vorticity,  $\zeta$ , is given by

$$\zeta = K_s V - (\partial V / \partial n) \tag{1}$$

where  $K_s$  is the streamline curvature. In (1) the definition of lateral shear vorticity includes the negative sign; e.g., a flow with slower current to the left represents negative lateral shear but positive lateral shear vorticity. Then, with the usual assumption, the law of conservation of potential vorticity in the ocean may be written

$$(f+\zeta)/h' = constant (2)$$

where h' is the vertical thickness of a parcel element. When the constant is evaluated at a streamline inflection where values are denoted by the subscript "0", and use is made of eq. (1), eq. (2) may be expanded to give

$$\partial V/\partial n = K_s V + (f - f_0 h'/h'_0) + (\partial V/\partial n)_0 (h'/h'_0) \quad (3)$$

Hence for parcel elements initially in the speed axis at an inflection of a meandering current, eq. (3) reduces to

$$\partial V/\partial n = K_s V + (f - f_0 h'/h'_0)$$
 (4)

Therefore, in order that the sign of the lateral shear of the parcel follows the sign of its flow curvature, it is necessary and sufficient for the curvature term in (4) to have a magnitude larger than the Coriolis term. This condition may be rephrased. From eqs. (1) and (4) the term inside the parentheses is seen equal to the negative of the relative vorticity,

$$(f - f_0 h'/h'_0) = -\zeta \tag{5}$$

Consequently, the condition is equivalent to the following inequality in absolute magnitudes,

$$|K_s V| > |\zeta| = |K_s V - \partial V/\partial n| \neq 0 \tag{6}$$

where  $\zeta=0$  is excluded, for reasons that will be given later. Accordingly, in addition to the requirement of a sign difference between the curvature and lateral shear vorticities, the inequality (6) will hold when the absolute magnitudes of the individual change of the two vorticities are given by

$$|(D/Dt)(K_s V)| > |(D/Dt)(-\partial V/\partial n)|$$
 (7)

614 F. CHEW

Thus for a flow where potential vorticity is conserved, and for a parcel initially located in the speed axis at an inflection of the flow, the conditions (6) and (7) must be met, if the sign of the lateral shear is to follow the sign of the flow curvature. The two derivatives in (7) have been discussed by Chew (1974). These are first reviewed, starting off with the equation governing the individual change of curvature or turning vorticity, called the turning equation.

## The turning equation

The turning equation, whose derivation is detailed by Chew (1974), is

$$(D/Dt) K_s V = (\partial/\partial n) (DV/Dt) - (f + K_s V) \nabla \cdot \mathbf{V}$$
Banking Divergence
$$- K_s V (\partial V/\partial s) - Df/Dt$$
Curvature Beta (8)

The individual change of the turning vorticity is a function of four terms: the beta term; a curvature-acceleration term, a product of the curvature and the downstream acceleration; a divergence term, similar to the corresponding term in the relative vorticity equation but without the shear vorticity; and the banking term that involves the cross-stream change of the downstream acceleration, hence of the downstream pressure gradient force, and thus represents a pressure torque.

The banking mechanism has both barotropic and baroclinic components. The first is derived from changes in the height of the sea surface, and the second from changes in the subsurface density field. For steady state motion, the barotropic component of the banking term may be written,

$$(\partial/\partial n) (DV/Dt)_h = -(g/V)_h (\partial w/\partial n)_h$$
$$+g(w/V^2)_h (\partial V/\partial n)_h \tag{9}$$

where all the terms are evaluated at the sea surface, h. Thus the barotropic component of the banking mechanism is negative when, e.g., the sea surface, especially one with negative lateral shear, rises faster on the left than on the right. A differential raising of the sea surface across the stream will pile up mass to the sides at

different rates. This will tend to turn the speed axis of the current away from the side where the sea surface is rising faster, simply because that side of the current is losing kinetic energy more rapidly.

The nature of the baroclinic component of the banking mechanism in a steady flow may be seen from the downstream component of the equation of frictionless motion for a parcel at a subsurface height, z, in the form:

$$DV/Dt = (g/\varrho) \int_{z}^{h} (w/V) (\partial \varrho/\partial z) dz - g(w/V)_{h}$$
 (10)

where the integration extends to the sea surface, h. As only stable stratification is considered, the sign of the baroclinic term in (10) is determined by the sign of the vertical motion. In general, the sign of the vertical motion in a water column may change with height, but in the height interval (h-z) where the sign is the same, parcel decelerates when ascending and accelerates when descending. Hence vertical motion plays a central role in the banking mechanism, which also affects the lateral shear vorticity, as we see next.

#### The lateral shear equation

The procedure used in deriving the turning eq. (8) also gives the equation governing the individual change of lateral shear vorticity,

$$\begin{array}{l} (D/Dt) \left( -\partial V/\partial n \right) = -\partial/\partial n \right) \left( DV/Dt \right) + \left( \partial V/\partial n \right) \boldsymbol{\nabla} \cdot \boldsymbol{\mathbf{V}} \\ & \quad \quad \text{Divergence} \\ \\ + \boldsymbol{K_s} \left( V(\partial V/\partial s) + (\partial w/\partial n) \right) \left( \partial V/\partial z \right) \\ & \quad \quad \quad \text{Curvature} \end{array}$$

In this equation the important feature is the presence of both the banking and curvature terms but with signs opposite to their counterparts in the turning eq. (8); therefore they serve to transform curvature vorticity to lateral shear vorticity and vice versa. But since lateral shear is the negative of lateral shear vorticity, the presence of the banking and curvature-acceleration mechanisms in both (8) and (11) ensures the simultaneous generation of curvature and shear of the same sign. However, their rates of generation will be different.

# The rate of curvature and shear vorticities changes

The operation (D/Dt), representing the individual change following the three-dimensional motion of a parcel, may be decomposed into a horizontal time change (d/dt), and a vertical advection. That is, D/Dt = d/dt + $w(\partial/\partial z)$ . In cases where there is conservation following the parcel, the vertical advection is equal in magnitude to the horizontal time change and may not be neglected. However, this is not the case for curvature and shear vorticities changes. For the portion of the Florida Current located between sections M and N in Fig. 5, and except for the vertical advection term. Table 1 reproduces the estimates given by Chew (1974) of the different terms in eqs. (8) and (11). In the Table, the notation (-1) (eq. 11) means a multiplication by (-1)to change eq. (11) into an equation for lateral shear.

The estimate of the vertical advection listed in the Table is made as follows. East of section M in Fig. 5 the drogue formation accelerated downstream. The concurrent descending motion indicated by eq. (10) for steady flow is assumed reflected in the downstream lowering of the 28C and 29C isotherms between sections M and N in Fig. 6. For an average lowering of 15 m over 30 hours, the descending speed was 0.015 cm/s at the level of the drogues. Then for a curvature of  $(1/150~{\rm km})$ , assumed constant with height, and a vertical shear of  $10^{-2}/s$ , the resulting vertical advection of  $K_s V$  is

$$w(\partial K_s V/\partial z) = wK_s(\partial V/\partial z) = -0.1 \times 10^{-10}/s^2$$
(12)

This represents an over-estimate, since the shear, corresponding to the disappearing of a surface current of 200 cm/s at a 200 m depth, is an extreme assumption. Yet, the magnitude of (12) is still an order smaller than that of the horizontal time change.

In Table 1, the entry for vertical advection of lateral shear is assumed equal to (12). Errors for these estimates are no less than the probable errors of  $\pm 46\,\%$  for the larger terms in Table 1. For each estimate of  $K_s$  or V, the error is 10%, so that an estimate of, say, the curvature-acceleration term entails a compounding of errors as in a binomial expansion with exponent

Table 1. Estimates of the terms in the equations for curvature vorticity and lateral shear changes for the Florida Current

Term	Curvature vorticity (eq. 8) (10 <sup>10-</sup> /s <sup>2</sup> )	Lateral shear $(-1)$ (eq. 11) $(10^{-10}/s^2)$	
Horizontal time change	1.2	1.0	
Vertical advection	-0.1	-0.1	
Banking	1.0	1.0	
Divergence	1.0	0.2	
Curvature-acceleration	-0.1	-0.1	
Beta effect	0.1		
Twisting		?	

4. Within these error bounds, it is possible to balance the sum of the contributions of the various terms in the Table. However, this is not done; rather, the view of large tolerance is adopted.

Two conclusions may be drawn from Table 1. The first is that the horizontal time change (d/dt)represents most of the individual changes in curvature and shear; hence these changes are adequately revealed by changes in a drogue formation. Second, the dominant mechanisms changing curvature vorticity are the banking and divergence mechanisms, while the banking mechanism is the only important one in lateral shear change. This difference follows directly from the absence of the Coriolis parameter in eq. (11). In curvature vorticity change, vertical motion provided the necessary link in the reinforcement observed between the banking and the divergence mechanisms. Where vertical motion is present in a shallow layer bounded on the top by the sea surface, its magnitude is least at the top so that the motion varies with height. Hence, in this layer where, e.g., descending motions accompany horizontal convergence, the pattern of descending motion that makes the banking term positive also makes the divergence term positive. Accordingly, as a parcel in the surface layer moved from its initial position in the speed axis at an inflection, the turning vorticity of the parcel changed more rapidly than its lateral shear. Thus primarily by means of the banking mechanism, both conditions (6) and (7) are fulfilled, and the observed movement across the speed axis is consistent with the constraint of potential vorticity conservation.

616 F. CHEW

The sum of the turning eq. (8) and the shear vorticity eq. (11) is the relative vorticity equation which, in turn, is a differential form of the conservation eq. (2). Hence the banking and the curvature-acceleration mechanisms contained in the processes represented in (8) and (11) are implicit in the process that maintains the conservation of potential vorticity. Both ageostrophic and geostrophic mechanisms are contained in eqs. (8) and (11), and are hence implicit in the conservation eq. (2). Thus, depending on the strength of various mechanisms, the regime of potential vorticity conservation encompasses a wide variety of motion systems. A system where the sign of the lateral shear may follow the sign of the curvature is one. Another is the system of geostrophie potential vorticity.

## Geostrophic potential vorticity

In the idealization of geostrophic current where the Coriolis acceleration exactly balances the horizontal pressure gradient force, the ageostrophic components of centripetal and downstream accelerations are zero at all times. Thus in a geostrophic flow  $(\mathbf{V}_g = V_g \mathbf{s})$ , the eqs. (8) and (11) in  $(s, n, \varrho, t)$  coordinates reduce respectively to

$$\nabla \cdot \mathbf{V}_{q} = -(1/f)Df/Dt \tag{13}$$

$$\nabla \cdot \mathbf{V}_{g} = -\left(\partial V_{g}/\partial n\right)^{-1} (D/Dt) \left(\partial V_{g}/\partial n\right) \tag{14}$$

where all variables are evaluated along constant (potential) density surfaces. When the geostrophic divergence is expressed in terms of the vertical thickness, h', of a parcel element, the two equations can then be integrated to give, respectively

$$f/h' = C_1 \tag{15}$$

and

$$-\left(\partial V_{\rho}/\partial n\right)/h' = C_2 \tag{16}$$

where the C's are integration constants. Eq. (15) is often taken as representing the potential vorticity of all parcel elements in all geostrophic flows. In fact, eq. (15) is limited to two cases: the restricted one where individual parcels are in the geostrophic speed axis and the anomalous

one where all parcels are without lateral sidear and hence a geostrophic current of infinite lateral extent. The latter is sometimes applied to an idealized ocean interior.

In general, the constant  $C_2$  in eq. (16) is not zero. For geostrophic anticyclonic shear is limited only by the inertial stability of the flow, according to Bjerkness (1951), while geostrophic cyclonic shear can be larger than f. Thus as long as the flow is stable, eq. (16) states that the lateral shear of a parcel in geostrophic motion can not change sign; that is, there can be no crossing of the speed axis. Hence eqs. (15) and (16) may be combined. One combination is

$$(f - \partial V_{\alpha}/\partial n)/h' = C_3 \tag{17}$$

which is the law of conservation of geostrophic potential vorticity. The lateral shear in (17) is somewhat different from the lateral shear that Schmitz used in his potential vorticity equation, but the form of his equation is exactly that of (17). Hence the artifact that Schmitz introduced into his model is the constraint of geostrophic balance on cross-stream movement.

#### Discussion and conclusion

The lateral shear vorticity is the negative of the lateral shear. Hence where the curvature and the lateral shear have the same sign, the corresponding vorticities have opposite signs. But this tendency to offset does not mean that the resulting relative vorticity may be taken constant or zero. In a three-dimensional flow, where horizontal divergence does not vanish, the relative vorticity of a meandering parcel must necessarily change, according to eqs. (8) and (11).

In a sluggish current, whether meandering or not, the relative vorticity is small because both the curvature and the shear vorticities are individually small. But in a fast, meandering current where curvature vorticity is large, the relative vorticity can remain small only when lateral shear vorticity of the opposite sign is present. Thus the contribution of the banking mechanism to the turning process has a two-fold effect: a turning of the current and a concurrent damping of the amplitude of the

resulting relative vorticity change. A parcel entering the left flank from the speed axis on approaching an anticyclonic turn gains positive (cyclonic) shear vorticity that offsets part of negative curvature vorticity gained in turning. Likewise, a parcel entering the right flank from the speed axis on approaching a cyclonic turn gains negative (anticyclonic) shear vorticity that offsets part of the positive curvature vorticity gained in turning. Hence, in crossing the speed axis, a meandering parcel is engaging in the process of keeping the magnitude of its relative vorticity change small.

In damping the amplitude of relative vorticity change, the banking mechanism acts through vertical motion and hence through individual change in horizontal speed. Therefore the amplitude of speed changes is generally larger than the amplitude of relative vorticity changes. Accordingly, the field of relative vorticity is generally a poor indicator of the intensity of the concurrent field of acceleration or of kinetic energy change. In particular, kinetic energy change will be underestimated in a model using geostrophic relative vorticity (Holton, 1972).

In a diagnostic study of a motion system, it is desirable to exhibit all the important mechanisms at work. In this sense, the choice of potential vorticity conservation is poor because it represents the net, integrated effect of different mechanisms. It is, of course, useful to know the net effect, but of even more importance to understanding the dynamics of the ocean is to know what are the different mechanisms and how they interact to achieve the net

effect. For only such knowledge will lead to accurate prediction. In this context, it is also desirable to exhibit the mechanisms in terms of deterministic laws rather than in terms of statistical probability. In the framework of Reynolds equation of motion, an instantaneous motion field is replaced by the sum of a mean and a fluctuation field. What is not resolved by the mean field is automatically relegated to the fluctuation field whose representation is usually in terms of Reynolds stresses. By nature, these stresses are statistical, depending on correlations of flow components. Hence to the extent that the interaction process is represented by Reynolds stresses, the deterministic law governing the process is replaced by a statistical probability. But deterministic laws are more informative than statistical probabilities. Moreover, such processes as the interaction between curvature and lateral shear vorticities can be significant contributors to Reynolds stresses. Therefore, it is important in the study of interaction processes that we go beyond the routine computation of Reynolds stresses to find the governing deterministic laws, as was attempted here in the case of the interaction between curvature and lateral shear vorticities.

## Acknowledgements

I would like to thank Drs D. V. Hansen, A. Leetmaa, H. Mofjeld, and R. L. Molinari for reading the manuscript.

#### REFERENCES

Bjerknes, J. 1951. Extratropical cyclones. In Compendium of Meteorology, American Meteor. Soc., Boston, pp. 1334.

Brown, D. 1959. Diagram on drag forces on components of parachute drogues. Scripps Institution

of Oceanography, La Jolla, Calif.

Chew, F. 1974. The turning process in a meandering current, a case study. J. Physical Oceanography 4, 27-57. Chew, F. & Berberian, G. A. 1972. Neighbor diffusivity as related to lateral shear in the Florida Current. Deep Sea Res. 19, 493-506.

Holton, J. R. 1972. An introduction to dynamic meteorology. Academic Press, New York, pp. 319. Schmitz, W. J., Jr. 1969. On the dynamics of the Florida Current, J. Marine Research 27, 121–150.

## ВЗАИМОДЕЙСТВИЕ МЕЖДУ КРИВИЗНОЙ И БОКОВЫМ СДВИГОМ ВО ФЛОРИДСКОМ ТЕЧЕНИИ ПРИ СРЕДНЕМ И МГНОВЕННОМ СОСТОЯНИЯХ. СРАВНЕНИЕ

Путем сравнения двух случаев, относящихся к Флоридскому течению, рассматривается вопрос о том, насколько динамика мгно-

венного течения сохраняется в модели, выводимой из среднего состояния. В средней модели элементы жидкости не могут пересекать

Tellus XXVII (1975), 6

ось скорости. Однако наблюдения мгновенной картины течения обнаруживают взаимодействие вихрей, связанных с кривизной и боковым сдвигом, которое сопровождается систематическим перемещением элементов жидкости через ось скорости. Эта разница расматривается с двух точек зрения. В начале рассматриваются уравнения, управляющие процессом взаимодействия, в частности, ме-

ханизм превращения завихренности, связанной с кривизной, в завихренность, связанную с боловым сдвигом скорости и наоборот. Далее рассматривается динамика геострофического потенциального вихря. Делается вывод, что из-за геострофического приближения средняя модель не воспроизводит процесс взаимодействия.

Tellus XXVII (1975), 6

# Estimation of the Depth of Sunlight Penetration in the Sea for Remote Sensing

Howard R. Gordon and W. R. McCluney

The penetration depth of light in the sea is defined for remote sensing purposes as the depth above which 90% of the diffusely reflected irradiance (excluding specular reflectance) originates. It is demonstrated that for a homogeneous ocean, this is the depth at which the downwelling in-water irradiance falls to 1/e of its value at the surface. Penetration depths as a function of wavelength are presented for a variety of water types, and a mean penetration depth  $z_{90}$  for a broadband sensor is defined and applied to the MSS on ERTS-1. The maximum  $z_{90}$  expected for ERTS-1 is found to be somewhat less than 20 m.

#### Introduction

A number of investigators are using the Multispectral Scanner Subsystem (MSS) on NASA's Earth Resources Technology Satellite (ERTS-1) for remote sensing of water resources.1 In many of these investigations it is necessary to have a rough idea of the effective penetration depth of imagery in each of the spectral bands employed by the MSS. Klemas has devised a slanting board with painted stripes chosen to match the two visible channels of the MSS and calibrated to give a visual estimate of this penetra-tion depth.<sup>2</sup> Other investigators use a white circular disk, called a Secchi disk, lowered into the water until it disappears from view in order to obtain approximate information as to the penetration of sunlight into the water. The Secchi disk has been widely employed in oceanography for the estimation of water transparency. In this paper we will define a penetration depth that can be directly determined from in-water irradiance measurements. This penetration depth is applicable to oceanic sensing in areas in which the water is sufficiently deep that reflection from the bottom does not contribute to the diffuse reflectance observed above the surface.

# Penetration Depth (Approximate Theory)

An approximate theory of the penetration depth can be easily effected using the quasi-single-scatter-

ing approximation<sup>3</sup> to the radiative transfer. In this approximation, single scattering equations are used throughout, but the beam attenuation coefficient c is everywhere replaced by  $c(1-\omega_0 F)$ , where  $\omega_0$  is the ratio of the scattering coefficient b to c, and F is the fraction of b scattered in the forward direction. Now, consider a layer of ocean water of thickness z illuminated by collimated irradiance  $H_0$  from the zenith. Then the radiance  $N_z(\mu')$  due to this layer (excluding specular reflection from the surface) leaving the ocean surface making an angle  $\cos^{-1}(\mu')$  with the zenith is given by

$$N_{z}(\mu') = \frac{4H_{0}}{n(n+1)^{2}} \frac{T(\mu,\mu')}{1+\mu} P(-\mu) \frac{\omega_{0}}{1-\omega_{0}F} \times \{1 - \exp[-z_{C}(1-\omega_{0}F)(1+\mu)/\mu]\}, (1)$$

where n = refractive index of water;

 $T(\mu,\mu')$  = Fresnel transmittance from an angle  $\cos^{-1}(\mu)$  to  $\cos^{-1}(\mu')$ ;

 $P(-\mu)$  = phase function for scattering through an angle  $\cos^{-1}(\mu)$  from the incident beam;  $\mu^2 = 1 - n^2(1 - {\mu'}^2)$  (i.e., Snell's law).

We now define the effective penetration depth  $[z_{90}(\mu')]$  for each emerging angle  $\cos^{-1}(\mu')$  as the layer thickness from which 90% of the total radiance originates, i.e.,

$$[N_{s_{90}}(\mu')]/[N_{\bullet}(\mu')] = 0.9$$

$$= 1 - \exp[-cz_{90}(\mu')(1 - \omega_0 F)(1 + \mu)/\mu]$$
or
$$z_{90}(\mu')c(1 - \omega_0 F) = 2.30\mu/(1 + \mu).$$

But  $c(1 - \omega_0 F)$  is just the quasi single-scattering approximation to K(0,-), the attenuation coefficient of downwelling irradiance just beneath the surface<sup>4</sup> so

H. R. Gordon is with the Department of Physics Optical Physics

Laboratory & Rosenstiel School of Marine and Atmospheric Sciences, University of Miami, Coral Gables, Florida 33124. W. R. McCluney is with the Hydrolegy and Oceanography Branch, NASA Goddard Space Flight Center, Greenbelt, Maryland 20771.

Received 15 July 1974.

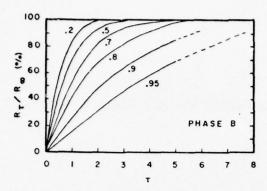


Fig. 1.  $R_{\tau}/R_{-}$  for layers of optical thickness  $\tau$ . The parameter next to each curve is  $\omega_0$ .  $\tau_{90}$  is the value of  $\tau$  for which  $R_{\tau}/R_{-}=0.9$ .

$$z_{90}(\mu')K(0,-) = 2.30\,\mu/(1 + \mu).$$
 (2)

Direct substitution into Eq. (2) shows that  $z_{90}(\mu')K(0,-)$  is almost independent of  $\mu'$ , and in fact

$$z_{90}(\mu')K(0,-) \cong 1.$$
 (3)

The near independence of  $z_{90}(\mu')$  and  $\mu'$  suggests an alternate definition of the penetration depth that is independent of  $\mu'$ . This is

$$R_{\bullet 0}/R_{\bullet} = 0.9,$$

where  $R_z$  is the diffuse reflectance of the ocean due to a surface layer of thickness z and is given by

$$R_{z} = 2\pi \int_{0}^{1} N_{z}(\mu') \mu' d\mu' / H_{0}$$

for an axisymmetric incident radiance distribution. It is clear that in the quasi-single-scattering approximation,

$$z_{90}K(0,-) \cong 1.$$
 (3')

# Comparison of Eq. (3') with Exact Calculations

In studying the influence of a reflecting bottom on the diffuse reflectance of the ocean, Gordon and Brown<sup>5</sup> have computed  $R_{\tau}$  (where  $\tau=cz$  is the optical depth) using Monte Carlo techniques as a function of  $\tau$  for the three scattering phase functions given in Ref. 3. They have also computed  $K(\tau,-)/c$  for the same phase functions, so it is possible to compare Eq. (3') with the results of their exact calculations.

To effect such a comparison,  $\tau_{90}$  is first determined by plotting  $R_\tau/R_\infty$  against  $\tau$  for each phase function and various values of  $\omega_0$ . An example of this for phase function  $B^3$  is shown in Fig. 1.  $\tau_{90}$  can be read directly from the curves for each value of  $\omega_0$  (e.g., from Fig. 1  $\tau_{90} \simeq 1$  for  $\omega_0 = 0.2$ ). Then since  $\tau_{90} = cz_{90}$ .

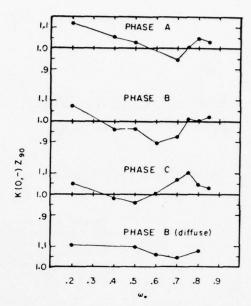


Fig. 2. Comparison of  $K(0,-)z_{90}$  with unity as a function of  $\omega_0$  for the three phase functions for the case of collimated incident irradiance from the zenith and for perfectly diffuse incident irradiance [phase B (diffuse)].

$$\tau_{90}[K(0,-)/c] = z_{90}K(0,-)$$

is formed and compared to unity. The result is shown in Fig. 2 for the three phase functions  $A,\,B,\,$  and C with collimated incident irradiance from the zenith (top three curves) and an incident field of completely diffuse irradiance [labeled phase B (diffuse)] to simulate skylight. It is seen that Eq. (3') is satisfied to within  $\pm 10\%$ , even accounting for the complete effects of multiple scattering as well as skylight in the incident irradiance. This of course indirectly implies the validity of Eq. (3). Hence we can conclude that in a homogeneous ocean the depth above which 90% of the diffusely reflected radiance originates is 1/K (0,–) or, more generally, the depth at which the downwelling irradiance falls to 1/e of its value at the surface.

#### **Applications**

From the work of Preisendorfer $^8$  it is readily shown that

$$a(z) \leq K(z,-),$$

where a(z) is the absorption coefficient of the medium at depth z. Applying this to the present case of a homogeneous ocean we find

and hence the maximum penetration depth is the inverse of the absorption coefficient of the medium (i.e., the absorption optical depth).

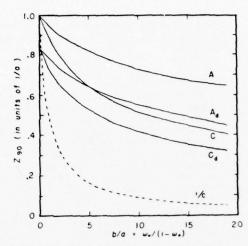


Fig. 3. 290 as a function of b/a for phase functions A and C, for collimated incident irradiance from the zenith, and an incident field of perfectly diffuse irradiance (identified by the subscript d).

To demonstrate the relative influence of absorption and scattering on z90, Fig. 3 gives z90 (in units of 1/a) as a function of the ratio of scattering to absorption for phase functions A and C for both collimated incident irradiance from the zenith and an incident field of uniform radiance (identified by the subscript d). It is seen that for  $b \approx 0$ ,  $z_{90}$  for the collimated cases is 1/a, while for diffuse incidence  $z_{90} \approx 0.8/a$ . Increasing b/a from 0 to 20 (keeping a fixed) changes z90 by only a factor of 2-3, while the turbidity of the water (c) increases by a factor of 20. Also, note that increasing a by a factor n decreases  $z_{90}$  by a factor n, and so variations in a have a much stronger influence on 290 than do variations in b. (1/c is also plotted on Fig. 3 and is evidently a poor estimate of the penetration depth except in the trivial case b = 0.) Hence we see not only that the limiting penetration depth is given by 1/a, but that in most cases the penetration depth will be determined to a large part by the absorption coefficient alone.

Jerlov9 has classified oceanic and coastal water types on the basis of their irradiance attenuation coefficient spectra. These spectra provide the necessary information to determine 290 as a function of wavelength  $[z_{90}(\lambda)]$  for various water types. The result of this determination is shown in Fig. 4 where the Roman numerals refer to Jerlov's oceanic water types and the Arabic numerals to his coastal water types. For type I water (for example, the Sargasso Sea) the maximum 290 is about 55 m near 475 nm, while for type 9 coastal water, the maximum 290 is only about 1.5 m at 600 nm. The shift of the wavelength of maximum penetration toward the red is due to progressively higher concentrations of the socalled yellow substances10 that are characteristic of decaying organic material and absorb strongly in the

There are two reasonable ways to define the mean penetration depth for broad wavelength band sensors such as the MSS on ERTS-1. The first is to integrate Eq. (1) over wavelength and angle and define, in analogy to

 $R_{*90}/R_{*} = 0.90,$ 

the mean penetration depth,  $\bar{z}_{90}$  as the value of z for

$$\begin{split} \int_0^1 \! \int_{\lambda_1}^{\lambda_2} G(\mu, \mu', \lambda) &\{ 1 - \exp[-z K_{\lambda}(0, -)(1 + \mu)/\mu] \} \mu' d\lambda d\mu' \\ &= 0.9 \! \int_0^1 \! \int_{\lambda_1}^{\lambda_2} G(\mu, \mu', \lambda) \mu' d\lambda d\mu', \end{split}$$

$$G(\mu, \mu', \lambda) = \frac{4H_0}{n(n+1)^2} \frac{T(\mu, \mu')}{1 + \mu} \frac{P(-\mu)\omega_0}{1 - \omega_0 F}$$

$$\begin{split} \int_0^1 \int_{\lambda_1}^{\lambda_2} G(\mu, \mu', \lambda) \, \exp[-z K_{\lambda}(0, -)(1 + \mu)/\mu] \mu' d\lambda d\mu' \\ &= 0.1 \int_0^1 \int_{\lambda_1}^{\lambda_2} G(\mu, \mu', \lambda) \mu' d\lambda d\mu'. \end{split}$$

$$= 0.1 \int_0^t \int_{\lambda_t}^{\lambda_2} G(\mu, \mu', \lambda) \mu' d\lambda d\mu'.$$

Now  $(\mu + 1)/\mu$  in the exponent varies from 2 to 2.512 as  $\mu'$  varies from 1 to 0, and if we replace  $(\mu + 1)/\mu$  by its mean (2.26), assuming  $H_0$  is independent of wavelength, we find

$$\int_{\lambda_1}^{\lambda_2} R_{\infty}(\lambda) \exp[-zK_{\lambda}(0,-)2.26] d\lambda = 0.1 \int_{\lambda_1}^{\lambda_2} R_{\infty}(\lambda) d\lambda, \quad (4)$$

which can be solved by trial and error for  $z \ (= \bar{z}_{90})$ given  $R_{\infty}(\lambda)$  and  $K_{\lambda}(0,-)$ .

In the second method, 290 is weighted at each

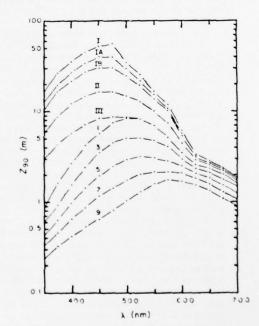


Fig. 4. Variation of zan with wavelength for various water types given by Jerloy in Ref. 9

Table I. Mean Penetration Depths in Meters for ERTS-1 MSS Bands

Location	Band 4 (500–600 nm)	Band 5 (600-700 nm)
Crater Lake	18.5	2.7
San Vicente Reservoir	1.9	1.5

wavelength by the upwelling irradiance  $R_{\omega}(\lambda)H_0(\lambda)$ , i.e.,

$$\overline{z}_{90} = \int_{\lambda_1}^{\lambda_2} z_{90}(\lambda) R_{\infty}(\lambda) H_0(\lambda) d\lambda / \int_{\lambda_1}^{\lambda_2} R_{\infty}(\lambda) H_0(\lambda) d\lambda$$

so that penetration depths at those wavelengths for which the upwelling irradiance is large contribute strongly to  $\tilde{z}_{90}$ . If we again assume  $H_0$  is independent of wavelength, this reduces to

$$\overline{z}_{90} = \int_{\lambda_1}^{\lambda_2} z_{90}(\lambda) R_{\bullet}(\lambda) d\lambda / \int_{\lambda_1}^{\lambda_2} R_{\bullet}(\lambda) d\lambda.$$
 (5)

Jerlov does not give  $R_{\infty}(\lambda)$  in his classifications, so neither Eqs. (4) nor (5) can be used to compute  $\tilde{z}_{90}$  for the water types in Fig. 4. Tyler and Smith<sup>11</sup> however have measured the in-water reflectance function R(z,-) as a function of  $\lambda$  for various waters, and to a very good approximation the spectrum of R(z,-) for small z differs from that of  $R_{\infty}$  by a wavelength independent constant. (Remember that specular reflectance from the sea surface is not included in  $R_{\infty}$ .) Hence  $R_{\infty}$  in Eqs. (4) and (5) can be replaced by R(z,-), where z is near the surface (z  $\sim$  few meters), and the Tyler and Smith measurements may then be used to determine  $\tilde{z}_{90}$  for the broadband MSS on ERTS-1.

The sensors of interest view the ocean in the 500-600-nm band (MSS-4) and the 600-700-nm band (MSS-5). Using the data presented by Tyler and Smith for Crater Lake and San Vicente Reservoir, it is found that Eqs. (4) and (5) yield identical values of \$90 to within about 3%. These are tabulated in Table I. The Crater Lake \$290's probably represent the largest penetration depths obtainable with ERTS-1, since the lake is known to have optical properties similar to the Sargasso Sea12 and has been called the "natural analog of distilled water." 13 The San Vicente Reservoir on the other hand contains vast quantities of phytoplankton and zooplankton, is quite turbid ( $c = 2.12 \text{ m}^{-1}$  at 530 nm), and hence its 290's in Table II are probably among the smallest ERTS-1 penetration depths.

We wish to emphasize here that for a given wavelength,  $z_{90}$  is the depth at which the downwelling irradiance falls to 1/e of its value at the surface and can be determined only through direct measurements with an irradiance meter, i.e., through measurements made in the water. Furthermore, for broadband sensing systems,  $\tilde{z}_{90}$  can be determined only from spectral irradiance measurements of the type presented in Ref. 11. A rough estimate of  $\tilde{z}_{90}$  for bands 4 and 5 can be obtained, however, by measuring  $z_{90}(\lambda)$ , where  $\lambda = 525$  nm for clear water and 545 nm for turbid water in band 4, and  $\lambda = 650$  nm for both

clear and turbid water in band 5. For these wavelengths,  $z_{90}(\lambda)$  equals the penetration depths in Table I.

#### Conclusions

The penetration depth of light in the sea has been defined for remote sensing purposes as that depth above which 90% of the diffusely reflected irradiance (excluding specular reflectance) originates. It is demonstrated that for a homogeneous ocean, this is the depth at which the downwelling in-water irradiance falls to 1/e of its value at the surface. This is then used to show that z90 is for the most part controlled by the absorption coefficient of the medium. Penetration depths as a function of wavelength are presented for a variety of water types, indicating that a maximum penetration depth of about 55 m near 475 nm can be expected in the clear water of the Sargasso Sea. A mean penetration depth for broadband sensors is defined and applied to the MSS on ERTS-1 showing the maximum mean penetration depth expected for band 4 is somewhat less than 20 m, while for band 5 the result is about 2 m.

Contribution No. 1800 University of Miami Rosenstiel School of Marine and Atmospheric Sciences.

This work was in part supported by the National Aeronautics and Space Administration, Earth Resources Survey Program, Contract Number T-4713B.

#### References

- Proceedings of the Symposium on Significant Results Obtained from the Earth Resources Technology Satellite-1, 5-9
  March 1973, NASA/Goddard Space Flight Center, Greenbelt,
  Md. 20771, publication NASA SP-327.
- V. Klemas, J. F. Borchardt, and W. M. Treasure, Rem. Sens. Environ. 2, 205 (1973).
- H. R. Gordon, Appl. Opt. 12, 2803 (1973); W. R. McCluney, Appl. Opt. 13, 2422 (1974).
- 4. If H(z, -) is the downwelling irradiance at a depth z beneath the sea surface, the downwelling irradiance attenuation coefficient K(z, -) is defined by

$$K(z,-) = -[1/H(z,-)](d/dz)H(z,-).$$

- H. R. Gordon and O. B. Brown, Appl. Opt. 13, 2153 (1974). In this paper R, was referred to as R<sub>1</sub>.
- O. B. Brown and H. R. Gordon, Trans. Am. Geophys. Union 54, 318 (1973).
- Although only a few calculations have been carried out for inhomogeneous media [O. B. Brown and H. R. Gordon, Trans. Am. Geophys. Union 55, 287 (1974)], it appears that for these media the more general value of z<sub>90</sub> is correct.
- 8. R. W. Preisendorfer, Monogr. U. G. G. L., No. 10, 11 (1961).
- N. G. Jerlov, Optical Oceanography (Elsevier, Amsterdam, 1968), 194 pp.
- 10. K. Kalle, Oceanogr. Mar. Biol. 4, 91 (1966).
- J. E. Tyler and R. C. Smith, Measurements of Spectral Irradiance Underwater (Gordon and Breach, New York, 1970), p. 41ff.
- R. C. Smith, J. E. Tyler, and C. R. Goldman, Limnol. Oceanogr. 18, 189 (1973).
- 13. R. C. Smith and J. E. Tyler, J. Opt. Soc. Am. 57, 589 (1967).

Reprinted from: Bulletin of the American Meteorological Society 56, No. 9, 997-998.

Progress in Oceanography, Volume 6, Edited by B. A. Warren. Pergamon Press, New York, 1973, 193 pages. Handbound.

This most recent addition to the Progress in Oceanography series begun in 1963 is a collection of longer papers, mostly on observational studies of ocean currents and circulation. Many physical oceanographers have been aware of these studies, but have not previously had convenient access to details. Articles of particular interest to marine and global meteorology, including current interest in the role of the ocean in climate, relate to the equatorial current systems and the response of ocean thermal structure to atmospheric exchange.

The only contribution with substantial theoretical or mathematical content is a presentation by M. C. Hendershott of a mathematical theory of scattering by bathymetric features of barotropic tidal energy into internal modes, and its observational testing near the diurnal inertial latitude (30°). The model development is straightforward, but complex. As happens all too frequently in oceanography, a sharp result is not possible because of the problems of acquiring an adequate data base.

Two contributions address observations of the equatorial current systems of the Pacific. Y. Magnier, H. Rotschi, P. Rual, and C. Colin describe current measurements taken between 4°S and 4°N on 170°E during 1967-8, on a series of cruises called the "Cyclone" cruises. The temporal and spatial patterns observed in the Equatorial Current, the North Equatorial Countercurrent, and the Equatorial Undercurrent found in the Western Pacific are presented in a set of detailed figures. Although the method employed does not provide absolute measurements, careful evaluation of the evidence suggests a dual core structure of the Equatorial Undercurrent in this region as distinguished from the single core previously observed in the central Pacific, and a westward flowing deep equatorial current lying beneath the Equatorial Undercurrent. A companion article by B. A. Taft and J. H. Jones describes measurement of the Equatorial Undercurrent in the eastern Pacific during the Piquero Expedition (June-August, 1969). On this expedition observations of currents and water properties were made from shipboard across and along the equator between 84°W and 11.5°W. Evidence for a double core in the undercurrent is found here also, but it appears unlikely that it is directly related to that found in the western Pacific. Probably the most interesting aspect of this contribution is that, in comparison to earlier observations, it suggests an inverse correlation between undercurrent transport and the strength of the trade winds. Taken together, these two contributions amply portray the complexity of temporal and spatial variation of the equatorial current systems.

In a most timely and useful contribution, D. F. Bumpus describes the circulation on the U.S. Atlantic continental shelf. It is unfortunate that the charts which are the meat of the article, showing the average currents at the surface and bottom as inferred from use of Lagrangian drift devices, are reduced in size almost to the point of illegibility. They deserve better rendition, but much of the information thereon is available elsewhere. Much valuable material, which is not effectively collected elsewhere, is to be found in Bumpus' distillation of information gathered during many years of research in this region. This chapter alone should establish the book as a useful reference in coastal oceanography for some time to come.

The concluding article, by T. Sankey, describes convective processes in the western Mediterranean Sea, especially the observations made during the international MEDOC campaigns in 1969–70. In this operation, detailed observations were made of deep penetrative convection forced by loss of buoyancy of surface water due to cooling and evaporation, especially under the influence of the mistrals. As opposed to upwelling, for instance, this process has had relatively little study in recent years. The observations reported here are particularly interesting to those concerned with synoptic scale sea-air interaction, and provide guidance as to the kind of observations required to document the process in other parts of the ocean.

As suggested by the dates mentioned, none of the material presented in the book is very new. For the most part, selected aspects of the work have been reported elsewhere, but the periodical literature does not permit the extensive graphic detail that is contained here. The book is an important one for the oceanographic library, and a useful one for the specialist in tropical oceanography or coastal circulation.—Donald Hansen

11 Reprinted from: NOAA Data Report MESA-1, 177 pages.

NOAA Data Report MESA-1

NEW YORK BIGHT PROJECT,
WATER COLUMN SAMPLING CRUISES #6-8
OF THE NOAA SHIP FERREL,
APRIL-JUNE 1974

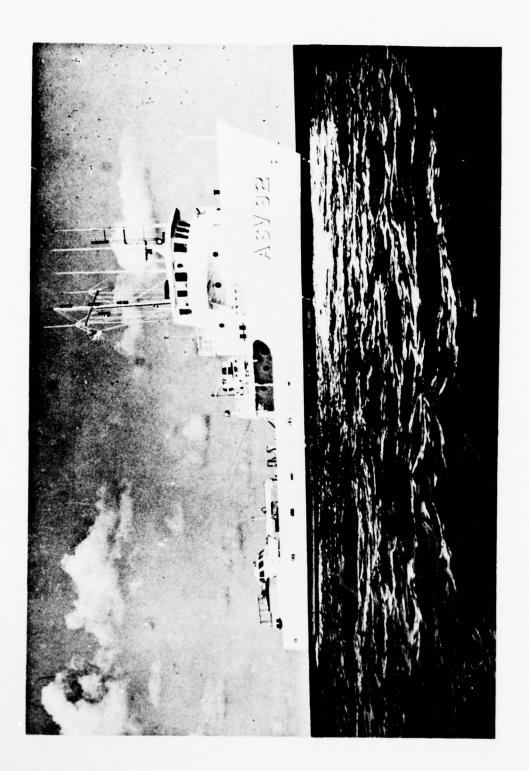
John B. Hazelworth Byron L. Kolitz Robert B. Starr Robert L. Charnell George A. Berberian Maxine A. Weiselberg

Marine EcoSystems Analysis Program Office Boulder, Colorado January 1975

UNITED STATES
DEPARTMENT OF COMMERCE
Frederick B. Dent, Secretary

NATIONAL OCEANIC AND ATMOSPHERIC ADMINISTRATION Robert M. White, Administrator Environmental Research Laboratories Wilmot N. Hess, Director





173

# CONTENTS

ABS	TRACT	Page 1
1.	INTRODUCTION	1
2.	INSTRUMENTATION	5
3.	DATA COLLECTION	6
4.	DATA PROCESSING	7
5.	DATA PRESENTATION	16
6.	ACKNOWLEDGMENTS	16
7.	REFERENCES	23
8.	STATION DATA	25
9.	ERRATA (MESA Report No. 74-2)	176
10.	ADDENDUM	177

# DISCLAIMER

The NOAA Environmental Research Laboratories do not approve, recommend, or endorse any proprietary product or proprietary material mentioned in this publication. No reference shall be made to the NOAA Environmental Research Laboratories, or to this publication furnished by the NOAA Environmental Research Laboratories, in any advertising or sales promotion which would indicate or imply that the NOAA Environmental Research Laboratories approve, recommend, or endorse any proprietary product or proprietary material mentioned herein, or which has as its purpose an intent to cause directly or indirectly the advertised product to be used or purchased because of this NOAA Environmental Research Laboratories publication.

NEW YORK BIGHT PROJECT,
WATER COLUMN SAMPLING CRUISES #6-8 OF THE NOAA SHIP FERREL,
April-June 1974

John B. Hazelworth Byron L. Kolitz Robert B. Starr Robert L. Charnell George A. Berberian Maxine A. Weiselberg

#### ABSTRACT

During the period April-June 1974, three oceanographic cruises, denoted 6, 7, and 8, were made by the NOAA ship Ferrel in the New York Bight. The objective of the cruises was to supply data to provide a base for analysis of the water movements on the highly impacted ecosystem. This report presents the corrected physical and chemical data from these cruises and describes the parameters measured, the measurement methods, and the corrections applied to the data.

Key Words: MESA, New York Bight, Physical Oceanographic Data, Nutrient Data

#### 1. INTRODUCTION

During 1973, the National Oceanic and Atmospheric Administration (NOAA) began an intensive investigation of the marine ecosystem of New York Bight. This project is the first regional project of the Marine Ecosystem Analysis (MESA) program and includes a data collection phase in each of the major oceanographic disciplines of biology, geology, chemistry, and physics. The prime purpose in this field phase is to provide baseline data on existing conditions and mechanisms from which changes in the environment can be analyzed and guidelines for future assessment of man-produced activity in the marine environ-

ment can be developed. The direct measurement program, based on a total of 43 current meters at 12 stations, was designed to provide data on the time and space scale of water motion in the apex and to test the circulation hypothesis proposed by Charnell et al. (1972).

To supplement these data, a series of cruises was planned that would provide data on density and quality of water in the apex. The cruises were designed to coincide with the transits of the Earth Resources Technology Satellite (ERTS). These remotely sensed data were to help in an evaluation of the potential for satellite monitoring of water quality changes in near-surface waters (cf. Charnell and Maul, 1973, and Charnell et al. 1974).

From August to November 1973, NOAA conducted the first five of these cruises. These water-sediment chemistry (WSC) cruises consisted of 25 stations that were occupied on an approximately monthly basis by the NOAA ship Ferrel. Results of these cruises were reported by Hazelworth et al. (1974). From April to June 1974, NOAA conducted an additional three cruises, covering the same 25 stations (fig. 1) again aboard the NOAA ship Ferrel. Cruise dates are given in table 1. Those staff members who participated in the field work are also listed in table 1. The sampling program was similar to the one used during the first five cruises.

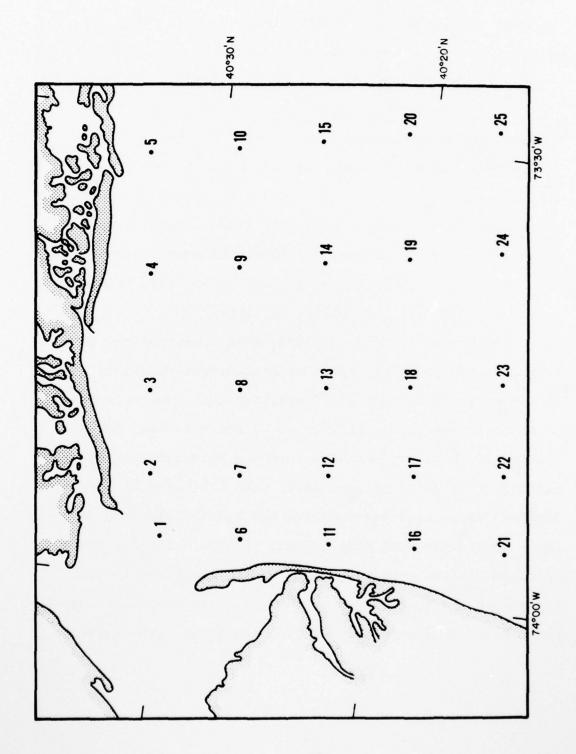


Figure 1. Locations of stations in the New York Bight area.

Table 1. Water-Sediment Chemistry Cruises by the NOAA Ship  $\underline{\mathsf{Ferrel}}$ 

Cruise	se Date	
6	April 16-20, 1974 ERTS Day, April 20	R. Starr G. Berberian D. Segar
7	May 6-9, 1974 ERTS Day, May 8	R. Starr G. Berberian L. Keister
8	June 10-13, 1974 ERTS Day, June 13	J. Hazelworth D. Segar M. Weiselberg
6	Station 7 occupied twice	
7	Station 7 occupied twice Station 16 no data availa Station 21 no data availa Station 22 no data availa Station 23 no data availa	able able able
8	Station 3 occupied twice Station 7 occupied twice	

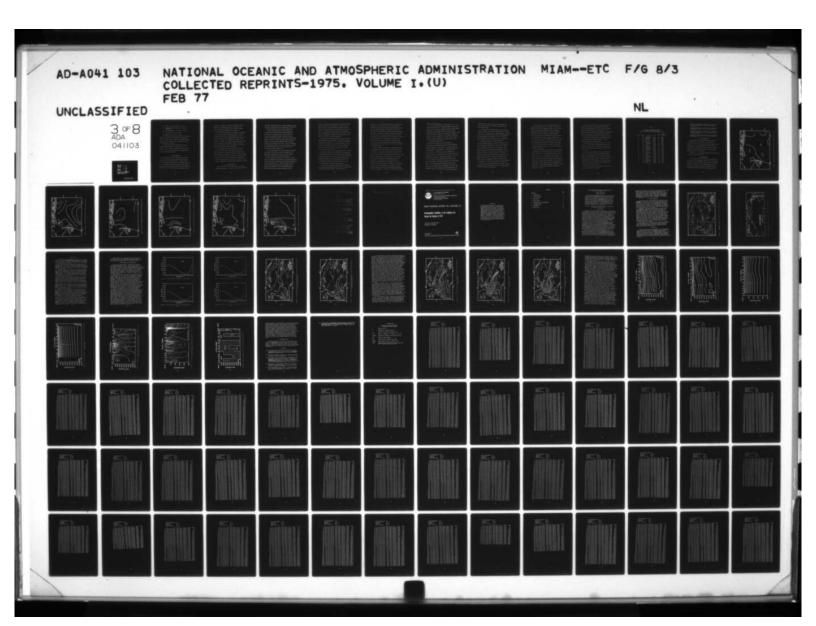
Only the physical and nutrient data obtained from the water column measurements on these three cruises are presented in this report. Water samples were also taken for other chemical analyses, but will be the subject of a separate report.

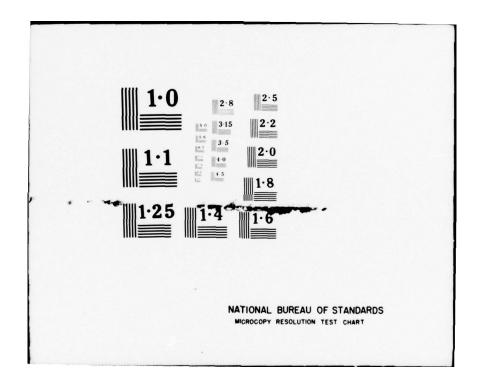
## 2. INSTRUMENTATION

The primary instrument used aboard the <u>Ferrel</u> for water column sampling was the Inter Ocean Model 513-10 CSTD, with added sensors for measuring turbidity, dissolved oxygen, pH, and Redox (Eh). The system is equipped with a digital display to monitor sensor functions during a cast. Data from the sensors were logged, one set per second, on a Kennedy magnetic-tape-recording system. As a backup system, the data were also printed out on a strip chart, in engineering units, by a digital recorder. The ship was also equipped to collect water samples by means of Niskin bottles with attached reversing thermometers. Ship's position was usually determined by Raydist, although horizontal sextant angles or radar were occasionally used.

The manufactures specifications on the sensors are as follows:

- (a) Depth, 0 to 300 m, ± 1 m,
- (b) Temperature,  $-5^{\circ}$  to  $45^{\circ}$ C,  $\pm 0.02^{\circ}$ C,
- (c) Conductivity, 0 to 65 m mhos, + 0.05 m mhos,





- (d) Salinity, 0 to 40 °/00, + 0.05 °/00;
- (e) Turbidity, 0 to 100 percent, ± 3-percent transmission,
- (f) Dissolved oxygen, 0 to 20 ppm, + 0.2 ppm
- (g) pH, 2 to 12 pH,  $\pm$  0.1 pH, and
- (h) Redox (Eh), -2 to +2 V,  $\pm$  5 mV.

Time constants for most of the sensors are relatively short, varying between 10 and 400 ms. Exceptions are oxygen, which has a time constant of 10 s, and salinity, which has a time constant of 1.4 s, caused by the use of slow-response thermistors.

The sensor package was calibrated by the Coast
Guard Instrumentation Center, Washington, D.C., in
February 1974. Periodic calibration checks were made,
on site, by the National Oceanographic Instrumentation
Center (NOIC) between cruises.

# 3. DATA COLLECTION

The normal plan of daily operations was to occupy six to nine stations each day, depending upon weather, depth of water, and travel distance. At each station, the sensor package was lowered to just below the water surface, and readings were logged from the digital readout for each sensor. The sensor package was then lowered to the bottom at a rate of about 6 m/min, slow enough to permit

the sensors to respond to gradients existing at the time. Another set of readings was taken at the bottom. The sensor package was then raised to the surface, stopping to take readings and samples at 10-m intervals.

Water samples were taken at the surface, at the bottom, and at 10-m intervals by using Niskin bottles. Reversing thermometers were used to record temperature near the surface and bottom. These temperature data were sufficient to check the accuracy of the temperature sensor and to compute a correction. In addition, water samples were drawn and analyzed for dissolved oxygen, salinity, pH, and Eh. These data were used to check the accuracy of the sensors and when necessary to compute calibrations.

At each sample depth, a water sample for nutrient analysis was drawn into an aged 125-ml plastic bottle with polyseal cap and was then immediately frozen. Other water samples were filtered, with both the filtrate and the filter pad saved, by freezing, for various chemical analyses. At the end of each cruise, the samples were transported in freezer chests, packed with dry ice, to a freezer at the Atlantic Oceanographic and Meteorological Laboratories (AOML).

#### DATA PROCESSING

After each cruise, the raw data tapes were returned to AOML for processing. In general, only the down-cast data

were used. During cruise WSC-8, a power fluctuation caused the loss of data during part of the down-cast on station 22. In this case, data from the up-cast were substituted.

Noise pulses were apparent in the original data, caused in part by power fluctuations and intermittent instrument noise associated with a faulty digitizer.

This noise was removed by separate numerical filters during the computer processing. First, the data were passed through a gate filter which eliminated extreme unrealistic values. Next, the data were passed through a gradient filter which eliminated noise spikes. Last, each parameter was plotted against depth and visually examined; any spikes which had been missed by the first two filters were removed during the final computer run.

To the extent possible, all sensor-measured parameters were checked for accuracy. Depth was compared to the meter-wheel reading at the winch, during casts having no wire angle, and appeared to be accurate within 1 m.

Salinity could be determined by two methods. Salinity values, as computed by the instrument, were recorded directly. Salinity also could be computed from the measured temperature and the conductivity value. After each cruise, salinity values were determined from the water samples using a Plessey 6220 salinometer. The two separately measured salinity profiles were plotted and compared with the

salinity values from the water samples. The sensor-recorded salinity values were inconsistent and, therefore, are not reported herein. This poor result for directly recorded salinity is caused by the long time constant of the salinity sensor. On the other hand, the salinity values computed from the temperature and conductivity gave acceptable results because the temperature thermistor has a time constant comparable to that of the conductivity sensor.

Computed salinity values compare well with the salinity determined from the water samples. The correction required was constant for each cruise. For cruise WSC-6, the correction factor was  $-0.37^{\rm O}/_{\rm OO}$ , for cruise WSC-7 was  $-0.36^{\rm O}/_{\rm OO}$ , and for cruise WSC-8 was  $-0.44^{\rm O}/_{\rm OO}$ . The final recorded salinity values with corrections applied are considered accurate to within  $\pm$  0.05  $^{\rm O}/_{\rm OO}$ .

During each cruise, reversing thermometers were attached to the surface and bottom Niskin bottles. For cruise WSC-6, the mean difference between the bottom reversing thermometers and temperature sensor was 0.02°C. For cruise WSC-7, the mean difference between top and bottom reversing thermometers and temperature sensor for all stations was 0.02°C. For cruise WSC-8, the mean difference was 0.04°C. Only for cruise WSC-8 was the correction factor applied.

Eh values were recorded during all cruises. However, no Eh meter was available during cruise WSC-6 to check sensor readings against water samples. Thus, no values are

presented. During cruises WSC-7 and WSC-8, an Eh meter was available and a reading was made on all water samples.

Whenever there was a constant difference between the sensor and water sample readings at all depths at a station, a correction (assuming the water sample readings were correct) was applied. Otherwise the sensor readings were discarded. For cruise WSC-7, a constant correction factor of -0.7 mV was applied to all values which were accepted after filtering. During cruise WSC-8, all Eh values were accepted. The first day's values had a correction of -0.34 mV applied, but the second and third days readings needed no correction. All recorded values are believed to be well within manufacturers' specifications.

During cruises WSC-6 and WSC-7, no oxygen probe values were recorded. After cruise WSC-7, it was discovered that the common bus of the Model 514 DM Display had a 5-V ground to the chassis. Recorded values for these cruises are from the water samples. The surface and 10-m values for cruise WSC-6 are above accepted saturation levels, but a recheck of the chemical procedure and standardization chemicals indicates no source of error. Dissolved oxygen was recorded and is presented for cruise WSC-8. A constant correction factor of +0.088 ml/1 was applied. It was noticed that the ship, while maneuvering in the vicinity of the station, churned up the water and introduced large amounts of small air bubbles. On occasion, the sensor package passed

through this disturbed water. On stations 21, 22, 17, 18, 4, 3, 11, and 12, near-surface dissolved oxygen values vary between 6.54 and 7.44 ml/l. Saturation points at these temperatures and salinities vary between 5.70 and 6.00 ml/l. Apparently, the air bubbles adhere to the oxygen sensor, causing an above normal reading. As the sensor is lowered, the bubbles wash away. By about 10 m, the sensor is recording correctly. With the exception of the above casts, after the correction factor is applied, all oxygen values fall well within instrument specifications.

pH has always exhibited an erratic behavior. cruise WSC-6, individual station corrections were computed. Some stations were discarded because no reliable correction could be computed. On cruise WSC-7, a depth-dependent linearregression equation was computed as a correction factor. On cruise WSC-8, a constant of -0.41 was computed as a correction factor. The accuracy of the pH values varies from cruise to cruise. For cruise WSC-6, all data fall within an accuracy of ± 0.1 pH. On cruises WSC-7 and WSC-8, it is estimated that 70 percent of the observations are within + 0.2 pH. Even this is misleading; further analysis indicates that on cruise WSC-8 all observations are within 0.1 pH, except for the near-surface observations at stations 22, 7, and 17. It is postulated that contaminants in the water were the cause of the erratic results of the pH measurements. On a subsequent cruise, the sensor probe was carefully cleaned

before each cast. Also the probe used to determine pH from the water sample was carefully cleaned before each water sample reading.

On cruise WSC-10, the erratic behavior definitely decreased. However, the pH sensor readings taken at stations 1. and 18, in the vicinity of the sludge dump area, were completely out of acceptable range, whereas pH readings from the water samples were acceptable. Thus it is believed that contaminants, probably organic, when in contact with the pH sensor, will tend to falsify the reading.

The turbidity probe on the profiling system is a 10-cm path-length transmissometer. Even for the coastal area where the water is highly turbid, values from the probe are in the operating range from 70 to 90 percent. While this is not the range of most sensitive operation (Drake et al., in press), the profiles provide useful data on the relative turbidity in the water column. The system was originally calibrated using clean-filtered seawater for the upper transmittance level. Periodic calibration checks showed the system to drift no more than 1 percent in the operating range. Consequently, accuracy of the measured data is considered to be within specifications of ± 3 percent.

Turbidity was not recorded during cruise WSC-8. A short in the bridle cable connecting the sensor to the data cable precluded collection of usable data.

For profiling data, there were generally two to five observations recorded per meter. Several interpolation methods were tried for computation values at 1-m intervals. The more sophisticated techniques—such as Lagrangian interpolation formulas—tended to introduce overshoots, especially at the top and bottom of large gradients. A linear interpolation was considered the most acceptable. The form used was the normal one with a modification: if a reading occurred at an interpolation depth, the accepted value would be the mean of the reading itself and the value determined from the linear interpolation performed as if the reading were absent. Values of sigma—t were interpolated rather than calculated from the interpolated temperature and salinity.

During cruise WSC-6, extreme variability was observed in measurements of near-surface waters. Normal survey procedure was to lower the sensor package into the water to a depth of 1 to 2 m; it would remain there for about 3 min, allowing the sensors to equilibrate before lowering to the bottom. During this period, the magnetic tape recorded all observations. Upon listing these data, it was noted that large variations were occurring within each parameter at some stations. For example, temperature changes of 0.05°C or greater were recorded between consecutive observations taken only 1 s apart.

For the normal processed tape, one set of parameter values was recorded at the shallowest recorded depth.

Then one set of observations at the next greater recorded depth was selected, and so on to the bottom. In this particular case, this method was considered to be unreliable. Instead, a mean value for each parameter was computed, using all recorded values at each 0.1 m between 1 and 2 m.

Table 2 gives selected means and standard deviations for each parameter at several stations, as examples, indicating the situation that occurred.

Water samples were analyzed for dissolved nitrates  $(NO_3-N)$ , nitrites  $(NO_2-N)$ , orthophosphates  $(PO_4-P)$ , and silicates  $(SiO_3-Si)$  with a four-channel Technicon Autoanalyzer, generally within a period of 6 wk after their collection.

The analytical procedures used in the analyses for nitrate and nitrite are described by Armstrong et al. (1967). The orthophosphate procedure is described by Grasshoff (1965), and the silicate procedure is described by Strickland and Parsons (1968). The water used for standardization, blank determinations, and wash between samples is filtered Gulf Stream water obtained from the surface of the Straits of Florida.

The detection limits and accuracies of analysis for the four nutrients are as follows:

Table 2.

# Selected Means and Standard Deviations for Each Recorded Parameter Occurring Between 1 and 2 M During Cruise WSC-6

				No.	
				of	Standard
Station	Depth	Parameter	Mean	obs.	deviation
no.	(m)				
1	1.0	temperature	8.12	1	0.00
1	1.5	temperature	8.24	39	0.11
1	1.4	salinity	23.44	32	0.84
1	1.0	salinity	24.75	1	0.00
1	1.7	salinity	24.07	3	1.20
1	1.1	рН	8.63	5	0.08
1	1.7	turbidity	70.77	3	0.55
2	1.6	temperature	8.31	52	0.27
2	1.6	salinity	29.28	52	0.81
2	1.6	рН	8.78	52	0.03
2 2 2 2 3 3	1.6	turbidity	73.70	52	3.11
3	1.5	temperature	9.27	4	0.26
3	1.5	salinity	27.17	4	0.17
3	1.3	turbidity	71.97	4	0.57
11	1.6	temperature	8.36	32	0.05
11	1.4	salinity	25.91	20	0.65
11	1.4	рН	8.70	20	0.04
11	1.4	turbidity	68.57	20	1.88
4	1.3	temperature	8.93	8	0.42
4	1.3	salinity	28.72	8	0.37
4	1.4	рН	8.78	31	0.03
4	1.4	turbidity	77.54	31	0.67
8	1.5	temperature	8.20	77	0.27
8	1.5	salinity	27.20	77	1.33
8	1.5	рН	8.51	77	0.03
8	1.3	turbidity	71.95	15	3.33
9	1.2	temperature	8.38	78	0.36
9	1.1	salinity	25.91	18	0.98
9	1.1	рH	8.71	18	0.06
9	1.1	turbidity	72.09	18	1.76

NO<sub>3</sub>-N 0.1 to 40  $\mu$ gat/L. Coefficient of variation-95-percent confidence level at 15  $\mu$ gat NO<sub>3</sub>-N/L-0.17 percent;

NO<sub>2</sub>-N 0.1 to 20  $\mu$ gat/L. Coefficient of variation-95-percent confidence level at 3.2  $\mu$ gat NO<sub>2</sub>-N/L-1.2 percent;

PO<sub>4</sub>-P 0.05 to 20  $\mu$ gat/L. Coefficient of variation-95-percent confidence level at 0.64  $\mu$ gat PO<sub>4</sub>-P/L-1.6 percent; and

 $SiO_3$ -Si 0.1 to 50  $\mu$ gat/L. Coefficient of variation-95-percent confidence level at 33  $\mu$ gat  $SiO_3$ -Si/L--2.3 percent.

### DATA PRESENTATION

The interpolated data and corresponding profiles of temperature, salinity, sigma-t, and turbidity are given in section 8, Station Data and Surface Contours. The codes used in the table headings are from the National Oceanographic Data Center Manual Series (1964). Profiles were made from the smoothed raw data, with identifying symbols located at 5-m intervals.

Figures 2 to 7 are contoured temperatures and salinities at the 3-m depth for each cruise.

# 6. ACKNOWLEDGMENTS

The authors express their thanks to the officers and crew of the NOAA ship <u>Ferrel</u>, under Comdr. Phillip Johnson, for the long and diligent hours they devoted to collecting these data. Thanks also go to Kathleen Phlips who prepared the data layout and typed the manuscript and to Alan Herman who wrote several of the data processing rou-

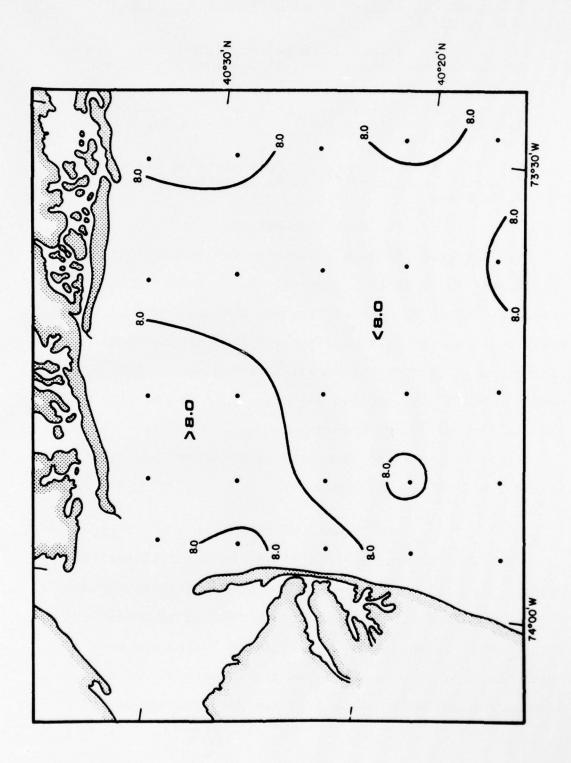


Figure 2. Cruise WSC-6, temperature (°C) contours at 3-m depth, April 16-20, 1974.

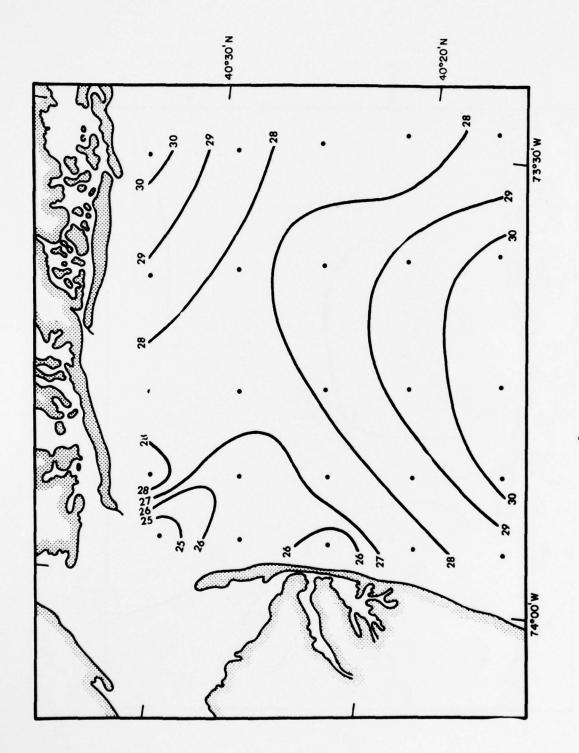


Figure 3. Cruise WSC-6, salinity (%/00) contours at 3-m depth, April 16-20, 1974.

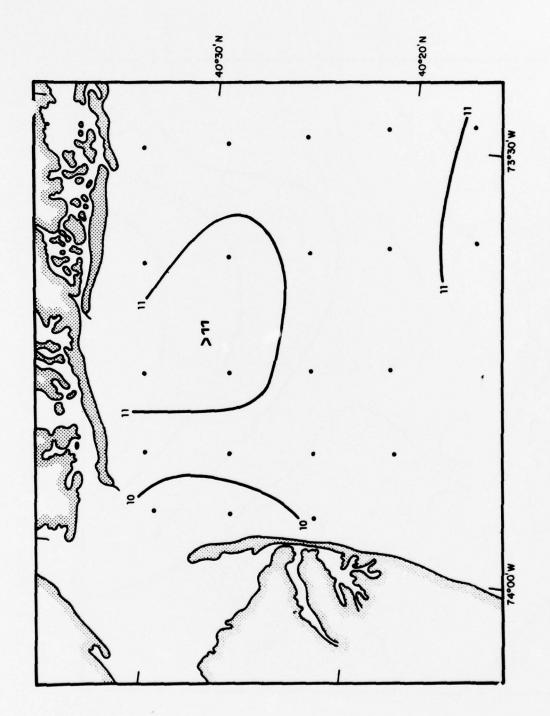


Figure 4. Cruise WSC-7, temperature (°C) contours at 3-m depth, May 6-9, 1974.

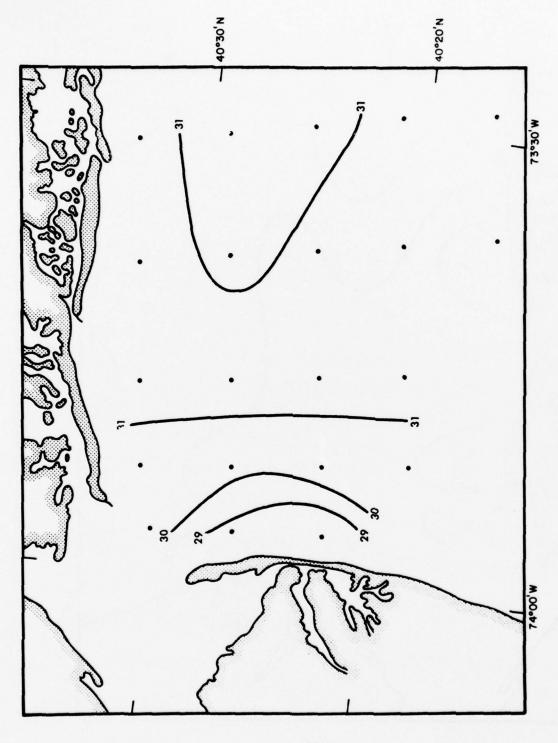


Figure 5. Cruise WSC-7, salinity (°/00) contours at 3-m depth, May 6-9, 1974.

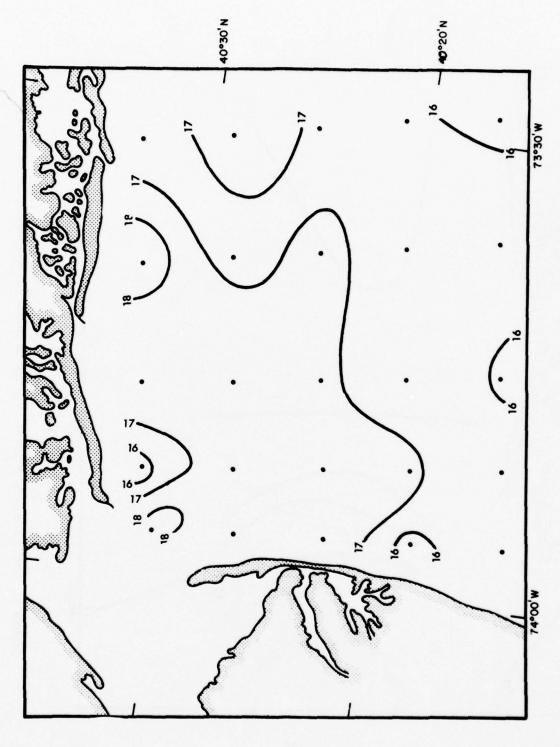


Figure 6. Cruise WSC-8, temperature  $\binom{0}{C}$  contours at 3-m depth, June 10-13, 1974.

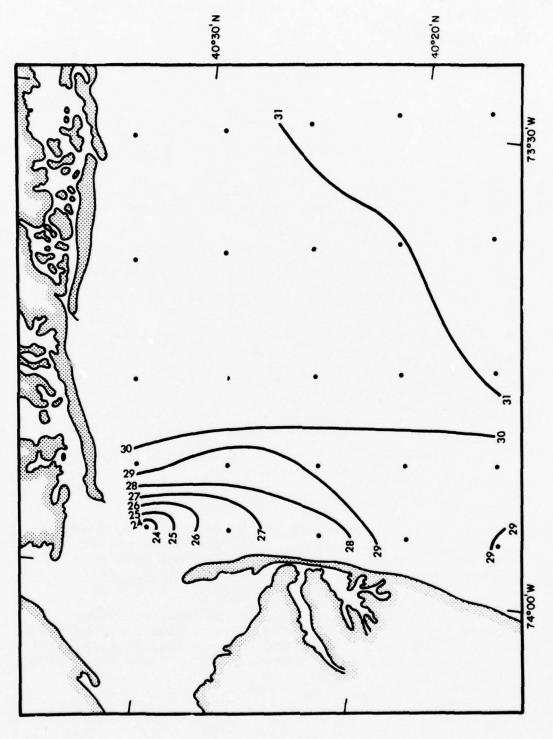


Figure 7. Cruise WSC-8, salinity (%)00) contours at 3-m depth, June 10-13, 1974.

times. The effort was sponsored by NOAA and funded in part by the NOAA Environmental Research Laboratories and the MESA program.

# 7. REFERENCES

- Armstrong, F. L. J., C. R. Stearns, and J. D. H. Strickland [1967]: the measurement of upwelling and subsequent processes by means of the Technicon Antography and associated equipment, Deep-Sea Res. Cusanog. Apstr. 14 (3): 381-389.
- Charnell R. L. and G. A. Maul (1973): Oceanic observation of New York Bight by ERTS 1, Nature 242 (5398):
- The directs of Waste Disposal in the New York Bight, chapter as report to the U.S. Army Corps of Engineers, Marianal Marine Fisheries Service, Sandy Hook Lab-
- Charman, M. L. J. R. Apel, W. H. Manning, III, and R. H. Quelogt (274): Utility of ERTS-1 for coastal coar observation: the New York Bight example. The New York Bight example.
- Drake Drake B. A. Segar, R. L. Charnell, and G. A. Maul
  Comparison of optical measurements and
  Supponded soluis concentrations in the ocean, Report
  The bidity Workshop, National Oceanographic Instrumentation Center Rockville, Md., 19 pp.
- Grassburg (1965): Technician Symposium, 304 pp.
- Hazelworth, c. B., B. L. Kolitz, R. B. Starr, R. L. Charnell, and G. A. Berberian (1974): New York Bight project, water column sampling cruises #1-5 of the NOAA ship Forkel, August-November 1973, MESA Report No. 74-2, U.S. Govel Print. Off., Washington, D. C., 191 pp.
- National Oceanographic Data Center Manual Series (1964):
  Plocessing physical and chemical data from oceanographic atations, Part 1. Coding and keypunching, Publications
  H-2 revised, U.S. Naval Oceanographic Office, Washington, D.C., 117 pp.

Strickland, J. D. H., and T. R. Parsons (1968): A practical handbook of seawater analysis, <u>Bulletin 167</u>, Fisheries Research Board of Canada, Ottawa, Ont., Canada, 311 pp.

12 Reprinted from: NOAA Technical Report ERL 344-AOML 20, 144 p.



U.S. DEPARTMENT OF COMMERCE Rogers C. B. Morton, Secretary

NATIONAL OCEANIC AND ATMOSPHERIC ADMINISTRATION
Robert M. White, Administrator
ENVIRONMENTAL RESEARCH LABORATORIES
Wilmot N. Hess, Director

### NOAA TECHNICAL REPORT ERL 344-AOML 20

# Oceanographic Conditions in the Caribbean Sea During the Summer of 1971

JOHN B. HAZELWORTH ROBERT B. STARR

BOULDER, COLO. July 1975



#### DISCLAIMER

The NOAA Environmental Research Laboratories do not approve, recommend, or endorse any proprietary product or proprietary material mentioned in this publication. No reference shall be made to the NOAA Environmental Research Laboratories, or to this publication furnished by the NOAA Environmental Research Laboratories, in any advertising or sales promotion which would indicate or imply that the NOAA Environmental Research Laboratories approve, recommend, or endorse any proprietary product or proprietary material mentioned herein, or which has as its purpose an intent to cause directly or indirectly the advertised product to be used or purchased because of this NOAA Environmental Research Laboratories publication.

#### CONTENTS

	Page
ABSTRACT	1
1. INTRODUCTION	1
2. DATA COLLECTION	2
3. NAVIGATION	2
4. DENSITY DATA	5
5. PRELIMINARY DATA PRESENTATION	6
6. ACKNOWLEDGMENTS	23
7. REFERENCES	23
8. SERIAL DATA	25

#### OCEANOGRAPHIC CONDITIONS IN THE CARIBBEAN SEA DURING THE SUMMER OF 1971

John B. Hazelworth Robert B. Starr

The NOAA ship <u>Discoverer</u> conducted a physical oceanographic program in the Caribbean Sea as part of CICAR (Cooperative Investigation of the Caribbean and Adjacent Regions) in July, August, and September 1971. The primary objective of the <u>Discoverer</u> cruise was to investigate the dynamics of the formation of the Yucatan Current. This report describes the measurements taken and the methods applied to correct and analyze the hydrographic station data. It also makes the results of these data available to other researchers who are working on problems in the Caribbean.

Key Words: Discoverer, STD Data, CICAR, Caribbean Sea, Oceanographic Observations

#### 1. INTRODUCTION

Scientists from the Atlantic Oceanographic and Meteorological Laboratories (AOML) of the National Oceanic and Atmospheric Administration (NOAA) conducted a two-ship investigation in the northwestern Caribbean Sea (Cayman Sea) and southern Gulf of Mexico during July, August, and September 1971. Additionally, stations were occupied and data taken through the Windward Passage and across the eastern end of the Caribbean Sea. The study was undertaken as part of the Declared National Program, CICAR (Cooperative Investigation of the Caribbean and Adjacent Regions), a program of the Intergovernmental Oceanographic Commission. Many of the stations were occupied on standard sections, defined for this international program.

Two ships of the NOAA National Ocean Survey were used in the AOML investigation. The NOAA ship Discoverer occupied hydrographic stations in the Caribbean Sea and planted and recovered deep-sea tide gages and current meters. The NOAA ship Researcher collected both Lagrangian current data and density data in the Caribbean Sea and the Gulf of Mexico. The results of the Researcher data collection program have been reported by Molinari (1973). The primary objectives of the study were to investigate the formation of the Yucatan Current and to map the distribution of various chemical elements.

This report provides salinity-temperature-density (STD) measurements and data taken by the <u>Discoverer</u> during July, August, and September 1971. The sections that follow describe the collection and analytical procedures applied and present some preliminary description of the results. These sections are presented to inform other users of these data, to describe the

methods used to analyze and correct the data before the measurements were submitted to the National Oceanographic Data Center (NODC) of the NOAA Environmental Data Service, and to interrelate the results. Water samples were 2350 collected and analyzed for nutrient content, but these results will be the subject of a separate report. Expendable bathythermograph (XBT) data were also collected by both the Researcher and Discoverer and are on file at the NODC.

#### DATA COLLECTION

Two cruises of the CICAR program were completed by the Discoverer during 1971. The first one was run from July 18 to August 20. During this cruise, designated as RP9, 97 STD casts were made. The cruise track and positions of the STD casts are given in figure 1. The second cruise, designated as RP11, was run from September 10 to September 19. During the second cruise, 22 STD casts were taken in an area farther east of the first cruise. The cruise track and positions of

the STD stations are given in figure 2.

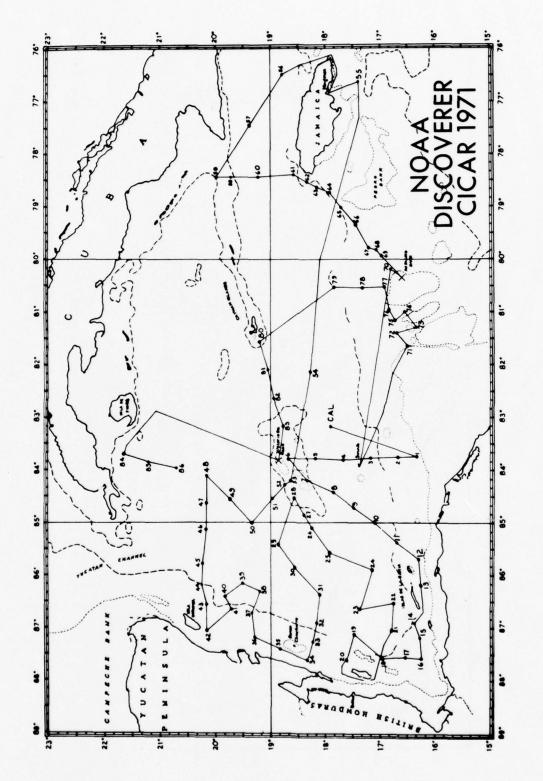
Temperature and salinity measurements were made while the Discoverer stopped on station, using the Plessey STD model 9006. Attached on the side of the STD cage was a General Oceanics Rosette Multi-Sampler. During each cast, nine water samples were taken. Ordinarily, the STD was lowered to 2,000 meters, depth permitting. On the return to the surface, water samples were collected at 2,000 and 15,000 meters and at the 6°, 10°, 13°, 16°, 18°, 22°, and 26°C isotherms. For depth and temperature checks, reversing thermometers were attached to four of the Niskin bottles. At the completion of a cast, water samples were drawn for measurement of salinity and oxygen. Additional water samples were drawn and then frozen. At the completion of the cruise, the frozen samples were returned to Miami where they were analyzed for nutrient content.

During the cast, the raw data were recorded in frequency count on magnetic tape. Simultaneously, the raw data were fed to the computer, translations into engineering units made, calibrations applied, and data recorded on punched

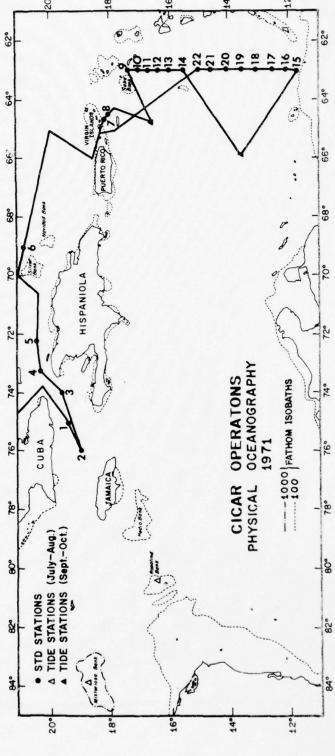
paper tape and typewriter printouts.

#### 3. NAVIGATION

Satellite navigation was the primary position determination system used on board the Discoverer. The system was inoperative from July 22 to 27. On the average, about 16 fixes a day could be obtained with this system. Loran A and Omega were available as backup. Although Loran A coverage is poor in most of the area, the Omega worked well; and fixes were normally taken at 15-minute intervals. The agreement between the satellite and Omega fixes was generally on the order of 1 mile.



Discoverer cruise track and STD station location for RP9.



Discoverer cruise track and STD station location for RP11. 83 Figure

#### 4. DENSITY DATA

Standard physical oceanographic procedures, as outlined in the <u>U.S. Naval Oceanographic Office Publ. No. 607</u> (1968), were used to correct the reversing thermometers for computations of temperature and depth. Salinity samples were analyzed on an inductive salinometer.

Mean differences were computed between the temperature and depth as recorded by the reversing thermometer and simultaneously as recorded by the STD. The mean depth difference was 3.9 meters, with a standard deviation of 4.13 meters. The mean temperature difference was  $0.03^{\circ}\text{C}$ , with a standard deviation of  $0.04^{\circ}\text{C}$ .

A similar check of salinity difference revealed a need for a salinity correction. The required salinity correction was constant throughout the cruises. A third-degree polynomial fit of the difference between STD salinity and water sample salinity as a function of depth was made and used for calibration. After the correction formula was applied to the salinity data, the mean difference was  $0.03^{\circ}/\circ\circ$ , with a standard deviation of  $0.04^{\circ}/\circ\circ$ .

For stations 8 through 17 and 73 through 84, selected values were coded from the typewriter output. These data were put on punch cards and then recorded on magnetic tape in the same format as the rest of the data. A new data tape was created containing only the down cast with an end of file at the end of each cast, and stations 8 through 17 and 73 through 84 were inserted in their proper chronological order.

These data were edited for noise by a series of filters. Temperature-Salinity (T-S) curves from the edited tape were plotted. These plots indicated residual small magnitude noise and gaps in the data. The noise was edited out point by point. To the extent possible, gaps in the data were filled in from the typewriter output.

The edited temperature and salinity data were smoothed by a linear regression computation. The regression was performed in 10-meter increments in overlapping 5-meter segments, and a new tape containing the smoothed data interpolated at 10-meter intervals was created. The standard NODC heading card for electronically obtained serial stations, containing cruise number, cast number, position, date, time, and weather data, were added to identify each cast.

Because of an insufficient number of observations, stations 8 through 17 and 73 through 84 were not subjected to the edit-regression interpolation procedure described above. They were quality-controlled and corrected by hand.

Using the edited data, sigma-t, specific volume anomaly, sound velocity, thermosteric anomaly, dynamic height, and transport function were computed at 20-meter intervals. Stations 8 through 17 and 72 through 84 were interpolated by the three-point Lagrangian interpolation method before the computations could be made.

Section 8 lists in chronological order the entire set of cruise stations with the abovementioned computations. For brevity, only selected depths are printed. The complete set of 10-meter interval data is on file at the NODC.

#### 5. PRELIMINARY DATA PRESENTATION

Four mean T-S curves (fig. 3 through 6) of various areas were computed and plotted. Area 1 is the mean curve of stations 9 through 22 (fig. 2) taken during cruise RP11 just west of the Lesser Antilles during September 1971. Area 2 is the mean curve of stations 56 through 61 taken during cruise RP9. These stations lie north of Jamaica. Area 3 includes stations 62 through 79 taken during cruise RP9. This area lies southwest of Jamaica. Area 4 comprises stations 40 through 49 and 84 through 86, covering the area east of the Yucatan Peninsula toward Cuba. Locations for these stations

are shown in figure 1.

The mean T-S curves were obtained by averaging the STD salinity values in 1/2°C intervals. In general, they agree very well with the T-S curve of the Caribbean Sea presented by Wüst (1964), but with some slight differences. Area 1 exhibits the highest mean salinity maximum of 36.81°/..., indicating its closeness to the source of the Subtropical Underwater. It also exhibits the lowest mean salinity of 34.72°/... for the Antarctic Intermediate Water (fig. 13). The mean minimum salinities of the three other areas are greater than 34.80°/..., indicating mixing of the Antarctic Intermediate Water as the water proceeds downstream. Area 1 also has the lowest mean surface salinity of 34.53°/..., with numerous values less than 34.00°/... and relatively low surface temperatures (fig. 12 and 13). The low salinity reflects the influence of the Amazon and Orinoco Rivers discharge combined with the equatorial low-salinity belt (Wüst).

combined with the equatorial low-salinity belt (Wüst).

The waters represented by the T-S curve of Area 2
were sampled to define the input through the Windward Passage.
Therefore, this curve should relate to the characteristics
of the waters that have entered through the Windward Passage
from the North Atlantic while that of Area 3 should reflect
modifications that occur to the water column as it transits
the Caribbean from Area 1. The surface water of Area 3 reflects the modifications experienced during this transit.
However, the surface of Area 2 is warmer and more saline than
that of Area 3 and, between 24° and 28°C, is fresher than
Area 3 (fig. 4, 5, 7, and 8). The T-S characteristics of
Area 4 should be indicative of the waters that are about to
exit the Caribbean through the Yucatan Channel. Areas 2 and
4 are essentially identical. It was expected that in the
near surface layer Area 4 would reflect T-S characteristics
intermediate between Areas 2 and 3, but it does not. Like
Area 2, Area 4 is appreciably fresher between 24° and 28°C
and is warmer at the surface than Area 3.

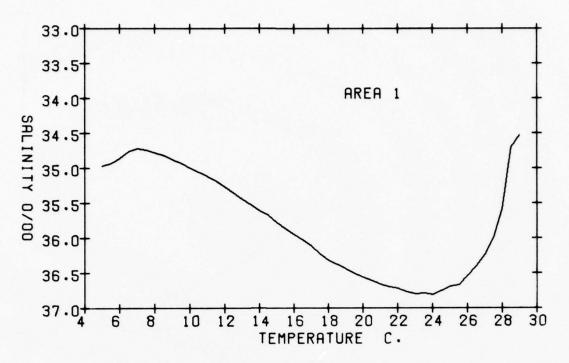


Figure 3. Mean T/S curve, stations 9-22, cruise RP11.

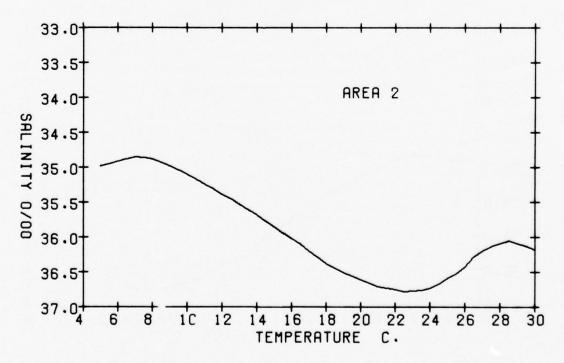


Figure 4. Mean T/S curve, stations 56-61, cruise RP9.

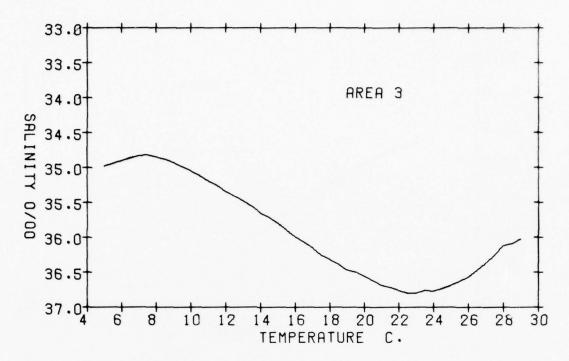


Figure 5. Mean T/S curve, stations 62-79, cruise RP9.

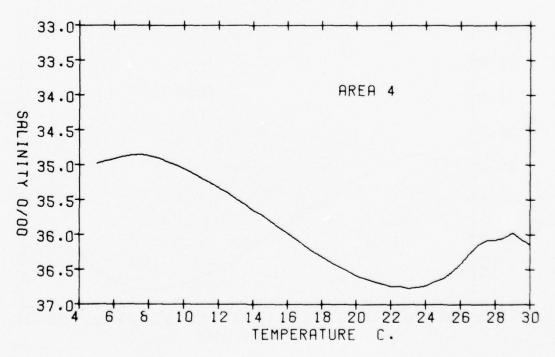
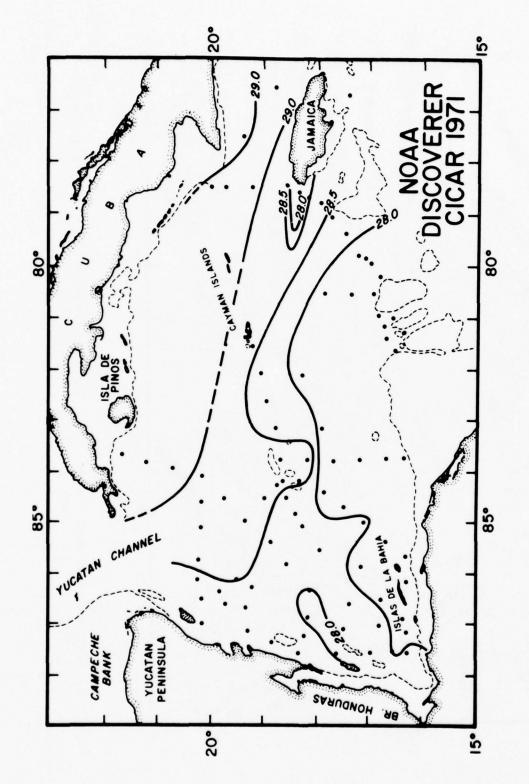
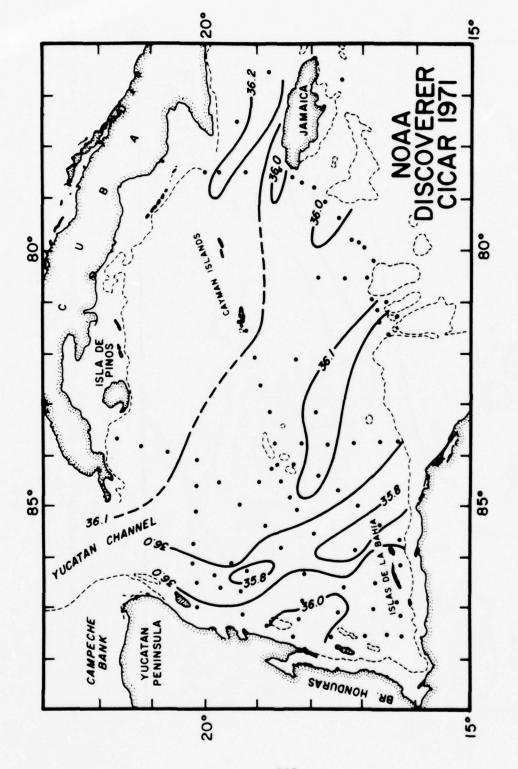


Figure 6. Mean T/S curve, stations 40-49 and 84-86, cruise RP9.



Surface temperature in degrees Celsius derived from the STD observations during July/August 1971. Figure 7.

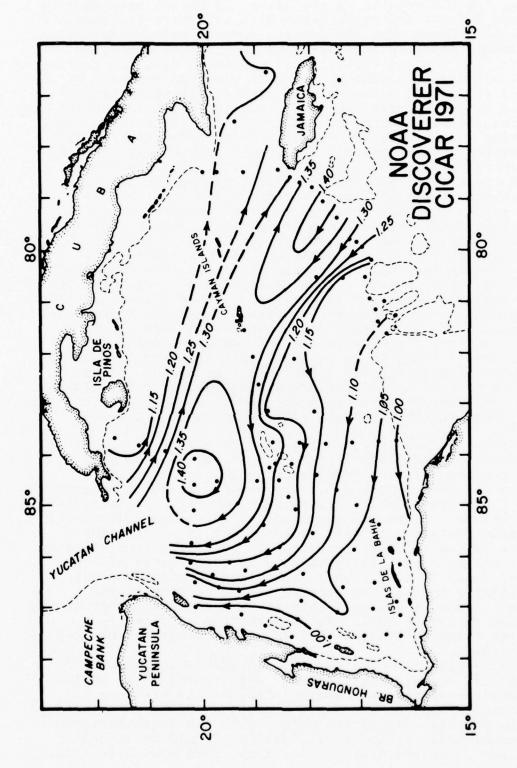


Surface salinity in parts per thousand derived from STD observations during July/August 1971. Figure 8.

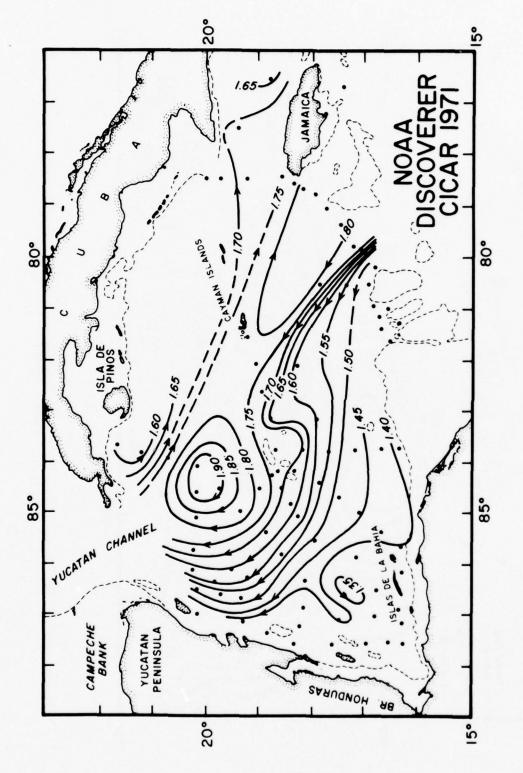
The T-S differences in the upper 150 meters between Area 3 and Areas 2 and 4 are explainable with reference to figures 9 These show the surface current pattern determined from dynamic topography relative to 500, 1,000, and 1,800 This current system is in agreement with the Lagrangian current measurements made at the same time and reported by Molinari (1973) and with the hydrographic stations and geomagnetic electrokinetograph (GEK) measurements taken during the same time and reported by Emilsson (1971). There is striking similarity in the surface current structure relative to the three depths, but Emilsson's GEK results agree best with the surface relative to 500 meters depth (fig. 9). The higher surface temperature and salinity north of Jamaica can be attributed to water that has flowed out from the Gulf of Mexico around Cabo San Antonio, the most westerly point of This higher temperature and salinity result from the additional heating and evaporation this water has been subjected to relative to that southwest of Jamaica, caused by a longer time in tropical conditions as it transits the Cayman Sea and the Loop Current of the eastern Gulf of Mexico. The longer route is suggested rather than a route just around the anticyclonic gyre between the Yucatan Channel and Misteriosa Bank because of the fresher water between 24° and 28°C. This is the only place where the T-S curves of Areas 2 and 4 differ, Area 4 being slightly less salty and therefore nearer the source of dilution for subsurface freshening. It is suggested that this relative freshening results from dilution as the Loop Current entraps colder, lower salinity shelf waters along the northern and eastern margins of the Gulf of Mexico.

Between 5° and 18°C, Area 1 is less saline than Area 3; and between 7° and 22°C, Area 3 is less saline than Area 2. The increasing salinity downstream, suggested by these segments of the T-S curves, covers a depth range of roughly 200 to 1,000 meters which brackets the Antarctic Intermediate Water minimum. Since the magnitude of the minimum decreases downstream continuously with distance due to mixing, the increase in the adjacent waters above and below is attributed to this mixing also. This suggests that the water of Area 2, north of Jamaica, has travelled the longest path from the open Atlantic and has the longest residence time in the Caribbean Sea of the waters sampled from the Discoverer during the CICAR survey of 1971. No contribution of water from the North Atlantic through the Windward Passage can be seen in these data.

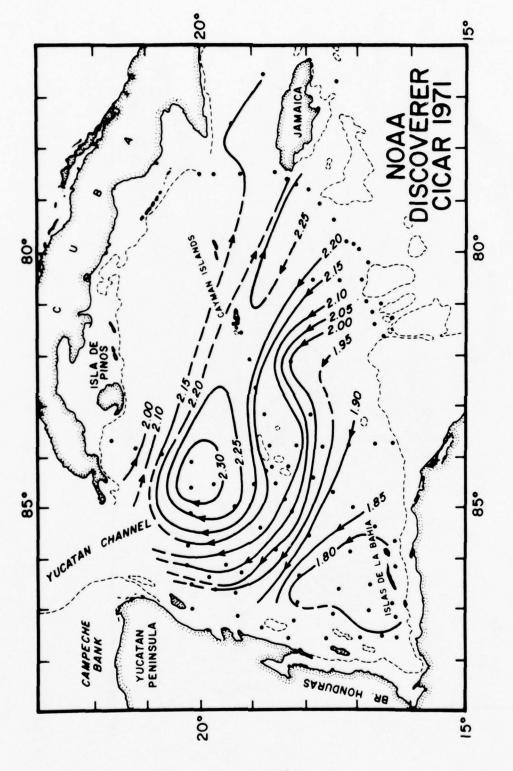
The section along 63° West longitude is a standard CICAR section. It extends the length of the Grenada Basin on the eastern slope of the Aves Ridge. Many of the stations of this eastern transect are depth-limited by banks associated with the Antilles Arc at the north, with the South American continental shelf at the south, and in the middle by the Aves Ridge. Consequently, the sections presented here (fig. 12)



Geostrophic current pattern at surface in dynamic meters relative to 500-meter level. Figure 9.



Geostrophic current pattern at surface in dynamic meters relative to 1,000-meter level. Figure 10.



Geostrophic current pattern at surface in dynamic meters relative to 1,800-meter level. Figure 11.

through 18) are drawn, at most, to 1,000-meter depth. temperature and salinity distributions shown in figures 12 and 13 depict the water structure quite well because gradients below 1,000 meters were very weak. The deepest values measured by the STD at 2,000 meters were 4.1°C for temperature and

34.98°/.. for salinity.

Analogous to the surface charts of dynamic topography for the Cayman Sea, the dynamic topography relative to 500 and 1,000 meters determined from these observations is shown in figures 14 and 15. Too few stations penetrated to 1,800 meters to make it worthwhile producing a section relative to that depth. Because 1,000 meters is deeper than the sill depths of the passages with the dominant flow (Stalcup and Metcalf, 1972), figure 15 is probably fairly indicative of the zonal flow through this section. The strongest gradients in figures 14 and 15 indicative of the maximum flow are centered on station 21, while counterflows are suggested at

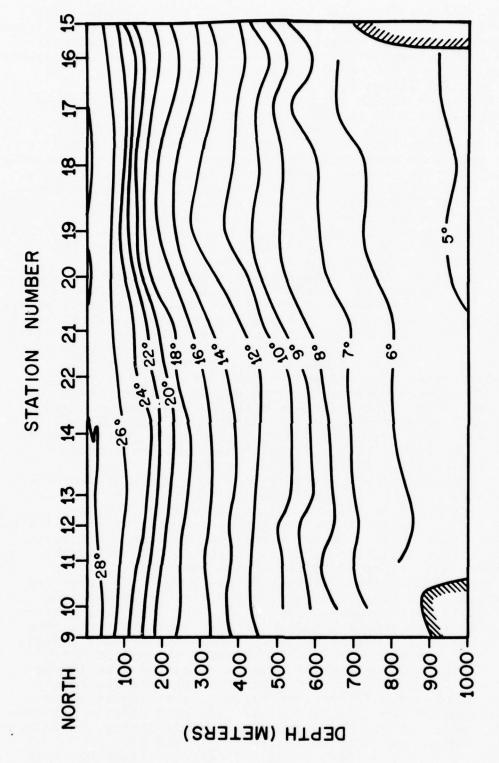
the northern and southern ends of the section.

Figures 16 and 17 confirm this interpretation and show the current structure in detail relative to 1,000 and 500 meters. The 1,000-meter depth allows a more accurate portrayal of the currents, but the 500-meter depth permits an extension shallower stations at the ends of the section. The difference in current structure relative to the two depths is quite significant. In this section, the Caribbean Current as discussed by Wüst (1964) and Gordon (1967) is a westwardflowing, bifurcate stream evident on the surface between stations 14 and 19 with an easterly flowing countercurrent underneath between stations 14 and 21 (fig. 16). To the north and south are easterly flowing currents penetrating to the surface with westerly flowing countercurrents below (fig. 16 and 17). At the extreme southern stations, a strong westerly flow is evident in figure 17 which can be correlated with the westward transport through the Grenada Passage reported by Stalcup and Metcalf (1972). It is difficult to explain the east-flowing currents on each side of the Caribbean Current based on only one section. However, they may represent arms of gyres in the lee of the Lesser Antilles and upstream from the Aves Ridge crest.

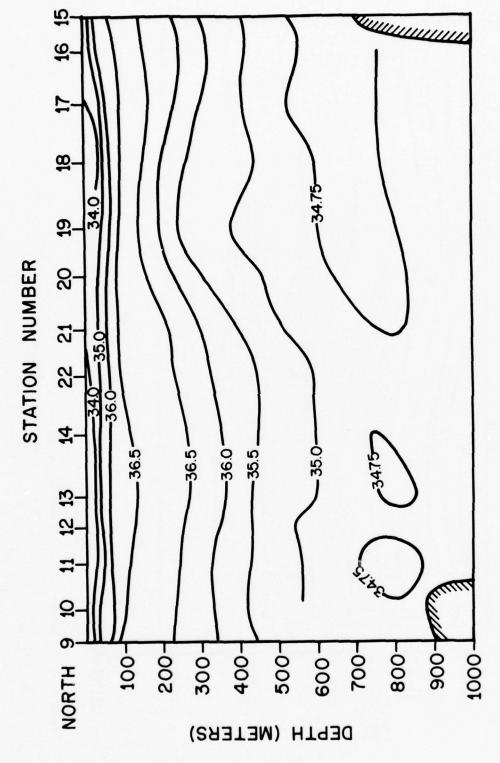
Several interesting relations are apparent between the temperature and salinity sections and the current section relative to 1,000 meters (fig. 12, 13, and 16). The surface water is warmer and less saline in the countercurrents than in the Caribbean Current or flow through the Grenada Passage, suggesting warming and dilution relative to surface water from outside the Antilles Arc due to retention time in the Caribbean. Also the core of Antarctic Intermediate Water, as defined by the 34.75°/00 isohaline, is strongest where the subsurface westerly current is indicated between stations 18 and 17 and is absent where the subsurface easterly counter-

flow is demonstrated between stations 14 and 21.

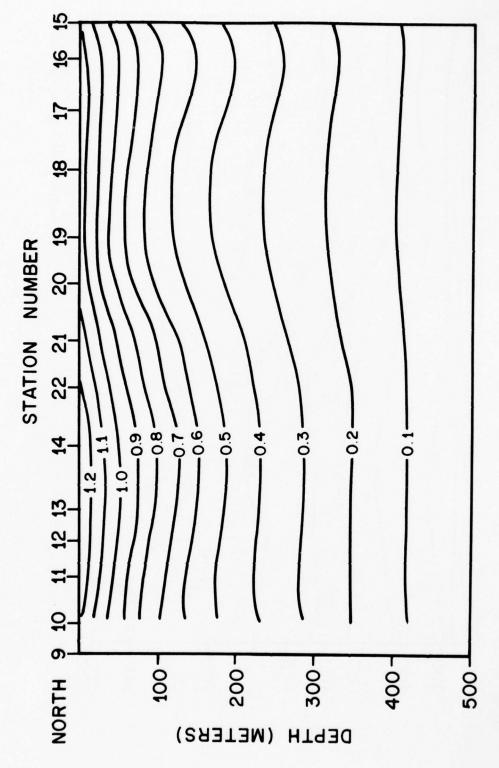
The volume transport across 63°West longitude has been computed to 1,000 meters or to the deepest depth of the shallower stations and is presented in figure 18. The total



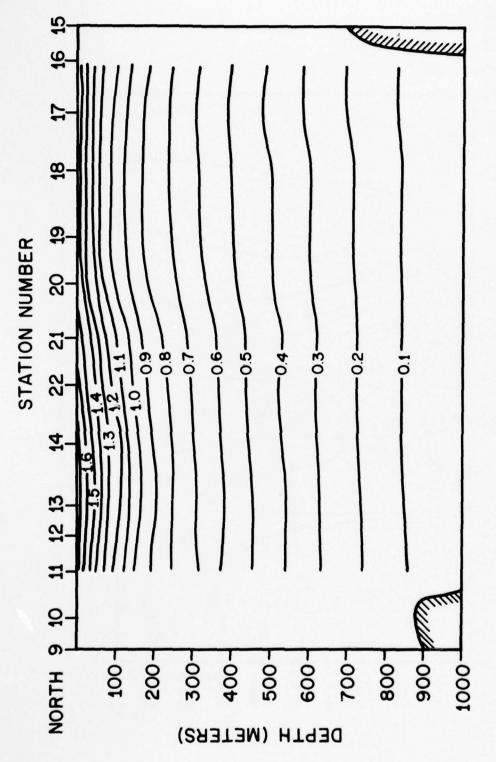
Temperature distribution in degrees Celsius observed during September 1971 along 63° West longitude. Figure 12.



Salinity distribution in parts per thousand observed during September 1971 along 63° West longitude. Figure 13.



Dynamic topography in dynamic meters relative to 500 meters along 63° West longitude. Figure 14.



Dynamic topography in dynamic meters relative to 1,000 meters along 63° West longitude. Figure 15.

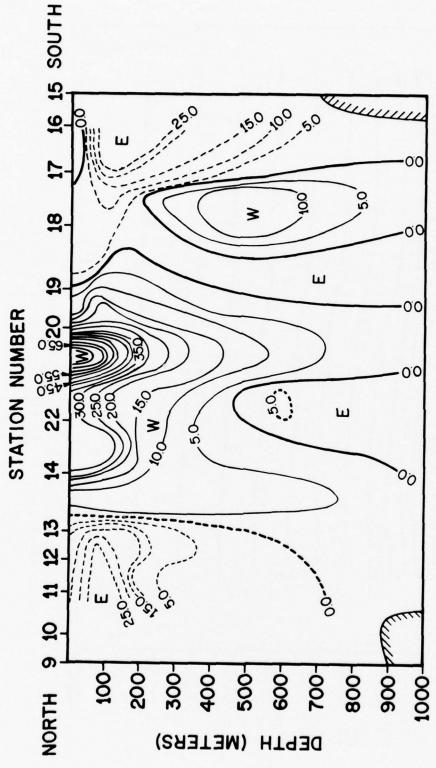


Figure 16. Isotachs of current velocity in centimeters per second relative to 1,000-meter depth along 63° West longitude.

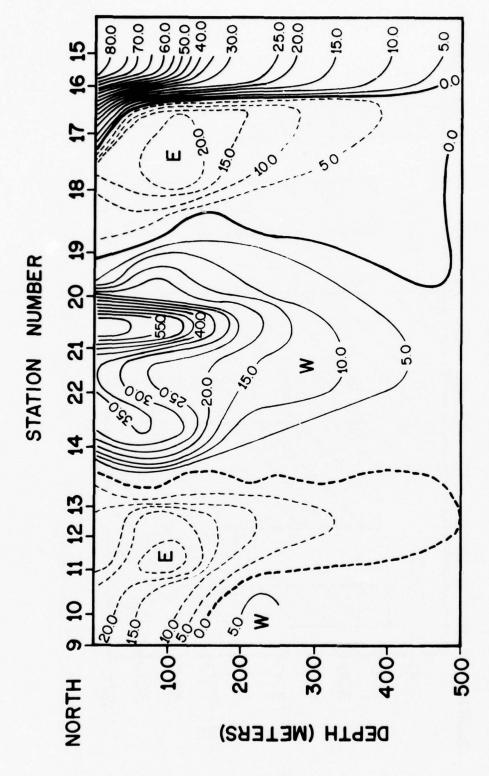


Figure 17. Isotachs of current velocity in centimeters per second relative to 500-meter depth along 63° West longitude.

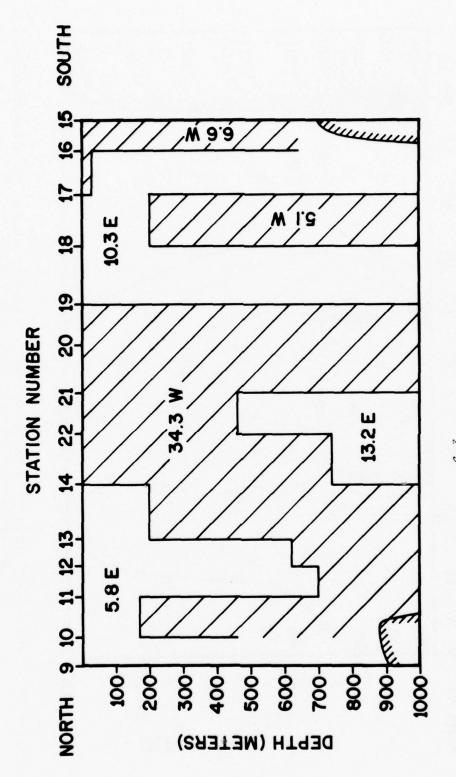


Figure 18. Volume transport X  $10^6 \text{m}^3/\text{sec}$  along 63° West longitude.

westward transport is 46.0x106 m3/sec, and eastward transport is  $29.3 \times 10^6$  m<sup>3</sup>/sec for a net transport of  $16.7 \times 10^6$  m<sup>3</sup>/sec westward. This net transport is considerably less than the 26x106 m3/sec reported by Gordon (1967) for the Eastern Venezuela Basin or the same volume reported by Stalcup and Metcalf (1972) for the major passages through the Lesser Antilles. However, the 34.3x106 m<sup>3</sup>/sec for the core of the Caribbean Current is appreciably greater than their values, whereas  $6.6 \times 10^6$  m<sup>3</sup>/sec for the flow through the Grenada Passage agrees reasonably well with the 3.8 to 15.9x106 m<sup>5</sup>/sec range reported by Stalcup and Metcalf. So the discrepancy lies principally in the magnitude of the countercurrents apparent in this section and a possible appreciable flow below 1,000 meters. This section would be more usable for this type of analysis if located 50 kilometers farther to the east to permit current computation relative to a deeper level.

#### ACKNOWLEDGMENTS

The authors express their thanks to the officers and crew of the <u>Discoverer</u> for the long and diligent hours they devoted to collecting these data. Thanks are also due Alan Herman of AOML for writing very difficult data processing programs. The work was funded in part by the National Science Foundation under International Decade of Ocean Exploration grant AG-253.

#### 7. REFERENCES

- Emilsson, Ingvar (1971), Note on the Countercurrent in the Yucatan Channel and the Western Cayman Sea, Geofisica Internacional, Revista de la Union Geofisica Mexicana, Mexico, 11 (3), pp. 139-149.
- Gordon, Arnold L. (1967), Circulation of the Caribbean Sea, Journal of Geophysical Research, 72 (24), pp. 6207-6623.
- Molinari, Robert L. (1973), Data From the Lagrangian Current-Measurement Project Conducted Aboard the NOAA Ship Researcher During CICAR Survey Month 1, NOAA Technical Memorandum ERL AOML 19, U.S. Department of Commerce, National Oceanic and Atmospheric Administration, Environmental Research Laboratories, Miami, Fla., 81 pp.
- Stalcup, Marvel C., and William G. Metcalf (1972), Current Measurements in the Passages of the Lesser Antilles, Journal of Geophysical Research, 77 (6), pp 1032-1049.
- U.S. Naval Oceanographic Office (1968), Instruction Manual for Obtaining Oceanographic Data, Third Edition, NOO Publ. No. 607, Washington, D.C., 188 pp.

Wüst, Georg (1964), Stratification and Circulation in the Antillean Caribbean Basins, Part One, Spreading and Mixing of the Water Types, With an Oceanographic Atlas, Columbia University Press, New York, N.Y., 201 pp.

#### 8. SERIAL DATA

## Explanation of Column Headings in the Serial Data Listings

Z	Depth in meters
T	Temperature in degrees Celsius
S	Salinity in parts per thousand (°/00)
SIG T	Sigma $t = (density at 0 pressure -1) x 1,000$
T ANOM	Thermosteric Anomaly in centiliters per ton
SVA	Specific Volume Anomaly
SVEL	Sound Velocity in meters per second
DYNHGT	Dynamic Depth Anomaly in dynamic meters
TRANS	Transport Function summed from the surface downward in dynamic meters times meters

```
17 54
    LATITUDE
                         83 08
   LONGITUDE
    DEPTH TO BOTTOM
                         3475 M
                  SIGT
                         TANOM
                                SVA
                                      SVEL
                                              DYNHGT
                                                       TRANS
   0 27.91 36.11 23.28
                         460.7 460.7 1542.81
                                               .0000
                                                           . 0
 20 27.84 36.15 23.52
                                               .0919
                         457.1 457.9 1543.00
                                                           .9
                         451.6 453.3 1543.05
 40 27.71 36.15 23.38
                                                         3.7
                                               .1830
 60 27.57 36.17 23.44
                         445.8 448.3 1543.09
                                               .2731
                                                         8.2
 80 26.89 36.28 23.74
                         416.9 420.3 1542.00
                                                        14.6
                                               . 3600
                         376.5 380.7 1540.32
100 25.95 36.45 24.16
                                                        22.6
                                               .4401
                         342.2 347.7 1538.92
120 25.16 36.59 24.52
                                               .5129
                                                        32.1
                                               .5791
140 24.23 36.70 24.88
                         307.6 313.8 1537.10
                                                        43.0
 160 23.15 36.77 25.25
                         272.8 279.3 1534.82
                                               .6384
                                                        55.2
180 21.81 36.77 25.63
                         236.6 243.3 1531.73
                                               .6907
                                                        68.5
                         200.7 208.0 1527.76
200 20.23 36.69 26.01
                                               . /358
                                                        82.7
220 19.23 36.62 26.23
                         180.1 189.0 1525.24
                                               .7755
                                                        97.9
                                               .8120
240 18.42 36.54 26.58
                        165.5 175.7 1523.19
                                                       113.7
                        154.7 165.9 1521.36
260 17.71 36.45 26.49
                                               .8461
                                                       130.3
280 17.09 36.35 26.57
                         147.8 159.4 1519.78
                                                       147.6
                                               .8787
                         144.7 156.0 1518.45
300 16.58 36.24 26.60
                                               .9102
                                                       165.4
                         134.1 142.8 1513.49
340 14.88 35.92 26.71
                                               .9711
                                                       203.1
                         117.2 125.7 1506.98 1.0246
380 12.80 35.59 26.89
                                                       243.0
420 11.25 35.33 27.01
                         106.2 116.4 1502.01 1.0728
                                                       285.0
460 11.11 35.31 27.02
                         105.2 116.2 1502.14 1.1105
                                                       328.8
500 10.22 35.27 27.04
                         103.2 114.9 1501.72 1.1661
                                                       374.5
540 10.12 35.15 27.07
                         100.3 112.2 1499.71 1.2117
                                                       422.1
580
      9.43 35.07 27.12
                          95.1 107.1 1497.75 1.2556
                                                       471.4
      8.91 35.03 27.18
620
                          90.0 102.3 1496.43 1.2972
                                                       522.5
      8.12 34.94 27.23
                          85.0
                                97.0 1494.00 1.3371
                                                       575.2
661)
700
                          82.3
                                93.8 1491.51 1.3753
      7.54 34.85 27.26
                                                       629.4
      6.70 34.79 27.32
7411
                          76.8
                                88.0 1489.62 1.4116
                                                       685.2
      6.25 34.79 27.38
780
                          71.1
                                82.2 1488.49 1.4457
                                                       742.3
                                74.3 1487.39 1.4769
                                                       8.00A
820
      5.80 34.82 27.46
                          63.4
860
      5.49 34.85 27.52
                          57.5
                               68.5 1486.83 1.5054
                                                       R60.4
900
      5.26 34.87 27.56
                          53.3
                                64.4 1486.58 1.5319
                                                       921.2
941
      5.01 34.89 27.61
                          49.0
                                60.1 1486.24 1.5567
                                                       983.0
980
      4.87 34.90 27.63
                          46.7
                                58.0 1486.33 1.5802
                                                      1045.7
      4.77 34.91 27.65
                          44.9
                                56.4 1486.59 1.6030
1020
                                                      1109.4
      4.65 34.92 27.67
                          42.9
                               55.0 1487.41 1.6473
1100
                                                      1239.4
      4.49 34.95 27.70
1200
                          40.4
                                53.2 1488.40 1.7009
                                                      1406.8
1300
      4.40 34.94 27.72
                          38.7
                               52.3 1489.69 1.7532
                                                      1579.5
      4. 14 34.94 27.72
                          39.1
                                52.4 1491.08 1.8055
1400
                                                      1757.5
      4.29 34.95 27.74
                          36.8
1500
                               52.0 1492.53 1.8577
                                                      1940.6
      4.26 34.95 27.74
                          36.5
                               52.5 1494.05 1.9098
1600
                                                      2129.0
1700
      4.23 34.95 27.74
                          36.2
                                53.1 1495.58 1.9626
                                                      2322.6
1800
      4.21 34.96 27.75
                          35.3
                                53.0 1497.17 2.0153
                                                      2521.5
1900
      4.20 34.96 27.75
                          35.2
                                53.8 1498.78 2.0687
                                                      2725.7
```

STD STATION NUMBER

JULY 18, 1971

2000

4.18 34.97 27.76

C

13.5 /

53.7 1500.37 2.1221

2935.2

54.2

```
01.5 7
    JULY 19, 1971
                         16 20
    LATITUDE
                         85 46
    LONGITUDE
    DEPTH TO BOTTOM
                          865 M
                                                        TRANS
                   SIGI
                         TANOM
                                SVA
                                       SVEL
                                              DYNHGT
                                                           .0
   0 28.00 36.00 23.17
                         471.4 471.4 1542.91
                                                .0000
                                                . 11940
 20 27.88 35.00 23.21
                         467.6 468.5 1542.97
                                                           .9
                         436.4 438.1 1541.97
 40 27.22 36.15 23.53
                                                .1846
                                                          3.7
  60 25.67 36.38 24.20
                         373.1 375.6 1538.97
                                                          8.2
                                                .2660
  80 25.00 36.49 24.49
                         345.5 348.8 1537.81
                                                . 5384
                                                         14.3
 100 24.21 36.61 24.82
                         314.1 318.2 1536.34
                                               .4051
                                                         21.7
                                                .4633
 120 22.33 36.66 25.40
                         258.2 263.0 1532.01
                                                         30.4
                         206.7 211.9 1526.63
 140 20.20 36.60 25.95
                                                         40.1
                                               .5107
 160 18.78 36.47 26.22
                         180.9 186.6 1522.88
                                               .5506
                                                         50.8
 180 17.09 36.37 26.34
                         169.2 175.5 1520.83
                                                         62.1
                                               .5868
200 16.95 36.21 26.50
                                               .6205
                                                         74.2
                         154.5 161.2 1517.63
                         145.2 152.2 1515.03
                                                         86.9
220 15.94 36.06 26.59
                                               .6518
                                               .6815
240 15.15 35.94 26.68
                         137.0 144.4 1512.76
                                                        100.3
                                                .7096
260 14.20 35.77 26.76
                         129.7 137.3 1509.87
                                                        114.2
280 13.23 35.62 26.94
                         121.5 129.2 1506.85
                                               .7363
                                                        128.6
300 12.36 35.44 26.91
                         115.2 123.1 1504.09
                                               .7615
                                                        143.6
340 11.20 35.34 27.01
                         106.2 114.4 1500.88
                                               .8091
                                                        175.0
380 10.65 35.24 27.04
                         102.5 111.3 1499.15
                                               .8545
                                                        208.3
421)
      9.88 35.13 27.09
                          97.8 107.0 1496.89
                                                .8981
                                                        243.4
                          92.8 102.1 1494.72
                                               .9399
460
      9.14 35.04 27.15
                                                        280.1
500
      8.58 34.97 27.18
                          89.5
                                 99.1 1493.19
                                               .9802
                                                        318.5
      8.24 34.94 27.21
                                96.7 1492.52 1.0192
                                                        358.5
540
                          86.7
580
      7.58 34.90 27.23
                          84.5
                                94.8 1491.74 1.0575
                                                        400.1
      7.40 34.87 27.28
620
                          80.1
                                90.5 1490.51 1.0947
                                                        443.1
      6.94 34.84 27.32
                                86.6 1489.33 1.1301
                                                        487.6
660
                          76.2
700
      6.53 34.84 27.36
                                 82.8 1488.77 1.1641
                                                        533.5
                          72.1
740
      6.74 34.84 27.40
                          68.5
                                79.2 1488.27 1.1964
                                                        580.7
790
      5.88 34.85 27.47
                          62.1
                                72.7 1487.10 1.2270
                                                        629.2
      5.70 34.86 27.50
820
                          58.9
                                69.7 1487.03 1.2554
                                                        678.8
      5.55 34.87 27.53
                          56.5
                                67.5 1487.10 1.2828
                                                        729.6
860
 900
      5.40 34.88 27.55
                          54.2
                                65.4 1487.17 1.3094
                                                        781.4
940
      5.25 34.89 27.58
                          51.9
                                63.3 1487.24 1.3351
                                                        A34.3
9811
                          49.6
                                 61.1 1487.30 1.3600
                                                        888.2
      5.11 34.90 27.60
      4.76 34.91 27.63
                          47.3
                                59.0 1487.36 1.3840
                                                        943.1
1020
1100
      4.56 34.93 27.68
                          42.6
                                54.7 1487.48 1.4295
                                                       1055.7
```

1

STD STATION NUMBER

Z	T	5	SIGT	TANOM	SVA	SVEL	NYNHGT	TRANS
(	27,97	36.01	23.18	469.7	469.7	1542.85	.0000	• 0
21	27.95	36.02	23.20	468.4	469.2	1543.14	.11939	• 9
4(	27.92	36.05	23.23	465.3	467.0	1543.43	.1875	3.8
60	27.24	36.06	23.46	443.5	446.0	1542.26	.2788	8.4
R	25.96	36.28	24.03	388.9	392.2	1539.88	. 5626	14.8
100	25.02	36.50	24.49	345.4	349.5	1538.19	.4368	22.8
120	23.82	36.64	24.96	300.9	305.7	1535.73	.5023	32.2
140	22.56	36.70	25.37	261.6	267.1	1532.95	.5596	42.8
160	20.58	36.61	25.85	215.7	221.7	1528.00	.6085	54.5
190	18.58	36.42	26.23	179.7	186.0	1522.58	.6493	67.1
201	17.98	36.24	26.46	157.6	164.3	1518.35	.6843	80.4
221	16.117	36.08	26.58	146.6	153.7	1515.45	.7161	94.4
241	14.79	35.87	26.71	134.5	141.8	1511.55	.7456	109.1
26!	14.00	35.74	26.78	127.9	135.4	1509.19	.7734	124.2
281	13,25	35.62	26.84		129.6	1506.91	.7999	140.0
300	12.47	35.49	26.90	116.5	124.5	1504.47	.8253	156.2
341	11.41	35.53	26.98	109.0	117.4	1501.29	.8734	190.2
381	A STATE OF THE PARTY NAMED IN	35.16	27.05	101.7	110.2	1497.62	.9189	226.1
421	9.38	35.06	27.12	95.1	103.8	1494.98	.9620	263.7
461	8.77	34.90	27.17	90.9	99.9	1493.28	1.0027	303.0
501	8.27	34.94	27.21	87.2	96.4	1491.98	1.0419	343.9
541	7.87	34.90	27.23	84.4	94.0	1491.06	1.0800	386.3
580	7.45	34.89	27.26	82.1	92.1	1490.85	1.1172	430.3
651	7.28	34.86	27.29	79.2	89.4	1490.03	1.1536	475.7
660	6.78	34.84	27.34	74.1	84.3	1488.71	1.1882	522.5
700			27.39	69.9	80.1	1487.81	1.2211	570.7
740	6.09	34.84	27.44	65.4	75.8	1487.28	1.2522	620.2
781	5.78	34.85	27.48	60.9	71.3	1486.70	1.2815	670.9
821	5.96	34.87	27.54	55.6	66.1	1486.09	1.3088	722.7
861	5.27	34.88		52.7	63.3	1485.98	1.5347	775.6
900	5,15	34.89	27.59	50.6	61.5	1486.16	1.3598	829.4
941		34.89	27.60	49.4	60.5	1486.36	1.5842	884.3
980		34.90	27.62	47.5	58.9	1486.62	1.4080	940.2
1020	4.86	34.91	27.64	45.9	57.6	1486.96	1.4314	997.0
1100			27.67	43.4	55.6	1487.62	1.4764	1113.3
1200	4.51	34.93	27.70	40.6	53.4	1488.49	1.5307	1263.7
1300			27.71	38.9	52.5	1489.77	1.5837	1419.4
1400			27.72	38.2	52.6	1491.12	1.6363	1580.4
1500	•		27.73	37.9	53.1	1492.64	1.6891	1746.6
1600			27.73	37.8	54.0	1494.25	1.7426	1918.2
1700	4.31	34.95	27.73	37.1	54.2	1495.91	1.7967	2095•2

JULY 19, 1971		19.5	19.5 %						
LATITUDE			17 12						
LONGITUDE			85 141	85 144					
DEPTH TO BOTTOM			2304 M						
	2	T	5	SIGT	TANOM	SVA	SVEL	TYNHGT	TRANS
	()	27.89	36.04	23.23	465.1	465.1	1542.70	.0000	• 0
:	20	27.39	36.04	23.23	465.1	465.9	1543.03	.0931	.9
	40	27.71	36.11	23.35	454.4	456.1	1543.02	.1853	3.7
(	61)	27.28	36.13	23.50			1542.41	.2751	8.3
	9()	26.55	36.28	23.85	406.6	410.0	1541.23	. 5604	14.7
1	00	25.45	36.44	24.51	362.3	366.4	1539.15	.4380	22.7
1:	20	24.44	36.58	24.15	322.8	327.7	1537.19	.5074	32.1
1	411	23.34	36.67	25.12	285.3	290.9	1534.89	.5693	42.9
1	60	21.41	36.65	25,65	234.4	240.5	1530.25	.6224	54.8
1	91)	20.67	36.50	25.81	219.4	226.2	1528.54	.6691	67.7
2	00		36.40			192.1		.7109	81.5
2	20	_	36.21		159.1	166.4	1518.55	.7468	96.1
2	110	15.56	35.96	26.58	146.4	154.0	1514.38	.7788	111.3
2	50		35.85				1511.34	.8082	127.2
2	80	14.12	35.74	26.75		138.5		.8361	143.7
3	on	13.34	35.60	26.81	125.1	133.4	1507.51	.8633	160.7
3	40	11.78	35.3R	26.94	111.9	120.5	1502.63	.9132	196.2
3	An.	10.68	35.20	27.01	105.9	114.A	1499.20	.9601	233.7
4;	20	9.17	35.08	27.07	99.8	108.8		1.0046	273.0
4	50	8.86	34.97	27.14	93.7	102.8		1.046R	314.0
5	nn	8.40	34.92	27.17	90.5	99.9	1492.45	1.0873	356.7
5	40	7.78	34.86	27.22	86.1	95.6	1490.66	1.1263	401.0
5	30	7.17	34.81	27.27	81.5	90.9	1488.89	1.1634	446.8
6	20	6.12	34.80	27.31	77.6	87.2	1488.16	1.1991	494.0
6	50	6.40	34.80	27.36	72.2	81.9	1487.16	1.2330	542.7
7	00	6.20	34.83	27.41	67.5	77.5	1487.05	1.2647	592.6
7	40	5.46	34.84	27.47	62.6	72.6	1486.36	1.2946	643.8
-			01-	07 10	10 -				

59.5

55.7

54.1

51.7

49.1

47.0

44.7

42.7

40.7

38.9

38.1

36.7

36.3

35.3

35.0

34.9

54.1

69.7 1486.22 1.5231

66.2 1486.13 1.3502

64.8 1486.21 1.3765

62.6 1486.27 1.4019

60.3 1486.54 1.4264

58.3 1486.42 1.4500

56.1 1486.51 1.4728

54.7 1487.33 1.5168

53.6 1488.53 1.5709

52.5 1489.77 1.6242

52.4 1491.08 1.6768

51.9 1492.49 1.7290

52.3 1493.97 1.7811

52.1 1495.51 1.8336

52.6 1497.04 1.8859

53.3 1498.66 1.9387

53.5 1500.33 1.9919

696.2

749.6

804.2

859.7

916.3

973.8

1032.3

1151.9

1306.3

1466.1

1631.1

1801.4

1976.9

2157.6

2343.6

2534.8

2731.4

STD STATION NUMBER

780

820

860

900

040

988

1020

1100

1200

1300

1400

1500

1600

1700

1800

1900

2000

5.66 34.85 27.50

5.47 34.87 27.54

5.33 34.87 27.55

5.18 34.88 27.58

5.08 34.90 27.61

4.89 34.90 27.63

4.75 34.91 27.65

4.63 34.92 27.68

4.52 34.95 27.70

4.42 34.94 27.71

4.54 34.94 27.72

4.28 34.95 27.74

4.24 34.95 27.74

4.21 34.96 27.75

4.18 34.96 27.76

4.17 34.96 27.76

4.17 34.97 27.77

```
STD STATION NUMBER

JULY 19, 1971 17.1 7

LATITUDE 17 42

LONGITUDE 83 48

DEPTH TO ROTTOM 5249 M
```

```
DYNHGT
                                                        TRANS
                         TANOM SVA
                  SIGT
                                       SVEL
  0 27.88 36.14 23.31
                         457.6 457.6 1542.77
                                                           .0
                                               .0000
                                                           .9
 20 27.51 36.13 23.43
                         446.8 447.6 1542.27
                                               .0905
  40 27.35 36.12 23.47
                         442.6 444.3 1542.23
                                               .1797
                                                          3.6
 60 27.05 36.18 23.61
                         429.0 431.6 1541.94
                                               .2673
                                                          8.1
 80 26,59 36.26 23.82
                         409.3 412.6 1541.30
                                               . 3517
                                                         14.3
100 26.01 36.39 24.10
                         382.5 386.6 1540.41
                                               .4316
                                                         22.1
120 24.19 36.64 24.85
                         311.4 316.2 1536.64
                                               .5019
                                                         31.4
140 22.57 36.78 25.43
                         256.1 261.6 1533.04
                                               .5597
                                                         42.1
160 21.14 36.72 25.78
                         222.2 228.4 1529.59
                                                         53.7
                                               .6087
                         199.7 206.4 1527.30
190 20.18 36.69 26.02
                                                         66.3
                                               .6522
                         185.4 192.7 1525.25
200 19.35 36.60 26.17
                                               .6921
                                                         79.8
220 18.79 36.52 26.25
                                               .7299
                         177.5 185.3 1523.92
                                                         94.0
240 17.85 36.39 26.39
                         164.5 172.8 1521.41
                                                .7657
                                                        109.0
                                               .7994
260 17.12 36.28 26.48
                         155.6 164.3 1519.47
                                                        124.6
280 16.56 36.18 26.54
                         150.2 159.3 1518.01
                                               .8318
                                                        140.9
300 16.32 36.17 26.59
                         145.6 155.3 1517.59
                                               .8632
                                                        157.9
340 15.06 35.95 26.71
                         134.4 144.8 1514.10
                                               .9232
                                                        193.6
38n 13.77 35.73 26.82
                         124.0 134.9 1510.36
                                               .9791
                                                        231.7
420 12.56 35.56 26.91
                         115.0 126.2 1507.12 1.0313
                                                        271.9
460 11.66 35.40 26.98
                         108.3 119.8 1504.17 1.0806
                                                        314.1
500 10.53 35.23 27.06
                         101.2 112.6 1500.64 1.1272
                                                        358.3
540 10.05 35.19 27.11
                          96.2 108.1 1499.51 1.1713
                                                        404.3
      9.30 35.10 27.17
580
                          90.8 102.8 1497.31 1.2134
                                                        452.0
      8.03 34.91 27.22
                          85.0
                                97.1 1492.97 1.2534
620
                                                        501.3
                          82.4
                                93.3 1490.91 1.2914
660
      7.35 34.83 27.26
                                                        552.2
                          75.6
700
      6.67 34.80 27.33
                                86.3 1488.87 1.3274
                                                        604.6
                          69.0
      6.32 34.83 27.40
                                79.7 1488.17 1.3607
7411
                                                        658.4
                                74.1 1487.50 1.3913
780
                          63,3
      5.08 34.85 27.46
                                                        713.4
      5.72 34.86 27.50
                          59.4
450
                                70.3 1487.12 1.4203
                                                        769.6
      5.40 34.88 27.55
                          54.2
                                65.0 1486.51 1.4474
860
                                                        827.0
900
      5.26 34.88 27.57
                          52.6
                                63.7 1486.59 1.4731
                                                        885.4
940
      5.06 34.90 27.61
                          48.A
                                60.0 1486.46 1.4978
                                                        944.8
980
      4.94 34.90 27.62
                          47.5
                                58.9 1486.62 1.5216
                                                       1005.2
1020
      4.85 34.91 27.64
                          45.8
                                57.4 1486.92 1.5448
                                                       1066.6
1100
      4.71 34.92 27.67
                          43.5
                                55.7 1487.66 1.5897
                                                       1191.9
      4.54 34.93 27.69
                          41.0
1200
                                53.8 1488.61 1.6446
                                                       1353.7
      4.44 34.94 27.71
                          39.2
1300
                                52.8 1489.85 1.6977
                                                       1520.8
1400
      4.36 34.94 27.72
                          38.3
                                52.7 1491.16 1./504
                                                       1693.2
      4.30 34.95 27.74
1500
                          37.0
                                52.1 1492.57 1.8028
                                                       1870.9
      4.26 34.96 27.75
                          35.9
                                51.8 1494.07 1.8550
                                                       2053.8
1600
                                                       2241.9
      4.24 34.96 27.75
                          35.6
                                52.5 1495.64 1.9077
1700
      4,21 34.96 27.75
                          35.3
                                53.0 1497.17 1.9605
1800
                                                       2435.3
      4.20 34.97 27.76
                          34.4
1900
                                53.0 1498.79 2.0137
                                                       2634.0
      4.19 34.97 27.76
                          34.3
2000
                                53.8 1500.41 2.0671
                                                       2838 . 1
```

```
STD STATION NUMBER
JULY 19, 1971 23.1 2
LATITUDE 18 16
LONGITUDE 85 43
DEPTH TO BUTTOM 5157 M

T S SIGT TANOM
```

```
SVA
                         TANOM
                                              DYNHGT
                                                        TRANS
                                       SVEL
                         496.9 496.9 1544.75
   0 28.95 36.02 22.90
                                               .0000
                                                           • 0
  20 28.74 36.07 22.98
                         489.8 490.6 1544.88
                                               .0987
                                                          1.0
  40 28.61 36.03 22.49
                         488.5 490.2 1544.90
                                               .1968
                                                          3.9
                         447.1 449.6 1541.85
                                               .2908
  60 27.10 35.95 23.42
                                                          8.8
  80 26.43 35.99 23.67
                         423.8 427.2 1540.69
                                               .3785
                                                         15.5
 100 25,45 36.07 23.88
                         403.1 407.2 1539.94
                                               .4619
                                                         23.9
 120 25.28 36.26 24.23
                         370.2 375.2 1538.92
                                               .5402
                                                         33.9
 140 24.27 36.59 24.78
                         317.3 322.9 1537.11
                                               .6100
                                                         45.4
                         265.5 271.8 1534.09
 160 22.36 36.76 25.33
                                               .6695
                                                         58.2
 180 22.05 36.74 25.54
                         244.9 251.9 1532.32
                                                         72.1
                                               .7218
                                               . 1683
                                                         87.0
 200 20.28 36.65 25.96
                         205.1 212.6 1527.86
                         186.3 194.3 1525.50
 220 19.33 36.58 26.16
                                               0000
                                                        102.8
                         175.5 184.1 1523.92
 240 18.68 36.51 26.27
                                               .8468
                                                        119.4
                                               .8829
 260 18.24 36.47 26.35
                         167.9 177.0 1522.94
                                                        136.7
 280 17.80 36.40 26.41
                         162.6 172.2 1521.91
                                               .9178
                                                        154.7
                                               .9517
 300 17.42 36.36 26.47
                         156.6 166.8 1521.08
                                                        173.4
 340 16.39 36.15 26.56
                         148.6 159.6 1518.43 1.0170
                                                        212.8
 380 15.53 36.04 26.67
                         137.8 149.7 1516.31 1.0790
                                                        254.7
                         127.4 139.7 1512.58 1.1370
 420 14.23 35.81 26.78
                                                        299.0
 460 12.74 35.55 26.89
                         117.2 129.5 1508.02 1.1909
                                                        345.6
 500 11.90 35.41 26,94
                         111.9 124.5 1505.65 1.2414
                                                        394.2
 540 10.78 35.23 27.01
                         105.4 118.0 1502.17 1.2899
                                                        444.9
      9.99 35.12 27.08
 580
                          98.7 111.3 1499.49 1.3355
                                                        497.4
      8.77 34.98 27.16
                          91.6 103.7 1495.84 1.3786
 620
                                                        551.7
                                99.3 1494.36 1.4192
 660
      8.22 34.95/27.21
                          87.2
                                                        607.6
      7.65 34.87 27.24
 700
                          83.5
                                95.6 1492.76 1.4581
                                                        665.2
 740
      7.22 34.85 27.29
                          79.2
                                91.2 1491.72 1.4954
                                                        724.3
 780
      6.89 34.84 27.33
                          75.5
                                87.7 1491.07 1.5312
                                                       784 · 8
 620
      6.59 34.83 27.36
                          72.4
                                84.7 1490.53 1.5657
                                                       H46.7
 860
      6.19 34.82 27.41
                          68.1
                                80.3 1489.59 1.5988
                                                       910.0
 900
      5.82 34.84 27.47
                          62.1
                                74.2 1498.79 1.6295
                                                       974.6
 940
      5.40 34.87 27.55
                          54.9
                                66.8 1487.79 1.6576
                                                      1040.4
 980
      5.18 34.88 27.58
                          51.7
                                63.5 1487.57 1.6835
                                                      1107.2
                          48.3
      5.01 34.90 27.62
                                60.3 1487.55 1.7083
1020
                                                      1175.0
                                                      1313.6
      4.78 34.91 27.65
                          45.0
                                57.4 1487.93 1.7550
1100
      4.58 34.94 27.70
                          40.6
1200
                                53.6 1488.79 1.8108
                                                      1491.9
      4.47 34.93 27.70
                                53.9 1489.96 1.8649
1300
                          40.2
                                                      1675.7
      4.39 34.94 27.72
1400
                          38.6
                                53.1 1491.28 1.9179
                                                      1864.8
                          37.4
      4.34 34.95 27.73
                                52.7 1492.74 1.9711
                                                      2059.3
1500
      4.29 34.95 27.74
1600
                          36.8
                                53.0 1494.18 2.0239
                                                      2259.0
      4.25 34.96 27.75
                          35.7
                                52.6 1495.68 2.0764
                                                      2464.0
1700
1800
      4.24 34.96 27.75
                          35.6
                                53.4 1497.29 2.1293
                                                      2674.3
1900
      4.22 34.97 27.76
                          34.6
                                53.3 1498.87 2.1829
                                                      2889.9
5000
      4.20 34.97 27.76
                          34.4
                                54.0 1500.45 2.2365
                                                      3110.9
```

STD STATION NUMBER	006
JULY 20, 1971	04.7 7
LATITUDE	18 31
LONGITUDE	83 46
DEPTH TO ROTTOM	1554 M

7.	Т	5	SIGT	TANOM	SVA	SVEL	TYNHGT	TRANS
()	28.74	36.06	22.97	490.5	490.5	1544.55	.0000	• 0
50	28,68	36.06	22.99	488.6	489.4	1544.75	.0980	1.0
411	28.15	36.06	23.16	471.8	473.5	1543.93	.1943	3.9
60	27.78	36.07	23.29	459.5	462.0	1543.46	.2878	8.7
80	27.02	36.00	23.44	441.0	444.4	1542.04	.3785	15.4
100	26.15	36.07	23.81	409.7	413.8	1540.45	.4643	23.8
120	25.54	36.21	24.11	381.5	386.4	1539.48	.5443	33.9
140	25.10	36.40	24.39	354.9	360.6	1538.94	.6190	45.5
160	23.38	36.68	24,47	299.7	306.2	1536.56	.6857	58.6
180	22.118	36.77	25.56	243.6	250.6	1532.42	. 7414	72.9
200	20.71	36.70	25.88	212.5	220.1	1529.07	.7884	88.2
550	19.53	36.60	26.12	189.9	197.9	1526.07	.8302	104.3
240	18.53	36.51	26.31	171.9	180.4	1523.49	.8681	121.3
260	18.05	36.46	26.39	164.1	173.2	1522.38	.9034	139.0
280	17.79	36.42	26.43	160.9	170.5	1521.90	.9378	157.4
300	17.51	36.37	26.46	158.0	168.2	1521.36	.9717	176.5
349	16.89	36.26	26.52	151.8	163.1	1520.05	1.0378	216.7
390	16.34	36.17	26.59	146.0	158.3	1518.94	1.1021	259.5
420	15.61	36.02	26.64	141.0	154.1	1517.18	1.1645	304.9
460	14.10	35.78	26.79	127.0	140.3	1512.77	1.2234	352.6
500	12.56	35.51	26.RY	116.7	130.0	1508.01	1.2772	402.7
540	11.73	35.42	26.09	108.1	121.6	1505.72	1.3271	454.8
580	10.46	35.20	27.05	102.2	115.4	1501.64	1.5743	508.8
620	9.51	35.07	27.11	96.4	109.3	1498.69	1.4192	564.7
6611	8.67	34.97	27.17	90.9	103.5	1496.10	1.4616	622.3
700	7.39	34.89	27.22	85.4	97.8	1493.70	1.5020	681.6
740	7.58	34.89	-	81.8	94.4	1493.15	1.5402	742.4
780	7.14	34.85	27.30	78.1	90.7	1492.06	1.5775	804.8
650	6.58	34.83	27.35	73.5	86.0	1490.89	1.6127	₽68•6
860	6.12	34.83	27.42	66.5	78.6	1489.32	1.6456	933.8
900	5.87	34.84	27.46	62.7	74.9	1488.99	1.6763	1000.2
941	5.47	34.87	27.54	55.7	67.7	1488.08	1.7046	1067.8
980	5.21	34.89	27.58	51.3	63.2	1487.70	1.7308	1136.5
1050	4.38	34.90	27.62	48.0	59.9	1487.43	1.7552	1206.3
100	4.74		27.66	43.8	56.1	1487.78	1.8017	1348.6
1500		34.93	27.69	41.2	54.1	1488.69	1.8565	1531.5
1300	4.79		27.72	38.6	52.1	1489.64	1.9092	1719.8
400	4.30	34.95	27.74	37.0	51.2	1490.92	1.9608	1913.3

STD STATION NUMBER	007
JULY 20, 1971	09.9 2
LATTIUDE	18 19
LONGITUDE	84 02
DEPTH TO BOTTOM	4/37 M

Z	Т	S	SICT	TANOM	SVA	SVEL.	DYNHAT	TRANS
0	28.66	36.06	22.99	487.9	487.9	1544.38	•0000	•0,
50	28.66	36.06	22.99	487.9	488.8	1544.70	.0977	1.0
40	28.08	36.00	23,14	473.9	475.6	1543.73	.1941	3.9
60	26.84	35.98	23.53	457.0	439.5	1541.29	.2856	8.7
80	26.25	36.03	23,75	415.6	418.9	1540.32	.5715	15.3
100	25.68	36.12	24.00	392.1	396.2	1559.41	.4530	23.5
120	25.07	36.38	24.38	355.5	360.4	1538.53	.5286	33.3
140	24.02	36.64	24.90	306.5	312.2	1536.55	.5959	44.6
160	22.50	36.75	25.42	256.4	262.1	1533.16	.6534	57.1
180	21.19	36.73	25.78	222.8	229.7	1530.06	. 1026	70.6
500	20.22	36.67	25.99	202.1	200.6	1527.72	. 1465	85.1
220	19.33	36.69	26,18	184.9	192.9	1525.51	. 7868	100.4
240	18.52	36.49	26.30	173.1	181.6	1523.44	.8242	116.6
260	18.00	36.44	26.39	164.4	173.4	1522.21	.8597	133.4
280	17.69	36.41	26.45	159.3	168.9	1521.60	·8940	150.9
300	17.33	36.36	26.50	154.6	164.7	1520.81	.9273	169.1
340	16.53	36.22	26.58	146.6	157.7	1518.92	.9918	207.5
380	15.36	35.99	26.67	157.8	149.6	1515.73	1.0531	248.4
420	13.71	35.71	26.81	124.3	136.2	1510.78	1.1103	291.7
460	12.07		26.93			1505.61	1.1619	337.2
500	11.55	35.36	26.97	109.3	121.6	1504.38	1.2110	384.6
540	11.20	35.31	27.00	106.8		1503.74	1.2504	434.1
580	10.59	35.21	27.03	103.7		1502.11	1.3068	485.4
620	9,91		27.08	99.1		1500.21	1.3525	538.6
660			27.12	94.9	108.2	1498.06	1.3966	593.6
790	8.46			88.5	101.6	1495.95	1.4384	650.3
740	7.48		27.26	81.9	94.4	1492.74	1.4776	708.6
780	6.84		27.53	75.6	87.7	1490.87	1.5139	768.4
820	6.29		27.40	68.6	80.4	1489.35	1.5477	829.7
860	5.00		27.47	62.3	74.0	1488.48	1.5786	892.2
900	5.54		27.51	58.5	70.2	1488.10	1.6076	955.9
940	5.51		27.53	56.2	68.2	1488.24	1.6352	1020.8
980	5.29		27.57	52.9	65.0	1488.01	1.6618	1086.7
1020	5.03		27.61	48.5	60.5	1487.64	1.6869	1153.7
1100	4.76		27.66	44.1	56.4	1487.87	1.7333	1290.5
1200	4.56		27.69	41.2	54.1	1488.69	1.7882	1466.6
1300	4.45		27.71	39.3		1489.89	1.8413	1648.1
1400			27.73	37.5	51.8	1491.13	1.8936	1934.9
1500	4.54	34.95	27.73	37.4	52.7	1492.74	1.9456	2026.8

STD STATION NUMBER	OUB
JULY 20, 1971	16.4 /
LATITUDE	17 52
LONGITUDE	84 24
DEPTH TO BOTTOM	4938 M

```
S
                   SIGT
                                              TYNHGT
                                                        TRANS
                         TANOM
                               SVA
                                       SVEL
  0 27.70 36.14 23.37
                         452.0 452.0 1542.38
                                                .0000
                                                           .0
                                                .0902
 20 27.62 36.14 23.40
                         449.5 450.3 1542.52
                                                            .9
                                                .1788
 40 27.20 36.17 23.56
                         434.1 435.8 1541.95
                                                          3.6
                         420.5 423.0 1541.44
                                                .2647
 60 26.82 36.20 23.70
                                                          8.0
 80 26.57 36.28 23.84
                         407.0 410.3 1541.28
                                                . 5481
                                                         14.2
                                                         21.9
100 26,29 36.36 23.99
                         393.0 397.2 1541.03
                                                .4288
120 24.93 36.59 24.58
                         336.5 341.5 1538.38
                                                .5027
                                                         31.2
                                                .5653
140 23.33 36.76 25.19
                         278.6 284.3 1534.93
                                                         41.9
160 21.44 36.75 25.72
                         228.0 234.1 1530.41
                                                .6171
                                                         53.7
180 20.12 36.66 26.01
                         200.6 207.3 1527.12
                                                         66.5
                                                .6612
                         190.6 197.9 1525.93
200 19.59 36.61 26.12
                                                .7018
                                                         80.2
220 18.66 36.51 26.28
                         175.4 183.2 1523.54
                                                .7399
                                                         94.6
                         165.1 173.4 1521.98
240 18.03 36.44 26.38
                                                .7755
                                                        109.7
                         155.7 164.5 1520.06
260 17.30 36.33 26.48
                                                .8093
                                                        125.6
                         145.9 155.0 1516.79
                                                .8413
280 16.18 36.12 26.59
                                                        142.1
                         141.2 150.6 1515.03
                                                .8718
300 15.54 36.00 26.64
                                                        159.2
                                                .9293
340 14.02 35.73 26.76
                         129.2 139.0 1510.51
                                                        195.2
380 13.44 35.64 26.82
                         124.1 134.7 1509.17
                                                .9836
                                                        233.5
420 12.75 35.48 26.83
                         122.7 133.9 1507.32 1.0371
                                                        273.9
460 12.04 35.37 26.88
                         117.7 129.4 1505.44 1.0889
                                                        316.4
 500 10.84 35.31 27.06
                         100.8 112.5 1501.84 1.1365
                                                        361.0
      9,98 35.15 27.09
 5411
                          97.8 109.6 1499.22 1.1801
                                                        407.3
 580
      8.37 34.93 27.18
                          89.4 100.2 1493.62 1.2219
                                                        455.4
      7.69 34.85 27.22
                          85.4
620
                                 96.1 1491.59 1.2612
                                                        505.0
                          90.9
660
      7.13 34.81 27.27
                                 91.5 1490.02 1.2988
                                                        556.2
 700
                          76.1
                                 87.0 1489.54 1.3343
      6.83 34.82 27.32
                                                        608.9
 740
      6.50 34.83 27.37
                          71.2
                                 82.2 1488.89 1.3682
                                                        662.9
                          67.4
 780
                                 78.6 1488.57 1.4004
      6.25 34.84 27.41
                                                        718.3
 820
      5.30 34.84 27.46
                                 74.2 1487.81 1.4309
                          63.1
                                                        774.9
                          59.9
860
      5.70 34.85 27.49
                                 71.2 1487.69 1.4601
                                                        832.8
      5.48 34.86 27.53
900
                          56.7
                                 68.2 1487.47 1.4880
                                                        391.7
940
                          52.9
                                 64.6 1487.44 1.5145
                                                        951.8
      5.31 34.88 27.57
980
      5.09 34.89 27.60
                          49.9
                                 61.6 1487.22 1.5397
                                                       1012.9
1020
      4.96 34.90 27.62
                          47.A
                                 59.7 1487.37 1.5639
                                                       1075.0
      4.75 34.92 27.66
                          43.9
1100
                                 56.2 1487.84 1.6105
                                                       1201.9
      4.59 34.93 27.69
                          41.5
                                 54.5 1488.82 1.6657
1200
                                                       1365.8
      4.45 34.94 27.71
                          39.3
1300
                                 52.9 1489.90 1.7192
                                                       1535.0
1400
      4.36 34.95 27.73
                          37.6
                                 52.0 1491.18 1.7716
                                                       1709.6
      4.31 34.96 27.74
                          36.3
1500
                                 51.5 1492.63 1.8235
                                                       1889.3
      4.27 34.96 27.75
                          35.9
1600
                                 52.0 1494.11 1.8752
                                                       2074.3
                          35.5
1700
      4.23 34.96 27.75
                                 52.4 1495.60 1.9274
                                                       2264.4
                          35.3
1800
      4.21 34.96 27.75
                                 53.0 1497.17 1.9801
                                                       2459.8
1900
      4.20 34.97 27.76
                          34.4
                                 53.0 1498.79 2.0334
                                                       2660.4
2000
      4.17 34.97 27.77
                          34.1
                                 53.5 1500.33 2.0866
                                                       2866.4
```

STD STATION NUMBER	009
JULY 20, 1971	22.6 7
LATITUDE	17 29
LONGITUDE	84 43
DEPTH TO ROTTOM	4823 M

Z	T	5	SIGT	TANOM	SVA	SVEL	TYNHGT	TRANS
0	27.89	36.03	23.23	465.8	465.8	1542.69	.0000	• 0
50	27.88		23.25	463.6	464.5	1543.03	.0930	•9
40		36.09	23.33	_		1543.00	.1852	3.7
60	27.12	36.16	23.57	432.6	435.1	1542.08	.2745	8.3
90	25.73	36.35	24.15		380.5	1539.40	.3561	14.6
100	24.69	36.51	24.59			1537.42	.4280	22.5
120	23.78	36.64	24.07	290.0	304.8	1535.62	.4925	31.7
140	22.75	36.71	25.32	266.0	271.6	1533.44	.5501	42.1
160	21.52	36.60	25.66	234.2	240.4	1530.57	.6013	53.6
180	19.87	36.58	56.05	200.0		1526.35	.6460	66 • 1
200	18.84	36.40	26.15	187.4	194.5	1523.63	.6861	79.4
220	17.53	36.30	26.40	163.3	170.8	1520.06	.7227	93.5
240	16.58	36.17	26.53			1517.41	.7557	108.3
260	15,92	36.08	26.61	145.2	151.5	1515.62	.7868	123.7
280	14.99	35.92	26.70	-	143.3	1512.89	.8163	139.7
300	14.56	35.84	26.74	131.8	140.7	1511.75	.8447	156.3
340	13.30	35.61	26.82		21 44 144 64	1508.04	.8997	191.2
380	11.70	35.40	26.07	109.1		1503.00	.9498	228.2
420	10,92	35.27	27.02	105.2		1500.78	.9970	267.2
460	9.86	35.13	The Court of the C	97.7		1.497 • 47	1.0417	308.0
500	9.07	35.01	27.13	93.9		1495.05	1.0840	350.5
540	8.62	20 (2)	27.17	90.9		1493.98	1 -1248	394.6
580	7.04	34.90	27.22	85.5	95.8	1491.98	1.1641	440.4
620	7.39	34.86	27.27	80.7	91.1	1490.46	1.2014	487.7
660	6.88	34.83	27.32	76.2	86.5	1489.09	1.2371	536.5
700	6.41	San S Contract	27.39	70.2	80.5	1487.89	1.2706	586 • 7
740	6.08	34.83	27.43	66.2	76.5	1487.22	1.3022	638 • 1
7811	5.70	34.86	27.50	59.1	69.4	1486.38	1.3312	690 • 8
820	5.45	34.87	27.54	55.6	66.0	1486.06	1.35R2	744.6
860	5.24	34.88	27.57	52.3	62.8	1485.87	1.3841	799.5
900	5.06	34.90	27.61	48.9	59.6	1485.83	1.4086	855.3
940	4.89	34.90	27.63	47.0	57.9	1485.78	1.4321	012.1
980	4.79	34.92	27.66	44.4	55.5	1486.03	1.4548	969.9
1020	4.70	34.93	27.68	42.6	54.0	1486.33	1.4767	1028-5
1100	4.59	34.94	27.70	40.7	52.7	1487.20	1.5196	1148.4
1200	4.48	34.94	27.71	39.5	52.2	1488.36	1.5720	1302.9
1300	4.38	34.95	27.73	37.A	51.3	1489.63	1.6237	1462.7
1400	4.33	34.95	27.73	37.3	51.6	1491.05	1.6752	1627.7
1500	4.29	34.96	27.74	36.1	51.3	1492.55	1.7264	1797.8
1600	4.26	34.96	27.75	35.8	51.8	1494.07	1.7779	1973.0
1700	4.23	34.96	27.75	35.5	52.3	1495.59	1.8300	2153.4
1800	4.21		27.75	35.3	53.0	1497.17	1.8826	2539.0
1900	4.18	34.97	-	34.3	52.8	1498.72	1.9358	2529.9
5000	4.16	34.91	27.77	34.0	53.4	1500.29	1.9889	2726•2

STD STATION NUMBER	010
JULY 21, 1971	02.9 /
LATITUDE	16 59
LONGITUDE	85 01
DEPTH TO BOTTOM	4402 M

```
S
                   SIGT
                         TAMOM SVA
                                       SVEL
                                               PYNHGT
                                                         TRANS
   0 28.04 35.96 23.12
                         475.5 475.5 1542.96
                                                .0000
                                                            .0
  20 28.01 35.98 23.15
                         472.8 473.6 1543.24
                                                            .9
                                                . 11949
  40 27.73 36.04 23.29
                         459.9 461.6 1542.99
                                                           3.8
                                                .1884
  60 26.99 36.08 23.56
                         434.0 436.5 1541.71
                                                .2783
                                                          8.4
  80 26.13 36.31 24.00
                         392.0 395.3 1540.30
                                                . 3614
                                                          14.8
 100 25.23 36.48 24.41
                         353.0 357.1 1538.67
                                                .4367
                                                         22.8
 120 23.38 36.70 25.13
                         284.5 289.3 1534.70
                                                .5013
                                                         32.2
 140 21.57 36.67 25.63
                         237.0 242.3 1530.37
                                                .5545
                                                         42.8
 160 19.92 36.60 26.02
                         200.0 205.9 1526.20
                                                         54.3
                                                .5993
 180 18.40 35.44 26.29
                         173.9 180.2 1522.08
                                                .6379
                                                         66.7
 200 17.59 36.32 26.40
                         163.6 170.5 1519.94
                                                         79.8
                                                .6730
 220 17.07 36.26 26.48
                         155.6 163.0 1518.65
                                                .7063
                                                         93.6
 240 16.53 36.18 26.55
                         149.5 157.4 1517.28
                                                .7384
                                                        108.0
 260 15.34 36.05 26.61
                         143.5 151.7 1515.36
                                                . 1693
                                                        123.1
 280 15.21 35.93 26.66
                         139.0 147.6 1513.58
                                                . 7992
                                                        138.8
 300 14.62 35.86 26.73
                         131.9 140.8 1511.95
                                                .8281
                                                         155.1
 340 13.13 35.58 26.84
                         122.1 131.5 1507.43
                                                .8834
                                                        189.3
 380 11.72 35.35 26.93
                         113.0 122.5 1503.04
                                                .9339
                                                        225.7
 420 10.67 35.22 27.02
                         104.4 114.1 1499.83
                                                .9814
                                                        264.0
 460 10.19 35.17 27.07
                         100.2 110.4 1498.68 1.0261
                                                         304.1
      9.31 35.08 27.15
500
                          92.4 102.7 1496.04 1.0687
                                                         346.0
      8.46 34.97 27.20
                          87.7
                                 97.9 1493.37 1.1087
 540
                                                         389.6
                          84.7
 580
      7.88 34.90 27.23
                                 94.9 1491.75 1.1474
                                                        434.7
 620
      7.33 34.85 27.28
                          80.4
                                 90.7 1490.20 1.1844
                                                        481.3
      6.91 34.83 27.32
 660
                          76.6
                                 87.0 1489.19 1.2199
                                                        529.4
      6.47 34.85 27.38
 700
                          71.1
                                 81.5 1488.13 1.2537
                                                        578.9
      6.17 34.85 27.42
 7411
                          67.0
                                 77.5 1487.60 1.2855
                                                        629.7
                          61.4
 780
      5.82 34.85 27.48
                                 71.9 1486.86 1.3154
                                                        681.7
      5,50 34.86 27.52
                                 67.7 1486.23 1.5433
 1158
                          57.2
                                                        734.9
                          52.3
 860
      5.22 34.88 27.57
                                 62.8 1485.79 1.3694
                                                        789.2
      5.04 34.90 27.61
                          48.6
900
                                                        844.4
                                 59.3 1485.71 1.3938
                          46.7
 940
      4.96 34.90 27.63
                                 57.5 1485.66 1.4171
                                                        900.6
 980
      4.78 34.91 27.65
                          44.7
                                 55.8 1485.99 1.4398
                                                        957.8
1020
      4.69 34.93 27.67
                          42.7
                                                       1015.8
                                 54.1 1486.28 1.4618
1100
      4.59 34.93 27.69
                          41.5
                                 53.4 1487.18 1.5047
                                                       1134.5
1200
      4.51 34.94 27.70
                          39.9
                                 52.7 1488.51 1.5575
                                                       1287.6
1300
      4.43 34.95 27.72
                          38.3
                                 51.9 1489.83 1.6699
                                                       1446.0
1400
      4.36 34.95 27.73
                          37.6
                                 52.0 1491.18 1.6618
                                                       1609.6
1500
      4.31 34.95 27.73
                          37.1
                                 52.3 1492.62 1.7139
                                                       1778.3
      4.26 34.96 27.75
                                 51.9 1494.08 1.7663
                          35.9
1600
                                                       1952.4
1700
                          35.5
      4.23 34.96 27.75
                                 52.3 1495.59 1.8183
                                                       2131.6
                          35.2
1800
      4.20 34.96 27.75
                                 52.9 1497.13 1.8709
                                                       2316.0
1900
      4.19 34.97 27.76
                                 52.9 1498.75 1.9239
                          54.3
                                                       2505 • 8
2000
      4.16 34.98 27.77
                          33.3
                                 52.7 1500.30 1.9769
                                                       2700.8
```

STU STATION NUMBER	11
JULY 21, 1971	07.3 /
LATITUDE	16 42
LONGITUDE	A5 22
DEPTH TO ROTTOM	970 M

7.	T	S	SIGT	TANOM	SVA	SVEL	TOPHY	TRANS
0	27.92	35.64	22.92	494.8	494.8	1542.40	.0000	• 0
20	27.95	35.70	22.96	491.4	492.2	1542.84	.0987	1.0
40	27.96	35.98	23.20	468.2	469.9	1543.22	.1949	3.9
60	26.35	36.24	23.88	403.2	405.7	1540.42	.2825	8.7
BO	25.16	36.48	24.43	350.9	354.2	1538.18	.3585	15.1
100	23.98	36.65	24.92	304.7	308.7	1535.81	.4248	22.9
150	22.49	36.74	25.42	256.6	261.4	1532.48	.4818	32.0
140	21.20	36.68	25.74	226.6	232.0	1529.39	.5311	42.1
160	19.60	36.57	26.08	194.1	199.9	1525.28	.5743	53.2
180	18.15	36.37	26.30	173.0	179.2	1521.31	.6122	65.1
2011	16.94	36.24	26.50	154.4	161.1	1517.93	.6462	77.6
220	15.91	36.07	26.61	144.1	151.1	1514.93	.6775	90.9
240	15.16	35.94	26.68	137.3	144.7	1512.79	.7071	104.7
260	14.57	35.85	26.74	131.0	138.8	1511.14	.7354	119.1
280	13.66	35.68	26.80	125.6	133.5	1508.34	. 1626	134.1
300	12.57	35.55	26.89	117.1	125.1	1505.19	.7885	149.6
340	11.60	35.35	26.96	110.8	119.3	1501.97	.8374	182.2
389	10.64	35.22	27.93	103.A	112.6	1499.09	.8837	216.6
420	9.76	35.12	27.09	98.1	107.3	1496.83	.9276	252.8
460	9.15	35.04	27.14	93.1	102.5	1494.76	.9697	290.8
500	8.65	35.00	27.19	88.3	97.9	1493.50	1.0098	330.4
540	8.11	34.93	27.22	85.6	95.4	1492.01	1.0498	371.5
580	7.13	34.90	27.26	82.4	92.5	1491.17	1.0863	414.3
62n	7.43	34.88	27.28	79.7	90.1	1490.64	1.1231	458.4
660	7.29	34.86	27.29	79.1	90.0	1490.73	1.1591	504.1
790	6.68	34.84	27.36	72.8	83.4	1488.95	1.1940	551.2
740	6.41	34.83	27.39	70.1	81.0	1488.53	1.2268	599.6
780	6.14		27.43	66.0	77.0	1488.11	1.2586	649.3
820	5.75	34.87	27.50	59.0	70.0	1487.26	1.2877	700.2
860	5.60	34. PH	27.53	56.7	67.9	1487.33	1.3153	752.3
900	5.46	34.89	27,55	54.4	65.7	1487.40	1.3420	805.4
940	5.51		27.58	52.1	63.6	the second second second	1.3679	859.6
980	5.16		27.60	49.0	61.5	1487.53	1.3929	914.8
1050	5.01		27.62	47.5	59.4		1.4171	471.0
1100	4.72	34.93	27.67	42.9	55.1	1487.72	1.4629	1086.3

STD STATION NUMBER	012
JULY 21, 1971	14.0 /
LATITUDE	16 14
LONGITUDE	85 41
DEPTH TO ROTTOM	0988 M

Z	т	S	SIGT	TANOM	SVA	SVEL	TOHNYC	TRANS
n	27.58	35.90	23,23	465.5	465.5	1541.90	.0000	•0
20	27.53			464.9	465.8	1542.35	.0931	•9
40	27.58		23,30	458.5	460.2	1542.63	.1857	3.7
60	26.96	36.14	23.61	429.5	432.1	1541.71	.2750	8.3
80	25.29	36.44	24.36	357.2	360.5	1538.45	.3542	14.6
100	24.44	35.54	24.75	322.0	326.1	1536.88	.4229	22.4
120	23.40	36.69	25,12	285.7	290.5	1534.73	.4845	31.5
140	22.07	36.73	25.53		251.9	1531.72	.5388	41.7
160	20.00	36.53	25.94	207.1	213.0	1526.35	.5853	52.9
180	18.31		26.28	174.9	181.2	1521.77	.6247	65.0
200	17.09	36.22	26.45	159.2	165.9	1518.35	.6594	77.9
220	16.01	36.05	26.57	147.6	154.6	1515.22	.6914	91.4
240	14.79	35.88	26.71	134.2	141.4	1511.55	.7210	105.5
260	13,91	35.72	26.78	127.4	134.8	1508.87	. 1487	120.2
280	12.73	35.52	26.87	119.3	126.9	1505.07	.7748	135.4
300	11,76	35.42	26.94	111.9	119.6	1502.65	. 7995	151.2
340	11.25	35.34	27.01	105.8	114.0	1500.73	.8463	184.1
390	10.49	35.22	27.06	101.2	109.9	1498.56	.8910	218.9
420	9.73	35.10	27.10	97.5	106.5	1496.31	.9345	255.4
460	9.20	35.04	27.14	93.5	102.9	1494.92	.9763	293.6
500	8.70	34.98	27.17	90.4	100.1	1493.66	1.0168	333.5
540	8.39	34.95	27.20	88.1	98.3	1493.09	1.0565	374.9
580	7.42	34.92	27.24	83.6	94.0	1491.93	1.0949	418.0
620	7.59	34.90	27.26	82.1	92.9	1491.66	1,1323	462.5
660	7.08	34.83	27.30	78.6	89.2	1489.88	1.1689	508.5
790	6.59	34.84	27.37	71.3	81.8	1488.61	1.2031	556.0
740	6.20	34.85	27.43	66.r	76.5	1487.72	1.2347	604.7
780	5.87		27.47	62.0	72.6	1487.07	1.2645	654.7
820	5.70	34.86	27.50	59.2	70.0	1487.04	1.2929	705.9
860	5.43	34.87	27.54	55.3	66.2	1486.61	1.5203	758 • 1
900	5.19	34.89	27,59	51.0	62.0	1486.32	1.3459	811.5

LATITUDE			16 1	4				
1	ONGITE	IDE .		85 4	1			
r	PEPTH T	TO BOT	МОТ	988 *	A			
Z.	T		SIGT	TANOM	SVA	SVEI.	DYNHGT	TRANS
0	27.57	35.94	23,23	465.4	465.4	1542.13	.0000	• 0
20	27.64	35.98	23.27	461.3	462.1	1542.42	.0928	• 9
40	27.65		23.30	458.7	460.4	1542.80	.1850	3.7
60	26,92		23.64		429.1	1541.62	.2739	8.3
80	25.40		24.33	360.0	363.3	1538.71	. 3532	14.6
100	24.54	36.61	24.78	318.0	322.1	1536.64	.4217	22.3
120	25.47	36.68	25.09	288.4	293.2	1534.90	.4P33	31.4
140	21.87	36.63	25.51			1531,11	.5379	41.6
160	19.95	36.52	25.95	506:5	212.1	1526.20	.5844	52.8
180	18.45	36.44	26.28	175.1	181.4	1,522.23	.6238	64.9
500	17.51	36.29	26.40	163.8	170.7	1519.68	.6590	77.7
550	16.10	36.09	26.58	146.5	153.6	1515.54	.6914	91.2
240	14.97	35.90	26.69	136.1	143.4	1512.17	./211	105.3
260	13.76	35.79	26.80	126.1	133.5	1508.37	.7488	120.0
280	13.11	35.62	26.87	119.1	126.9	1506.45	. 1748	135.3
300	12.14	35.42	26.91	115.3	123.1	1503.29	.7998	151.0
340	11,11	35.31	27.02	105.2	113.3	1500.21	.8465	184.0
380	10.32	35.20	27.07	99.8	108.4	1497.91	.8911	218.7
420	9.58	35.10	27.12	95.5	104.4	1495.75	.9337	255.2
460	9.18	35.04	27.14	93.1	102.5	1494.87	.9751	293.4
500	8.67	34.98	27.17	90.1	99.8	1493.54	1.0156	333.2
540	8.35	34.94	27.19	88.5	98.6	1492.91	1.0551	374.6
580	7.94	34.90	27.23	85.2	95.5	1491.97	1.0938	417.6
620	7.46	34.87	27.27	80.7	91.2	1490.76	1.1310	462.1
660	6.94	34.84	27.32	76.0	86.4	1489.35	1.1665	508 • 1
700	6.53	34.85	27.39	70.2	80.6	1488.38	1.1998	555.4
740	6.27	34.85	27.42	67.0	77.7	1488.02	1.2314	604.0
780	5.93	34.86	27.47	61.9	72.6	1487.32	1.2616	653.9
820	5.75	34.87	27.50	59.1	70.1	1487.25	1.2901	704.9
010		7" "7	77 47	L	. 7 .		. 4.7/	767 1

56.4

52.0

48.4

47.2

46.1

43.7

67.5 1486.99 1.3176

63.1 1486.61 1.5438

59.7 1486.68 1.3681

58.8 1487.02 1.3918

57.9 1487.36 1.4152

40.8 53.8 1488.89 1.5158 1239.8

56.1 1488.04 1.4608 1090.9

757.1

R10.3

P64.6

919.8

975.9

15.5 /

STD STATION NUMBER A12

JULY 21, 1971

860

900

940

980

1020

1100

1200

5.52 34.87 27.53

5.26 34.89 27.58

5.11 34.91 27.61

5.03 34.92 27.63

4.95 34.92 27.64

4.80 34.93 27.66

4.50 34.94 27.70

```
JULY 21, 1971
                         19.0 /
    LATITUDE
                         16 16
                         86 11
    LONGITUDE
    DEPTH TO BOTTOM
                         1372 M
                                                       TRANS
             5
                  SIGT
                         TANOM SVA
                                      SVEL
                                              JANHEL
   0 27.55 36.16 23.43
                        445.9 445.9 1542.06
                                                         • 0
                                               .0000
                                                          .9
  20 27.44 36.17 23.48
                        441.8 442.6 1542.16
                                               . 11880
  40 27.42 36.17 23.48
                        441.3 443.0 1542.44
                                                         3.6
                                               .1774
  60 27.14 36.17 23.57
                        432.6 435.1 1542.14
                                               .2652
                                                         8.0
 80 26.47 36.24 23.84
                        406.8 410.3 1541.02
                                               .3498
                                                        14.1
 100 24.52 36.61 24.79
                        316.8 320.9 1536.60
                                               .4229
                                                        21.9
                         271.7 276.4 1533.63
 12n 22.95 36.71 25.26
                                               .4826
                                                        30.9
 140 21.21 36.66 25.72
                        228.4 233.7 1529.40
                                                        41.1
                                               .5336
 160 19,47 36.55 26.10
                        191.6 197.5 1524.89
                                               .5767
                                                        52.2
 180 18.52 36.43 26.30
                        172.8 179.1 1521.83
                                               .6144
                                                        64.1
 200 17.11 36.23 26.45
                        159.0 165.7 1518.43
                                               .6489
                                                        76.7
 220 16.19 36.13 26.59
                        145.3 152.4 1515.87
                                              ·6807
                                                        90.0
                                              .7105
 240 15.47 36.01 26.66
                        138.7 146.2 1513.84
                                                       103.9
 260 14.61 35.86 26.74
                        131.8 139.6 1511.29
                                              . 7391
                                                       118.4
 280 13.27 35.60 26.82
                        124.0 131.7 1506.94
                                              . 7662
                                                       133.5
                         116.1 124.0 1504.50
                                              . /918
 300 12.47 35.50 26.90
                                                       149.1
 340 11.47 35.36 26.09
                                              . 4397
                         197.7 116.1 1501.54
                                                       181.7
 380 10.18 35.17 27.07
                         99.9 108.4 1497.40
                                               .8851
                                                       216.2
 420
      9.71 35.09 27.09
                          98.1 107.0 1496.23
                                               .9280
                                                       252.5
 460
      9.10 35.04 27.15
                          92.2 101.5 1494.57
                                              .9693
                                                       290.4
                               98.0 1492.90 1.0096
      8.50 34.97 27.19
                          88.5
 500
                                                       330.0
 5411
      8.18 34.94 27.22
                          45.9
                                95.8 1492.29 1.0482
                                                       571.2
      7.54 34.89 27.28
 SAU
                          80.4
                                90.3 1490.42 1.0855
                                                       413.8
      7.01 34.86 27.33
                          75.5
 620
                                85.5 1489.00 1.1208
                                                       458.0
                          70.7
 660
      6.56 34.85 27.38
                                80.6 1487.85 1.1542
                                                       503.5
 700
      6.32 34.85 27.41
                          67.5
                                77.7 1487.56 1.1856
                                                       550.3
 740
      6.11 34.85 27.44
                          64.9
                                75.3 1487.39 1.2163
                                                       598.3
 781
      5.90 34.86 27.48
                          61.5
                                72.2 1487.18 1.2457
                                                       647.6
820
      5.70 34.86 27.50
                          58.9
                                69.7 1487.04 1.2742
                                                       598.0
861
      5.51 34.88 27.54
                          55.5
                                66.6 1486.97 1.3014
                                                       749.5
      5.26 34.89 27.58
ann
                          51.6
                                62.7 1486.60 1.3273
                                                       802.0
 941)
      5.08 34.90 27.61
                          49.9
                                60.2 1486.52 1.3518
                                                       A55.6
      4.97 34.91 27.63
 980
                          47.0
                                58.5 1486.77 1.3756
                                                       910.2
      4.18 34.92 27.65
                                57.1 1487.07 1.3986
1020
                          45.4
                                                       965.7
                          44.5
      4.90 34.92 27.66
                                56.9 1488.04 1.4442
                                                      1079.4
1100
      4.77 34.93 27.67
                          43.4
                                56.9 1489.56 1.5008
1200
                                                     1226.6
                                56.1 1490.74 1.5577
                          41.9
1300
      4.66 34.93 27.68
                                                     1379.6
                         38.9 53.5 1491.53 1.6125
1400
      4.45 34.94 27.72
                                                     1538 • 1
```

STD STATION NUMBER

JULY 222, 1971 LATT TUDE LONGTTUDE BEPT** TO 901TOM  Z T S SIGT TANOM SVA SVEL OYNHGT IRANS O 27, 94 36.15 23.30 458.7 458.7 1542.91 .0000 20 27, 68 36.14 23.38 451.3 452.2 1542.66 .0911 .9 40 27, 47 36.17 23, 47 442.8 444.5 1542.55 .1808 3.6 60 26, 63 36.17 23, 47 442.8 444.5 1542.55 .1808 3.6 60 26, 63 36.17 23, 47 416.8 419.2 1540.99 .2671 81 210 23, 96 36.65 24, 92 303.9 307.9 1535.77 .4146 21.9 120 22, 47 36.72 25, 41 257.7 262.4 1532.42 .4716 50.7 140 21, 55 36.71 25, 72 228.4 253.8 1529.81 .5212 40.6 160 19, 32 36.60 26.05 197.1 203.0 1525.91 .5649 515 180 18.08 36.35 26.33 170.4 176.7 1521.10 .6029 63.2 200 17, 20 36.50 26, 48 155.9 162.7 1518.76 .6368 88.6 220 16, 99 36.15 26, 77 147.8 154.9 1516.17 .6686 88.6 220 16, 99 36.15 26, 77 147.8 154.9 1516.17 .6686 88.6 220 16, 90 36.15 26, 77 147.8 154.9 1516.17 .6686 88.6 220 16, 93 35.03 26, 66 139, 4 146.9 1514.20 .6988 102.3 260 14, 61 35.86 26.74 131.7 139.5 1511.30 .7274 116.6 280 13, 90 35.72 26, 78 127.4 135.4 1509.17 .7549 131.4 300 15, 20 35.61 26, 84 121, 4 129.7 1507.07 .7814 146.8 340 11, 93 35.41 26, 94 112, 4 121.1 1503.18 .8318 179.3 340 10, 35.16 27.08 98.2 108.2 1497.72 .9225 249.3 420 10, 10 35.16 27.08 98.2 108.2 1497.72 .9225 249.3 420 10, 10 35.16 27.08 98.2 108.2 1497.72 .9225 249.3 420 10, 10 35.16 27.08 98.2 108.2 1497.72 .9225 249.3 420 10, 10 35.16 27.08 98.2 108.2 1497.72 .9225 249.3 420 10, 10 35.16 27.08 98.2 108.2 1497.72 .9225 249.3 420 10, 10 35.16 27.08 98.2 108.2 1497.72 .9225 249.3 420 10, 10 35.16 27.08 98.2 108.2 1497.72 .9225 249.3 420 10, 10 35.16 27.08 98.2 108.2 1497.72 .9225 249.3 420 10, 10 35.16 27.08 98.2 108.2 1497.72 .9225 249.3 420 10, 10 35.16 27.08 98.2 108.2 1497.72 .9225 249.3 420 10, 10 35.16 27.08 98.2 108.2 1497.72 .9225 249.3 420 10, 10 35.16 27.08 98.2 108.2 1497.72 .9225 249.3 420 10, 10 35.16 27.08 98.9 108.2 1497.72 .9225 249.3 420 10, 10 35.16 27.08 98.9 108.2 1497.72 .9225 249.3 420 10, 10 35.16 27.08 98.9 108.2 1497.72 .9225 249.3 420 10, 10 35.16 27.08 149.2 149.2 149.2 149.2 149.2 149.2 149.2	SID STATION NUMBER			014							
LONGTINDE   R6   54   3219   M	JULY 22, 1971			00.0 /							
The color of the	LATITUDE			16 27	16 22						
Z         T         S         S16T         TANOM         SVA         SVEL         OYNHGT         TRANS           0         27.94         36.15         25.30         458.7         458.7         1542.91         .0000         .0           20         27.68         36.14         23.58         451.3         452.2         1542.65         .1608         3.6           60         26.63         36.17         23.74         416.8         419.2         1540.99         .2671         8.1           80         25.62         36.40         22.23         370.4         373.7         1539.19         .3464         14.2           100         23.96         36.65         24.92         303.9         307.9         1535.77         .4146         21.9           120         22.47         36.67         25.71         228.4         233.8         1529.91         .649         50.7           140         21.35         36.50         26.05         197.1         203.0         1525.91         .649         51.5           180         18.83         34.98         26.33         170.4         176.7         151.5         66.36         85.6           200         17.2	t	ONGTI	JDE		86 54						
Z         T         S         S16T         TANOM         SVA         SVEL         OYNHGT         TRANS           0         27.94         36.15         25.30         458.7         458.7         1542.91         .0000         .0           20         27.68         36.14         23.58         451.3         452.2         1542.65         .1608         3.6           60         26.63         36.17         23.74         416.8         419.2         1540.99         .2671         8.1           80         25.62         36.40         22.23         370.4         373.7         1539.19         .3464         14.2           100         23.96         36.65         24.92         303.9         307.9         1535.77         .4146         21.9           120         22.47         36.67         25.71         228.4         233.8         1529.91         .649         50.7           140         21.35         36.50         26.05         197.1         203.0         1525.91         .649         51.5           180         18.83         34.98         26.33         170.4         176.7         151.5         66.36         85.6           200         17.2	Γ	DEPT :	10 901	TOM	3219	M					
0 27, 94 36.15 25.30											
20 27,68 36.14 23.38	2	T	S	SIGT	TANOM	SVA	SVEL	PYNHGT	TRANS		
40 27,47 36.17 23,47 442.8 444.5 1542.55 .1808 8.1 80 25.62 36.40 24.23 370.4 373.7 1539.19 .3464 14.2 100 23.96 36.65 24.92 303.9 307.9 1535.77 .4146 21.9 120 22.47 36.72 25.41 257.7 262.4 1532.42 .4716 30.7 140 21.5 36.71 25.72 228.4 233.8 1529.81 .5212 40.6 160 19.32 36.60 26.05 197.1 203.0 1525.91 .5649 51.5 180 18.08 36.59 26.56 197.1 203.0 1525.91 .5649 51.5 180 18.08 36.59 26.56 197.1 203.0 1525.91 .5649 51.5 180 18.08 36.59 26.56 197.1 203.0 1525.91 .5649 51.5 180 18.08 36.59 26.66 139.4 146.9 1514.20 .6029 36.13 26.57 147.8 154.9 1516.17 .6686 88.6 20 16.29 36.13 26.57 147.8 154.9 1516.17 .6686 88.6 20 16.29 36.13 26.57 147.8 154.9 1516.17 .6686 88.6 26 14.61 35.86 26.74 131.7 139.5 1511.30 .7274 116.6 280 13.90 35.72 26.78 127.4 135.4 1509.17 .7549 131.4 300 13.20 35.61 26.84 121.4 122.7 1507.07 .7814 146.8 340 11.93 35.41 26.94 112.4 121.1 1503.18 .8318 179.0 38.10.73 35.24 27.05 103.7 112.6 1490.43 .8783 213.2 420 10.10 35.16 27.08 103.7 112.6 1490.43 .8783 213.2 420 10.10 35.16 27.08 198.7 108.2 1497.72 .9225 249.3 460 9.33 35.07 27.14 93.8 103.3 1495.44 .9649 287.0 500 8.68 34.98 27.17 90.2 99.9 1493.56 1.0054 326.4 500 8.68 34.98 27.17 90.2 99.9 1493.56 1.0054 326.4 500 8.68 34.98 27.17 90.2 99.9 1493.56 1.0054 326.4 500 8.68 34.98 27.17 90.2 99.9 1493.56 1.0054 326.4 500 8.66 34.84 27.37 71.2 61.1 1487.85 1.1508 499.3 700 6.24 34.86 27.37 75.7 85.6 1489.01 1.1175 4540.0 60.9 34.86 27.43 75.7 85.6 1489.01 1.1175 4540.0 60.9 34.86 27.45 67.3 77.3 1485.87 1.2917 744.3 90.0 4.99 34.91 27.63 47.3 57.9 1485.91 1.225 793.9 780 5.61 34.89 27.65 53.8 64.1 1485.81 1.2268 69.1 149.9 34.90 27.65 44.9 44.9 34.90 27.75 51.86.6 14.95.91 1.225 1.3154 99.1 1000 4.99 34.90 27.76 38.2 49.9 1486.81 1.4223 107.05 1000 4.99 34.90 27.75 38.2 49.9 1486.81 1.4223 107.05 1000 4.00 34.96 27.74 36.6 50.0 1489.47 1.5222 1364.9 1200 4.01 34.99 27.76 38.2 49.9 1486.81 1.4223 107.05 1000 4.20 34.96 27.75 38.2 49.9 1486.81 1.4223 107.05 1000 4.20 34.96 27.77 36.6 50.0 1489.47 1.5222 1364.9 1200 4.10 34.99 27.77 36.6 50.0 1489.4	n	27.94	36.15	23,30	458.7	458.7	1542.91	.0000	• 0		
40 27,47 36.17 23,47 442.8 444.5 1542.55 .1808 8.1 80 25.62 36.40 24.23 370.4 373.7 1539.19 .3464 14.2 100 23.96 36.65 24.92 303.9 307.9 1535.77 .4146 21.9 120 22.47 36.72 25.41 257.7 262.4 1532.42 .4716 30.7 140 21.5 36.71 25.72 228.4 233.8 1529.81 .5212 40.6 160 19.32 36.60 26.05 197.1 203.0 1525.91 .5649 51.5 180 18.08 36.59 26.56 197.1 203.0 1525.91 .5649 51.5 180 18.08 36.59 26.56 197.1 203.0 1525.91 .5649 51.5 180 18.08 36.59 26.56 197.1 203.0 1525.91 .5649 51.5 180 18.08 36.59 26.66 139.4 146.9 1514.20 .6029 36.13 26.57 147.8 154.9 1516.17 .6686 88.6 20 16.29 36.13 26.57 147.8 154.9 1516.17 .6686 88.6 20 16.29 36.13 26.57 147.8 154.9 1516.17 .6686 88.6 26 14.61 35.86 26.74 131.7 139.5 1511.30 .7274 116.6 280 13.90 35.72 26.78 127.4 135.4 1509.17 .7549 131.4 300 13.20 35.61 26.84 121.4 122.7 1507.07 .7814 146.8 340 11.93 35.41 26.94 112.4 121.1 1503.18 .8318 179.0 38.10.73 35.24 27.05 103.7 112.6 1490.43 .8783 213.2 420 10.10 35.16 27.08 103.7 112.6 1490.43 .8783 213.2 420 10.10 35.16 27.08 198.7 108.2 1497.72 .9225 249.3 460 9.33 35.07 27.14 93.8 103.3 1495.44 .9649 287.0 500 8.68 34.98 27.17 90.2 99.9 1493.56 1.0054 326.4 500 8.68 34.98 27.17 90.2 99.9 1493.56 1.0054 326.4 500 8.68 34.98 27.17 90.2 99.9 1493.56 1.0054 326.4 500 8.68 34.98 27.17 90.2 99.9 1493.56 1.0054 326.4 500 8.66 34.84 27.37 71.2 61.1 1487.85 1.1508 499.3 700 6.24 34.86 27.37 75.7 85.6 1489.01 1.1175 4540.0 60.9 34.86 27.43 75.7 85.6 1489.01 1.1175 4540.0 60.9 34.86 27.45 67.3 77.3 1485.87 1.2917 744.3 90.0 4.99 34.91 27.63 47.3 57.9 1485.91 1.225 793.9 780 5.61 34.89 27.65 53.8 64.1 1485.81 1.2268 69.1 149.9 34.90 27.65 44.9 44.9 34.90 27.75 51.86.6 14.95.91 1.225 1.3154 99.1 1000 4.99 34.90 27.76 38.2 49.9 1486.81 1.4223 107.05 1000 4.99 34.90 27.75 38.2 49.9 1486.81 1.4223 107.05 1000 4.00 34.96 27.74 36.6 50.0 1489.47 1.5222 1364.9 1200 4.01 34.99 27.76 38.2 49.9 1486.81 1.4223 107.05 1000 4.20 34.96 27.75 38.2 49.9 1486.81 1.4223 107.05 1000 4.20 34.96 27.77 36.6 50.0 1489.47 1.5222 1364.9 1200 4.10 34.99 27.77 36.6 50.0 1489.4					451.3	452.2	1542.66	.0911	.9		
60 26,63 36,17 23,74 416,8 419,2 1540,99 .2671 8.1 80 25,62 36,40 24,23 370,4 373,7 1539,19 .3464 14.2 100 23,96 36,65 24,92 303,9 36,70 1535,77 .4146 21.9 120 22,47 36,72 25,41 25,77 262,4 1532,42 .4716 30.7 140 21,35 36,71 25,72 228,4 233,8 1529,81 .5212 40.6 160,19,42 36,60 26,05 197,1 203,0 1525,91 .5649 51.5 180 18,08 36,58 26,33 170,4 176,7 1521,10 .6029 63.2 200 17,20 36,50 26,48 155,9 162,7 1518,76 .6368 75,6 220 16,29 36,13 26,57 147,8 154,9 1516,17 .6686 88.6 220 16,29 36,13 26,57 147,8 154,9 1516,17 .6686 88.6 260 14,61 35,86 26,74 131,7 139,5 1511,30 .7274 116.6 280 13,90 35,61 26,84 121,4 129,7 1507,07 .7814 146,8 300 13,20 35,61 26,84 121,4 129,7 1507,07 .7814 146,8 300 11,93 35,41 26,94 112,4 121,1 1503,18 .8318 179,0 380 10,73 35,24 27,03 103,7 112.6 1499,43 .8783 213,24 27,03 400 9,33 35,07 27,14 93,8 103,3 1495,44 .9649 287,0 500 8,68 34,98 27,17 90,2 99,9 1490,18 1.0622 249,3 400 8,16 34,91 27,21 86,4 96,2 1491,80 1.0449 367,4 500 7,48 34,88 27,27 81,1 90,9 1490,18 1.0622 410,0 5,91 34,86 27,37 71,2 61,1 1487,85 1.508 499,3 700 6,24 34,86 27,33 75,7 85,6 1489,01 1.1175 454,0 90,4 99,3 4,91 27,42 67,3 77,3 1487,24 1.1225 593,9 90,4 4,0 34,90 27,67 45,0 50,0 1485,77 1.360 90,4 99 34,91 27,67 45,0 50,2 60,6 1485,77 1.360 90,4 90,4 34,96 27,72 38,2 49,9 1486,81 1.223 1000 4,9 34,96 27,72 38,2 49,9 1486,81 1.223 1000 4,9 34,96 27,72 38,2 49,9 1486,81 1.223 1000 4,9 34,96 27,72 38,2 49,9 1486,81 1.223 1000 4,9 34,96 27,72 38,2 49,9 1486,81 1.223 1000 4,9 34,96 27,72 38,2 49,9 1486,81 1.223 1000 4,9 34,96 27,72 38,2 49,9 1486,81 1.223 1000 4,9 34,96 27,77 36,2 50,5 1496,99 1.7750 2189,1 1000 4,13 34,96 27,77 36,2 50,5 1496,99 1.7750 2189,1 1000 4,13 34,96 27,77 35,3 50,9 1496,99 1.7750 2189,1 1000 4,13 34,99 27,77 35,3 50,9 1496,99 1.7750 2189,1 1000 4,13 34,99 27,77 35,3 50,9 1496,99 1.7750 2189,1 1000 4,13 34,99 27,77 35,3 50,9 1496,99 1.7750 2189,1 1000 4,13 34,99 27,77 35,3 50,9 1496,99 1.7750 2189,1 1000 4,13 34,99 27,77 35,3 50,9 1496,99 1.7750 2189,1 1000 4,13 34,99 27,77 35,3 50,9 1496,99 1.					442.8	444.5	1542.55		3.6		
80 25.62 36.40 24.23 370.4 373.7 1539.19 .5464 14.2 100 22.96 36.65 24.92 303.9 307.9 1535.77 .4146 21.9 120 22.47 36.72 25.41 257.7 262.4 1532.42 .4716 30.7 140 21.35 36.71 25.72 228.4 233.8 1529.81 .5212 40.6 16.19 .42 36.60 26.05 197.1 203.0 1525.91 .5649 51.5 180 18.08 36.35 26.35 170.4 176.7 1521.10 .6029 30.2 200 17.20 36.50 26.48 155.9 162.7 1518.76 .6368 75.6 20 16.29 36.13 26.57 147.8 154.9 1516.17 .6686 88.6 20 16.29 36.13 26.67 147.8 154.9 1516.17 .6686 88.6 20 16.29 36.13 26.66 139.4 146.9 1514.20 .6988 102.3 26.14 13.5 86 26.74 131.7 139.5 1511.30 .7274 116.6 280 13.90 35.72 26.78 127.4 135.4 1509.17 .7549 131.4 300 15.20 35.61 26.84 121.4 129.7 1507.07 .7814 146.8 340 11.93 35.41 26.94 112.4 121.1 1503.18 .8318 179.0 380 10.73 35.24 27.03 103.7 112.6 1499.43 .8773 213.2 420 10.10 35.16 27.08 98.2 108.2 1497.72 .9225 249.3 460 9.33 35.07 27.14 93.8 103.3 1495.44 .9649 287.0 500 8.68 34.94 27.17 90.2 99.9 1493.56 1.0054 326.4 150.0 6.66 6.56 34.84 27.47 90.2 99.9 1493.56 1.0054 326.4 10.0 6.56 34.84 27.47 90.2 99.9 1493.56 1.0054 326.4 10.0 6.56 34.84 27.47 90.2 99.9 1493.56 1.0054 326.4 10.0 6.66 6.56 34.84 27.47 90.2 99.9 1493.56 1.0054 326.4 10.0 6.56 34.84 27.47 90.2 99.9 1493.56 1.0054 326.4 10.0 6.66 6.56 34.84 27.47 90.2 99.9 1493.56 1.0054 326.4 10.0 6.56 34.84 27.47 90.2 99.9 1493.56 1.0054 326.4 10.0 6.34 34.85 27.47 90.2 99.9 1493.56 1.0054 326.4 10.0 6.34 34.85 27.47 90.2 99.9 1493.56 1.0054 326.4 10.0 6.34 34.85 27.47 90.2 99.9 1493.56 1.0054 326.4 10.0 6.34 34.85 27.47 90.2 99.9 1493.56 1.0054 326.4 10.0 6.34 34.89 27.60 50.5 1495.60 1.2125 593.9 1490.0 14.4 34.9 34.9 27.60 50.5 1495.60 1.2125 593.9 1490.0 14.2 34.85 27.47 50.2 57.3 67.5 1486.60 1.2125 593.9 1490.0 14.9 34.9 27.60 50.2 60.6 1495.47 1.2217 744.3 10.0 4.84 34.9 27.7 34 35.0 51.5 1486.81 1.4223 1070.5 1020 4.61 34.94 27.69 45.0 50.5 1485.96 1.2404 643.0 90.5 1490.9 1490.					416.8	419.2	1540.99		8.1		
100 23,96 36.65 24.92 303,9 307.9 1535.77 .4146 21.9 120 22,47 36.72 25.41 257.7 262.4 1532.42 .4716 30.7 140 21.5 36.71 25.72 228.4 233.8 1529.81 .5212 40.6 160 19.32 36.60 26.05 197.1 203.0 1525.91 .5649 51.5 180 18.08 36.58 26.33 170.4 176.7 1521.10 .6029 63.2 200 17.20 36.50 26.48 155.9 162.7 1518.76 .6368 2816 220 16.29 36.13 26.57 147.8 154.9 1516.17 .6686 88.6 240 15.58 36.03 26.66 139.4 146.9 1514.20 .6988 102.3 260 14.61 35.86 26.74 131.7 139.5 1511.30 .7274 116.6 280 13.90 35.72 26.78 127.4 135.4 1509.17 .7549 131.4 300 13.20 35.61 26.84 121.4 129.7 1507.07 .7814 146.8 340 11.93 35.41 26.94 112.4 129.7 1507.07 .7814 146.8 340 11.93 35.42 27.03 103.7 112.6 1499.43 .8783 213.2 420 10.10 35.16 27.08 98.9 108.2 1497.72 .9225 249.3 460 9.33 35.07 27.14 93.8 103.3 1495.44 .9649 287.0 500 8.68 34.98 27.17 90.2 99.9 1490.18 1.0054 326.4 500 666 6.56 34.84 27.37 71.2 61.1 149.356 1.0054 326.4 500 6.24 34.84 27.37 71.2 61.1 1487.85 1.1508 499.3 700 6.24 34.86 27.37 71.2 61.1 1487.85 1.1508 499.3 700 6.24 34.88 27.47 62.0 72.5 1486.60 1.2125 593.9 780 5.61 34.87 27.52 57.3 67.5 1496.06 1.2125 593.9 94.8 27.60 5.39 34.88 27.56 53.8 64.1 1485.81 1.2668 693.1 860 5.14 30.89 27.60 50.2 60.6 1485.47 1.2917 744.3 90.0 4.99 34.91 27.63 47.3 57.9 1485.57 1.3381 849.5 980 4.71 34.93 27.67 43.0 54.0 1485.70 1.3600 903.5 980 4.71 34.93 27.67 43.0 54.0 1485.70 1.3600 903.5 980 4.71 34.93 27.67 43.0 54.0 1485.70 1.3600 903.5 980 4.71 34.93 27.67 43.0 54.0 1485.70 1.3600 903.5 980 4.71 34.93 27.67 43.0 54.0 1485.70 1.3600 903.5 980 4.71 34.93 27.67 43.0 54.0 1485.70 1.3600 903.5 980 4.71 34.93 27.67 43.0 54.0 1485.70 1.3600 903.5 980 4.71 34.93 27.67 43.0 54.0 1485.70 1.3600 903.5 980 4.71 34.93 27.67 43.0 54.0 1485.70 1.3600 903.5 980 4.71 34.93 27.67 43.0 54.0 1485.70 1.3600 903.5 980 4.71 34.93 27.67 43.0 54.0 1485.70 1.3600 903.5 980 4.71 34.93 27.67 43.0 54.0 1485.97 1.3600 903.5 980 4.71 34.93 27.67 43.0 50.0 1489.47 1.5222 1364.9 140.0 4.30 34.96 27.74 36.2 50.5 1496.99 1.7750 2189.1 1000 4.13 34.99 27.77 35.3 50.9 149	80	25.62	36.40	24.23	370.4	373.7	1539.19	. 3464	14.2		
120 22.47 36.72 25.41 257.7 262.4 1532.42 .4716 40.6 19.32 36.60 26.05 197.1 203.0 1525.91 .5649 51.5 180 18.08 36.38 26.33 170.4 176.7 1521.10 .6029 63.2 200 17.20 36.50 26.48 155.9 162.7 1518.76 .6368 75.6 220 16.29 36.13 26.57 147.8 154.9 1516.17 .6686 88.6 27.0 15.58 36.03 26.66 139.4 146.9 1514.20 .6088 102.3 26.0 14.61 35.86 26.74 131.7 139.5 1511.30 .7274 116.6 280 13.90 35.72 26.78 127.4 135.4 1509.17 .7549 131.4 300 13.20 35.61 26.94 112.4 129.7 1507.07 .7614 146.8 340 11.93 35.41 26.94 112.4 129.7 1507.07 .7614 146.8 340 11.93 35.42 27.03 103.7 112.6 1499.43 .8763 213.2 420 10.10 35.16 27.08 98.9 108.2 1497.72 .9225 249.3 460 9.33 35.07 27.14 93.8 103.3 1495.44 .649 287.0 500 8.68 34.98 27.17 90.2 99.9 1493.56 1.0054 326.4 500 7.48 34.87 27.27 81.1 90.9 1490.18 1.0822 410.0 6.66 6.56 34.84 27.37 71.2 31.1 1487.85 1.1508 499.3 700 6.24 34.84 27.37 71.2 31.1 1487.85 1.1508 499.3 700 6.24 34.84 27.42 67.3 77.3 1487.24 1.125 593.9 700 6.24 34.84 27.42 67.3 77.3 1487.24 1.125 593.9 700 6.24 34.84 27.45 62.0 7.02 34.86 27.53 75.7 85.6 1480.01 1.1175 \$46.0 6.26 434.84 27.45 62.0 7.02 34.86 27.53 75.7 85.6 1480.01 1.1175 \$46.0 6.94 34.84 27.45 62.0 7.02 34.86 27.53 75.7 85.6 1480.01 1.1175 \$46.0 6.94 34.84 27.45 62.0 7.02 34.86 27.53 75.7 85.6 1480.01 1.1175 \$46.0 6.94 34.84 27.45 62.0 7.02 34.86 27.53 75.7 85.6 1480.01 1.1175 \$46.0 6.94 34.84 27.45 62.0 7.25 1486.60 1.2125 593.9 780 5.61 34.89 27.65 50.5 1485.81 1.2668 693.1 760 4.34 34.99 27.65 45.0 50.5 1485.81 1.2668 693.1 760 4.40 34.99 27.65 44.0 1485.70 1.3600 903.5 1020 4.61 34.99 27.65 44.0 1485.70 1.3600 903.5 1020 4.61 34.99 27.65 44.0 1485.70 1.3600 903.5 1020 4.61 34.99 27.65 44.0 1485.70 1.3600 903.5 1020 4.61 34.99 27.65 44.0 1485.70 1.3600 903.5 1020 4.61 34.99 27.65 44.0 1485.70 1.3600 1.3600 903.5 1020 4.61 34.99 27.76 44.0 1485.70 1.3600 1.370.5 1100 4.49 34.96 27.77 36.2 50.5 1498.06 1.4722 1215.2 1300 4.30 34.96 27.74 36.2 50.5 1498.96 1.5725 1519.6 1400 4.30 34.96 27.77 36.5 50.5 1492.91 1.5230 1679.4 1600 4.20 34.97 27.76 34.4 50.3 1493	100	23.96	36.65	24.92	303.9	307.9	1535.77	.4146	21.9		
140 21.35 36.71 25.72 228.4 253.8 1529.81 .5212 40.6 160 19.3 36.60 26.05 197.1 203.0 1525.91 .5649 51.5 200 17.20 36.50 26.48 155.9 162.7 1518.76 .6368 75.6 220 16.29 36.13 26.57 147.8 154.9 1516.17 .6686 88.6 240 15.58 36.03 26.66 13.94 146.9 1514.20 .6088 102.3 26.14 13.58.6 26.74 131.7 133.5 1511.30 .7274 116.6 280 13.90 35.72 26.78 127.4 135.4 1509.17 .7549 131.4 300 13.20 35.61 26.94 121.4 129.7 1507.07 .7614 146.8 340 11.93 35.41 26.94 112.4 121.1 1503.18 .8318 179.0 380 10.73 35.24 27.03 103.7 112.6 1494.43 .8783 213.2 420 10.10 35.16 27.08 98.2 108.2 1497.72 .9225 249.3 460 9.33 35.07 27.14 93.8 103.3 1495.44 .9649 287.0 50.0 8.68 34.98 27.17 90.2 99.9 1493.56 1.064 326.4 410.0 26.0 34.86 27.33 75.7 85.6 1489.01 1.1175 454.0 66.6 6.56 34.84 27.37 71.2 31.1 1487.85 1.1508 499.3 700 6.24 34.86 27.35 75.7 85.6 1489.01 1.1175 454.0 66.6 6.56 34.84 27.47 62.0 72.5 1486.60 1.2125 534.0 80.6 34.87 27.27 81.1 90.9 1490.18 1.0622 410.0 8.0 5.0 34.88 27.56 50.2 60.6 1495.47 1.2917 744.3 94.0 4.94 34.92 27.65 50.2 60.6 1495.47 1.2917 744.3 94.0 4.94 34.92 27.65 45.0 57.3 67.5 1486.06 1.2125 533.9 94.0 4.94 34.96 27.72 38.0 50.9 1485.52 1.3154 796.4 94.0 4.94 34.92 27.65 45.0 55.8 1485.57 1.3381 849.5 94.0 4.94 34.96 27.72 38.0 50.5 1486.81 1.223 1070.5 1200 4.40 34.96 27.72 38.0 50.5 1486.81 1.322 1215.2 1300 4.30 34.96 27.74 36.2 50.5 1489.06 1.4223 1070.5 1200 4.40 34.96 27.74 36.2 50.5 1489.06 1.4223 1070.5 1200 4.40 34.96 27.74 36.2 50.5 1489.06 1.4223 1070.5 1200 4.40 34.96 27.74 36.2 50.5 1489.06 1.4722 1215.2 1300 4.30 34.96 27.74 36.2 50.5 1490.96 1.5725 1519.6 1600 4.20 34.97 27.76 34.4 50.3 1493.84 1.6734 1844.2 1700 4.10 34.97 27.76 34.4 50.3 1493.84 1.6734 1844.2 1700 4.10 34.97 27.76 34.4 50.3 1493.84 1.6734 1844.2 1700 4.10 34.97 27.76 34.4 50.3 1493.84 1.6734 1844.2 1700 4.10 34.97 27.76 34.4 50.3 1493.84 1.6734 1844.2 1700 4.10 34.97 27.76 34.4 50.3 1493.84 1.6734 1844.2 1700 4.10 34.97 27.76 34.4 50.3 1493.84 1.6734 1844.2 1700 4.10 34.97 27.76 34.4 50.3 1493.84 1.6734 1844.2 1700 4.10 34.97 27.7											
160       19.82       36.60       26.05       197.1       203.0       1525.91       .5649       51.5         180       18.08       36.30       26.48       155.9       162.7       1518.76       .6029       63.2         200       17.20       36.50       26.48       155.9       162.7       1518.76       .6368       75.6         220       16.29       36.13       26.57       147.8       154.9       1516.17       .6686       88.6         240       15.58       36.03       26.66       139.4       146.9       1514.20       .6988       102.3         260       14.61       35.86       26.74       131.7       139.5       1511.30       .7274       116.6         280       13.90       35.61       26.84       121.4       129.7       1507.07       .7814       146.8         340       11.93       35.41       26.94       112.4       121.1       1503.18       .8783       213.2         420       10.10       35.16       27.08       98.2       108.2       1497.72       9225       249.3         460       9.33       35.07       27.14       93.8       103.3       1495.44       .964											
180       18.08       34.58       26.33       170.4       176.7       1521.10       .6029       63.2         200       17.20       36.50       26.48       155.9       162.7       1518.76       .6368       75.6         240       15.58       36.13       26.66       139.4       146.9       1514.20       .6988       102.3         260       14.61       35.86       26.74       131.7       139.5       1511.30       .7274       116.6         280       13.90       35.72       26.78       127.4       135.4       1509.17       .7549       131.4         300       13.20       35.61       26.84       121.4       129.7       1507.07       .7814       146.8         340       11.93       35.41       26.94       112.4       121.1       1503.1a       .8783       179.0         380       10.73       35.16       27.08       98.2       108.2       1497.72       .9225       249.3         420       10.10       35.16       27.08       98.2       108.2       1497.72       .9225       249.3         450       9.33       35.07       27.14       93.8       103.2       1497.72       .9											
200       17.20       36.50       26.48       155.9       162.7       1518.76       .6368       75.6         220       16.29       36.13       26.57       147.8       154.9       1516.17       .6686       88.6         240       15.58       36.03       26.66       139.4       146.9       1514.20       .6988       102.3         260       14.61       35.86       26.78       127.4       135.4       1509.17       .7549       131.4         300       13.90       35.72       26.78       127.4       135.4       1509.17       .7549       131.4         300       15.20       35.61       26.84       121.4       129.7       1507.07       .7814       146.8         340       11.93       35.41       26.94       112.4       121.1       1503.18       .8318       179.0         380       10.73       35.24       27.03       103.7       112.6       1499.43       .8783       213.2         420       10.10       35.16       27.08       98.2       108.2       1497.72       .9225       249.3         460       9.35       35.07       27.14       93.8       103.3       1497.44       .											
220       16.29       36.13       26.57       147.8       154.9       1516.17       .6686       88.6         240       15.58       36.03       26.66       139.4       146.9       1514.20       .6988       102.3         260       14.61       35.86       26.78       131.7       139.5       151.30       .7274       116.6         280       13.90       35.72       26.78       127.4       135.4       1509.17       .7549       131.4         300       13.20       35.61       26.84       121.4       129.7       1507.07       .7814       146.8         340       11.93       35.41       26.94       112.4       121.1       1503.18       .8783       137.2         420       10.10       35.16       27.08       98.2       108.2       1497.72       .9225       249.3         460       9.33       35.07       27.14       93.8       103.3       1495.44       .9649       287.0         500       8.68       34.98       27.17       90.2       99.9       1493.56       1.0654       287.0         500       7.48       34.87       27.27       81.1       90.9       1490.18       1.082<											
240       15.58       36.03       26.66       139.4       146.9       1514.20       .6988       102.3         260       14.61       35.86       26.74       131.7       139.5       1511.30       .7274       116.6         280       13.90       35.72       26.78       127.4       135.4       1509.17       .7549       131.4         300       13.20       35.61       26.78       127.4       135.4       1509.17       .7549       131.4         300       13.20       35.61       26.84       121.4       129.7       1507.07       .7814       146.8         340       10.73       35.42       27.03       103.7       112.6       1499.43       .8783       213.2         420       10.10       35.16       27.08       98.2       108.2       1497.72       .9225       249.3         460       9.33       35.07       27.14       93.8       103.3       1495.44       .9649       287.0         500       8.68       34.98       27.17       90.2       99.9       1493.56       1.0054       326.4         500       7.48       34.87       27.27       81.1       90.9       1490.18       1.04											
260       14.61       35.86       26.74       131.7       139.5       1511.30       .7274       131.4         280       13.90       35.72       26.78       127.4       135.4       1509.17       .7549       131.4         300       13.20       35.61       26.84       121.4       129.7       1507.07       .7614       146.8         340       11.93       35.41       26.94       112.4       121.1       1503.18       .8318       179.0         380       10.73       35.24       27.03       103.7       112.6       1494.43       .8783       213.2         420       10.10       35.16       27.08       98.2       108.2       1497.72       .9225       249.3         460       9.33       35.07       27.14       93.8       103.3       1495.44       .9649       287.0         500       8.68       34.98       27.17       90.2       99.9       1493.56       1.0054       286.4         540       8.16       34.91       27.27       81.1       90.9       1490.18       1.0822       410.0         620       7.02       34.86       27.37       71.2       31.1       1487.85       1.1508											
280       13,90       35,72       26,78       127,4       135,4       1509,17       .7549       131,4         300       13,20       35,61       26,84       121,4       129,7       1507,07       .7814       146,8         340       11,93       35,41       26,94       112,4       121,1       1503,18       .8318       179.0         380       10,73       35,24       27,03       103,7       112,6       1494,43       .8783       213,2         420       10,10       35,16       27,08       98,2       108,2       1497,72       .9225       249,3         460       9,33       35,07       27,14       93,8       103,3       1495,44       .9649       287,0         500       8,68       34,98       27,17       90,2       99,9       1493,56       1,0054       326,4         540       8,16       34,91       27,27       81,1       90,9       1490,18       1,049       367,4         590       7,48       34,87       27,27       81,1       90,9       1490,18       1,049       367,4         500       7,02       34,86       27,37       71,2       31,1       1487,24       1,175											
300       13,20       35,61       26,84       121,4       129,7       1507,07       .7814       146,8         340       11,93       35,41       26,94       112,4       121,1       1503,18       .8318       179,0         380       10,73       35,24       27,03       103,7       112,6       1499,43       .8763       213,2         420       10,10       35,16       27,08       98,2       108,2       1497,72       .9225       249,3         460       9,33       35,07       27,14       93,8       103,3       1495,44       .9649       287,0         500       8,68       34,98       27,17       90,2       99,9       1493,56       1,0054       326,4         540       8,16       34,91       27,27       81,1       90,9       1491,80       1,0449       367,4         580       7,48       34,87       27,27       81,1       90,9       1490,18       1,0822       410,0         620       7,02       34,86       27,37       75,7       85,6       1489,01       1,175       454,0         740       5,91       34,87       27,42       67,3       77,3       1487,24       1,1625											
340       11.93       35.41       26.94       112.4       121.1       1503.18       .8318       179.0         380       10.73       35.24       27.03       103.7       112.6       1490.43       .8783       213.2         420       10.10       35.16       27.08       98.2       108.2       1497.72       .9225       249.3         460       9.33       35.07       27.14       93.8       103.3       1495.44       .9649       287.0         500       8.68       34.98       27.17       90.2       99.9       1493.56       1.0054       326.4         540       8.16       34.91       27.27       81.1       90.9       1490.18       1.0622       410.0         620       7.02       34.86       27.33       75.7       85.6       1489.01       1.1175       454.0         660       6.56       34.84       27.37       71.2       31.1       1487.24       1.1225       546.0         740       5.91       34.85       27.47       62.8       72.5       1486.60       1.2125       593.9         780       5.61       34.87       27.52       57.3       67.5       1486.60       1.2404											
380       10.73       35.24       27.03       103.7       112.6       1499.43       .8783       213.2         420       10.10       35.16       27.08       98.2       108.2       1497.72       .9225       249.3         460       9.33       35.07       27.14       93.8       103.3       1495.44       .9649       287.0         500       8.68       34.98       27.17       90.2       99.9       1493.56       1.0649       367.4         580       7.48       34.81       27.21       86.4       96.2       1491.80       1.0449       367.4         580       7.48       34.87       27.27       81.1       90.9       1490.18       1.0822       410.0         620       7.02       34.86       27.33       75.7       85.6       1487.85       1.1508       499.3         700       6.24       34.84       27.37       71.2       31.1       1487.85       1.1508       499.3         700       6.24       34.84       27.42       67.3       77.3       1486.60       1.2125       593.9         780       5.61       34.87       27.52       57.3       67.5       1486.60       1.2268							AND DESCRIPTION OF THE PARTY OF				
420       10.10       35.16       27.08       98.7       108.2       1497.72       .9225       249.3         460       9.33       35.07       27.14       93.8       103.3       1495.44       .9649       287.0         500       8.68       34.98       27.17       90.2       99.9       1493.56       1.0649       326.4         580       7.48       34.87       27.27       86.4       96.2       1491.80       1.0449       367.4         580       7.48       34.87       27.27       81.1       90.9       1490.18       1.0449       367.4         580       7.48       34.87       27.27       81.1       90.9       1490.18       1.0449       367.4         580       7.02       34.86       27.37       71.2       31.1       1487.85       1.1508       499.3         700       6.24       34.84       27.47       62.0       72.5       1486.60       1.2125       593.9         780       5.61       34.87       27.52       57.3       67.5       1486.60       1.2404       643.0         820       5.39       34.88       27.60       50.2       60.6       1485.47       1.2917											
460       9.33       35.07       27.14       93.8       103.3       1495.44       .9649       287.0         500       8.68       34.98       27.17       90.2       99.9       1493.56       1.0054       326.4         540       8.16       34.91       27.21       86.4       96.2       1491.80       1.0449       367.4         580       7.48       34.87       27.27       81.1       90.9       1490.18       1.0822       410.0         620       7.02       34.86       27.33       75.7       85.6       1489.01       1.1175       454.0         660       6.56       34.84       27.37       71.2       81.1       1487.85       1.1508       499.3         700       6.24       34.84       27.37       71.2       81.1       1487.85       1.1508       499.3         740       5.91       34.85       27.47       62.0       72.5       1486.60       1.2125       593.9         780       5.39       34.88       27.56       53.8       64.1       1485.81       1.2668       693.1         860       5.14       30.89       27.60       50.2       60.6       1485.47       1.2917											
500       8.68       34.98       27.17       90.2       99.9       1493.56       1.0054       326.4         540       8.16       34.91       27.21       86.4       96.2       1491.80       1.0449       367.4         580       7.48       34.87       27.27       81.1       90.9       1490.18       1.0622       410.0         620       7.02       34.86       27.33       75.7       85.6       1489.01       1.1175       454.0         660       6.56       34.84       27.37       71.2       31.1       1487.85       1.1508       499.3         700       6.24       34.84       27.42       67.3       77.3       1487.85       1.1508       499.3         740       5.91       34.85       27.42       67.3       77.5       1486.60       1.2125       593.9         780       5.61       34.87       27.52       57.3       67.5       1486.60       1.225       593.9         780       5.61       34.87       27.52       57.3       67.5       1486.60       1.225       593.9         80       5.39       34.88       27.56       53.8       64.1       1485.81       1.2668 <t< td=""><td></td><td></td><td></td><td></td><td></td><td></td><td></td><td></td><td></td></t<>											
540       8.16       34.91       27.21       86.4       96.2       1491.80       1.0449       367.4         580       7.48       34.87       27.27       81.1       90.9       1490.18       1.0822       410.0         620       7.02       34.86       27.33       75.7       85.6       1489.01       1.1175       454.0         660       6.56       34.84       27.37       71.2       31.1       1487.85       1.1508       499.3         700       6.24       34.84       27.42       67.3       77.3       1487.24       1.1625       546.0         740       5.91       34.85       27.47       62.4       72.5       1486.60       1.2125       593.9         780       5.61       34.87       27.52       57.3       67.5       1436.06       1.2404       643.0         820       5.39       34.88       27.56       53.8       64.1       1485.81       1.2668       693.1         860       5.14       34.89       27.60       50.2       60.6       1485.47       1.2917       744.3         940       4.94       34.93       27.65       45.0       55.8       1485.57       1.5381											
580       7.48       34.87       27.27       81.1       90.9       1490.18       1.0822       410.0         620       7.02       34.86       27.33       75.7       85.6       1489.01       1.1175       454.0         660       6.56       34.84       27.37       71.2       31.1       1487.85       1.1508       499.3         700       6.24       34.84       27.42       67.3       77.3       1487.24       1.1g25       546.0         740       5.91       34.85       27.47       62.4       72.5       1486.60       1.2125       593.9         780       5.61       34.87       27.52       57.3       67.5       1486.06       1.2404       643.0         820       5.39       34.88       27.56       53.8       64.1       1485.81       1.2668       693.1         860       5.14       34.89       27.60       50.2       60.6       1485.47       1.2917       744.3         940       4.99       34.91       27.63       47.3       57.9       1485.52       1.3154       796.4         940       4.84       34.93       27.67       43.0       54.0       1485.93       1.3613								-			
620       7.02       34.86       27.33       75.7       85.6       1489.01       1.1175       454.0         660       6.56       34.84       27.37       71.2       31.1       1487.85       1.1508       499.3         700       6.24       34.84       27.42       67.3       77.3       1487.24       1.1825       546.0         740       5.91       34.85       27.47       62.8       72.5       1486.60       1.2125       593.9         780       5.61       34.87       27.52       57.3       67.5       1486.06       1.2404       643.0         820       5.39       34.88       27.56       53.8       64.1       1485.81       1.2668       693.1         860       5.14       38.89       27.60       50.2       60.6       1485.47       1.2917       744.3         900       4.99       34.91       27.63       47.3       57.9       1485.52       1.5154       796.4         940       4.84       34.92       27.65       45.0       55.8       1485.57       1.5381       849.5         980       4.71       34.93       27.67       43.0       54.0       1485.98       1.3813											
660       6.56       34.84       27.37       71.2       31.1       1487.85       1.1508       499.3         700       6.24       34.84       27.42       67.3       77.3       1487.24       1.1e25       546.0         740       5.91       34.85       27.47       62.4       72.5       1486.60       1.2125       593.9         780       5.61       34.87       27.52       57.3       67.5       1486.06       1.2404       643.0         820       5.39       34.88       27.56       53.8       64.1       1485.81       1.2668       693.1         860       5.14       34.89       27.60       50.2       60.6       1485.47       1.2917       744.3         900       4.99       34.91       27.63       47.3       57.9       1485.52       1.5154       796.4         940       4.84       34.92       27.65       45.0       55.8       1485.57       1.5381       849.5         980       4.71       34.93       27.67       43.0       54.0       1485.70       1.5600       903.5         1020       4.61       34.94       27.72       38.2       49.9       1486.81       1.4223											
700       6.24       34.84       27.42       67.3       77.3       1487.24       1.1825       546.0         740       5.91       34.85       27.47       62.8       72.5       1486.60       1.2125       593.9         780       5.61       34.87       27.52       57.3       67.5       1486.60       1.2404       643.0         820       5.39       34.88       27.56       53.8       64.1       1485.81       1.2668       693.1         860       5.14       38.82       27.60       50.2       60.6       1485.47       1.2917       744.3         900       4.99       34.91       27.63       47.3       57.9       1485.52       1.3154       796.4         940       4.84       34.92       27.65       45.0       55.8       1485.57       1.3381       849.5         940       4.84       34.93       27.67       43.0       54.0       1485.70       1.3600       903.5         1020       4.61       34.94       27.69       41.3       52.5       1485.98       1.3813       958.3         1100       4.49       34.96       27.72       38.2       49.9       1486.81       1.4223											
740       5.91       34.85       27.47       62.4       72.5       1486.60       1.2125       593.9         780       5.61       34.87       27.52       57.3       67.5       1486.06       1.2404       643.0         820       5.39       34.88       27.56       53.8       64.1       1485.81       1.2668       693.1         860       5.14       34.89       27.60       50.2       60.6       1485.47       1.2917       744.3         900       4.99       34.91       27.63       47.3       57.9       1485.52       1.3154       796.4         940       4.84       34.92       27.65       45.0       55.8       1485.52       1.3154       796.4         940       4.84       34.92       27.65       45.0       55.8       1485.57       1.381       849.5         980       4.71       34.93       27.67       43.0       54.0       1485.70       1.3600       903.5         1020       4.61       34.94       27.69       41.3       52.5       1485.98       1.3813       958.3         1100       4.49       34.96       27.72       38.2       49.9       1486.81       1.4223											
780       5.61       34.87       27.52       57.3       67.5       1436.06       1.2404       643.0         820       5.39       34.88       27.56       53.8       64.1       1485.81       1.2668       693.1         860       5.14       34.89       27.60       50.2       60.6       1485.47       1.2917       744.3         900       4.99       34.91       27.63       47.3       57.9       1485.52       1.3154       796.4         940       4.84       34.92       27.65       45.0       55.8       1485.52       1.3154       796.4         940       4.84       34.92       27.65       45.0       55.8       1485.57       1.3600       903.5         980       4.71       34.93       27.67       43.0       54.0       1485.70       1.3600       903.5         1020       4.61       34.94       27.69       41.3       52.5       1485.98       1.3813       958.3         1100       4.49       34.96       27.72       38.2       49.9       1486.81       1.4223       1070.5         1200       4.40       34.96       27.74       36.6       50.0       1489.47       1.5222											
820 5.39 34.88 27.56 53.8 64.1 1485.81 1.2668 693.1 860 5.14 34.89 27.60 50.2 60.6 1485.47 1.2917 744.3 900 4.99 34.91 27.63 47.3 57.9 1485.52 1.3154 796.4 940 4.84 34.92 27.65 45.0 55.8 1485.57 1.3381 849.5 980 4.71 34.93 27.67 43.0 54.0 1485.70 1.3600 903.5 1020 4.61 34.94 27.69 41.3 52.5 1485.98 1.3813 958.3 1100 4.49 34.96 27.72 38.2 49.9 1486.81 1.4223 1070.5 1200 4.40 34.95 27.72 38.0 50.5 1486.06 1.4722 1215.2 1300 4.34 34.96 27.74 36.6 50.0 1489.47 1.5222 1364.9 1400 4.50 34.96 27.74 36.2 50.5 1490.96 1.5725 1519.6 1500 4.23 34.96 27.75 35.5 50.5 1492.31 1.6230 1679.4 1600 4.20 34.97 27.76 34.4 50.3 1493.84 1.6734 1844.2 1700 4.19 34.97 27.76 34.4 50.3 1493.84 1.6734 1844.2 1700 4.19 34.97 27.76 34.3 51.1 1495.45 1.7240 2014.1 1800 4.16 34.98 27.77 33.3 50.9 1496.99 1.7750 2189.1 1900 4.13 34.98 27.78 33.0 51.3 1498.52 1.8261 2369.1											
860 5.14 34.89 27.60 50.2 60.6 1485.47 1.2917 744.3 900 4.99 34.91 27.63 47.3 57.9 1485.52 1.3154 796.4 940 4.84 34.92 27.65 45.0 55.8 1485.57 1.3381 849.5 980 4.71 34.93 27.67 43.0 54.0 1485.70 1.3600 903.5 1020 4.61 34.94 27.69 41.3 52.5 1485.98 1.3813 958.3 1100 4.49 34.96 27.72 38.2 49.9 1486.81 1.4223 1070.5 1200 4.40 34.95 27.72 38.0 50.5 1486.06 1.4722 1215.2 1300 4.34 34.96 27.74 36.6 50.0 1489.47 1.5222 1364.9 1400 4.50 34.96 27.74 36.2 50.5 1490.96 1.5725 1519.6 1500 4.23 34.96 27.75 35.5 50.5 1492.31 1.6230 1679.4 1600 4.20 34.97 27.76 34.4 50.3 1493.84 1.6734 1844.2 1700 4.19 34.97 27.76 34.4 50.3 1493.84 1.6734 1844.2 1700 4.19 34.97 27.76 34.3 51.1 1495.45 1.7240 2014.1 1800 4.16 34.98 27.77 33.3 50.9 1496.99 1.7750 2189.1 1900 4.13 34.98 27.78 33.0 51.3 1498.52 1.8261 2369.1											
900 4.99 34.91 27.63 47.3 57.9 1485.52 1.3154 796.4 940 4.84 34.92 27.65 45.0 55.8 1485.57 1.3381 849.5 980 4.71 34.93 27.67 43.0 54.0 1485.70 1.3600 903.5 1020 4.61 34.94 27.69 41.3 52.5 1485.98 1.3813 958.3 1100 4.49 34.96 27.72 38.2 49.9 1486.81 1.4223 1070.5 1200 4.40 34.95 27.72 38.0 50.5 1486.06 1.4722 1215.2 1300 4.34 34.96 27.74 36.6 50.0 1489.47 1.5222 1364.9 1400 4.50 34.96 27.74 36.2 50.5 1490.96 1.5725 1519.6 1500 4.23 34.96 27.75 35.5 50.5 1492.31 1.6230 1679.4 1600 4.20 34.97 27.76 34.4 50.3 1493.84 1.6734 1844.2 1700 4.19 34.97 27.76 34.4 50.3 1493.84 1.6734 1844.2 1700 4.19 34.97 27.76 34.3 51.1 1495.45 1.7240 2014.1 1800 4.16 34.98 27.77 33.3 50.9 1496.99 1.7750 2189.1 1900 4.13 34.98 27.78 33.0 51.3 1498.52 1.8261 2369.1											
940 4.84 34.92 27.65 45.0 55.8 1485.57 1.3381 849.5 980 4.71 34.93 27.67 43.0 54.0 1485.70 1.3600 903.5 1020 4.61 34.94 27.69 41.3 52.5 1485.98 1.3813 958.3 1100 4.49 34.96 27.72 38.2 49.9 1486.81 1.4223 1070.5 1200 4.40 34.95 27.72 38.0 50.5 1488.06 1.4722 1215.2 1300 4.34 34.96 27.74 36.6 50.0 1489.47 1.5222 1364.9 1400 4.50 34.96 27.74 36.2 50.5 1490.96 1.5725 1519.6 1500 4.23 34.96 27.75 35.5 50.5 1492.31 1.6230 1679.4 1600 4.20 34.97 27.76 34.4 50.3 1493.84 1.6734 1844.2 1700 4.19 34.97 27.76 34.4 50.3 1493.84 1.6734 1844.2 1700 4.19 34.97 27.76 34.3 51.1 1495.45 1.7240 2014.1 1800 4.13 34.98 27.77 33.3 50.9 1496.99 1.7750 2189.1											
980       4.71       34.93       27.67       43.0       54.0       1485.70       1.3600       903.5         1020       4.61       34.94       27.69       41.3       52.5       1485.98       1.3813       958.3         1100       4.49       34.96       27.72       38.2       49.9       1486.81       1.4223       1070.5         1200       4.40       34.95       27.72       38.0       50.5       1486.06       1.4722       1215.2         1300       4.34       34.96       27.74       36.6       50.0       1489.47       1.5222       1364.9         1400       4.50       34.96       27.74       36.2       50.5       1490.96       1.5725       1519.6         1500       4.23       34.96       27.75       35.5       50.5       1492.31       1.6230       1679.4         1600       4.20       34.97       27.76       34.4       50.3       1493.84       1.6734       1844.2         1700       4.19       34.97       27.76       34.3       51.1       1495.45       1.7240       2014.1         1800       4.16       34.98       27.77       33.3       50.9       1496.99       1											
1020       4.61       34.94       27.69       41.3       52.5       1485.98       1.3813       958.3         1100       4.49       34.96       27.72       38.2       49.9       1486.81       1.4223       1070.5         1200       4.40       34.95       27.72       38.0       50.5       1486.06       1.4722       1215.2         1300       4.34       34.96       27.74       36.6       50.0       1489.47       1.5222       1364.9         1400       4.50       34.96       27.74       36.2       50.5       1490.96       1.5725       1519.6         1500       4.23       34.96       27.75       35.5       50.5       1492.31       1.6230       1679.4         1600       4.20       34.97       27.76       34.4       50.3       1493.84       1.6734       1844.2         1700       4.19       34.97       27.76       34.3       51.1       1495.45       1.7240       2014.1         1800       4.16       34.98       27.77       33.3       50.9       1496.99       1.7750       2189.1         1900       4.13       34.98       27.78       33.0       51.3       1498.52 <td< td=""><td></td><td></td><td></td><td></td><td></td><td></td><td></td><td></td><td></td></td<>											
1100       4.49       34.96       27.72       38.2       49.9       1486.81       1.4223       1070.5         1200       4.40       34.95       27.72       38.0       50.5       1488.06       1.4722       1215.2         1300       4.34       34.96       27.74       36.6       50.0       1489.47       1.5222       1364.9         1400       4.50       34.96       27.74       36.2       50.5       1490.96       1.5725       1519.6         1500       4.23       34.96       27.75       35.5       50.5       1492.31       1.6230       1679.4         1600       4.20       34.97       27.76       34.4       50.3       1493.84       1.6734       1844.2         1700       4.19       34.97       27.76       34.3       51.1       1495.45       1.7240       2014.1         1800       4.16       34.98       27.77       33.3       50.9       1496.99       1.7750       2189.1         1900       4.13       34.98       27.78       33.0       51.3       1498.52       1.8261       2369.1			-								
1200     4.40     34.95     27.72     38.0     50.5     1498.06     1.4722     1215.2       1300     4.34     34.96     27.74     36.6     50.0     1489.47     1.5222     1364.9       1400     4.50     34.96     27.74     36.2     50.5     1490.96     1.5725     1519.6       1500     4.23     34.96     27.75     35.5     50.5     1492.31     1.6230     1679.4       1600     4.20     34.97     27.76     34.4     50.3     1493.84     1.6734     1844.2       1700     4.19     34.97     27.76     34.3     51.1     1495.45     1.7240     2014.1       1800     4.16     34.98     27.77     33.3     50.9     1496.99     1.7750     2189.1       1900     4.13     34.98     27.78     33.0     51.3     1498.52     1.8261     2369.1											
1300     4.34     34.96     27.74     36.6     50.0     1489.47     1.5222     1364.9       1400     4.50     34.96     27.74     36.2     50.5     1490.96     1.5725     1519.6       1500     4.23     34.96     27.75     35.5     50.5     1492.31     1.6230     1679.4       1600     4.20     34.97     27.76     34.4     50.3     1493.84     1.6734     1844.2       1700     4.19     34.97     27.76     34.3     51.1     1495.45     1.7240     2014.1       1800     4.16     34.98     27.77     33.3     50.9     1496.99     1.7750     2189.1       1900     4.13     34.98     27.78     33.0     51.3     1498.52     1.8261     2369.1									and the second second		
1400     4.30     34.96     27.74     36.2     50.5     1490.96     1.5725     1519.6       1500     4.23     34.96     27.75     35.5     50.5     1492.31     1.6230     1679.4       1600     4.20     34.97     27.76     34.4     50.3     1493.84     1.6734     1844.2       1700     4.19     34.97     27.76     34.3     51.1     1495.45     1.7240     2014.1       1800     4.16     34.98     27.77     33.3     50.9     1496.99     1.7750     2189.1       1900     4.13     34.98     27.78     33.0     51.3     1498.52     1.8261     2369.1											
1500 4.23 34.96 27.75 35.5 50.5 1492.31 1.6230 1679.4 1600 4.20 34.97 27.76 34.4 50.3 1493.84 1.6734 1844.2 1700 4.19 34.97 27.76 54.3 51.1 1495.45 1.7240 2014.1 1800 4.16 34.98 27.77 33.3 50.9 1496.99 1.7750 2189.1 1900 4.13 34.98 27.78 33.0 51.3 1498.52 1.8261 2369.1		-									
1600     4.20     34.97     27.76     34.4     50.3     1493.84     1.6734     1844.2       1700     4.19     34.97     27.76     54.3     51.1     1495.45     1.7240     2014.1       1800     4.16     34.98     27.77     33.3     50.9     1496.99     1.7750     2189.1       1900     4.13     34.98     27.78     33.0     51.3     1498.52     1.8261     2369.1		The state of the s					The Control of the Co	The same same			
1700 4.19 34.97 27.76 54.3 51.1 1495.45 1.7240 2014.1 1800 4.16 34.98 27.77 33.3 50.9 1496.99 1.7750 2189.1 1900 4.13 34.98 27.78 33.0 51.3 1498.52 1.8261 2369.1		_									
1800 4.16 34.98 27.77 33.3 50.9 1496.99 1.7750 2189.1 1900 4.13 34.98 27.78 33.0 51.3 1498.52 1.8261 2369.1											
1900 4.13 34.98 27.78 33.0 51.3 1498.52 1.8261 2369.1											
2000 4.11 34.98 27.78 32.8 51.9 1500.10 1.8777 2554.3											
	2000	4.11	54.9p	27.18	25.4	51.9	1500.10	1.8777	2554.3		

STO STATION NUMBER 114

STD STATION NUMBER	015
JULY 22, 1971	04.5 7
LATITUDE	16 16
LONGITUDE	87 10
PEPTH TO HOTTOM	1899 M

```
SVEL
                                                        TRANS
             S
                  SIGT
                         TANOM
                               SVA
                                              TYNHET
  0 27,97 35.89 23.09
                         478.4 478.4 1542.74
                                               .0000
                                                          • 0
                         477.3 478.2 1543.05
 20 27,96 35,90 23,11
                                               .0957
                                                          1.0
                         464.6 466.3 1543.17
 40 27.82 36.02 23.24
                                               .1901
                                                          3.8
                         399.7 402.2 1540.17
 60 26.24 36.25 23.42
                                               .2769
                                                          8.5
 80 25.29 36.49 24.40
                         353.8 357.1 1538.50
                                                         14.8
                                               . 3529
100 24.13 36.63 24.86
                         310.4 314.4 1536.16
                                                         22.5
                                               .4200
                         264.1 268.9 1532.71
                                               .4784
                                                         31.5
120 22.60 36.68 25.34
140 20.80 36.71 25.87
                         214.1 219.4 1528.35
                                                         41.6
                                               .5272
160 19.21 36.52 26.14
                         188.2 194.0 1524.15
                                                         52.5
                                               .5685
180 17.79 36.34 26.37
                         166.7 172.9 1520.21
                                               .6052
                                                         64.2
200 16.90 36.24 26.51
                         153.5 160.2 1517.79
                                               .6385
                                                         76.7
                         145.1 152.2 1515.57
                                               .6698
220 16.10 36.11 26.60
                                                         89.8
240 15.65 36.01 26.62
                         142.9 150.5 1514.41
                                               .7000
                                                        103.5
                         134.2 142.1 1512.21
                                               .7293
                                                        117.8
260 14.89 35.90 26.71
                         130.7 138.9 1510.28
                                               .7574
                                                        132.6
280 14.23 35.76 26.75
                         121.8 130.1 1506.95
300 13.17 35.60 26.84
                                               .7843
                                                        148.0
340 12.12 35.41 26.90
                         115.9 124.7 1503.83
                                               .8347
                                                        180.4
                                                        214.8
380 10.86 35.25 27.01
                         105.6 114.6 1499.91
                                               .8822
                                               .9266
                          99.9 109.2 1497.77
                                                        251.0
420 10.12 35.15 27.07
      9.40 35.08 27.13
                                               .9692
                                                        288.9
                          94.0 103.6 1495.72
461
                          90.9 100.7 1493.93 1.0100
                                                        328.5
500
      8.77 34.99 27.17
                          87.7
                                97.7 1492.57 1.0496
                                                        369.7
541
      8.26 34.95 27.20
580
      7.61 34.86 27.24
                          83.7
                                93.7 1490.66 1.0880
                                                        412.4
      6.98 34.84 27.32
                          76.7
                                86.5 1488.83 1.1243
                                                        456.7
620
660
      6.65 34.83 27.36
                          72.9
                                82.9 1488.17 1.1582
                                                        502.3
                          69.2
                                79.4 1487.84 1.1906
                                                        549.3
700
      6.39 34.84 27.40
                          64.6
                                                        597.5
740
      6.09 34.85 27.44
                                75.0 1487.28 1.2214
      5.80 34.85 27.48
                                71.2 1486.77 1.2507
                                                        647.0
780
                          60.8
                                66.5 1486.12 1.2783
                                                        697.6
820
      5.47 34.87 27.54
                          55.8
                                62.3 1485.82 1.3039
                                                        749.2
860
      5.03 34.89 27.58
                          51.8
                                60.1 1485.97 1.3284
                          49.3
                                                        801.9
900
      5.10 34.90 27.61
                                57.9 1486.09 1.3520
940
      4.96 34.91 27.63
                          46.0
                                                        855.5
                                56.7 1486.43 1.3749
980
      4.39 34.92 27.65
                          45.4
                                                        910.0
1020
      4.74 34.92 27.66
                          43.9
                                55.4 1486.50 1.3973
                                                        965.5
      4.57 34.94 27.70
1100
                          40.5
                                52.4 1487.12 1.4403
                                                       1079.0
      4.45 34.95 27.72
                          38.5
                                51.2 1488.27 1.4923
                                                       1225.6
1200
      4.34 34.95 27.73
                          37.4
                                50.7 1489.46 1.5432
                                                       1377.4
1300
      4.29 34.96 27.74
                                50.3 1490.91 1.5935
1400
                          36.1
                                                       1534.2
      4.26 34.96 27.75
1500
                          35.8
                                50.9 1492.43 1.6441
                                                       1696.1
      4.24 34.97 27.76
                          34.9
                                50.8 1494.01 1.6950
                                                       1863.1
1600
      4.20 34.97 27.76
                          34.4
                                51.2 1495.49 1.7460
1700
                                                       2035.1
```

STD ST	ATION !	UMBER	016	
JULY 2	2, 197	1	08.9 7	,
LATITU	DE		16 15	,
LONGIT	UDE		97 34	
DEPTH	TO BOT	ТОМ	1591	•
Т	S	SIGT	TANOM	
1 28.30	35.79	22.91	495.0	-
28.13			488.0	

7.	Т	S	SIGT	TANOM	SVA	SVEL	DYNHGT	TRANS
n	28.30	35.79	22.91	495.0	495.9	1543.36	.0000	• 0
20	28.13	35.82	22.99	488.0	488.8	1543.34	.0985	1.0
40	27.32	36.00	23.23	465.3	467.0	1543.15	.1941	3.9
60	26.42	36.14	23.78	413.0	415.5	1540.49	.2823	8.7
9.0	25,56	36.39	24.23	369.6	372.9	1539.05	.3612	15.1
100	24.30	36.64	24.82	314.2	318.3	1536,59	.4303	23.0
120	22.74	36.71	25.53	265.7	270.5	1533.08	.4891	32.2
140	21.14	36.70	25.77	223.5	228.9	1529.26	.5391	42.5
160	19.58	36.52	26.05	196.7	202.6	1525.19	.5822	53.7
180	18.03	36.37	26.33	170.3	176.5	1520.96	.6201	65.7
200	16.62	36.18	26.53	151.6	158.2	1516.91	.6536	78.5
550	15.77	36.03	26.61	143.3	150.3	1514.47	.6845	91.9
240	14.93	35.92	26.72	133.7	141.0	1512.06	.7136	105.8
260	14.17	35.78	26.77	128.2	135.8	1509.79	.7413	120.4
2811	13.52	35.67	26.85	123.1	131.0	1507.86	. 1680	135.5
300	12.85	35.58	26.89	117.1	125.2	1505.86	. 1936	151.1
340	11.57	35.36		109.9	118.3	1501.87	.8420	183.8
380	10.45	35.24		99.4	108.1	1498.44	.8876	218.4
420	9.71		27.12	95.6	104.6	1496.29	.9303	254.8
460	9.00	35.04		90.7	99.9	1494.20	.9710	292.8
500	8.44	34.94		86.7	96.2	1492.69	1.0103	332.4
540	8.17		27.23	84.5	94.4	1492.28	1.0485	373.6
580	7.61	34.91		80.0	90.0	1490.74	1.0854	416.3
620	7.04		27.34	74.9	84.B	1489.12	1.1205	460.4
660	6.61		27.39	69.7	79.7	1488.10	1.1533	505.9
700	6.37	34.87	-	66.6	76.8	1487.77	1.1846	552.7
740	6.17	34.87	and the same of th	64.1	74.7	1487.62	1.2149	600.7
780	5.88	34.88		60.0	70.6	1487.13	1.2440	649.8
820	5.60		27.53	56.5	67.2	1486.66	1.2715	700 • 1
860	5.41	34.90		53.0	63.9	1486.57	1.2978	751.5
900	5.17	34.93		48.1	59.1	1486.27	1.3223	803.9
940	5.03	34.94		45.2	56.3	1486.39	1.3454	857.3
980	4.89		27.67	43.1	54.4	1486.48	1.3675	911.6
1020	4.78		27.68	42.1	53.7	1486.67	1.3891	966 • 7
1100	4.69	-	27.69	41.0	53.3	1487.62	1.4319	1079.5
1200	4.53	34.97	27.13	37.8	50.6	1488.61	1.4834	1225.3

```
STD STATION NUMBER 017
JULY 22, 1971 13.4 /
LATITUDE 16 32
LONGITUDE 87 32
DEPTH TO BOITOM 2586 M
```

```
S
                   SIGT
                         TANOM SVA
                                       SVEL
                                               DYNHGT
                                                         TRANS
  0 27.00 36.05 23.24
                         464.7 464.7 1542.73
                                                .0000
                                                           .0
  20 27.71 36.05 23.23
                                                .0931
                         465.0 465.8 1543.08
                                                           .9
  40 27.93 36.05 23.23
                         465.8 467.5 1543.46
                                                          3.7
                                                .1864
  60 26.68 36.09 23.66
                         424.1 426.6 1541.04
                                                .2758
                                                          8.3
  80 25.94 36.30 24.06
                         386.7 390.0 1539.85
                                                . 3575
                                                          14.7
 100 24.47 36.50 24.72
                         323.0 327.1 1536.95
                                                .4292
                                                          22.5
 120 22.52 36.79 25.45
                                                .4877
                         253.9 258.6 1532.60
                                                          31.7
                         218.6 223.9 1528.48
                                                .5360
 140 20.86 36.67 25.82
                                                         42.0
 160 19.14 36.52 26.16
                         186.0 191.8 1523.93
                                                          53.1
                                                .5776
 180 17.98 36.40 26.37
                         166.7 172.9 1520.84
                                                .6140
                                                          65.0
 200 17.02 36.28 26.51
                         153.2 159.9 1518.19
                                                .6473
                                                         77.6
                                                .6788
 220 16.44 36.17 26.56
                         148.2 155.4 1516.67
                                                         90.9
                                                . 1097
 240 16.03 36.08 26.59
                         145.5 153.2 1515.66
                                                        104.8
                                                .7394
 269 15.27 35.99 26.69
                         136.1 144.2 1513.50
                                                        119.3
                                                .7677
 280 14.36 35.81 26.76
                         129.9 138.2 1510.77
                                                        134.3
                                                . 1945
 300 13.39 35.66 26.84
                                                        149.9
                         121.6 130.0 1507.75
                                                .8449
 349 11.97 35.44 26.95
                         111.2 119.9 1503.34
                                                        182.7
                                                .8915
 390 10.66 35.21 27.02
                         104.9 113.7 1499.15
                                                        217.5
                                                .9352
 420
      9.62 35.08 27.10
                          97.1 106.0 1495.90
                                                        254.0
                                               .9764
 450
      8.82 35.01 27.17
                          90.4
                                 99.4 1493.49
                                                        292.3
 500
      8.56 34.96 27.21
                          87.0
                                 96.4 1492.35 1.0154
                                                        332.1
      8.16 34.94 27.23
                                 94.2 1491.84 1.0535
 540
                          84.4
                                                        373.5
                          82.0
      7.76 34.91 27.26
 580
                                 92.2 1491.29 1.0909
                                                        416.4
 620
      7.30 34.86 27.28
                          79.7
                                 90.0 1490.12 1.1271
                                                        460.7
      6.91 34.85 27.33
                          75.0
 660
                                 85.4 1489.24 1.1623
                                                        506.5
                                 83.9 1488.88 1.1959
      6.66 34.83 27.35
                          73.3
 700
                                                        553.7
 740
      6.40 34.84 27.40
                          69.2
                                 80.1 1488.51 1.2288
                                                        602.2
 780
      6.00 34.84 27.45
                          64.0
                                 74.8 1497.58 1.2598
                                                        652.0
 820
      5.55 34.87 27.52
                          57.9
                                 68.6 1486.86 1.2885
                                                        702.9
 860
      5.40 34.88 27.56
                          53.9
                                                        755.0
                                 64.8 1486.52 1.5153
      5.16 34.90 27.60
 900
                          50.0
                                 60.9 1486.22 1.3403
                                                        808.1
 940
      4.98 34.90 27.62
                          47.9
                                 58.9 1486.12 1.3643
                                                        862.2
 980
      4.83 34.92 27.65
                          44.9
                                 56.1 1486.19 1.3873
                                                        917.3
      4.71 34.94 27.68
                          42.3
                                 53.7 1486.37 1.4092
                                                        973.2
1020
      4.52 34.95 27.71
                                 51.1 1486.93 1.4509
1100
                          39.2
                                                       1087.6
1200
      4.44 34.95 27.72
                          58.4
                                 51.0 1488.23 1.5018
                                                       1235.2
      4.38 34.96 27.74
                           37.0
                                 50.5 1489.63 1.5529
1300
                                                       1388.0
      4.32 34.96 27.74
1400
                          36.4
                                 50.7 1491.03 1.6035
                                                       1545.8
      4.27 34.96 27.75
                                                       1708.7
                           35.9
                                 51.0 1492.47 1.6544
1500
      4.23 34.97 27.76
                          34.7
                                 50.6 1493.95 1.7051
                                                       1876.7
1600
1700
      4.21 34.97 27.76
                          34.5
                                 51.3 1495.53 1.7561
                                                       2049.7
1800
      4.18 34.98 27.77
                          33.5
                                 51.1 1497.07 1.8073
                                                       2227.9
      4.16 34.98 27.77
                                 51.7 1498.64 1.8587
1900
                          33.3
                                                       2411.2
      4.13 34.98 27.78
                                 52.2 1500.19 1.9107
2000
                          33.0
                                                       2599.7
```

STD STATION NUMBER	018
JULY 22, 1971	18.3 /
LATITUDE	16 57
LONGITUDE	87 34
DEPTH TO BOTTOM	2414 M

Z	T	S	SIGT	TANOM	SVA	SVEL	DYNHGT	TRANS
U	28.13	36.04	23.15	472.6	472.6	1543.22	.0000	• 0
20	28.98	36.04	23.17	471.0	471.9	1543.44	.0944	• 9
40	28.06	36.04	23.18	470.4	472.1	1543.72	.1888	3.8
60	27.33	36.09	23.45	444.1	446.6	1542.49	.2807	8.5
80	25.79	36.35		378.8	382.1	1539.54	.3636	14.9
100	24.42	36.58	24.75	385.3	326.3	1536.82	. 4344	22.9
120	22.65		25.35	263.5	268.3	1532.81	.4939	32.2
140	20.86	36.66	25.81	219.3	224.6	1528.47	.5432	42.6
160	19.24	36.54	26.15	187.0	192.8	1524.24	.5849	53.8
180	18.45	36.47		172.9	179.5	1522.26	.6221	65.9
Sou	17.51	36.36	26.43	161.0		1520.03	.6569	78.7
550	16.71		26.52	152.1	159.4	1517.52	.6896	92.2
240	15.70	36.04	26.63	141.5	149.0	1514.59	.7204	106.3
260	14.79	35.88	26.71	133.8	141.7	1511.88	. 7495	121.0
280	14.23		26.78	127.4	135.6	1510.33	.7772	136.2
300	13.30	35.65	26.85	120.6	129.0	1507.44	.8037	152.0
341	11.77	35.41	26.97	109.6	118.1	1502.63	.8530	185.2
380	10.50	35.23	27.06	100.7	109.4	1498,60	.8988	220.2
420	9.73	35.13	27.12	95.4	104.4	1496.35	.9416	257.0
460	9.31	35.07	27.14	93.2	102.7	1495.38	.9829	295.5
500	8.44	34.98	27.21	86.7	96.1	1492.68	1.0229	335.6
540	7.71	34.91	27.27	81.4	90.8	1490.46	1.0604	377.3
580	7.38	34.84	27.30	78.3	88.1	1489.81	1.0961	420.5
620	7.15	34.88	27.32	76.0	86.1	1489.56	1.1310	465.0
660	6.75		27.36	72.2	82.4	1488.62	1.1649	510.9
700	6.67		27.37	71.2	81.8	1488.95	1.1977	558.2
740	6.16		27.44	64.7	75.3	1487.58	1.2294	606.7
780	5.07		27.47	62.4	73.2	1487.48	1.2592	656.5
820	5.64	The second secon	27.52	57.0	67.8	1486.83	1.2874	707.4
860	5.43		27.57	53.0	64.0	1486.66	1.3139	759.5
000	5.13	34.91	27.61	48.0	59.7	1486.11	1.5390	812.5
940	4.98	34.92	27.64	46.5	57.5	1486.16	1.3624	866.5
980	4.91	34.92	27.64	45.7	57.0	1486.53	1.3853	921.5
1030	4.42		27.66	44.0	55.6	1486.82	1.4079	977.4
1100	4.65	34.94	27.69	41.4	53.5	1487.45	1.4515	1091.8
1200	4.51	34.95	27.71	39.1	52.0	1488.52	1.5042	1239.6
1300	4.41		27.73	37.3	50.9	1489.76	1.5558	1392.6
1400	4.32	34.96	27.74	36.4	50.7	1491.03	1.6064	1550.7
1500	4.26	34.97		35.0	50.1	1492.44	1.6571	1713.9
1600	4.23	34.97		34.7	50.7	1493.96	1.7074	1882.1
1700	4.20		27.76	34.4	51.2	1495.49	1.7583	2055.4
1800	4.17		27.77	33.4	51.0	1497.03	1.8094	2233.7
1900	4.14		27.78	33.1	51.5	1498.56	1.8604	2417.2
2000	4.12	34.99	27.79	32.1	51.4	1500.15	1.9119	2605.8

STD STATION NUMBER	019
JULY 23, 1971	00.1 /
LATTTUDE	17 28
LONGITUDE	87 08
DEPTH TO BOTTOM	3625 M

```
TOHNY
                                                        TRANS
                         TANOM SVA
                                       SVEL
       T
                   SIGT
                         483.5 483.5 1543.04
  0 28.11 35.88 23.04
                                                           • 0
                                                .0000
                                                .0963
 20 27.97 35.88 23.09
                         479.1 479.9 1543.06
                                                          1.0
 40 27.95 35.96 23.15
                         472.7 474.4 1543.41
                                                .1918
                                                          3.8
                         450.9 453.4 1542.79
                                                .2846
 60 27.48 36.06 23.38
                                                          8.6
                                                .3720
                         417.3 420.6 1541.34
 80 26.4 36.17 23.73
                                                         15.2
                         364.7 368.9 1539.15
 100 25.46 36.41 24.29
                                                .4509
                                                         23.4
 120 24.44 35.60 24.74
                         321.4 326.3 1537.21
                                                .5204
                                                         33.1
                         252.7 258.1 1532.10
 140 22.23 36.70 25.46
                                                         44.1
                                                .5789
 160 19.98 36.56 25.97
                         204.0 209.9 1526.31
                                                .6257
                                                         56.2
 180 18.24 36.41 26.31
                         172.2 178.6 1521.59
                                                .6645
                                                         69.1
                                                .6988
                         157.2 163.9 1518.71
                                                         82.7
 200 17.19 36.28 26.47
 220 16.19 36.12 26.58
                         146.3 153.4 1515.86
                                                .7305
                                                         97.0
                         138.5 146.0 1513.47
                                                        111.9
240 15.36 35.98 26.66
                                                .7604
                         131.4 139.1 1511.01
260 14.53 35.84 26.74
                                                .7889
                                                        127.4
                                                .8159
280 13.64 35.71 26.83
                         122.9 130.9 1508.30
                                                        143.4
 300 12.97 35.60 26.88
                         117.9 126.1 1506.28
                                                .8416
                                                        160.0
                                                .8003
 340 11,28 35,33 27,00
                         106.7 115.0 1500.83
                                                        194.7
                                                .9346
 380 10.03 35.15 27.08
                          98.8 107.2 1496.82
                                                        231.2
                                                .9762
      9.14 35.04 27.15
                          92.8 101.3 1494.07
                                                        269.4
420
                          90.9 100.0 1493.68 1.0163
 460
      8.97 35.01 27.17
                                                        309.2
 500
                          88.6
                                98.2 1493.16 1.0559
      8.57 34.98 27.19
                                                        350.7
 540
      8.06 34.91 27.21
                          86.4
                                 96.1 1491.79 1.0949
                                                        393.7
      7.31 34.86 27.29
                          79.6
                                 89.2 1489.50 1.1319
 580
                                                        438.2
 620
      6.65 34.83 27.36
                          72.9
                                 82.3 1487.46 1.1662
                                                        484.2
      6.32 34.82 27.30
                          69.7
                                 79.3 1486.87 1.1984
                                                        531.5
 660
                          63.B
 700
      6.02 34.85 27.45
                                73.5 1486.36 1.2288
                                                        580.1
 740
      5.72 34.86 27.50
                          59.4
                                 69.3 1485.82 1.2573
                                                        629.8
                                                        680.6
 781
      5.36 34.89 27.57
                          53.0
                                 62.8 1485.06 1.2836
                          49.7
                                 59.7 1484.83 1.3080
820
      5.14 34.90 27.60
                                                        732.4
                          47.4
      5.00 34.91 27.63
 860
                                 57.6 1484.93 1.3314
                                                        785.2
                          44.9
      4.84 34.92 27.65
                                 55.2 1484.94 1.3539
                                                        838.9
900
940
      4.74 34.94 27.68
                          42.3
                                 52.9 1485.20 1.3755
                                                        893.5
                          40.6
 980
      4.65 34.95 27.70
                                 51.5 1485.50 1.3966
                                                        949.0
      4.60 34.95 27.70
                          40.1
                                                       1005.3
1020
                                 51.3 1485.95 1.4172
1100
      4.50 34.95 27.71
                          39.0
                                 50.8 1486.84 1.4583
                                                       1120.3
      4.40 34.95 27.72
                          38.0
                                 50.5 1488.06 1.5088
                                                       1268 . 6
1200
      4.32 34.96 27.74
                          36.4
                                 49.7 1489.39 1.5588
                                                       1422.0
1300
1400
      4.27 34.96 27.75
                          35.9
                                 50.0 1490.82 1.6087
                                                       1580.4
      4.23 34.97 27.76
1500
                          34.7
                                 49.7 1492.31 1.6585
                                                       1743.8
      4.20 34.97 27.76
                          34.4
                                 50.3 1493.84 1.7085
                                                       1912.1
1600
      4.18 34.98 27.77
                          33.5
                                 50.2 1495.42 1.7590
1700
                                                       2085.5
1800
      4.15 34.98 27.78
                          33.2
                                 50.7 1496.95 1.8096
                                                       2263.9
1900
                          33.9
                                 51.3 1498.52 1.8604
                                                       2447.4
      4.13 34.98 27.78
2000
      4.11 34.99 27.79
                          32.0
                                 51.2 1500.11 1.9116
                                                       2636.0
```

```
T S SIGT TANOM

T S SIGT TANOM

127.94 36.03 23.21 467.4 (27.92 36.03 23.22 466.7
```

```
TANOM SVA
                                       SVEL
                                              TYNHGT
                                                        TRANS
   0 27.94 36.03 23.21
                         467.4 467.4 1542.80
                                                           .0
                                                .0000
  20 27.92 36.03 23.22
                         466.7 467.6 1543.08
                                                           .9
                                                . 0935
  40 27.98 36.04 23.24
                         464.8 466.5 1543.33
                                                .1869
                                                          3.7
  60 27.08 36.10 23.54
                         435.7 438.2 1541.94
                                                .2774
                                                          8.4
                         380.3 383.6 1539.66
  80 25.84 36.35 24.12
                                                .3596
                                                         14.8
                         320.1 324.2 1536.85
 100 24.42 36.61 24.75
                                                .4303
                                                         22.6
                         264.0 268.7 1533.00
 120 22.70 36.72 25.34
                                                .4896
                                                         31.8
                         227.8 233.1 1529.50
 140 21.24 36.68 25.72
                                                .5398
                                                         42.1
 160 19.62 36.57 26.08
                         194.3 200.1 1525.33
                                                         53.4
                                                .5831
 190 18.29 36.42 26.30
                         172.7 179.0 1521.75
                                                         65.4
                                                .6211
 200 17.71 36.30 26.45
                         158.5 165.2 1519.09
                                                .6555
                                                         78.2
 220 16.52 36.18 26.55
                         149.3 156.5 1516.92
                                                .6877
                                                         91.6
 240 15.56 36.03 26.66
                         139.2 146.7 1514.14
                                                .7180
                                                        105.7
 260 14.79 35.90 26.73
                         132.4 140.2 1511.90
                                                .7467
                                                        120.3
 280 13.18 35.61 26.85
                         121.2 129.0 1506.67
                                                . 7736
                                                        135.5
 300 12.32 35.49 26.93
                         113.7 121.6 1503.97
                                                . 7986
                                                        151.2
 340 11.36 35.36 27.01
                         105.9 114.3 1501.15
                                                .8458
                                                        184.1
 380 10.46 35.22 27.06
                         100.8 109.4 1498.45
                                                        218.9
                                                .8906
 420
      9,54 35.10 27.13
                          94.6 103.5 1495.62
                                                .9331
                                                        255.3
 460
      8.85 35.02 27.18
                          89.8
                                 98.9 1493.62
                                                . 9734
                                                        293.5
      8.34 34.97 27.22
 500
                          86.n
                                 95.3 1492.29 1.0121
                                                        533.2
      7.71 34.90 27.26
                          82.1
 540
                                 91.6 1490.45 1.0496
                                                        374.4
                          77.6
 580
      7.27 34.88 27.31
                                87.2 1489.37 1.0853
                                                        417.1
      6.93 34.86 27.34
                          74.5
620
                                84.4 1488.67 1.1195
                                                        461.2
      6.62 34.86 27.38
                          70.5
                                80.5 1488.11 1.1526
660
                                                        506.7
                          68.1
      6.37 34.85 27.41
 700
                                 78.4 1487.75 1.1843
                                                        553.4
      6.04 34.86 27.46
 740
                          63.3
                                73.6 1487.11 1.2146
                                                        601.4
 780
      5.72 34.87 27.51
                          58.7
                                 69.1 1486.49 1.2430
                                                        650.6
 820
      5.36 34.89 27.57
                          53.0
                                63.3 1485.71 1.2693
                                                        700.8
860
      5.31 34.89 27.57
                          52.4
                                63.1 1486.16 1.2944
                                                        752.1
900
      5.18 34.91 27.60
                          49.4
                                60.4 1486.31 1.5192
                                                        804.4
940
      5.07 34.91 27.62
                          48.2
                                 59.4 1486.51 1.3431
                                                        857.6
      4.76 34.91 27.63
 980
                          47.0
                                58.4 1486.72 1.3667
                                                        911.8
                                                        966.9
1020
      4.79 34.93 27.67
                          43.6
                                55.2 1486.70 1.3893
      4.69 34.94 27.68
                                54.0 1487.61 1.4331
1100
                          41.9
                                                       1079.8
1200
      4.54 34.95 27.71
                          39.5
                                 52.4 1488.64 1.4865
                                                       1225.8
      4.48 34.96 27.72
1300
                          38.1
                                 51.8 1490.05 1.5389
                                                       1377.1
      4.41 34.95 27.72
                          38.1
1400
                                52.6 1491.39 1.5914
                                                       1533.6
                                51.8 1492.71 1.6435
1500
      4.73 34.96 27.74
                          36.5
                                                       1695.4
1600
      4.20 34.97 27.76
                          34.4
                                50.3 1493.84 1.6950
                                                       1862.3
```

```
87 05
    LONGITUDE
    DEPTH TO RUTTOM
                         3310 M
                                       SVEI.
       T
                         TANOM SVA
                                              DYNHGT
                                                        TRANS
             S
                   SIGI
                         475.0 475.0 1543.45
                                                           • 0
  0 28.23 36.05 23.13
                                               .0000
  20 28.15 36.06 23.20
                         468.7 469.5 1543.39
                                               . 11945
                                                           .9
  40 27.04 36.05 23.22
                         465.9 467.6 1543.47
                                               .1882
                                                          3.8
                                               .2774
  60 26.79 36.16 23.68
                         422.5 425.0 1541.34
                                                          8.4
 80 25.56 36.37 24.22
                         370.6 373.9 1539.03
                                                         14.8
                                               .3573
                                               .4280
 100 24.58 36.55 24.66
                         329.0 333.1 1537.18
                                                         22.6
                         276.1 280.9 1533.74
 120 23.01 36.67 25.22
                                               .4894
                                                         31.8
 140 21.27 36.68 25.72
                         228.5 233.9 1529.58
                                               .5419
                                                         42.1
 160 19.68 36.57 26.06
                         195.8 201.6 1525.50
                                               .5845
                                                         53.4
 180 18.18 36.40 26.32
                         171.5 177.8 1521.41
                                               .6224
                                                         65.4
200 17.01 36.24 26.48
                         156.0 162.7 1518.14
                                               .6565
                                                         78.2
220 16.02 36.08 26.59
                         145.5 152.6 1515.30
                                               .6880
                                                         91.7
                         137.2 144.6 1513.04
240 15.23 35.96 26.68
                                               .7177
                                                        105.7
260 14.43 35.81 26.74
                         131.5 139.2 1510.66
                                               .7461
                                                        120.4
280 13.41 35.65 26.83
                         122.8 130.6 1507.48
                                               . /731
                                                        135.5
300 12.77 35.56 26.89
                         117.0 125.1 1505.57
                                               .7986
                                                        151.3
340 11.59 35.36 26.96
                         110.0 118.5 1501.95
                                               .8477
                                                        184.2
                                                        219.0
                                               .8933
380 10.41 35.19 27.05
                         102.1 110.8 1498.23
                                               .9365
420
      9.74 35.11 27.10
                          97.1 106.1 1496.36
                                                        255.6
                                               .9779
460
      8.77 34.99 27.17
                          90.9
                                99.9 1493.28
                                                        293.9
500
      8.11 34.92 27.21
                          86.3
                                95.5 1491.35 1.0171
                                                        333.8
540
      7.62 34.89 27.26
                          81.6
                                91.0 1490.09 1.0544
                                                        375.3
                                87.6 1489.49 1.0901
580
      7.30 34.88 27.30
                          78.0
                                                        418.2
      7.12 34.8H 27.33
620
                          75.6
                               85.6 1489.44 1.1247
                                                        462.5
      6. 12 34.86 27.34
                          74.4
                                64.8 1489.28 1.1589
                                                        508.1
660
                          69.5
700
      6.48 34.85 27.39
                                79.9 1488.19 1.1917
                                                        555.1
      5.74 34.86 27.47
740
                          62.1
                                72.2 1486.71 1.2224
                                                        603.4
      5.52 34.88 27.54
7811
                                65.6 1485.70 1.2500
                                                        652.9
                          55.6
nsa
      5.24 34.90 27.59
                                                        703.4
                          50.9
                                61.0 1485.24 1.2753
860
                          47.1
                                                        754.9
      5.04 34.92 27.63
                                57.4 1485.10 1.2989
900
                                54.6 1484.99 1.3213
      4.35 34.93 27.66
                          44.3
                                                        AU7.3
9411
      4.72 34.94 27.68
                          42.1
                                52.7 1485.12 1.3429
                                                        860.6
1100
      4.62 34.94 27.69
                          41.1
                                51.8 1485.36 1.3638
                                                        914.7
1020
      4.55 34.94 27.70
                          40.3
                                51.3 1485.73 1.3845
                                                        969.7
      4.45 34.95 27.72
                          38.5
                                50.2 1486.63 1.4248
1100
                                                       1082.1
      4. 14 34.96 27.74
                                49.0 1487.83 1.4743
1200
                          36.6
                                                       1227.0
      4.28 34.96 27.75
                          36.0 49.2 1489.22 1.5234
                                                       1376.9
1300
      4.25 34.97 27.76
                          34.9
                                49.0 1490.75 1.5723
                                                       1531.7
1400
      4.23 34.97 27.76
                          34.7
1500
                                49.7 1492.31 1.6217
                                                       1691.4
1600
      4.21 34.97 27.76
                          34.5
                                50.4 1493.88 1.6716
                                                       1856.0
      4.18 34.97 27.76
                                50.9 1495.41 1.7221
                                                       2025.7
1700
                          34.2
1800
      4.15 34.98 27.78
                          53.2
                                50.7 1496.95 1.7730
                                                       2200.5
1900
      4.13 3".9" 27.78
                          33.0
                                51.3 1498.52 1.8240
                                                       2380.3
```

STD STATION NUMBER

JULY 23, 1971

LATITUDE

2000

4.12 34.99 27.79

021 21.7 Z

16 44

51.4 1500.15 1.8753

2565.3

32.1

,	STD STA	TION	UMBER	022	
	JULY 24	1, 197	1	02.4	,
t	ATT TUE	DE		16 4	4
l	ONGITU	IDE		86 3	1
ſ	DEPTH	O BOT	TOM	4589	4
	т	S	SIGI	TANOM	S
0	27.86	36.0P	23.27	461.3	46
n	27.33	36.08	23.28	460.3	46
0	27.82	36.10	23.30	458.6	461
1	26.95	36.17	23.67	423.0	425
	25 70	76 17	24 16	777 "	201

STD STATION NUMBER	23
JULY 24, 1971	15.5 %
LATITUDE	17 22
LONGTTUDE	86 35
DEPTH TO ROTTOM	3845 M

Z.	т	5	SIGT	TANOM	SVA	SVEL	NYNHGT	TRANS
	28.08		23.15			1543.09	.0000	•0
20	-	36.01	23.17	-	471.8	1543.26	.0945	• 9
	27.34	35.08	23.28		462.3	1543.28	.1879	3.8
	27.08		23.58	432.1		1541.98	.2776	8.4
80	25.80	36.33	24.12	380.5		1539.55	.3595	14.8
100	24.35	36.60	24.77	318.8	322.9	1536.67	.4301	22.7
120	22.91	35.67	25.24	273.4	278.1	1533.49	.4902	31.9
140	21.02	36.64	25.75		230.2	1528.88	.5411	42.2
160	19.50	36.56	26.10	192.0	197.9	1524.99	.5839	53.5
180	18.27	36.43	26.32	171.5	177.8	1521.70	.6215	65.5
200	16.89	36.21	26.49	155.4	162.1	1517.75	.6554	78.3
220	15,56	36.02	26.65	139.9	146.8	1513.81	.6863	91.7
240	14.60	35.86	26.74	131.3	138.5	1510.93	.7149	105.7
560	13.56	35.75	26.84	121.8	129.2	1508.07	.7416	120.3
280	12.76	35.55	26.88	117.6	125.1	1505.20	.7671	135.4
300	11.75	35.37	26.04	112.1	119.7	1501.87	.7916	150.9
340	10.40		27.114	102.7	110.4	1497.54	.8375	183.5
380	9.58	35.11	27.13	94.5	102.6	1495.13	.8797	217.9
420	8.90	35.02	27,17	90.6	98.9	1493.16	.9201	253.9
460	8.36	34.96	27.21	87.0	95.6	1491.70	.9589	291.5
590	7.89	34.90	27.23	84.7	93.6	1490.49	.9966	330.6
540	7.42	34.88	27.29	19.6	88.7	1489.31	1.0329	371.2
SAN	7.11	34.87	27.32	76.2	85.6	1488.74	1.0676	413.2
620	6,67		27.37	71.9	81.4	1487.64	1.1009	456.6
660	6.26		27.43	66.0	75.5	1486.68	1.1324	501.2
700	5.04	34.86	27.48	60.9	70.4	1485.66	1.1614	547.1
740	5.59	2 000	27.53	56.4	66.1	1485.33	1.1887	594.1
780	5.22	34.91	27.60	49.9	59.5	1484.52	1,2138	642.2
820	4.99		27.64	45.8	55.5	1484.26	1.2367	691.2
860	4.86		27.66	44.4	54.3	1484.38	1.2587	741.1
900	4.72	34.94	27.68	42.1	52.2	1484.47	1.2799	791.9
940	4.61	34.95	27.70	40.2	50.5	1484.68	1.3004	843.5
980	4.55		27.71	39.6	50.2	1485.09	1.3205	895.9
1020	4.52	34.96	27.72	38.5	49.5	1485.63	1.3404	949.1
1100	4.42	34.96	27.73 27.75	37.4	49.0	1486.53	1.3795	1057.9
1200	4.30	34.97	27.75	36.0 35.4	48.4	1487.89	1.4284	1198.3
	4.26	34.97	27.76	35.0		1489.32	1.4769	1493.7
1500	4.22	34.97	27.76	34.6	49.2	1490.79	1.5256	1648.7
1600	4.20	34.97	27.76	34.4	50.3	1492.27	1.6247	1808.7
1700	4.18		27.77	33.5	50.2	1495.42	1.6746	1973.7
1800	4.15	34.98	27.78	35.2	50.7	1496.95	1./250	2143.7
1900	4.13	34.98	27.78	33.0	51.3	1498.52	1.7761	2318.7
5000	4.12		27.79	32.1	51.4	1500.15	1.8272	2498.9
2.000	7.12	04.7		02.1	31.4	1300.13	1.0515	2.47047

STD STATION NUMBER	024
JULY 24, 1971	21.3 7
LATITUDE	17 15
LONGITUDE	86 11
DEPTH TO ROTTOM	4180 M

```
TOHNY
                         TANOM SVA
                   SIGT
                                       SVEI.
                                                        TRANS
   0 27.94 35.70 22.96
                         491.1 491.1 1542.50
                                                .0000
                                                            .0
  20 27.77 36.02 23.26
                         462.8 463.6 1542.75
                                                .0955
                                                          1.0
                                                          3.8
 40 27.68 36.10 23.35
                         454.2 455.9 1542.94
                                                .1874
                                                          8.4
 60 27.25 36.14 23.52
                         438.0 440.6 1542.35
                                                .2771
                                                .3587
 80 25.68 36.39 24.20
                         372.7 376.0 1539.32
                                                         14.8
 100 24.46 36.62 24.75
                         320.5 324.6 1536.95
                                                .4288
                                                         22.7
 120 23.09 35.69 25.21
                         276.9 281.7 1533.96
                                                .4894
                                                         31.8
 140 21.16 36.66 25.73
                         227.1 232.5 1529.27
                                                .5408
                                                         42.1
                         197.8 203.7 1525.81
                                                . 5844
 160 19.79 36.58 26.04
                                                         53.4
 180 18.70 36.47 26.24
                         178.9 185.3 1522.97
                                                .6233
                                                         65.5
200 17.68 36.35 26.40
                         163.4 170.3 1520.23
                                                .6589
                                                         78.3
220 16.87 36.23 26.51
                         153.5 160.8 1518.03
                                                .6920
                                                         91.8
 240 16,29 36,14 26,57
                         147.1 154.9 1516.51
                                                . 7236
                                                        106.0
 260 15.56 36.01 26.64
                         140.6 148.8 1514.44
                                                .7539
                                                        120.7
                                                .7828
280 14.62 35.86 26.74
                         131.8 140.1 1511.64
                                                        136.1
 300 13.78 35.71 26.80
                         125.7 134.3 1509.08
                                                .8103
                                                        152.0
340 12,20 35,47 26,93
                         113.0 121.8 1504.18
                                                .8612
                                                        185.5
                                                .90R5
 380 11.19 35.32 27.01
                         105.9 115.1 1501.15
                                                        220.9
 420 10.23 35.19 27.08
                          99.1 108.5 1498.23
                                                .9532
                                                        258 . 1
                                                        297.1
 460
      9.50 35.10 27.13
                          94.0 103.6 1496.12
                                                .9956
      8.19 34.94 27.22
 500
                          86.0
                                95.2 1491.68 1.0357
                                                        337.7
                          79.4
                                 88.4 1489.23 1.0722
 540
      7.40 34.88 27.29
                                                        379.9
                          74.8
 580
      6.89 34.85 27.34
                                 83.9 1487.86 1.1067
                                                        423.5
                          70.4
      6.55 34.85 27.38
                                 79.7 1487.17 1.1393
                                                        468.4
650
      6.25 34.85 27.42
660
                          66.6
                                 76.1 1486.63 1.1704
                                                        514.6
      5.84 34.87 27.49
700
                          60.1
                                 69.6 1485.67 1.1996
                                                        562.0
      5.55 34.88 27.54
 7411
                          55.9
                                 65.5 1485.17 1.2267
                                                        610.5
780
      5.32 34.90 27.58
                          51.P
                                 61.5 1484.91 1.2520
                                                        660.1
 820
      5.23 34.90 27.59
                          50.8
                                 60.8 1485.20 1.2765
                                                        710.7
      5.08 34.91 27.62
                          48.3
861
                                 58.6 1485.25 1.3003
                                                        762.2
      4.93 34.92 27.64
                          45.9
                                                        814.7
 900
                                 56.4 1485.30 1.3233
940
      4.81 34.93 27.66
                          43.8
                                 54.6 1485.48 1.3454
                                                        868.1
980
      4.76 34.94 27.68
                          42.6
                                 53.6 1485.94 1.3670
                                                        922.3
      4.56 34.94 27.69
1020
                          41.5
                                 52.8 1486.18 1.3883
                                                        977.4
      4.54 34.95 27.71
                          39.5
                                 51.3 1487.01 1.4301
                                                       1090.2
1100
      4.42 34.96 27.73
                          37.4
1200
                                 50.0 1488.16 1.4808
                                                       1235.7
      4.34 34.96 27.74
                                 50.0 1489.47 1.5308
                                                       1386.3
1300
                          36.6
      4.29 34.98 27.76
                          34.6
                                 48.8 1490.93 1.5802
                                                       1541.9
1400
      4.23 34.97 27.76
                          34.7
                                 49.7 1492.31 1.6298
                                                       1702.4
1500
1600
      4.20 34.98 27.77
                          33.7
                                 49.5 1493.85 1.6797
                                                       1867.8
1700
      4.18 34.98 27.77
                          33.5
                                 50.2 1495.42 1.7295
                                                       2038.3
```

STD STATION NUMBER			025							
JULY 25, 1971			05.5 7							
LATITUDE			17 5	17 55						
LONGITUDE			85 3	85 33						
(	DEPTH '	TO BOT	TOM	3804 4	•					
7.	T	S	SIGT	TANOM	·SVA	SVEL	DYNHGT	TRANS		
	28.06	35.91	23.08	479.7	479.7	1542.95	.0000	• 0		
	28.07					1543.31	.0960	1.0		
	27.94					1543.37	.1916	3.8		
	27.52					1542.88	.2846	8.6		
	26.64					1541.35	.3720	15.2		
			24.23			1539.54	.4513	23.4		
			24.92				.5207	33.1		
			25.31			1533.60	.5799	44.1		
			25.78			1529.50	.6300	56.2		
			25.49			1527.38	.6739	69.3		
	19.37									
						1525.27	.7145	83.1		
	18.33					1522.54	.7520	97.8		
	17.71					1520.97	.7871	113.2		
	16.66					1518.01	.8202	129.3		
	15.96					1516.09	.8513	146.0		
	15.38				146.8	1514.51	.8812	163.3		
	14.14					1510.99		199.7		
	12.69					1506.57	.9905	238.3		
	10.97					1500.98		278.9		
	10,14					1498.52		321.3		
500			27.14			1495.70	1.1261	365.5		
540		34.93				1492.20	1.1659	411.4		
580		34.92		82.1		1491.50	1.2036	458 • 8		
620		34.87		77.5		1489.77	1.2397	507.6		
660	6.56	34.84	27.37	71.2	81.2	1487.84	1.2735	557.9		
700	6.22	34.85	27.43	66.2	76.3	1487.16	1.3050	609.5		
740	5.80	34.88	27.50	58.9	68.9	1486.17	1.3341	662.3		
780	5.46	34.80	27.55	54.1	64.1	1485.47	1.3607	716.2		
820	5.22	34.91	27.60	49.0	60.0	1485.17	1.3854	771 • 1		
860	5.08	34.91	27.62	48.3	58.6	1485.25	1.4091	827.0		
900	4.09	34.93	27.65	44.7	55.1	1485.15	1.4319	883.8		
940	4.78	34.93	27.67	43.5				941.5		
980			27.68	41.9		1485.69		1000.1		
1020		34.94		41.2		1486.06		1059.5		
			27.71			1487.00				
1200		34.96		37.5		1488.20	1.5883	1337.2		
1300		34.96		36.8	50.3	1489.55	1.6384	1498.5		
1400		34.96		36.2	50.4	1490.94	1.6886	1664.8		
1500			27.76	35.0	50.1	1492.44	1.7388	1836.2		
1600	_	34.97		34.7	50.7	1493.96	1.7892	2012.6		
1700	4.21	34.98		33.8	50.6	1495.54	1.8402	2194.1		
1100	4	3-076	_,,,	20.0	30.0	1475.54		2174.1		

STD STATION NUMBER 025

STD STATION NUMBER	026
JULY 25, 1971	12.7 %
LATITUDE	18 15
LONGITUDE	85 04
DEPTH TO HOTTOM	2979 M

2	Т	5	SIGT	TANOM	SVA	SVEL	CYNHST	TRANS
0	28.38	36.UR	23.10	477.6	477.6	1543.80	.0000	• 0
50	28,27	36.08	23.14	474.1	475.0	1543.89	.0953	1.0
40	27.04	36.13	23.28	460.2	461.9	1543.54	.1889	3.8
60	27.40	36.11	23.45	444.8	447.4	1542.66	.2799	8.5
80	26.45	36.27	23.81	410.4	413.7	1541.45	.3660	14.9
100	26.91	36.42	24.12	380.3	384.5	1540.44	.4458	23.1
120	25.15	36.56	24.49	344.9	349.A	1538.87	.5192	32.7
140	24.54	35.64	24.74	321.4	327.1	1537.81	.5869	43.8
160	23.51	36.71	25.16	281.5	287.9	1535.17	.6484	56.1
190	21.92	36.76	25.60	240.0	247.0	1532.00	.7019	69.6
500	20.75	36.71	25.28	212.8	220.4	1529.19	.7487	84.1
530	19.47	35.57	26.12	190.5	198.6	1525.88	. 7905	99.5
240	18.62	36.51	26.29	174.1	182.6	1523.75	.8287	115.7
2611	17.97	36.43	26.39	164.4	173.4	1522.12	.8643	132.6
240	17.42	36.34	26.46	158.1	167.6	1520.74	.8984	150.3
300	16.51	36.21	26.58	146.9	156.7	1518.21	.9308	168.6
340	15.95	36.11	26.65	139.6	150.4	1516.73	.9055	207.0
380	14.74	35.90	26.74	131.3	142.7	1513.67	1.0507	247.9
420	12.79	35.59	26.87	119.0	130.5	1508.26	1.1058	291.0
460	11.37	35.35	27.00	106.A	118.1	1503.10	1.1558	336.3
500	10.41	35.20	27.06	101.4	112.7	1500.17	1.2021	383.4
540	9.56	35.08	27.11	96.4	107.8	1497.60	1.2461	432.4
5811	8.01	35.01	27.16	91.5	103.0	1495.76	1.2883	483.1
620	8.39	34.96	27.20	87.4	99.0	1494.39	1.3286	535.4
660	7.31	34.91	27.25	82.A	94.4	1492.78	1.3673	589.4
700	7.29	34.87	27.30	78.6	90.1	1491.37	1.4042	644.8
740	6.75	34.85	27.36	72.9	84.5	1489.89	1.4391	701.7
780	6.57	34.85	27.41	68.1	79.5	1489.05	1.4718	759.9
850	5.99	34.86	27.46	62.7	74.0	1488.20	1.5027	819.4
860	5.73	34.87	27.51	5A. 8	70.2	1487.82	1.5316	880.1
900	5.52	34.80	27.55	54.9	66.4	1487.66	1.5589	941.9
940	5.24	34.90	27.59	50.9	62.4	1487.19	1.5848	1004.8
ORO	5.10	34.91	27.61	48.5	60.3	1487.28	1.6002	1068.7
1020	4.94	34.92	27.54	46.0	57.9	1487.30	1.6327	1133.5
1100	4.70	34.94	27.68	41.9	54.1	1487.65	1.6772	1265.9
1200	4.54	34.95	27.71	39.5	52.4	1488.64	1.7304	1436.3
1300	4.42	34.96		37.4	51.0	1499.80	1.7821	1611.9
1400	4.74	34.96		36.6	51.0	1491.11	1.8331	1792.7
1500	4.29	34.97	27.75	35.3	50.5	1492.56	1.8840	1978.6
1600	4.25	34.97	27.76	34.9	50.9	1494.04	1.4347	2169.5
1700	4.20	34.98		33.7	50.5	1495.50	1.9858	2365.5
1800	4.16	34.90	27.77	33.3	50.8	1496.99	2.0364	2566.6
1000	4.15	34.99	27.78	32.4	50.9	1498.61	2.0872	2772.8

STD STATION NUMBER	027
JULY 25, 1971	17.1 2
LATITUDE	18 25
LONGITUDE	84 50
DEPTH TO BOTTOM	2280 M

Z	T	5	SIGT	TANOM	SVA	SVEI	PYNHGT	TRANS
n	28.49	36.09	23.07	480.4	480.4	1544.04	.0000	• 0
20	28.40	36.00	23.10	477.5	478.4	1544.17	.0959	1.0
40	28.10	36.10	23.21	467.3	469.1	1543.86	.1906	3.8
60	27.14	36.03	23.47	442.6	445.1	1542.01	.2820	8.6
80	26.30	36.03	25.74	417.1	420.4	1540.43	.3686	15 * 1
100	25.74	36.13	23.09	393.1	397.3	1539,56	.4503	23.2
120	24.93	36.44	24.47	347.1	352.0	1538.25	.5253	33.0
140	23.40	36.70	24.98	298.8	304.5	1536.30	.5909	44.2
160	23.16	36.76	25.24	273.8	280.2	1534.84	.6494	56.6
180	21.77	36.77	25.65	235.3	242.2	1531.62	.7016	70 • 1
500	20.19	36.69	26.02	199.9	207.4	1527.65	. 1466	84.6
550	19.47	36.63	26.16	186.2	194.2	1525.93	. 1867	99.9
240	18. 3	36.56	26.27	175.5	184.1	1524.39	.8246	116.0
<b>560</b>	18.18	36.49	26.39	165.0	174.1	1522.78	.8604	132.9
280	17.57	36.40	26.47	157.2	166.8	1521.24	.8945	150.4
300	16.99	36.29	26.52	151.9	161.9	1519.73	.9274	168.6
340	16.30	36.19	26.61	143.7	154.7	1518.19	.9907	207.0
380	15.44	36.05	26.70	135.1	147.0	1516.04	1.0510	247.8
450	14.43	35.88	26.79	126.4	138.8	1513.30	1.1082	291.0
460	13.44	35.72	26.88	118.2	131.1	1510.55	1.1623	336.4
500	11,96	35.47	26.98	108.6	121.3		1.2131	384.0
540	11.45	35.42	27.114	103.1	116.4	1504.75	1.2606	433.4
580	10.23	35.22	27.10	96.9	109.9	1500.84	1.3062	484.8
620		35.03		92.2	104.6	1496.95	1.3492	537.9
660	8.50	34.98	27.20	87.6	100.1	1495.48	1.3900	592.7
700	7.68		27.26	82.5	94.6	1492.90	1.4288	649.1
740	7.16		27.31	77.6	89.6	1491.50	1.4657	707.0
780	6.74	34.84	27.35	73,6	85.5	1490.49	1.5006	766.3
820		34.85	27.40	69.1	81.2	1490.01	1.5340	827.0
860	6.15		27.44	65.4	77.5	1489.47	1.5658	889.0
900	5.99	34.86	27.48	61.5	73.7	1489.10	1.5960	952.2
941	5.72	-	27.51	58.7	71.1	1489.08	1.6250	1016.6
980	5.50		27.55	54.6	67.1	1488.88	1.6526	1082.2
1020	5.24	34.90	27.59	50.9	6333	1488.49	1.6785	1148.8
1100	4.88		27.66	44.6	57.2	1488.37	1.7267	1285.1
1200	4.61		27.70	40.2	53.3	1488.93	1./821	1460.5
1300	4.45		27.73	37.8	51.4	1489.92	1.8346	1641.4
1400	4.36		27.74	36.A	51.2	1491.19	1.8860	1827.4
1500	4.28		27.75	35.2	50.4	1492.52	1.9364	2018.5
1600	4.25		27.76	34.9	50.9	1494.04	1.9869	2214.7
1700	4.22	34.98	100	33.0	50.7	1495.58	2.0379	2415.9
1800	4.20		27.77	33.7	51.4	1497.15	2.0889	2622.3
1900	4.16	34.99	21.18	32.5	51.0	1498.65	2.1407	2833.7

STD STATION NUMBER	28
JULY 25, 1971	23.1 7
LATITUDE	18 36
LONGITUDE	84 42
DEPTH TO BOTTOM	2577 M

```
SIGT
                         TANOM SVA
                                               PYNHGI
                                                        TRANS
                                       SVEL
   0 28,20 36.05 23.14
                         474.1 474.1 1543.38
                                                .0000
                                                           . 0
  20 28.08 36.07 23.19
                         468.9 469.7 1543.47
                                                .0944
                                                            .9
  40 27.64 36.06 23.33
                         455.9 457.5 1542.82
                                                .1871
                                                          3.8
 60 27.04 36.06 23.52
                         437.3 439.9 1541.81
                                                .2769
                                                          8.4
  80 26.25 36.03 23.75
                         415.6 418.9 1540.32
                                                .3627
                                                         14.8
                         399.9 404.0 1539.82
                                                .4450
100 25.87 36.09 23.92
                                                         22.9
120 25.31 36.30 24.25
                         36R.2 373.2 1539.02
                                                .5227
                                                         32.5
140 24.24 36.63 24.82
                         313.5 319.2 1537.07
                                                .5920
                                                         43.7
 160 22.84 36.75 25.33
                         265.7 272.0 1534.03
                                                .6511
                                                         56.1
 180 21.61 36.78 25.70
                         230.3 237.2 1531.21
                                                .7020
                                                         69.7
200 21.05 36.75 25.83
                         217.7 225.4 1530.02
                                                .7483
                                                         84.2
220 19.83 36.63 26.07
                         195.2 203.3 1526.93
                                                         99.6
                                                . /911
240 18.66 36.52 26.29
                         174.3 182.9 1523.87
                                                        115.8
                                                .8297
                         166.7 175.8 1523.08
260 18.28 36.50 26.37
                                                        132.7
                                                .8656
                         164.1 173.8 1522.60
                                                . 4006
280 18.02 36.45 26.39
                                                        150.4
 300 17.67 36.41 26.45
                         158.8 169.1 1521.87
                                                . 9349
                                                        168.7
 340 16.76 36.24 26.54
                         150.3 161.5 1519.64 1.0010
                                                        207.5
380 15,52 36.02 26.66
                         139.0 150.9 1516.26 1.0637
                                                        248.8
420 14.24 35.81 26.78
                         127.6 139.9 1512.61 1.1219
                                                        292.5
460 13.00 35.59 26.87
                         119.2 131.7 1508.94 1.1764
                                                        338.5
500 12,33 35.53 26.95
                         111.0 124.0 1507.26 1.2271
                                                        386.5
540 11.31 35.36 27.02
                         105.0 118.1 1504.19 1.2756
                                                        436.6
      9.93 35.14 27.09
580
                          97.9 110.5 1499.66 1.3212
                                                        488.5
      9.15 35.05 27.15
620
                          92.2 104.7 1497.34 1.3638
                                                        542.2
      8.81 35.01 27.18
                          90.0 102.9 1496.68 1.4053
6611
                                                        597.6
700
      8.35 34.95 27.20
                          87.6 100.6 1495.52 1.4461
                                                        654.7
740
      7.77 34.90 27.25
                          83.0
                                 95.9 1493.90 1.4853
                                                        713.3
780
      7.28 34.86 27.29
                          79.2
                                 92.0 1492.62 1.5228
                                                        773.5
820
      6.85 34.85 27.34
                          74.2
                                 87.0 1491.58 1.5585
                                                        835.1
      6.58 34.84 27.37
                          71.5
860
                                 64.4 1491.16 1.5928
                                                        898 · 1
      6.14 34.85 27.44
900
                          65.2
                                 77.9 1490.08 1.6251
                                                        962.5
940
      5.80 34.86 27.49
                          60.4
                                 73.0 1489.39 1.6552
                                                       1028.1
ORO
      5.34 34.90 27.58
                          52.0
                                 64.2 1488.24 1.6825
                                                       1094.9
                          49.1
      5.15 34.91 27.61
1020
                                 61.4 1488.14 1.7076
                                                       1162.7
                          42.8
1100
      4.78 34.94 27.67
                                 55.2 1497.97 1.7538
                                                       1301.1
                          39.7
1200
      4,56 34.95 27.71
                                 52.6 1486.72 1.4077
                                                       1479.2
      4.43 34.96 27.73
                                 51.2 1489.84 1.8597
1300
                          37.5
                                                       1662.6
      4.34 34.96 27.74
                                 51.0 1491.10 1.9105
1400
                          36.6
                                                       1851 . 1
1500
      4.29 34.97 27.75
                          35.3
                                 50.5 1492.56 1.9614
                                                       2044.7
1600
      4.25 34.97 27.76
                          34.0
                                 50.9 1494.04 2.0121
                                                       2243.4
                          33.9
                                 50.7 1495.58 2.0631
1700
      4.22 34.99 27.77
                                                       2447.2
      4.20 34.9P 27.77
                          33.7
                                 51.4 1497.15 2.1143
1800
                                                       2656.0
                                 51.3 1498.74 2.1656
1900
      4.18 34.99 27.78
                          32.7
                                                       2470.0
                          32.5
5000
      4.16 34.99 27.78
                                 51.9 1500.31 2.2172
                                                       3089.2
```

STD STATION NUMBER	029
JULY 26, 1971	17.5 /
LATITUDE	18 52
LONGITUDE	85 24
PEPTH TO ROTTOM	4419 M

```
S
                   SIGI
                         TANOM SVA
                                       SVEL
                                               TANHET
                                                        TRANS
   1) 28.38 36.06 23.119
                         479.0 479.0 1543.78
                                                .0000
                                                           • 0
                                                .0957
  20 28.33 36.07 23.11
                         476.7 477.6 1544.01
                                                          1.0
                                                .1899
                                                          3.8
  40 27.72 36.00 23.26
                         462.7 464.3 1542.94
  60 27.13 35.98 23.43
                         445.9 448.4 1541.94
                                                .2811
                                                          8.5
  80 26.44 36.06 23.72
                         419.1 422.4 1540.78
                                                . 3682
                                                         15.0
                         399.6 403.8 1539.93
 100 25.91 36.11 23.92
                                                .4508
                                                         23.2
 120 25.56 36.21 24.10
                         382.1 387.0 1539.53
                                               .5209
                                                         33.0
                                               .6026
 140 24.10 36.52 24.60
                         334.6 340.4 1538.09
                                                         44.3
                         283.7 290.1 1535.66
 160 23,49 36.75 25.14
                                                .6657
                                                         57.0
 180 22.54 36.79 25.44
                                                . 7209
                         254.6 261.7 1533.62
                                                         70.9
 200 21.14 36.76 25.81
                         219.4 227.0 1530.27
                                                . 1697
                                                         85.8
 220 20.01 36.67 26.05
                         196.8 205.0 1527.46
                                                ·8129
                                                        101.6
 241 18,96 36.59 26,26
                         176.5 185.2 1524.79
                                                ·8519
                                                        118.3
 260 18.34 36.54 26.38
                         165.2 174.3 1523.29
                                               .9879
                                                        135.7
 280 17.80 36.47 26.46
                         157.5 167.2 1521.98
                                               .9220
                                                        153.8
 300 17.37 36.41 26.52
                         151.9 162.0 1520.98
                                               .9550
                                                        172.5
 340 16.67 36.29 26.60
                         144.6 155.8 1519.42 1.U185
                                                        212.0
 380 15.63 36.07 26.69
                         135.6 147.5 1516.34 1.0793
                                                        254.0
 420 14.22 35.83 26.80
                         125.7 138.0 1512.57 1.1366
                                                        298.3
 460 13.14 35.64 26.48
                         118.3 130.9 1509.46 1.1006
                                                        344.9
 500 12.10 35.51 26.97
                                                        393.5
                         109.3 122.2 1506.66 1.2411
 540 10.97 35.34 27.06
                         100.6 113.4 1502.97 1.2881
                                                        444.1
 580 10.29 35.25 27.12
                          95.7 108.7 1501.09 1.3323
                                                        496.5
 621
      9.93 35.04 27.16
                          91.1 103.5 1496.89 1.3748
                                                        550.7
      8.59 34.97 27.21
                                99.0 1495.05 1.4154
 660
                          86.7
                                                        606.5
      1.78 34.90 27.25
 700
                          85.1
                                95.4 1493.30 1.4545
                                                        663.9
 740
      7.47 34.89 27.29
                          79.6
                                92.0 1492.74 1.4920
                                                        722.8
 780
      7.05 34.87 27.33
                          75.4
                                 87.9 1491.74 1.5280
                                                        783.2
 650
      6.62 34.85 27.37
                          71.3
                                83.6 1490.68 1.5622
                                                        845.0
      6.11 34.85 27.44
 860
                          64.9
                                76.9 1489.31 1.5944
                                                        908.1
      5.80 3/.87 27.50
                          59.6
                                71.7 1486.75 1.6242
 ann
                                                        472.5
                          54.1
 9411
      5.46 34.89 27.55
                                66.1 1488.06 1.6518
                                                       1038.1
      5.24 34.91 27.60
980
                          50.1
                                62.1 1487.85 1.6774
                                                       1104.6
      5.04 34.92 27.63
1020
                          47.1
                                59.2 1487.70 1./015
                                                       1172.2
      4.76 34.94 27.68
                          42.6
                                54.9 1487.89 1.7469
                                                       1310.2
1100
      4.58 34.95 27.71
                          39.9
                                                       1487.6
                                52.9 1488.80 1.8006
1200
      4.46 34.96 27.73
                          37.9
                                51.6 1489.96 1.8525
1300
                                                       1670.2
      4.37 34.96 27.74
                          36.0
                                51.4 1491.23 1.9040
1400
                                                       1858 - 1
15011
      4.32 34.97 27.75
                          35.7
                                 50.9 1492.68 1.9548
                                                       2051.0
      4.27 34.97 27.76
                          35.1
1600
                                 51.2 1494.12 2.0059
                                                       2249.0
                          34.1
      4.24 34.98.27.77
                                 51.0 1495.66 2.0571
                                                       2452.2
1700
1800
      4.21 34.98 27.77
                          33.8
                                 51.5 1407.19 2.1083
                                                       2660.5
1900
      4.19 34.90 27.78
                          32.3
                                51.5 1498.78 2.1599
                                                       2973.9
      4.18 34.99 27.78
                          32.7
                                52.2 1500.40 2.2117
                                                       3092.4
2000
```

STD STATIO	N NUMBER	030
JULY 26, 1	971	23.4 /
LATTTUDE		18 27
LONGITUDE		85 53
DEPTH TO B	MOTTO	4394 M
T C	CTCT	TANION

Z	T	S	SIGT	TANOM	SVA	SVEL	DYNHGT	TRANS
0	28.41	35.80	22.95	492.2	492.2	1543.69	.0000	• 0
20	28.08	35.89	23.06	481.8	482.7	1543.30	.0975	1.0
40	28.07	35.93	23.119	478.6	480.3	1543.64	.1938	3.9
60	27.94	36.03	23.24	464.2	466.8	1543.56	.2685	8.7
80	26.94	36.13	23.61	429.3	432.6	1541.98	. 3784	15.4
100	26.28	36.25	23.91	400.6	404.8	1540.91	.4622	23.8
120	25.55	36.45	24.27	365.9	370.9	1539.70	.5397	33.8
140	24.45	36.56	24.71	324.6	330.3	1537.52	.6099	45.3
160	23.11	36.71	25.22	276.0	282.4	1534,67	.6711	58 • 1
180	22.17	36.73	25.50	248.9	255.9	1532.62	.7249	72.1
500	20,93	36.60	25.84	216.3	223.9	1529.38	.7729	87.1
550	19.91	36.61	26.03	198.6	206.8	1527.13	.8160	102.9
240	18.88	36.49	26.21	181.8	190.4	1524.47	.8557	119.7
2611	17.87	36.36	26.36	167.1	176.1	1521.76	.8924	137.1
280	16.95	36.23	26.49	155.3	164.6	1519.23	.4264	155.3
300	15.92	36.08	26.61	143.3	152.9	1516.27	.9582	174.2
3411	14.22	35.81	26.78	127.2	137.2	1511.26	1.0164	213.7
380	12.95	35.50	26.40	116.4	126.6	1507.15	1.0694	255.4
420	11.13	35.32	27.02	104.8	114.9	1501,58	1.1177	299.2
460	9.95	35.13	27.10	97.4	107.3	1497.43	1.1620	344.8
500	8.95	35.02	27.16	91.4	101.3	1494.63	1.2036	392.1
540	8.24		27.22	86.0	96.0	1492.53	1.2431	441.0
580	7.58		27.27	81.1	91.0	1490.58	1.2605	491.5
620	7.13	34.87	27.32	76.5	86.5	1489.46	1.3160	543.4
660	6.78	34.86	27.36	72.6	82.8	1488.73	1.3498	596 • 7
700	6.24	34.86	27.43	65.7	75.8	1487.25	1.3815	651.4
740	5.91	34.87	27.48	60.0	71.1	1486.60	1.4110	707.2
780	5.64	34.88	27.52	57.0	67.2	1486.18	1.4386	764.2
820	5.42	311.89	27.56	53.7	64.1	1485.95	1.4648	822.3
860	5.23	34.91	27.60	50.0	60.6	1485.86	1.4897	881 • 4
900	4.98	34.93	27.64	45.7	56.3	1485.52	1.5130	941.5
OHO	4.86	34.93	27.66	44.4	55.2	1485.68	1.5353	1002.4
980	4.78	34.911	27.67	42.8	53.9	1486.02	1.5570	1064.3
1020	4.68	34.95	27.69	40.9	52.3	1486.27	1.5783	1127.0
1100	4.53	34.97	27.73	37.A	49.7	1486.99	1.6194	1254.9
1200	4.41	34.96	27.73	37.3	49.9	1488.12	1.6695	1419.4
1300	4.73	34.97	27,75	35.8	49.3	1489.44	1.7188	1763.1
1400	4.27	34.97	27.76	35.1		1490.83	1.7680	
1500	4.53	34.98	27.77	34.0	49.0	1492.32	1.8668	2126.6
1600	4.0		27.77 27.78	33.7 32.7	49.5	1495.43	1.9163	2315.8
1700	4.18	34.99	27.78	32.3	49.8	1496.92	1.9660	2509.9
1800	4.13	34.90	27.79	32.2	50.6	1498.53	2.0162	2709.0
2000	4.11	35.00		31.3	50.5	1500.12	2.0667	2913.1
61,111	4.11	3.7.00	61.66	51.5	20.3	1000.12		

```
STD STATION NUMBER 031

JULY 27, 1971 05.9 /

LATITUDE 18 07

LONGITUD 86 22

DEPTH TO BOTTOM 4122 M
```

Z.	T	S	SIGT		SVA	SVEL	DYNHGT	TRANS
U		36.03	23.19	469.2	469.2	1542.93	•0000	• 0
50	27.99	36.02	23.19	469.6	470.5	1543.23	.0940	• 9
40	27,97	36.03	23.20	468.3	470.0	1543.52	.1880	3.8
60	27.48	36.06	23.38	450.9	453.4	1542.79	.2804	8.4
80	26.45	36.17	23.79	411.5	414.8	1540.90	.3672	14.9
100	25.42	36.3H	24.28	365.7	369.8	1539.03	.4457	23.0
150	24.29	36.60	24.79	317.1	322.0	1536.85	.5148	32.7
147	22.76	36.69	25.30	267.A	273.3	1533.45	.5744	43.5
160	21.37	36.67	25.68	231.9	238.0	1530.16	.6255	55.5
180	19.70	36.55	26.04	197.7	204.3	1525.86	.6697	68.5
500	18.20	35.41		171.3	178.3	1521.80	.7080	82.3
220	17.53	36.29	26.44	159.7	167.1	1519.46	. 1425	96.8
240	16.57	36.14	26.56	148.9	156.7	1516.75	. 1749	112.0
260	15.41	36.00	26.67	138.1	146.2	1513.96	.8052	127.8
280	14.52	35.84	26.74	131.2	139.5	1511,30	.8338	144.1
300	15.43	35.66	26.93	122.4	130.8	1507.88	.8608	161.1
340	11.57	35.33	26.98	108.3	116.6	1501.15	.9101	196.5
380	9.76	35.12	27.11	96.6	104.8	1495.80	.9540	233.8
420	9.21	35.06	27.15	92.4	101.0	1494.36	.9951	272.8
460	8.54	34.90	27.20	87.4	96.2	1492.42	1.0345	313.4
500	7.90	34.92	27.25	83.3	92.3	1490.55	1.0722	355.5
540	7.56	34.88	27.29	7A. 9	87.8	1489.08	1.1081	399.1
580	6.92	34.85	27.33	75.2	84.3	1487.97	1.1425	444.2
620	6.53	34.85	27.39	70.1	79.4	1487.09	1.1752	490.5
660	6.11	34.86	27.45	64.1	73.5	1486.09	1.2059	538.2
700	5.75	34.87	27.50	59.0	68.4	1485.31	1.2343	587.0
740	5.40	34.89		53.4	62.8	1484.58	1.2605	636.9
780	5.25	34.90	27.59	51.0	60.6	1484.63	1.2852	687.8
850	5.04	34.92	27.63	47.1	56.9	1484.45	1.3087	739.7
860	4.88	34.93	27.66	44.6	54.6	1484.46	1.3310	792.5
900	4.78	34.93	27.67	43.5	53.7	1484.70	1.3526	846.1
ott ()	4.68	34.94	27.69	41.7	52.2	1484.96	1.3737	900.7
980	4.61	34.95	27.70	40.2	51.0	1485.34	1.3944	956 • 0
10Su	4.53	34.95	27.71	39.3	50.4	1485.66	1.4146	1012.2
1100	4.42	34.97	27.74	36.7	48.3	1486.54	1.4544	1127.0
1200	4.52	34.96	27.74	36.4	48.7	1487.75	1.5031	1274.8
1300	4.27	34.97	27.76	35.1	48.3	1489.19	1.5515	1427.6
1400	4.23	34.97	27.76	34.7	48.8	1490.67	1.5999	1585.1
1500	4.20	34.97	27.76	34.4	49.3	1492.19	1.6489	1747.6
1600	4.15	34.98	27.78	33.2	48.9	1493.64	1.6980	1914.9
1700	4.15	34.98	27.78	33.2	49.8	1495.29	1.7472	2087.2
1800	4.15	34.98	27.78	33.2	50.7	1496.95	1./974	2264.4
1900	4.14	34.99	27.78	32.3	50.7	1498.58	1.8480	2446.7
0000	4.12	31.99	27.79	32.1	51.4	1500.15	1.8989	2634.0

STD STATION NUMBER	n32
JULY 27, 1971	11.7 /
LATITUDE	18 10
LONGITUDE	86 50
DEPTH TO BOTTOM	3990 M

	Z	T	5	SIGT	LANOW	SVA	SVEL	~YNHGT	TRANS
	n	27.90	36.07	23.25	463.2	463.2	1542.75	•0000	• 0
	50	27.90	36.06	23.25	464.7	464.8	1543.07	.0928	• 9
	40	27.81	36.05	23.27	461.9	463.6	1543.19	.1856	3.7
	60	26.94	36.11	23.59	430.7	433.2	1541.63	.2753	8.3
	an	26.12	35.25	23.06	395.A	399.2	1540.22	. 3586	14.7
	1011	25.30	36.4A	24.39	355.0	359.1	1538.83	.4344	22.6
	120	23.27	36.63	24.90	305.8	310.7	1536,09	.5014	31.9
	140	21.91	36.66	25.52	246.9	252.4	1531.24	.5577	42.5
	160	19.08	34.57	25.98	205.3	209.2	1526.32	.6038	54.2
	180	18.31	36.40	26.28	174.6	181.0	1521.79	.6428	66.6
	500	17.13	36.26	26.47	157.2	164.0	1518,51	.6773	79.8
	550	16.24	36.14	26.59	146.0	153.1	1516.03	.7090	93.7
	240	15.36	35.99	26.67	137.8	145.3	1513.48	.7389	108.2
	26n	14.71	35.88	26.73	132.2	140.0	1511.63	.7674	123.2
	5811	13.86	35.73	26.40	125.A	133.9	1509.04	.7948	138.9
	300	13.20	35.63	26.86	120.1	128.5	1507.08	.8210	155.0
	340	11.02	35.43	26.96	110.8	119.5	1503.17	· 4705	188.8
	380	10.73	35.26	27.05	102.4	111.2	1499.46	.9166	224.6
	420	9.85	35.13	27.10	97.4	106.5	1496.78	•9600	262.1
	460	9.04	35.03	27.15	45°U	101.2	1494.33	1.0013	301.4
	500	8.44	34.97	27.20	87.4	96.9	1492.66	1.0410	342.2
	540	7.02	34.92	27.24	83.5	93.3	1491.28	1.0790	384.6
	5811	7.37	34.87	27.28	79.7	89.4	1489.75	1.1155	428.5
	620	6.97	34.85	27.33	75.A	85.7	1488.81	1.1506	473.8
	660	6.44	34.83	27.38	70.5	80.2	1487.36	1.1839	520.5
	700	6.19	34.84	27.44	55.4	75.2	1486.63	1.2151	568.5
	7411	5.79	34.87	27.50	59.5	69.5	1486.12	1.2441	617.7
	780	5.41	34.88	27.55	54.3	64.2	1485.25	1.2708	668.0
	850	5.20	34.90	27.59	50.4	60.4	1485.08	1.2057	719.4
	860	4.97	34.91	27.63	47.1	57.2	1484.80	1.3192	771.7
	900	4.81	34.93	27.66	43.R	54.1	1484.83	1.3413	824.9
	04(1	4.67	34.94	27.69	41.6	52.0	1484.92	1.3626	878.9
	98Ú	4.57	34.95	27.71	39.0	50.4	1485,17	1.3832	933.9
	020	4.51	34.95	27.71	39.1	50.1	1485.58	1.4032	989.6
	100	4.43	34.96	27.73	37.5	49.2	1486.57	1.4430	1103.4
-	500	4.34	34.96	27.74	36.6	49.0	1487.83	1.4919	1250.2
	300	4.30	34.97	27.75	35.4	48.7	1489.32	1.5409	1401.8
	400	4.27	34.97	27.76	35.1	49.3	1490.83	1.5899	1558.4
	500	4.24	34.97	27.76	34.8	49.9	1492.35	1.6396	1719.8
	600	4.22	34.97	27.76	34.6	50.5	1493.92	1.6898	1886.3
	700	4.21	34.97	27.76	34.5	51.3	1495.53	1.7406	2057.8
	800	4.19	34.98	27.77	33.6	51.3	1497.11	1.7914	2234.4
	000	4.15	34.98	27.78	33.2	51.6	1498.60	1.8429	2416.1
5	000	4.14	34.94	27.78	32.3	51.6	1500.24	1.8942	2603.0

STD STATION NUMBER	033
JULY 27, 1971	16.5 /
LATITUDE	18 15
LONGITUDE	87 15
DEPTH TO BOTTOM	990 M

2	T	5	SIGT	TANIOM	SVA	SVEL	TNHGT	TRANS
- 0	28.12	35.99	23.12	475.9	475.9	1543.16	.0000	• 0
50	28.06	36.02	23.16	471.8	472.7	1543.38	. 11949	• 9
40	28.113	36.02	23.17	470.0	472.6	1543.64	.1894	3.8
60	27.49	36.10	23.41	448.3	450.9	1542.85	.2817	8.5
90	26.30	36.27	23.92	399.8	403.1	1540.65	. 3671	15.0
100	25.20	36.40	24.43	351.3	355.5	1538.61	.4430	23.1
120	23.22	36.63	25.12	284.8	289.6	1534.23	.5075	32.6
140	20.93	36.65	25.79	221.9	227.2	1528.65	.5592	43.3
160	19.31	34.55	26.13	189.5	195.3	1524.43	.6014	54.9
180	17.86	36.36	26.37	106.0	173.1	1520.44	.6383	67.3
500	16.71	36.21	26.53	151.4	158.0	1517.21	.6714	80.4
550	15.46	36.00	26.61	143.5	150.5	1515.12	.7022	94.1
240	15.08	35.94	26.70	135.5	142.9	1512.54	.7315	108.4
560	14.02	35.74	26.77	128.3	135.8	1509.25	. 7594	123.3
580	13.13	35.65	26.97	118.8	126.5	1506.53	. 1857	138.8
300	12.13	35.56	26.90	116.3	124.4	1505.43	.8107	154.8
340	12.10	35.47	26.95	111.1	119.9	1503.83	.8595	188.2
380	10.13	35.18	27.09	98.2	106.7	1497.21	.9047	223.5
420	9.66	35.12	27.12	95.0	104.0	1496.08	.9468	260.5
460	9.21	35.07	27.16	91.7	101.1	1495.01	.9878	299.2
500	8.70	35.00	27.19	89.1	98.8	1493.68	1.0277	339.5
540	8.21	34.95	27.22	85.5	95.5	1492.41	1.0667	381.4
590	7.57	34.89	27.27	80.9	90.9	1490.54	1.1040	424.8
620	6.04	34.86	27.34	74.7	84.5	1488.71	1.1390	469.7
660	6.66	34.85	27.37	71.R	81.8	1488.25	1.1722	515.9
700	6.48	34.84	27.40	69.0	79.2	1487.78	1.2043	563.4
740	6.98	34.86	27.45	63.8	74.2	1487.26	1.2351	612.2
7911	5.00	34.87	27.50	59.6	70.1	1486.81	1.2637	662.2
8211	5.32	34.40	27.58	51.9	62.0	1485.56	1.2903	713.3
860	5.15	34.91	27.61	49.1	59.5	1485.54	1.3146	765.4
900	4.31	34.93	27.66	43.8	54.1	1484.83	1.3378	818.5

STD STATION NUMBER	0.34
JULY 27, 1971	20.3 /
LATITUDE	18 19
LONGITUDE	87 34
DEPTH TO BOTTOM	962 M

Z	T	5	SIGT	TANOM	SVA	SVEL	DYNHGT	TRANS
0	28,25	35.98	23.07	480.7	480.7	1543.43	.0000	• 0
Sil	28.08	36.03	23.16	471.7	472.6	1543.43	.0953	1.0
40	27.95	36.04	23.21	467.0	468.7	1543.48	.1895	3.8
60	27.15	36.11	23.53	436.5	439.0	1542.06	.2802	8.5
80	25.31	36.44	24.35	358.2	361.5	1538.50	.3603	14.9
100	23.42	36.6ª	25,10	286.8	290.8	1534.45	.4255	22.8
120	21.52	36.68	25.65	235.1	239.8	1529.92	.4786	31.8
140	19.33	36.55	26.14	188.5	193.6	1524.18	.5219	41.8
160	18.11	36.43	26.36	167.7	173.5	1520.92	.5586	52.6
180	17.28	36.29	26.45	158.5	164.6	1518.67	.5924	64.1
200	16.56	36.18	26.54	150.2	156.7	1516.72	.6245	76.3
220	15.82	36.08	26.64	141.1	148.1	1514.68	.6550	89.1
240	15.06	35.94	26.70	135.1	142.4	1512.48	.6841	102.5
260	13.97	35.76	26.80	125.8	133.4	1509.12	.7116	116.4
280	12.94	35.61	26.90	116.6	124.3	1505.87	. /374	130.9
300	12.43	35.54	26.94	112.1	120.0	1504.40	.7618	145.9
340	11.75	35.41	26.97	109.2	117.8	1502.56	.8097	177.3
380	10.02	35.29	27.113	103.4	112.4	1500.17	.8555	210.7
420	10.13	35.18	27.09	98.2	107.6	1497.86	.8994	245.8
460	9.32	35.07	27.14	93.4	102.9	1495.42	.9415	282.6
500	8.58	34.99	27.20	88.0	97.6	1493.21	.9815	321.0
540	8.38	34.97	27.21	86.5	96.7	1493.08	1.0204	361.1
5811	8.10	34.94	27.23	84.7	95.3	1492.63	1.0589	402.7
620	7.68	34.90	27.26	81.7	92.5	1491.62	1.0965	445.8
660	7.31	34.88	27.30	78.1	89.1	1490.82	1.1326	490.4
700	7.00	34.87	27.34	74.7	85.9	1490.25	1.1675	536.4
740	6.55	34.87	27.40	68.9	80.0	1489.14	1.2007	583.7
780	5.49	34.87	27.47	61.9	72.7	1487.57	1.2317	632.4
820	5.59	34.88	27,53	56.4	67.1	1486.63	1.2594	682.2
860	5,15	34.91	27,61	49.1	59.5	1485.54	1.2851	733.1

STD STATION NUMBER	35
JULY 28, 1971	00.5 /
LATITUDE	18 50
LONGITUDE	87 25
DEPTH TO BOTTOM	658 M

2	T	S	SIGT	TANOM	SVA	SVEL	TYNHGT	TRANS
n	28.24	36.05	23.13	475.3	475.3	1543.47	.0000	• 0
20	28.13	36.05	23.16	471.9	472.7	1543.56	.0948	•9
40	27.16	36.07	23.30	458.9	460.6	1543.09	.1881	3.8
60	26.03	36.24	24.01	391.0	393.5	1539.71	.2735	8.4
80	25.01	36.46	24.46	348.0	351.2	1537.81	.3480	14.6
100	23.58	35.67	25.05	292.0	296.0	1534.84	.4127	22.2
120	21.93	36.72	25.56	243.1	247.8	1531.02	.4671	31.0
140	20.68	36.67	25.97	213.9	219.2	1528.00	.5138	40.8
160	19.36	36.57	26.14	187.8	193.6	1524.61	.5551	51.5
180	18.45	36.48	26.31	172.2	17R.5	1522.27	.5923	63.0
200	17.41	36.53	26.45	158.6	165.4	1519.42	.6267	75.2
220	16,55	36.20	26.56	148.5	155.7	1517.04	.6588	88.0
240	15.53	36.03	26.66	138.5	146.0	1514.05	.6890	101.5
26n	14.26	35.81	26.77	128.0	135.7	1510.11	.7172	115.6
280	13.26	35.65	26.86	119.8	127.6	1506.98	.7435	130.2
300	12.75	35.58	26.91	115.2	123.3	1505.52	.7686	145.3
340	11.72	35.41	26.98	108.7	117.2	1502.46	.8169	177.0
380	10.62	35.26	27.07	100.5	109.3	1499.07	.8623	210.6
420	9.79	35.13	27.11	96.4	105.5	1496.57	.9053	246.0
460	9.56	35.11	27.13	94.2	103.9	1496.35	.9471	283.0
500	9.21	35.07	27.16	91.7	101.9	1495.66	.9881	321.7
540	8.47	34.98	27.21	87.1	97.4	1493.43	1.0281	362.1
580		34.92		82.3	92.6	1491.58	1.0661	403.9
620	7.18	34.88	27.32	76.4	86.5	1489.67	1.1020	447.3

JULY 28, 1971			05.2	05.2 /					
LATTTUDE				19 1	7				
LONGITUDE				87 09	4				
		PEPTH 1		TOM	1545	и			
		T		SIGI	TANCM	SVA	SVEL	THHET	TRANS
	n	28.16	36.03	23.14	474.3	474.3	1543.28	.0000	• 0
	20	28.16	36.04	23.15	473.5	474.4	1543.61	.0949	.9
	40	27,91	36.05	23.23	465.0	466.7	1543.40	.1890	3.8
	60	26,98	36.14	23.60	429.8	432.3	1541.75	.2789	8.5
	80	25.59	36.40	24.24	369.3	372.6	1539.12	. 3594	14.8
	100	23.41	36.66	25.119	287.9	291.9	1534.41	.4258	22.7
	120	21.05	36.67	25.77	223.5	228.1	1528.67	.4778	31.7
	140	19.18	36.53	26.16	186.3	191.3	1523.74	.5198	41.7
	160	18.14	36.45	26.36	167.0	172.6	1521.02	.5561	52.5
	180	17,21	36.32	26.49	154.7	1.60.8	1518.49	.5895	63.9
	200	16.58	36.21	26.56	148.4	155.0	1516.81	.6211	76.0
	550	15.78	36.12	26.63	141.7	148.8	1515.21	.6514	88.8
	24(1	15.40	35.01	26.68	137.2	144.7	1513.62	.6808	102.1
	260	14.68	35.89	26.75	130.8	138.6	1511.54	.7091	116.0
	280	13.92	35.76	26.81	124.8	132.9	1509.27	.7363	130.4
	300	13.30	35.66	26.86	119.9	128.3	1507.45	.7624	145.4
	340	11.68	35.41	26.99	107.0	116.5	1502.32	.8115	176.9
	380	11,05	35.31	27.03	104.2	113.3	1500.65	.8576	210.3
	420	10.64	35.26	27.06	100.8	110.6	1499.78	.9023	245.5
	460	10.60	35.25	27.06	190.0	111.5	1500.27	. 446P	282.5
	500	10.03	35.17	27.10	97.3	108.3	1498.77	.9909	321.2
	540	9.25	35.07	27.15	92.3	103.3	1496.45	1.0334	361.7
	580	8.75	35.01	27.19	89.1	100.4	1495.17	1.0740	403.9
	620	8.38	34.97	27.21	86.5	98.1	1494.57	1.1138	447.6
	660	7.89		27.25		94.9		1.1524	
	700	7.21	34.87	27.31	77.5	89.0	1491.07		
	740		34.85		71.8	83.0	1489.54	1.2235	538 • 1
	700	1 10	7. 01	01 110		77 0		1 07	

66.5

60.7

55.0

53.3

48.9

47.0

44.5

41.5

36.4

34.0

77.8 1488.79 1.2557

71.9 1487.82 1.2857

67.1 1487.37 1.5134

64.7 1487.13 1.3398

60.2 1486.76 1.3645

58.6 1487.02 1.3883

56.2 1487.03 1.4112

53.6 1487.49 1.4551

51.8 1488.48 1.5074

49.9 1489.69 1.5583

637.7

688.5

740.5

793.5

R47.6

902.7

958.7

1073.3

1221.5

1374 . 8

STD STATION NUMBER 36

780

1158

660

0011

0411

990

1020

1100

1200

1300

6.30 34.86 21.42

5.09 34.87 27.49

5.61 34.89 27.54

5.39 34.89 27.56

5.13 34.91 27.61

5.03 34.92 27.63

4.87 34.93 27.66

4.66 34.94 27.69

4.50 34.95 27.71

4.39 34.97 27.74

```
LATTTUDE
                         19 21
                         86 44
    LONGITUDE
                         4023 M
    DEPTH TO BOTTOM
                         TANOM SVA
                                              DYNHGT
                                                        TRANS
                   SIGT
                                       SVEI
  0 28.17 35.89 23.03
                         484.6 484.6 1543.17
                                               .0000
                                                           .0
  20 28.18 35.89 23.03
                         484.9 465.8 1543.52
                                               .0970
                                                          1.0
                                               .1939
  40 28.07 35.89 23.06
                         481.5 483.2 1543.61
                                                          3.9
  60 27.15 36.09 23.51
                         438.6 441.1 1542.09
                                               .2864
                                                          8.7
  80 26.49 36.32 23.90
                         401.9 405.3 1541.13
                                               . 3710
                                                         15.3
 100 25.10 36.54 24.49
                         344.8 348.9 1538.41
                                               .4464
                                                         23.4
                                               .5103
                                                         33.0
 120 23.50 34.73 25.12
                         285.4 290.2 1535.02
 140 22.07 36.77 25.56
                         243.3 248.8 1531.75
                                               .5642
                                                         43.7
                                               .6104
 160 20.41 36.71 25.95
                         206.6 212.7 1527.89
                                                         55.5
                         187.9 194.5 1525.30
 180 19.48 36.61 26.14
                                               .6511
                                                         68.1
 200 18.35 36.47 26.33
                         170.5 177.6 1522.29
                                               .6883
                                                         31.5
 220 17.58 36.38 26.45
                         158.9 166.4 1520.29
                                                         95.6
                                               . 1227
 240 17.03 36.29 26.51
                         152.8 160.8 1518.89
                                               .7554
                                                        110.4
                         147.2 155.7 1517.39
 260 16.46 36.19 26.57
                                               .7871
                                                        125.8
 280 15.40 36.07 26.63
                         141.4 150.3 1515.57
                                               .8177
                                                        141.9
                                               .8470
 300 15.04 35.95 26.71
                         133.9 143.1 1513.39
                                                        158.5
 340 14.02 35.77 26.80
                                               .9028
                                                        193.5
                         126.1 135.9 1510.57
                                               .9553
 38n 12.90 35.59 26.89
                         117.3 127.6 1507.32
                                                        230.7
 420 11.98 35.45 26.96
                                                        209.9
                         110.4 121.1 1504.69 1.0050
 460 11.28 35.34 27.01
                         106.0 117.1 1502.77 1.0525
                                                        311.1
 500 10.72 35.27 27.06
                         101.5 113.1 1501.36 1.0988
                                                        354.1
 540 10.15 35.18 27.09
                                                        398.9
                          98.6 110.5 1499.86 1.1437
      9.54 35.00 27.12
 580
                          95.4 107.5 1498.18 1.1873
                                                        445.6
      8.74 35.00 27.16
                          91.2 103.3 1496.13 1.2296
                                                        493.9
 6211
                                97.3 1494.07 1.2696
 660
      8.14 34.94 27.23
                                                        543.9
                          85.3
      7.70 34.90 27.26
                                94.1 1492.99 1.3080
 700
                          82.0
                                                        595.4
                                89.7 1491.34 1.3449
 7411
      7.12 34.85 27.30
                          77.0
                                                        648.5
                                83.9 1490.06 1.3796
 78n
      6.63 34.84 27.36
                          72.1
                                                        703.0
      0.19 34.85 27.43
 6511
                          65.9
                                77.5 1488.98 1.4119
                                                        758.8
                          59.7
 860
      5.81 34.87 27.50
                                71.3 1488.15 1.4417
                                                        P15.9
 000
      5.55 34.88 27.54
                          55.9
                                67.5 1487.76 1.4694
                                                        874.1
 940
      5.36 34.89 27.57
                          53.0
                                64.7 1487.66 1.4957
                                                        933.4
 ORD
      5.04 34.92 27.63
                          47.1
                                58.7 1487.05 1.5205
                                                        93.8
1020
      4.08 34.95 27.66
                          44.6
                                56.4 1487.07 1.5436
                                                       1055.1
                          40.2
                                52.2 1487.29 1.5868
1100
      4.61 34.95 27.70
                                                       1180.3
1200
      4.47 34.96 27.73
                          38.0
                                50.7 1488.36 1.6382
                                                       1341.6
      4.37 34.96 27.74
1300
                          36.9
                                50.4 1489.59 1.6888
                                                       1507.9
      4.71 34.98 27.76
1400
                          34.8
                                49.1 1491.01 1.7388
                                                       1679.3
      4.28 34.97 27.75
1500
                          35.2
                                50.4 1492.52 1.7890
                                                       1855.7
1600
      4.24 34.97 27.76
                          34.8
                                50.8 1494.00 1.8393
                                                       2037.1
      4.22 34.98 27.77
                          33.9
                                50.7 1495.58 1.8900
1700
                                                       2223.6
                                51.1 1497.07 1.9410
      4.18 34.98 27.77
                          33.5
1800
                                                       2415.1
1900
      4.11 34.99 27.79
                          32.n
                                50.3 1498.45 1.9916
                                                      2611.7
      4.10 34.99 27.79
                          31.9
2000
                                51.1 1500.07 2.0421
                                                       2813.4
```

10.7 /

STD STATION NUMBER

JULY 28, 1971

```
JULY 28, 1971
                         15.7 /
                         19 15
    LATITUDE
                         86 17
    LONGITUDE
    DEPTH TO HOTTOM
                         4406 M
                  SIGT
                         TANOM SVA
                                       SVEL
                                              TYNHGT
                                                        TRANS
  0 28.07 35.72 22.93
                         493.7 493.7 1542.80
                                               .0000
                                                           .0
 20 28.46 35.73 22.94
                         492.7 493.5 1543.11
                                               .11987
                                                          1.0
                                               .1959
 40 27.30 35.84 23.11
                         476.6 478.3 1542.97
                                                          3.9
 60 27.74 36.06 23.30
                         459.0 461.5 1543.36
                                                          8.8
                                               .2899
 80 27.22 36.13 23.52
                         457.8 441.2 1542.60
                                               .3802
                                                         15.5
 100 26.15 34.23 23.93
                         398.2 402.3 1540.59
                                               .4645
                                                         23.9
120 25.42 36.44 24.32
                         361.4 366.3 1539.41
                                               .5414
                                                         34.0
 140 24.73 35.62 24.82
                         314.0 319.6 1537.04
                                                         45.5
                                               .6100
                         270.7 277.1 1534.19
160 22.92 36.71 25.27
                                               . 6697
                                                         58.3
180 21.30 36.68 25.71
                         229.3 236.2 1530.30
                                               .7210
                                                         72.2
                         203.5 211.0 1527.61
200 20.19 36.64 25.98
                                               . 1657
                                                         87.1
220 19.35 36.57 26.15
                         187.6 195.6 1525.54
                                                        102.8
                                               .8064
                         172.2 180.6 1522.75
240 18.30 36.43 26.31
                                               .8440
                                                        119.3
260 17.60 36.35 26.42
                         161.5 170.4 1520.96
                                               .8791
                                                        136.5
280 16.93 36.22 26.51
                         153.3 162.6 1518.86
                                               .9124
                                                        154.5
                                               . 9443
300 16.28 36.14 26.58
                         146.9 156.6 1517.44
                                                        173.0
340 15.04 35.92 26.69
                         136.1 146.5 1514.00 1.0049
                                                        212.0
                         123.9 134.7 1510.07 1.0609
380 13.69 35.71 26.82
                                                        253.3
420 12.47 35.52 26.42
                         114.3 125.4 1506.43 1.1127
                                                        296.8
460 11.34 35.34 27.00
                         107.0 118.2 1502.98 1.1615
                                                        342.3
    10.67 35.24 27.04
                         102.8 114.4 1501.15 .. 2080
                                                        389.7
      9.76 35.11 27.10
                          97.4 108.9 1498.36 1.2526
                                                        438.9
540
                          93.1 104.9 1496.92 1.2952
                                                        489.9
 580
      9.21 35.05 27.14
6211
      8.58 34.98 27.19
                          88.8 100.6 1495.13 1.3362
                                                        542.5
660
      7.96 34.95 27.25
                          83.4
                                95.2 1493.38 1.3752
                                                        596.7
      7.31 34.88 27.30
                                89.7 1491.46 1.4123
 700
                          78.1
                                                        652.5
 740
      6.98 34.86 27.33
                          75.2
                                86.9 1490.81 1.4476
                                                        709.7
 791
      6.55 34.85 27.38
                          70.4
                                82.0 1489.76 1.4814
                                                        768.3
      6.07 34.86 27.45
820
                          63.6
                                75.1 1488.52 1.5129
                                                        A28.2
      5.75 34.87 27.50
                          59.0
                                70.5 1487.90 1.5421
                                                        R89.3
860
 ann
      5. 6 34.89 27.55
                          54.1
                                65.6 1487.41 1.5693
                                                        951.5
      5.23 34.90 27.59
940
                          50.8
                                62.3 1487.15 1.5947
                                                       1014.8
                                58.3 1486.93 1.6187
OAO
      5.01 34.92 27.63
                          46.8
                                                       1079.1
      4.86 34.93 27.66
                          44.4
                                56.1 1486.98 1.6415
1020
                                                       1144.3
      4.62 34.95 27.70
                          40.3
                                52.4 1487.33 1.6848
1100
                                                       1277.3
1200
      4.47 34.96 27.73
                          38.0
                                50.7 1488.36 1.7364
                                                       1448.4
      4.40 34.96 27.73
1300
                          37.2
                                50.8 1489.71 1.7869
                                                       1624.6
                          35.8
                                50.1 1491.08 1.8377
1400
      4.33 34.97 27.75
                                                       1805.8
                                                       1992.1
1500
      4.28 34.97 27.75
                          35.2
                                50.4 1492.52 1.8g80
      4.24 34.97 27.76
                          34.P
                                50.8 1494.00 1.9386
1600
                                                       2183.4
      4.11 34.98 27.77
                                50.6 1495.54 1.9890
                          33. R
                                                       2379.8
1700
                                51.3 1497.11 2.0400
                                                       2581.2
1800
      4.19 34.98 27.77
                          33.6
                                51.2 1498.70 2.0012
1900
      4.17 34.99 27.78
                          32.6
                                                       2787.8
      4.15 34.99 27.78
                                51.8 1500.27 2.1427
                                                       2999.5
2000
                          32.4
```

STD STATION NUMBER

STD STATION NUMBER	59
JULY 29, 1971	NU.5 Z
LATITUDE	19 31
LONGITUDE	86 1"
DEPTH TO BOTTOM	4431 M

Z	т	S	SIGT	TANOM	SVA	SVEL	DYNHGT	TRANS
0	28.70	36.08	23.00	487.8	487.8	1544.48	.0000	• 0
20	28.40		23.07	480.4	481.3	1544.14	.0969	1.0
40	27.78		23.25	463.8	465.5	1543.08	.1916	3.9
60	27.47		23.43	446.3	448.8	1542.82	.2830	8.6
80	26.68	36.16	23.71	419.2	422.5	1541.42	. 5701	15.1
100	26.24	36.37	24.01	390.8	395.0	1540.92	.4519	23.4
120	25.19	36.54	24.41	353.3	358.3	1539.42	.5272	33.1
140	23.95	36.68	24.95	301.7	307.3	1536.41	.5938	44.4
160	22.81	36.77	25.35	263.4	269.7	1533.97	.6515	56.8
180	21.92	36.75	25.62	238.0	245.0	1531.73	.7030	70.3
500	20.55	36.64	25.94	207.1	214.6	1527.99	.7489	84.9
220	19,58	36.60	26.11	191.1	199.1	1526.21	.7903	100.3
240	18.99	36.52	26.20	182.3	191.0	1524.81	.8293	116.5
260	18.34	35.45	26.31	171.7	180.8	1523.21	.8665	133.4
280	17.74	35.36	26.39	164.1	173.7	1521.70	.9019	151.1
300	16.91	36.24	26.50	153.7	163.7	1519.44	.9357	169.5
340	15.50	36.01	26.66	139.3	149.9	1515,54	.9981	208•2
380	14.42	35.83	26.76	129.A	141.1	1512.57	1.0560	249.3
420	12.98	35.58	26.88	117.7	129.0	1507.88	1.1097	292.6
460	12.50	35.55	26.94	112.7	124.8	1507.21	1.1605	338.0
500	11.22	35.33	27.01	105.7	117.7	1503.19	1.2094	385.4
540	10.63		27.06	101.4	113.8	1501.66	1.2558	434.7
580	9.81	35.14	27.11	96.0	108.4	1499.23	1.3002	485 • 8
620	9.01	35.04	27.17	90.8	103.2	1496.81	1.5427	538 • 7
700	8.47	34.98 34.93	27.21	87.1	99.6	1495.37	1.3833	593.2
740	7.80 7.08		27.33	81.2 75.8	93.5	1493.41	1.4222	649.3
780	6.76	34.85	27.35	73.1	87.7 85.1	1491.21	1.4587	707•0 766•0
820	6.40	34.85	27.40	68.5	80.5	1489.81		826.4
860	5.96	34.86	27.47	62.3	74.1	1488.73	1.5267	888.1
900	5.64	34.88	27.52	57.0	68.8	1488.13	1.5861	951.0
940	5.37	34.89	27.57	53.1	64.9	1487.70	1.6129	1015.0
980	5.09	34.91	27.61	48.4	60.1	1487.24	1.6379	1080.0
1020	4.04	34.92	27.64	46.0	57.9	1487.30	1.6614	1146.0
1100	4.70	34.94	27.68	41.9	54.1	1487.65	1.7060	1280.7
1200	4.52	34.95	27.71	39.2	52.1	1488.55	1.7590	1453.9
1300	4.42	34.96	27.73	37.4	51.0	1489.79	1.8103	1632.4
1400	4.35	34.96	27.74	36.7	51.1	1491.15	1.8614	1816.0
1500	4.29	34.97	27.75	35.3	50.5	1492.56	1.9124	2004.7
1600	4.25	34.97	27.76	34.9	50.9	1494.04	1.9631	2198.5
1700	4.22	34.97	27.76	34.6	51.5	1495.57	2.0144	2397.3
1800	4.20	34.98	27.77	33.7	51.4	1497.15	2.0655	2601.3
1900	4.18	34.98	27.77	33.5	52.0	1498.72	2.1170	2810.5
5000	4.17	34.99	27.78	32.6	52.1	1500.36	2.1691	3024.8

STD STATION NUMBER	40
JULY 29, 1971	15.7 7
LATITUDE	19 44
LONGITUDE	86 20
DEPTH TO ROTTOM	4418 M

7	T	S	SIGT	TANOM	SVA	SVEL.	DYNHGT	TRANS
0	28. 30	35.82	22.93	493.R	493.8	1543.39	.0000	• 0
50	28.13	35.79	22.97	490.6	491.4	1543.32	.0985	1.0
40	27.81	35.96	23.20	468.3	470.0	1543.10	.1947	3.9
60	27.33	36.10	23.46	443.4	445.9	1542.50	.2863	8.7
80	26.93	36.24	23.73	418.0	421.4	1541.83	.3730	15.3
100	25.48	36.50	24.29	364.7	368.9	1539.74	.4520	23.6
120	24.57	36.61	24.71	324.4	329.3	1537,53	.5218	33.3
140	23.78	36.72	25.03	294.0	299.6	1536.02	.5847	44.4
160	22.75	36.77	25.37	261.7	268.1	1533.82	.6415	56.6
180	20.92	36.67	25.80	220.1	227.0	1529.28	.6910	70.0
500	19.93	36.66	26.06	195.5	202.9	1526.91	. /340	84.2
220	19,12	36.57	26.21	181.9	189.8	1524.90	. 7733	99.3
240	18.35	36.46	26.32	171.2	179.7	1522.92	.8102	115.1
260	17.58	36.34	26.42	161.8	170.7	1520.89	.8453	131.7
280	16.98	36.26	26.50		163.2	1519.35	.8786	148.9
300	16,68	36.23	26.55	149.2	159.1	1518.74	.9109	166.8
340	15.66	36.06	26.66	139.1	149.8	1516.09	.9728	204.5
380	14.57	35.88	26.76	129.3	140.6	1513.11	1.0307	244.6
420	13.40	35.68	26.86	120.4	132.1	1509.73	1.0851	286.9
460	12.35	35.51	26.44	112.A	124.8	1506,66	1.1365	331.3
500	11.39	35.35	26.09	107.2	119.4	1503.81	1.1854	377.8
540	10,51	35.22	27.05	101.6	113.9	1501.20	1.2320	426.1
580	9.76	35.12	27.11	96.6	109.1	1499.02	1.2766	476.3
6211	9.38	35.07	27.13	94.3	107.1	1498.21	1.3198	528.2
660	8,45	34.96	27.19	88.3	100.7	1495.27	1.3614	581.9
700	7.90	34.91	27.24	84.1	96.5	1493.77	1.4008	637.1
740	7.37	34.87	27.28	74.7	92.0	1492.33	1.4384	693.9
780	6.39	34.86	27.34	74.0	86.2	1491.10	1.4741	752.2
820	6.38	34.85	27.41	68.2	80.2	1489.74	1.5073	811.8
860	6.00	34.86	27.46	62.8	74.7	1488.89	1.5383	872.7
900	5.50	34.84	27.53	56.5	68.2	1487.96	1.5668	934.8
940	5.19	34.90	27.57	52.6	64.4	1487.80	1.5933	998.0
980	5,11	34.91	27.61	48.7	60.4	1487.32	1.6183	1062.3
1020	4,93	34.93	27.65	45.2	57.0	1487.27	1.6418	1127.5
1100	4.65	34.95	27.70	40.6	52.7	1487.46	1.6856	1260.6
1200	4.49	34.96	27.72	38.2	51.0	1488.45	1./375	1431.8
1300	4.38	34.96	27.74	37.0	50.5	1489.63	1.7882	1608.0
1400	4.31	34.97	27.75	35.6	49.8	1491.00	1.8384	1789.4
1500	4.27	34.97	27.76	35.1	50.3	1492.48	1.8885	1975.7
1600	4.23	34.97	27.76	34.7	50.7	1493.96	1.9389	2167.1
1700	4.20	34.98	27.77	33.7	50.5	1495.50	1.9890	2363.5
1800	4.18	34.9R	27.77	33.5	51.1	1497.07	2.0398	2564.9
1900	4.16	34.99	27.78	32.5	51.0	1498.66	2.0908	2771.5
2000	4.15	34.99	27.78	32.4	51.8	1500.27	2.1422	2983.1

OOL1 271 1711					16.0					
LATITUDE				19 50						
LONGITUDE					86 37					
DEPTH TO BOTTOM				1902 M						
				OF	1 11/2					
	2	T	5	SIGT	MOMAT	SVA	SVEL	DYNHGT	TRANS	
	0	28,21	35.85	22.99	488.A	488.8	1543.22	.0000	• 0	
	20	28.16	35.92	23.05	482.2	483.0	1543.50	. 0972	1.0	
	40	27.72	36.11	23.34	454.7	456.4	1543.04	.1911	3.9	
	60	27.11	36.17	23.58	431.6	434.1	1542.07	.2802	8.6	
	80	26,17	36.30	23.98	395.7	397.1	1540.38	. 3633	15.0	
	100	24.71	36.55	24.62	332.A	336.9	1537.49	.4367	23.0	
	120	and the same of th	36.61	24.42		309.3	1535.83	.5013	32.4	
	140	21.93	36.67	25.52		252.2	1531.30	.5575	43.0	
	160	20.20	34.64	25.08		8.005	1526.99	.6037	54.6	
	180	19.40	36.61	26.16	185.9		1525.08	.6434	67.1	
	200	18.48	36.48	26.50	172.9		1522.67	.6811	80.3	
	220	17.48		26.42	162.0	100.5	1520.57	.7161	94.3	
	240	17.02	36.27	26.50		162.0	1518.84	. 1402	108.9	
	260	16.74		26.55			1518.30	.7812	124.2	
	290	16.33		26.60		154.1	1517.31	· A124	140.2	
	300	15.77	35.UH	26.65	140.1	149.5	1515.81	. 8428	156.7	
	340	14.72	35.90	26.74		141.1	1512.97	.9008	191.6	
	380	13.60	35.71	26.94	122.1	132.9	1509.78	.4555	228.7	
	420	12.65	35.55	26.91	115.5		1507.08	1.0075	268.0	
	460	11.05	35.44	26.46	110.6	122.3	1505.21	1.0573	309.3	
	500	11.20		27.01	105.3	117.4	1503,13	1.1051	352.6	
	5411	10.12	35.17	27.08	98.8	110.7	1499.74	1.1508	397.7	
	580	9.48	35.00	27.13	94.4	106.5	1497.96	1.1043	444.6	
	620	9.00	35.01	27.15	92.9	105.2	1496.74	1.2368	493.2	
	660	8. 17	34.95	27,20	87.0	100.2	1494.95	1.2777	543.5	
	700	7.51	34.88	27.27	90.0	92.7	1492.24	1.3165	595.4	
	740	7.25	34.87	27.30	78.1	90.2	1491.87	1.5529	648.8	
	780	6.25	34.85	27.34	74.2	86.4	1490.93	1.3885	703.6	
	820	6.25	34.85	27.42	66.6	78.4	1489.22	1.4213	759.8	
	860	5.85	34.86	27.48	61.0	72.6	1488.29	1.4516	R17.3	
	900	5.48	34.89	27.55	54.4	65.9	1487.50	1.4701	875.9	
	9411	5.25		27.60	50.2	61.8	1487.24	1.5046	935.6	
	980	4.85	34.93	27.66	44.3	55.5	1486.29	1.5274	96.2	
	1020	4.34	34.43	27.66	44.2	55.8	1486.90	1.5497	1057.8	
	1100	4.65		27.69	41.4		1487.44	1.5932	1183.5	
	1200	4.49		27.72	3A.9	51.7	1486.43	1.6452	1345.4	
			24 111	27 34	27 0	E 0 E		1 6000		

12.3 /

STD STATION NUMBER

JULY 29, 1971

50.5 1492.48 1.7967

1512.5

1684.6

1861.8

1300 4.38 34.96 27.74 37.0 50.5 1489.63 1.6960

1400 4.33 34.97 27.75 35.8 50.1 1491.08 1.7465

35.1

1600 4.20 34.98 27.77 33.7 49.5 1493.85 1.8466 2044.0 1700 4.17 34.99 27.78 32.6 49.3 1495.39 1.8964 2231.1 1800 4.16 34.99 27.78 32.5 50.1 1497.00 1.9465 2423.2

1500 4.27 34.97 27.76

```
STD STATION NUMBER
                         42
   JULY 29, 1971
                        18.3 7
                        20 04
   LATITUDE
                        87 04
   LONGITUDE
   DEPTH TO BOTTOM
                         614 M
                 SIGI
                        TANOM
                              SVA
                                     SVEL
                                             DYNHGT
                                                      TRANS
 0 28.19 36.03 23.13
                        475.2 475.2 1543.34
                                              .0000
                                                        • 0
                                              .0949
 20 28.12 36.03 23.15
                        473.0 473.9 1543.52
                                                         .9
 40 27.36 36.08 23.27
                        461.3 463.0 1543.32
                                              .1886
                                                        3.8
60 27.19 36.12 23.52
                        437.6 440.2 1542.20
                                              .2789
                                                        8.5
811 25.76 36.36 24.15
                        377.2 380.5 1539.48
                                              . 5610
                                                       14.9
100 23.90 36.65 24.92
                        303.9 307.9 1535.60
                                              .4298
                                                       22.8
                        241.3 245.9 1530.84
120 21.56 36.72 25.58
                                              .4852
                                                       31.9
140 19.71 35.59 26.07
                        195.1 200.2 1525.28
                                              .5298
                                                       42.1
160 18.21 36.46 26.55
                        167.9 173.5 1521.24
                                              .5672
                                                       53.0
                        158.3 164.4 1519.26
180 17.46 36.35 26.46
                                                       64.7
                                              .6010
200 16.70 36.23 26.55
                        149.7 156.3 1517.20
                                                       77.1
                                              .6331
220 16.11 36.13 26.61
                        143.8 150.9 1515.62
                                              .6638
                                                       90.0
240 15.60 36.06 26.67
                        137.9 145.4 1514.30
                                              .6934
                                                      103.6
                        133.9 141.9 1512.75
260 15.04 35.95 26.71
                                              . 7221
                                                      117.8
280 14.21 35.81 26.79
                                              . 7498
                        127.0 135.2 1510.27
                                                      132.5
                                              . 1764
3nn 13.57 35.71 26.84
                        121.5 130.0 1508.39
                                                      147.7
                        115.9 125.1 1506.15
                                                      179.8
340 12.75 35.57 26.90
                                              .H273
                                              . 8751
380 11.18 35.33 27.02
                        105.0 114.1 1501.13
                                                      213.9
420 10.00 35.16 27.10
                        97.6 106.8 1497.37
                                              . 4194
                                                      249.8
                                             .9608
460 9.11 35.06 27.17
                         90.9 100.2 1494.63
                                                      287.4
500 8.60 35.00 27.20
                        87.6 97.2 1493.30 1.0002
                                                      326.6
```

STD STATION NUMBER	43
JULY 29, 1971	22.5 /
LATITUDE	20 nm
LONGITUDE	86 31
DEPTH TO BOITOM	988 M

7	T	5	SIGT	TANOM	SVA	SVEL	TNHGT	TRANS
n	28.33	35.91	22.99	488.2	488.2	1543.54	.0000	• 0
20	28.00	36.06	23.21	467.1	467.9	1543.28	.0956	1.0
40	27.33	36.09	23.45	444.1	445.8	1542.16	.1870	3.8
60	26.58	36.18	23.76	414.7	417.2	1540.88	.2733	8.4
89	25.74	36.37	24.17	375.9	379.2	1539.45	.3529	14.6
100	24.46	36.62	24.75	320.5	324.6	1536.95	.4233	22.4
120	23.10	36.68	25,20	277.9	282.7	1533.98	.4840	31.5
140	21.61	36.77	25.69	231.0	236.4	1530.55	.5360	41.7
160	20.45	36.67	25.44	207.5	213.5	1527.64	.5809	52.9
180	19.15	36.55	26.18	184.1	190.6	1524.32	.6214	64.9
500	18.20	36.46	26.36	167.7	174.7	1521.85	.6579	77.7
220	17.51	36.30	26.45	158.9	166.4	1520.38	.6920	91.2
240	17.20	36.33	26.50	153.A	161.9	1519.44	. 7248	105.3
260	16.93	36.27	26.55	149.7	158.3	1518.59	.7568	120.2
<b>23</b> n	16,48	36.21	26.58	146.2	155.4	1517.80	. 1882	135.6
300	16,05	36.14	26.62	142.4	152.1	1516.83	.8189	151.7
341	14.88	35.92	26.72	132.9	143.1	1513.50	.8779	185.6
390	13.86	35.74	26.81	125.1	136.0	1510.66	.9337	221.9
420	12.77	35.58	26.91	115.6	126.9	1507.52	.9859	260.3
460	12.31	39.51	26.04	112,1	124.1	1506.53	1.0362	300.7
500	11.61	35.38	26.08	108.9	121.3	1504.61	1.0857	343.1
540	10.67	35.26	27.06	101,3	113.8	1501.82	1.1325	387.5
590	10.14	35.18	27.09	98,4	111.2	1500.47	1.1777	433.7
620	9.05	35.04	27.16	91.4	103.8	1496.96	1.2207	481.7
660	8.44	31.97	27.20	87.4	99.8	1495.24	1.2614	531.3
700	7.99	34.92	27.25	83.2	95.6	1493.74	1.3004	582.6
740	7.15	34.86	27.31	77.5	89.4	1491.47	1.3376	635.4
780	-6.50	34.86	and the same of th	69.0	80.6	1489.57	1.3717	689.6
850	6,19	311.86	27.44	65.1	76.8	1489.00	1.4034	745.1

STD STATION NUMBER	44
JULY 30, 1971	01.9 /
LATITUDE	20 15
LONGITUDE	86 12
DEPTH TO BOTTOM	1999 4

```
SIGT
                         TANOM SVA
                                                        TRANS
       T
                                       SVEL
                                               PANHET
   0 28.23 35.86 22.99
                         488.7 488.7 1543.28
                                                .0000
                                                           • 0
                                                .0963
  20 27.96 35.96 23.15
                         473.0 473.9 1543.11
                                                          1.0
                         451.4 453.1 1542.93
  40 27.56 36.13 23.38
                                                .1890
                                                          3.8
  60 27.09 36.00 23.53
                         436.7 439.2 1541.95
                                                .2782
                                                          8.5
  80 25.89 36.14 23.95
                         396.9 400.2 1539.59
                                                . 5621
                                                         14.9
 100 25.25 36.44 24.37
                         356.4 360.5 1538.68
                                                .4382
                                                         22.9
 120 24.73 36.61 24.66
                         329.0 333.9 1537.91
                                                .5077
                                                         32.4
 140 23.91 36.66 24.94
                         302.0 307.6 1536.29
                                                .5718
                                                         43.1
 160 22.09 36.74 25.53
                         246.0 252.2 1532.10
                                                .6278
                                                         55.1
 180 20.73 36.69 25.87
                         213.8 220.6 1528.79
                                                .6751
                                                         68.2
 200 19.43 36.60 26.15
                         187.4 194.7 1525.47
                                                         82.1
                                                .7166
                                                .7548
 220 18.99 36.56 26.23
                         179.4 187.4 1524.52
                                                         96.8
 240 18.56 36.51 26.30
                                                .7917
                         172.6 181.1 1523.57
                                                        112.3
 260 18.07 36.45 26.38
                         165.3 174.4 1522.43
                                                .8272
                                                        128.5
                         161.4 171.0 1521.87
 280 17.78 36.41 26.42
                                                        145.3
                                                .8617
 300 17.56 36.3F 26.45
                         158.4 168.7 1521.51
                                                        162.9
                                                .8957
 340 16.52 36.21 26.57
                         147.1 158.2 1518.88
                                                .9613
                                                        200.1
 380 15.87 36.09 26.63
                         141.5 153.5 1517.42 1.0233
                                                        239.8
 420 14.93 35.94 26.73
                         132.4 145.1 1514.96 1.0827
                                                        281.9
 460 14.05 35.78 26.80
                         126.0 139.3 1512.61 1.1399
                                                        326.4
 500 11.70 35.39 26.97
                         109.8 122.2 1504.94 1.1923
                                                        373.0
 540 10.71 35.26 27.05
                         102.0 114.5 1501.96 1.2391
                                                        421.7
 580
      9.98 35.16 27.10
                          97.2 109.9 1499.87 1.2841
                                                        472.1
 620
      9.12 35.05 27.16
                          91.7 104.2 1497.23 1.3268
                                                        524.3
 660
      8.41 34.98 27.22
                          86.2
                                98.6 1495.14 1.5673
                                                        578.2
 700
      7.74 34.92 27.26
                          81.6
                                93.9 1493.32 1.4060
                                                        633.7
      7.25 34.88 27.31
 740
                          77.3
                                89.5 1491.88 1.4424
                                                        690.7
      6.75 34.86 27.36
 780
                          72.2
                                84.2 1490.56 1.4774
                                                        749.1
      6.35 34.85 27.41
 620
                          67.8
                                79.8 1489.62 1.5102
                                                        808.8
      5.97 34.86 27.47
                          62.4
                                74.3 1488.77 1.5410
 860
                                                        869.9
 900
      5.66 34.88 27.52
                          57.2
                                69.0 1488.21 1.5697
                                                        932.1
941
      5.28 34.91 27.59
                          50.6
                                                        995.4
                                62.2 1487.36 1.5960
980
      4.99 34.92 27.63
                          46.6
                                58.1 1486.85 1.6199
                                                       1059.7
      4.83 34.94 27.67
                          43.3
                                55.0 1486.87 1.6426
                                                       1125.0
1020
1100
      4.66 34.95 27.70
                          40.7
                                52.9 1487.50 1.6858
                                                       1258.1
      4.50 34.94 27.71
1200
                          39.A
                                52.6 1488.46 1.7383
                                                       1429.3
      4.39 34.97 27.74
                                49.9 1489.68 1.7890
1300
                          36.4
                                                       1605.7
      4.33 34.97 27.75
                          35.8
1400
                                50.1 1491.08 1.8395
                                                       1787.1
      4.27 34.97 27.76
1500
                          35.1
                                50.3 1492.48 1.8897
                                                       1973.6
      4.24 34.97 27.76
                          34.8
                                50.8 1494.00 1.9402
                                                       2165.1
1600
      4.22 34.98 27.77
                          33.9
1700
                                50.7 1495.58 1.9908
                                                       2361.6
                          53.7
      4.20 34.98 27.77
1800
                                51.4 1497.15 2.0419
                                                       2563.3
                                                       2770.0
      4.18 34.99 27.78
                          32.7
                                51.3 1498.74 2.0932
1900
                                                       2981.9
2000
      4.12 34.99 27.79
                          32.1
                                51.4 1500.15 2.1445
```

STD STATION NUMBER	045
JULY 30, 1971	07.9 1
LATITUDE	20 12
LONGITUDE	85 411
DEPTH TO BOTTOM	4413 M

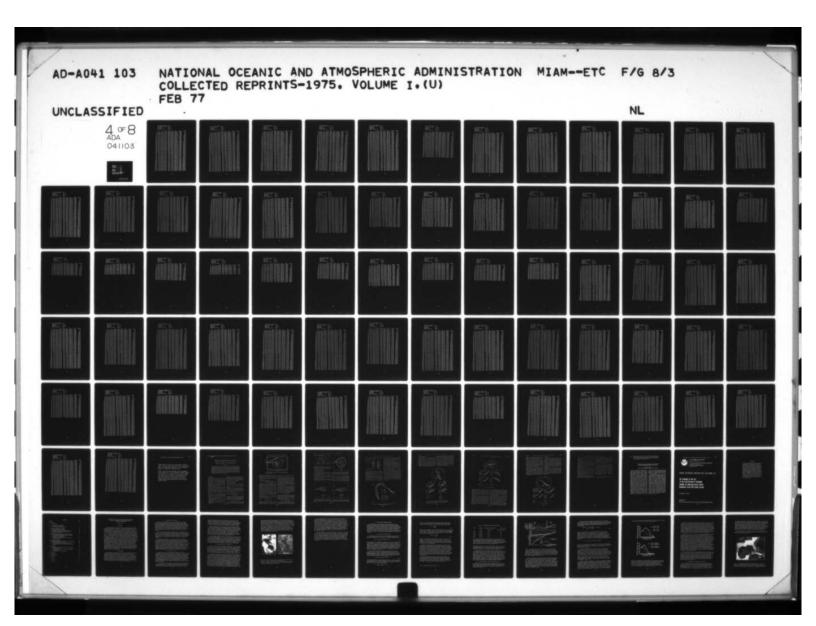
Z	T	S	STOT	TANOM	SVA	SVEL	DYNHET	TRAMS
0	28.67	36.07	23.00	487.5	487.5	1544.41	.0000	• 0
50	28.66	36.07	23.00	487.2	488.1	1544.71	.0976	1.0
40	28.35	36.07	23.10	477.4	479.1	1544.37	.1943	3.9
60	27.53	36.03	23.34	454.6	457.1	1542.88	.2879	8.7
80	26.62	36.01	23.62	428.1	431.5	1541.15	.3768	15.4
100	26.02	36.06	23.85	406.5	410.6	1540.14	.4610	23.7
120	25.76	36.12	23.47	394.5	399.4	1539.92	.5420	33.8
140	25.50	36.53	24.21	371.7	377.4	1539.82	.6197	45.4
160	24.40	36.58	24.71	324.6	331.1	1537.98	.6905	58.5
180	23.25	36.73	25.19	278.4	285.6	1535.36	. 1522	72.9
200	22.15	36.77	25.54	244.9	252.7	1532.87	.8060	88.5
550	21,22	36.74	25.78	222.0	231.5	1530.79	.8544	105.1
240	20.52	36.70	25.99	202.5	211.5	1528.66	.8087	122.6
260	19.58	36.62	26.13	189.7	199.2	1526.87	.9308	141.0
280	18.46	36.52	26.29	174.3	184.3	1524.51	.9781	160.2
300	17.09	35.44	26.39	164.1	174.5	1522.83	1.0100	180.1
3411	17.05	36.30	26.52	152.5	163.9	1520.57	1.9816	222.0
380	15.72	36.07	26.65	139.7	151.7	1516.93	1.1449	266.6
420	14.32	35.82	26.77	128.5	140.8	1512.88	1.2033	313.6
460	12.97	35.60	26.88	117.9	130.4	1508.85	1.2576	362.8
500	11.94	35.44	26.96	110.4	123.1	1505.82	1.5082	414.1
540	10.97	35.24	27.04	102.5	115.2	1502.56	1.3560	467.4
590	9.81	35.14	27.11	96.0	108.4	1499.22	1.4009	522.5
620	8.79	35.01	27.18	89.7	101.8	1495.95	1.4429	579.4
660	8.13	34.94	27.23	85.1	97.1	1494.03	1.4825	637.9
700	7.39	34.86	27.27	80.7	92.4	1491.74	1.5203	698.0
740	6.01	34.84	27.33	75.8	87.4	1490.50	1.5562	759.5
780	6.56	34.86	27.39	69.9	81.5	1489.81	1.5900	822.5
820	6.05	34.85	27.45	64.1	75.6	1489.42	1.6215	886.7
861	5.80	34.87	27.50	59.6	71.2	1498.10	1.6509	952.2
000	5.49	34.80	27.55	54.5	66.0	1487.53	1.6781	1018.7
941	5.18	34.91	27.60	49.11	60.9	1486.96	1.7035	1086.4
out	4.77	34.92	27.64	46.3	57.8	1486.77	1./271	1155.0
1020	4.77	34.94	27.68	42.7	54.2	1486.63	1.1495	1224.5
1100	4.56	34.95	27.71	39.7	51.6	1487.08	1./916	1366.2
1200	4."2	34.96	27.73	37.4	50.0	1498.15	1.8421	1547.9
1300	4.74	34.97	27.75	35.9	49.3	1489.48	1.8918	1734.6
1400	4.29	34.97	27.75	35.3	49.6	1490.91	1.9412	1926.2
1500	4.27	34.97	27.76	35.1	50.3	1492.47	1.4912	2122.9
1600	4.25	34.98	27.77	34.2	50.2	1494.05	2.0417	2324.5
1700	4.25	34.47	27.76	54.9	51.9	1495.69	5.11050	2531.2
1800	4.24	311.94	27.77	34.1	52.0	1497.31	2.1445	2743.1
Tàûu	4.24	34.9P	27.77	34.1	52.9	1498.97	2.1970.	2960.1
5000	4.24	34.98	27.77	34.1	53.8	1500.63	2.2503	3182.5

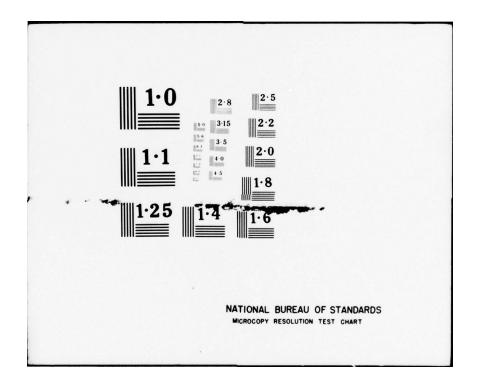
STO STATION NUMBER	46
JULY 30, 1971	13.8 7
LATTTUDE	20 11
LONGITUDE	85 NA
DEPTH TO BOTTOM	4416 M
T 5 5161	TANOM
20 00 76 00 20 00	1107 11

7.	T	5	SIGI	TANOM	SVA	SVEL.	DYNHGT	TRANS
n	28.70	36.09	22.94	493.4	493.4	1544.92	.0000	• 0
50	28.90	36.09	22.94	493.4	494.3	1545.24	.0988	1.0
40	28.93	36.09	22.93	494.4	496.1	1545.63	.1978	4.0
60	28.26	36.02	23.10	478.1	480.7	1544.46	.2955	8.9
80	27.14	35.98	23.43	446.2	449.5	1542.29	. 3885	15.7
100	26.51	35.98	23.63	427.n	431.1	1541.19	.4766	24.4
150	26.13	36.02	23.78	412.7	417.6	1540.68	.5615	34.8
140	25.76	36.13	23.98	393.7	399.5	1540.25	.6432	46.8
160	25.29	36.37	24.31	362.6	369.2	1539.68	. 1200	60.4
180	24.39	36.54	24.75	320.7	328.0	1538.05	. 7898	75.5
500	25.46	34.75	25.15	282.9	290.9	1536.23	.8516	91.9
220	22.26	35.78	25,51	247.7	256.3	1533.54	.9064	109.5
240	21.13	36.13	25.79	221.3	230.4	1530.86	.9550	128.1
560	20.25	35.67	25,49	202.4	212.1	1528.71	.9993	147.7
Sau	19.40	36.60	26.16	186.6	196.8	1526.67	1.0402	168.1
300	18.68	36.51	26.27	175.5	186.2	1524.88	1.0785	189.3
340	17.39	34.35	26.47	156.7	168.2	1521.62	1.1488	233.8
380	16.30	35.17	26.59	145.1	157.4	1518.81	1.2141	281.1
420	15,30	35.99	26.69	136.5	149.5	1516.18	1.2755	330.9
460	14.02	35.77	26.80	126.1	139.4	1512.50	1.3335	383.1
500	12.40	35.51	26.43	113.8	126.8	1507.47	1.3870	437.5
5411	11,50	35.35	27.01	105.6	118.7	1504.14	1.4360	494.0
580	10,39	35.23	27.08	98.8	111.9	1501.42	1.4823	552.4
650	9.49	35.10	27.14	93.8	106.8	1498.65	1.5260	612.5
661	8.13	35.01	27.19	88.8	101.6	1496.38	1.5677	674.4
700	8.01	34.92	27.23	84.9	97.4	1494.20	1.6075	737.9
740	7.45	34.87	27.27	80.8	93.2	1492.64	1.6457	803.0
780	6.81	34.84	27.34	74.5	86.5	14 76	1.6816	869.5
650	6.37	34.83	27.39	69.6	81.5	1489.66	1./152	937.5
860	5.36	34.85	27.46	63.0	74.9	1488.71	1.7465	1006.7
äüu	5.64	34.8A	27.52	57.0	68.8	1488.12	1.7754	1077.2
OTT ()	5.39	34.90	27.57	52.6	64.4	1487.79	1.8019	1148.7
980	5.14	34.91	27.61	49.0	60.8	1487.44	1.8270	1221.3
050	4.08	34.92	27.64	46.5	58.4	1487.46	1.8506	1294.8
100	4.67	34.94	27.69	41.6		1487.52	1.8954	1444.7
1200	4.50	34.95	27.71	39.0	51.8	1488.47	1.9480	1636.9
1300	4.40	34.96	27.73	57.2	50.8	1489.71	1.9993	1834.3
1400	4.32	34.96	27.74	36.4	50.7	1491.02	2.0400	2036.7
LSnn	4.28	34.97	27.75	35.2	50.4	1492.51	2.1001	2244.2
1600	4.24	34.97	27.76	34.8	50.8	1494.00	2.1507	2456.8
1700	4.21	34.98	27.77	33.8	50.6	1495.54	2.2015	2674 • 4
1800	4.19		-	33.6	51.3	1497.11	2.2524	2897.1
1900	4.17	54.94	27.78	32.6	51.2	1498.69	2.3039	3124.9

```
JULY 30, 1971 19.8 Z
LATITUDE 20 10
LONGITUDE 84 39
DEPTH TO BOTTOM 4418 M
T S SIGT TANOM
```

```
SIGT
                         TANOM SVA
                                      SVEL
                                              MYNHIGT
                                                        TRANS
                                               .0000
                                                           .0
   0 28.80 36.04 22.93
                         493.8 493.8 1544.66
  20 28.74 36.06 22.97
                         490.5 491.3 1544.87
                                               . 0985
                                                          1.0
  40 28.51 36.01 23.01
                         486.8 488.5 1544.66
                                                          3.9
                                               .1965
  60 27.35 35.97 23.36
                         453.3 455.9 1542.42
                                               .2909
                                                          8.8
  80 26.70 35.97 23.56
                         433.5 436.8 1541.29
                                               .3802
                                                         15.5
 100 26.37 36.05 23.73
                         417.7 421.9 1540.94
                                               .4661
                                                         24.0
 120 26.10 36.09 23.84
                         406.7 411.7 1540.68
                                               .5494
                                                         34.1
 140 25.94 36.19 23.97
                         394.8 400.6 1540.72
                                               .6306
                                                         45.9
 160 25.49 34.31 24.20
                         372.9 379.4 1540.10
                                                         59.3
                                               . 1086
 180 24.97 36.46 24.47
                         346.8 354.2 1539.33
                                                         74.2
                                               .7820
                         328.6 336.7 1538.83
 200 24.59 36.56 24.66
                                               .8511
                                                         90.6
                         299.7 308.6 1537.53
 220 23.88 36.68 24.97
                                               .9156
                                                       108.2
                         256.0 265.5 1534.57
 240 22,54 36.77 25.43
                                               .9730
                                                       127.1
 260 21.63 36.76 25.68
                         232.3 242.3 1532.53 1.0238
                                                       147.1
 28n 20.90 36.72 25.85
                         216.0 226.6 1530.89 1.0707
                                                       168.0
300 20.35 36.67 25.96
                         205.4 216.6 1529.68 1.1150
                                                       189.9
                                                       236.1
 340 18.61 36.50 26.28
                         174.6 186.6 1525.32 1.1957
 380 17.54 36.50 26.47
                         157.2 170.2 1522.75 1.2669
                                                       285.4
420 16.49 36.19 26.57
                         147.9 161.5 1520.06 1.3334
                                                       337.4
460 15.32 36.00 26.69
                         136.2 150.4 1516.89 1.3958
                                                       392.0
 500 14.13 35.79 26.79
                         126.9 141.3 1513.52 1.4542
                                                       449.0
 540 12.00 35.59 26.89
                         117.3 131.9 1509.89 1.5086
                                                        508.3
 580 11.70 35.39 26.97
                         109.8 124.2 1506.22 1.5598
                                                        569.7
 620 10.25 35.20 27.08
                          98.7 112.5 1501.53 1.6071
                                                       633.0
      9.27 35.07 27.15
 66n
                          92.6 106.1 1498.45 1.6509
                                                        698.2
                                96.7 1494.21 1.6913
      8.01 34.93 27.24
 700
                          84.2
                                                        765.0
                                90.7 1492.18 1.7289
                          78.4
      7.33 34.88 27.30
 740
                                                        833.4
                                83.8 1490.43 1.7639
 780
      6.72 34.86 27.37
                          71.8
                                                       903.3
      6.39 34.86 27.41
 820
                          67.6
                                79.6 1489.78 1.7965
                                                       974.5
 8611
      5.98 34.86 27.47
                          62.5
                                74.4 1488.81 1.8274
                                                      1047.0
900
                          57.8
      5.65 34.87 27.52
                                69.6 1488.15 1.8559
                                                      1120.7
                          53.8
 940
      5.43 34.89 27.56
                                65.7 1487.94 1.8829
                                                      1195.5
 9811
      5.19 34.91 27.60
                          49.5
                                61.5 1487.65 1.9684
                                                      1271.3
1020
      5.00 34.92 27.63
                          46.7
                                58.7 1487.54 1.9323
                                                      1348.1
1100
      4.68 34.94 27.69
                          41.7
                                53.9 1487.56 1.9770
                                                      1504.5
                          37.9
1200
      4.46 34.96 27.73
                                50.6 1488.32 2.0288
                                                      1704.8
                                                      1910.2
1300
      4.35 34.97 27.75
                          36.0
                                49.4 1489.51 2.0790
                                49.0 1490.96 2.1285
1400
      4.30 34.98 27.76
                          34.7
                                                      2120.6
      4.25 30.97 27.76
                          34.9
                                50.0 1492.39 2.1782
1500
                                                      2335.9
                                49.9 1493.97 2.2280
      4,23 34.98 27.77
                          34.0
                                                      2556.2
1600
      4.20 34.98 27.77
                                50.5 1495.49 2.2782
1700
                          33.7
                                                      2781.5
1800
      4.18 34.98 27.77
                          33.5
                                51.1 1497.06 2.3290
                                                      3011.9
1900
      4.16 34.99 27.78
                          32.5
                                51.0 1498.65 2.3798
                                                      3247.3
2000
      4.14 34.99 27.78
                          32.3
                                51.6 1500.23 2.4311
                                                      3487.9
```





```
STD STATION NUMBER 048
SEPTEMBER 31, 1971 01.7 2
LATITUDE 20 12
LONGLIUDE 84 05
DEPTH TO ROTTOM 4354 M
```

```
S
                         TANOM
                                SVA
                                       SVEL
                                              DYNHGT
                                                        TRANS
                   SIGT
                                               .0000
                         494.4 494.4 1544.98
                                                           .0
  0 28.93 36.09 22.93
  20 28.90 36.09 22.94
                         493.4 494.3 1545.24
                                               .0989
                                                          1.0
                         485.6 487.3 1544.70
  40 28.52 36.03 23.02
                                                          3.9
                                               .1970
  60 27.17 35.97 23.41
                         447.8 450.3 1542.02
                                               .2908
                                                          8.8
  80 26.57 35.98 23.61
                         428.8 432.1 1541.00
                                               .3790
                                                         15.5
 100 26.17 36.04 23.79
                         412.4 416.6 1540.47
                                               .4639
                                                         24.0
 120 26.48 36.54 23.01
                         400.2 405.2 1541.77
                                               .5461
                                                         34.1
140 25,90 36.35 24.10
                         382.1 387.9 1540.77
                                               .6254
                                                         45.8
160 25.14 36.45 24.41
                         352.5 359.0 1539.40
                                               .7001
                                                         59.0
 180 24.43 36.58 24.73
                         322.6 329.9 1538.14
                                               .7690
                                                         73.7
 200 23.86 36.67 24.97
                         299.8 307.9 1537.15
                                               .8328
                                                         89.7
220 23.30 36.73 25.18
                         279.8 288.6 1536.13
                                                        107.0
                                               .8924
                         258.4 267.8 1534.72
                                                .9481
240 22.40 36.76 25.40
                                                        125.4
260 22.08 36.76 25.55
                         244.3 254.4 1533.70 1.0003
                                                        144.9
280 21.08 36.70 25.78
                         222.1 232.8 1531.35 1.0490
                                                        165.4
300 19.86 36.63 26.06
                         195.9 207.0 1528.30 1.0930
                                                        186.8
340 18.32 36.48 26.34
                         169.1 181.0 1524.46 1.1708
                                                        232.1
380 17.31 36.35 26.49
                         154.8 167.6 1522.03 1.2406
                                                        280.3
420 16.29 36.12 26.56
                         148.5 162.1 1519.38 1.3062
                                                        331.3
460 14.86 35.87 26.69
                         136.0 149.8 1515.30
                                              1.3680
                                                        384.8
500 13.57 35.69 26.83
                         123.0 137.0 1511.58 1.4251
                                                        440.6
540 12.31 35.49 26.93
                         113.5 127.6 1507.79 1.4783
                                                        498.7
580 11.14 35.31 27.01
                         105.7 119.6 1504.18 1.5281
                                                        558.9
620 10.35 35.20 27.07
                         100.4 114.3 1501.89 1.5749
                                                        620.9
      9.43 35.08 27.13
                          94.4 108.0 1499.05 1.6193
                                                        684.8
660
      8.73 35.00 27.18
                          89.5 103.1 1497.01 1.6615
700
                                                        750.4
      8.07 34.93 27.23
740
                          85.0
                                98.3 1495.08 1.7017
                                                        817.7
      7.53 34.88 27.27
                          81.1
                                94.3 1493.60 1.7404
780
                                                        886.5
058
                                89.2 1492.37 1.7771
      7.05 34.86 27.32
                          76.1
                                                        956.9
860
      6.43 34.84 27.39
                          69.6
                                82.2 1490.56 1.8115
                                                       1028.7
900
      6.05 34.86 27.46
                          63.4
                                75.9 1489.73 1.8431
                                                       1101.8
940
      5.67 34.87 27.51
                          58.1
                                70.4 1488.88 1.8725
                                                       1176.1
990
      5.40 34.8P 27.55
                          54.2
                                66.5 1488.46 1.9001
                                                       1251.5
      5.16 34.90 27.60
                          50.0
1020
                                62.3 1488.16 1.9256
                                                       1328 - 1
                                55.8 1487.92 1.9726
      4.77 34.93 27.67
                                                       1484.0
1100
                          43.4
      4.55 34.95 27.71
                          39.6
                                52.5 1488.67 2.0265
                                                       1684.0
1200
      4.41 34.96 27.73
                                                       1889.3
                          37.3
                                50.9 1489.75 2.0781
1300
      4.33 34.97 27.75
                                50.1 1491.07 2.1287
                                                       2099.6
                          35.8
1400
      4.28 34.97 27.75
                                                       2315.0
                                50.4 1492.51 2.1789
1500
                          35.2
                                50.8 1493.99 2.2294
1600
      4.24 34.97 27.76
                          34.8
                                                       2535.4
      4.21 34.98 27.77
1700
                          33.8
                                50.6 1495.53 2.2797
                                                       2760.8
      4.18 34.98 27.77
                                51.1 1497.06 2.3305
                                                       2991.3
1800
                          33.5
1900
      4.15 34.99 27.78
                          32.4
                                50.9 1498.61 2.5813
                                                       3226.9
2000
      4.14 34.99 27.78
                          32.3
                                51.6 1500.23 2.4324
                                                       3467.6
```

JULY 31, 1971			07.3						
LATITUDE			19 4	19 44					
LONGITUDE			84 30						
DEPTH TO BOTTOM			4420 M						
	JEL (-)	10 601	City	4420	•				
2	Т	5	SIGT	TANOM	SVA	SVEL	NYNHGT	TRANS	
	28.92	36.08	22.96	491.6	491.6	1544.74	.0000	• 0	
	28.80				492.5	1545.01	.0984	1.0	
	28.71							3.9	
					492.0	1545.13	.1969		
	27.60					1542.98	.2924	8.8	
	26.93				443.8	1541.81	.3832	15.6	
	26.44			419.A	424.0	1541.10	.4699	24.1	
120	26.40	36.27	23.89	402.8	407.8	1541.53	.5531	34.3	
140	25.01	36.28	24.05	387.4	393.2	1540.73	.6332	46.2	
	25.32			363.5	370.1	1539.76	. 1005	59.6	
	24.98				350.1	1539.13	.7816	74.5	
	24.40					1538.41	8493	90.9	
	23.71				303.0	1537.12	.9124	108.5	
			25.39			1534.87	.9696	127.3	
	21,25				235,1	1531.50	1.0201	147.2	
	19.99				208.1	1528.35	1.0644	168.0	
300	19.31	36.60	26.18	184.4	195.3	1526.74	1.1048	189.7	
340	17.92	36.42	26.40	163.0	175.7	1523.25	1.1785	235.4	
380	17.06	34.32	26.53	151.3	164.0	1521.26	1.2462	283.9	
	15.80					1517.83		335 • 1	
	14.46					1513.98		388.7	
500		35.57				1509.12		444.5	
5411		35.45			125.1	1506.78	1.4757	502.6	
580		35.30				1504.16	1.5247	562 • 6	
620		35.15				1500.57	1.5709	624.5	
6611		35.0R			108.5	1499.16	1.6151	688.2	
700		35.04				1498.32	1.6579	753.7	
740		34.94			100.6	1495.81	1.6994	820.8	
780	7.77	34.90	27.25	83.0	96.6	1494.55	1./300	P89.6	
820	7.10	34.87	27.52	76.1	89.2	1492.58	1.7761	959.9	
860	6.56	34.85	27.38	70.5	83.4	1491.09	1.8107	1031.6	
900	5.09	34.86	27.46	62.7		the state of the s	1.8423	1104.7	
940		34.84		57.0				1179.0	
980		34.90		52.3			1.8980	1254.4	
1020		34.92		47.6		1487.86		1330.8	
		34.94						1486.5	
1100	4.13	34.94	27.70	42.4			1.9687		
		34.96	and the same of th			1488.65		1686.0	
1300		34.96		37.3		1489.75		1890.8	
1400		34.97		35.7		1491.03		2100.6	
1500		34.97		35.1	50.3	1492.47	2.1736	2315.5	
1600		34.9P		34.1	50.1	1494,01	2.2239	2535.3	
1700		34.94		53.7	50.5	1495.49	2.2741	2760.2	
1800	4.18	35.00	27.79	32.0	49.7	1497.09	2.3246	2990.2	
1000		70 00		40 F		1400 65		****	

49 07.3 2

STD STATION NUMBER

JULY 31, 1971

1900 4.16 34.99 27.78 32.5 51.0 1498.65 2.3753 3225.2 2000 4.15 34.99 27.78 32.4 51.8 1500.27 2.4267 3465.3

STD STATION NUMBER	50
JULY 31, 1971	14.2 /
LATITUDE	19 20
LONGITUDE	84 52
PEPTH TO ROTTOM	4415 M

```
SIGT
                                                        TRANS
             S
                         TANOM
                                SVA
                                               TYNHGT
                                       SVEI.
   0 28.79 36.09 22.97
                         489.9 489.9 1544.68
                                                .0000
                                                           .0
  20 28.79 36.09 22.97
                         489.9 490.8 1545.01
                                                .0981
                                                          1.0
                                                .1963
                         489.7 491.4 1545.26
  40 28.76 36.08 22.98
                                                          3.9
                                                .2925
                         468.1 470.7 1543.53
  60 27.85 35.98 23.20
                                                          8.8
                         439.7 443.1 1541.82
  80 26.93 35.98 23.50
                                                . 5839
                                                         15.6
 100 26.37 36.03 23.71
                         419.2 423.3 1540.92
                                                .4705
                                                         24.1
 120 25.94 36.07 23.88
                         403.4 408.3 1540.29
                                                .5537
                                                         34.4
 140 25.57 36.19 24.09
                         383.9 389.5 1539.86
                                                         46.2
                                                .6335
 160 25.17 36.38 24.35
                         358.4 364.9 1539.41
                                                .7089
                                                         59.7
 180 24.11 36.67 24.89
                         306.9 314.2 1537.44
                                                .7768
                                                         74.5
                                                         90.6
                                                .8342
 200 22.31 36.75 25.48
                         251.2 259.0 1533.32
 220 21.24 36.74 25.77
                         223.4 231.8 1530.84
                                                .8832
                                                        107.8
 240 20.29 36.70 26.00
                         201.7 210.7 1528.58
                                                .9275
                                                        125.9
 260 19.49 36.62 26.15
                         187.4 196.9 1526.62
                                                .9683
                                                        144.9
 280 18.62 36.51 26.29
                         174.1 184.0 1524.39 1.0063
                                                        164.6
 300 18.14 36.47 26.38
                         165.5 176.0 1523.29 1.0423
                                                        185.1
 340 17.41 36.37 26.48
                         155.7 167.2 1521.70 1.1109
                                                        228.2
 390 16.37 36.19 26.59
                         145.2 157.5 1519.05 1.1755
                                                        273.9
420 15.44 36.00 26.66
                         138.8 151.8 1516.63 1.2378
                                                        322.2
 460 14.05 35.77 26.79
                         126.7 140.0 1512.60 1.2959
                                                        372.9
 500 13.37 35.66 26.85
                         121.3 135.1 1510.89 1.3510
                                                        425.8
 540 12.19 35.46 26.93
                         113.5 127.4 1507.34 1.4038
                                                        480.9
580 10.81 35.25 27.02
                         104.5 118.0 1502.94 1.4527
                                                        538.0
620 10.02 35.16 27.09
                          97.9 111.4 1500.65 1.4986
                                                        597.1
660
      9.16 35.05 27.15
                          92.4 105.7 1498.02 1.5420
                                                        657.9
 700
                          89.2 102.5 1496.34 1.5834
      8.56 34.97 27.18
                                                        720.4
740
      7.71 34.90 27.26
                          82.1
                                95.0 1493.67 1.6229
                                                        784.5
780
                          78.7
      7.30 34.87 27.29
                                                        850.2
                                91.6 1492.70 1.6600
      6.77 34.85 27.35
820
                          73.2
                                85.8 1491.27 1.6953
                                                        917.3
860
      6.46 34.84 27.39
                          70.0
                                82.6 1490.68 1.7288
                                                        985 . 8
900
      6.01 34.85 27.45
                          63.7
                                76.1 1489.56 1.7606
                                                       1055.6
940
      5.63 34.88 27.53
                          56.9
                                69.1 1488.73 1.7895
                                                       1126.6
980
      5.38 34.89 27.56
                          53.2
                                65.5 1488.39 1.8165
                                                       1198.7
                          49.2
1020
      5.16 34.91 27.61
                                61.5 1488.18 1.8419
                                                       1271.9
                          43.7
      4.80 34.93 27.66
1100
                                56.2 1488.04 1.888R
                                                       1421.2
                          39.7
      4.56 34.95 27.71
                                52.6 1498.72 1.9429
1200
                                                       1612.8
1300
      4.43 34.96 27.73
                          37.5
                                51.2 1489.83 1.9947
                                                       1809.7
                          35.9
1400
      4.34 34.97 27.75
                                50.2 1491.12 2.0454
                                                       2011.7
      4.29 34.94 27.76
1500
                          34.6
                                49.8 1492.57 2.0955
                                                       2218.7
1600
      4.25 34.98 27.77
                          34.2
                                50.2 1494.05 2.1458
                                                       2430.8
                                50.7 1495.58 2.1963
      4.22 34.98 27.77
                          33.9
                                                       2647.9
1700
      4.20 34.98 27.77
                          33.7
                                51.4 1497.15 2.2473
1800
                                                       2870 • 1
      4.17 34.99 27.78
                                51.2 1498.69 2.2985
1900
                          32.6
                                                       3097.4
2000
      4.16 35.00 27.79
                          31.8
                                51.2 1500.33 2.3498
                                                       3329.8
```

```
STD STATION NUMBER 51
JULY 31, 1971 21.7 2
LATITUDE 18 59
LONGITUDE 84 32
DEPTH TO BOTTOM 2743 M
```

```
SVEL
                                              PYNHGT
                                                        TRANS
                   SIGT
                         TANOM SVA
             5
   n 28.89 36.09 22.94
                         493.1 493.1 1544.89
                                               .0000
                                                           • 0
  20 28.90 36.09 22.94
                         493.4 494.3 1545.24
                                               .0987
                                                          1.0
  40 28.90 36.08 22.93
                         494.2 495.9 1545.56
                                               .1978
                                                          4.0
                                               .2942
  60 27.72 35.95 23.22
                         466.2 468.8 1543.22
                                                          8.9
  80 26.77 35.97 23.54
                         435.6 438.9 1541.45
                                               . 3850
                                                         15.7
 100 26.26 36.01 23.73
                         417.3 421.4 1540.65
                                               .4710
                                                         24.2
                         400.7 405.6 1540.27
120 25.42 36.10 23.91
                                               .5537
                                                         34.5
 140 25.60 36.23 24.11
                         381.8 387.6 1539.97
                                                         46.3
                                               .6330
                         352.6 359.2 1539.34
160 25.12 36.44 24.41
                                                         59.7
                                               .7077
 180 24.03 36.69 24.93
                         303.2 310.5 1537.26
                                                         74.6
                                               . 1747
 200 22.81 36.75 25.33
                         264.8 272.8 1534.60
                                                         90.6
                                               .8330
 220 21.74 36.75 25.64
                         235.9 244.4 1532.17
                                               . 8647
                                                        107.8
 240 20.56 36.71 25.93
                         207.9 217.0 1529.32
                                               .9309
                                                        126.0
 260 19,56 36,61 26,12
                         189.9 199.4 1526.81
                                               .9725
                                                        145.0
 280 18.83 36.54 26.26
                         177.0 187.0 1525.01 1.0111
                                                        164.9
                         166.5 176.9 1523.02 1.0475
 300 18.06 36.43 26.37
                                                        185.4
 340 16.69 36.23 26.55
                         149.5 160.6 1519.41 1.1146
                                                        228.7
 380 15.26 35.99 26.69
                         135.7 147.4 1515.41 1.1762
                                                        274.5
 420 13.74 35.72 26.82
                         124.2 136.1 1510.89 1.2329
                                                        322.7
 460 12.49 35.52 26.92
                         114.7 126.8 1507.14 1.2855
                                                        373.1
                         105.8 117.7 1502.58 1.3343
 500 11.06 35.29 27.01
                                                        425.5
 540 10.23 35.19 27.08
                          99.1 111.2 1500.16 1.3798
                                                        479.8
 580
      9.54 35.09 27.12
                          95.4 107.5 1498.18 1.4236
                                                        535.9
 620
      9.03 35.03 27.16
                          91.8 104.2 1496.87 1.4660
                                                        593.7
      8.49 34.97 27.20
                          88.2 100.6 1495.43 1.5070
 660
                                                        653.1
                                95.8 1493.41 1.5463
 700
      7.81 34.90 27.24
                          83.6
                                                        714.2
      7.65 34.89 27.26
                          82.1
                                94.8 1493.43 1.5843
 740
                                                        776.8
                                89.6 1491.79 1.6211
      7.07 34.85 27.31
                          77.1
 780
                                                        H40.9
                          73.6
 820
      6.74 34.84 27.35
                                86.1 1491.14 1.6560
                                                        906.5
                          68.1
                                80.6 1490.34 1.6893
                                                        973.4
 860
      6.37 34.85 27.41
 900
      5.37 34.85 27.47
                          62.0
                                74.1 1489.00 1.7204
                                                       1041.6
 940
      5.54 34.88 27.54
                          55.A
                                67.9 1488.37 1.7485
                                                       1111.0
      5,26 34.90 27.59
 980
                                63.1 1487.92 1.7747
                          51.1
                                                       1181.4
      5.07 34.91 27.62
1020
                          48.2
                                60.3 1487.81 1.7994
                                                       1252.9
1100
      4.73 34.94 27.68
                          42.2
                                54.5 1487.77 1.8447
                                                       1398.7
      4.53 34.95 27.71
                          39.3
1200
                                52.2 1488.59 1.8976
                                                       1585.8
                          37.3
      4.41 34.96 27.73
                                50.9 1489.75 1.9488
1300
                                                       1778.2
      4.34 34.97 27.75
                          35.9
                                50.2 1491.12 1.9996
1400
                                                       1975.6
1500
      4.28 34.97 27.75
                          35.2
                                50.4 1492.51 2.0409
                                                       2178.1
      4.25 34.98 27.77
                          34.2
                                50.2 1494.05 2.1003
1600
                                                       2385.6
1700
      4.21 34.98 27.77
                          33.0
                                50.6 1495.54 2.1506
                                                       2598.1
1800
      4.18 34.98 27.77
                          33.5
                                51.1 1497.07 2.2015
                                                       2815.7
1900
      4.17 35.00 27.79
                          31.0
                                50.4 1498.71 2.2522
                                                       3038.4
                          32.4
2000
      4.15 34.99 27.78
                                51.8 1500.27 2.3035
                                                       3266.2
```

STD STATION NUMBER	52
AUGUST 01. 1971	01.9 7
LATITUDE	18 45
LONGITUDE	84 15
DEPTH TO BOTTOM	2575 M

7	T	5	SIGT	TANOM	SVA	SVEL	CYNHGT	TRANS
n	28.88	36.05	22.91	495.7	495.7	1544.84	.0000	• 0
50	28.89		22.92	495.3	496.1	1545.19	.0992	1.0
40	28.61	36.02	22.98	489.2	490.9	1544.89	.1979	4.0
60	27.47	35.98	23.33	456.3	458.9	1542.70	.2929	8.9
80	26.67	35.99	23.59	431.1	434.4	1541.24	. 3822	15.6
100	26.17	36.09	23.82	408.8	413.0	1540.51	.4669	24.1
120	25.78	36.18	24.01	390.7	395.7	1540.02	.5478	34.3
140	25.32	36.36	24.29	364.2	370.0	1539.42	.6244	46.0
160	24.52	36.60	24.78	318.0	324.5	1537.56	.6938	59.2
180	22.80	36.77	25.35	263.1	270.3	1534.26	. /533	73.6
200	21.80	36.76	25.63	236.8	244.5	1532.01	.8048	89.2
220	20.73	36.72	25.89	211.6	219.9	1529.46	.8512	105.8
240	19.76	36.62	26.08	194.1	203.0	1527.05	.8935	123.2
260		36.51		174.8	184.0	1524.15	.9322	141.5
280	17.76	36.39	26.41	162.4	172.0	1521.79	.9678	160.5
300	17.08	36.27	26.49	155.4	165.4	1519.98	1.0015	180.2
340	15.83	36.07	26.63	142.1	152.9	1516.63	1.0650	221.5
380	14.71	35.89	26.74	131.4	142.8	1513.56	1.1241	265.3
420	13.54	35.69	26.85	122.4	134.2	1510.20	1.1795	311.4
460	12.39	35.50	26.92	114.3	126.3	1506.78	1.2314	359.6
500	11.45	35.35	26.98	108.2	120.5	1504.02	1.2806	409.9
540	10.51	35.22	27.05	101.6	113.9	1501.20	1.3274	462.0
580	9.83	35.12	27.09	97.8	110.2	1499.27	1.5722	516.0
620	9.31	35.06	27.13	94.0	106.7	1497.94	1.4155	571.8
660	8.76	35.01	27.18	89.2	102.1	1496.49	1.4573	629.2
700	8.31	34.96	27.22	86.3	99.2	1495.38	1.4975	688.3
740	7.83	34.90	27.24	83.A	96.8	1494.13	1.5367	749.0
790	7.20	34.86	27.30	78.1	90.8	1492.31	1.5741	811.2
820	6.55			71.0	84.1	1490.38	1.6092	874.9
860		34.85	27.45	64.1	76.1	1489.07	1.6412	939.9
900	5.71	34.88	27.52	57.8	69.7	1488.41	1.6704	1006.2
940	5.45		27.56	54.0	66.0	1488.02	1.6977	1073.5
980	5.16		27.61	49.2	61.1	1487.53	1.7231	1142.0
1020	4.94	34.93	27.65	45.3	57.1	1487.31	1.7467	1211.4
1100	4.69	34.94	27.68	41.8	54.0	1487.60	1.7911	1352.9
1200	4.53		27.72	38.6	51.5	1488.61	1.8437	1534.6
<b>13</b> 00	4.39	34.96		37.1	50.7	1489.67	1.8949	1721.6
1400	4.33	34.97		35.8	50.1	1491.08	1.9451	1913.6
1500	4.27		27.76	35.1	50.3	1492.47	1.9951	2110.6
1600	4.22		27.77	33.9	49.8	1493.93	2.0450	2312.6
1700	4.20		27.77	33.7	50.5	1495.50	2.0951	2519.6
1800	4.18		27.78	32.7	50.4	1497.08	2.1457	2731.7
1900		34.99		32.4	50.9		2.1962	2948.7
2000	4.13	34.99	27.79	32.2	51.5	1500.19	2.2475	3170.9

```
AUGUST 01, 1971 06.5 / LATITUDE 18 37 LONGITUDE 84 10 DEPTH TO BOTTOM 1015 M
```

7	T	S	SIGI	TANOM	SVA	SVEL	TYNHET	TRANS
0	28.77	36.08	22.97	490.0	490.0	1544.63	.0000	• 0
	28.83		22.95	491.9	492.8	1545.08	.119A3	1.0
40	28.66	36.06	22.99	487.9	489.6	1545.03	.1965	3.9
60	27.78	36.01	23.25	463.R	466.3	1543.41	.2921	8.8
80	26.57	36.01	23.64	426.6	430.0	1541.03	.3817	15.6
100	26.06	36.06	23.A3	407.7	411.8	1540.23	.4659	24.0
120	25.54	36.24	24.13	379.3	384.3	1539.51	.5455	34.1
140	24.78	36.48	24.55	339.8	345.6	1538.25	.6185	45.8
160	23.42	34.60	25.11	286.0	292.5	1535.43	.6823	58.8
180	21,60	36.75	25.68	232.2	239.1	1531.15	.7355	73.0
Sou	20.27	35.67	25.98	203.4	210.9	1527.85	.7805	88.1
550	19.46	35.61	26.15	187.4	195.4	1525.89	.8211	104.1
240	18.86	36.59	26.29	174.1	182.7	1524.50	.8589	120.9
560	18.16	36.50	26.40	163.8	172.9	1522.73	.8945	138.5
280	17.68	36.41	26.45	159.0	168.7	1521.57	.9286	156.7
300	17.33	36.36	26.50	154.6	164.7	1520.81	.9620	175.6
340	16.99	36.35	26.57	147.5	158.9	1520,44	1.0267	215.4
380	15.66	36.0P	26.67	137.7	149.6	1516.75	1.0885	257.7
420	14.26	35.83	26.79	126.6	138.9	1512.70	1.1461	302.4
460	12.80	35.60	26.92	114.7	127.1	1508.28	1.1992	549.3
500	11.80	35.42	26.97	100.4	121.9	1505.32	1.2488	398.3
540	11.02	35.31	27.03	103.7	116.5	1503.11	1.2964	449.2
580	10.07	35.17	27.09	98.0	110.7	1500.20	1.3421	502.0
650	9.53	3=.11	27.14	93.7	106.7	1498.81	1.3854	556.5
660	8,96	35.03	27.17	90.0	103.9	1497.26	1.4275	612.8
700	8.02	34.93	27.24	84.3	96.9	1494.25	1.4675	670.7
740	7.40	34.88	27.29	79.4	91.7	1492.46	1.5051	730.2
780	6.79	34.85	27.35	73.5	85.5	1490.70	1.5405	791 • 1

```
      STD. STATION NUMBER
      54

      AUGUST 01, 1971
      18.2 %

      LATITUDE
      18 21

      LONGITUDE
      82 04

      DEPTH TO BOTTOM
      4206 M
```

```
TRANS
                         TANOM SVA
                                               DYNHGT
             S
                   SIGT
                                       SVEL.
       T
  0 27.61 36.07 23.35
                         454.2 454.2 1542.12
                                                .0000
                                                           .0
                         446.9 447.7 1542.04
  20 27.42 36.09 23.42
                                                .11902
                                                           .9
  40 27.04 36.11 23.56
                         433.9 435.4 1541.53
                                                .1785
                                                          3.6
  60 26.62 36.23 23.79
                         412.3 414.8 1541.02
                                                .2635
                                                          8.0
  80 26.11 36.36 24.05
                         387.6 391.0 1540.29
                                                . 3441
                                                         14.1
 100 25.38 36.52 24.39
120 24.27 36.70 24.87
                         354.5 358.6 1539.06
                                                .4191
                                                         21.7
                         309.3 314.2 1536.88
                                                .4864
                                                         30.8
 140 23.19 36.79 25.25
                         272.4 278.0 1534.62
                                                .5456
                                                         41.1
 160 22.45 36.80 25.48
                         251.4 257.7 1533.08
                                                .5092
                                                         52.5
 180 21.55 36.76 25.70
                         230.1 237.1 1531.03
                                                .6486
                                                         65.0
                                                .6940
 200 20.53 36.68 25.92
                         209.3 216.8 1528.57
                                                         78.4
 220 19.81 36.62 26.07
                         195.4 203.5 1526.87
                                                .7361
                                                         92.7
 240 18.84 36.51 26.23
                         179.4 188.0 1524.37
                                                .7752
                                                        107.9
 260 18.04 36.42 26.37
                         166.8 175.8 1522.31
                                                .8116
                                                        123.7
 280 17.42 36.35 26.47
                         157.4 166.9 1520.75
                                                .8459
                                                        140.3
 300 16.60 36.22 26.56
                         148.2 158.0 1518.49
                                               .8783
                                                        157.5
                                               .9399
 340 15.67 36.06 26.66
                         139.3 150.0 1516.12
                                                        193.9
 380 14.96 35.94 26.72
                         133.0 144.5 1514.41
                                                .9989
                                                        232.7
 420 14.21 35.80 26.78
                         127.7 140.0 1512.51 1.0559
                                                        273.8
 460 13.89 35.75 26.81
                         124.9 138.1 1512.06 1.1115
                                                        317.1
 500 13.28 35.65 26.86
                         120.2 134.1 1510.59 1.1660
                                                        362.7
 540 11.37 35.33 26.98
                         108.3 121.4 1504.36 1.2173
                                                        410.4
      8.93 34.99 27.14
                          93.3 104.7 1495.81 1.2625
 580
                                                        460.0
      7.87 34.90 27.23
                          84.4
                                95.4 1492.35 1.3025
620
                                                        511.3
 660
      7.12 34.84 27.30
                          78.6
                                89.2 1490.03 1.5392
                                                        564.1
 700
      6.93 34.84 27.34
                          74.7
                                85.6 1489.55 1.3741
                                                        618.4
      6.59 34.85 27.38
                          70.9
                                82.0 1489.27 1.4077
 740
                                                        674.0
      6.29 34.84 27.41
                          67.8
 780
                                79.1 1488.72 1.4399
                                                        731.0
 820
      5.92 34.86 27.47
                          61.8
                                73.0 1487.92 1.4703
                                                        789.2
      5.71 34.87 27.51
 860
                          58.6
                                69.9 1487.74 1.4989
                                                        848.6
 900
      5.48 34.89 27.55
                          54.4
                                65.9 1487.50 1.5261
                                                        909.1
 940
      5.14 34.91 27.61
                          49.0
                                60.3 1486.80 1.5512
                                                        970.7
                          45.2
      4.93 34.93 27.65
 980
                                 56.6 1486.62 1.5746
                                                       1033.2
      4.79 34.94 27.67
                          42.9
1020
                                54.4 1486.71 1.5969
                                                       1096.6
      4.58 34.96 27.71
                          39.1
1100
                                 51.1 1487.18 1.6388
                                                       1226.1
                          37.8
      4.45 34.96 27.73
1200
                                 50.4 1488.28 1.6894
                                                       1392.5
                                 49.7 1489.60 1.7392
1300
      4.37 34.97 27.74
                          36.2
                                                       1563.9
      4.31 34.97 27.75
                          35.6
                                                       1740.3
1400
                                 49.8 1491.00 1.7890
1500
      4.27 34.98 27.76
                          34.4
                                 49.5 1492.49 1.8386
                                                       1921.7
                          34.1
1600
      4.24 34.98 27.77
                                 50.1 1494.01 1.8884
                                                       2108.1
      4.22 34.99 27.78
                                 50.0 1495.59 1.9388
                                                       2299.4
                          33.1
1700
      4.20 34.99 27.78
                          32.9
                                                       2495.8
                                 50.7 1497.17 1.9892
1800
      4.17 34.99 27.78
                          32.6
                                 51.2 1498.70 2.0401
                                                       2697.3
1900
2000
      4.15 35.01 27.80
                          30.9
                                 50.3 1500.30 2.0907
                                                       2903.8
```

AUGUST 03, 1971	04.1	7
LATITUDE	17	25
LONGITUDE	76	34
DEPTH TO BOTTOM	1970	*4

```
S
                   SIGT
                         TANOM
                                SVA
                                       SVEL
                                               TNHGT
                                                        TRANS
  7
       T
  0 27.56 36.02 23.33
                         456.2 456.2 1541.96
                                                           .0
                                                .0000
  20 27.57 36.01 23.32
                         457.3 458.1 1542.30
                                                           .9
                                                .0914
  40 27.49 36.16 23.45
                         444.0 445.7 1542.58
                                                .1818
                                                          3.6
  60 27.08 36.20 23.62
                         428.5 431.0 1542.03
                                                .2695
                                                          8.2
  80 26.75 36.26 23.77
                         414.1 417.5 1541.66
                                                .3543
                                                         14.4
 100 26.27 36.36 23.99
                         392.4 396.6 1540.98
                                                .4358
                                                         22.3
 120 25.73 36.45 24.23
                         369.8 374.8 1540.14
                                                .5129
                                                         31.8
 140 25.09 36.56 24.51
                         343.1 348.8 1539.05
                                                .5853
                                                         42.8
 160 24.38 36.65 24.80
                         316.1 322.6 1537.75
                                                .6524
                                                         55.1
 180 23.28 36.74 25.19
                                                . /132
                         278.5 285.7 1535.45
                                                         68.8
 200 21.85 36.76 25.62
                         238.1 245.9 1532.14
                                                .7664
                                                         83.6
 220 20.99 36.73 25.86
                         215.0 223.4 1529.90
                                                .8133
                                                         99.4
 240 19.91 36.65 26.06
                         195.7 204.6 1527.49
                                                .8561
                                                        116.1
 260 19.03 36.54 26.21
                         181.9 191.2 1525.26
                                                .8957
                                                        133.6
 280 18.31 36.48 26.34
                         168.8 178.7 1523.47
                                                .9327
                                                        151.9
 300 17.82 36.43 26.43
                         160.9 171.2 1522.32
                                                .9677
                                                        170.9
 340 16.99 36.30 26.53
                         151.1 162.5 1520.39 1.0341
                                                        210.9
 380 15.77 36.10 26.66
                         138.6 150.6 1517.12 1.0969
                                                        253.6
 420 14.79 35.92 26.74
                         130,9 143.5 1514.50 1.1559
                                                        298.6
 460 13.91 35.74 26.80
                         126.1 139.3 1512.11 1.2126
                                                        346.0
 500 12.63 35.53 26.90
                         116.6 129.9 1508.27 1.2662
                                                        395.6
 540 11.56 35.38 26.99
                         108.0 121.3 1505.08 1.3162
                                                        447.3
 580 10.34 35.29 27.05
                         102.0 115.6 1503.10 1.3637
                                                        500.9
 620 10.21 35.21 27.10
                          97.3 111.1 1501.40 1.4090
                                                        556.3
660
      9.19 35.09 27.18
                          89.9 103.3 1498.19 1.4518
                                                        613.5
 700
      8.33 35.00 27.24
                          83.6
                                96.6 1495.51 1.4918
                                                        672.4
      7.91 34.95 27.27
                          81.2
                                94.4 1494.50 1.5301
 740
                                                        732.9
 780
      7.30 34.90 27.32
                          76.5
                                89.4 1492.75 1.5668
                                                        794.8
 820
      6.87 34.87 27.36
                          73.0
                                85.8 1491.68 1.6018
                                                        858.2
      6.48 34.87 27.41
                                80.7 1490.80 1.6352
 860
                          68.0
                                                        922.9
      6,21 34.86 27.44
 900
                          65.4
                                 78.2 1490.37 1.6669
                                                        989.0
 940
      5.83 34.87 27.49
                          60.0
                                72.6 1489.52 1.6971
                                                       1056.3
 980
      5.59 34.89 27.54
                          55.6
                                 68.4 1489.24 1.7252
                                                       1124.7
      5.44 34.90 27.56
1020
                          53.2
                                 66.1 1489.30 1.7522
                                                       1194.3
      5.01 34.93 27.64
1100
                          46.0
                                 59.0 1488.90 1.8020
                                                       1336.5
1200
      4.67 34.96 27.70
                          40.1
                                 53.3 1489.18 1.8579
                                                       1519.5
1300
      4.43 34.97 27.74
                          36.8
                                 50.4 1489.85 1.9094
                                                       1707.9
1400
      4.33 34.98 27.76
                          35.0
                                 49.4 1491.09 1.9589
                                                       1901.3
                          34.0
1500
      4.23 34.98 27.77
                                 49.0 1492.32 2.0082
                                                       2099.6
                          33.3
      4.16 34.98 27.77
1600
                                 49.0 1493.68 2.0571
                                                       2302.9
1700
      4.11 34.99 27.79
                          32.0
                                 48.5 1495.14 2.1059
                                                       2511.1
1800
      4.09 34.98 27.78
                          32.6
                                 49.9 1496.69 2.1553
                                                       2724.1
1900
      4.17 34.99 27.78
                          32.6
                                 51.2 1498.70 2.2051
                                                       2942.1
```

STD STATION NUMBER	56
AUGUST 10, 1971	03.3 7
LATITUDE	18 46
LONGITUDE	76 24
DEPTH TO BOTTOM	3015 M

```
S
                   SIGT
                         MOMAT
                                SVA
                                       SVEL
                                              DYNHGT
                                                        TRANS
   0 29.21 36.24 22.95
                         492.6 492.6 1545.70
                                               .0000
                                                           . 0
  20 29.09 36.22 22.97
                         490.2 491.1 1545.75
                                                .0984
                                                          1.0
  40 28.74 36.20 23.07
                         480.4 482.1 1545.32
                                                          3.9
                                                .1957
  60 27.17 36.25 23.65
                         427.7 430.2 1542.27
                                               .2869
                                                          8.8
  80 25.75 36.36 24.16
                         376.9 380.2 1539.46
                                                .3680
                                                         15.3
 100 24.73 36.51 24.58
                         336.2 340.3 1537.51
                                                .4400
                                                         23.4
 120 23.98 36.64 24.94
                         302.6 307.4 1535.88
                                                .5048
                                                         32.8
                         273.7 279.3 1534.43
 140 23.13 36.75 25.24
                                               .5635
                                                         43.5
 160 22.33 36.80 25.51
                         248.1 254.4 1532.77
                                                .6168
                                                         55.3
 180 21.53 36.78 25.72
                         228.2 235.1 1531.00
                                                .6658
                                                         68.1
 200 20.45 36.69 25.95
                         206.6 214.1 1528.36
                                                .7107
                                                         81.9
                                                .7521
220 19.60 36.60 26.11
                         191.6 199.6 1526.27
                                                         96.5
                                               .7907
 240 18.68 36.48 26.25
                         177.7 186.2 1523.89
                                                        112.0
260 17.85 36.38 26.38
                         165.2 174.2 1521.72
                                               .8267
                                                        128.1
280 17.24 36.31 26.48
                         156.1 165.6 1520.18
                                                        145.0
                                                .8607
 300 16.70 36.22 26.54
                         150.4 160.3 1518.79
                                               .8933
                                                        162.5
 340 15.93 36.12 26.64
                         140.6 151.5 1516.99
                                                        199.5
                                               .9555
                         131.0 142.7 1514.96 1.0143
 380 15.11 36.01 26.74
                                                        238.9
                         124.1 136.5 1512.95 1.0701
420 14.32 35.8H 26.82
                                                        280.6
 460 13.65 35.75 26.86
                         120.2 133.2 1511.27 1.1238
                                                        324.5
 500 12.57 35.60 26.96
                         110.3 123.6 1508.15 1.1751
                                                        370.5
 540 12.12 35.54 27.00
                                                        418.5
                         106.4 120.3 1507.20 1.2238
 580 11.54 35.46 27.05
                                                        468.4
                         101.7 116.1 1505.76 1.2711
 620 10.98 35.38 27.09
                          97.8 112.5 1504.35 1.3169
                                                        520.1
 660 10.57 35.29 27.13
                          94.1 109.0 1502.72 1.3611
                                                        573.7
 700
      9.53 35.18 27.19
                          88.5 103.2 1500.20 1.4038
                                                        629.0
 740
      8.52 35.04 27.25
                          83.4
                                97.5 1496.93 1.4439
                                                        686.0
 780
      7.25 34.91 27.33
                          75.1
                                87.9 1492.57 1.4811
                                                        744.5
      6.37 34.87 27.42
                                78.6 1489.72 1.5141
                                                        804.4
820
                          66.6
      5.86 34.87 27.49
                                                        865.6
860
                          60.3
                                72.0 1488.34 1.5443
 900
      5.60 34.88 27.53
                          56.5
                                68.2 1487.96 1.5723
                                                        927.9
940
      5.32 34.90 27.58
                          51.8
                                63.5 1487.51 1.5987
                                                        991.3
980
                          49.1
      5.15 34.91 27.61
                                60.9 1487.49 1.6235
                                                       1055.8
      5.00 34.92 27.63
                                58.7 1487.54 1.6475
1020
                          46.7
                                                       1121.2
      4.77 34.93 27.67
1100
                          43.4
                                55.8 1487.92 1.6929
                                                       1254.8
1200
      4.59 34.96 27.71
                          39.2
                                52.3 1488.86 1.7468
                                                       1426.9
1300
      4.49 34.97 27.73
                          37.4
                                51.2 1490.10 1.7984
                                                       1604.1
1400
      4.37 34.98 27.75
                          35.4
                                49.9 1491.26 1.8491
                                                       1786.5
1500
      4.30 34.98 27.76
                          34.7
                                49.9 1492.61 1.8990
                                                       1973.9
      4.31 35.00 27.77
1600
                          33.3
                                49.6 1494.33 1.9484
                                                       2166.3
1700
      4.27 35.00 27.78
                          32.9
                                50.0 1495.81 1.9981
                                                       2363.6
1800
                          32.4
                                50.2 1497.26 2.0482
                                                       2565.9
      4.22 35.00 27.78
1900
      4.19 35.00 27.79
                          32.1
                                50.7 1498.79 2.0987
                                                       2773.3
      4.17 35.00 27.79
                          31.9
                                51.4 1500.37 2.1497
                                                       2985.7
2000
```

```
STD STATION NUMBER 57
AUGUST 10, 1971 16.0 Z
LATITUDE 19 24
LONGITUDE 77 26
DEPTH TO BOTTOM M

T S SIGT TANOM
```

```
SIGT
                         TANOM
                                SVA
                                       SVEI.
                                              TYNHET
                                                        TRANS
   0 28.82 36.16 23.02
                         485.8 485.9 1544.81
                                                .0000
                                                           • 0
  20 28.07 35.98 23.13
                         475.0 475.9 1543.36
                                                .0962
                                                          1.0
  40 27.30 36.04 23.43
                         446.8 448.5 1542.05
                                                .1886
                                                          3.8
  60 26.92 36.11 23.60
                                                .2767
                         430.1 432.6 1541.59
                                                          8.5
  80 26.29 36.26 23.91
                                                . 5603
                         400.2 403.5 1540.62
                                                         14.8
 100 25.60 36.38 24.22
                         371.0 375.1 1539.45
                                                .4382
                                                         22.8
 120 24.77 36.49 24.56
                         358.8 343.7 1537.91
                                               .5101
                                                         32.3
 140 24.18 36.58 24.80
                         315.4 321.1 1536.88
                                               .5766
                                                         43.2
 160 23.54 36.66 25.05
                         291.6 298.0 1535.70
                                                         55.3
                                               .6385
 180 22.58 36.73 25.39
                         260.0 267.1 1533.67
                                               .6950
                                                         68.7
                         227.8 235.5 1531.12
                                               . 7452
 200 21.46 36.76 25.72
                                                         83.1
                                                .7898
 220 20.35 36.72 26.00
                         201.8 210.1 1528.44
                                                         98.4
 240 19.49 36.66 26.18
                         184.5 193.3 1526.34
                                                .8301
                                                        114.6
 260 18.91 36.60 26.31
                         172.2 181.5 1524.69
                                               . 9676
                                                        131.6
 280 18.34 36.54 26.38
                         165.2 175.0 1523.61
                                                .9032
                                                        149.3
 300 17.99 36.50 26.44
                         159.9 170.2 1522.89
                                               .9378
                                                        167.7
 340 17.37 35.41 26.52
                         151.9 163.4 1521.63 1.0045
                                                        206.6
 380 16.71 36.28 26.58
                         146.3 158.8 1520.17 1.0689
                                                        248.0
 420 15.74 36.10 26.67
                         137.9 151.2 1517.67 1.1309
                                                        292.0
 460 14.38 35.87 26.80
                         126.1 139.6 1513.77 1.1891
                                                        338.4
 500 13.48 35.74 26.89
                         117.5 131.6 1511.35 1.2433
                                                        387.1
 540 12.60 35.60 26.96
                         110.9 125.2 1508.90 1.2947
                                                        437.9
 580 11.59 35.45 27.03
                         103.4 117.8 1595.92 1.3434
                                                        490.6
 620
     10.77 35.32 27.08
                          98.6 113.1 1503.53 1.3894
                                                        545.3
      9.71 35.16 27.15
 660
                          92.9 106.9 1500.18 1.4335
                                                        601.8
                          87.4 100.9 1496.89 1.4749
 700
      8.69 35.02 27.20
                                                        659.9
 740
      8.23 34.97 27.24
                          84.4
                                97.9 1495.74 1.5145
                                                        719.7
 780
      7.63 34.93 27.29
                          78.8
                                92.2 1494.06 1.5524
                                                        781.1
 820
                          75.2
      7.15 34.89 27.33
                                88.5 1492.80 1.5885
                                                        843.9
      6.53 34.86 27.39
                                82.2 1490.99 1.6229
 860
                          69.4
                                                        908.1
 900
      6.11 34.86 27.45
                                76.8 1480.98 1.654R
                          64.1
                                                        973.7
 940
      5.75 34.86 27.49
                          59.8
                                72.3 1489.19 1.6847
                                                       1040.5
 980
      5.51 34.88 27.54
                          55.5
                                68.0 1488.90 1.7127
                                                       1108.4
      5.20 34.90 27.59
1020
                          50.4
                                62.8 1488.33 1.7389
                                                       1177.5
      4.81 34.93 27.66
                          43.A
1100
                                56.3 1488.08 1.7858
                                                       1318.5
      4.60 34.95 27.70
                          40.1
1200
                                                       1499.8
                                53.1 1488.88 1.8403
                          37.9
      4.46 34.96 27.73
                                51.6 1489.96 1.8923
1300
                                                       1686.5
      4.37 34.97 27.74
1400
                          36.2
                                50.6 1491.24 1.9438
                                                       1878.3
1500
      4.32 34.97 27.75
                          35.7
                                 50.9 1492.68 1.9945
                                                       2075.2
                          34.3
      4.26 34.98 27.76
                                                       2277.2
1600
                                 50.4 1494.09 2.0453
      4.23 34.98 27.77
1700
                          34.0
                                50.9 1495.62 2.0959
                                                       2484.2
1800
      4.22 34.99 27.78
                          33.1
                                 51.0 1497.25 2.1467
                                                       2696.4
1900
      4.20 34.99 27.78
                          32.9
                                 51.6 1498.82 2.1981
                                                       2913.6
      4.18 35.00 27.79
                          32.0
                                 51.5 1500.41 2.2496
2000
                                                       3136.0
```

```
      STD STATION NUMBER
      58

      AUGUST 10, 1971
      21.3 Z

      LATITUDE
      19 57

      LONGITUDE
      78 27

      DEPTH TO ROTTOM
      1756 M
```

			5			SVA	-	DANHEL	TRANS
		29.17					1545.49	•0000	• 0
		28.97		22.97			1545.45	.0993	1.0
	411	28.32		23.14	474.3		1544.34	.1960	3.9
		27.10					1541.72	.2675	8.8
	80	25.99	36.17	23.97		398.0	1539.62	.3712	15.4
	100	25.15					1538.39	.4472	23.6
	150	24.28	36.60				1536.82	.5155	33.2
	140	23.39					1535.06	.5766	44.1
	160	25.09	36.77				1532.05	.6304	56.2
	180	21.02	34.75	25.84	216.9	223.8	1529.62	.6777	69.2
	500	19.35	36.60	26.11	191.3	198.7	1526.72	.7199	83.2
	220	18.95	36.61	26.28	174.8	182.8	1524.45	.7581	98.0
	2411	18.50	36.57	26.37	166.8	175.4	1523.46	.7939	113.5
	560	18.17	36.53	26.42	161.9	171.0	1522.79	.8285	129.7
	280	17.94	36.50	26.45	158.6	168.3	1522.42	· P624	146.7
	300	17.65	36.46	26.49	154.7	165.0	1521.86	.8958	164.2
	3411	16.91	36.33	26.57	147.1	158.5	1520.18	.9602	201.4
	380	16.37	36.24	26.63	141.6	153.9	1519,10	1.0226	241.0
	4211	15.15	35.99	26.72	133.3	146.2	1515.71	1.0825	283.1
	460	14.25	35.84	26.80	125.6	139.1	1513.32	1.1397	327.6
	500	13.14	35.67	26.90	116.1	129.8	1510.14	1.1931	374.2
	541	12.19	35.53	26.48	108.4	122.3	1507.43	1.2435	423.0
	580	11.21	35.38	27.05	101.8	115.8	1504.51	1.2913	473.7
	650	10.24	35.23	27.11			1501.54	1.5365	526.3
	660	9.35		27.17	90.0	104.5	1498.80	1.3792	580.6
	700	8.58		27.21	86.5	99.9	1496.46	1.4201	636.6
	740	7.92		27.27	81.4	94.5	1494.54	1.4590	694.1
	780	7.16		27.32	76.1	88.8	1492.18	1.4957	753.2
	850	6.13	34.86	27.37	71.9	84.5	1491.13	1.5303	813.8
	860	6.30	34.86	27.42	66.5	78.9	1490.08	1.5629	875.6
	900	5.91		27.48	60.9	73.2	1489.19	1.5934	938 • 8
	940	5.58		27.54	55.5	67.7	1488.55	1.6215	1003.1
	980	5.25	34.91	27.60	50.2	62.3	1487.89	1.6477	1068.5
	1020	5.01	34.93	27.64	46.0	58.1	1487.60	1.6717	1134.9
	1100	4.70		27.69	41.2	53.4	1487.66	1.7165	1270 • 4
	1200	4.47	34.96	27.73	38.0	50.7	1488.36	1.7683	1444.7
	1300	4.75	34.97		36.0	49.4	1489.52	1.8181	1624.0
	1400	4.28		27.76	34.5	48.7	1490.88	1.8672	1808.3
-	1500	4.24		27.77	34.1	49.1	1492.36	1.9161	1997.4
	1600	4.21		27.78	33.0	48.9	1493.90	1.9653	2191.5
	1700	4.23	34.98	27.77	34.0	50.9	1495.62	2.0148	2390.5

STD STATION NUMBER	59
AUGUST 11, 1971	04.7 7
LATITUDE	19 41
LONGITUDE	78 24
DEPTH TO BOTTOM	1756 M

7			CICI	TANOM	CVA	CVC	DVNILICT	TOANE
	T		SIGT			SVEL	TYNHGT	TRANS
	29.42		22.85			1546.11	.0000	• 0
	29.19	36.20			495.7	1545.95	.0997	1.0
	28.84		23.01		488.2	1545.50	.1981	4.0
	27.08		23.53	437.1		1541.92	.2909	8.9
80	26.13	36.21	23.93	399.0		1540.21	.3751	15.5
100	25.1R	36.42	24.38		359.9	1538.50	.4513	23.8
120	24.13	36.62			316.0	1536.47	.5189	33.5
140	23.09	36.75		272.6		1534.33	.5783	44.5
160	22.04		25.56	243.2		1531.99	.6311	56.6
180	21.24		25.77		230.3	1530.20	.6791	69.7
200	20.42	36.71	25.97	204.3	and the same of the same	1528.30	.7233	83.7
550	19.48	36.63			194.5	1525.96	. 1639	98.6
240	18.54	36.52	26.32		179.9	1523.53	.8014	114.2
560	17.98	36.47			170.8	1522.19	.8364	130.6
280	17.46		26.48		165.6	1520.90	.8701	147.7
300	17.47		26.51	152.7	162.9		.9029	165.4
340	17.07		26.57		159.3	1520.70	.9673	202.8
380	16,17	36.16			155.2	1518.41	1.0304	242.7
420	15.41		26.71		146.8	1516.60	1.0910	285.2
460	14.67		26.78	127.7	141.4	1514.77	1.1486	330.0
500	13.35		26.88		131.8	1510.87	1.2033	377.0
540	12.72	35,60	26.93	113.2	127.6	1509.30	1.2550	426.2
580	the second second	35.44	27.01		120.4	1506.25	1.3047	477.4
650	10.90		27.07	100.1	114.7	1504.01	1.3518	530.5
660	10.20	35.24	27.12	94.9	109.6	1502.05	1.3966	585.5
700	9.42	35.14	27.18	89.8	104.3	1499.74	1.4395	642.2
740	8.45		27.23	84.6	98.5	1496.62	1.4801	700.6
780	7.45	34.93	27.32	76.3	89.4	1493.37	1.5179	760.6
820		34.89	27.39	70.1	82.7	1491.28	1.5523	822.0
860	6.04	34.88	27.47	61.A	73.8	1489.08	1.5841	884.7
900	5.60	34.90	27.55	55.0	66.8	1487.99	1.6121	948.7
940	5.29	34.91	27.59	50.7	62.3	1487.40	1.6378	1013.7
980	5.19	34.91	27.60	49.5	61.5	1487.65	1.6626	1079.7
1020	4.99		27.64	45.8	57.A	1487.51	1.6865	1146.7
1100	4.63		27.70	40.4	52.5	1487.37	1.7305	1283.4
1200	-		27,73	37.9	50.6	1488.32	1.7815	1459.0
1300	4.36		27,75	36.1	49.5	1489.56	1.8311	1639.6
1490	4.29		27,76	34.6	48.8	1490.93	1.8801	1825.2
1500	4.24	34.99	27.77	33.3	48.4	1492.38	1.9287	2015.6

```
78 27
    LONGITUDE
    DEPTH TO BOTTOM
                         5523 M
             S
                  SIGT
                                              THHET
                                                        TRANS
       T
                         TANOM SVA
                                      SVEL
  0 29.01 36.15 22.95
                         492.7 492.7 1545.20
                                                          • 0
                                               .0000
 20 28.79 36.12 23.00
                         487.8 488.6 1545.03
                                               . 981
                                                          1.0
 40 28.07 36.07 23.20
                         468.6 470.3 1543.77
                                               .1940
                                                          3.9
 60 26.85 36.05 23.58
                         432.3 434.8 1541.38
                                               .2845
                                                          8.7
 80 26.05 36.13 23.89
                         402.4 405.7 1539.95
                                               .3686
                                                         15.2
 100 25.68 36.26 24.10
                         382.0 386.1 1539.53
                                               .4477
                                                         23.4
120 24.97 36.52 24.52
                         342.5 347.4 1538.41
                                                         33.1
                                               .5211
140 24.02 36.65 24.90
                         305.8 311.5 1536.55
                                                         44.2
                                               .5870
                         272.3 278.7 1534.63
 160 23.08 36.75 25.26
                                                         56.5
                                               .6460
 180 21.74 36.77 25.65
                         234.5 241.4 1531.54
                                                         69.9
                                               .6980
200 20.70 36.73 25.91
                                               .7439
                         210.1 217.6 1529.07
                                                         84.3
220 19.75 36.66 26.11
                         191.0 199.1 1526.74
                                                         99.6
                                               .7856
240 19.07 36.60 26.24
                         178.5 187.2 1525.11
                                               .8242
                                                        115.7
260 18.49 36.53 26.34
                         169.5 178.7 1523.71
                                               .8608
                                                        132.6
280 17.97 36.47 26.42
                         161.5 171.2 1522.48
                                               .8958
                                                        150.2
300 17.67 36.45 26.48
                         155.9 166.2 1521.90
                                               .9295
                                                       168.4
340 16.86 36.32 26.58
                         146.7 158.0 1520.02
                                               .9948
                                                       206.9
380 16.54 36.25 26.60
                         144.6 157.1 1519.63 1.0580
                                                       248.0
420 15.44 36.03 26.68
                         136.6 149.6 1516.66 1.1194
                                                       291.5
460 14.44 35.87 26.78
                         127.3 140.9 1513.97 1.1774
                                                       337.5
500 13.28 35.67 26.87
                         118.8 132.6 1510.61 1.2322
                                                        385.7
540 12.15 35.49 26.96
                         110.6 124.5 1507.24 1.2835
                                                        436.0
580 11.17 35.34 27.03
                         104.1 118.0 1504.32 1.3320
                                                       488.3
620 10.75 35.23 27.09
                          98.2 112.1 1501.93 1.3779
                                                        542.5
      9.74 35.16 27.14
                          93.4 107.5 1500.29 1.4219
                                                       598.5
660
700
      8.40 35.03 27.19
                          88.3 102.0 1497.31 1.4640
                                                       656.2
740
      8.16 34.95 27.23
                          84.8
                                98.3 1495.45 1.5041
                                                        715.6
                          80.1
780
      7.40 34.87 27.28
                                93.1 1493.09 1.5423
                                                       776.5
                          74.7
      6.71 34.82 27.34
820
                                87.1 1490.99 1.5784
                                                       838.9
                          70.3
      6.37 34.82 27.38
860
                                82.8 1490.30 1.6123
                                                       902.8
      6.07 34.85 27.45
900
                          64.4
                                76.9 1489.80 1.6442
                                                       967.9
940
      5.69 34.87 27.51
                          58.3
                                                      1034.3
                                70.7 1488.96 1.6735
980
      5.41 34.90 27.57
                          52.A
                                65.2 1488.53 1.7007
                                                      1101.7
1020
      5.10 34.92 27.62
                          47.A
                                60.0 1487.95 1.7257
                                                      1170.3
      4.75 34.95 27.69
1100
                          41.7
                                54.1 1487.86 1.7712
                                                      1310.2
1200
      4.53 34.96 27.72
                                51.5 1488.61 1.8240
                                                      1490.0
                          38.6
1300
      4.41 34.97 27.74
                                50.2 1489.77 1.8749
                                                      1674.9
                          36.6
1400
      4.34 34.98 27.76
                          35.1
                                49.5 1491.13 1.9248
                                                      1864.9
      4.27 34.98 27.76
                                49.5 1492.49 1.9741
1500
                          34.4
                                                      2059.9
                                48.8 1494.08 2.0237
      4.25 35.00 27.78
                          32.7
                                                      2259.7
1600
1700
      4.22 35.00 27.78
                          32.4
                                49.3 1495.61 2.0731
                                                      2464.6
1800
      4.20 34.99 27.78
                          32.9
                                50.7 1497.16 2.1230
                                                      2674.4
                                50.4 1498.71 2.1735
      4.17 35.00 27.79
                          31.9
```

60 13.9 /

19 10

STD STATION NUMBER

AUGUST 11. 1971

LATITUDE

1900

2000

4.17 35.00 27.79

51.4 1500.37 2.2244

31.9

2889.2

3109.1

STD STATION NUMBER	A60
AUGUST 11, 1971	17.5 /
LATTIUDE	19 12
LONGITUDE	78 24
PEPTH TO BOTTOM	31172 M

7	T	5	SICI	TANOM	SVA	SVEL	TYNHGT	TRANS
0	29.29	36.15	22.85	501.7	501.7	1545.79	•0000	• 0
50	28,92	36.12	22.95	491.9	492.8	1545.31	.0994	1.0
40	28.39	36.09	23.11	477.2	478.9	1544.48	.1966	4.0
60	27.38	36.05	23.41	448.5	451.0	1542.56	.2896	8.8
80	26.36	36.10	23.77	413.8	417.1	1540.63	. 5764	15.5
100	25,20	36.19	24.01		394.7	1539.75	.4576	23.8
120	25.23	36.43	24.37	356.5	361.5	1538.95	.5332	33.7
140	23.03	36.64	24.92	304.0	309.6	1536.32	.6004	45.1
160	22.56	36.75	25.41	258.0	264.3	1533.32	.6577	57.6
180	21.53	36.76	25.70	229.6	236.6	1530.98	.7078	71.3
200	20.58	36.71	25.93	208.4	216.0	1528.73	.7531	85.9
550	19.85	36.66	26.08	193.5	201.6	1527.01	. 1949	1.01 - 4
241)		36.60	26.22	180.5	189.1	1525.33	.8339	117.7
260	18.56	36.53	26.32	171.2	180.4	1523.91	.8709	134.7
280	17.98	36.46	26.41	162.5	172.2	1522.50	.9061	152.5
300	17.54	36.40	26.47	156.5	166.7	1521.47	.9400	171.0
340	16.85	36.29	26.56	148.7	160.0	1519.96	1.0054	209.9
380	16.09	36.15	26.63	141.9	154.1	1518.15	1.0682	251.3
420	14.38	35.96	26.73	131.0	144.7	1515.14	1.1276	295.3
460	14.05	35.74	26.80	125.2	138.5	1512.62	1.1545	341.5
500	12.77	35.57	26.90	116.3	129.7	1508.79	1.2381	390.0
540	11.76	35.41	26.97	109.4	122.9	1505.81	1.2884	440.5
580	10.92	35.30	27.114	102.7	116.5	1503.39	1.5361	493.0
650	10.23	35.20	27.119	98.4	112.2	1501.46	1.5819	547.4
661	9.64	35.12	27.13	94.7	108.7	1499.87	1.4260	603.5
700	8.08	35.03	27.18	A9.6	103.3	1497.61	1.4684	661.4
740	8.06	34.95	27.23	84.9	98.2	1495.05	1.5086	721.0
780	7.36	34.87	27.29	79.6	92.5	1492.94	1.5468	782.1
820	6.79	34.83		75.0	87.6	1491.32	1.5827	844.7
860	6.37	34.83	27.39	69.6	82.1	1490.32	1.6167	908.7
900	6.08	34.86	27.45	63.8	76.3	1489.86	1.6484	974.0
940	5.68	34.88	27.52	57.5	69.8	1488.94	1.6775	1040.5
980	5.42	34.89	27.56	53.7	66.0	1488.55	1.7045	1108.2
<b>1</b> 050	5.13	34.91	27.61	48.0	61.1	1488.06	1./299	1176.9
1100	4.72		27.68	42.1	54.4	1487.73	1.7757	1317.1
1500	4.53		27.72	38.6	51.5	1488.61	1.8284	1497.3
1300	4.40	34.97	27.74	36.5	50.1	1489.72	1.8790	1682.7
14110	4.53		27.76	35,0	49.4	1491.09	1.9290	1873.1
1500	4.27	34.98	27.76	34.4	49.5	1492.49	1.9784	2068.5

```
AUGUST 12, 1971 01.5 / LATITUDE 18 39 LONGITUDE 78 24 DEPTH-TO BOITOM 4655 M
```

```
TRANS
                         TANOM SVA
                                      SVEL
                                              TYNHGT
                         492.5 492.5 1544.17
  0 28.60 35.97 22.95
                                              ·uono
                                                          • 0
                         459.6 460.5 1543.12
                                                         1.0
 20 27.90 36.12 23.29
                                              .0953
 40 27.14 36.06 23.49
                         440.4 442.1 1541.71
                                                         3.8
                                               .1856
                        429.9 432.4 1541.51
 60 26.39 36.10 23.60
                                               .2730
                                                         8.3
  90 26.76 36.15 23.68
                         422.3 425.7 1541.59
                                               . 3588
                                                        14.7
 100 26.08 36.23 23.80
                        411.1 415.3 1541.58
                                               .4429
                                                        22.7
                                              .5241
                         391.4 396.4 1540.97
120 26.14 36.32 24.01
                                                        32.4
                         347.4 353.2 1539.14
                                              .5990
140 25.14 36.52 24.47
                                                        43.6
 160 23.00 36.69 24.97
                        299.5 306.0 1536.62
                                              .6650
                                                        56.2
                                              . 7225
 180 22.79 36.78 25.36
                        262.1 269.3 1534.25
                                                        70.1
                                              .7731
200 21.60 36.79 25.71
                        229.3 237.0 1531.51
                                                        85.1
220 20.119 36.76 25.99
                        202.5 210.8 1528.85
                                              .8179
                                                       101.0
240 19.53 35.67 26.18
                        184.8 193.6 1526.46
                                              .8583
                                                       117.7
260 18.77 36.58 26.33
                        170.2 179.5 1524.27
                                              .8956
                                                       135.3
280 18.18 35.53 26.42
                        162.1 171.9 1523,14
                                              .9308
                                                       153.5
                        156.0 166.4 1522.32
                                              .9646
300 17.80 36.40 26.48
                                                       172.5
340 17.29 36.41 26.54
                        150.0 161.5 1521.39 1.0304
                                                       212.4
                         143.6 156.1 1519.71 1.0941
                                                       254.9
380 16.56 36.27 26.61
420 15.31 36.15 26.69
                         135.8 149.1 1517.94 1.1551
                                                       299.9
460 14.72 35.96 26.79
                         126.5 140.3 1514.96 1.2132
                                                       347.2
500 13.60 35.78 26.89
                         117.0 131.1 1511.79 1.2674
                                                       396.9
                        106.0 120.0 1507.58 1.3175
                                                       448.6
540 12.22 35.57 27.01
580 11.34 35.43 27.07
                         100.4 114.5 1505.02 1.3643
                                                       502.2
620 10.61 35.33 27.12
                         95.2 109.4 1502.98 1.4091
                                                       557.7
      9.03 35.24 27.17
                          90.5 104.9 1501.08 1.4518
                                                       614.9
660
                          85.6 99.5 1498.00 1.4927
700
      8.96 35.10 27.22
                                                       673.8
740
      7.03 34.95 27.27
                          81.5
                               94.7 1494.58 1.5316
                                                       734.3
                          76.9
 781
      7.22 34.88 27.31
                               89.6 1492.41 1.5684
                                                       796.3
      6.84 34.87 27.36
                          72.6
                               85.4 1491.57 1.6035
                                                       859.8
820
      6.31 34.84 27.41
                                80.5 1490.09 1.6367
                                                       924.6
860
                          68.1
                                                       990.7
900
      6.01 34.87 27.47
                          62.2
                               74.6 1489.59 1.6678
                                68.6 1488.57 1.6964
      5,59 34.88 27.53
                                                      1057.9
940
                          56.4
      5.33 34.90 27.58
                                64.1 1488.20 1.7229
                          51.9
                                                      1126.3
980
                                60.1 1487.99 1.7478
      5.11 34.92 27.62
                          47.9
                                                      1195.8
1020
      4.89 34.94 27.66
                          44.0
                                56.6 1488.42 1.7944
                                                      1337.5
1100
1200
      4.69 34.95 27.69
                          41.0
                                54.3 1489.25 1.8499
                                                      1519.7
1300
      4.51 34.96 27.72
                          38.4
                                52.2 1490.16 1.9029
                                                      1707.4
                                50.9 1491.32 1.9541
1400
      4.39 34.97 27.74
                          36.4
                                                      1900.2
      4.32 34.98 27.76
                          34.9 50.2 1492.69 2.0046
                                                      2098.2
1500
```

```
STD STATION NUMBER 62
AUGUST 12, 1971 08.9 /
LATITUDE 18 21
LONGITUDE 78 34
DEPTH TO BOTTOM 2210 M

T S SIGT TANOM SVA
1 27.68 36.03 23.29 459.3 459.3
1 27.64 36.03 23.31 458.0 458.9
1 27.26 36.07 23.46 443.4 445.1
2 27.04 36.14 23.58 431.6 434.1
2 26.78 36.22 23.73 417.9 421.3
```

STD STATION NUMBER	63
AUGUST 12, 1971	17.2 /
LATTIUDE	18 1"
LONGITUDE	78 39
PEPTH TO ROTTOM	2250 M

```
DYNHGT
                   SIGT
                         TANIOM
                                SVA
                                       SVEL
                                                        TRANS
   0 29.12 36.23 22.97
                         490.4 490.4 1545.50
                                                .0000
                                                           .0
  20 28.55 36.16 23.11
                         477.3 478.1 1544.56
                                                .11969
                                                          1.0
  40 27.84 36.02 23.23
                         465.0 466.6 1543.22
                                                .1913
                                                          3.9
  60 27.59 36.13 23.40
                         449.3 451.8 1543.10
                                                .2832
                                                          8.6
 80 27.20 36.15 23.54
                         435.8 439.2 1542.58
                                                . 5723
                                                         15.2
                         415.1 419.2 1541.87
 100 26.71 36.23 23.76
                                                .4581
                                                         23.5
 120 26.44 36.26 23.87
                         404.7 409.7 1541.61
                                                         33.4
                                                .5410
                         384.0 389.8 1540.85
 140 25.94 36.34 24.08
                                                         45.1
                                                .6210
 160 25.17 36.45 24.40
                         353.3 359.9 1539.47
                                                .6959
                                                         58.2
 180 24.53 36.59 24.77
                         319.0 326.3 1537.90
                                                . 7646
                                                         72.8
200 23.31 36.72 25.17
                         280.8 288.8 1535.83
                                                .8261
                                                         88.7
                         244.5 253.0 1533.23
220 22.14 36.78 25.55
                                                .8802
                                                        105.8
240 21.11 36.75 25.81
                         219.3 228.4 1530.83
                                                .9284
                                                        123.9
260 19.76 35.65 26.10
                         192.0 201.5 1527.40
                                                .9714
                                                        142.9
 280 18.92 36.57 26.26
                         177.0 187.0 1525.30 1.0103
                                                        162.7
 300 18.42 36.51 26.34
                         169.3 179.8 1524.14 1.0469
                                                        183.3
 340 17.32 36.36 26.50
                         154.3 165.8 1521.43 1.1163
                                                        226.6
 380 16.39 36.20 26.60
                         144.9 157.3 1519.12 1.1g06
                                                        272.5
                                                        321.0
420 15.33 36.04 26.72
                         133.5 146.5 1516.33 1.2413
460 14.38 35.89 26.P1
                         124.6 138.2 1513.79 1.2982
                                                        371.7
500 13.24 35.65 26.97
                         119.5 133.2 1510.45 1.3526
                                                        424.8
                                                        479.9
 540 12.25 35.51 26.95
                         111.0 125.0 1507.61 1.4041
 580 11.75 35.45 27.00
                         106.2 120.8 1506.47 1.4528
                                                        537.1
620 10.97 35.35 27.07
                          99.8 114.5 1504.27 1.5000
                                                        596.1
      9.83 35.17 27.13
                          94.1 108.5 1500.62 1.5446
                                                        657.0
660
                          89.3 103.2 1497.93 1.5868
 7011
      8.96 35.05 27.18
                                                        719.6
 740
      8.20 34.95 27.22
                          85.4
                                98.9 1495.60 1.6271
                                                        783.9
 789
      7.46 34.88 27.28
                          80.2
                                93.3 1493.34 1.6655
                                                        849.8
820
      6.95 34.85 27.33
                          75.6
                                88.5 1491.97 1.7020
                                                        917.1
                          69.5
860
      6.36 34.83 27.39
                                82.0 1490.27 1.7362
                                                        985.9
 900
      6.07 34.83 27.43
                          65.9
                                78.4 1489.77 1.7682
                                                       1056.0
      5.73 34.65 27.49
940
                          60.3
                                72.7 1489.09 1.7984
                                                       1127.3
080
      5.43 34.89 27.56
                          53.8
                                66.2 1488.59 1.8261
                                                       1199.8
1020
      5. 12 34.89 27.57
                          52.5
                                65.2 1488.80 1.8524
                                                       1273.4
      4.94 34.93 27.65
                          45.3
                                58.0 1488.61 1.9013
                                                       1423.6
1100
1200
      4.64 34.95 27.70
                          40.5
                                53.7 1489.05 1.9571
                                                       1616.5
      4.49 34.96 27.72
1300
                          38.2
                                 52.0 1490.08 2.0098
                                                       1814.9
1400
      4.41 34.96 27.73
                          37.3
                                 51.9 1491.39 2.0614
                                                       2018.5
      4.34 34.97 27.75
1500
                          35.9
                                 51.2 1492.76 2.1127
                                                       2227.2
      4.29 34.97 27.75
                          35.3
                                 51.5 1494.20 2.1640
1600
                                                       2441.0
                                                       2659.9
      4.25 34.98 27.77
                          34.2
                                 51.2 1495.70 2.2149
1700
                                 50.4 1497.08 2.2655
      4.18 34.99 27.78
                          32.7
                                                       2884 · U
1800
      4.14 34.90 27.78
                                 50.7 1498.57 2.3158
1900
                          32.3
                                                       3113.0
2000
      4.13 35.00 27.79
                          31.5
                                 50.8 1500.20 2.3662
                                                       3347.1
```

```
      STD STATION NUMBER
      A63

      AUGUST 12, 1971
      20.7 /

      LATITUDE
      18 10

      LONGITUDE
      78 39

      DEPTH TO BOTTOM
      2250 M
```

```
TANO" SVA
                                             DYNHGT
                                                       TRANS
 Z
             5
                  SIGT
                                      SVE
                         492.3 492.3 1545.68
                                                          .0
  0 29.20 36.24 22.95
                                               .0000
  20 28.56 36.24 23.16
                        471.8 472.7 1544.65
                                               . 0965
                                                         1.0
 40 28.18 36.20 23.26
                        462.7 464.4 1544.12
                                                         3.8
                                               .1902
 60 27.53 36.17 23.45
                        444.5 447.1 1543.00
                                               .2814
                                                         8.5
 80 27.25 36.15 23.52
                        437.3 440.7 1542.69
                                               .3701
                                                        15.1
 100 26.91 36.18 23.66
                        424.7 428.9 1542.28
                                               .4571
                                                        23.3
                        410.9 415.9 1542.01
120 20.62 36.25 23.80
                                               . 5416
                                                        33.3
140 26.02 36.25 23.99
                         392.8 398.6 1540.96
                                                        45.0
                                               .6230
160 25.23 36.45 24.39
                         355.1 361.7 1539.61
                                               . 6001
                                                        58.2
180 24.36 36.58 24.75
                         320.5 327.9 1537.97
                                               . 7680
                                                        72.9
200 23.30 36.73 25.18
                         279.9 287.8 1535.81
                                               .8296
                                                        8.88
                        245.0 253.6 1533.51
                                               .8837
229 22.24 36.81 25.54
                                                       106.0
                                               .9322
240 21.50 36.78 25.78
                         222.1 231.3 1531.36
                                                       124.1
260 19.39 36.69 26.10
                         192.3 201.9 1527.79
                                               .9755
                                                       143.2
280 18.43 36.58 26.29
                         174.1 184.1 1525.05 1.0141
                                                       163.1
300 18.31 36.53 26.38
                         165.2 175.7 1523.84 1.0501
                                                       183.7
                        152.9 164.4 1521.55 1.1182
340 17.35 36.39 26.51
                                                       227.1
380 16.28 36.21 26.63
                        141.P 154.U 1518.79 1.1817
                                                       273.1
420 15.28 36.06 26.74
                        131.0 144.0 1516.19 1.2413
                                                       321.6
460 14.16 35.83 26.91
                        124.5 137.9 1513.02 1.2979
                                                       372.4
500 12.92 35.59 26.88
                         117.7 131.2 1509.32 1.3517
                                                       425.4
                         107.7 121.2 1505.65 1.4023
                                                       480.5
540 11.71 35.42 26.99
580 11.28 35.42 27.07
                         100.1 114.2 1504.80 1.4493
                                                       537.5
                         97.2 111.3 1502.56 1.4944
620 10.51 35.2P 27.10
                                                       596.4
      9.56 35.12 27.14
                          93.5 107.3 1499.58 1.5380
                                                       657.1
660
                         89.4 103.1 1497.37 1.5799
700
      8.82 35.02 27.18
                                                       719.4
                               98.7 1495.36 1.6203
740
      8.14 34.94 27.23
                          85.3
                                                       783.4
780
      7.57 34.86 27.28
                          80.4
                                93.4 1492.96 1.6588
                                                       849.0
                          75.8
1158
      6.80 34.82 27.33
                                88.5 1491.34 1.6953
                                                       916.1
1193
      6.43 34.82 27.38
                          71.1
                                83.7 1490.54 1.7298
                                                       984.6
900
      5.98 34.83 27.44
                          64.A
                                77.1 1489.42 1.7618
                                                      1054.4
                          57.8
941
      5.65 34.87 27.52
                                70.1 1488.90 1.7913
                                                      1125.5
980
      5.44 34.88 27.55
                                67.0 1488.62 1.8189
                          54.6
                                                      1197.7
1020
      5.26 34.90 27.59
                          51.1
                                63.6 1488.57 1.8451
                                                      1271.0
      4.94 34.92 27.64
                          46.0
                                58.8 1488.60 1.8941
                                                      1420.6
1100
      4.64 34.94 27.69
1200
                          41.3
                                54.4 1489.03 1.9498
                                                      1612.8
      4.47 34.96 27.73
                                51.7 1490.00 2.0029
                                                      1810.5
1300
                          38.0
      4.38 34.97 27.74
                                50.8 1491.28 2.0544
                                                      2013.3
1400
                          36.3
1500
      4.34 34.97 27.75
                          35.9
                                51.2 1492.76 2.1052
                                                      2221.3
```

```
      STD STATION NUMBER
      64

      AUGUST 12, 1971
      23.7 /

      LATITUDE
      17 56

      LONGITUDE
      78 45

      DEPTH TO BOTTOM
      970 M
```

7	T	S	SIGT	TANOM	5VA	SVEL	DYNHGT	TRANS
0	29,20	34.23	22.94	493.0	493.0	1545.67	.0000	• 0
20	28.62	36.23	23.14	474.4	475.3	1544.77	.0968	1.0
40	27.30	35.13	23.33	455.7	457.3	1543.24	.1901	3.8
60	27.27	36.06	23.45	444.4	446.9	1542.33	.2805	8.5
80	27.22	36.07	23.47	442.2	445.5	1542.55	. 5698	15.0
100	26.36	36.14	23.64	426.1	430.3	1542.13	.4573	23.3
150	26.52	36.24	23.83	408.6	413.6	1541.77	.5417	33.3
140	26.19	36.33	24.00	392.2	398.0	1541.42	.6229	45.0
160	25.91	36.42	24.15	377.3	384.0	1541.18	.7011	58.2
190	25.34	36.52	24.41	353.3	560.7	1540.26	. 1756	73.0
200	24.08	34.71	24.93	303.2	311.3	1537.72	.8428	89.1
550	22.46	36.82	25.49	250.2	258.9	1534.09	.8998	106.6
240	21.14	35.74	25.80	8.025	230.0	1530.90	.9487	125.1
260	19.75	36.63	26.09	193.2	202.7	1527.35	.9919	144.5
Sau	19.03	36.59	26.25	178.2	188.3	1525.63	1.0310	164.7
300	18.37		26.38	165.9	176.5	1524.02	1.0675	185.7
340	17.33	36.40	26.53	151.7	163.2	1521.50	1.1357	229.8
380	16.41	36.21	26.60	144.6	157.0	1519.19	1.1997	276.5
420	15.43	36.02	26.68	137.1	150.1	1516.62	1.2608	325.7
460		35.73		127.0	140.2	1512.13	1.3185	377.3
500	12.61	35,51	26.88	117.7	130.9	1508.18	1.3727	431.1
540	11.73	35.38	26.05	111.0	124.5	1505.67	1.4237	487.0
580	10.73		27.02	104.6	118.0	1502.63	1.4720	545.0
650	9.85		27.08	98.8	112.2	1499,98	1.5180	604.8
660	9.12	35.02		94.0	107.2	1497.84	1.5620	666 • 4
700	8.41		27.18	89.2	102.3	1495.73	1.6040	729.7
740	7.52		27.25	83.2	95.7	1492.88	1.6436	794.7
790	7.03		27.29	79.6	92.0	1491.58	1.6811	861.2
820	6.51	34.82		72.1	84.5	1490.20	1.7162	929.1
860	6.21		27.40	68.3	80.6	1489.67	1.7492	998•4
900	5.82		27.47	62.1	74.2		1.7801	1069.0
940	5.64	34.87	27.52	57.7	70.0	1488.76	1.8087	1140.8

		ATION P		65				
AUGUST 13, 1971				05.3				
	ATITU	(100)		17 4	5			
L	ONGITE	IDE		79 01				
(	DEPTH	to Bot.	ГОМ	951	4			
Z	т	S	SIGT	TANOM	SVA	SVEL	~YNHGT	TRANS
2.0	28.26		22.96	491.1	491.1	1543.32	.0000	•0
20		35.86		477.7		1542.84	.0970	1.0
40		35.96					.1909	3.8
60	27.39		23.39		452.8	1542.57	.2824	8.6
80	27.29			446.5		1542.68	.3726	15.1
100	27.25			444.5		1542.92	.4625	23.5
120	27.16	36.04		438.9	443.9	1543.08	.5517	33.6
140	27.07	36.14	registration and the	432.5		1543.25	.6400	45.5
160	26.75	36.19		-	425.8	1542.90	.7264	59.2
180	26.00	36.33			393.9	1541.63	.8084	74.6
200	24.94	36.44		347.4		1539.56	.8833	91.5
220	22.02				280.2	1535.15	.9469	109.8
240	21.28		25.75		236.5	1531.23	.9986	129.2
260	19.84	36.63			205.0	1527.60	1.0427	149.6
280	18.30	36.52	26.25	177.7		1524.91	1.0820	170.9
300	18.18	36.47		166.5	176.9		1.1184	192.9
341)	17.14	36.33		152.4	163.8	1520.86	.1860	239.0
380	16.18	36.15		143.9		1518.43	1.2500	287.7
420	15,19	35.96		136.4	149.3	1515.80	1.5109	338.9
460	13.30	35.73	26.81	124.6	137.7	1511.74	1.3683	392.5
5nn	13,16	35.67	26.90	116.4	130.2	1510.21	1.4218	448.3
540	12.16	35.53	26.99	107.0	121.8	1507.32	1.4721	506.2
580	11.20	35.38	27.05	101.6	115.6	1504.47	1.5197	566.1
620	10.46	35.27	27.10	97.1	111.2	1502.37	1.5648	627.8
660	9.05	35.01	27.14	93.6	106.8	1497.56	1.6083	691.2
700	8.58	34.95	27.20	88.0	101.1	1495.63	1.6496	756.4
740	7.71	34.88	27.24	83.6	96.4	1493.65	1.6801	823.2
780	7.24	34.85	27.29	79.11	92.1	1492.44	1./269	891.5
820	6.62	34.82	27.35	73.5	85.8	1490.64	1.7626	961.3
860	6.32		27.39	69.7	82.1	1490.10	1.7962	1032.5
900	6.10		27.43	65.5	78.1	1489.91	1.8283	1105.0
940	5.64	34.87	27.52	57.7	70.0	1488.76	1.8579	1178.7

•	STD STA	MOIT!	NUMBER	66						
	AUGUST	13, 19	971	15.1	,					
ı	ATITUE	DE		17 2	17 27					
1	ONGIT	IDE		79 19	3					
	PEPTH 1		TOM	1189	4					
2	T	5	STOT	TANOM	SVA	SVEL.	TONHET			
0	28.18	35.99	23.10	477.A	477.8	1543.29	.0000			
20	27.94	35.90	23.18	470.2	471.1	1543.09	.0949			
40	27.88	36.00	23.27	461.2	462.9	1543,37	.1883			
60	27.84	36.11	23.30	458.5	461.0	1543.63	.2807			
80	27.86	36.17	23.34	454.8	458.2	1544.05	. 3726			
100	27.76	36.15	23.36	453.1	457.4	1544.14	.4642			
120	27.22	36.04	23.49	440.7	445.8	1543,22	.5545			
140	26.64	36.18	23.74	416.5	422.4	1542.32	.6413			
160	25.78	36.33	24.13	379.9	386.6	1540.80	. 7222			
180	24.15	36.62	24.84	311.7	319.0	1537.49	.7927			
500	23.11	36.83	25.31	267.3	275.3	1535.42	.8521			
220	22.15	36.85	25.60	239.1	247.7	1533.26	.9045			
240	20.05	36.62	26.00	201.4	210.3	1527.85	.9503			
260	18.86	36.51	26.23	179.9	189.2	1524.75	.9902			
290	18.56	36.46	26.32	171.5	181.3	1523.59	1.0273			
300	17.84	34.39	26.39	164.2	174.6		1.0629			
340	17.75	36.26	26.49	155.4	166.8	1520.52	1.1311			
380	16.10	36.10	26.59	145.8	158.0	1518.13	1.1958			

80.6

75.4

70.3

64.7

61.6

55.3

52.1

46.6

420 15.13 35.96 26.70

460 13.56 35.69 26.85

500 12.25 35.46 26.92

540 10.90 35.25 27.01 580 10.08 35.15 27.07

620

660

700

780

P20

860

900

940

980

1020

1100

9.52 35.0H 27.11

8.90 35.00 27.15

8.29 34.94 27.20

7.75 34.88 27.24

7.27 34.84 27.28

6.71 34.81 27.33

6.31 34.81 27.38

5.07 34.83 27.44

5.84 34.85 27.48

5.50 34.88 27.54

5.28 34.89 27.58

4.29 34.92 27.63

TRANS

.9 3.8

8.5

15.0 23.4

33.6 45.5

59.1

74.3

108.3

126.9

146.3

166.4

187·3 231·2

277.8

326.8

378.3

431.9

487.6

545.1

604.5

665.6

728.5

792.9

858.9

926.3

1065.4

1209.5

1283.2

1433.6

135.1 147.9 1515.61 1.2571

122.8 135.7 1510.91 1.3139

114.6 127.6 1506.90 1.3667

106.0 118.7 1502.61 1.4161

99.6 112.4 1500.21 1.4623

95.8 108.7 1498.74 1.5068

92.1 105.1 1497.00 1.5496

87.5 100.4 1495.28 1.5908

84.2 97.0 1493.80 1.6304

93.3 1492.55 1.6685

87.9 1490.98 1.7048

82.7 1490.05 1.7390

77.0 1489.38 1.7709

74.2 1489.53 1.8010

67.9 1488.86 1.8295

64.6 1488.64 1.8560

59.4 1488.80 1.9047

2	T	5	SIGT	TANOM	SVA	SVEI	TOHNY	TRANS
n	27.74	36.07	23.51	458.2	458.2	1542.40	.0000	• 0
20	27.63	36.UH	23.35	454.1	455.0	1542.49	.0913	• 9
40	27.58	36.11	23.49	450.4	452.1	1542.73	.1820	3.6
60	27.50	36.11	23.41	447.9	450.5	1542.88	.2723	8.2
an	27.14	36.16	23.60	430.2	433.5	1542.23	.3607	14.5
100	26.66	36.25	23.77	413.5	417.7	1541.76	.445A	22.6
120	26.55	36.20	23.85	405.9	410.9	1541.89	.52R7	32.3
140	26.18	34.34	24.01	391.2	397.0	1541.41	.6095	43.7
160	25. 14	36.44	24.38	355.4	362.0	1539.91	.6854	56.7
180	25.39	36.74	25.16	281.5	288.8	1535.72	.7504	71.0
500	21.82	36.75	25.62	238.0	245.8	1532.05	.8039	86.6
550	20.15	36.67	26.01	200.4	208.5	1527.85	. 9493	103.1
240	19.58	36.57	26.09	193.3	202.0	1526.51	.8904	120.5
260	17.38	36.36	26.36	167.4	176.3	1521.79	.9292	138.7
500	16.58	36.17	26.53	151.4	160.5	1518.06	.9619	157.6
300	16.19	36.12	26.58	146.3	156.0	1517.14	.9036	177.1
340	15.71	36.05	26.64	140.0	151.7	1516.23	1.0551	218.1
380	15.11	35.93	26.68	136.9	148.5	1514.87	1.1154	261.5
4211	13.52	35.61	26.82	123.5	135.3	1510.11	1.1722	307.3
461)	12.63	35.52	26.89	117.3	129.5	1507.62	1.2255	355.2
500	11.92	35.43	26.96	110.8	123.5	1505.74	1.2758	405.3
540	11.29	35.33	27.00	106.0	120.0	1504.08	3245	457.3
540	10.21	35.17	27.07	100.3	113.2	1500.71	1.5713	511.2
650	9.66	35.10	27.11	96.5	104.6	1499.27	1.4158	567.0
660	9.28	35,05	27.13	94.2	107.7	1498.47	1.4592	624.5
700	8.52	34.94	27.17	90.9	104.1	1496.15	1.5017	683.7
740	8.08	34.92	21.22	85.9	99.2	1495.11	1.5419	744.6
790	7.74	34.88	27.24	84.1	97.6	1494.41	1.5814	807.0
650	7.17	34.84	27.29	74.2	92.5	1492.81	1.6196	971.1
690	6.51	34.81	27.56	72.9	85.6	1490.84	1.6554	936.6
900	5.09	34.81	27.42	66.4	78.7	1489.43	1.6883	1003.4
940	5.01	34.83	27.45	63.0	76.7	1489.79	1.7192	1071.6
989	5.78	34.84	27.48	61.6	74.7		1.7495	1141.0
1020	5.1.9		27.54	55.2	68.2	1489.47	1.7779	1211.5
1100	4.19	34.92	27.63	46.6	59.4	1488.80	1.9047	1433.6

```
AUGUST 14, 1971 02.2 / LATITUDE 17 03 10061TUDE 79 49 1061 M
```

7.	•	S	SIGT	MONAT	SVA	SVEL	DYNHET	TRANS
n	27.69	36.09	23.54	455.3	455.3	1542.31	.0000	• 0
50	27.58	36.08	23.36	452.6	453.4	1542.38	.0909	• 9
411	27.47	36.08	23.40	449.1	450.8	1542.46	.1813	3.6
60	27.19	36.15	23.54	435.5	43R.0	1542.23	.2702	8.1
20	26.06	36.20	23.66	424.B	428.2	1542.08	.3568	14.4
100	26.75	36.25	23.77	414.2	418.4	1541.93	.4415	22.4
120	26.59	36.55	23.43	398.2	403.2	1541.56	.5236	32.0
149	26.17	36.42	24.10	382.1	387.9	1541.22	.6027	43.3
160	25.17	34.59	24.51	343.3	349.9	1539.59	.6765	56.1
180	23.71	35.15	25.116	291.3	298.5	1536.51	. 7414	70.3
Suu	22.20	35.75	25.51	248.2	256.1	1533.04	.7968	85.7
550	19.07	36.60	26.03	198.4	206.5	1527.01	.8431	102.1
240	18.51	36.47	26.26	176.8	185.3	1523.68	.8822	119.3
260	17.58	36.34	26.42	161.8	170.7	1520.89	.9178	137.5
280	17.02	36.28	26.46	157.9	167.3	1520.09	.9516	156.0
300	16.39	36.15	26.56	148.6	158.3	1517.78	.9842	175.4
3111	15.72	36.05	26.64	141.2	151.9	1516.26	1.0458	216.0
380	14.93	35.91	26.71	134.5	146.1	1514.28	1.1054	259.0
420	14.00	35.76	26.79	126.4	138.5	1511.78	1.1624	304.4
4611	13.22	35.61	26.84	122.0	134.7	1509.69	1.2175	352.0
500	12.10	35.44	26.93	113.3	126.2	1506.37	1.2697	401.7
540	11.08	35.27	26.99	107.6	120.5	1503.27	1.3194	453.5
590	10.11		27.07	100.1	112.9	1500.32	1.5661	507.2
620	9.53	35.07	27.11	96.7	109.6		1.4107	562.8
660	8.74	34.98	27.16	91.1	103.9	1496.38	1.4531	620.0
700	7.86	34.88	27.22	85.7	98.1	1493.57	1.4937	679.0
740	7.52	34.86	27.26	82.5	95.0	1492.89	1.5321	739.5
780	7.24	34.84	27.28	80.2	92.9	1492.43	1.5696	801.5
820	6.89	34.82	27.31	77.0	89.8	1491.70	1.6061	865.1
860	6.60	34.81	27.34	74.0	86.9	1491.19	1.6417	930.0
900	6.21		27.41	67.6	80.4	1490.33	1.6751	996.4
940	6.00	34.84		64.3	77.2	1490.16	1.7067	1064.0
980	5.55		.27.54	55.9	68.5	1489.06	1.7357	1132.9
1020	4. 5	-	27.67	43.5	55.2	1486.95	1.7603	1202.8
1100	4.09	34.92	27.63	46.6	59.4	1488.80	1.9047	1433.6

STD STATION NUMBER	A68
AUGUST 14. 1971	05.7 2
LATITUDE	17 03
LONGITUDE	79 44
DEPTH TO BOTTOM	1061 M

7.	T	S	SIGT	TANOM	SVA	SVE	DYNHGT	TRANS
0	27.54	36.06	23.36	452.7	452.8	1541.95	.0000	• 0
20	27.51	36.08	23,39	450.4	451.2	1542.23	.0904	• 9
40	27.41	36.13	23.46	443.7	445.4	1542.38	.1801	3.6
60	27.27	36.15	23.52	437.9	440.5	1542.41	.2686	8.1
80	26.93	36.21	23.67	423.2	426.6	1542.03	.3554	14.3
100	26.49	36.31	23.89	402.6	406.8	1541.44	.4387	22.3
120	26.18	36.39	24.05	387.6	392.6	1541.13	.5186	31.8
140	25.75	36.55	24.29	364.7	370.5	1540.58	.5949	43.0
160	25.27	36.58	24.47	346.9	353.5	1539.82	.6673	55.6
180		36.69	24.94	302.4	309.7	1537.19	.7336	69.6
200	23.33	36.77	25,20	277.R	285.8	1535.92	.7932	84.9
220	21.57	36.72	25.66	233.6	242.0	1531.69	.8460	101.3
240	19.78	36.58	26.04	197.5	206.4	1527.07	.8908	118.6
260	18.67	36.44	26.25	177.5	186.7	1524.18	.9301	136.9
280	17.69	36.33	26.38	165.1	174.7	1521.52	.9663	155.8
300	17.05	36.25	26.48	156.1	166.2	1519.87	1.0003	175.5
340	15.59	36.02	26.64	140.5	151.2	1515.83	1.0636	216.8
380	The same of the sa		26.71	134.0	145.4	1513.60	1.1232	260.5
420	13.93	35.74	26.79			1511.53	1.1800	306.6
460	13.02	35.57	26.85	121.1	133.6	1508.98	1.2348	354.9
500	12.56	35.50	26.89	117.5	130.7	1508.00	1.2873	405.3
540	11.59	35.35	26.96	110.7	124.1	1505.15	1.5383	457.9
580	10.36	35.16	27.03	103.5	116.5	1501.23	1.3865	512.4
620	9.17	34.99	27.10	97.0	109.5	1497.34	1.4318	568.7
660	7.74	34.87	27.23	84.8	96.3	1492.46	1.4726	626.8
700	7.61	34.87	27.25	83.0	95.0	1492.60	1.5107	686.5
740	7.42	34.85	27.26	81.9	94.2	1492,49	1.5486	747.7
780	7.14	34.82	27.28	80.3	92.9	1492.02	1.5859	810.4
820	6.74	34.81	27.33	75.8	88.3	1491.09	1.6220	874.5
860	6.50	34.82	27.37	72.0	84.7	1490.81	1.6564	940 • 1
900	6.15	34.82	27.41	67.6	80.3	1490.08	1.6897	1007.0
940	5.87	34.84	27.46	62.7	75.4	1489.64	1./206	1075.2
980	5.15	34.89	27.59	50.6	62.4	1487.46	1.7485	1144.6
1020	4.85	34.94	27.67	43.5	55.2	1486.95	1.7718	1215.1

STD STATION NUMBER	69
AUGUST 14, 1971	19.7 /
LATITUDE	16 52
LONGTTUDE	79 57
DEPTH TO BOTTOM	900 M

Z	T	S	SIGT	TANOM	SVA	SVEL	TYNHGT	TRANS
0	27.55	36.08	23.37	451.6	451.6	1541.99	.0000	• 0
50	27.55	36.08	23.37	451.6	452.5	1542.32	. 0904	•9
40	27.53	36.08	23.38	451.0	452.7	1542,60	.1809	3.6
60	27.16	36.14	23.55	435.3	437.8	1542.15	.2700	8.1
80	26.79	36.24	23.74	415.8	420.1	1541.74	. 3558	14.4
100	26.20	36.38	24.03	388.0	393.1	1540.84	.4371	22.3
120	25.39	36.57	24.43	351.2	356.1	1539,45	.5120	31.8
140	24.07	36.65	24.65	350.2	336.0	1538,61	.5812	42.7
160	24.24	36.70	24.88	308.5	315.0	1537,46	.6463	55.0
180	24.07	36.72	24.94	302.2	309.5	1537.38	.7088	68.6
200	22.51	36.64	25.31	267.3	275.2	1533,99	.7672	83.3
220	20.36	36.65	25.44	207.1	215.4	1528,40	.8163	99.2
240	19.03	35.50	26.18	184.8	193.4	1524.90	.8572	115.9
260	18.34	36.42	26.29	173.9	183.0	1523.18	.8948	133.4
280	17.54	36.32	26.41	162.3	171.9	1521.07	.9303	151.7
300	16.79	36.21	26.51	153.2	163.1	1519.05	.9638	170.6
340	15.40	35.99	26.66	138.7	149.2	1515,21	1.0258	210.4
380	13.94	35.74	26.79	126.7	137.6	1510,92	1.0838	252.6
420	12.84	35.53	26.85	120.6	131.9	1507.69	1.1378	297.1
460	11.98	35.42	26.94	112.6	124.3	1505,29	1.1884	343.6
50n	11.08	35.25	26.97	109.1	121.0	1502.61	1.2376	392.1
540	10.81	35.24	27.02	105.2	117.8	1502.29	1.2852	442.6
580	10.19	35.16	27.06	100.7	113.6	1500.62	1.3317	494.9
620	9.78	35.09	27.08	99.2	112.4	1499.70	1.3769	549.1
660	9.37	35.02	27.09	97.9	111.4	1498.76	1.4215	605.0
700	8.13	34.92	27.21	86.6	99.3	1494.65	1.4630	662.8
740	7.26	34.83	27.27	81.2	93.3	1491.85	1.5018	722.1
780	6.96	31.83	27.31	77.2	89.5	1491.33	1.5382	782.9
820	5.95	34.84	27.45	63.7	74.9	1488.01	1.5707	845.1
860	6.50	34.82	27.37	72.0	84.7	1490.82	1.6010	908.5

3.6.											
AUGUST 14, 1971					19.7	19.7 /					
LATITUDE				16 46							
LONGITUDE				80 08							
	Г	EPTH 1	TO BOT	TOM	708 *	1					
	7	T	S	SIGT	TANOM	SVA	SVEL	DYNHGT	TRANS		
	0	27.66	36.14	23.38	450.7	450.7	1542.29	0000	• 0		
	50	27.41	36.10	23.44	445.0	446.7	1542.03	.0897	.9		
	40	27.36	36.11	23.46	443.6	445.3	1542.25	.1789	3.6		
	50	27.10	36.16	23.58	432.0	434.5	1542.04	.2669	8.0		
	80	26.82	36.25	23.74	417.0	420.3	1541.81	.3524	14.2		
	100	26.72	36.27	23.78	412.5	416.7	1541.93	.4361	22.1		
	120	26.56	36.30	23.86	405.5	410.5	1541.92	.5188	31.7		
	140	26.20	36.34	24.114	388.2	394.0	1541.50	.5993	42.9		
	160	26.07	36.44	24.12	380.7	387.3	1541.57	.6774	55.6		
	180	25.41	36.40	24.36	357.5	364.9	1540.40	. 1526	69.9		
	500	22.35	35.63	25.38	261.0	268.8	1533.32	.8160	85.6		
	220	20.50	36.61	25.87	213.6	221.9	1528.74	.8651	102.4		
	241	19.18	36.50	26.14	188.5	197.1	1525.32	.9070	120.1		
	260	17.74	36.33	26.37	166.3	175.2	1521.35	. 4442	138.6		
	580	17.03	36.23	26.47	157.1	166.5	1519.47	. 9794	157.9		
	300	16.44	36.16	26.55	149.0	158.7	1517.94	1.0100	177.8		
	340	15.34	37.96	26.65	139.6	150.1	1514.99	1.0726	219.4		
	380	13.18	35.59	26.85	122.7	133.2	1508.25	1.1290	263.5		
	420	11.45	35.41	26.95	111.0	121.6	1504.19	1.1795	309.7		
	460	10.56	35.22	27.114	102.4	113.0	1500.09	1.2271	357.8		
	500	9.10	34.99	27.11	95.9	105.9	1495.14	1.2712	407.8		
	540	8.08	34.92	27,22	85.0	95.7	1491.88	1.3109	459.4		
	580	7.63	34.87	27.25	83.3	93.2	1490.74	1.3487	512.6		
	620	7.22	34.85	27.29	79.2	89.3	1489.78	1.5848	567.3		
	660	6.90	34.83	27.31	77.2	87.6	1489.39	1.4202	623.4		
	700	8.13	34.92	27.21	86.6	99.3	1494.65	1.4563	680.9		

STD STATION NUMBER 70

SID STATION NUMBER			71							
1	NUGUST	16, 19	971	03.5 /						
LATTTUDE				16 3	16 3"					
1	ONGIT	JUE		81 39	4					
		TO BOT		•	4					
Z	T	S	STGT	TANOM	SVA	SVEL	TYNHGT	TRANS		
0	27.59	36.09	23.43	446.0	446.0	1541.65	.0000	• 0		
20	27.25	36.10	25.49	440.0	441.8	1541.67	.0888	•9		
40	26.73	36.21	23.74	417.1	418.8	1540.93	.1748	3.5		
61	26.58	36.26	23.82	409.0	411.5	1540.96	.2579	7.9		
80	26.13	36.37	24.05	387.5	390.8	1540.35	. 3381	13.8		
100	25.29	36.54	24.44	350.4	354.5	1538.86	.4126	21.3		
120	23.75	36.60	24.95	301.2	306.1	1535.48	.4787	30.2		
140	20.63	36.55	25.79	221.3	226.6	1527.75	.5319	40.3		
160	18.91	36.44	26.16	146.2	191.9	1523.22	.5738	51.4		
180	18.35	36.40	26.27	175.6	181.9	1521,90	.6112	63.2		
200	17.97	35.31	26.30	173.1	180.0	1521.04	.6474	75.8		
550	16.40	36.13	26.54	150.2	157.4	1516.51	.6811	89.1		
240	15.42	34.01	26.67	137.6	145.1	1513.69	.7114	103.0		

STD STATION NUMBER				72						
AUGUST 16, 1971				06.8 Z						
LATITUDE				16 41	1					
		JDE		81 12	?					
	DEPTH 1	TO BOT	OM	241	4					
Z	т	S	SIGT	TANOM	SVA	SVEL	TYNHGT	TRANS		
		36.06				1542.39		• 0		
		36.08		451.3	452.2	1542.29	.0911	.9		
		36.12		441.6	443.3	1542.17	.1807	3.6		
60	27.24	36.14	23.52	437.7	440.3	1542.33	.2690	8.1		
80	25.98	36.35	24.08	384.5	387.8	1539.98	.3518	14.3		
100	24.83	36.51	24.55	339.1	343.2	1537.75	.4249	22.1		
120	24.71	36.52	24.60	334.9	339.8	1537.79	.4932	31.3		
140	22.64	36.60	25.27	271.0	276.5	1533.07	.5549	41.8		
160	18.52	36.45	26,25	177.5	183.2	1522.10	.6008	53.3		
180	17.61	36.33	26.40	163.2	169.4	1519.68	.6361	65.7		
200	17.97	36.31	26,30	173.1	180.0	1521.04	.6710	78.8		

SID STATION NUMBER			13					
AUGUST 16, 1971			12.4	,				
LATITUDE			16 1					
	ONGIT			81 1				
	EPTH			265				
	Cr 111	.0 60.		200				
Z	T	S	SIGT	TANOM	SVA	SVEL	TYNHGT	TRANS
	27.45			459.9	459.8	1542.15	.0000	• 0
			23.35	453.7	454.5	1542.37	. 9914	• 9
	27.54			450.7	452.4	1542.62	.1821	3.6
	-		23,43	446.6	449.1	1542.64	.2723	8.2
80	26.69	36.37	23.87	404.3	407.6	1541.62	. 3579	14.5
100	26.25	36.53	24.13	379.7	383.9	1541.09	.4371	22.4
120	24.72	36.75	24.75	320.3	325.2	1538.00	.5080	31.9
140	24.07	36.71	24.93	302.0	308.6	1536.73	.5714	42.7
160	18,90	36.53	26.24	179.2	184.8	1523.27	.6207	54.6
180	17.45	36.36	26.47	157.0	163.1	1519.24	.6555	67.4
200	16.119	36.16	26.64	141.2	147.7	1515.27	.6866	80.8
550	15.59	36.07	26.68	137.4	143.8	1513.97	.7158	94.8
240	15.24	36.00	26.70	135.0	141.6	1513.12	. 7443	109.4
260	14.49	35.94	26.73	152.7	139.5	1512.26	. 7724	124.6
280	14.54	35.87	26.75	130.3	137.5	1511.39	.8001	140.3
300	14.18	381	26.78	128.n	135.5	1510.50	.8274	156.6
340	13.48	35.67	26.82	123.3	131.9	1508.70	.8809	190.8
380	12.78	35.54	26.87	118.7	128.6	1506.85	.9330	227.0

STO STATION NUMBER				A73		7			
AUGUST 16, 1971				14.6 /					
L	ATTTU	DE		16 1	7				
		JDE		81 14	4				
DEPTH TO BOTTOM			265	265 M					
Z	т	5	SIGT	TANOM	SVA	SVEL	TNHGT	TRANS	
		36.07		462.3	462.3	1542.69	.0000	• 0	
20	27.66	36.07	23.33	455.R	456.6	1542.55	.0919	. 9	
40	27.52	36.08	23.38	450.7	452.4	1542.57	.1828	3.7	
60	27.35	36.11	23.46	443.4	445.9	1542.54	.2726	8.2	
80	26.76	36.25	23.76	414.9	418.3	1541.69	.3590	14.5	
100	25.34	36.5R	24.45	349.1	353.3	1539.00	.4362	22.5	
120	23.40	36.72	25.14	283.2	288.0	1534.76	.5003	31.9	
140	22.32	36.80	25.51	247.7	253.2	1532.41	. 5544	42.4	
160	19.67	36.69	26.16	186.0	192.5	1525.58	.5990	53.9	
		36.12		135.4	141.1	1513.68	.6324	66.3	

STD STAT	74			
AUGUST 1	5, 19	971	19.	4 1
LATITUDE			16	27
LONGITUD	80	56		
DEPT TO	49	9 4		
-	S	STGT	TAN	014

7	Т	S	SIGT	TANOM	SVA	SVEI	TOHOT	TRANS
0	28.08	36.11	23.22	466.0	466.0	1543.18	.0000	• 0
50	27.77	34.15	23.34	455.0	455.9	1542.85	.0922	.9
40	27.69	35.12	23.36	453.3	455.0	1542.99	.1833	3.7
60	27.52	36.11	23.38	451.3	453.8	1543.15	.2742	8.3
80	27.59	36.12	23.39	450.1	453.4	1543.41	. 3649	14.6
100	27.12	36.16	23.57	432.6	436.8	1542.73	.4539	22.8
150	25.02	36.59	24.28	365.5	370.5	1540.71	.5346	32.7
140	24.65	36.70	24.82	314.0	319.8	1538.20	.6037	44.1
160	23.07	36.75	24.99	297.3	303.8	1536.83	.6660	56.8
130	22.14	36.70	25.51	247.7	254.5	1532.25	.7219	70.7
500	20.25	36.71	26.02	500.0	207.5	1527.83	.7681	85.6
	18.26			159.7	167.5	1522.47	.8056	101.3
241	17.53	36.39	26.47	157.1	165.3	1520.46	.8388	117.8
560	16.18	36.20	26.64	140.5	148.9	1516.56	.8703	134.8
280	14.50	35.96	26.84	121.9	130.3	1511.38	.8982	152.5
300	13.34	35.72	56.40	116.5	124.9	1507.63	.9237	170.7
340	12.15	35.49	26.96	110.5	119.3	1504.01	.9735	208.7
380	10.00	35.18	27.11	95.A	104.2	1496.76	1.0173	248.5
420	8.51	35.07	27.26	85.5	90.4	1492.13	1.0569	290.0
460	9. "4	35.04	27.15	92.3	100.8	1494.36	1.0949	333.1

STD STATION NUMBER AUGUST 16, 1971 LATITUDE LONGITUDE DEPTH TO POITOM				971	A74 20.7 16 2 80 56 499	,			
	Z	т	5	SIGI	TANOM	SVA	SVEL	NYNHGT	TRANS
		28.11					1543.27	.0000	• 0
	20	27.76	36.17	23.38			1542.85		.9
	40	27.69	36.13	23.36	452.7	454.4	1542.99	.1823	3.7
	60	27.61	35.12	23.38	450.7	453.2	1543.13	.2731	8.2
	80	27.35	36.18	23.51	438.3	441.7	1542.94	.3626	14.6
1	100	26.59	36.37	23.90	401.4	405.6	1541.72	.4473	22.7
1	120	26.06	36.45	24.13	379.4	384.4	1540.91	.5263	32.4
1	4(1	25.10	36.71	24.62	332.6	338.4	1539.20	.5986	43.7
1	160	24.21	36.79	24.95	301.3	307.9	1537.47	.6632	56.3
1	180	25.45	36.82	25.20	277.6	284.8	1535.92	.7225	70.1
2	500	21.56	36.85	25.81	219.6	226.5	1530.92	.7736	85.1
	Fr. mark char		A TOTAL CONTRACTOR OF THE PARTY	The same of the sa					

220 19.15 36.62 26.22 180.3 186.7 1525.02

240 17.15 36.33 26.51 153.1 160.3 1519.28

260 15.45 36.03 26.68 136.7 144.9 1514.11

290 14.36 35.90 26.82 123.5 131.8 1510.84

300 13.02 35.68 26.93 113.0 121.3 1506.54 340 11.15 35.36 27.05 101.9 110.2 1500.41

.8150

. 8496

.8802

.9078

.9331

. 4788

101.0

117.6

134.9

152.8

171.2

STD STATION NUMBER	75
AUGUST 16, 1971	23.8 7
LATITUDE	16 45
LONGITUDE	81 07
DEPTH TO BOTTOM	512 "

7.	T	5	SIGT	TANOM	SVA	SVEI.	TNHGT	TRANS
1)	27.06	36.12	23.27	461.5	461.5	1542.93	.0000	• 0
20	27.58	36.11	25.39	450.2	451.0	1542.41	.0913	•9
40	27.47	36.11	23.42	447.1	448.8	1542.48	.1812	3.6
60	27.40	36.11	23.44	444.9	447.5	1542.66	.2709	8.2
80	26.83	36.24	23.73	418.1	421.4	1541.82	. 3577	14.4
100	26.02	36.43	24.13	379.9	384.1	1540.47	.4383	22.4
120	25.88	36.46	24.19	373.7	378.6	1540.49	.5146	31.9
140	25.72	36.51	24.28	365.2	371.0	1540.49	.5895	43.0
160	23.56	36.69	25.07	289.6	296.0	1535.78	.6562	55.4
180	22.30	36.72	25.46	253.3	260.3	1532.95	./119	69.1
500	19.23	36.50	26.13	189.7	196.9	1524.82	.7576	83.8
550	13.49	36.43	26.26	176.4	184.2	1522.97	.7957	99.3
540	16.52	36.23	26.59	145.8	153.5	1517.30	.8295	115.6
2611	15.46	36.03	26.68	137.0	145.1	1514.15	.8593	132.5
280	14.98	35.95	26.73	132.2	140.8	1512.87	.8879	150.0
300	14.63	35.88	26.75	130.2	139.2	1512.03	.9159	168.0
340	12,61	35.60	26.95	110.9	120.1	1505.71	.9687	205.7
380	10.66	35.27	27.07	100.4	109.3	1499.22	1.0144	245.4
420	10.06	35.20	27.12	95.3	104.6	1497.62	1.0572	286.8
460	9.00	35.0A	27.20	88.2	97.3	1494.24	1.0973	329.9
500	8.52	35.01	27.22	86.1	95.3	1493.01	1.1358	374.6
540	8.14	34.94	27.24	84.0	93.4	1491.76	1.1735	420.8
590	7.56	34.88	27.26	81.9	91.7	1490.49	1.2105	468.4

AUGUST 17, 1971			03.2	,					
LATITUDE				16 49	4				
LONGITUDE				80 57					
		0 BOTT		395					
	CF (A)	0 601	OM	343					
Z	т	S	SIGT	TANOM	SVA	SVEL	DYNHGT	TRANS	
0	27.54	36.04	23.35	454.2	454.2	1541.93	.0000	• 0	
20	27.35	36.13	23.48	441.5	442.3	1541.88	.0897	• 9	
		36.17				1541.89	.1774	3.6	
60	26.07	36.24	23.68			1541.81	.2633	8.0	
		36.40	-			1540.84		14.1	
		36.40				1540.10	.4227	21.7	
		36.68				1538.53	.4942	30.9	
		36.73				1537.87	.5598	41.4	
160	24.22	36.75	24.92	304.4	310.9	1537.45	.6230	53.3	
180	22.24	36.85	25.56	243.5	250.6	1532.89	.6791	66.3	
200	21.03	36.71	25.80	220.6	228.1	1529.94	.7270	30.4	
220	20.29	36.6P	25.99	202.9	211.2	1528.24	.7709	95.3	
240	17.73	36.38	26.41	162.4	170.6	1521.05	.8001	111.1	
260	15.84	36.04	26.64	141.3	148.9	1515.41	.8411	127.6	
540	14.35	35.83	26.77	128.0	136.3	1510.74	.8696	144.7	
300	13.84	35.76	26.83	123.1	131.6	1509.35	.8964	162.4	
340	11.33	35.41	27.05	101.9	110.2	1501.10	.9441	199.2	
380	10,96	35.28	27.04			1499.93	·daba	237.9	

STD STATION NUMBER 76

STD STATION NUMBER				77				
AUGUST 17, 1971			08.3	,				
	ATITU	DE						
	LONGIT			80 3	1			
	DEPTH T	TO BOT	MOT	371	•			
Z	τ	5	SIGT	TANOM	SVA	SVEL	TNHGT	TRANS
0	27.78	36.UR	23.30	458.8	458.8	1542.50	.0000	•0
20	27.75	36.09	23.32	457.0	457.8	1542.77	.0917	
40	27.47	35.13	23.44	445.6	447.3	1542.51	.1822	3.7
60	26.79	35.24	23.74	416.3	418.9	1541.41	.2688	
80	26,36	36.38	23.48	393.8	397.1	1540.87	. 3504	14.4
100	25.90	36.48	24.20	372.7	376.9	1540.24	.4278	22.1
120	25.55	36.55	24.36	357.2	362.1	1539.81	.5017	31.4
140	24.47	36.65	24.62	353.3	339.0	1538.85	.5718	42.2
160	23.36	36.92	25.51	267.5	273.9	1535.47	.6331	54.2
190	21.96	36.99	25.76	224.6	231.8	1532.31	.6837	67.4
500	20,90	36.81	25.92	204.2	216.8	1529.66	. 7285	81.5
220	19.57	36.57	26.09	193.0	200.8	1526.16	.7703	96.5
2411	17.57	36.45	26.50	155.7	162.1	1520.63	.8066	112.3

260 16.78 36.25 26.62 142.6 151.1 1517.21

280 15.57 36.09 26.70 135.2 144.0 1514.86

300 14.95 36.00 26.77 128.1 137.3 1513.15

340 11.53 35.41 27.05 101.0 110.2 1501.10

.8379

.8674

.8955

.9441

128.7

145.8

163.4

STD STATION NUMBER	A77
AUGUST 17, 1971	08.3 /
LATITUDE	16 53
LONGITUDE	80 31
DEPTH TO BOTTOM	371 M

Z	Т	S	SIGT	TANOM	SVA	SVEL	TNHGT	TRANS
	27.75			457.1	457.1	1542.44	.0000	• 0
20	27.74	36.09	23.32	456.7	457.6	1542.75	.0915	• 9
40	27.26	36.20	23.56	434.0	435.7	1542.11	.1808	3.6
60	26.83	36.26	23.74	416.6	419.1	1541.52	.2663	8.1
80	26.39	36.38	25.97	394.6	397.9	1540.95	. 5480	14.3
100	25.96	36.47	24.18	375.0	379.2	1540.38	.4257	22.0
120	25.44	36.54	24.39	354.9	359.9	1539.54	.4006	31.2
140	24.76	36.73	24.74	321.4	327.1	1538.40	.56P3	41.9
160	23.25	36.88	25.31	267.6	274.0	1535.17	.6284	53.9
180	22.07	36.85	25.62	257.7	244.7	1552.47	.6803	67.0
200	21.05	36.83	25.89	212.0	219.6	1530.10	.7267	81.0
220	18.33	36.51	26.36	167.1	174.7	1522.58	.7662	96.0
240	16.72	36.27	26.57	147.4	155.3	1517.92	.7992	111.6
260	16.18	36.13	26.59	145.4	153.8	1516.48	.8301	127.9
280	15.07	35.99	26.73	132.5	140.4	1513.21	.8505	144.8
300	14.12	35.86	26.84	121.9	129.9	1510.34	.8865	162.3
340	11.33	35.41	27.05	101,9	110.2	1501.10	.9441	199.2

STD STATION NUMBER	78
AUGUST 17, 1971	14.0 %
LATITUDE	17 21
LONGITUDE	80 29
DEPTH TO BOTTOM	1595 M

7	T	5	SIEL	TANOM	SVA	SVEL	TNHGT	TRANS
0	27.71	36.02	23.28	460.9	460.9	1542.29	.0000	• 0
20	27.64	36.03	23.31	457.9	458.8	1542.47	.0920	• 9
40	27.25	36.15	23.53	437.0	438.7	1542.04	.1817	3.7
60	26.47	36.35	23.92	399.2	401.7	1540.80	.2657	8.1
80	25.91	36.47	24.19	373.7	377.1	1539.93	.3436	14.2
100	25.44	36.49	24.29	364.3	368.4	1539.64	.4182	21.8
120	25.08	36.63	24.57	337.8	342.7	1538.75	.4893	30.9
140	23.56	36.85	25.19	278.4	284.1	1535.59	.5520	41.3
160	21.52	36.83	25.76	224.5	230.7	1530.69	.6u34	52.9
180	20.79	36.73	25.88	212.8	219.6	1529.00	.6485	65.4
200	20.58	36.71	25.93	208.4	216.0	1528.73	.6920	78.8
550	19.76	36.63	26.09	193.4	201.4	1526.75	.7338	93.1
240	18.16	36.44	26.36	167.8	176.1	1522.35	.7715	108.1
260	17.90	36.41	26.40	164.0	173.0	1521.90	.8064	123.9
280	17.52	36.3P	26.46	157.B	167.3	1521.06	.8405	140.4
300	16.42	36.29	26.56	148.0	157.9	1519.21	.8730	157.5
340	15,53	36.02	26.66	139.2	149.9	1515.65	.4349	193.7
380	13.76	35.75	26.85	122.4	133.2	1510.35	.9921	232.2
420	11.82	35.41	26.96			1504.11	1.0426	272.9
460	10.56	35.25	27.07	100.5		1500.13	1.0893	315.6
500	9.72	-	27.13	93.9		1497.60	1.1326	360.0
540	8.57	35.00	27.20	87.4	97.8	1493.82	1.1731	406.1
580	7.62	34.89	27.26	81.7		1490.73	1.2110	453.8
651)	7.59		27.29	79.1		1490.49	1.2474	503.0
660	7.10		27.30	78.3		1489.97	1.2830	553.6
700	6.40		27.33	75.n		1489.43	1.3179	605.6
7411	6.29	34.86	27.43	66.1	76.8	1488.09	1.3507	659.0
780	5.97		27.47	62.6		1487.48	1.3804	713.6
850	5.66		27.53	56.5		1486.90	1.4080	769.4
850	5.34		27.58	51.9	62.7	1486.29	1.4337	826.2
900	5.17	34.91	27.61	49.1	60.0	1486.25	1.4581	884 • 1
940	4.98	34.92	27.54	46.1	57.1	1486.15	1.4813	942.9
980	4.84	34.94	27.67	43.4	54.6	1486.24	1.5036	1002.6
1050	4.68		27.70	40.2	51.5	1486.29	1.5248	1063.1
1100	4.54		27./2	38.7		1487.02	1.5660	1186.8
1200	4.46		27.73	37.7	50.4	1488.30	1.6165	1345.9
1300	4.39		27.74	36.5	50.0	1489.69	1.6671	1510.1
1400	4.33	-	27.75	35.3	49.7	1491.09	1.7172	1679.3
1500	4.27	34.97	27.76	34.8	49.9	1492.47	1.7670	1853.5

STD STATION NUMBER	178
AUGUST 17, 1971	17.7 7
LATITUDE	17 19
LONGITUDE	80 3.4
DEPTH TO BOTTOM	1606 M

		T		SIGT			SVEL	JANHEL	TRANS
				23.25			1542.57	•0000	• 0
		27.75		23.33			1542.78	.0920	• 9
4			36.16				1541.99	.1815	3.7
		26.53	36.31	23.H4			1541.11	.2662	8.1
100000		The second second	36.41	24.08			1540.34	.3458	14.3
10			36.52	24.35	358.9		1539.44	.4209	21.9
12				24.62	332.4	337.3	1538.53	.4909	31.0
14		23.93		25.02	295.0	300.7	1536.44	.5547	41.5
16	U	22."4	36.91	25.55	244.4	250.7	1533.28	·POOR	53.1
18	U	21.29	36.74	25.78	255.0	229.0	1530.36	.6578	65.8
50	Ü	20.36	36.71	25.49	202.6	210.0	1528.13	.7017	79.4
55	0	18.68	36.51	26.28	175.3	183.1	1523.61	. 7410	93.8
24	0	18.06	36.42	26.36	167.0	175.3	1522.04	. 1769	109.0
26	n	17.98	36.41	26.38	165.9	174.9	1522.13	.8119	124.9
28	0	17.33	36.58	26.39	164.8	174.4	1521.98	.8468	141.5
30	n	16.59	36.25	26.59	145.5	155.4	1518.50	. 479A	158.8
34	0	14.74	35.88	26.72	133.0	143.3	1513.01	.9396	195.2
38	0	11,93	35.45	26.97	109.4	119.1	1503.86	.9923	233.8
42	()	11.20	35.33	27.01	105.3	115.5	1501.82	1.0394	274.5
46		10.46	35.22	27.116	100.7	111.2	1499.75	1.0848	316.9
50	1)	9.48	35.10	27.14	93.4	103.9	1496.71	1.1278	361.2
54	0	8.50	34.98	27,20	87.5	97.8	1493.54	1.1680	407.1
59	()	7.52	34.90	27.29	79.5	89.4	1490.36	1.2058	454.6
65	0	7.38	34.87	27.28	80.0	90.3	1490.43	1.2419	503.6
66	11	7.11	34.82	27.28	79.0	90.6	1489.95	1.2783	554.0
70	U	6.52	34.84	27.38	70.7	81.2	1488.32	1.3125	605.8
74	0	6.16	34.82	27.41	67.4		1487.52	1.3436	658.9
78	0	5.90	34.86	27.48	61.4	72.1	1497.21	1.3735	713.3
85	9	5.50	34.92	27.56	53.7	64.5	1486.73	1.4610	768.8
86	n	5.45	34.80	27.56	53.8	64.7	1486.73	1.4267	825.3
àti	()	5.16	34.92	27.62	48.2	59.1	1486.25	1.4512	R82.9
94	0	4.95	34.93	27.65	45.2	56.2	1486.05	1.4743	941.4
99	(1	4.81	34.93	27.66	43.9	55.0	1486.13	1.4967	1000.8
102	1)	4.70	34.94	27.69	41.6	53.0	1486.35	1.5182	1061.1
110	0	4.55	34.95	-	39.3	51.2	1487.03	1.5597	1184.2
120	ŋ	4.45	34.95	27.72	38.1	50.8	1488.26	1.6105	1342.7
130	11	4.35	34.96	27.74	36.5	50.0	1480.57	1.6606	1506.3
140	n	4.32	34.97	27.75	35.6	49.9	1491.04	1.7109	1674.9
150	n	4.28	34.97	27.75	35.2	50.4	1492.52	1.7613	1848.5

```
BU 24
   LONGITUDE
   DEPTH TO BOTTOM
                         2926 M
             5
                  SIGI
                         MOMAI
                               SVA
                                      SVEL
                                              DYNHGT
                                                       TRANS
  0 27.09 36.07 23.22
                         466.1 466.1 1542.95
                                               .0000
                                                           • 0
                                                           .9
 20 27.74 36.07 23.30
                         458.5 459.3 1542.72
                                               .11925
                         448.1 449.8 1542.64
 40 27.53 36.12 23.41
                                               .1835
                                                          3.7
 60 27.39 36.14 23.47
                         142.3 444.9 1542.67
                                               .2729
                                                         8.2
 80 27.43 36.15 23.50
                         439.7 443.1 1542.86
                                                        14.6
                                               . 3617
100 26.98 36.16 23.62
                         428.4 432.6 1542.42
                                               . 4493
                                                        22.7
120 26.31 36.37 23.99
                         392.6 397.6 1541.40
                                                         32.5
                                               .5323
140 26.07 36.44 24.12
                         380.7 386.5 1541.24
                                                        44.0
                                               .6107
160 25.92 36.48 24.20
                         372.9 379.6 1541.25
                                               .6873
                                                        56.9
181 24.78 36.58 24.62
                         332.9 339.9 1538.99
                                               .7593
                                                        71.4
                                                         87.2
200 23.13 36.76 25.25
                         273.1 281.1 1535.41
                                               .8214
                                               .8733
220 21.64 35.81 25.71
                         229.0 237.5 1531.95
                                                       104.2
241 20.15 36.67 26.112
                         200.1 209.0 1528.16
                                               .9179
                                                        122.1
260 18.75 36.49 26.24
                         178.8 188.1 1524.43
                                               .9576
                                                       140.8
                         164.5 174.1 1521.76
280 17.76 36.36 26.39
                                               .9938
                                                       160.3
300 17.43 36.32 26.44
                         159.5 169.7 1521.06 1.0282
                                                       180.6
340 16.14 36.12 26.59
                         145.5 156.4 1517.64 1.0931
                                                       223.0
380 15.27 35.97 26.68
                         137.2 149.0 1515.42 1.1534
                                                       267.9
420 14.33 35.80 26.75
                         130.3 142.6 1512.87 1.2122
                                                       315.2
46n 13.41 35.63 26.82
                         123.9 136.7 1510.35 1.2687
                                                       364.9
500 12.08 35.43 26.03
                         113.7 126.5 1506.30 1.3212
                                                       416.7
540 11.17 35.31 27.01
                                                        470.5
                         105.9 118.9 1503.63 1.3704
580 10.36 35.20 27.06
                         100.6 113.6 1501.28 1.4172
                                                       526.3
     9.19 35.03 27.13
                          94.2 106.8 1497.45 1.4617
620
                                                       583.9
6611
     8.30 31.92 27.19
                          89.1 101.3 1494.64 1.5031
                                                       643.2
      7.12 34.80 27.26
700
                          81.7
                                92.9 1490.61 1.5418
                                                       704.1
     6.44 34.81 27.37
740
                          71.6
                               82.5 1488.63 1.5767
                                                       766.5
780
     6.10 34.83 27.42
                          66.5
                                77.4 1487.93 1.6087
                                                       A30.2
820
      5.98 34.84 27.45
                               75.3 1488.12 1.6391
                                                       895.1
                          64.0
660
      5.37 34.84 27.46
                          62.R
                               74.5 1488.36 1.6688
                                                       961.3
ann
      5.50 34.87 27.53
                          56.3
                                67.8 1487.56 1.6972
                                                      1028.6
      5.16 34.90 27.60
940
                          49.9
                                61.2 1486.87 1.7227
                                                      1097.0
      4.95 34.92 27.64
                          46.3
                                57.7 1486.67 1.7467
980
                                                      1166.4
                          41.8
      4.12 34.94 27.68
                                53.2 1496.44 1.7690
                                                      1236.7
1020
      4.49 34.96 27.72
                          39.2
                                50.0 1486.83 1.8099
                                                      1379.9
1100
      4.44 34.97 27.74
                                49.5 1488.24 1.8598
                                                      1563.4
1200
                          36.8
                                50.2 1489.73 1.9099
1300
      4.40 34.97 27.74
                          36.6
                                                      1751.9
```

79

21.3 /

STD STATION NUMBER

4.35 34.97 27.75

4.28 34.98 27.76

4.76 34.98 27.76

4.23 34.98 27.77

4.19 35.00 27.78

4.17 34.99 27.79

4.14 34.99 27.79

1400

1500

1600

1700 1800

1900

0000

1UGUST 17, 1971

LATTIUDE

50.4 1491.15 1.9604

50.0 1492.52 2.0104

50.4 1494.09 2.0604

50.8 1495.63 2.1105

50.1 1497.13 2.1609

50.8 1498.70 2.2116

51.4 1500.24 2.2626

1945.4

2143.9

2347.5

2556.0

2769.6

2988.2

3211.9

36.0

34.3

34.3

33.9

32.4

32.3

```
      STD STATION NUMBER
      80

      AUGUST 18, 1971
      06.5 /

      LATITUDE
      19 13

      LONG*TUDE
      81 34

      DEPTH TO BOTTOM
      1955 M
```

```
MOMAT
                                       SVEL
                                               DYNHGT
                                                        TRANS
                   SIGT
                                SVA
   0 28.84 36.15 23.00
                         487.2 487.2 1544.84
                                                ·uonu
                                                           • 0
  20 28.66 36.14 23.06
                         481.8 482.6 1544.77
                                                .0970
                                                          1.0
  40 28.17 36.19 23.25
                         463.1 464.8 1544.09
                                                .1917
                                                          3.9
  60 27.07 36.26 23.67
                         423.7 426.2 1542.07
                                                .2808
                                                          8.6
  80 26.80 36.26 23.75
                         415.4 418.8 1541.79
                                                . 3653
                                                         15.0
                                                .4408
                                                         23.2
 100 26.85 36.20 23.69
                         421.6 425.8 1542.15
 120 26.39 36.33 23.93
                         398.3 403.3 1541.55
                                                .5327
                                                         33.0
                                                         44.5
 140 25.31 36.48 24.23
                         369.8 375.6 1540.69
                                                .6106
                                                .6844
 160 25.37 36.50 24.38
                         355.7 362.3 1539.99
                                                         57.4
 180 24.77 36.67 24.70
                         325.6 333.0 1539.03
                                                . 7539
                                                         71.8
 200 23.75 36.90 25.17
                         280.4 288.5 1537.08
                                                .8160
                                                         87.5
 220 22.60 37.04 25.61
                         238.3 247.1 1534.62
                                                .8696
                                                        104.3
                                                .9158
 240 21.08 34.93 25.96
                         205.6 214.8 1530.89
                                                        122.2
                                                .9574
 260 20.10 36.78 26.11
                         191.3 201.0 1528.44
                                                        140.9
 280 19.07 36.61 26.25
                         177.9 188.0 1525.76
                                                .9963
                                                        160.5
 300 18.16 36.49 26.39
                         164.6 175.1 1523.36 1.0326
                                                        180.8
 340 17.15 36.28 26.48
                         156.4 167.8 1520.84 1.1002
                                                        223.4
 380 16.31 35.16 26.58
                         146.1 158.4 1518.82 1.1645
                                                        268.7
 420 15.10 35.02 26.76
                         129.9 142.7 1515.58 1.2247
                                                        316.5
                         116.2 128.9 1510.04 1.2790
 460 13.29 35.71 26.90
                                                        366.6
 500 12.12 35.48 26.96
                         110.7 123.5 1506.50 1.3295
                                                        418.8
 54n 11.39 35.42 27.05
                         102.0 115.3 1504.54 1.3766
                                                        472.9
                                                        528.9
 580 10.62 35.26 27.07
                         100.5 113.8 1502.28 1.4229
      9.65 35.12 27.13
                          94.6 107.7 1499.26 1.4661
 650
                                                        586.7
                          89.7 102.7 1496.99 1.5081
 660
      8.89 35.03 27.18
                                                        646.2
      8.42 34.94 27.18
                          89.5 102.7 1495.77 1.5489
 700
                                                        707.3
 740
      7.99 34.91 27.22
                          85.7
                                98.9 1494.76 1.5895
                                                        770.1
 789
      7.25 34.90 27.33
                          75.6
                                88.4 1492.56 1.6266
                                                        M34.4
 820
      6.56 34.91 27.43
                          66.0
                                78.4 1490.54 1.6599
                                                        900.2
                                 76.7 1489.88 1.6915
      6.24 34.88 27.45
                          64.3
 860
                                                        967.2
      5.97 34.84 27.45
                                 76.0 1489.38 1.7218
 900
                          63.6
                                                       1035.5
      5.74 34.86 27.50
 940
                          59.4
                                 71.8 1489.14 1.7515
                                                       1104.9
                          53.1
 980
      5.46 34.90 27.57
                                 65.6 1488.73 1.7788
                                                       1175.5
                          48.4
      5.22 34.93 27.61
                                 60.9 1488.46 1.8043
1020
                                                       1247.2
      4.85 34.95 27.67
                          42.8
                                55.4 1488.28 1.8491
                                                       1393.4
1100
      4.63 34.96 27.71
                          39.4
                                52.5 1489.00 1.9038
                                                       1581.0
1200
                          39.0
      4.56 34.96 27.71
                                53.0 1490.39 1.9561
                                                       1774.0
1300
                          36.7
                                 51.3 1491.44 2.0075
1400
      4.42 34.97 27.74
                                                       1972.2
      4.37 34.98 27.75
                          35.7
                                 51.2 1492.90 2.0590
                                                       2175.5
1500
      4, 16 34.98 27.75
1600
                          35.3
                                 51.7 1494.51 2.1103
                                                       2384.0
      4.74 34.98, 27.76
1700
                          34 . R
                                 52.1 1496.07 2.1620
                                                       2597.6
                          33.9
                                52.1 1497.57 2.2140
1800
      4.30 34.99 27.77
                                                       2816.4
```

```
      STD STATION NUMBER
      81

      AUGUST 10, 1971
      11.5 /

      LATITUDE
      19 06

      LONGITUD
      82 02

      DEPTH TO BOTTOM
      2149 M
```

```
TANOM SVA
                  SICT
                                      SVEL
                                              DYNHGT
                                                       TRANS
  0 28.22 36.00 23.10
                         478.3 478.3 1543.38
                                               .0000
                                                           .0
                                               .0940
 20 27.83 36.07 23.27
                         461.2 462.1 1542.91
                                                          .9
                                                         3.7
 40 27.41 36.16 23.48
                         441.6 443.3 1542.40
                                               .1846
 60 27.18 36.20 23.58
                         431.9 434.5 1542.26
                                               .2723
                                                         8.3
 80 26.08 36.24 23.68
                                               . 3584
                         422.8 426.1 1542.16
                                                        14.6
                         412.5 416.7 1542.04
100 26.76 35.29 23.78
                                               .4427
                                                        22.6
                         400.4 405.4 1541.82
120 26.50 36.34 23.91
                                               .5249
                                                        32.3
                                               ·6u52
140 26.29 36.38 24.00
                         391.9 397.8 1541.70
                                                        43.6
160 25.45 36.50 24.23
                         369.8 376.5 1541.10
                                               .6827
                                                        56.5
180 24.87 36.70 24.69
                         326.4 333.8 1539.29
                                               . 1537
                                                        70.8
200 23.32 36.98 25.36
                         262.7 270.6 1536.08
                                               .8141
                                                        86.5
220 21.44 36.99 25.90
                         211.2 219.4 1531.58
                                               .8631
                                                        103.3
240 20.10 36.83 26.15
                         187.2 196.2 1528.16
                                               .9047
                                                       121.0
                                               .9431
260 19.26 36.67 26.25
                         178.2 187.6 1526.02
                                                       139.4
                                               .9798
                         169.5 179.5 1524.49
280 18.63 35.58 26.34
                                                       158.7
300 17.9 36.50 26.47
                         157.3 167.6 1522.59 1.0145
                                                       178.6
340 16.74 35.34 26.62
                         142.7 153.9 1519.68 1.0796
                                                       220.5
380 15.93 36.18 26.69
                                                       264.9
                         136.0 148.2 1517.70 1.1412
                         131.9 144.5 1514.89 1.2002
420 14.91 35.94 26.73
                                                       311.8
460 13.72 35.75 26.84
                         121.6 134.6 1511.50 1.2555
                                                       360.9
                         130.4 146.7 1513.52 1.3127
                                                       412.2
500 14.15 35.72 26.75
540 11.66 35.43 27.00
                         106.2 119.7 1505.50 1.3669
                                                       465.9
590 10.96 35.29 27.02
                         104.3 118.0 1503.51 1.4148
                                                       521.5
                          96.4 109.8 1500.14 1.4605
      9.48 35.15 27.11
                                                       579.0
621
660
      9.19 35.05 27.14
                          93.1 106.5 1498.12 1.5042
                                                       638.3
      8.90 35.02 27.17
                          90.4 104.2 1497.66 1.5464
                                                       699.3
700
      7.82 34.88 27.23
740
                                98.1 1494.05 1.5864
                                                       762.0
                          85.1
      7.37 34.84 27.26
                                95.1 1492.94 1.6252
780
                                                       826.2
                          82.2
058
      6.28 34.84 27.33
                                87.9 1491.68 1.6619
                                                       892.0
                          75.1
      6.24 34.85 27.41
860
                          68.1
                                80.4 1489.81 1.6959
                                                       959.1
      5.78 34.86 27.49
900
                          60.2
                                72.2 1488.65 1.7268
                                                      1027.6
9411
      5.56 34.89 27.54
                          55.6
                                67.7 1488.47 1.7548
                                                      1097.2
980
      5.30 34.90 27.58
                          51.4
                                63.6 1488.07 1.7811
                                                      1167.9
      5.13 34.92 27.62
                                60.3 1488.07 1.8059
                                                      1239.7
1020
                          48.1
      4.84 34.93 27.66
                          44.2
                                56.7 1488.22 1.8524
                                                      1386.0
1100
      4.51 34.95 27.71
                          39.3
                                52.1 1488.52 1.9067
                                                      1574.0
1200
      4.49 34.96 27.73
                          38.0
                                51.8 1490.11 1.9591
1300
                                                      1767.3
      4.45 34.97 27.73
1400
                          37.1
                                51.8 1491.59 2.0108
                                                      1965.8
1500
      4.42 34.97 27.74
                                52.3 1493.09 2.0625
                                                      2169.5
                          36.7
      4.38 34.97 27.75
                                52.5 1494.56 2.1150
                                                      2378.3
1600
                          36.0
1700
      4.34 34.98 27.75
                          35.4
                                52.7 1496.07 2.1669
                                                      2592.4
1200
      4.30 35.00 27.77
                          33.5
                                51.7 1497.60 2.2189
                                                      2811.7
                          34.0
                                53.0 1499.20 2.2712
1900
      4.29 34.99 27.77
                                                      3036.2
                                51.1 1500.28 2.3237
2000
      4.15 35.00 27.79
                          31.7
                                                      3266.0
```

```
      STD STATION NUMBER
      A81

      AUGUST 18, 1971
      14.6 7

      LATITUDE
      19 05

      LONGITUDE
      82 07

      DEPTH TO ROITOM
      2305 M
```

```
TANOM SVA
                  SIGI
                                      SVEL
                                              LOHNAL
                                                       TRANS
  0 27.89 35.99 23.20
                                               .0000
                         468.7 468.7 1542.66
                                                          • 0
                         462.P 463.6 1542.56
 20 27.70 35.99 23.26
                                                          .9
                                               .0932
                         452.0 453.7 1542.50
 40 27.50 36.05 23.37
                                               .1850
                                                         3.7
 60 27.25 36.09 23.48
                         441.4 444.0 1542.31
                                               .2747
                                                         8.3
 80 27.04 35.14 23.59
                         431.2 434.5 1542.21
                                                        14.7
                                               . 3626
                         424.0 428.1 1542.26
 100 26.90 36.19 23.66
                                               .44RR
                                                        22.8
                         408.1 413.2 1542.04
120 26.52 36.29 23.83
                                               .5330
                                                        32.6
140 26.12 36.39 24.06
                         386.0 391.8 1541.31
                                               .6135
                                                        44.1
160 25.59 36.49 24.31
                         362.4 369.1 1540.49
                                               .6896
                                                        57.1
180 29.35 36.48 23.23
                         465.6 487.9 1549.12
                                               .7753
                                                        71.8
200 30.57 36.55 22.94
                        493.2 523.8 1552.01
                                               · H764
                                                        88.3
220 25.03 36.84 24.76
                         319.8 330.2 1540.43
                                               .9618
                                                       106.7
240 15.91 37.09 27.56
                               77.2 1516.26 1.0026
                          54.1
                                                       126.3
260 16.06 36.91 27.35
                         73.9 94.7 1516.85 1.0198
                                                       146.5
280 18.42 36.61 26.42
                         161.8 171.7 1523.90 1.0464
                                                       167.2
                         156.7 167.0 1522.50 1.0A03
300 17.86 36.50 26.47
                                                       188.5
340 16.97 36.28 26.52
                         151.8 163.1 1520.31 1.1470
                                                       233.0
                         141.3 153.5 1518.07 1.2102
380 16.06 36.15 26.63
                                                       280.2
420 14.93 35.91 26.71
                         134.3 147.0 1514.94 1.2706
                                                       329.8
460 13.79 35.76 26.84
                         122.2 135.3 1511.74 1.3272
                                                       381.8
500 12.60 35.56 26.92
                         114.1 127.4 1508.21 1.5796
                                                       435.9
540 11.67 35.40 26.98
                                                       492.1
                         108.6 122.0 1505.50 1.4294
580 10.63 35.29 27.09
                         98.3 111.7 1502.36 1.4765
                                                       550.2
620 10.00 35.17 27.10
                          96.9 110.4 1500.61 1.5204
                                                       610.1
660
      9.20 35.06 27.15
                          92.2 105.6 1498.19 1.5638
                                                       671.8
      8.58 34.97 27.19
 700
                          89.4 102.7 1496.43 1.6049
                                                       735.2
      8.04 34.92 27.22
740
                                98.8 1494.96 1.6449
                          85.5
                                                       A00.2
      7.48 34.88 27.28
780
                          80.3
                                93.4 1493.40 1.6834
                                                       866 · 8
      7.02 34.85 27.32
820
                                89.1 1492.23 1./200
                                                       934.9
                          76.1
      6.21 34.87 27.44
                                77.1 1489.73 1.7533
860
                          64.9
                                                      1004.3
900
      5.95 34.86 27.47
                          61.9
                                74.3 1489.33 1.7832
                                                      1075.1
      5.59 34.89 27.54
9411
                          55.3
                                67.6 1488.57 1.8113
                                                      1147.0
980
      5.75 34.91 27.58
                          51.5
                                63.7 1488.28 1.8376
                                                      1219.9
1020
      5.10 34.93 27.63
                          47.2
                                59.4 1487.97 1.8629
                                                      1294.0
     5.02 34.94 27.64
1100
                          45.6
                               58.6 1488.95 1.9085
                                                      1444.8
      4.62 34.96 27.71
                          39.5
                               52.6 1488.98 1.9631
1200
                                                      1638.4
     4.50 34.96 27.72
                          38.1
1300
                                52.0 1490.14 2.0155
                                                      1837.4
     4.45 34.97 27.74
1400
                                51.5 1491.58 2.0670
                          36.7
                                                      2041.5
      4.27 34.98 27.76
1500
                               49.4 1492.48 2.1176
                          54.3
                                                      2250.7
```

STD STATION NUMBER	082
AUGUST 19, 1971	18.3 /
LATITUDE	18 5/
LONGITUDE	R2 36
DEPTH TO BOTTOM	2354 M

Z.	т	5	SICT	TANCM	SVA	SVEL	TNHGT	TRANS
0		36.06				1543.18	.0000	• 0
20		35.06	23.26		463.1	1542.95	.0933	• 9
40	27.51		23.37		453.8	1542.78	.1850	3.7
611	27.50	36.06	23.38		454.1	1542.84	.2758	8.3
Rn	27.33		23.45	100	447.9	1542.79	.3660	14.7
100	26.86		23.71		424.0	1542.22	.4532	22.9
120	26.20	36.41	24.06		391.5	1541.19	.5347	32.8
140	25.66	35.52	24.31		368.5	1540.36	.6107	44.3
160	24.13		24.72	323.1	329.8	1538.63	.6306	57.2
180	23.55	36.87	25.18	279.4		1536.48	.7422	71.4
200	22.04		25.69		238.8	1532.77	.7948	86.8
220	20.31		25.97		212.8	1529.78	.8400	103.1
240	19.85	36.75	26.15	187.0	195.9	1527.41	.8809	120.3
260	19.04	36.66	26.29	173.9	183.2	1525.41	.9188	138.3
290	18.28	36.55	26.41	162.9	172.7	1523.45	. 9544	157.1
300	17.74	36.47	26.48	155.A	166.1	1522.14	.9883	176.5
340	16.00	36.20	26.57	147.7	158.9	1519.80	1.0534	217.3
390	15.79	34.13	26.68	137.1	149.1	1517,22	1.1151	260.7
420	14.78	35.95	26.77	128.1	140.7	1514.49	1.1725	306.5
460	13.30	35.70	26.86	120.0	133.1	1511.80	1.2273	354.5
500	12.30	35.63	26.94	112.4	125.9	1508.96	1.2788	404.6
540	11,45	35.41	27.03	103.5	116.8	1504.75	1.3271	456.7
580	10./1	35.30	27.08	99.1	112.4	1502.65	1.3732	510.7
650	9.97	35.22	27.16	91.3	104.8	1500.18	1.4167	566.6
660	9.05	35.07	27.19	89.0	102.2	1497.65	1.4586	624 • 1
700	8.24	34.98	27.25	83.4	96.3	1495.15	1.4980	683.2
740	7.50	34.92	27.29	79.0	91.7	1493.28	1.5354	743.9
780	7.119	34.84	27.33	75.n	87.5	1491.93	1.5713	806.0
820	0.67	34.85	27.37	71.8	84.2	1490.90	1.6057	869.6
860	6.25	34.86	27.43	66.0	78.5	1489.90	1.6383	934.4
900	5.80	34.87	27.50	59.6	71.7	1488.76	1.6693	1000.6
940	5.45	34.80	27.55	54.4	66.3	1488.03	1.6958	1067.9
980	5.20	34.92	27.61	48.0	60.9	1497.70	1.7214	1136.2
1020	4.49	34.92	27.64	46.3	58.3	1487.49	1.7452	1205.5
1100	4.75	34.94	27.68	42.4	54.8	1487.87	1.7902	1347.0
1200	4.56	34.96	27.72	38.9	51.9	1489.82	1.8438	1528•7 1715•7
		34.97	27.76	36.7	50.4		1.8949	1907.6
1500	4.28	34.98	27.75	35.0 35.2	49.4 50.4	1491.09	1.9447	2104.6
1600	4.24	34.98	27.76	34.4	50.4	1494.01	2.0444	2306.5
1700	4.21	34.98	27.77	53.8	50.6	1495.53	2.0943	2513.4
1800	4.19	34.90	27.78	32.8	50.5	1497.12	2.1449	2725.4
1900	4.18	34.99	27.78	32.7	51.3	1498.74	2.1958	2942.4
2000	4.16	35.00		51.8	51.3	1500.34	2.2468	3164.5
				-1.00			•	

STD STATION NUMBER	83		
AUGUST 19, 1971	23.2 /		
LATITUDE	18 46		
LONGITUDE	83 05		
DEPTH TO BOTTOM	1673 M		

2	T	S	SIGT	TANOM	SVA	SVEL	DYNHGT	TRANS
0	28.18	36.04	23.14	474.2	474.2	1543.33	.0000	• 0
50	27.90	36.11	23.28	460.6	461.5	1543.12	.0936	.9
40	27.62	36.10	23.36	452.5	454.2	1542.81	.1851	3.7
60	27.04	36.17	23.61	429.3	431.8	1541.92	.2737	8.3
80	26.77	36.25	23.16	415.3	418.6	1541.69	.3588	14.6
100	25.92	36.51	24.22	371.2	375.3	1540.31	.4382	22.6
120	24.88	36.64	24.64	331.1	335.9	1538.30	.5093	32.1
140	22.99	36.91	25.41	258.1	263.6	1534.21	.5693	42.9
160	21.73	36.91	25.77	223.8	250.0	1531.31	.6186	54.7
190	20.81	36.88	25.49	202.4	209.2	1529.17	.6625	67.6
500	19.87	36.76	26.15	187.1	194.5	1526.84	.7029	81.2
550	19.20	36.62	26.23	180.2	188.1	1525.17	.7412	95.7
240	18.64	36.54	26.31	172.4	180.9	1523.83	.7781	110.8
260	17.92	36.48	26.44	159.4	168.4	1522.02	.8130	126.8
580	17.32	36.44	26.56	148.7	158.2	1520.54	.8457	143.3
300	16.99	36.31	26.54	150.4	160.5	1519.77	.8775	160.6
340	15.99	36.15	26.65	139.7	150.6	1517.19	. 4309	196.9
380	15.10	36.02	26.75	130.1	141.8	1514.96	.4986	235.7
420	13.96	35.86	89.65	118.2	130.3	1511.76	1.0533	276.8
460	13,03	35.65	26.91	115.2	127.7	1509.11	1.1059	320.0
500	11.81	35.48	27.01	105.5	118.1	1505.43	1.1547	365.2
540	11.11	35.32	27.02	104.6	117.5	1503.46	1.2020	412.3
580	10.30		27.119			1501.09	1.2475	461.3
650	9.84	35.14	27.11	96.7	110.0	1499.97	1.2018	512.1
660	9.12	35.04	27.15	92.7	106.0	1497.88	1.3350	564.6
700	8.56	35.00	27.21	86.7	100.1	1496.40	1.3763	618.9
740	7.77	34.95	27.29		92.0	1493.97	1.4146	674.7
780	7.09	34.91	27.35	73.3	85.9	1491.94	1.4505	732.0
820	6.52	34.80	27.38	71.0		1490.25	1.4840	790.7
860	6.31	34.84	27.41	68.1	80.5	1490.09	1.5170	850.7
900	5.75		27.47	62.5	74.8	1489.35	1.5482	912.0
940	5.51		27.56	53.4		1488.28	1.5762	974.5
980	5.23		27.60	50.0	62.0	1487.83	1.6015	1038 • 1
1050	5.11	34.92	27.62	48.3	60.5	1488.00	1.6261	1102.6
1100	4.71	34.95	27.69	41.4	53.7	1487.70	1.6718	1234.6
1200	4.51		27.71	39.1	52.0	1488.51	1.7240	1404.4
1300	4.37		27.75	35.4		1489.62	1.7749	1579.4
1400	4.31		27.75	35.5	49.8	1490.99	1.8246	1759.3
1500	4.25	_	27.76	34.2	49.3	1492.41	1.8743	1944.3
1600	4.23	34.97	27.76	34.8	50.7	1493.96	1.9240	2134.2

STD STATION NUMBER	084
AUGUST 20, 1971	10.7 7
LATITUDE	21 49
LONG! TUD=	85 39
DEPTH TO BOTTOM	2631 M

```
S
                   SIGT
                         TANCM
                                SVA
                                       SVEL
                                              TUHET
                                                        TRANS
   0 29,29 36.15 22.85
                         501.7 501.7 1545.79
                                               .0000
                                                           • 0
  20 29.29 36.15 22.85
                                               .1004
                         501.7 502.6 1546.12
                                                          1.0
                                                ·Súue
                                                          4.0
  40 29.14 36.14 22.90
                         497.4 499.2 1546.11
                                               .2939
  60 27.47 36.32 23.58
                         431.8 434.4 1543.00
                                                          9.0
 .80 25.68 36.59 24.35
                         358.6 361.9 1539.50
                                                         15.6
                                                .3736
 100 24.38 36.72 24.85
                         311.1 315.2 1536.84
                                               .4413
                                                         23.8
 120 23.28 36.90 25.32
                         266.6 271.5 1534.61
                                                .5000
                                                         33.2
 140 22.25 34.95 25.64
                                                         43.7
                         235.6 241.1 1532.37
                                                .5512
 160 21.58 34.87 25.83
                         217.5 223.6 1530.37
                                                .5977
                                                         55.2
 180 20.36 36.79 26.05
                         197.2 204.0 1527.88
                                                .6405
                                                         67.6
                                                .6803
200 19.72 36.70 26.15
                         187.0 194.3 1526.36
                                                         80.8
 220 19.09 36.64 26.27
                                               . /182
                         176.4 184.3 1524.88
                                                         94.8
240 18.46 35.5P 26.38
                         165.2 173.7 1523.37
                                                .7539
                                                        109.5
                                               . 1882
 260 17.90 36.46 26.44
                         160.2 169.2 1521.95
                                                        124.9
                                               .8216
 280 17.46 36.40 26.49
                         154.8 164.3 1520.91
                                                        141.0
 300 17.97 36.33 26.53
                                                .8541
                         151.0 161.0 1520.01
                                                        157.8
 340 16.25 35.23 26.65
                         139.7 150.7 1518.09
                                                .9167
                                                        193.2
                         133.2 144.9 1515.44
 380 15.26 36.02 26.72
                                                .9759
                                                        231.1
420 14.65 35.96 26.P1
                         125.1 137.6 1514.09 1.0330
                                                        271.2
 460 14.05 35.83 26.83
                         122.5 135.8 1512.67 1.0882
                                                        313.7
                         117.3 131.0 1510.03 1.1417
 500 13.11 35.65 26.89
                                                        358.3
 540 12.30 35.52 26.46
                         110.8 124.9 1507.80 1.1927
                                                        405.0
580 11.52 35.42 27.02
                         104.7 119.0 1505.64 1.2416
                                                        453.7
620 10.86 35.33 27.07
                         99.8 114.3 1503.87 1.2886
                                                        504.3
660 10.37 35.18 27.05
                         102.0 117.1 1502.57 1.3348
                                                        556.7
                          89.7 103.8 1498.60 1.3795
700
      9.13 35.08 27.18
                                                        611.0
      7.19 34.95 27.37
                          71.5
                                83.7 1491.75 1.4162
740
                                                        667.0
      6.50 34.92 27.44
780
                          64.7
                                76.4 1489.64 1.4482
                                                        724.3
      6.07 34.90 27.49
820
                          60.5
                                72.1 1488.60 1.4777
                                                        782.8
      5.90 34.89 27.50
 R50
                          59.1
                                70.9 1488.55 1.5064
                                                        942.5
      5.65 34.91 27.55
                                66.8 1488.21 1.5339
900
                          54.0
                                                        903.3
940
      5.58 34.92 27.59
                          51.0
                                62.9 1487.80 1.5598
                                                        965.1
090
      5.08 34.93 27.63
                          46. R
                                58.5 1497.23 1.5841
                                                       1028.0
1050
      4.02 34.95 27.68
                          42.4
                                54.0 1486.83 1.6065
                                                       1091.8
      4.52 34.96 27.72
                          38.5
                                50.4 1486.95 1.6481
1100
                                                       1222.1
      4.35 34.97 27.75
1200
                          36.0
                                48.4 1487.88 1.6969
                                                       1389.3
      4.26 34.9H 27.77
1300
                          34.1
                                47.3 1489.17 1.7451
                                                       1561.4
                          34.1
1400
      4.23 34.98 27.77
                                48.2 1490.68 1.7934
                                                       1738.3
                          33.A
                                48.7 1492.24 1.8418
      4.21 34.98 27.77
                                                       1920.1
1500
      4.17 34.98 27.77
                          33.4
                                49.2 1493.73 1.8906
                                                       2106.7
1600
      4.16 34.99 27.78
                                49.5 1495.34 1.9396
1700
                          32.9
                                                       2298.2
      4.15 34.99 27.78
                                50.0 1496.96 1.9805
                          32.4
                                                       2494.7
1800
                          32.3
                                50.7 1498.57 2.0399
1900
      4.14 34.99 27.78
                                                       2696.2
2000
      4.13 35.00 27.79
                          31.5
                                50.8 1500.21 2.0901
                                                       2902.6
```

```
83 45
    LONGITUDE
    DEPTH TO BOTTOM
                         4114 M
                         TANOM SVA
                                              -YNHGT
       T
             5
                   SIGT
                                       SVE
                                                        TRANS
   0 29.51 36.16 22.85
                         501.6 501.6 1545.84
                                                .0000
                                                          • 0
  20 29,24 36,15 22,87
                         500.1 500.9 1546.01
                                                .1003
                                                          1.0
                         485.2 466.9 1544.73
  40 28.53 36.04 23.02
                                                .1990
                                                          4.0
                                                . Sous
  60 26.78 36.08 23.62
                         428.0 430.5 1541.25
                                                          8.9
  90 25.40 36.34 24.25
                         368.0 371.3 1538.62
                                                . 5710
                                                         15.5
 100 24.18 36.59 24.81
                         314.7 318.8 1536.25
                                                .4400
                                                         23.6
 120 22.81 36.71 25.30
                         267.7 272.5 1535.27
                                                .4991
                                                         33.0
                                                .5498
 140 21.56 36.70 25.71
                         229.5 234.8 1529.84
                                                         43.5
 160 20.23 36.67 25.99
                         202.4 208.4 1527.10
                                                . 5941
                                                         54.9
 180 19.62 36.62 26.12
                         190.6 197.3 1525.70
                                                .6347
                                                         67.2
 200 18.96 36.55 26.23
                         179.4 186.6 1524.11
                                                .6731
                                                         80.3
                                                . 7098
 220 18.57 36.51 26.30
                         172.9 180.7 1523.28
                                                         94.1
                                                . 1455
 240 18.19 36.46 26.36
                         167.4 175.8 1522.46
                                                        108.7
                                                . 7802
 260 17.75 36.39 26.42
                         162.1 171.1 1521.44
                                                        123.9
                                                .8137
 280 17.14 36.29 26.49
                         155.3 164.7 1519.86
                                                        139.9
                                                . 4458
 300 16.23 36.13 26.58
                         146.5 156.2 1517.28
                                                        156.5
                         135.5 146.0 1514.39
                                               .9056
 340 15.15 35.96 26.70
                                                        191.5
                                                .9622
                                                        228.9
 390 14.43 35.82 26.79
                         126.7 137.8 1511.95
 420 13.40 35.68 26.86
                         120.4 132.1 1509.73 1.0164
                                                        268.5
 460 12.52 35.54 26.92
                         113.8 125.9 1507.27 1.0676
                                                        310.1
 500 11.64 35.36 26.46
                         110.0 123.3 1504.69 1.1177
                                                        353.9
 540 10.62 35.23 27.04
                         102.7 115.1 1501.60 1.1649
                                                        399.5
      9.40 35.13 27.00
                          98.2 110.7 1499.54 1.2008
                                                        447.0
 580
                          92.6 105.2 1497.61 1.2533
                                                        490.3
 650
      9,22 35.06 27.15
                          90.3 103.1 1496.55 1.2951
      8.78 35.00 27.17
                                                        547.3
 660
 700
      8.22 34.94 27.21
                          86.4
                                99.3 1495.02 1.3356
                                                        599.9
                                 94.6 1493.19 1.3744
 740
      7.59 34.88 27.26
                          82.0
                                                        554.1
 7811
                          75.9
      7.03 34.86 27.32
                                 88.3 1491.65 1.4111
                                                        709.8
 820
      6.61 34.85 27.37
                          71.1
                                 83.5 1490.64 1.4454
                                                        766.9
 8611
      6.30 34.85 27.42
                          67.2
                                 79.6 1490.07 1.4779
                                                        R25.4
 900
      6.05 34.87 27.46
                          62.6
                                 75.2 1489.75 1.5086
                                                        885.1
 9411
                                 68.4 1488.75 1.5373
                                                        946.1
      5.63 34.89 27.53
                          56.1
                          51.1
 980
      5.33 34.91 27.59
                                 63.3 1488.22 1.5638
                                                       1008.1
1020
                                 59.9 1487.91 1.5886
      5.09 34.92 27.62
                          47.7
                                                       1071.1
                          42.1
      4.72 34.94 27.68
                                 54.4 1487.73 1.6343
                                                       1200.1
1100
      4.18 34.96 27.72
                                 50.8 1488.40 1.6863
                          38.1
1200
                                                       1366.1
      4. 49 34.96 27.73
                          37.1
                                 50.7 1499.67 1.7371
                                                       1537.3
1300
      4.53 34.97 27.75
                          55. P
                                 50.1 1491.08 1.7873
                                                       1713.5
1400
1500
      4.77 34.97 27.76
                          35.1
                                 50.3 1492.48 1.8375
                                                       1894.8
1600
      4.24 34.98 27.77
                          34.1
                                 50.1 1494.01 1.8877
                                                       2081.0
      4.21 34.98 27.77
                          33. R
                                 50.6 1495.54 1.9380
                                                       2272.3
1700
      4.19 34.90 27.78
                          32.A
                                 50.5 1497.12 1.9887
1800
                                                       2468.7
                                                       2670.1
1000
      4.17 34.90 27.78
                          32.6
                                 51.2 1495.70 2.0395
```

85 15.8 /

21 04

STD STATION NUMBER

4.15 35.00 27.79

2000

AUGUST 20, 1971

LATITUDE

31.7

51.1 1500.29 2.0906

```
AUGUST 20, 1971 18.9 / LATITUDE 21 15 10NG1TUDE 85 50 DEPTH TO BOTTOM 3823 M
```

```
S
                  SIGT
                         TANOM SVA
                                      SVEL
                                              DYNHIGT
                                                        TRANS
   0 29.45 36.15 22.80
                         506.8 506.8 1546.12
                                                          .0
                                               .uono
 20 29.23 36.13 22.96
                         501.2 502.0 1545.97
                                               .1009
                                                          1.0
 40 28.21 34.05 23.12
                         475.8 477.5 1544.04
                                               .1988
                                                          4.0
 60 26.71 36.05 23.62
                         428.0 430.5 1541.06
                                               .2897
                                                          8.9
                                               . 5719
 80 25.87 36.25 24.04
                         388.4 391.7 1539.64
                                                         15.5
100 24.75 36.48 24.56
                         339.0 343.1 1537.53
                                               .4453
                                                         23.7
120 25.41 36.68 25.11
                         286.5 291.3 1534.75
                                               .5088
                                                         33.2
140 22.12 36.73 25.52
                         247.5 253.0 1531.85
                                                         43.9
                                               .5632
160 20.84 36.68 25.83
                         217.3 223.4 1528.76
                                                         55.7
                                               .6108
180 19.47 36.65 26.07
                         194.7 201.4 1526.42
                                                         68.3
                                               .6533
200 19.32 36.59 26.17
                         185.4 192.6 1525.16
                                               .6927
                                                         81.8
                                               . 7305
220 18.76 36.52 26.26
                         176.8 184.6 1523.83
                                                         96.0
24n 18.26 35.48 26.36
                         167.6 176.1 1522.68
                                               .7665
                                                        111.0
260 17.90 36.41 26.42
                         161.9 170.8 1521.60
                                               .8012
                                                        126.7
290 17.40 36.36 26.48
                                               . 8349
                         156.2 165.7 1520.70
                                                        143.0
300 16.04 36.27 26.52
                         152.2 162.2 1519.57
                                               .8676
                                                        160.0
340 15.86 36.08 26.63
                         142.0 152.8 1516.73
                                               .9306
                                                        196.0
                                               .9888
380 14.45 35.85 26.76
                         129.0 140.2 1512.69
                                                        234.4
420 13.38 35.66 26.84
                         121.5 133.2 1509.64 1.0434
                                                        275.1
460 12.61 35.54 26.91
                         115.5 127.7 1507.58 1.0956
                                                        317.9
500 11.68 35.38 26.96
                         110.1 122.6 1504.86 1.1458
                                                        362.7
540 10.62 35.23 27.04
                         102.7 115.1 1501.60 1.1932
                                                        409.5
590
     9.93 35.13 27.08
                          98.7 111.2 1499.65 1.2383
                                                        458.1
      9.25 35.04 27.13
                          94.5 107.1 1497.70 1.2819
620
                                                        508.5
      8.63 34.98 27.18
660
                          89.5 102.1 1495.97 1.3234
                                                        560.6
700
      8.10 34.92 27.22
                          86.2
                                98.9 1494.54 1.3635
                                                        614.4
740
      7.55 34.87 27.26
                          82.2
                                94.7 1493.02 1.4021
                                                       669.7
790
      7.12 34.86 27.33
                          75.7
                                88.1 1491.61 1.4386
                                                        726.5
                          71.1
1158
      6.55 34.84 27.38
                                83.4 1490.39 1.4731
                                                        784.7
260
      6.21 34.86 27.44
                          65.4
                                77.6 1489.73 1.5053
                                                        844.3
ann
      5.08 34.89 27.48
                          61.0
                                73.5 1489.49 1.5356
                                                        905.1
940
      5.62 34.89 27.53
                          56.0
                                68.3 1488.71 1.5640
                                                        967.1
      5.30 34.90 27.58
                          51.5
ORN
                                63.7 1488.08 1.5905
                                                       1030.2
      5.07 34.92 27.62
1020
                          47.5
                                59.6 1487.83 1.6152
                                                      1094.4
                          42.1
                                54.4 1487.73 1.6609
      4.72 34.94 27.68
                                                      1225.4
1100
1200
      4.51 34.95 27.71
                          39.1
                                52.0 1488.51 1.7135
                                                      1394.2
                                50.9 1489.75 1.7647
1300
      4.41 34.96 27.73
                          37.3
                                                       1568 • 1
1400
      4.34 34.97 27.75
                          35.9
                                50.2 1491.12 1.8154
                                                       1747.1
1500
      4.28 34.97 27.75
                          35.2
                                50.4 1492.52 1.8657
                                                      1931.1
```

```
STD STATION NUMBER 86
AUGUST 20, 1971 22.8 7
LATITUDE 20 43
LONGITUDE 83 58
DEPTH TO ROTTOM 4393 M
```

```
THHET
                         TANIO
                                                        TRANS
                   SIGT
                               SVA
                                       SVEL
  n 29.27 36.14 22.85
                         501.7 501.7 1545.74
                                               .0000
                                                           • 0
  20 29.18 34.13 22.87
                         499.6 500.4 1545.86
                                               .1002
                                                          1.0
  40 29.05 36.10 22.89
                         497.5 499.3 1545.89
                                               .2002
                                                          4.0
                         477.1 479.7 1544.63
                                               .2981
  60 28.32 36.06 23.11
                                                          9.0
                         448.6 452.0 1542.83
                                               .3912
  80 27.36 36.04 23.41
                                                         15.9
                         425.7 429.9 1541.79
 100 26.73 36.09 23.65
                                               .4794
                                                         24.6
 120 25.99 36.21 23.97
                         394.9 399.8 1540.53
                                                         35.0
                                               .5624
 140 25.17 36.30 24.36
                         357.7 363.4 1539.10
                                                         47.0
                                               .6387
                         290.7 297.1 1535.63
 160 23.51 36.66 25.06
                                               . /048
                                                         60.5
 190 22,40 36.77 25.47
                         252.2 259.3 1533.25
                                               . 7604
                                                         75.1
200 21.22 36.72 25.76
                         224.3 232.0 1530.45
                                               .8096
                                                         90.8
220 20.12 36.66 26.01
                         200.3 208.5 1527.75
                                               . A5 36
                                                        107.4
240 19.33 36.59 26.17
                         185.6 194.3 1525.83
                                               .8939
                                                        124.9
                         174.1 183.3 1524.07
260 18.62 36.51 26.29
                                               .9316
                                                        143.2
290 18.06 36.45 26.38
                         165.1 174.8 1522.72
                                               .9675
                                                        162.2
                         159.9 170.1 1521.49 1.0020
                                                        181.9
 300 17.56 35.36 26.44
                         148.8 159.9 1518.89 1.0677
 340 16.53 36.19 26.56
                                                        223.3
380 15.51 36.01 26.65
                         139.5 151.4 1516.21 1.1297
                                                        267.2
                         127.0 140.1 1512.15 1.1877
420 14.11 35.77 26.78
                                                        313.6
460 13.03 35.59 26.86
                         119.8 132.3 1509.04 1.2420
                                                        362.2
500 12.20 35.48 26.94
                         112.2 125.2 1506.76 1.2933
                                                        412.9
 540 11.32 35.35 27.01
                         105.9 119.1 1504.21 1.3423
                                                        465.6
                         101.7 114.8 1501.69 1.5891
 580 10.47 35.21 27.05
                                                        520.2
 620
      9.61 35.11 27.12
                          95.0 108.1 1499.10 1.4337
                                                        576.7
 660
      9.44 35.04 27.16
                          91.3 104.4 1497.57 1.4761
                                                        634.9
                          86.3
      8. 11 34.96 27.22
                                99.2 1495.38 1.5169
                                                        694.8
 700
      7.86 34.93 27.26
                                95.1 1494.29 1.5557
 740
                                                        756.2
                          82.0
                                89.2 1491.88 1.5924
 780
                                                        819.2
      7.09 34.86 27.32
                          76.7
                                83.5 1490.64 1.6268
                                                        883.6
 820
      6.61 34.85 27.37
                          71.1
                                76.7 1489.70 1.6590
      6.20 34.87 27.45
 860
                          64.5
                                                        949.3
                                71.1 1488.81 1.6885
900
      5.01 34.8P 27.50
                          59.0
                                                       1016.3
      5.51 34.90 27.56
940
                          54.0
                                66.0 1488.28 1./159
                                                       1084.4
                          49.6
 980
      5.26 34.92 27.60
                                61.7 1487.95 1.7416
                                                       1153.5
1020
      5.04 34.93 27.64
                          46.4
                                58.5 1487.72 1.7656
                                                       1223.7
      4.72 34.95 27.69
1100
                          41.4
                                53.7 1487.74 1.8105
                                                       1366.7
      4.52 34.96 27.72
                          3A.5
1200
                                51.4 1488.57 1.8630
                                                       1550 . 4
      4.39 34.97 27.74
1300
                          36.4
                                49.9 1499.68 1.9138
                                                       1739.3
      4. 12 34.97 27.75
                          35.7
                                50.0 1491.04 1.9637
                                                       1933.1
1400
      4.27 34.97 27.76
                                50.3 1492.47 2.0137
1500
                          35.1
                                                       2132.0
      4.23 34.98 27.17
                          34.0
                                49.9 1493.97 2.0634
1699
                                                       2335.9
                          53. n
      4.21 34.99 27.78
                                49.9 1495.55 2.1136
1700
                                                       2544.7
      4.19 34.98 27.17
                                51.3 1497.11 2.1643
1800
                          33.6
                                                       2758.6
      4.17 35.00 27.79
1000
                          31.0
                                50.4 1498.71 2.2152
                                                       2977.6
      4.14 35.00 27.79
2000
                                50.9 1500.24 2.2662
                          31.6
                                                       3201.6
```

```
I ONG ! TUDE
                         75
                             Ort
    DEPTH TO ROTTOM
                         3566 M
                   SIST
                         TANOM
                                SVA
                                       SVEL.
                                              PYNHGT
                                                        TRANS
             S
                         499.7 499.7 1546.21
   0 29.45 36.25 22.87
                                                .0000
                                                           • 0
  20 29.29 35.25 22.93
                         494.5 495.4 1546.20
                                                .0995
                                                          1.0
  40 28.90 35.27 23.11
                         477.3 479.0 1545.51
                                                          4.0
                                                .1969
                         426.5 429.1 1542.31
  60 27.18 36.27 23.64
                                                .2878
                                                          8.8
  80 25.60 36.43 24.26
                         367.4 370.7 1539.17
                                                         15.4
                                                . 3677
                                                .4369
 100 24.34 36.62 24.79
                         317.1 321.2 1536.66
                                                         23.4
 120 23.01 36.68 24.96
                         300.5 305.4 1535.99
                                                .4996
                                                         32.8
                                                .5585
 149 23.26 36.74 25.20
                         278.0 283.6 1534.75
                                                         43.4
 160 22.26 36.79 25.52
                         247.0 253.3 1532.58
                                                .6122
                                                         55.1
 180 21.00 36.78 25.87
                         214.3 221.1 1529.59
                                                .6596
                                                         67.8
 200 19.06 36.70 26.09
                         193.4 200.8 1527.03
                                               .7018
                                                         81.4
 220 18.90 36.59 26.27
                         176.1 184.0 1524.41
                                                .7403
                                                         95.8
 240 18.50 36.55 26.35
                         168.3 176.8 1523.44
                                                .7763
                                                        111.0
                         160.7 169.8 1522.36
 260 18.03 34.50 26.03
                                                .8110
                                                        126.9
                         156.3 166.0 1521.84
                                                .8446
 280 17.75 34.47 26.48
                                                        143.4
 300 17.35 36.41 26.53
                                                .8773
                                                        160.6
                         151.4 161.6 1520.92
 340 16.74 36.31 26.60
                         144.8 156.0 1519.65
                                                .9408
                                                        197.0
 380 15.92 36.17 26.68
                         136.8 148.9 1517.65 1.0018
                                                        235.9
420 15.16 34.03 26.75
                         130.6 143.5 1515.78 1.0605
                                                        277.1
460 13.83 35.77 26.84
                         122.3 135.4 1511.88 1.1162
                                                        320.6
 500 13.00 35.65 26.91
                         114.8 128.4 1509.65 1.1689
                                                        366.4
 540 11.89 35.47 26.99
                         107.3 121.0 1506.33 1.2188
                                                        414.1
 58n 11.18 35.39 27.06
                         100.5 114.5 1504.42 1.2656
                                                        463.8
 620 10.40 35.30 27.14
                          93.9 107.9 1502.20 1.3100
                                                        515.3
      9.76 35.23 27.19
                          88.5 102.7 1500.45 1.3521
                                                        568.6
 660
      9.15 35.16 27.24
 700
                          84.1
                                 98.3 1498.78 1.3922
                                                        623.5
      8.38 35.06 27.28
                          79.9
                                93.7 1496.43 1.4305
                                                        679.9
 740
      7.76 34.97 27.31
                          77.6
                                 91.3 1494.61 1.4676
                                                        737.9
 780
 820
      7.18 34.94 27.37
                          71.9
                                 85.5 1492.99 1.5031
                                                        797.3
      6.58 34.90 27.42
 860
                          67.0
                                 80.0 1491.24 1.5362
                                                        858.1
                                                        920.2
900
      6.20 34.90 27.47
                          62.2
                                 75.1 1490.39 1.5672
      5. 24 34.91 27.52
                                                        983.4
 940
                          57.1
                                 69.8 1489.62 1.5961
      5.43 34.93 27.59
                                                       1047.8
 980
                          50.8
                                63.2 1488.65 1.6227
1020
      5.26 34.96 27.63
                          46.6
                                 59.2 1488.65 1.6472
                                                       1113.2
      4.16 34.97 27.69
                                 54.0 1486.34 1.6920
                                                       1246.8
1100
                          41.4
                                49.7 1489.51 1.7437
                                                       1418.7
1500
      4.73 35.02 27.74
                          36.2
1300
      4.50 35.01 27.76
                          34.5
                                48.4 1490.19 1.7928
                                                       1595.5
1400
      4.44 35.02 27.78
                          33.1
                                47.9 1491.60 1.8407
                                                       1777.2
      4,53 35.02 27.79
                                 47.4 1492.79 1.8882
                                                       1963.6
1500
                          52.0
      4.28 35.03 27.80
                                 47.0 1494.25 1.9355
                                                       2154.8
1600
                          30.7
1700
      4.24 35.02 27.80
                          31.1
                                 48.1 1495.72 1.9833
                                                       2350.7
      4.21 35.03 27.81
1800
                          30.0
                                 47.9 1497.26 2.0311
                                                       2551.5
                          29.7
1900
      4.18 35.03 27.81
                                 48.4 1498.79 2.0793
                                                       2757.0
```

STD STATION NUMBER

SEPTEMBED 10, 1971

4.17 35.04 27.82

2000

LATITUDE

001

17.6 7

19 26

28.9

48.5 1500.43 2.1278

```
STD STATION NUMBER 002
SEPTEMPER 11, 1971 00.1 /
LATITUDE 19 00
LONGITUDE 75 59
DEPTH TO BOITOM 2845 M
```

```
TYNHET
                         TANOM SVA
                                                        TRANS
                  SIGT
                                       SVEI
  0 29.52 35.24 22.84
                         502.7 502.7 1546.34
                                               .0000
                                                          • 0
  20 29.49 36.24 22.85
                         501.7 502.6 1546.60
                                                          1.0
                                               ·1005
                                               .2003
  40 29.22 36.23 22.93
                         493.7 495.4 1546.36
                                                          4.0
  60 28.28 36.27 23.08
                         479.9 482.5 1546.00
                                               .2981
                                                          9.0
  80 27.74 36.25 23.43
                         446.7 450.1 1543.84
                                                         15.9
                                               . 5014
 100 25.98 36.39 24.11
                         381.6 385.7 1540.34
                                                         24.6
                                               .4750
 120 24.38 36.57 24.58
                         336.3 341.2 1538.24
                                                         34.8
                                               .5476
 140 23.81 36.63 24.95
                         301.3 307.0 1536.02
                                               .6125
                                                         46.4
 160 22.00 36.78 25.59
                         240.7 246.9 1531.90
                                               .6678
                                                         59.2
 180 20.39 36.77 25.86
                         214.7 221.6 1529.56
                                                . /147
                                                         73.0
                                               . 1570
 200 20.00 36.71 26.08
                         193.7 201.1 1527.15
                                                         87.7
 220 19. 12 36.65 26.22
                                                . 1960
                                                        103.3
                         181.0 189.0 1525.53
                         169.5 178.0 1523.49
                                               .8327
                                                        119.5
 240 18.52 36.54 26.34
 2611 18.04 36.50 26.43
                         161.0 170.0 1522.39
                                               .8675
                                                        136.5
 280 17.57 36.44 26.50
                                               .9009
                         154.3 163.9 1521.28
                                                        154.2
 300 17.27 36.39 26.53
                                               . 9334
                         151.0 161.1 1520.67
                                                        172.6
 340 16.52 36.26 26.61
                         143.5 154.6 1518.93
                                               .9065
                                                        211.2
 380 15.70 36.12 26.69
                         135.6 147.6 1516.92 1.0569
                                                        252.3
 420 14.95 35.98 26.78
                         127.8 140.5 1514.75 1.1145
                                                        295.7
 460 13.70 35.79 26.88
                         118.2 131.3 1511.48 1.1691
                                                        341.4
 500 12.70 35.64 26.97
                         109.8 123.2 1508.64 1.2200
                                                        389.2
                          98.5 111.6 1504.00 1.2659
 540 11.03 35.43 27.09
                                                        438.9
 580 11.07 35.38 27.08
                          99.4 113.2 1504.02 1.5109
                                                        490.4
620 10.19 35.25 27.13
                          94.0 107.8 1501.38 1.3549
                                                        543.7
660
      9.51 35.17 27.19
                          89.0 102.8 1490.46 1.3068
                                                        598.8
                          84.2
                                97.9 1497.46 1.4369
 700
      8.82 35.09 27.24
                                                        655.5
                                91.5 1494.76 1.4746
 741
      7.96 35.00 27.30
                          78.2
                                                        713.7
                          74.1
 780
      7.18 34.91 27.34
                                86.8 1492.30 1.5103
                                                        773.4
                          69.0
620
      6.56 34.87 27.40
                                81.3 1490.47 1.5439
                                                        834.5
      6.08 34.87 27.46
                          63.0
 850
                                75.1 1489.22 1.5750
                                                        A96.9
      5.64 34.89 27.53
                                68.0 1488.14 1.6037
                                                        960.5
900
                          56.2
0411
      5.35 34.91 27.58
                          51.4
                                63.1 1487.65 1.6209
                                                       1025.1
980
      5.17 34.93 27.62
                          47.A
                                59.7 1487.60 1.6544
                                                       1090.8
1020
      4.07 34.95 27.66
                          44.1
                                56.1 1487.46 1.6776
                                                       1157.5
      4.75 34.97 27.70
                          40.2
1100
                                52.6 1487.89 1./211
                                                       1293.4
1200
      4.52 34.98 27.74
                          37.1
                                49.9 1488.60 1./721
                                                       1468 - 1
1300
      4.42 35.00 27.76
                          34.4
                                48.1 1480.85 1.8210
                                                      1647.8
      4.77 35.01 27.78
                          33.2
                                47.7 1491.30 1.8602
1400
                                                       1432.3
                          32.6
1500
      4.32 35.01 27.78
                                48.0 1492.74 1.9171
                                                      2021.6
      4.25 35.02 27.80
1600
                          31.2
                                47.3 1494.11 1.9646
                                                      2215.7
      4.00 35.02 27.80
                          30.7
1700
                                47.6 1495.55 2.0119
                                                      2414.5
                          30.5
1800
      4.18 35.02 27.80
                                48.2 1497.12 2.0598
                                                       2618.1
1900
      4.17 35.02 27.81
                          30.4
                                49.0 1498.74 2.1084
                                                       2826.5
```

STD STATION NUMBER	003
SEPTEMBER 11, 1971	10.4 7
LATITUDE	19 39
LONGITUDE	74 05
PEPTH TO BOTTOM	2900 M

```
SIGT
                         TANOM
       T
             S
                                 SVA
                                       SVEL
                                              DYNHET
                                                        TRANS
  0 29.17 36.24 22.96
                         491.3 491.3 1545.61
                                                .0000
                                                           • 0
  20 29.16 36.23 22.95
                         491.7 492.6 1545.91
                                                .0984
                                                          1.0
                         476.0 477.7 1545.02
                                                .1954
 40 28.50 36.20 23.12
                                                          3.9
  60 27.78 36.20 23.39
                         450.2 452.7 1543.58
                                                .2885
                                                          8.8
  80 26.58 36.31 23.86
                         405.4 408.7 1541.32
                                                . 3746
                                                         15.4
 100 25.78 36.46 24.22
                         370.6 374.7 1539.94
                                                .4530
                                                         23.7
 120 24.65 36.59 24.67
                         328.2 333.1 1537.71
                                                         33.4
                                                .5237
 140 23.67 36.70 25.05
                         292.3 298.0 1535.74
                                                         44.5
                                                .5868
 160 23.16 36.74 25.23
                         275.2 281.6 1534.82
                                                .6448
                                                         56.9
 180 22.25 36.79 25.53
                         246.7 253.8 1532.88
                                                .6983
                                                         70.3
 200 21.42 36.75 25.73
                         227.4 235.1 1531.00
                                                .7472
                                                         84.7
                                                . 1907
 220 19.48 36.63 26.11
                         191.4 199.5 1526.52
                                                        100.1
 240 18.05 36.61 26.28
                         174.8 163.5 1524.78
                                                .8290
                                                        116.3
 260 18.53 36.56 26.35
                         168.3 177.5 1523.86
                                                .8651
                                                        133.3
                                                .8999
 290 18.06 36.51 26.43
                         160.7 170.5 1522.78
                                                        150.9
                         154.5 164.8 1521.83
 300 17.64 36.46 26.50
                                                . 4334
                                                        169.2
                                                .9982
 340 17.08 36.37 26.56
                         148.1 159.5 1520.73
                                                        207.9
 380 16.37 36.24 26.63
                         141.6 153.9 1519.10 1.0608
                                                        249.1
 420 15.28 36.06 26.74
                         131.0 144.0 1516.19 1.1193
                                                        292.7
460 14.43 35.91 26.82
                         124.2 137.8 1513.98 1.1760
                                                        338.6
 500 13.54 35.76 26.89
                         117.3 131.3 1511.57 1.2297
                                                        386.7
 540 12.59 35.61 26.97
                         110.0 124.3 1508.88 1.2808
                                                        436.9
 580 11.59 35.45 27.03
                         103.4 117.8 1505.92 1.3294
                                                        489.1
 620 10.72 35.33 27.10
                          97.0 111.4 1503.37 1.5751
                                                        543.2
      9.72 35.19 27.17
 660
                          90.8 104.9 1500.25 1.4183
                                                        599.1
 700
      9.08 35.10 27.20
                          87.4 101.5 1498.44 1.4595
                                                        656.7
 740
      8. +1 35.03 27.25
                          82.5
                                96.4 1496.50 1.4991
                                                        715.8
      7.67 34.96 27.31
                          77.1
 780
                                                        776.6
                                 90.6 1494.25 1.5365
      7.30 34.93 27.34
                          74.3
 820
                                 87.8 1493.44 1.5722
                                                        838.7
 860
      6.90 34.91 27.38
                          70.4
                                 83.9 1492.51 1.6067
                                                        902.3
 900
      6.43 34.89 27.43
                          65.9
                                                        967.2
                                 79.1 1491.28 1.6391
 940
      5.97 34.89 27.49
                          60.2
                                 73.1 1490.11 1.6699
                                                       1033.4
      5.67 34.91 27.54
                          55.1
 980
                                 68.0 1489.59 1.6980
                                                       1100.8
      5.72 34.90 27.60
                          49.7
1020
                                 63.3 1490.55 1./241
                                                       1169.2
      5.03 34.98 27.68
                          42.5
1100
                                 55.6 1489.05 1.7718
                                                       1309.1
                          38.6
1200
      4.31 35.00 27.72
                                 52.3 1489.81 1.8253
                                                       1489.0
1300
      4.67 35.02 27.75
                          35.6
                                 50.0 1490.91 1.8759
                                                       1674.1
1400
      4.45 35.03 27.78
                          32.5
                                 47.3 1491.66 1.9247
                                                       1864.1
1500
      4.35 35.03 27.79
                          31.5
                                 47.0 1492.89 1.9718
                                                       2058.9
1600
      4.31 35.03 27.80
                          31.0
                                 47.4 1494.37 2.0194
                                                       2258.5
                                                       2462.8
1700
      4.23 35.02 27.80
                          31.0
                                 48.0 1495.68 2.0674
1800
      4.18 35.02 27.80
                          30.5
                                 48.2 1497.12 2.1154
                                                       2672.0
1900
      4.16 35.02 27.81
                          30.3
                                 48.8 1498.70 2.1639
                                                       2835.9
      4.15 35.03 27.82
                          29.4
2000
                                 48.9 1500.33 2.2123
                                                       3104.7
```

```
      STD STATION NUMBER
      004

      SEPTEMBED 11, 1971
      16.5 %

      LATITUDE
      20 12

      LONGITUDE
      75 14

      DEPTH TO BOITOM
      1360 M
```

7	т	5	SIGT	TANOM	SVA	SVEL	THHET	TRANS
	27.05		23.68			1542.08	.0000	•0
	27.45		25.69		422.8	1542.42	.0845	.8
40	-		23.65		427.0	1542.44	.1695	3.4
60			23.88			1541.65	.2528	7.6
80			24.03			1541.02	.3326	13.5
-	25.40		24.43			1539.16	.4073	20.9
	24.90		24.63			1538.35	4765	29.7
140	22 3		24.93	The state of the s		1536.64	.5411	39.9
	23.28		25.24			1535.18	.6001	51.3
180			25.68		238.6	1531.57	.6520	63.8
200	_		26.12			1526.92	.6956	77.3
250			26.31			1524.36	.7333	91.6
240			26.41		171.0	1522.94	.7685	106.6
260			26.47			1522.24	.8022	122.3
280			26.50			1521.71	.8352	138.7
300	and the second		26.53		161.0	1521.26	.8676	155.7
340			26.61			1519.86	.9308	191.7
380	15.82		26.69	136.0		1517.32	.9916	230.1
420			26.78	128.0	140.7	1515.03	1.0495	271.0
460	15.91	35.82	26.86	120.2	133.5	1512.20	1.1044	314.0
500	13.07	35.69	26.93	113.2	126.9	1509.93	1.1562	359.3
540	12.23	35.58	27.01	105.5	119.5	1507.62	1.2052	406.5
580	11.38	35.45	27.07	99.6	113.8	1505.19	1.2520	455.6
620	10.28	35.30	27.16	91.4	105.8	1501.77	1.2960	506.6
660	9.74	35.25	27.21	86.7	100.9	1500.40	1.3370	559.3
700	9.40	35.20	27,23	85.0	99.6	1499.75	1.3770	613.6
740			27.26	82.1	96.7	1498.19	1.4162	669.4
780			27.31	77.0	91.0	1495.51	1.4535	726.8
850			27.33	75.6	89.6	1494.48	1.4895	785.7
860			27.39	69.7	83.5	1493.22	1.5241	A46.0
900			27.44	65.4	79.7	1493.54	1.5565	907.6
940			27.49	50.5	74.1	1491.49	1.5873	970.5
980			27.51	58.1	72.1	1491.64	1.6165	1034.5
1020			27.54	55.4	69.5	1491.42	1.6451	1099.8
1100			27.66	43.7	56.6	1488.90	1.6971	1233.5
1200	4.31	35.00	27.72	38.6	52.3	1489.82	1.7505	1406.0

```
STD STATION NUMBER 005
SEPTEMBER 11, 1971 22,4 7
LATITUDE 20 19
LONGITUDE 72 11
DEPTH TO ROTTOM 3950 M
```

```
TANOM SVA
                                      SVEL
                                                        TRANS
                   SIGT
                                              DYNHGT
   0 28.48 36.40 23.31
                         457.8 457.8 1544.29
                                               .0000
                                                           • 0
                         434.4 434.9 1543.18
                                               . 0893
  20 27.80 36.43 23.55
                                                           .9
  40 27.13 36.47 23.80
                         411.1 412.3 1542.04
                                               .1740
                                                          3.5
  60 26.45 36.50 24.04
                         387.8 390.1 1540.87
                                               .2542
                                                         7.8
  An 25.26 36.61 24.50
                         344.5 347.8 1538.53
                                               .3280
                                                         13.6
                                               . 3954
 100 24.54 36.63 24.75
                         322.1 326.2 1537.15
                                                        20.9
 120 24.19 36.65 24.85
                         310.7 315.5 1536.65
                                               .4596
                                                         29.4
 140 23.22 36.76 25.22
                         275.4 281.0 1534.67
                                               .5192
                                                         39.2
 160 22.03 36.83 25.62
                         237.9 244.1 1532.02
                                               .5718
                                                         50.1
 180 21.19 36.83 25.85
                         215,6 222.5 1530,14
                                               .6184
                                                         62.0
 200 20.20 36.74 26.05
                         196.6 204.0 1527.72
                                               .6611
                                                         74.8
 220 19.31 36.68 26.24
                         178.6 186.6 1525.53
                                               .7001
                                                         88.4
 240 18.71 36.62 26.35
                         168.3 176.9 1524.11
                                               .7365
                                                        102.8
                                               .7713
 260 18.34 36.58 26.41
                         162.3 171.5 1523.33
                                                       117.9
 280 18.03 36.54 26.46
                         157.8 167.6 1522.72
                                               .8052
                                                       133.6
 300 17.79 36.50 26.49
                         155,1 165,4 1522,30
                                               .8385
                                                       150.1
 340 17.29 36.43 26.56
                         148.6 160.1 1521.41
                                               .9033
                                                       184.9
 380 16.85 36.34 26.60
                         145.1 157.7 1520.65
                                               .9668
                                                       222.3
 420 15.03 36.01 26.76
                         129.3 142.2 1515.35 1.0277
                                                       262.2
 460 14.88 35.99 26.78
                         127.7 141.6 1515.50 1.0848
                                                       304.5
 500 14.14 35.86 26.84
                         121.9 136.5 1513.64 1.1407
                                                       349.0
 540 12.78 35.66 26.97
                         109.9 124.4 1509.57 1.1934
                                                       395.7
                         106.9 122.1 1508.69 1.2431
 580 12.35 35.59 27.00
                                                       444.4
 620 11.40 35.45 27.07
                         100.0 115.2 1505.90 1.2905
                                                       495.1
 669 10.47 35.33 27.15
                          92.8 107.8 1503.13 1.3351
                                                        547.6
 700
      9.92 35.26 27.20
                          87.3 102.4 1501.35 1.3772
                                                       601.9
      9.07 35.16 27.25
                               97.7 1499.13 1.4172
 7411
                          82.8
                                                       657.8
      8.49 35.11 27.30
 780
                          77.A
                                92.6 1497.55 1.4552
                                                        715.2
 820
      7.78 35.05 27.34
                          74.8
                                89.5 1496.20 1.4915
                                                       774.1
      7.53 35.02 27.38
                          70.7
                                                       834.5
 860
                                85.4 1495.09 1.5265
 900
      6.61 34.93 27.44
                                78.8 1492.05 1.5595
                          65.2
                                                       896.2
      6.21 34.92 27.48
                          60.9
 940
                                74.3 1491.11 1.5898
                                                       959.2
 989
      5.71 34.92 27.55
                                67.8 1489.76 1.6183
                          54.8
                                                      1023.4
      5.41 34.93 27.59
1020
                          50.6
                                63.4 1489.22 1.6441
                                                      1088.6
                                54.8 1489.28 1.6914
1100
      5.08 35.00 27.69
                          41.6
                                                      1222.1
1200
      4.77 35.03 27.75
                          35.9
                                49.5 1489.69 1.7435
                                                      1393.9
      4.61 35.04 27.77
                                47.7 1490.69 1.7921
1300
                          33.4
                                                      1570.7
      4.42 35.03 27.79
                          32.2
                                46.9 1491.53 1.8396
                                                      1752.3
1400
      4.20 35.02 27.80
                          30.7
                                45.7 1492.25 1.8859
1500
                                                      1938.6
1600
      4.11 35.02 27.81
                          29.8
                                45.4 1493.53 1.9313
                                                      2129.4
                          29.1
1700
      3.97 35.01 27.82
                                45.1 1494.58 1.9762
                                                      2324.8
                                44.1 1495.65 2.0210
                          27.7
1800
      3.83 35.01 27.83
                                                      2524.7
1900
      3.71 35.01 27.85
                                43.3 1496.81 2.0647
                                                      2729.0
                          26.6
2000
      3.61 35.01 27.96
                          25.6
                                42.7 1498.05 2.1077
                                                      2937.6
```

STD STATION NUMBER	006
SEPTEMBE: 12, 1971	14.4 7
LATTTUDE	50 Eu
LONGITUDE	69 05
DEPTH TO BOTTOM	3590 M

7	T	5	SIGT	TANOM	SVA	SVEL	DANHEL	TRAMS
0	28.51	34.54	23.25	465.1	463.1	1544.30	•0000	• 0
50	28.47	34.41	23.52	456.8	457.6	1544.60	.0921	• 9
40	28.45	36.44	23.36	453.3	455.1	1544.86	.1833	3.7
60	27.77	36.47	23.60	430.4	433.0	1543.78	. 2721	8.2
80	25.56	36.56	24.57	356.9	360.2	1539.19	. 3515	14.5
100	24.52	36.61	24.72	323.0	327.1	1537.09	.4202	22.2
120	23.91	36.58	24.88	307.7	312.6	1535.90	.4842	31.2
140	23.52	36.61	25.02	294.6	300.2	1535.29	. 5454	41.5
160	23.74	34.75	25.18	274.5	285.9	1535.28	.6041	53.0
190	22.47	35.84	25.50	249.1	256.2	1533.49	.6583	65.6
200	21.30	36.85	25.84	217.0	224.7	1530.77	. 1064	79.3
550	20.15	36.75	26.06	195.5	203.7	1527.85	.7492	93.8
2411	19.53	36.66	26.22	180.6	189.5	1525.89	. 7885	109.2
260	18.33	36.61	26.31	171.9	181.2	1524.76	.8255	125.4
280	18.48	36.59	26.39	164.0	174.8	1524.06	· 8611	142.2
300	13.16	36.55	26.44	160.2	170.7	1523.43	.8957	159.8
3411	17.68	36.44	26.51	153.2	164.9	1522.62	. 4627	197.0
380	17.19	36.42	26.58	147.0	159.8	1521.75	1.0276	236.8
420	16.75	35.35	26.62	143.1	156.9	1520.93	1.0909	279.1
460	15.76	36.19	26.69	136.2	150.8	1519.08	1.1524	324.0
500	15.24	36.07	26.76	129/4	144.8	1517.37	1.2116	371.3
540	13.95	35.85	26.87	118.8	134.4	1513.65	1.2677	420.9
580	13.13	35.72	26.04	112.2	128.1	1511.46	1.3201	472.7
620	12.21	35.59	27.02	104.3	120.4	1508.86	1.5697	526.5
660	11.27	35.45	27.09	97.7	113.7	1506.09	1.4163	582.2
700	10.36	35.33	27.17	91.0	106.8	1503.38	1.46.04	639.7
740	9.85	35.26	27.20	87.7	103.7	1502.10	1.5024	699.0
780	9.03	35.16	27.26	82.2	97.8	1499.63	1.5429	759.9
820	8.44	35.10	27.30	77.R	93.2	1496.00	1.5811	822.4
860	7.75	35.04	27.36	72.3	87.3	1495.96	1.6170	P86 • 4
900	7.31	35.00	27.40	69.2	84.1	1494.86	1.6512	951.7
940	7.36	35.08	27.45	63.9	79.7	1495.81	1.6838	1018.4
980	6.73	30.06	27.52	57.0	72.2	1493.99	1.7144	1086.4
1020	5.74	35.07	27.64	46.4	60.5	1491.53	1.7415	1155.5
1100	5.59	35.06	27.67	42.0	57.4	1491.42	1.7806	1296.8
1200	5.07	35.06	27.74	37.0	51.4	1490.96	1.8440	1478.5
1300	4.73	35.05	27.77	34.0	48.6	1491.19	1.8936	1665.4
1400	4.41	35.05	27.40	30.6	45.3	1491.52	1.9406	1857.2
1500	4.17	35.03	27.81	29.6	44.5	1492.14	1.9857	2053.5
1600	4.00	35.03	27.85	21.0	43.2	1493.08	2.0294	2254.3
1700	5.08	35.02	27.84	27.5	43.2	1494.22	2.0723	2459.3
1800	3.75	35.02	27.95	26.0	42.0	1495.25	2.1149	2668.7
1900	3.61	35.02	27.R6	24.9	41.2	1496.40	2.1562	2882.3
2000	3.50	35.02	27.87	23.8	40.5	1497.60	2.1958	3099.9

STD STATION NUMBER	007
SEPTEMBE: 15, 1971	02.2 7
LATITUDE	18 1"
LONGITUDE	64 40
DEPTH TO POTTOM	0727 M

Z	T	5	SIGI	TANOM	SVA	SVEI.	PYNHGT	TRANS
()	28.39	35.34	22.54	531.1	531.1	1543.12	.0000	• 0
20	28,20	35.74	22.91	496.4	497.2	1543.42	.1028	1.0
$a_0$	27.83	36.09	23.29	459.6	461.3	1543.26	.1987	4.0
60	27.38	36.32	23.61	429.1	431.7	1542.80	.2880	8.9
80	26.18	36.54	24.16	376.9	380.1	1540.61	. 3692	15.5
100	25.42	34.65	24.48	346.3	350.4	1539.26	.4422	23.6
120	24.11	36.77	24.85	311.2	316.1	1537.52	.5089	33.1
140	23.74	35.81		266.8	272.4	1534.26	.5677	43.9
160	22.27	36.81	25.53	245.8	252.1	1532.62	.6202	55.8
180	20.66	35.77	25.95	206.2	213.0	1528.67	.6667	68.6
200	19.87	36.72	26.13	189.7	197.1	1526.80	.7077	82.4
220	19.79	36.61	26.32	171.0	178.8	1524.00	.7453	96.9
2411	18.48	36.58	26.38	165.6	174.1	1523.41	.7806	112.2
260	18.01	36.51	26.44	159.5	168.6	1522.31	.8148	128.1
280	17.58	34.45	26.50	153.8	163.4	1521.32	.8480	144.7
300	17.37	36.42	26.53	151.1	161.3	1520.99	.8205	162.0
340	16.92	36.34	26.58	146.6	158.0	1520.22	.9447	198.5
380	16.42	36.22	26.63	141.9	154.2	1518.93	1.0071	237.6
420	14.96	35.99	26.76	129.3	142.1	1515.11	1.0666	279.1
460	13.75	35.80	26.83	122.5	135.7	1512.31	1.1224	322.8
500	12,42	35.49	26.01	115.6	128.7	1507.52	1.1754	368.8
540	11.60	35.44	27.03	104.3	117.7	1505.29	1.2237	416.8
580	10.12	35.17	27.08	98.8	111.6	1500.38	1.2704	466.7
620	9.28	35.10	27.17	90.5	103.2	1497.89	1.5135	518.4
660	11.27	35.45	27.09	97.7	113.7	1506.10	1.3557	571.7

STD STATION NUMBER	กบล
SEPTEMBER 15. 1971	03.8 /
LATITUDE	18 05
LONGITUDE	64 36
DEPTH TO ROTTOM	2551 M

```
SIGT
                                              PYNHGT
                                                        TRANS
       T
                         TANOM
                                SVA
                                       SVEL
  0 28.27 35.65 22.82
                         505.0 505.0 1543.17
                                                .0000
                                                           . 0
 20 28,19 35.73 22.90
                                                .1003
                         496.8 497.6 1543.39
                                                          1.0
                                                          4.0
 40 27.88 36.17 23.33
                         455.4 457.1 1543.44
                                                .1957
 60 26,97 36.53 23,90
                         401.4 404.0 1542.06
                                                          8.7
                                                .2818
 80 25.94 36.71 24.36
                                                . 35P3
                         357.4 360.7 1540.20
                                                         15.1
 100 24.97 34.82 24.75
                         320.9 325.0 1538.34
                                                .4269
                                                         23.0
120 24.20 35.96 25.08
                         288.6 293.5 1536.93
                                                .4887
                                                         32.1
140 23.42 36.90 25.27
                         270.9 276.6 1535.28
                                                .5458
                                                         42.5
                                                .5989
160 22,51 36.86 25.50
                         248.7 255.0 1533.28
                                                         53.9
180 21.38 36.82 25.79
                         221.3 228.3 1530.64
                                                .6472
                                                         66.4
200 20,00 36.75 26.11
                         190.8 198.2 1527.18
                                                .6899
                                                         79.8
220 19.02 36.64 26.29
                         174.4 182.3 1524.68
                                                . 1279
                                                         94.0
                                                .7638
240 18.55 36.58 26.36
                         167.3 175.8 1523.61
                                                        108.9
260 17.96 36.50 26.45
                         159.1 168.1 1522.16
                                                        124.5
                                                . /981
280 17,57 36.45 26.51
                         153.6 163.2 1521.29
                                                .8313
                                                        140.8
300 17.31 36.41 26.54
                         150.5 160.6 1520.81
                                                .8637
                                                        157.7
                                                .9271
340 16.71 36.31 26.61
                         144.1 155.3 1519.56
                                                        193.6
                                                .9883
380 15.24 35.19 26.69
                         135.7 147.9 1517.74
                                                        231.9
420 14.63 35.94 26.80
                                              1.0454
                         126.1 138.7 1514.01
                                                        272.5
460 13.57 35.79 26.91
                         115.7 128.7 1511.06
                                              1.0990
                                                        315.4
500 12.78 35.68 26.98
                         108.4 121.9 1508.95
                                              1.1494
                                                        360.4
                         105.3 119.3 1507.59
                                                        407.4
 540 12.22 35.58 27.01
                                              1.1977
 580 11.11 35.42 27.10
                          97.1 111.0 1504.21 1.2437
                                                        456.2
62n 10.24 35.29 27.16
                          91.9 105.8 1501.61
                                              1.2870
                                                        506.8
      9.32 35.17 27.22
                          86.0
                                99.6 1498.77
                                                        559.1
660
                                              1.5278
700
      8.40 35.06 27.28
                          80.2
                                93.3 1495.86 1.3663
                                                        613.0
740
      8.08 35.03 27.31
                          77.7
                                91.2 1495.26
                                              1.4030
                                                        668.4
      7.67 35.01 27.35
780
                          73.4
                                 86.9 1494.32
                                              1.4385
                                                        725.2
820
      6.99 34.98 27.42
                          66.11
                                 79.5 1492.30 1.4718
                                                        783.4
      6.68 34.98 27.47
860
                          62.3
                                75.6 1491.74 1.5027
                                                        842.9
910
      6,35 34.99 27.52
                          57.4
                                70.6 1491.10 1.5319
                                                        903.6
                          53.9
      6.13 35.00 27.56
                                 67.3 1490.90 1.5597
 940
                                                        965.5
 980
      5.62 35.00 27.62
                          47.8
                                60.7 1489.51 1.5853
                                                       1028.4
      5,50 35.03 27.66
                          44.1
                                 57.3 1489.72 1.6091
                                                       1092.3
1020
      4.85 34.98 27.70
                          40.5
1100
                                 53.2 1489.32 1.6526
                                                       1222.8
1200
      4.60 34.98 27.73
                          37.8
                                 50.9 1488.93 1.7041
                                                       1390.6
1300
      4.19 35.00 27.75
                          35.2
                                 49.0 1490.14 1./540
                                                       1563.5
1400
      4.25 34.99 27.77
                          33.4
                                 47.6 1490.78 1.8024
                                                       1741.4
1500
      4.18 35.00 27.79
                          32.0
                                 46.9 1492.14 1.8501
                                                       1924.0
      4.12 35.00 27.79
1600
                          31.4
                                 47.0 1493.54 1.8974
                                                       2111.4
                          50.6
                                 46.8 1494.86 1.9439
1700
      4.04 35.00 27.80
                                                       2303.4
      3.89 35.01 27.83
                          28.3
                                 44.9 1495.91 1.9898
                                                       2500.2
1800
                          27.6
1900
      3.32 35.01 27.83
                                 44.8 1497.27 2.0345
                                                       2701.4
2000
      3.82 35.01 27.83
                          27.6
                                 45.6 1498.93 2.0798
                                                       2907.1
```

STD STATION NUMBER	009
SEPTEMBER 16, 1971	06.2 7
LATITUDE	17 20
LONGITUDE	62 59
DEPTH TO BOTTOM	0905 *

Z	т	5	SIGT	TANOM	SVA	SVEL	NYNHGT	TRANS
	28.49					1542.23	.0000	• 0
	28.49					1542.88	.1196	1.2
	28.00					1542.78	.2315	
	26.97			441.7	444.2	1541.57	.3290	10.3
	25.62					1539.23	.4104	17.7
100	24.60	36.68	24.75	320.2	324.3	1537.34	.4798	26.6
120	23.75	36.82	25.12	285.4	290.2	1535,66	.5413	36.8
140	22.74	36.90	25.47	252.1	257.7	1533.58	.5961	48.2
160	21.69	36.84	25.72	228.1	234.3	1531.15	.6453	60.6
180	20.17	36.69	26.02	199.4	206.1	1527.27	.6893	74.0
500	18.96	36.58	26.26	177.3	184.5	1524.13	.7284	88.1
220	18.27	36.52	26.39	165.0	172.7	1522.43	.7641	103.1
240	17.97	36.47	26.45	159.1	167.4	1521.54	.7981	118.7
260	17.54	36.43	26.50	154.3	163.2	1520.86	.8312	135.0
280	17.24	36.37	26.52	151.8	161.2	1520.24	.8636	151.9
300	16.79	36.30	26.58	146.6	156.6	1519.14	.8954	169.5
340	15.45	36.03	26.68	136.8	147.4	1515.41	.9564	206.6
380	14.07	35.77	26.78	127.1	138.1	1511.38	1.0137	246.0
420	12.79	35.58	26.40	115.9	127.3	1507.58	1.0668	287.6
460	13.57	35.79	26.91	115.7	128.7	1511.06	1.1173	331.3

STD STATION NUMBER	010
SEPTEMBEP 16, 1971	09.6 7
I.ATITUDE	17 0.5
LONGITUDE	63 01
DEPTH TO ROTTOM	0878 M

7.	T	5	SIGT	TANOM	SVA	SVEI	OYNHGT	TRANS
0	28.33	34.00	21.56	625.5	625.5	1541.52	.0000	• 0
20	28.39	34.83	22.16	567.7		1542.92	.1194	1.2
40	28.18	35.26	22.55	530.2	531.9	1543.24	.2294	4.7
60	27.53	35.73	23.12	476.2	478.7	1542.60	. 3305	10.3
80	26.91	36.10	23.60	430.5	433.8	1541.88	.4218	17.8
100	25.57	36.49	24.31	362.2	366.4	1539.48	.5018	27.0
120	24.37	36.72	24.85	310.8	315.7	1537.14	.5700	37.8
140	22.90	36.82	25.36	262.3	267,8	1533.91	.6283	49.7
160	21.61	36.80	25.71	228.8	235.0	1530.90	.6786	62.8
180	20.43	36.72	25.98	203.9	210.6	1528.01	.7232	76.8
200	19.59	36.61	26.17	185.7	192.9	1525.37	. 1635	91.7
550	18.81	36.54	26.26	176.5	184.4	1523.99	.8013	107.3
240	18.34	36.48	26.34	169.5	178.0	1522.91	·8375	123.7
260	17.83	36.42	26.42	161.9	170.8	1521.70	.8724	140.8
280	17.37	36.36	26.49	155.5	165.0	1520.61	.4060	158.6
300	16.93	36.29	26.54	150.5	160.5	1519.55	.9385	177.1
340	15.36	35.97	26.66	139.3	149.8	1515.06	1.0009	215.9
389	13.76	35.68	26.78	127.5	138.3	1510.27	1.0582	257.0
420	12.77	35.50	26.84	121.4	132.7	1507.42	1.1127	300.5
460	11.50	35.35	26.94	112.4	123.8	1503.87	1.1637	346.0
500	10.50	35.14	26.08	109.0	120.5	1500.77	1.2123	393.5
540	9.57	35.03	27.07	100.3	111.6	1497.57	1.2586	443.0
580	9.16	35.01	27.12	95.3	107.0	1496.68	1.3025	494.2
620	8.53	34.94	27.17	91.0	102.7	1494.89	1.3446	547.1
660	7.99	34.86	27.19	84.1	100.8	1493.40	1.3855	601.7
700	7.63	34.83	27.22	86.2	98.2	1492.63	1.4250	657.9
740	7.01	34.76	27.25	83.1	94.7	1490.79	1.4636	715.7
780	6.56	34.75	27.50	78.0	89.6	1489.66	1.5004	775.0

```
      STD STATION NUMBER
      011

      SEPTEMBER 16, 1971
      13.2 Z

      LATITUDE
      16 39

      LONGITUDE
      62 57

      DEPTH TO BOTTOM
      1239 M
```

```
SIGT
                         TANOM SVA
                                      SVE
                                              TYNHIGT
                                                       TRANS
       T
  0 28.05 34.01 21.66
                         616.0 616.0 1540.92
                                               .0000
                                                          • 0
  20 28.00 34.26 21.86
                         596.4 597.3 1541.43
                                               .1213
                                                         1.2
                                               .2383
  40 27.71 34.57 22.12
                         571.3 573.0 1541.91
                                                         4.8
  60 27.53 35.45 22.91
                         496.3 498.8 1542.33
                                               . 3455
                                                        10.6
 80 26.89 36.05 23.56
                         433.5 436.8 1541.79
                                               .4391
                                                        18.5
 100 25.88 36.36 24.12
                         380.8 384.9 1540.08
                                               .5213
                                                        28.1
 120 25.06 36.57 24.53
                         341.5 346.4 1538.67
                                               .5944
                                                        39.3
 140 23.94 36.75 25.00
                         296.3 302.0 1536.44
                                               .6592
                                                        51.8
 160 22.96 36.82 25.34
                         263.9 270.3 1534.39
                                               .7165
                                                        65.5
                         225.7 232.7 1531.23
 180 21.60 36.84 25.75
                                                        80.4
                                               .7668
                         200.2 207.7 1528.28
                                               .8108
 200 20.40 36.76 26.01
                                                        96.2
                                               .8502
 220 19.20 36.65 26.25
                         178.1 186.0 1525.19
                                                       112.8
                                               .8864
 240 18.41 36.53 26.36
                        167.6 176.1 1523.16
                                                       130.1
 269 17.85 36.46 26.44
                                               .9208
                         159.4 168.4 1521.80
                                                       148.2
 280 17.27 36.35 26.50
                                               .9540
                         153.9 163.4 1520.30
                                                       167.0
 300 16.54 36.21 26.57
                         147.5 157.4 1518.30
                                              .9861
                                                       186.4
 34n 15.09 35.95 26.70
                         135.0 145.4 1514.19 1.0467
                                                       227.0
 380 14.14 35.79 26.79
                         127.1 138.1 1511.62 1.1035
                                                       270.0
420 12.82 35.56 26.88
                         118.0 129.3 1507.66 1.1567
                                                       315.2
460 11.57 35.33 26.95
                         111.9 123.2 1503.77 1.2071
                                                       362.5
                                                       411.8
500 10.76 35.21 27.00
                         106.6 118.2 1501.43 1.2552
                         99.0 110.4 1497.82 1.3008
 540
     9.63 35.06 27.08
                                                       462.9
                          92.7 104.0 1495.46 1.3436
                                                       515.8
580
      8.84 34.98 27.15
                               98.5 1492.53 1.3840
      7.93 34.87 27.20
620
                          87.5
                                                       570.4
      7.50 34.85 27.24
                                95.6 1491.89 1.4228
660
                          84.3
                                                       626.5
                                94.1 1490.35 1.4607
700
     7.06 34.77 27.25
                          83.0
                                                       684.2
740
      6.45 34.72 27.29
                          78.9
                                89.6 1488.54 1.4974
                                                       743.3
      6.21 34.72 27.33
780
                          75.8
                                86.8 1488.23 1.5327
                                                       803.9
     5.39 34.73 27.36
820
                          12.4
                                83.6 1488.02 1.5669
                                                       865.9
     5.79 34.74 27.40
                          69.2
860
                                80.6 1487.88 1.5996
                                                       929.3
                          64.3
900
     5.63 34.78 27.45
                                76.0 1487.95 1.6310
                                                       993.9
                          59.8
940
     5.50 34.82 27.49
                                71.8 1488.13 1.6605
                                                      1059.7
GRA
     5.40 34.88 27.55
                          54.2
                                66.5 1488.46 1.6882
                                                      1126.7
     5.18 34.91 27.60
                                61.8 1488.26 1./138
1020
                          49.4
                                                      1194.7
     4.85 34.98 27.70
                                53.2 1488.32 1.7604
1100
                          40.5
                                                      1333.7
```

STD STATION NUMBER	012
SEPTEMBER 16, 1971	15.6 /
LATTIUDE	16 19
LONGITUDE	62 57
DEPTH TO ROTTOM	1286 4

Z	T	S	SIGT	TANOM	SVA	SVE	TYNHGT	TRANS
n	27.99	34.20	21.82	600.4	600.4	1541.01	•0000	• 0
20	27.86	34.63	22.18	565.5	566.3	1541.54	.1167	1.2
40	27.66	35.02	22.54	531.2	532.9	1541.85	.2266	4.6
60	27.23	35.71	23.20	468.3	470.8	1541.91	. 3270	10.1
80	26.45	36.15	23.72	419.0	422.3	1541.34	.4163	17.6
100	26.16	36.33	24.01	391.3	395.4	1540.70	.4921	26.7
120	25.62	36.47	24.28	365.1	370.1	1539.90	.5746	37.4
140	25.00	36.68	24.63	331.8	337.6	1538.94	.6454	49.6
160	24.45	36.79	24.89	307.4	314.0	1537.99	. /105	63.2
190	22.17	36.73	25.33	265.2	272.3	1534.15	. 1692	78.0
200	20.76	36.74	25.90	210.9	218.5	1529.24	.8182	93.9
550	19.70	36.68	26.14	188.3	196.4	1526.62	.8597	110.6
240	18.74	36.54	26.28	174.R	183.4	1524.11	.8977	128.2
260	18.09	36.47	26.39	164.3	173.4	1522.50	.9334	146.5
280	17.59	36.40	26.46	157.7	167.3	1521.30	.9674	165.5
300	16.97	36.29	26.53	151.4	161.4	1519.67	1.0003	185.2
340	15.67	36.06	26.66	139.3	150.0	1516.12	1.0622	226.5
380	13.85	35.72	26.79	126.3	137.2	1510.60	1.1197	270.1
420	12.99	35.58	26.86	119.0	131.2	1508.25	1.1731	316.0
460	11.27	35.26	26.95	111.7	122.8	1502.64	1.2242	364.0
500	10.02	35.07	27.112	104.6	115.5	1498.61	1.2717	413.9
540	9.33	34.90	27.08	99.5	110.5	1496.64	1.5165	465.6
580	8.55	34.89	27.12	95.0	106.0	1494.26	1.3597	519.2
650	8.35	34.94	27.19	88.3	99.9	1494.22	1.4010	574.4
660	7.96	34.84	27.21	87.2	98.9	1493.31	1.4410	631.2
700	7.24	34.82	27.26	81.7	93.1	1491.11	1.4795	689.7
740	6.32	34.78	27.29	79.1	90.5	1490.07	1.5162	749.6
780	6.51	34.77	27.33	75.8	87.4	1489.49	1.5518	810.9
820	6.25	34.74	27.37	71.8	83.5	1499.12	1.5861	873.7
860	6.01	34.77	27.39	69.6	81.4	1488.81	1.6192	937.8
900	5.75	34.81	27.46	63.5	75.4	1488.47	1.6506	1003.2
940	5.53	34.85	The same of the sa	57.9	70.0	1488.29	1.6797	1069.8
980	5.34	34.87		54.2	66.4	1488.20	1.7069	1137.6
1020	5.12		27.59	51.0	63.2	1487.97	1.7328	1206.3
1100	4.74	34.92	27.66	43.8	56.1	1487.78	1.7799	1346.9

STD STATION NUMBER	013
SEPTEMBER 16, 1971	18.8 7
LATITUDE	16 03
LONGITUDE	63 01
DEPTH TO BOTTOM	2076 M

```
SIGI
                         TANOM
                                SVA
                                       SVEL
                                               TYNHGT
                                                        TRANS
       T
  0 28.10 34.01 21.64
                         617.5 617.5 1541.03
                                                           .0
                                                .0000
 20 27.83 34.98 22.46
                         539.4 540.2 1541.86
                                                .1158
                                                          1 .2
 40 27.65 35.35 22.79
                         507.2 508.8 1542.17
                                                .2207
                                                          4.5
 60 27.00 35.96 23.46
                         443.3 445.8 1541.63
                                                .3161
                                                          9.9
 80 26.63 36.15 23.72
                         418.4 421.7 1541.29
                                                .4029
                                                         17.1
100 26.29 36.28 23.93
                                                .4854
                         398.8 402.9 1540.96
                                                         26.0
120 25.92 36.40 24.13
                         379.1 384.1 1540.54
                                                .5641
                                                         36.5
                                                .6385
140 25.43 36.54 24.39
                         354.5 360.3 1539.84
                                                         48.5
                         317.4 323.9 1538.48
                                                         61.9
160 24.65 36.74 24.78
                                                .7069
180 22.33 36.76 25.31
                                                         76.7
                         267.4 274.6 1534.58
                                                . 7668
                         226.2 233.9 1530.96
                                                         92.5
200 21.40 36.76 25.74
                                                .8176
220 20.38 36.73 26.00
                         201.9 210.1 1528.53
                                                .8620
                                                        109.3
240 19.43 36.63 26.17
                         185.2 193.9 1526.14
                                                .9024
                                                        127.0
                                                .9397
260 18.48 36.53 26.34
                         169.3 178.5 1523.68
                                                        145.4
                         160.4 170.1 1521.85
                                                .9745
280 17.77 36.42 26.43
                                                        164.5
300 17.35 36.38 26.51
                         153.6 163.7 1520.89 1.0079
                                                        184.3
                                                        226.0
340 16.04 36.08 26.59
                         145.9 156.8 1517.28 1.0721
                         131.7 143.2 1513.98 1.1316
380 14.83 35.92 26.74
                                                        270.0
420 13.05 35.57 26.84
                         121.7 133.1 1508.44 1.1867
                                                        316.4
460 11.74 35.39 26.96
                         110.5 122.0 1504.43 1.2375
                                                        364.9
500 10.99 35.27 27.01
                         106.1 117.9 1502.31 1.2855
                                                        415.4
                         101.0 112.9 1499.70 1.5316
540 10.12 35.14 27.06
                                                        467.7
      9.50 35.05 27.13
                          94.5 106.4 1497.25 1.3755
                                                        521.9
580
620
      8.59 34.95 27.16
                          91.1 103.0 1495.13 1.4175
                                                        577.7
      7.69 34.83 27.21
660
                          87.1
                                98.4 1492.21 1.4580
                                                        635.3
                          83.2
                                94.4 1490.42 1.4966
700
      7.08 34.77 27.25
                                                        694.3
      6.70 34.76 27.29
                          79.0
                                90.2 1489.57 1.5330
                                                        754.9
740
780
      6.35 34.74 27.32
                          76.1
                                 87.3 1488.82 1.5685
                                                        817.0
      6.10 34.75 27.36
8211
                          72.2
                                                        880.4
                                83.6 1488.49 1.6027
                          64.2
      5.45 34.75 27.40
                                                        945.2
860
                                80.7 1488.14 1.6357
                          63.6
900
      5.69 34.80 27.45
                                75.3 1488.22 1.6668
                                                       1011.2
      5.52 34.84 27.51
                          58.6
940
                                70.6 1488.24 1.6960
                                                       1078.5
OAN
      5.30 34.86 27.55
                          54.5
                                 66.6 1488.03 1.7234
                                                       1146.9
                          49.4
      5.74 34.89 27.60
                                                       1216.3
1020
                                 61.4 1487.66 1.7490
1100
      4.68 34.93 27.68
                          42.4
                                 54.6 1487.55 1.7950
                                                       1358 - 1
1200
      4.43 34.95 27.72
                          38.3
                                 50.9 1488.18 1.8474
                                                       1540.3
                          36.2
                                 49.5 1489.30 1.8973
1300
      4.30 34.96 27.74
                                                       1727.5
1400
      4.23 34.97 27.76
                          34.7
                                 48.8 1490.66 1.9464
                                                       1919.7
1500
      4.18 34.97 27.76
                          34.2
                                 49.1 1492.10 1.9953
                                                       2116.8
                          33.9
1600
      4.15 34.97 27.77
                                 49.6 1493.62 2.0447
                                                       2318.8
      4.12 34.97 27.77
                          33.6
                                 50.1 1495.15 2.0944
                                                       2525.8
1700
1800
      4.12 34.98 27.78
                          32.9
                                 50.3 1496.82 2.1443
                                                       2737.7
```

STD STATION NUMBE	R 014
SEPTEMBER 16, 197	1 23.3 /
LATTTUDE	15 29
! ONGITUDE	63 00
DEPTH TO HOTTOM	2171 4

Z	Т	5	SIGT	TANOM	SVA	SVE!	DYNHET	TRANS
0			21.70	The second second	_	1540.84	.0000	•0
20		34.71	22.16	567.5		1542.18	.1181	1.2
40		35.12	22.59		528.5	1542.15	.2277	4.6
60	26.95	35.96	23.48	441.8		1541.52	.3250	10.2
80	26.49	36.19	23.83	408.3		1540.78	.4106	17.5
100	25.06	36.36	24.09	383.1	387.3	1540.27	4905	26.5
120	25.69	36.44	24.27	365.8	370.7	1540.08	.5663	37.1
140	25.36	36.58	24.44	349.6	355.3	1539.71	.6389	49.2
160	24.43	36.60	24.69	326.2	332.7	1538.87	.1077	62.6
180	23.79	36.83	25.11	286.3	293.6	1536.79	. 1704	77.4
500	22.64	36.96	25.54	245.n		1534.34	.9250	93.4
220	18.74	36.51	26.26	177.0	184.8	1523.76	.8688	110.3
240	18.67	36.50	26.27	176.n	184.5	1523.88	.4057	128.0
260	18.71	36.51	26.27		185.5	1524.32	.9427	146.5
280	17.00	36.41	26.39	164.2		1522.22	.9787	165.7
300	17.22	36.52	26.49	154.9	165.0	1520.45	1.0126	185.6
340	15.89	36.0R	26.62	142.7	153.5	1516.82	1.0761	227.4
380	14.24	35.77	26.75	130.5	141.6	1511.93	1.1351	271.7
420	13.00	35.56	26.84	121.4	132.8	1508.26	1.1900	518.2
460	12.11	35.44	26.93	113.5	125.3	1505.76	1.2412	366.8
500	11.02	35.29	27.02	105.1	117.0	1502.44	1.2894	417.4
540	9.96	35.13	27.08	99.1	110.9	1499.11	1.5349	469.9
580	9.19	35.04	27.14	93.6	105.3	1496.83	1.3780	524.2
620	8.34	34.93	27.19	88.9	100.5	1494.17	1.4192	580.1
660	7.60	34.84	27.23	85.1	96.3	1491.88	1.4588	637.7
700	7.10	34.81	27.28	80.5	91.8	1490.56	1.4964	696.8
740	6.46	34.75	27.32	76.7	87.6	1488.62	1.5323	757.4
780	6.14		27.36	72.7	83.6	1488.00	1.5664	819.4
8211	5.96	34.76	27.40	68.6	79.6	1487.54	1.5991	882.7
860	5.57	34.81	27.48	61.4	72.5	1487.10	1.6297	947.3
900	5.48	34.85	27.50	58.9	70.3	1487.41	1.6585	1013.0
940	5.25	34.86	27.56	54.0	65.5	1487.17	1.6855	1079.9
080	5.09	34.89	27.60	49.0	61.6	1487.21	1.7109	1147.8
1020	4.82	34.92	27.65	44.7	56.3	1486.80	1.7345	1216.8
1100	4.57	34.94	27.70	40.5	52.4	1497.11	1./777	1357.3
1200	4.36		27.74	36.8	49.3	1487.91	1.8284	1537.6
1300	4.27		27.75	35.9	49.1	1489.17	1.8776	1722.9
1400	4.21	34.97	27.76	34.5	48.5	1490.58	1.9262	1913.1
1500	4.15	34.97	27.77	33.7	48.7	1491.98	1.9748	2108.1
1700	4.13	34.97	27.77	33.6	50.1	1495.15	2.0237	2512.9
1800	4.10		27.78	32.7	50.0	1496.74	2.0735	2722.8
1900	4.10		27.78	32.7	50.9	1498.39		2037.7
2000	4.10		27.78	32.7		1500.05	2.1743	3157.7
2000	4.10	34.30	21.10	36.1	21.0	1300.03	. 62230	3131.1

STD STATION NUMBER	015
SEPTEMBER 18, 1971	10.8 7
LATITUDE	11 45
LONGITUDE	63 02
DEPTH TO BOTTOM	700 M

7.	T	5	SIGT	TANOM	SVA	SVEL	DYNHGT	TRANS
0	27.72	34.35	55.05	581.2	581.2	1540.59	.0000	• 0
20	27.04	35.49	23.03	484.5	485.3	1541.07	.1067	1.1
40	26.02	36.25	23.99	392.A	394.5	1539.34	.1946	4 • 1
60	25.53	35.44	24.29	364.6	367.1	1538.69	.2708	8.7
80	24.26	36.52	24.75	322.0	325.3	1536.06	. 3400	14.8
100	21.86	36.58	25.48	251.4	255.3	1530.40	.3981	22.2
120	20.49	36.59	25.46	214.8	219.5	1527.09	.4455	30.7
140	19.119	36.51	26.17	185.5	190.6	1523.47	.4865	40.0
160	18.54	36.45	26.26	176.5	182.2	1522.18	.5238	50 • 1
180	17.05	36.36	26.34	169.0	175.2	1520.71	.5596	60.9
500	17.26	36.28	26.45	15R.R	165.5	1518.92	.5936	72.4
550	16.09	36.00	26.58	146.3	153.4	1515.52	.6255	84.6
240	15.17	35.93	26.67	138.1	145.5	1512.82	.6554	97.5
260	14.56	35.81	26.71	134.2	141.9	1511.07	.6842	110.8
280	14.13	35.75	26.76	129.A	137.9	1509.94	.7121	124.8
300	13.31	35.56	26.78	127.4	135.7	1507.37	.7395	139.3
340	11.52	35.30	26.93	113.2	121.6	1501.63	. /902	169.9
380	10.42	35.13	27.00	106.7	115.3	1498.19	.8376	202.5
420	9.35	34.96	27.05	102.0	110.6	1494.74	.8827	236.9
460	8.23	34.84	27.13	94.0	102.5	1491.06	.9252	273.1
500	7.64	34.7R	27.17	90.1	98.7	1489.37	.9654	310.9
540	7.16	34.72	27.21	86.7	95.3	1487.70	1.0042	350.3
580	6.75	34.69	27.23	84.9	93.7	1487.09	1.0419	391.2
620	6.37	34.6P	27.27	80.8	89.8	1486.23	1.0785	433.6

STD STATION NUMBER	916
SEPTEMBER 18, 1971	13.7 /
LATITUDE	12 03
LONGITUDE	63 00
DEPTH TO BOTTOM	2348 M

```
SIGT
                         MOMAT
                                SVA
                                       SVEL
                                              DYNHET
                                                        TRANS
       T
   0 27.74 34.12 21.84
                         598.4 598.4 1540.36
                                                .0000
                                                           .0
  20 27.08 35.10 22.79
                         507.6 508.4 1540.32
                                                .1107
                                                          1.1
  40 26,29 36.17 23.85
                         406.7 408.4 1539.89
                                                .2024
                                                          4.2
  60 25.97 36.32 24.06
                         386.3 388.8 1539.61
                                                .2821
                                                          9.1
 80 25.36 36.45 24.35
                                                .3572
                         358.9 362.2 1538.63
                                                         15.5
 100 23.55 36.67 25.06
                         291.1 295.2 1534.77
                                                .4229
                                                         23.3
                                                .4796
 120 22.83 35.73 25.31
                         266.8 271.6 1533.34
                                                         32.3
 140 21.02 36.61 25.73
                         227.1 232.4 1528.85
                                                         42.4
                                                .5300
 150 19.46 36.46 26.03
                         198.3 204.1 1524.78
                                                .5736
                                                         53.4
 180 18.37 36.36 26.24
                         179.0 165.3 1521.92
                                                .6126
                                                         65.3
200 17.83 36.30 26.33
                         170.5 177.4 1520.62
                                                .6488
                                                         77.9
                                                .6834
220 17.23 36.24 26.43
                         161.0 168.4 1519.11
                                                         91.2
240 16.36 36.07 26.50
                                                .7164
                         153.7 161.5 1516.65
                                                        105.2
260 15.47 35.93 26.60
                                                .7478
                         144.5 152.6 1514.08
                                                        119.9
280 14.74 35.80 26.66
                         138.6 147.0 1511.96
                                                .7778
                                                        135.1
300 13.42 35.67 26.74
                                                        151.0
                         131.4 140.0 1509.49
                                                .8065
 340 12.24 35.37 26.45
                         121.1 129.9 1504.19
                                                .8604
                                                        184.3
                                                .9104
 380 10.56 35.09 26.04
                         112.0 120.7 1498.64
                                                        219.7
      9.94 35.00 26.08
                                                . 4579
420
                         108.4 117.5 1496.94
                                                        257:1
460
      9.39 34.94 27.03
                         104.1 113.6 1495.51 1.0040
                                                        296.4
 500
      8.75 34.87 27.08
                          99.5 109.1 1493.69 1.0486
                                                        337.4
540
      7.88 34.77 27.15
                          94.2 103.7 1490.92 1.0914
                                                        380.2
580
      7.37 34.71 27.16
                          91.6 101.2 1489.53 1.1325
                                                        424.7
      6.58 34.66 27.23
                          84.9
651
                                 94.1 1487.03 1.1716
                                                        470.8
      5.99 34.64 27.29
                          79.1
660
                                88.1 1485.31 1.2080
                                                        518.4
                          73.5
700
      5.77 34.68 27.35
                                 82.7 1485.13 1.2422
                                                        567.4
                                                        617.7
740
      5.64 34.72 27.40
                          69.0
                                78.5 1485.31 1.2743
780
      5.49 34.77 27.46
                          63.5
                                73.4 1485.42 1.5045
                                                        669.3
820
      5. 35 34.82 27.51
                          58.1
                                68.3 1485.58 1.3330
                                                        722.1
860
      5.27 34.84 27.54
                          55.7
                                66.3 1485.93 1.3600
                                                        775.9
900
      5.08 34.88 27.59
                          50.6
                                61.3 1485.86 1.3854
                                                        830.8
040
      4.94 34.90 27.62
                                58.5 1485.97 1.4095
                          47.5
                                                        886.7
980
      4.85 34.91 27.64
                          45.8
                                57.0 1486.27 1.4327
                                                        943.6
1020
      4.72 34.92 27.67
                          43.6
                                55.0 1486.40 1.4550
                                                       1001.3
      4.49 34.94 27.71
1100
                          39.7
                                51.4 1486.79 1.4974
                                                       1119.5
      4.37 34.95 27.73
1200
                          37.7
                                50.1 1487.94 1.5477
                                                       1271.7
      4.27 34.96 27.75
1300
                          35.9
                                49.1 1489.18 1.5973
                                                       1429.0
      4.22 34.96 27.75
                                49.4 1490.61 1.6462
1400
                          35.4
                                                       1591.2
      4.17 34.96 27.76
                          34.9
1500
                                49.7 1492.05 1.6957
                                                       1758.3
1600
      4.14 34.97 27.77
                          33.8
                                49.5 1493.59 1.7452
                                                       1930.3
1700
      4.12 34.97 27.77
                                50.1 1495.16 1.7950
                          33.6
                                                       2107.3
      4.10 34.97 27.77
1800
                          33.4
                                50.7 1496.73 1.8453
                                                       2289.3
1900
      4.11 34.97 27.77
                          53.5
                                 51.8 1498.42 1.8965
                                                       2476.4
2000
      4.11 34.98 27.78
                          32.9
                                 51.9 1500.10 1.9482
                                                       2668.6
```

STD STATION NUMBER	017
SEPTEMBER 18, 1971	17.4 %
LATITUDE	12 30
LONGITUDE	63 00
DEPTH TO HOTTOM	5800 ₩

```
SIGT
                                                        TRANS
                         TANOM
                                SVA
                                       SVEL
                                               TNHGT
   0 27.93 34.03 21.71
                         610.8 610.8 1540.68
                                                .0000
                                                           .0
                                                .1209
  20 27.38 34.20 21.85
                         597.0 597.8 1541.09
                                                          1.2
  40 27.51 34.79 22.42
                         543.1 544.7 1541.27
                                                .2351
                                                          4.8
  60 26.63 35.93 23.56
                         434.2 436.7 1540.77
                                                . 3333
                                                         10.5
  80 25.29 36.37 24.31
                         362.6 365.9 1538.39
                                                .4135
                                                         17.9
 100 24.29 36.65 24.82
                         313.5 317.6 1536.56
                                                .4819
                                                         26.9
 120 22.35 36.78 25.49
                         250.1 254.9 1532.16
                                                .5391
                                                         37.1
 140 20.86 36.60 25.77
                         223.6 228.9 1528.42
                                                .5875
                                                         48.3
                                                         60.5
 160 19.56 36.54 26.07
                         194.9 200.8 1525.14
                                                .6305
 190 18.04 36.31 26.28
                         174.8 181.0 1520.92
                                                .6686
                                                         73.5
 200 16.23 36.11 26.56
                         147.9 154.4 1515.65
                                                         87.2
                                                .7022
 220 16.54 36.15 26.52
                         151.9 159.1 1516.95
                                                        101.6
                                                .7335
 240 15.32 35.93 26.63
                         141.3 148.8 1513.29
                                                . 7643
                                                        116.6
 260 14.47 35.78 26.71
                         134.5 142.2 1510.75
                                                .7934
                                                        132.1
                                                .8214
 280 13.42 35.67 26.76
                         129.4 137.4 1508.85
                                                        148.3
 300 13.14 35.54 26.80
                                                .8485
                                                        165.0
                         125.6 133.8 1506.78
                                                .8998
 340 11.78 35.33 26.91
                         115.6 124.2 1502.57
                                                        200.0
                                                .9482
 380 10.38 35.10 26.98
                         108.3 116.9 1498.01
                                                        236.9
 420
      9.26 34.95 27.06
                         101.3 109.9 1494.40
                                                .9035
                                                        275.8
 460
      8.45 34.85 27.11
                          96.5 105.1 1491.90 1.0366
                                                        316.4
 500
      7.73 34.77 27.15
                          92.1 100.8 1489.70 1.0777
                                                        358.7
 541
      6.86 34.69 27.21
                          86.3
                                94.7 1486.88 1.1168
                                                        402.6
      6.46 34.68 27.26
                          81.9
 580
                                90.4 1485.94 1.1536
                                                        448.0
      6.24 34.67 27.28
                          79.9
 620
                                88.7 1485.70 1.1896
                                                        494.8
      6.00 34.67 27.31
                          77.0
                                86.0 1485.39 1.2245
                                                        543.1
 660
      5.89 34.69 27.34
 700
                          74.2
                                83.6 1485.62 1.2584
                                                        592.8
 740
      5.55 34.72 27.40
                          69.1
                                78.7 1485.35 1.2908
                                                        643.8
      5.51 34.78 27.46
                          62.9
                                72.9 1485.52 1.3210
                                                        696.0
 780
                                                        749.4
 820
      5.34 34.83 27.52
                          57.2
                                67.4 1485.55 1.3493
                                                        803.9
860
      5.22 34.86 27.56
                          53.6
                                 64.1 1485.75 1.3755
900
      5.11 34.88 27.59
                          50.9
                                 61.7 1485.98 1.4005
                                                        859.5
                                 58.7 1486.05 1.4246
940
      4.96 34.90 27.62
                          47.7
                                                        916.0
                          45.6
                                56.7 1486.18 1.4477
                                                        973.4
980
      4.93 34.91 27.64
      4.72 34.93 27.67
                          42.9
                                54.3 1486.41 1.4698
                                                       1031.8
1020
      4.55 34.94 27.70
                                 51.9 1486.95 1.5125
                                                       1151.1
                          40.1
1100
      4.40 34.96 27.73
                                 49.8 1488.08 1.5633
                                                       1304.9
                          37.2
1200
      4.29 34.96 27.74
                                 49.3 1489.26 1.6130
                                                       1463.7
1300
                          36.1
1400
      4.24 34.97 27.76
                          34.8
                                 48.9 1490.71 1.6619
                                                       1627.4
      4.17 34.97 27.77
                                 48.9 1492.06 1.7108
                                                       1796.1
1500
                          34.1
      4.13 34.97 27.77
                          33.7
                                 49.3 1493.55 1.7508
                                                       1969.6
1600
                          33.6
                                 50.1 1495.15 1.8095
                                                       2148.1
1700
      4.12 34.97 27.77
                                 50.3 1496.82 1.8595
1800
      4.12 34.98 27.78
                          32.9
                                                       2331.5
1900
      4.11 34.98 27.78
                          32.P
                                 51.0 1498.44 1.9101
                                                       2520.0
2000
      4.11 34.98 27.78
                          32.A
                                51.9 1500.10 1.9617
                                                       2713.6
```

```
SEPTEMBER 18, 1971
                         21.0 /
                         13 02
   LATITUDE
   LONGITUDE
                         63 01
    DEPTH TO BOTTOM
                         1575 M
                         TANOM
                               SVA
                                       SVEL
                                              TYNHGT
                                                        TRANS
             S
                  SIGT
  0 27.94 34.01 21.69
                        612.5 612.5 1540.67
                                               .0000
                                                          • 0
 20 27,90 34.15 21.81
                         601.2 602.0 1541.08
                                                          1.2
                                               .1215
                         551.1 552.8 1541.47
 40 27.63 34.73 22.33
                                               .2369
                                                         4.8
 60 26.89 35.52 23.17
                         471.6 474.1 1540.96
                                               . 3396
                                                         10.6
                        377.4 380.7 1539.10
 80 25.62 36.30 24.15
                                               .4251
                                                         18.2
100 24.70 36.58 24.80
                         316.0 320.0 1536.29
                                               .4952
                                                         27.4
120 21.69 36.65 25.58
                        241.P 246.4 1530.34
                                               .5518
                                                         37.9
                                               . 5954
140 19.17 36.52 26.18
                        184.3 189.4 1523.42
                                                         49.4
160 17.55 36.29 26.39
                        164.7 170.2 1519.15
                                               .6313
                                                         61.6
                        149.9 155.7 1514.93
180 16.12 36.05 26.54
                                               .6639
                                                         74.6
                        138.7 144.9 1512.61
200 15.30 35.96 26.66
                                               .6940
                                                         88.2
220 14.84 35.85 26.68
                        137.1 143.7 1511.37
                                               .7229
                                                        102.3
240 13.61 35.60 26.75
                                               .7509
                        130.4 137.2 1507.44
                                                       117.1
                                               . 1774
260 12.63 35.48 26.86
                        120.3 127.2 1504.36
                                                       132.3
                                               .4024
280 12.55 35.47 26.90
                         115.8 123.1 1503.72
                                                       148.1
300 11.83 35.37 26.93
                         113.6 121.2 1502.15
                                                       164.4
                                               .8268
                         105.0 113.0 1499.04
340 10.90 35.24 27.02
                                                       198.5
                                               . 8740
                         102.3 110.7 1497.22
                                                       234.3
380 10.15 35.13 27.05
                                               .4192
420
     9.49 35.04 27.09
                          98.3 107.1 1495.36
                                              . 9627
                                                       272.0
     8.97 34.97 27.12
4611
                          95.4 104.5 1494.00 1.0049
                                                       311.3
                          91.8 101.1 1492.14 1.0461
590
     8.33 34.89 27.16
                                                        352.3
      7.61 34.79 27.19
                          0.88
                                98.2 1489.92 1.0860
                                                        395.0
540
      7.20 34.77 27.23
                                94.3 1488.95 1.1244
                          84.8
                                                       439.2
580
                          82.P
                                                        434.9
      6.93 34.75 27.25
                                92.5 1488.52 1.1618
650
      6.67 34.73 27.27
                          80.9
6611
                                90.8 1488.12 1.1985
                                                        532.1
      6.25 34.70 27.30
700
                          77.0
                                87.7 1487.07 1.2343
                                                        580.8
      5.97 34.72 27.56
                          72.9
                                                        630.9
740
                                83.0 1486.63 1.2683
      5.81 34.75 27.40
790
                          68.7
                                79.1 1486.68 1.3008
                                                        682.2
      5.54 34.77 27.45
                          64.0
                                74.5 1486.27 1.3318
                                                        734.9
820
      5.45 34.81 27.49
                                70.9 1486.62 1.3608
                                                        788 . 8
860
                          60.0
                                66.3 1486.67 1.3582
900
      5.29 34.85 27.54
                          55.2
                                                        843.7
                                63.8 1486.91 1.4142
940
      5.18 34.87 27.57
                          52.4
                                                       899.8
ORD
      4.99 34.90 27.62
                          48.1
                                59.6 1486.82 1.4390
                                                       956.9
1020
      4.83 34.92 27.65
                          44.9
                                56.4 1486.85 1.4622
                                                       1014.9
     4.59 34.94 27.70
                          40.7
                                52.7 1487.20 1.5057
                                                      1133.6
1100
     4.40 34.96 27.73
                          37.2
1200
                                49.8 1488.08 1.5568
                                                      1286.8
     4.30 34.97 27.75
                          35.4
                                48.7 1489.32 1.6060
                                                      1444.9
1300
     4.22 34.97 27.76
                          34.6
                                48.6 1490.63 1.654R
                                                      1608.0
1400
```

018

STD STATION NUMBER

STD STATION NUMBER 019
SEPTEMBER 19, 1971 01.1 /
LATITUDE 13 33
LONGITUDE 62 57
DEPTH TO BOTTOM 1165 M

2	T	5	SIGI	TANOM	SVA	SVEL	DYNHGT	TRANS
0	27.09	34.05	21.71	611.2	611.2	1540.83	.0000	• 0
50	27.95	34.12	21.77	604.9	605.8	1541.15	.1217	1.2
41)	27.67	34.64	22.25	558.9	560.5	1541.46	.2383	4.8
60	26.62	35.71	23.39	1149.7	452.2	1540.54	. 3396	10.6
80	25.00	36.21	24.28	365.7	368.9	1537,56	.4217	18.2
100	22.74	36.67	25.29	268.7	272.6	1532.74	.4859	27.3
120	21.14	36.63	25.71	228.7	233.5	1528.87	.5365	37.5
140	19.36	36.46	26.06	195.8	200.9	1524.18	.5799	48.7
160	17.41	36.20	26.35	168.0	173.5	1518.64	.6173	60.6
180	16,42	36.11	26.52	152.1	158.0	1515.91	.6505	73.3
500	15,52	35.93	26.59	145.6	151.9	1513,27	.6814	86.6
550	14.51	35.76	26.68	136.R	143.3	1510.21	.7110	100.6
2411	13.47	35.57	26.76	129.8	136.5	1506.94	.7390	115.1
260	12.49	35.42	26.84	122.0	128.9	1503.82	. 1655	130.1
580	11.47	35.33	26.49	117.2	124.3	1501.92	.7908	145.7
300	11.32	35.25	26.93	113.3	120.6	1500.23	.8153	161.7
3411	10.25	35.10	27.01	106.1	113.7	1496.90	.8623	195.3
380	9.52	35.00	27.05	101.7	109.7	1494.77	.9072	230.7
4211	9.18	35.01	27.12	95.6	104.2	1494.18	.9502	267.8
460	8.43	34.88	27.13	94.0	102.6	1491.86	.9919	306.7
500	8.11	34.84	27.15	92.3	101.3	1491.25	1.0328	347.2
5411	7.00	34.81	27.17	90.1	99.5	1490.67	1.0729	389.3
580	7.49		27,20	88.0	97.8	1490.09	1.1125	433.0
620	6.98		27,23	84.9	94.7	1488.69	1.1509	478.3
661	6.45		27.27	81.1	90.7	1487.20	1.1880	525.1
700	6.12		27.31	77.0	86.7	1486.54	1.2235	573.3
740	5.93	34.70	27.35	73.9	83.9	1486.45	1.2578	622.9
780	5.77		27.38	70.5	80.8	1486.48	1.2908	673.9
920	5.50		27.45	64.0	74.6	1486.53	1.3221	726.2
860	5.41		27.51	58.8	69.6	_		779.6
900	5.24		27.55	54.6	65.6			A34.2
9411	5.04		27.60	49.4	60.5		1.4034	889.8
980	4.38	_	27.65	45.4	56.6	and the same of th	1.4268	946.5
1020	4.74		27.67	43.1	54.5		1.4490	1004.0
1100	4.59	34.04	27.70	40.7	52.7	1487.20	1.5057	1133.6

STD STATION NUMBER	020
SEPTEMBER 19, 1971	04.6 /
LATTIUDE	14 03
LONGITUDE	63 02
DEPTH TO BOTTOM	1332 M

Z	Т	5	SIGT	TANOM	SVA	SVEL	CANHEL	TRANS
		31.22		601.5	601.5	1541.21	.0000	• 0
		34.58	22.14	569.7	570.5	1541.53	.1172	1.2
40	27.34	35.45	22.97	490.4	492.1	1541.58	.2235	4.6
60	26.44	36.18	23.81	410.5	413.0	1540.57	.3140	10.0
80	25.23	36.56	24.47	347.2	350.5	1538.41	.3903	17.0
100	24.20	36.77	24.94	302.3	306.4	1536.45	.4560	25.5
120	22.52	36.78	25.41	257.5	262.2	1532.85	.5129	35.1
140	20.75	36.68	25.86	214.5	219.8	1528.14	.5611	45.9
160	18.75	36.44	26.23	179.4	185.1	1522.80	.6015	57.5
180	17.35	36.26	26.41	162.3	168.4	1518.85	.6369	69.9
200	16.88	36.27	26.53	150.8	157.5	1517.78	.6695	83.0
220	16.23	36.11	26.56	147.9	155.1	1515.97	.7007	96.7
240	14.99	35.90	26.69	136.5	143.9	1512.22	.7306	111.0
260	14.39	35.81	26.75	130.7	138.4	1510.53	. 1589	125.9
280	13.75	35.68	26.78	127.3	135.3	1508.63	.7862	141.3
300	13.05	35.58	26.85	120.9	129.1	1506.53	.8127	157.3
340	12.06	35.43	26.93	113.4	122.1	1503.65	.8626	190.8
380	10.83	35.23	27.00	106.3	115.2	1499.77	.9102	226.3
420	10.11	35.13	27.05	101.6	110.9	1497.72	.9554	263.6
460	8.98	34.96	27.11	96.3	105.4	1494.02	.9986	302.7
500	8.26	34.87	27.15	92.2	101.4	1491.85	1.0398	343.5
540	7.78	34.82	27.19	89.1	98.5	1490.61	1.0798	385.9
580	7.42	34.74	27.21	86.3	96.0	1489.83	1.1187	429.8
620	7.05	34.76	27.24	83.6	93.5	1489.00	1.1566	475.3
660	6.51	34.75	27.28	80.1	90.0	1487.89	1.1934	522.3
700	6.22	34.70	27.31	77.4	87.3	1486.95	1.2290	570.8
740	6.01	34.70	27.34	74.9	85.0	1486.77	1.2635	620.6
780	5.86	34.13	27.38	70.8	81.3	1486.86	1.2065	671.8
820	5.64	34.74	27.41	67.5	78.1	1486.64	1.3283	724.3
860	5.53	34.78	27.46	63.2	74.1	1486.90	1.3589	778.1
900	5.37	34.82	27.51	58.3	69.5	1486.96	1.3877	833.0
940	5.10	34.88	27.59	50.8	62.0	1486.59	1.4140	889.1
980	4.89	34.91	27.64	46.2	57.5	1486.43	1.4380	946.1
1020	4.71	34.93	27.67	42.A		1486.37	1.4601	1004.1
1100	4.51	34.95	27.71	39.1	50.9	1486.88	1.5021	1122.6
1200	4.36	34.96	27.74	36.8	49.3	1487.91	1.5519	1275.3

```
STD STATION NUMBER 021
SEPTEMBER 19, 1971 09.3 /
LAFITUDE 14 32
LONGITUDE 65 00
DEPTH TO ROTTOM 1540 M
```

Z	T	S	SIGT	TANOM	SVA	SVEL	DYNHGT	TRANS
0	28.00	34.42	21.98	584.9	584.9	1541.29	.0000	• 0
50	28.13	34.77	22.23	560.7	561.5	1542.07	.1146	1.1
40	27.51	35.16	22.66	519.6	521.3	1541.88	.2229	4.5
60	26.50	36.17	23.78	413.0	415.5	1540.69	.3166	9.9
80	25.83	35.37		378.6	381.9	1539.65	. 3963	17.0
100	25,22	36.58	24.49	345.4	349.6	1538.73	.4695	25.7
120	24.63	36.81	24.84	311.7	316.7	1537.84	.5361	35.8
140	23.55	36.87	25.18	279.5	285.2	1535.83	.5963	47.1
160	22.72	36.93	25.50	249.4	255.8	1533.87	.6504	59.6
180	20.93	36.74	25.86	215.3	222.2	1529.37	.6982	73.0
200	19.59	36.60	26.11	191.3	198.7	1525.92	. 7403	87.4
220	18.63	36.51	26.29	174.3	182.1	1523.45	.7784	102.6
240	17.87	36.42	26.41	162.8	171.1	1521.49	.8137	118.5
260	17.13	36.30	26.50	154.3	163.1	1519.52	.8471	135.1
280	16.17	36.14	26,60	144.4	153.5	1516.78	.8787	152.4
300	15.33	36.00	26.69	136.4	145.7	1514.36	.9087	170.3
340	13.84	35.73	26.80	125.4	135.2	1509.94	.9649	207.8
380	12.70	35.56	26.90	115.7	125.9	1506.61	1.0167	247.4
420	11.61	35.35	26.95	111.1	121.5	1503.29	1.0661	289.1
460	10.14	35.12	27.04	102.9	113.0	1498.46	1.1131	332.6
500	9.35	35.02	27.10	97.5	107.8	1496.11	1.1574	378 • 1
540	8.72	34.94	27.14	93.8	104.3	1494.31	1.1999	425.2
580	8.15	34.86	27.16	91.4	101.9	1492.71	1.2409	474.0
650	7.62	34.80	27.19	88.3	98.9	1491.26	1.2811	524.5
660	7.20	34.76	27.22	85.6	96.3	1490.23	1.3201	576.5
700	6.99		27.26	82.0	93.1	1490.08	1.3581	630 • 1
740	6.61		27.30	77.9	88.9	1489.22	1.3946	685 • 1
780	6.26		27.34	74.2	85.3	1488.48	1.4294	741.6
820	5.84	34.75	27.40	69.1	80.0	1487.45	1.4627	799.5
860	5.70	34.79	27.45	64.4	75.7	1487.59	1.4938	858 • 6
900	5.54	34.83		59.6	71.1	1487.66	1.5232	918.9
940	5.35	34.86		55.1	66.8	1487.58	1.5506	980 • 4
980	5.10	34.90	27.61	49.3	61.0	1487.27	1.5762	1043.0
1020	4.90	34.91	27.64	46.3	58.1	1487.12	1.6001	1106.5
1100	4.58		27.71	39.9	51.8	1487.17	1.6439	1236.3
1200	4.41		27.73	37.3	49.9	1488.12	1.6947	1403.2
1300	4.26	34.97		35.0	48.2	1489.15	1.7440	1575.2
1400	4.22	34.97		34.6	48.6	1490.62	1.7922	1752.0
1500	4.17	34.97	27.77	34.1	48.9	1492.06	1.8408	1933.6

STO STATION NUMBER	022
SEPTEMBER 19, 1971	13.0 /
LATITUDE	14 59
LONGITUDE	62 54
DEPTH TO BOTTOM	1381 M

				******				TO
	T		SIGI			SVEL	TOHHET	TRANS
	27.87					1540.57	.0000	• 0
	27.94		21.87			1541.02	.1203	1.2
	27.66		22.54			1541.85	.2332	4.7
60			23.36			1541.46	. 1320	10.4
A ()	26.07		24.01		394.8	1540.14	.4170	17.9
100		36.54	24.42		356.0	1538.98	.4921	27.0
120	24.57		24.72	and the second s	328.6	1537.54	.5606	37.5
140	23.76		25.09	288.4		1536.03	.6228	49.3
160	22.82	36.84	25.40	258.6		1534.05	.6787	62.3
180	21.72		25.65		242.0	1532.06	.1294	76.4
500	20, 39		25.98	203.6		1528.21	.7747	91.5
550	19.08	36.52	26.18			1524.74	.8151	107.4
2411			26.40			1521.64	· 4515	124.0
260		34.57			168.0	1520.86	.8856	141.4
280	17.07		26.51			1519.66	.9186	159.4
300	16.50	36.20				1518.17	.9506	178.1
340	14.95					1513.73	1.0110	217.4
380	13.94	35.77		124.5		1510.95	1.0673	259.0
420	12,91	35.59	26.89	117.5		1508.00	1.1206	302.7
460	12.00	35.44	26.05	111.5	123.3	1505.38	1.1714	348.6
500	11.06	35.31	27.02	104.4		1502.61	1.2193	396.4
540	9.02	35.15	27.10	97.0		1498.99	1.2644	446.1
580	8.76	35.01	27.15	92.3	103.8	1495.94	1.306R	497.5
620	7.03		27.21	86.7		1492.55	1.3470	550.6
660	7.14	34.81	27.27	81.1		1490.07	1.3850	605.2
700	6.71	_	27.30	78.4	89.1	1488.98	1.4213	661.4
740	6.51		27.34	74.A	85.4	1488.02	1.4562	718.9
780	6.06		27.38	70.2	81.1	1487.71	1.4894	777.8
820	5,95		27.41	68.2	79.3	1487.93	1.5216	A3A.1
8611	5.77		27.44	64.5	75.9	1487.89	1.5525	899.5
900	5,58		27.49	60.0	71.6	1487.82	1.5822	962.2
949	5.34	34.84	27.56	53.5	65.2	1487.57	1.6097	1026.1
980	5.03		27.61	49.3	60.8	1486.97	1.6350	1091.0
1020	4.94		27.64	45.7	57.3	1486.87	1.65A4	1156.8
1100	4.57		27.70	40.5	52.4	1487.11	1.7022	1291.3
1500	4.38		27.73	37.A	50.3	1487.98	1.7532	1464.1
1300	4.26	34.97	27.76	35.0	48.2	1489.15	1.4024	1641.9

Hazelworth, John B.; Kolitz, Byron L.; Starr, Robert B.; Charnell, Robert L.; Berberian, George A.; Weiselberg, Maxine A. New York Bight Project, Water Column Sampling Cruises No. 9 - 12 of the NOAA Ship FERREL, July - November 1974. NOAA DR ERL MESA-3.

ABSTRACT: During the period July-November 1974, four oceanographic cruises, denoted 9, 10, 11, and 12, were made by the NOAA Ship <u>Ferrel</u> in the New York Bight. The objective of the cruises was to supply data to provide a base for analysis of the water movements on the highly impacted ecosystem. This report presents the corrected physical and chemical data from these cruises and describes the parameters measured, the measurement methods, and the corrections applied to the data.

# The Effect of Wind and Surface Currents on Drifters1

A. D. KIRWAN, JR., G. McNALLY, M.-S. CHANG AND R. MOLINARIS

(Manuscript received 15 August 1974, in revised form 9 December 1974)

#### ABSTRACT

The problem analyzed here is the motion of a drifter acted on by wind, surface and subsurface currents. From the condition of static equilibrium of all drag forces acting on the drifter, the effects of wind and surface current of arbitrary direction and magnitude and drogue characteristics are examined parametrically. Specific application is made to a recently developed drifter with 9.2 and 11.85 m parachute drogues and a window shade drogue. The calculations show that for some environmental conditions the deviation between the magnitudes of the drifter velocity and the water parcel velocity may exceed 50%. Furthermore, the direction of velocity vectors may differ by as much as 45°. Drifter data from an experiment conducted by the Atlantic Oceanographic and Meteorological Laboratories and the NOAA Data Buoy Office in the Gulf of Mexico Loop Current are examined in light of the theoretical results. The wind effects predicted by the theory were observed in the field. Thus wind corrections to the drifter velocity records which are based on the theory can significantly improve the velocity records.

## 1. Introduction

Preliminary plans for the First GARP Global Experiment (FGGE) call for a large number of free drifting platforms observing oceanic and atmospheric conditions. The data would be collected by a Random Access Measurement System (RAMS) aboard the TIROS N satellite. Because of the large deployment this component of FGGE has great potential for studying horizontal scales of ocean dynamics provided these vehicles can be effectively attached to representative water parcels by drogues.

Because of the need for an antenna, there must be a surface buoy. This, however, introduces some serious technical problems. Accelerations on the buoy due to waves, wind, and vertical shears between the buoy and drogue are different than those on the water parcel. In addition, the drogue may fishtail and kite. Unless accounted for all of these factors can lead to serious errors in interpretation of observations of drifter motion.

This report is restricted to one of the above questions; namely, how much can wind and surface drag affect a drifter system composed of a surface buoy with antenna and an attached drogue. Our results are

preliminary and apply to a simplified situation, yet they do provide some quantitative design criteria. If FGGE drifters are to be utilized for studying ocean currents, this study must be followed up by more detailed theoretical analysis and field tests of all of the technical problems mentioned above.

# 2. Formulation of problem

The following assumptions are made in this analysis:

- (i) The wind, surface and subsurface currents are steady.
- (ii) The " $V^2$ " drag law with a constant drag coefficient applies.
- (iii) Drag on the cable connecting the drag body at depth z to the surface vehicle is neglected. Thus our results apply only to drifters drogued to shallow depths. Beyond 500 m the drag on the cable may well be the most significant effect.

From assumptions (i) and (iii) the equations of motion for the drifter system reduce to

$$\mathbf{F}_{s} + \mathbf{F}_{s} + \mathbf{F}_{a} = 0. \tag{1}$$

In order, these terms are the drag acting at depth z on the drogue, the surface current drag acting on the wetted portion of the surface vehicle, and the wind drag exerted on the dry portion. Assumption (ii) asserts that each of the drag forces is given by

$$F_i = \rho_i C_{D_i} A_i |V_i - V| (V_i - V),$$
 (2)

where  $\rho_i$  is the fluid density (air and water) enveloping the *i*th component of the drifter system,  $C_{Di}$  the drag

<sup>&</sup>lt;sup>1</sup> Dedicated to W. Richardson and W. Hill and the crew of the R. V. Gulfstream, lost at sea 4 January 1975.

<sup>&</sup>lt;sup>3</sup> Department of Oceanography, Texas A&M University, College Station 77843

<sup>&</sup>lt;sup>2</sup> Scripps Institution of Oceanography, LaJolia, Calif. 92037.

Naval Ship Systems Research and Development Center, Carderock, Md.

<sup>&</sup>lt;sup>3</sup> Atlantic Oceanographic & Meteorological Laboratories, NOAA, Miami, Fla. 33149.

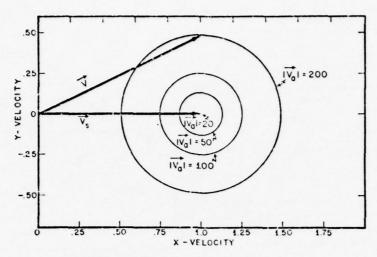


Fig. 1. The effect of wind on a Nova drifter drogued with a 9.2 m parachute at the surface. The locus for the drifter velocity for a given wind magnitude occurs on the appropriate circle.

coefficient for the *i*th component,  $A_i$  the area of the *i*th component as seen by the fluid streaming past it,  $V_i$  the velocity of the fluid at the *i*th part of the system with x and y components  $U_i$  and  $V_i$ , and V the velocity of the drifter system whose components are U and V.

Inserting (2) into (1) we obtain

$$\rho_{s}C_{Ds}A_{s}|V_{s}-V|(V_{s}-V)+\rho_{s}C_{Ds}A_{s}|V_{s}-V|(V_{s}-V) +\rho_{c}C_{Dc}A_{a}|V_{a}-V|(V_{a}-V)=0.$$
(3)

The effect of the wind and surface current can be investigated with (3) by regarding  $V_{ij}^{\mu}V_a$  and  $V_i$  as parameters of a solution for V. The other quantities  $\rho_i$ ,  $C_{Di}$  and  $A_i$  are known a priori. Note the formal similarity of this problem with the theory of the statics of structures. In the latter case the condition of equilibrium of forces provides a system of equations which is solved for the displacement vector in terms of prescribed loadings. In our case the equilibrium of forces determines the velocity.

The inversion of (3) for V is readily accomplished numerically once  $V_s$ ,  $V_s$  and  $V_a$  have been specified. We found a simple interation technique using complex arithmetic to be very efficient for the parameter ranges of interest.

An important special case is when the drifter is drogued at the surface. In this case (3) can be inverted analytically to obtain

$$V = (V_a + K^{\frac{1}{2}}V_a)/(1+K^{\frac{1}{2}}),$$
 (4)

where

$$K = \rho_a C_{Da} \cdot 1_a / (\rho_s C_{Ds} \cdot 1_s).$$

Thus for a wind of magnitude of  $|V_a|$  but of arbitrary direction the system velocity is given by a circle centered at  $V_a/(1+K^4)$  with a radius of  $K^4|V_a|/$ 

 $(1+K^4)$ . The center of the circle is the system velocity for no wind.

Eq. (4) indicates that the relative velocity error,  $(V-V_*)$ , depends upon the magnitude (and not the magnitude squared) of the air velocity even though the  $V^2$  drag law is applied. The effect of the increased drag when the wind is increased is compensated by an increase in the drag at the ocean surface.

Calculations are performed for a drifter developed at Nova University, Fort Lauderdale, Fla., for the NOAA Data Buoy Office (NDBO). This drifter has been proposed as the surface platform for many of the FGGE experiments.

Fig. 1 shows the effect of wind of various magnitudes and arbitrary directions on the Nova University drifter with a 9.2 m parachute drogue at the surface. (In this case  $A_t$  and  $C_{Dx}$  for the drifter are effectively that of the 9.2 m parachute; see Table 1.) The coordinate system is oriented in the direction of the surface current. Also the calculations have been normalized by the current magnitude. This graph demonstrates that the percentage error,

$$[|V-V_*|/|V|] \times 10^2$$

between the drifter velocity and the surface current may be of the order of 50% for a wind speed 200 times greater than the surface current. Note also that the drifter velocity vector may deviate as much as 30° from the surface current vector.

For high winds the percent error is approximately

$$[K^{\frac{1}{2}} | V_a| / |V| (1+K^{\frac{1}{2}})] \times 10^2$$
.

Thus for a wind of magnitude 200 times the surface current the percentage error is reduced to only 45% by changing from a 9.2 to an 11.85 m parachute. On

Table 1. Hydrodynamic characteristics of Nova University Drifter and drocues.

		Drifter	
		$10^{-1} \text{ m}^2$ , $C_{Da} = 1$ $(10^{-1} \text{ m}^2$ , $C_{Ds} = 1$	
		Drogues	
	9.2 m parachute	11.85 m parachute	Window shade
A, CD:	5.723×10 m <sup>2</sup> 1.35	9.448×10 m <sup>2</sup> 1.35	2.787×10 m <sup>2</sup> 1.9

the other hand, if the drifter loses its drogue,  $A_s$  and  $C_{Ds}$  become that of the buoy (see Table 1). The percentage error then exceeds 100% for a wind speed of only 50 times the surface current.

#### 3. Three-drag body problem

When the drifter is drogued at depth z, there are three drag bodies to consider and it is necessary to invert (3) numerically. Some examples of these calculations are given in Figs. 2-4.

These calculations are most conveniently depicted in a coordinate system oriented in the direction of the subsurface current  $V_i$ . Also, the magnitude of this current is fixed at unity.

The inputs for the calculation are the areas and drag coefficients for the three drag bodies (Table 1) and the magnitudes of the surface current and wind

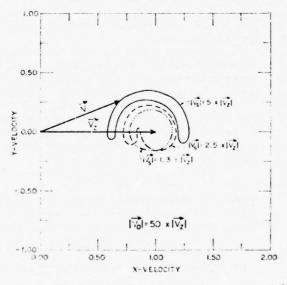


Fig. 2. The effect of surface current with a constant wind magnitude on a Nova drifter drogued at some subsurface depth by a 9.2 m parachute. The locus for the drifter velocity for a given surface current magnitude occurs within the indicated enclosed region.

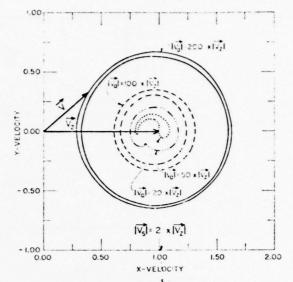


Fig. 3. The effect of wind with a constant surface current magnitude on a Nova drifter drogned at some subsurface depth by a 9.2 m parachute. The locus for the drifter velocity for a given wind speed occurs within the indicated enclosed region.

vector relative to  $V_z$ . The calculation is started with the wind and surface current aligned in the direction of the subsurface current. The numerical inversion of (3) for  $V_z$ , the drifter velocity, is then readily accomplished. The wind direction is varied in 30° increments for 360° with the solution for  $V_z$  being performed at each increment. Then the surface

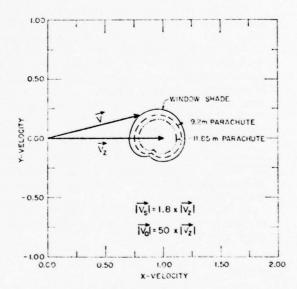


Fig. 4. The effect of various drogue sizes at constant wind and current magnitudes for a Nova drifter. The locus for the drifter velocity for a given drogue occurs within the indicated enclosed region.

TABLE 2. Hydrodynamic characteristics of drifters used in loop current study.

Drifter no.	Type	$A_a(m^2)$	.1 (n/2)
1)	1	Cylinder*	Parachute
21		$9.755 \times 10^{-1}$	$8.938 \times 10$
3	2	Cylinder	Cylinder
		$1.366 \times 10$	$1.343 \times 10$
4	3	Cylinder	Cylinder
		$3.581 \times 10$	1.375×10
			Rectangular pole
			4.297.10-1
5	4	Cylinder	Cylinder
		$3.581 \times 10$	1.375×10
			Vane
			4.262×10

<sup>•</sup> CD for cylinder is 1.2

current is changed by 30° increments for 180°. For each angle increment of current, the wind direction is varied 360° as before. This procedure produces an envelope containing 84 solutions for the drifter velocity for each set of parameters.

Fig. 2 shows the effect of surface current magnitude with a constant wind speed on the drifter velocity for a Nova University drifter with a 9.2 m parachute drogue. From this we see that if the wind and surface current are opposed to the subsurface current, the drifter velocity could deviate by more than 50% in the case of a surface speed five times the subsurface

speed. Under the same conditions, except that the wind and surface current are aligned with the subsurface current, the percentage error is of the order of 20%. For a shear ratio of 1.3 to 1, the velocity errors may still be in excess of 25%.

The results of calculations examining the effect of wind magnitude with a constant surface current magnitude on the drifter velocity are shown in Fig. 3. As before, the calculations apply to the Nova University drifter with a 9.2 m parachute drogue. For the most stringent case considered, the velocity error is of the order of 75%. Moreover, the direction of motion of the drifter in this case can be inclined 45° to that of the subsurface current.

The effect of varying the drogue type while holding the wind and current magnitude fixed is shown in Fig. 4. The calculations were performed for the Nova University drifter with a window shade drogue, a 9.2 m parachute drogue, and an 11.85 m parachute drogue. It is seen from this that the window shade with a cross-sectional area of only 29.9 m² is not as efficient as a drag body as either of the parachute drogues. In fact, it alone can cause an incremental increase of over 10% in the error in the velocity measurement when compared with measurements from the large parachute drogue.

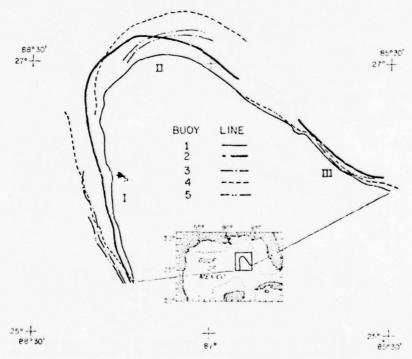


Fig. 5. Trajectories for comparison test in Gulf of Mexico. The three different legs are indicated by Roman numerals.

# 4. Experimental data

An experiment that sheds some light on the utility of the analytical and numerical results was conducted by the Atlantic Oceanographic and Meteorological Laboratories (AOML) for NDBO. The objective of this study was to evaluate the effect of wind and surface current on certain NDBO buoys by comparing their drift to the drift of a "calibration" drifter. The experiment was conducted in the eastern Gulf of Mexico Loop Current. Hydrodynamic data for the drifters used in this experiment are given in Table 2.

The navigational and positioning capability of the

tracking ship (R/V Virginia Key) along with the rapid dispersion of the drifters made it necessary to smooth the half-hourly positions. Successive groups of 13 fixes (6 h) were smoothed by fitting second-degree polynomial functions to the latitude-vs-time and longitude-vs-time values. Coordinate speeds were calculated by differentiating these functions. Finally, the velocity and position records were smoothed by a three-point running average to obtain hourly readings. The raw wind data observed on the Virginia Key were reduced in a similar manner.

The height that the wind observations were made

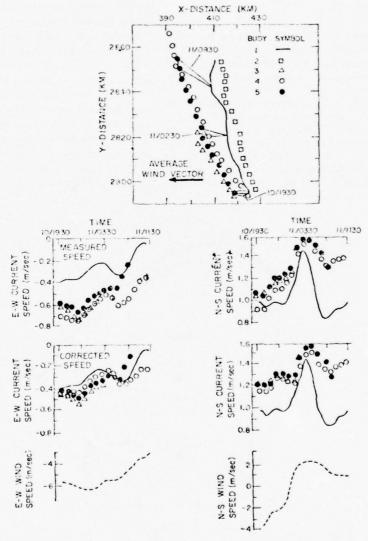


Fig. 6. Trajectories, currents and wind records for leg 1. The top panel shows trajectories of the five drifters. The bottom panels show the measured current components as well as the current components corrected in accordance with (4). Also shown are the components of the wind.

X-DISTANCE (KM)

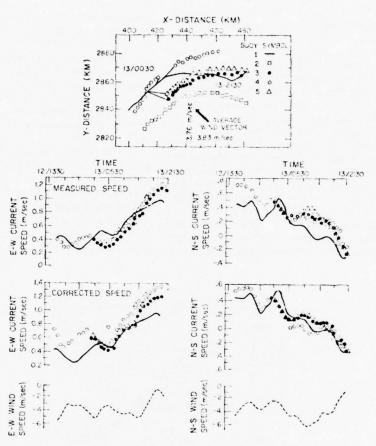


Fig. 7. As in Fig. 6 except for leg 2.

differed by about 5 m from the height of the buoys. Assuming a logarithmic velocity profile one finds that the velocity at the buoy is within 90% of that observed. Because the Virginia Key frequently was 10-20 km from some of the drifters and because the logarithmic profile indicated such a small difference, we elected not to make a height correction to the wind records.

Fig. 5 gives the smoothed trajectories determined from the analysis. The rapid separation of the drogued and non-drogued drifters is evident in this figure. As expected, the non-drogued drifters had a larger downwind displacement than did the drogued drifters. The separation between the two drogued drifters also varies but to a lesser degree. The cause of this separation could be due to small-scale diffusive processes, horizontal inhomogeneity of the currents (discussed below), or the result of the dynamics of turning currents (Chew, 1974).

Prifter type 1 has been used by AOML in a number of previous experiments. Here this type was drogued at 30 m by a 11.85 m parachute while the other types were not drogued. This disparity in coupling depths required a special assumption for analysis of the data, namely, that there was no vertical current shear between the surface and 30 m.

Note from Table 2 that the type 1 drifters have a much smaller K than the other types. For the wind speeds encountered in this experiment, the maximum wind effect for type 1, as computed from (4), was only 4% of the drifter velocity. Thus the velocity records for type 1 are regarded as the "true" surface current. For each of the other drifters listed in Table 2, a surface current is also computed from (4).

These computed surface currents are compared to the observed currents in Figs. 6, 7 and 8. Downstream and cross-stream current components are relative to the direction of the drogued drifters for that particular trajectory interval. Thus for leg 1 the downstream direction is N-S while for legs 2 and 3, it is E-W.

These figures show that the corrected cross-stream speed records are very similar for all of the drifters. This is true even though the uncorrected cross-stream speeds of drifter 4 during legs 1 and 2 are in some cases a factor of 2 greater than the velocities of drifter 1. After correction the speeds are within 15% over most of the trajectories. Drifter 4 was drogued during leg 3, and Fig. 7 indicates that the effect of wind on this drifter is greatly reduced as it tracks closely with the other drogued drifters.

The wind correction for the downstream components increases the velocity difference between drifters for legs 1 and 2. However, for all legs this was the weakest wind component. Vertical and horizontal shears in the intense Loop Current, rather than the wind, probably were the most dominant causes of the deviation of the velocity records. It was not possible to make a quantitative correction for this effect. However, a qualitative assessment shows that a horizontal shear correction would reduce the error.

# 5. Discussion

1) The theoretical calculations show that steady winds and surface currents can substantially bias velocity records obtained from drifter trajectories. The magnitudes of the parcel and drifter velocities can differ by 75% and the direction by 45% when there is a 200 to 1 ratio of wind speed to parcel velocity.

The theoretical results are substantiated by the field tests even though different drifters and K's were used in the latter. During leg 1 it is seen that  $K^4[V_a]/[V](1+K^3)$  for the field tests was the same as that used in the calculations which produced the errors indicated above.

2) The calculations also showed that the effect on a drifter of wind and/or surface currents depended upon direction. For a fixed magnitude the percent velocity error was larger when the surface current and/or wind opposed the subsurface current. The reason for this is that in opposed cases the relative velocity past the drifter system is greatest. Thus the drag is greater.

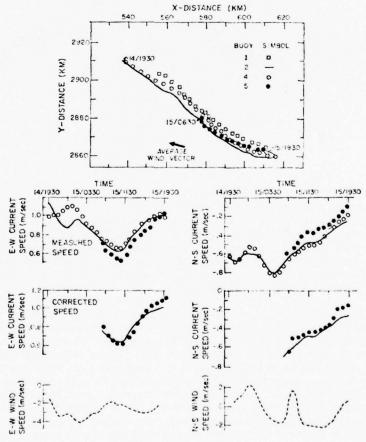


Fig. 8. As in Fig. 6 except for leg 3.

Also, for either a surface current or wind large with respect to the other, the theoretical solution approaches the two-body case.

3) The experimental data show that even for large differences in parcel and drifter velocities, wind corrections based on (4) can improve the results.

4) The experimental data also demonstrate that where there are large horizontal velocity gradients, another effect is observed. A very small wind can move the drifter into a completely different current regime. This horizontal shear effect enhances the turbulent dispersive processes.

The separation of the drifters during leg 1 (Fig. 6) exemplifies this type of effect. Here the northward motion of drifter 2 relative to 1 indicates that the current axis is to the west. Thus the east wind component caused the non-drogued drifters to move toward the axis. Although the east-west separation of the drogued and non-drogued drifters is a function of wind-induced motion, the north-south separation is caused by this horizontal current shear.

Because of this last type of effect, it is virtually impossible to correct a trajectory to obtain the true path of the water parcel originally tagged. Eq. (4) requires as input the observed drifter velocity and

wind speed to obtain the corrected speed. After the first time step the observed velocity at the "corrected" position is not known, and particularly in the case of large shears, the task of estimating this velocity is not trivial. In essence, a drifter integrates its instantaneous velocity to obtain its trajectory. Thus velocity errors accumulate in the trajectory.

Acknowledgments. This research was partially supported by the Office of International Decade of Ocean Exploration of the National Science Foundation and by the Ocean Science Division of the Office of Naval Research. The experimental portion of the research was supported by the NOAA Data Buoy Office. The assistance of Mr. E. Kerut in conducting the experiment is gratefully acknowledged. The success of the experiment was due principally to the efforts of Captain G. Hood and First Mate T. Morrissey of the R/V Virginia Key. Finally, we are deeply indebted to W. Richardson of Nova University for constructive criticism.

#### REFERENCE

Chew, F. 1974: The turning process in meandering currents. Δ case study. J. Phys. Oceanogr., 4, 27–57.

Reprinted from: Proc. of the Florida Red Tide Conference, Florida Marine Research Publication, Florida Department of Natural Resources, Marine Research Laboratory, Sarasota, Florida, October 10-12, No. 8, 9-10.

# CIRCULATION OF THE EASTERN GULF OF MEXICO AND ITS POSSIBLE RELATION TO RED TIDES

George A. Maul Atlantic Oceanographic and Meteorological Laboratories

Deep sea circulation in the eastern Gulf of Mexico is dominated by the Gulf Loop Current. This strongly baroclin'c flow enters the Gulf through the Yucatan Strait. It can penetrate into the basin as far north as the Mississippi Delta in summer. In early winter the flow tends to be from Yucatan almost directly to the west Florida Platform where it is known as the Florida Current. In its annual cycle of growth, eddy separation, and decay, the current interacts with the waters of the west Florida Shelf. Mesoscale eddies (20 km diameter) are known to detach from the current and drift onto the shelf. These eddies bring Gulf Loop Current water onto the shelf, and are capable of mixing the local Florida Shelf interacting with the Gulf Loop Current to cause a net southward drift along the shelf break. This averaged description is irregularly interrupted by local wind conditions, presence of the offshore current, and by tidal effects which dominate inlet zones.

Water from the west Florida Shelf is transported to the Keys where entrainment by the Florida Current carries it to the east coast and beyond. In summer, this water may find its way to the western Gulf of Mexico as an alongshore westerly drift west of the Mississippi Delta. This exported water must be

waters to the bottom. Interaction with the shelf waters at the shelf break is very strong and the Gulf Loop Current's behavior and presence is the offshore boundary condition for the shelf circulation.

In shallow waters away from tidal inlets, the wind dictates the current regime. High frequency (daily) winds drive the water in the upper layers in the direction of the wind. During periods of land breeze-sea breeze, the circulation is dominated by high variability in direction and speed. When the southeast trades are more constant, such as in summer, the flow is alongshore to the north from Cape Sable to Tarpon Springs. This produces a time-averaged cyclonic eddy on the west replaced by offshore water or upwelled water. In either case, foreign materials are introduced to the shelf by the action of mean wind stress and/or offshore currents, and upwelling along the shelf break. Summer stratification is strongly vertical whereas in the winter, near the coast, the stratification is horizontal. Summer conditions inhibit vertical mixing and Gulf Loop Current water can be seen to penetrate along the bottom onto the shelf into depths of 30 meters or less. Winter mixing exchanges estuarine water offshore to distances of at least 10 km.

Reprinted from: NOAA Technical Report ERL 335-AOML 18, 125 p.



U.S. DEPARTMENT OF COMMERCE Rogers C. B. Morton, Secretary

NATIONAL OCEANIC AND ATMOSPHERIC ADMINISTRATION
Robert M. White, Administrator
ENVIRONMENTAL RESEARCH LABORATORIES
Wilmot N. Hess, Director

# NOAA TECHNICAL REPORT ERL 335-AOML 18

An Evaluation of the Use of the Earth Resources Technology Satellite for Observing Ocean Current Boundaries in the Gulf Stream System

GEORGE A. MAUL

BOULDER, COLO. January 1975

# DISCLAIMER

The NOAA Environmental Research Laboratories do not approve, recommend, or endorse any proprietary product or proprietary material mentioned in this publication. No reference shall be made to the NOAA Environmental Research Laboratories, or to this publication furnished by the NOAA Environmental Research Laboratories, in any advertising or sales promotion which would indicate or imply that the NOAA Environmental Research Laboratories approve, recommend, or endorse any proprietary product or proprietary material mentioned herein, or which has as its purpose an intent to cause directly or indirectly the advertised product to be used or purchased because of this NOAA Environmental Research Laboratories publication.

C	10:	T	E	N'	rs

ABS	STRACT	Page 1
1.	INTRODUCTION	1
	<ul><li>1.1 Definition of the Problem</li><li>1.2 Choice of the Test Site</li><li>1.3 Prior Ocean Color Observations</li></ul>	2 2 3
2.	OPTICAL AND HYDROGRAPHIC PROGRAM 2.1 Background of Optical Theory 2.2 Optical Properties of the Loop Current Front 2.3 Background of Hydrographic Observations 2.4 Observation Program	6 8 12 14
3.	CURRENT PATTERNS AND THEIR SURFACE MANIFESTATIONS 3.1 Correlation Between Surface Optical Parameters and Subsurface Temperatures 3.2 Pathlines of the Current 3.3 Theoretical Relationship Between Surface and Subsurface Fronts	17 17 19
4.	RADIATION OBSERVATIONS 4.1 Theoretical Effect of Sea State on Upwelling Light 4.2 Spectroradiometer Observations 4.3 ERTS Observations of the Gulf Loop Current 4.4 Satellite Evidence of Fine-Scale Features in the Current	29 29 32 36
5.	DISCUSSION 5.1 Evaluation of Ocean Color Data for Locating the Gulf Loop Current 5.2 Some Features of the Current Usefully Observed From Satellites 5.3 Suggestions for Future Research	50 50 55 61
6.	CONCLUSION	63
7.	ACKNOWLEDGMENTS	66
8.	REFERENCES	67
9.	APPENDIXES	73
	APPENDIX A	73
	APPENDIX B	90

# AN EVALUATION OF THE USE OF THE EARTH RESOURCES TECHNOLOGY SATELLITE FOR OBSERVING OCEAN CURRENT BOUNDARIES IN THE GULF STREAM SYSTEM

George A. Maul

#### ABSTRACT

Remote sensing of ocean color to locate current boundaries has been tested in the eastern Gulf of Mexico. Infrared techniques fail there for several months of the year because surface thermal signatures are destroyed by summer insolation. A 1-year time history of the Gulf Loop Current has been made by ship in synchronization with the Earth Resources Technology Satellite (ERTS). Shipboard measurements of upwelling spectral irradiance show that the color change across the cyclonic boundary is associated with changes in chlorophyll-a concentrations and changes in the volume scattering function. Surface chlorophyll-a, temperature, and scattering observations show that color signature of the current is present when thermal indications are absent, and thus this flow can potentially be monitored by a combination of visible and infrared techniques. Shipboard observations indicate that seastate changes frequently occur at the cyclonic edge; this is recorded in ERTS images which show that the current's boundary can be detected by changes in either color or sea state. Theoretical spectra of upwelling irradiance confirm that surface reflectance changes due to meteorological conditions spectrally alter ERTS radiances. The gain settings for the satellite are not optimized for ocean radiances and hence computer enhancement of the data is required. The ship data demonstrate an annual cycle of growth, eddy separation, and decay of the Gulf Loop Current, but this could not be reproduced with ERTS due to the 18-day orbit cycle and because the sensors were not designed for ocean radiance levels or spectral distributions. This research supports the concept that a visible multispectral scanner, which supplies at least daily observations, is capable of providing triweekly pathlines of the Gulf Loop Current.

#### 1. INTRODUCTION

The objective of this report is to present an evaluation of the use of the Earth Resources Technology Satellite for observing ocean current boundaries. Definition of the problem is discussed first so that the purpose and direction of the research are pellucid at the outset. Choice of the test site and a brief discourse on earlier ocean color investigations complete the introduction. The latter subjects are discussed because the focus of the research is to examine the application of ocean color remote sensing to locating currents in the eastern Gulf of Mexico; Appendix A demonstrates the utility of visible scanning radiometer data in other parts of the Gulf Stream system from Cape Florida to Cape Hatteras.

#### 1.1 Definition of the Problem

The location of ocean currents by infrared radiometers in aircraft and satellites is operationally successful from aircraft over the Gulf Stream. The statistical correlation between the surface thermal signature of the Gulf Stream and the velocity core has been studied, and it has been shown (Hansen and Maul, 1970) that north of Cape Hatteras there is a thermal indication of the cyclonic edge (left-hand side facing downstream in the Northern Hemisphere) at all seasons. Atlases, however (e.g., Robinson, 1973), show that major portions of the Gulf Stream system have no surface thermal gradients caused by seasonal heating for as much as 4 months of the year.

The cyclonic edge of the Gulf Stream-type flows is frequently well defined and can often be observed by noting changes in temperature, salinity, color, and sea state (Stommel, 1966, pp. 62-65; Uda, 1938). Color changes imply that the optical properties of the ocean change in the vicinity of the cyclonic edge. If those optical properties are observable when the thermal signature is lost, a year-round remote sensing technique is potentially available.

Specifically, this research is to test the utility of the Earth Resources Technology Satellite, ERTS (supplemented by Skylab photography), for observing ocean currents from changes in the optical properties of the water across the cyclonic edge through information collected in a sequence of ground-truth research vessel cruises in synchronization with the satellite. The research relates upwelling irradiance spectra to the current's surface optical signature, evaluates the seasonality of parameters contributing to the surface optical signature, correlates the surface optical signature and the deeper thermal structure, obtains pathlines of the deeper thermal signature, tests whether ERTS data reproduce the circulation pattern, contributes to basic oceanographic knowledge in the test site, and examines the requirements for an optimum ocean-color-sensing satellite.

# 1.2 Choice of Test Site

Radiation data from the Earth Resources Technology Satellite's Multispectral Scanner (MSS) became available from mid-1972 onward, but almost exclusively over the United States because of limitations in on-board tape recorder capacity. Satellite tracking stations at Greenbelt, Maryland, and Goldstone, California, are able to receive signals over the Gulf of Mexico and into the Cayman Sea, an area that fits the problem definition and is logistically convenient. ERTS has an 18-day revisit time that requires the ocean feature to be studied as a slowly varying phenomenon. Data taken by the R/V DISCOVERER in 1969-70 showed that changes in the circulation patterns in this area were not rapid and that monthly observation schedules would be acceptable.

On the basis of these considerations, the eastern Gulf of Mexico was chosen as the test site. Here, the flow from the Yucatan Strait penetrates northward into the Gulf to a varying degree before exiting through the Straits of Florida. Leipper (1970) proposed an annual cycle of growth,

spreading, and decay of this current system, but it was based on data spaced at random intervals over 2 years including several cruises not designed to collect data on the current. The sequence of current patterns obtained in the present study was designed to provide a proper time series of the Gulf Loop Current from Yucatan to Key West. The surface vessel cruises are at 36-day intervals in synchronization with ERTS overpasses.

Routine monitoring of the Gulf Loop Current has several practical applications: The relatively sterile waters of the current mark a boundary of organic production important to the fishing industry (Austin, 1971). The high velocities in the current can have a marked effect on optimum ship routing. Sound propagation characteristics in the sea change significantly in the vicinity of the current's boundary, having implications for bathymetric surveying and national defense. The location of the Loop Current has been related to storm intensification (Leipper and Volgenau, 1970) in this hurricane fertile region. Environmentalists are concerned about the transport of hydrocarbons and wastes (Smith, 1974).

These data have already been used to document the first Florida east coast red tide (Murphy et al., 1974), wherein the organisms were transported by entrainment from Florida Bay to the Florida east coast. The impact of a recent accidental jettisoning of hundreds of cyanide canisters following a ship collision in the Yucatan Straits is being studied with these results (Corwin and Richardson, 1974). The Gulf of Mexico thus represents an area of regional interest where knowledge of surface current trajectories in real-time is an important contribution to the proper use of the oceans.

#### 1.3 Prior Ocean Color Observations

Early work on ocean color is summarized by Schott's 1935 map (Neumann and Pierson, 1966, p. 68) of Forel color for the Atlantic Ocean in figure 1. The contours of Forel scale number clearly separate the Sargasso Sea from the east coast of North America's coastal waters. Similarly, Joseph and Wattenbergs' 1944 map (Neumann and Pierson, 1966, p. 65) of the distribution of the vertical extinction coefficient in the Atlantic almost duplicates Schott's distribution of color (fig. 1): The Sargasso Sea is a clear, blue, water mass, juxtaposed with a green, more turbid coastal water mass.

Observations have shown that the temperature and salinity change at the cyclonic edge of the Gulf Stream is well correlated with a rapid change in horizontal velocity shear (e.g., Maul and Hansen, 1972). A color change is associated with this shear but the correlation was not established. In the summer of 1971, observations were taken by the author while on board the R/V KNORR in the Gulf Stream off New England. The Forel-scale color never failed to correlate with surface temperature changes: Forel number 0-1 were always recorded in the Stream with higher temperatures, and Forel numbers 4-5 were always observed at stations in the slope water outside of the Stream with lower surface temperatures. These changes were noted even if the station spacing inside and outside the boundary was only several kilometers apart. From these observations, it appears that color change is as viable an indicator of the cyclonic edge as temperature or salinity. Hanson (1972) reviewed the field of ocean remote sensing and discussed

the techniques for measuring temperature in the infrared or microwave, salinity and sea state in the microwave, and color by visible spectroscopy. The research effort discussed herein centers on the use of the visible and reflected infrared portion of the electromagnetic spectrum (400-1100 nm). Yentsch (1960) contributed to using remote spectral devices in this spectral region in his study on the influence of phytoplankton pigments on the color of the sea. That paper, and a later one (Yentsch, 1962), discussed changes in the absorption spectra of sea water due to chlorophylls and to particulates. The absorption spectra show a shift in the wavelength of maximum transparency toward the green with increasing chlorophyll concentrations; larger particle sizes cause higher attenuance of light in the shorter wavelengths of the spectrum. The Forel color shift in the ocean (fig. 1) is explained by these results.

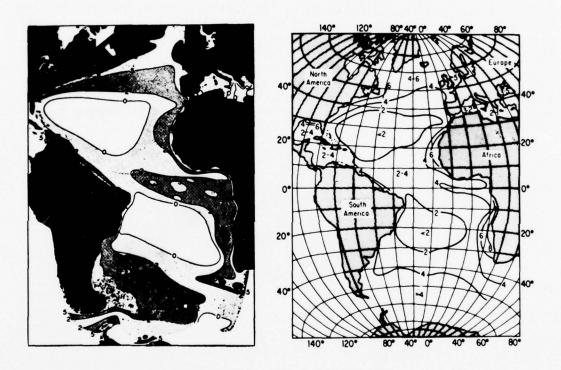


Figure 1.1a (left): Color of the sea as indicated in percent of yellow as indicated by the Forel scale, according to Schott.

Figure 1.1b (right): Distribution of the vertical extinction coefficient (x100) of the surface water, according to Joseph and Wattenberg (both figures after Neumann and Pierson, 1966).

Remote sensing of the color, on the other hand, is a corollary to the absorption spectra problem. Clark et al. (1970) obtained reflectance spectra of upwelling radiance from aircraft over the Sargasso Sea, the New England slope water, and Georges Bank. They related the spectra of back-scattered light to varying chlorophyll concentration and noted that anomalies in the spectra are related to other biochromes, suspended sediment, surface reflection, polarization, and air light. Chandrasekhar (1960) showed from radiative transfer theory that the reflectance spectra at the ocean's surface are a function of both the scattering and attenuation of the water itself and the materials suspended or dissolved in it. Chandrasekhar's theory gives a qualitative explanation of the spectra obtained by Clark et al.: Higher reflectances are caused by increased scattering, and shifts in the wavelength of maximum reflectance are due to absorption (see also Yentsch, 1960, 1962).

The results discussed above form the basis for this study. In the Gulf Stream off New England, a color change is associated with the cyclonic edge of the current. That color shift is associated with changes in the concentration of pigment forming molecules in the water, and it can be detected by airborne spectroradiometers. If similar results can be obtained in the test site, then ocean color can be used to delineate the boundary of the Gulf Loop Current. The following sections will discuss ocean spectra in light of more recent theoretical results and the application of the color sensors aboard the Earth Resources Technology Satellite to current boundary location.

# 2. OPTICAL AND HYDROGRAPHIC PROGRAM

The subsections of this chapter elucidate the background of the research. The optical theory necessary to interpret both the shipboard observations and satellite data is presented. An aircraft/ship experiment conducted before the satellite launch is used to test whether ERTS has the basic capability to observe ocean color, and what surface vessel measurements are required to obtain satisfactory ground truth. Previous hydrographic observations in the Gulf of Mexico are then researched, and a useful indicator of the Gulf Loop Current's deeper thermal signature is chosen for the time series. Finally, the observation program and measuring techniques are discussed.

# 2.1 Background of Optical Theory

The radiance (N ( $\lambda$ )) at the top of the atmosphere can be written as the sum of the ocean surface radiance (N<sub>S</sub> ( $\lambda$ )), the diffuse radiance from beneath the ocean (N<sub>d</sub> ( $\lambda$ )), and the radiance from the atmosphere (N<sub>g</sub> ( $\lambda$ )):

$$N(\lambda) = \alpha(\lambda)N_{s}(\lambda) + \gamma(\lambda)N_{d}(\lambda) + N_{a}(\lambda)$$
(2.1)

where  $\alpha(\lambda)$  and  $\gamma(\lambda)$  are atmospheric transmittance factors for  $N_s$  and  $N_d$ , and  $\lambda$  is wavelength. The effect of the atmosphere on ocean color sensing from space has been recently studied by Curran (1972). In this work, however, interest is in determining the boundary of these baroclinic flows by changes in the optical properties of the ocean  $(N_s, N_d)$ . The radiance of the atmosphere does not contribute to determining these ocean properties except to reduce the contrast, unless there is significant atmospheric spatial variability. The effect of sea state on  $N(\lambda)$  is to spectrally alter  $N_s$   $(\lambda)$ ; this will be discussed in section 4.2.

Gordon (1973) constructed a single scattering model for the ocean wherein he related the diffuse reflectance ( $R_d(0,-)$ ) just above the sea surface (defined as the ratio of the upwelling irradiance (H(0,+)) to the downwelling irradiance (H(0,-)) to several optical properties of the water and its suspended or dissolved materials.  $R_d(0,-)$  as defined here does not include the surface component and is proportional to  $N_d$ ,

$$N_d \propto R_d (0,-) \cdot H(0,-) = H(0,+)$$
, (2.2)

where the proportionality constant depends on angle. The optical parameters in Gordon's model are  $\omega_0$ , which is defined as the ratio of the beam scattering coefficient (b) to the total beam attenuation coefficient (c), and B, which is the fraction of backscattered light:

$$B \equiv 2\pi \int_{\pi/2}^{\pi} \frac{\beta(\Theta)}{b} \sin \Theta d\Theta. \qquad (2.3)$$

 $\beta(\Theta)$  in (2.3) is the volume scattering function which relates to the intensity of radiation (dJ( $\Theta$ )), singly scattered from a small sample volume (dv) when illuminated by an incident irradiance (H $_{\Theta}$ ) through

$$\beta(\Theta) = \frac{dJ(\Theta)}{H dv}$$
0 (2.4)

Examples of measurements of this variable are given later in section 2.2.It has been shown that  $\beta(45^{\circ})$  and b are well related in the ocean (Beardsley et al., 1970). In Gordon's model, for a semi-infinite ocean, the forward-scattered light is approximated by a delta function (cf., Jerlov, 1968), and the diffuse reflectance can be written

$$R_{d}(0,-) = \frac{k \omega_{0}B}{1-\omega_{0}F}$$
, (2.5)

where F is the fraction of forward-scattered light (1-B), and k is a constant. Each of the variables in (2.2), (2.3), (2.4), and (2.5) are dispersive, that is, they are wavelength dependent and will be tacitly assumed to be so hereforth.  $R_d$  is the contribution to the reflectance of photons from the atmosphere that penetrate the ocean's surface and are scattered back into the atmosphere.

Equation (2.5) allows spectra to be computed for comparison with observations. The important oceanic parameters are  $\omega_0$  and B. These independent variables provide an infinite set of possible contributions to the upwelling light, and they must be known to interpret observations. Unfortunately  $\omega_0$  is only imperfectly known even for pure water, and the contributions to B from particles alone (Bp) are unknown. From the behavior of Rd; Maul and Gordon (1974) were able to show that the spatial gradient of (2.1) in two ERTS bands can give quantitative information about the gradient of particle concentrations in the sea. This is a useful result for locating ocean currents from ERTS because there are large changes in the extinction coefficient (Joseph and Wattenburg)  $^{\rm l}$  across these boundaries.

ERTS is a polar-orbiting research and development satellite originally designed to return seven channels of data; one instrument failed (channels 1-3) early in the mission. The ground swath is 185 km wide and the revisit time is 18 days. The sensors of the multispectral scanner are in the visible and near infrared (reflected infrared) region. Pertinent details are summarized in table 2.1.

<sup>1</sup> Cited by Neumann and Pierson (1966), p. 65.

Table 2.1 Multispectral Scanner Specifications

Band	Bandpass	Nominal radiance response	Digital steps
	(nm)	$(mW cm^{-2}sr^{-1})$	(Quantized onboard)
MSS-4	500-600	0-2.48	128
MSS-5	600-700	0-2.00	128
MSS-6	700-800	0-1.76	128
MSS-7	800-1100	0-4.60	64

Note: The Earth Resources Technology Satellite's multispectral scanner is quantized onboard and the data relayed in a digital bit stream. An oscillating mirror system reflects upwelling radiation into six detectors for each channel so that six scanlines of the earth are observed simultaneously. Energy for each quantum step can be estimated by assuming a linear relationship over the 128 (64) steps (NASA, 1971).

The satellite does not receive any information from the blue portion of the spectrum (400-500 nm). It seems that this is a severe limitation for oceanography since most of the spectral information observed at the sea surface is contained in this spectral interval (see section 4.2).

The penetration depth of the ERTS sensors is important in data interpretation because, in the coastal zone, bottom reflection contributes to  $R_d$ . Gordon and McCluney (1974) have studied this and show that in the open ocean, the mean penetation depth is 15 to 18 m for MSS-4, and 3 m for MSS-5. In the coastal zone, these values will be even less because of larger values of the absorption coefficient ( $a_v$ ) due to yellow substance (Gelbstoff; Kalle, 1938). Charnell and Maul (1973) showed that, for MSS-6 and MSS-7, pure water is essentially opaque because of very large attenuation coefficients in the near infrared; therefore, any information from MSS-6 or MSS-7 can be considered surface data only, whereas some subsurface variability may be inferred from MSS-4 and MSS-5.

# 2.2 Optical Properties of the Loop Current Front

Figure 2.1 is a south-north section through the cyclonic front of the Gulf Loop Current near Dry Tortugas. These data were collected during a joint ship/aircraft experiment on 27-28 June 1972, and are representative of the variability in temperature, scattering, chlorophyll-a concentration, and spectra.

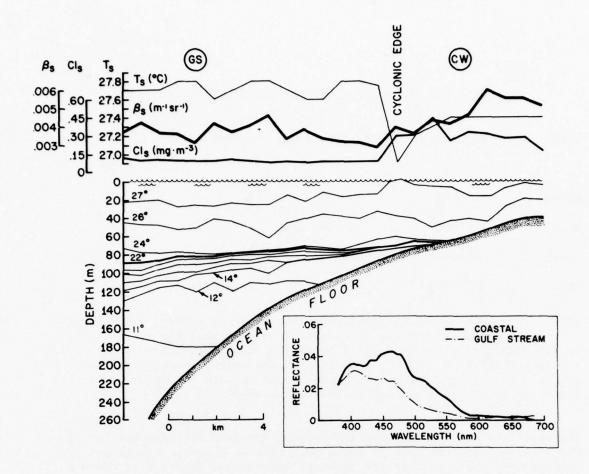


Figure 2.1 South-to-north (left to right) cross section of the Gulf Loop Current's cyclonic boundary. Isotherms in the thermal cross section are in degrees Celsius. The cyclonic edge marks not only where temperature, scattering, and chlorophyll values change, but also salinity, current velocity, and frequently sea state. Inset are reflectance spectra; one taken in the Gulf Stream (GS), the other taken in the coastal water (CW). Mixed layer depth suggests that the optical properties which affect spectra are homogeneous for at least 20 m.

The surface temperature field  $(T_s)$  shows a marked decrease near the current's edge. This is the thermal signature that completely disappears for 3 or 4 months when summer insolation makes these waters isothermal, thus rendering infrared techniques useless. The subsurface thermal field reflects early summer conditions: mixed layer depth of approximately 20 m, gentle slope of warmer isotherms (i.e., 22°C), and steeper slope of cooler isotherms (i.e., 14°C) when going toward the current. The core of the current is further offshore (to the left) than this section shows. Details of the boundary between the current and coastal waters are emphasized here to demonstrate use of visible techniques for remote sensing in tropical and subtropical waters.

Profiles of surface chlorophyll-a concentration (Cl $_{\rm S}$ ) and volume scattering function at 45° ( $\beta$ (45) $_{\rm S}$ ) made during the transect are shown along with the thermal signature. Light-scattering measurements were made during the experiment using a Brice-Phoenix light-scattering photometer and a blue (436 nm) filter. The volume-scattering function defined in (2.4) was calculated using

$$\beta(45^{\circ}) = \frac{a}{h \pi} \frac{D}{D} \frac{D}{(0^{\circ})} \tau \sin 45^{\circ},$$
(2.6)

where a is the ratio of the working standard diffuser to the reference standard diffuser,  $\beta(45$ °) is in units of m $^{-1} sr^{-1}$ , TD is the transmittance of the reference standard diffuser, h is the dimension of the irradiated element, D is the deflection of the galvonometer, and  $\tau$  is the transmittance of the neutral density filters. Chlorophyll-a measurements were made in vitro on a fluorometer calibrated with pure chlorophyll-a. The calibrations were checked on a spectrophotometer, and calculations were made using the S. C. O. R./ U. N. E. S. C. O. (Strickland and Parsons, 1968) equation:

$$C1 = 11.64 E_{663} - (2.16 E_{645} + 0.10 E_{630})$$
, (2.7)

where Cl is the chlorophyll-a concentration in mg m $^{-3}$ , E is the extinction (defined as the logarithm of the reciprocal of transmittance), and subscripts are the applicable wavelength in nanometers. These techniques are used for all values reported herein.

The profiles demonstrate that the general level of scattering is  $0.7 \times 10^{-3} \, \mathrm{m}^{-1} \, \mathrm{sr}^{-1}(18\%)$  more in the coastal water than in the current. Similarly the chlorophyll-a concentration is  $0.2 \, \mathrm{mg \ m}^{-3}(100\%)$  more in coastal water. This is the general situation observed in these transects especially near the coast; however, many times there were no distinct changes of these indicators of optical properties across the cyclonic edge, and there were instances where scattering from an isolated sample was higher in the current (see section 3.1). The slight peak in  $\mathrm{Cl_s}$  just before reaching the edge is a common feature (Lorenzen, 1971). Maul (1973) related these chlorophyll peaks to the edge of currents, and it appears to be a feature of the accumulation of materials so often observed near the cyclonic edge (e.g., \$tommel, 1966, p. iv).

Spectra of upwelling irradiance at 1-m depth and downwelling irradiance from the sun and sky 3 m above the water's surface were obtained during the ship/aircraft experiment. Reflectance ratios (uncorrected for the immersion effect, Tyler and Smith, 1970) are graphed as an inset on figure 2.1. Approximate location of these observations in the Gulf Stream (GS) and coastal waters (CW) are indicated on the top of the figure. The reflectance in coastal waters is generally higher than in the current, and the wavelength of maxium intensity is shifted to higher values. This is in agreement with color aerial photographs taken concurrently: A distinct discontinuity

in color from the green of the coastal water to the blue of the Gulf Stream occurred at the point labeled cyclonic edge in figure 2.1.

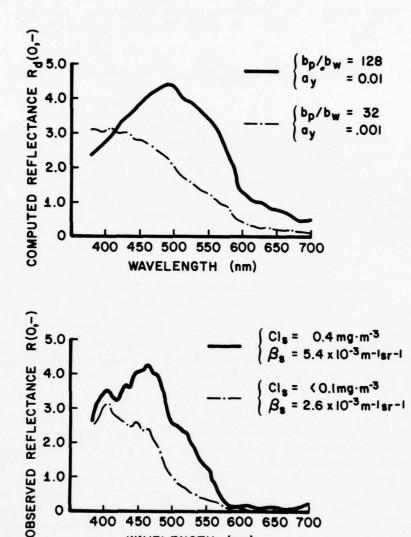


Figure 2.2a Theoretical spectra computed for ratio of particle scattering to water scattering of 128 (solid line) and 32 (dashed line). The beam attenuation coefficients were 0.01 and 0.001 (ay values at 550 nm), respectively, for this example of coastal and offshore water types. Figure 2.2b Observed reflectance spectra for coastal (solid line) and Gulf Stream (dashed line). The surface volume scattering is for blue light at 45°. See figure 2.1 for geographic location.

WAVELENGTH (nm)

450 500 550 600 650 700

2.0

1.0

0

400

Figure 2.2a contains the reflectance spectra for two water types. These spectra were calculated using the Monte Carlo technique by Gordon et al. (1974): (2.5) is a very good approximation to the full equation, which is a polynomial fit in powers of  $\beta\omega_0/1-\omega_0F$ . The solid curve is computed using a ratio of the particle-scattering coefficient (bp) to the pure-water scattering coefficient (bw)=128; the ratio b /bw is proportional to the concentration of suspended particles. The dashed line uses bp/bw=32, and hence is much lower in suspended materials. This is qualitatively analogous to the lowered-volume scattering function in the current. The values labeled ay are beam absorption coefficients (a=c-b) for yellow substance only. Range of ay is chosen to represent coastal and oceanic values. For comparison, the observed reflectance spectra in figure 2.2b are from the inset to figure 2.1.

Referring to (2.5), it is seen that at a given wavelength, if B remains constant, the reflectance is dependent on the scattering albedo ( $\omega_0$ ). As more and more particles are added to the suspension,  $\omega_{_{\mathrm{O}}}$  increases and the upwelling radiance increases. In figure 2.2b, it is seen that  $\beta(45)$  has doubled in going from the current into coastal water. Simply increasing  $a_{\mathbf{v}}$ would decrease  $\omega_0$  with a resultant decrease in N $_{
m d}$ . The absorption coefficient is very dependent on wavelength. This causes a shift in the spectral peak to a longer wavelength, i.e., the water appears green to the eye. This is not to say that the chlorophyll-a and the Gelbstoff produce quantitatively similar results; in general they will not. What it does imply is that the broad absorption bands in pigments, such as chlorophyll and Gelbstoff at shorter wavelengths (<600 nm), produce qualitatively similar effects in the spectra. In nature, however, such as in a plankton bloom or in coastal waters, increased amounts of chlorophyll are normally accompanied by increased particle concentrations (organisms which contain the chlorophy11) as well as increased amounts of Gelbstoff. Since a and b vary almost independently, the reflectance signature, which depends on  $\omega_0$  and B, is not unique and can be unraveled only when the variation of the optical properties of the individual components with wavelength is known.

The aircraft experiment thus established that the color signature of the Gulf Loop Current was identical with the thermal signature, that an optical signature was present in summer, and that appropriate surface parameters for identifying that signature were chlorophyll-a concentration and volume scattering function. The observed reflectance spectra showed that there was variation in the MSS-4 bandpass interval and that the color change was potentially observable from ERTS. These results suggested that the eastern Gulf of Mexico was an acceptable test site, and the background of hydrographic conditions was researched.

# 2.3 Background of Hydrographic Observations

Early hydrographic work in the Gulf of Mexico has been summarized by Galtsoff (1954) who edited a complete overview of the biology, chemistry, geology, and physics of the area: In 1895, Lindenkohl published a map of the temperature field at 250 fm (457 m), in degrees Fahrenheit, which is reproduced in figure 2.3. The warm waters of the Caribbean can be seen flowing northward into the Gulf and penetrating deeply into the ambient

thermal field; similarly the Gulf Stream, seen as a region of large horizontal temperature gradient, is flowing easterly and then northerly through the Straits of Florida. In an analysis of these data, Sweitzer, in 1898, reported that the circulation was a spreading of this inflow which resulted in an anticyclonic circulation around the entire Gulf basin. Parr, in 1935, reported the opposite conclusion using ATLANTIS data taken in 1933; he stated that the Gulf Stream takes the shortest path from Yucatan to the Straits of Florida. Leipper expressed this divergence of opinion as the state of knowledge in 1954 even after reviewing Dietrich's 1939 map of the salinity maximum core, which reflects the deep penetration seen in figure 2.3.

Work done in the 1960's, notably by Leipper, and others (Capurro and Reid, 1972), led Leipper to speculate that there was an annual cycle in the current patterns in the eastern Gulf.

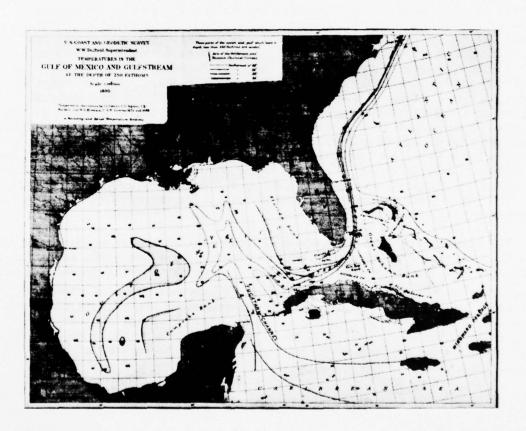
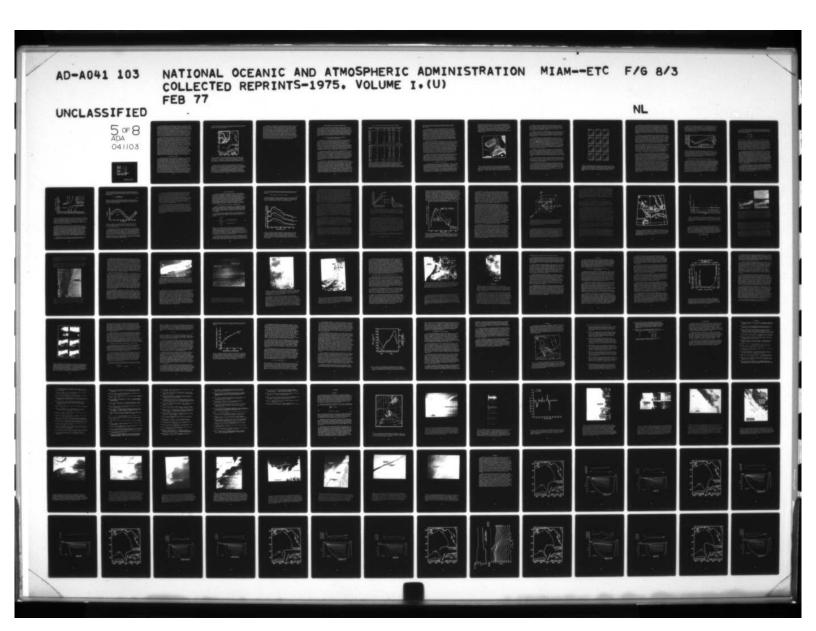
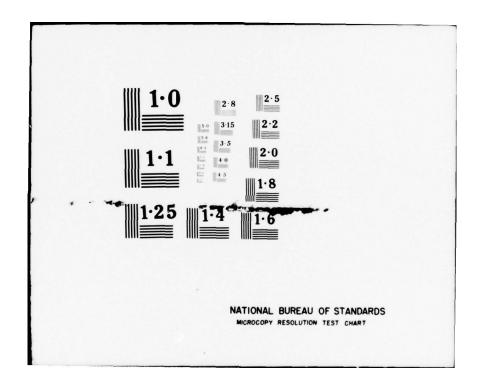


Figure 2.3 Lindenkohl's 1895 map of the temperature field (°F) at 250 fm in the Gulf of Mexico. Data are from soundings made by Sigsbee, Bartlett, and Brownson between 1874 and 1883. The shallow waters (<250 fm) of Campeche Bank and the west Florida Platform are stippled on the chart.





Bottom topography in the eastern Gulf of Mexico is dominated by a broad shallow shelf extending north of the Yucatan Peninsula, the Campeche Bank, and another broad shallow shelf west of Florida, the west Florida Platform. The continental slopes are marked by steep escarpments along the west Florida area and northeast of Campeche. Sill depth in the Yucatan Strait is 2000 m, and in the Straits of Florida is approximately 800 m (see inset to fig. 2.4). As the Yucatan Current flows over Campeche Bank, the bottom topography has been thought to control the flow as far north as 23°30'N (Molinari and Cochrane, 1972): Above that latitude, the flow is no longer so constrained. After leaving the confines of the Campeche Bank, the Gulf Loop Current makes an anticyclonic turn in the deep water of the basin, and once again is channeled by the Florida Platform and the Cuban Platform into the Straits of Florida.

The water masses in the eastern Gulf are essentially the same below the depth of the 17°C isotherm (Nowlin and McLellan, 1967) as evidenced by the temperature-salinity (T-S) relationship. The depth of this isotherm varies considerably, and as expected from simple dynamical considerations, 17 °C is several hundred meters deeper under the current and in the Yucatan Water. Above the 17 °C isotherm, the T-S relation for Gulf Loop Current Water and Eastern Gulf of Mexico Water, shows a distinct difference. The former has higher salinities, which reach a maximum near 22° C; the latter is generally cooler at the same saline level. Following the precedent of Wennekens (1959), all the water originating in the Yucatan Strait is referred to as Yucatan Water, the water along the continental shelves as Shelf Water, and the resident eastern Gulf of Mexico water as Eastern Gulf Water. The Yucatan Water is modified as it flows through the Gulf Loop Current (region of anticyclonic turning) and into the Straits of Florida, as evidenced by a decrease in the salinity maximum of the Subtropical Underwater (Wust, 1964). For consistency, the current regime is referred to by these three subdivisions: Figure 2.4, Yucatan Current as defined by the hydrographic sections from Cabo San Antonio, Cuba, to Isla Contoy, Mexico; Gulf Loop Current as the regime from the Yucatan section to the Key West, Florida, to Habana, Cuba, hydrographic section; Florida Current, eastward of the latter section.

# 2.4 Observation Program

Leipper showed that the 22°C isotherm at 100-m depth was a good incicator of the current in all seasons of the year. Adopting this as the basis for the tracking strategy, this isotherm is followed with expendable bathythermographs (XBTs). The first four cruises were started in St. Petersburg. On the day of every second overpass by ERTS, the ship occupied the suborbital track; XBT data along the NNE-SSW tending line in figure 2.4 typify the ground track. Upon reaching the Yucatan Strait, a Salinity-Temperature-Depth (STu) profile was made at each of nine stations. After observing this hydrographic section, a zig-zag tracking pattern was initiated heading downstream, so that the average speed of the ship was boosted 2 kt. Typically, hourly XBT's were taken. When the depth of the 22° C isotherm exceeded approximately 125 m, the ship's course was altered to the left. This course was run until the 22°C isotherm was less than 80 m, and then course was altered to the right. The pattern was continued from Yucatan around the Loop to Dry Tortugas, in all but a few cases, where weather or fuel considerations made it advisable to run for Key West. The Key West-Habana section of seven STD lowerings was occupied after a short refueling

stop. From January through the end of the project (eight cruises), the cruises originated from Miami, and the Key West-Havana section was done first; this section is also a suborbital track.

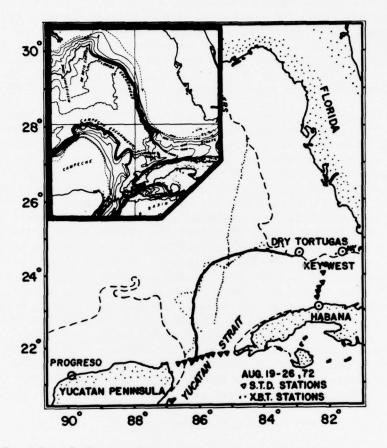


Figure 2.4 Example of the tracking technique is given in the main figure for August 1972. Dots are XBT drops and triangles are STD lowerings. The solid line is the pathline. (Inset) Bottom topography in the eastern Gulf of Mexico. Contours are in meters and show the topography of the deep eastern basin surrounded by the Florida, Campeche, and Cuban Platforms.

After each trip, the position data were replotted and a smooth plot constructed, which made a best fit to the estimated courses and speeds made good. Positioning was accomplished using Loran-A, radar, visual, and celestial observations. It is difficult to estimate errors, but based on Loran-A/radar comparisons, ±1 to 3 km seem reasonable. The expendable BT strip chart recorder was tested (and adjusted if necessary) before each cruise with a test canister. The average-surface-bucket temperature and the average-XBT-surface temperature (from the recorder) were calculated for each cruise, and the surface XBT temperature was adjusted for the difference in the average.

In addition to the routine XBT observations described above, continuous flow measurements of chlorophyll-a using the technique of Lorenzen (1966), modified to include a bubble trap, were recorded. An infrared radiometer with a special 10.5- to 12.5-µm bandpass filter recorded continuous near-surface measurements of radiation temperature for comparison with the NOAA-2 meteorological satellite (Maul and DeVivo, in preparation); these will be the first such comparison in the same wavelength interval. Volume scattering at 45°, 90°, and 135° was observed, using both blue (436 nm) and green (546 nm) light, on the suborbital track and at each STD station. During appropriate daylight hours, spectra of upwelling and downwelling irradiance were observed for correlation with the biological data and the optical data. STD stations were taken to a depth of 1000 m, or 100 m from the bottom, whichever was less. Surface calibration points were taken at each cast, and the lowering speed was about 50 m per minute. Station spacing was about 20 km, and no stations were closer than 22 km (12 n mi) to foreign coasts.

## 3. CURRENT PATTERNS AND THEIR SURFACE MANIFESTATIONS

To interpret the ERTS data, ground-truth cruises were conducted. This section opens with an analysis of the correlation of the annual cycle of the surface optical signature of the Gulf Loop Current and the relation of that surface expression to the deeper thermal signature. Details of the pathlines are then discussed for their contribution to the physical oceanography of the Gulf of Mexico. In the last section, the theoretical relationship between the surface and 200-m fronts of a two-layer model are explored, and the importance of curvature in the pathlines is analyzed. The potential contribution and limitations of surface observations to needs in ocean physics are examined.

# 3.1 Correlation Between Surface Optical Parameters and Subsurface Temperatures

During each of the transects of the Straits of Florida and the Yucatan Strait, profiles of surface-chlorophyll and surface-volume scattering function were made. The aircraft experiment summarized in figure 2.1 shows that the cyclonic edge is closely correlated to the maximum positive gradient in chlorophyll-a when proceeding toward the boundary from the current. Since this is the region of the current that an ocean color sensor will record as the boundary, the correlation between this maximum chlorophyll gradient and the deeper thermal structure must be established. Particularly, the correlation between the 22°C isotherm at 100-m depth is needed, and, for comparison with earlier work by Hansen and Maul (1970) in the Gulf Stream off New England, the 15°C isotherm at 200-m depth is also investigated.

The transect data, separated by months, are summarized in table 3.1. The first column is the month of the survey. The second column lists the horizontal separation in kilometers between the cyclonic edge at the surface (CE) and the 22°C isotherm at 100-m depth. Column three is similar to column two except being for the 15°C isotherm at 200 m. The fourth column is the average-surface chlorophyll-a concentration in the current (GS); the sixth column is the percent increase in chlorophyll-a concentration in the coastal water over that in the current. The volume-scattering function (not tabulated) showed general agreement with these trends in agreement with the discussion in section 2.2.

One reason that Leipper chose the 22°C isotherm as an indicator is evident from table 3.1. All blank entries, except January 1973, are caused by the indicator being aground; January is the one exception, in that no transects were made because of operational difficulties. The shallower indicator isotherm is more reliable in these waters as Leipper suggested. The horizontal separations are somewhat larger in the Yucatan Strait than in the Straits of Florida, possibly because of higher current velocities in the narrower Key West-Habana section. On the average, however, the separation is approximately 15 km, which is very close to the average value of 14.7 km reported by Hansen and Maul off New England between the maximum surface thermal gradient and the maximum thermal gradient at 200 m. This is unexpected, in that the ratio of the Coriolis parameter at Gulf of Mexico latitudes to New England is 0.6, and initially the separation would be expected to be larger in southern latitudes.

Table 3.1 Separation of Surface Front and Indicator Isotherm

YUCATAN	CE-22 @ 100 (km)	CE-15 @ 200 (km)	$C1_s(GS)$ $(mg.m-3)$	$C1_s(CW)$ $(mg.m^{-3})$	Difference %
AUG 72	2	_	0.13	0.89	(585)
SEP 72	-	_		-	_
O-N 72	6	_	0.85	1.24	46
DEC 72	10	-	0.34	0.64	88
JAN 73	-	-	_	-	-
FEB 73	8	-	0.36	0.48	33
MAR 73	23	19	0.14	0.16	14
A-M 73	-	_	0.20	0.23	15
JUN 73	20	6	0.18	0.32	78
JUL 73	25	-	0.31	0.49	58
AUG 73	37	61	0.40	0.55	38
SEP 73	28	18	0.37	0.51	38
ΑVE±σ	17.7±11.7	26.0±24.0	0.33±.21	0.55±.32	45±26
					(99 ± 172)
FLORIDA					
AUG 72	13	13	0.06	0.13	117
SEP 72	- ·	-	0.06	0.19	217
O-N 72	6	17	0.50	0.85	70
DEC 72	14	17	0.54	0.66	22
JAN 73		-	-	-	-
FEB 73	14	10	0.80	0.93	16
MAR 73	-		0.13	0.14	8
A-M 73			0.31	0.36	16
JUN 73	14	8	0.21	0.31	48
JUL 73	11	0	0.24	0.43	79
AUG 73	14	15	0.24	0.41	71
SEP 73	0	5	0.41	0.64	56
AVE±σ OVERALL	10.8±5.2	10.6±6.1	0.32±.23	0.46±.28	65±60
ΑVE±σ	14.4±9.6	15.8±15.4	0.32±.21	0.50±.29	56±48

Summary of separation of the cyclonic edge (CE) and the indicator isotherm (22°C @ 100 m and 15°C @ 200 m), and the surface chlorophyll-a ( $\rm Cl_S$ ) in the current (GS) and in coastal waters (CW). The percent difference between coastal and current chlorophyll values is computed by 100 (CW-GS) $\pm$ GS=%. Blank values are where data were not obtained or where indicator went aground.

The result implies that the current velocities must be less at higher latitudes, and this is indeed observed by Fuglister (1951) in his ship drift studies.

It is also useful to note that the average separation of the 15°C at 200 m is approximately the same as the 22°C at 100 m. If the relation between the 15°C isotherm at 200 m and the velocity core holds in these latitudes as it does off New England, then the pathlines to be discussed in section 3.2 are also pathlines of the velocity core maximum. The large standard deviations on the data in columns two and three reinforce earlier conclusions that these surface indicators of the current are complicated expressions of local wind and current conditions and should not be expected to be more precise indicators than they are. That is, for gross-scale features, they are reliable indicators (within 10-30 km) of the current's cyclonic edge, but for fine-scale analysis they may be misleading and must be used with caution. This is a fundamental limitation of remotely sensed ocean-current boundary location.

Average-surface chlorophyll-a concentrations in the current (GS) and in the coastal water (CW) are given in columns four and five of table 3.1. These values are in good agreement with those reported by Corcoran and Alexander (1963) in the Straits of Florida off Miami. Average values in the current are 0.32 mg m<sup>-3</sup>, whereas the mean value was 0.50 mg m<sup>-3</sup> in the coastal water. This represents an average increase of 56% in coastal water compared to that in the current. During several months of the spring of 1973, the % increase was markedly lower than in other months. Volume-scattering function values follow this trend also, which means that waters are spectrally similar and no ocean-color-sensing device could detect a boundary on the basis of color change alone. The data in the last column indicate that there is a maximum in the percent difference in the summer months, which is encouraging for remote sensing because that is when surface thermal signatures are lost.

Continuous-flow chlorophyll-a measurements were made during each cruise, including the current tracking to obtain the pathlines of the current. The general trend of surface values is not significantly different than that reported here. One exception is the summer of 1973 discussed below. Harbor and nearshore values were generally much higher than these reported here; estuarine water in general has entirely different chlorophyll and scattering values caused by suspended materials and Gelbstoff. These waters are easily distinguished in ERTS data as will be discussed in section 4.3.

#### 3.2 Pathlines of the Current

Conditions prior to the first cruise are summarized in figure 3.1. These data were obtained through the courtesy of Merrill (Texas A & M University), Molinari (National Oceanic and Atmospheric Administration, NOAA), Rinkel (Florida State University System Institute of Oceanography, SUSIO), and Brooks and Niiler (Nova University) from 6 to 18 May 1972. In this composite of their data, an anticyclonic eddy is in the process of separating as evidence-ed by the ridge in the topography of the 22°C isotherm extending northeast from Campeche Bank to the Florida Platform. Areas where the 22°C isotherm is deeper than 125 m are stippled; the indicator isotherm is the heavy line

outlining the main flow and the eddy. Here the tracking technique would show very short radii of curvature in the zone where the separation was taking place, or the eddy could be missed entirely (if it were not for the suborbital trackline, cf., fig. 2.4). Recirculation in the eddy is already quite extensive as evidenced by the closure of the isopleths. The process of eddy separation cannot be discussed with the pathlines of the 22°C isotherm except to confirm that this did indeed occur. This eddy was observed as late as December 1972 in the suborbital trackline near the west Florida Platform.

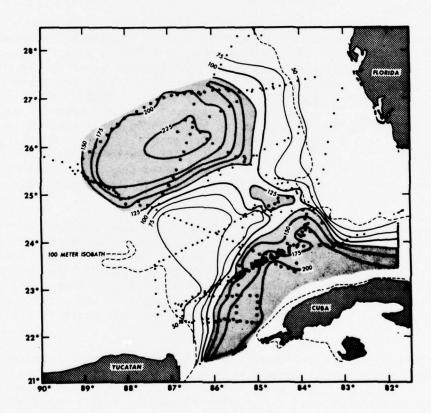


Figure 3.1 Depth of the 22°C isotherm in the project area, composited from data taken 6-18 May 1972. The eddy was actively separating from the main flow; and this figure required spatial smoothing, but it does illustrate the relation of the indicator (100-m depth contour heavy) to the thermal field. Stippled areas are where the isothermal surface was deeper than 125 m.

Pathlines of the 22°C isotherm at 100-m depth are given in figure 3.2. The series was obtained at 36-day intervals, coincidental with the 18-day period of ERTS. Dates of each survey are labeled on the appropriate pathline. The shortest tracking time was 3 days and the longest 6 days, so that near synopticity was accomplished. Hydrographic station transects of the straits added 2 to 3 days to each cruise.

By August 1972, the 22°C isotherm extended north from Yucatan and curved in a gentle anticyclonic arc, terminating tangent to the Florida Platform near Dry Tortugas (see also fig. 2.4). The suborbital trackline supports the earlier discussion that the eddy observed in May had completely separated, as evidenced by the 22°C isotherm being shallower than 30 m between the eddy and the main flow.

By September conditions had changed markedly. The initial current direction had a significant easterly component and flowed directly toward the west Florida shelf. There was evidence of Loop Current Water on the shelf, and the 22°C isotherm apparently went aground well north of Dry Tortugas. A red tide of Gymnodinium breve was reported on the west Florida shelf at this time. By late October the current had reformed to its southernmost extent, and evidence of Florida Bay Water flowing south through the Keys was noted in both the ship track and an ERTS image (see also fig. 4.9). Murphy et al. have used this evidence to document partially the source of the first reported Florida east coast red tide. It is hypothesized that the organisms were carried by the current through the Straits of Florida and exchanged with local coastal water north of Miami.

By December 1972, the current had swung to the west and had penetrated into the Gulf to the same latitude as during August. At 24°N, the stream flowed in a sharp anticyclonic turn to the east. January 1973 was the only month in which transects of the Straits were not obtained. This was caused by 25 m sec<sup>-1</sup> winds and high seas forcing the ship to turn back. Only four crossings were obtained, but sufficient detail permitted the observation that, for the first time in the series, the current penetrated north of Dry Tortugas (25°N).

The "spring intrusion" (Leipper, 1970) continued through February, March, April-May, and June when the current extended to 27°N. As the current penetrated deeper, it also swung farther to the west. North of 24°N, the isobaths curve sharply to the west, and the current flows into deeper water where different dynamics probably dominate.

A deep intrusion in July 1973, coupled with a marked cyclonic curvature off the west Florida shelf, led to expectation of an eddy separating by the following cruise. The deep intrusion from the east was not a sampling artifact; the R/V BELLOWS obtained concurrent hydrographic station data across the shelf and out into the main current throughout this area. The furthest western extent of the current also occurred in July. A vast area of green, high chlorophyll-content water was encountered along the western boundary opposite the intrusion from the east.

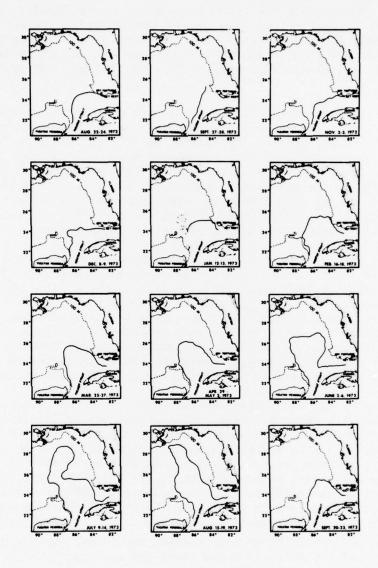


Figure 3.2 Pathlines of the 22°C isotherm at 100-m depth for the period August 1972 to September 1973. Dashed line is the 100 m isobath. Actual dates of each survey from Yucatan to Dry Tortugas, but excluding the time required for the STD sections, is given on the lower right of each figure. Sequence starts at the upper left and proceeds left to right, top to bottom.

By August 1973, the current system extended almost to the Mississippi Delta. The eddy had not separated. Very low salinity water (24°/00) was recorded by a simultaneous cruise of the R/V BELLOWS and the R/V VIRGINIA KEY all along the current edge off the Florida shelf. Surface salinities were less than 30°/00 along the cyclonic boundary in the Straits of Florida. Because the Loop Current was so close to the Mississippi Delta and there are no other large sources of fresh water, it seems probable that this was Mississippi River Water in origin. This water has been traced as far north as Georgia where salinities were still 32°/00 (D. Wallace, personal communication).

During the last cruise, September 1973, the current was found well to the south again, at approximately the same penetration as February. A track-line on the R/V BOWERS, from Ft. Myers west to 87°W and north to Pascagoula, confirmed that an anticyclonic eddy had indeed separated and that a significant change in the hydrography of the eastern Gulf had occurred in 1 month. There was no hint in the extensive August data that a recirculation had begun as a prelude to the eddy formation, although observations by Cochrane (personal communication, 1974), made between the April-May and June cruises, showed substantial closure in his isotherm field in this area.

These data support the possibility that the eddy separation is an annual event, but by no means does it occur at the same time each year. The May 1972 eddy and the September 1973 event are 16 months apart, whereas space-craft data, supported by recently obtained buoy tracks (W. S. Richardson, personal communication), suggest that an eddy had separated in April 1974, a 7-month time difference. Other eddies have separated in November 1970, and one again in July or August 1971 (J. Brucks, personal communication). Thus in each of the last 5 years, between the vernal and autumnal equinoxes, an anticyclonic eddy appears to have separated from the main current.

In figure 3.3, the northward penetration of the 22°C isotherm into the Gulf is compared with historical data. The dashed line is Fuglister's harmonic fit of annual and semiannual terms to ship drifts in the Straits of Florida. The solid line is Niiler and Richardson's (1973) fit of a sinusoid, with an annual term only, to the direct transport measurements in the Straits of Florida. The light line with triangles is the fit of the arc distance from Cabo San Antonio to the pathlines of the indicator. Cochrane (1965) did an analysis similar to Fuglister's and showed that the ship drifts in the western Yucatan Strait are essentially the same as in the Straits of Florida, except that the maximum drift through Yucatan leads that through Florida by l month. Niiler and Richardson's curve shows the same general feature of low transports in winter and high transports in summer. They noted that the week-to-week fluctuations in the current were as much as the annual range, and further that the transports lag the annual cycle of wind stress curl over the Atlantic Ocean by 4 months. Maul (1974) reported that the slope of the 17°C isotherm in the Yucatan Strait lagged the penetration by three to four cruises. The general agreement between the three curves in figure 3.3 suggests that the variations in the Gulf Loop Current are well correlated with the annual cycle of current velocity and transport. The annual cycle of current velocity is in phase with the annual cycle of trade wind stress (Fuglister, 1951).

These data form the basis upon which Leipper's suggestion has been investigated. The pathlines indicate that: (a) There is an annual cycle of growth and decay of the Gulf Loop Current, (b) a major exchange of heat, salt, and momentum from the current into the Gulf is made at least once a year through the separation of an anticyclonic eddy or current ring, and (c) the circulation in the eastern Gulf of Mexico is associated with the annual cycle of mass transport.

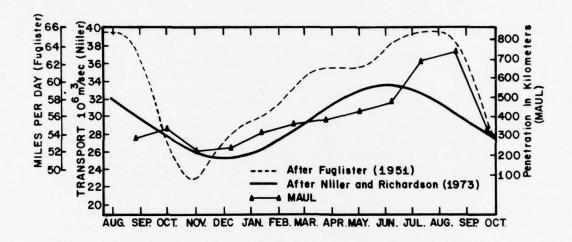


Figure 3.3 Annual cycle of surface drift velocity in the Straits of Florida between Cape Florida and 30°N (dashed), annual cycle in direct transport between Miami and Bimini (solid), and annual cycle of penetration of the Gulf Loop Current into the Gulf of Mexico (triangles) during 1972-73. The large decrease in penetration between August and September (right-hand side) represents the separation of an anticyclonic eddy and is a discontinuity in the penetration pattern.

#### 3.3 Theoretical Relationship between Surface and Subsurface Fronts

The statistical relationship between surface and subsurface indicators discussed in section 3.1 allows an interpretation of the pathlines discussed in section 3.2 in terms of satellite ground truth. The average separation of the surface and subsurface fronts and values of the Coriolis parameter imply specific current velocities in a geostrophically balanced system. Hansen and Maul showed that the horizontal distance between the maximum temperature gradient at 200-m depth and the maximum temperature gradient at the sea surface varied with curvature in the Gulf Stream meanders off Cape Hatteras. For anticyclonic curvature, the separation averaged 16.2  $^{\pm}$  13.4 km; for cyclonic curvature, the distance was 11.3  $^{\pm}$  8.1 km; and for inflection points, 14.2  $^{\pm}$  9.7 km. Even though the standard deviations ( $^{\pm}\sigma$ ) are large, the conclusion from the  $^{\pm}$  test is that the different values are statistically significant at the 95% confidence level.

To investigate the variability in separation of the surface front to the 200-m front, consider an unaccelerated, two-layer, frictionless model with the lower layer (2) at rest. The equations of motion for the upper layer (1) in natural coordinates are:

$$\frac{dV}{dt} + g\varepsilon \frac{\partial D}{\partial s} = 0 ,$$

$$KV^{2} + fV + g\varepsilon \frac{\partial D}{\partial n} = 0 ,$$
(3.1)

where g is gravity,  $\varepsilon \equiv \frac{\rho_1 - \rho_2}{\rho_2}$ ,  $\rho$  is density,D is the thickness of the upper layer,  $\vec{s}$  is the along-stream coordinate, and  $\vec{n}$  is the cross-stream coordinate taken positive to the left of the velocity vector facing downstream. The radius of curvature (1/K) is typically 100 km in the Gulf Stream meanders, reported on by Hansen (1970), and is positive for cyclonic curvature. Using (3.1) at a mean latitude of 39°, Hansen and Maul's data show that the average velocity in the anticyclonic turns is 155 cm sec<sup>-1</sup>, 149 cm sec<sup>-1</sup> in the inflections, and 158 cm sec<sup>-1</sup> in the cyclonic turns. The significance of curvature is apparent when the geostrophic velocities (k=0) are computed: 129 cm sec<sup>-1</sup> in the anticyclonic and 185 cm sec<sup>-1</sup> in the cyclonic meanders, or approximately  $\pm 16\%$  error, respectively.

The relatively constant velocity at first glance seems at variance with the drogue studies of Parker (1972) and Chew (1974). In both of these studies, drogue velocities decreased in anticyclonic turns and increased through the inflection points into the cyclonic turns. In Parker's work, however, as the velocity decreased, the drogues were found far (>20 km)to the right of the Gulf Stream's velocity core (as indicated by the 15°C isotherm at 200 m; Fuglister and Voorhis, 1965), and they sped up again in the cyclonic turn as they drifted over to the indicator isotherm. Similarly in Chew's Gulf of Mexico data, the deceleration in anticyclonic turns was associated with the drogues being to the left of the 22°C isotherm at 100 m; accelerations in inflections found the drogues to the right of the indicator isotherm. These velocity changes are consistent with the possibility of a statistically constant velocity in the core, but the velocity core is not a streamline.

The intersection with the sea surface of the density discontinuity in a two-layer model is analogous to the surface-temperature gradient maximum and/or surface-color change zone in the ocean. As a first approximation, a constant velocity of 150 cm sec<sup>-1</sup> is used to study the effects of curvature and latitude on the separation between the surface front and the front at 200-m depth. From Nowlin and McLellan's (1967) data,  $\rho_1$  is conservatively chosen to be 1.0255 and  $\rho_2 \approx 1.0265$ . Results for the latitudes of the Gulf of Mexico are given in figure 3.4.

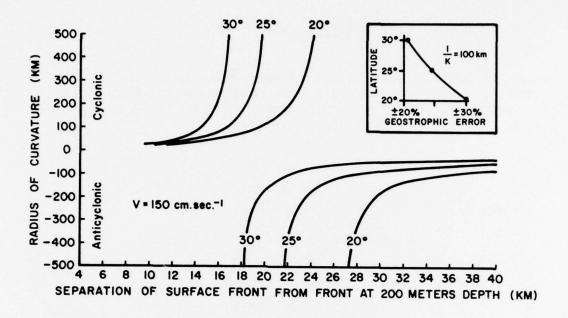


Figure 3.4 Theoretical separation of surface front from the front at 200-m depth versus the radius of curvature of Loop Current meanders. The curves are given for the bounding latitudes of the Gulf of Mexico (20°,25°, and 30°) and are for a velocity core speed of 150 cm sec<sup>-1</sup>. Inset is the error introduced by assuming the geostrophic approximation as a function of latitude for a  $K=10^{-7}$  cm<sup>-1</sup>; the error values are approximately symmetrical, but not exactly as seen in the main drawing.

Separation between the surface front and the 200-m front is a non-linear function of the radius of curvature and is inversely proportional to latitude. For large cyclonic curvature, the interface steepens. Conversely, the interface becomes very flat for the same curvature in the anticyclonic case. That is, for the same interface slope (pressure gradient) when the centripetal and Coriolis terms are additive (cyclonic curvature), the velocity will be less than for the anticyclonic case. The inset in figure 3.4 depicts the meridional dependence on the geostrophic approximation in meandering flow for a 100-km radius of curvature; this error becomes asymmetric for smaller radii. These results emphasize the need to account for curvature in interpreting maps of dynamic topography particularly in lower latitudes.

Typical amplitudes (a) for meanders in the Gulf Stream system are 50 km; wavelengths ( $\lambda$ ) are characteristically 400 km (Chew, 1974; Hansen

(1970). Using these values and assuming a sinusoidal meander path, the effect of curvature on the separation between the satellite-sensed front and the front at 200-m depth can be studied. Curvature is calculated along the meander by

$$K = -\frac{a k^2 \sin k n}{(1 + a^2 k^2 \cos^2 kn)^{3/2}},$$
(3.2)

where  $k \equiv 2\pi/\lambda$  and n is defined as before. Using (3.1) and (3.2), the curvature and the separation along the geodesics to the meander path can be computed. Figure 3.5 depicts the variability for V=100, 150, and 200 cm sec  $^{-1}$  at 25° North latitude.

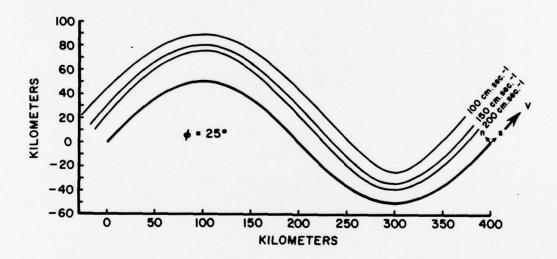


Figure 3.5 Skematic of separation of surface front from the front at 200-m depth (heavy line) as a function of curvature and velocity along a sinusoidal meander. The velocity is considered constant along V for each of the three cases.

Minimum radius of curvature for this model occurs at 100 and 300 km along the meander and is 81 km. The heavy line with the arrow in figure 3.5 is the meander pathline, and the other lines represent the location of the surface front with respect to the velocity core. Average separation for all velocities is 30.4 km in the anticyclonic turn. The minor effect of variations in the Coriolis parameter along the pathline (4%) have been neglected here; from figure 3.5, it is seen that  $\frac{\partial f}{\partial t}$  would reduce the anticyclonic

separation and increase the cyclonic separation. The net effect is to reduce the pathline variability in the separation for an east-west oriented meander, and to do so more strongly at higher latitudes.

In summary, the distance from the satellite-sensed cyclonic edge to the current core will have typical separations of 26 km in the cyclonic turns and 39 km in the anticyclonic turns during the autumn and early winter when current velocities are a minimum of 100 cm sec<sup>-1</sup>. During springtime when velocities have increased to 150 cm sec<sup>-1</sup>, the corresponding values are 16 km in the cyclonic turns and 30 km in the anticyclonic turns. During the maximum velocities, which Fuglister (1951) and Cochrance (1965) report to be mid-summer, the values are 11 km and 26 km for the cyclonic and anticyclonic turns, respectively. The average theoretical separation is 22 km, which is somewhat larger than the statistical value of 15 km observed in the straits; the latter value may be smaller because of channeling effects.

For practical applications, such as optimizing marine transportation, the average separation of the satellite-sensed current boundary and the velocity core for all current speeds is probably adequate. The large variances in the separation of the surface front and the indicator isotherm (table 3.1) suggest that factors other than curvature are important. The satellite data, which are discussed in the next sections, are useful in providing synoptic observations of the current, but they are limited in providing details of some aspects of the flow patterns. This underscores the aphorism that remote sensing is an ancillary technique for studying ocean physics.

### 4. RADIATION OBSERVATIONS

This section is devoted to analyzing the physics of the variables which relate to the satellite observations. First, the theoretical effect of the surface contribution to the upwelling radiance observed by ERTS is discussed and the importance of sea state is exemplified. Shipboard observations of ocean spectra are then studied to understand how different water types behave when integrated over the spectral response of the multispectral scanner's several channels. Next, actual ERTS observations are presented, and the technique for extracting useful oceanic information from the digital data by computer enhancement is discussed. Last, unexpected ERTS and Skylab data are used to show evidence of fine-scale features embedded in the current, as viewed by surface glitter patterns.

### 4.1 Theoretical Effect of Sea State on Upwelling Light

Equation 2.1 identified three components to the radiation received by a satellite: diffuse radiation from beneath the sea, atmospheric radiation which is mostly scattered light, and the radiation reflected from the sea surface itself. Because the surface component to N can dominate the scene (i.e., sunglint), sea-state effects on upwelling spectral irradiance must be investigated.

Let  $\rho(\theta)$  be the Fresnel reflectance from a calm surface where  $\theta$  is the zenith angle (angle of incidence). Then the total reflectance ( $\rho$ ) from the ocean's surface, in the absence of foam, white caps, and glitter, is given by:

$$\rho = \frac{\int_{0}^{2\pi} \int_{0}^{\pi/2} \rho(\theta) N_{a} \sin\theta \cos\theta d\theta d\psi}{\int_{0}^{2\pi} \int_{0}^{\pi/2} N_{a} \sin\theta \cos\theta d\theta d\psi},$$
(4.1)

where  $N_a$  is the radiance of the atmosphere, and the integration is over  $2\pi$  Steridians  $(\theta,\psi)$ . Even thought  $N_a$  is strongly dependent on wavelength, Sauberer and Ruttner (1941) have shown that for zenith angles less than  $40^\circ$ ,  $\rho$  is essentially nondispersive; therefore, Anderson's (1954) value of  $\rho=0.03$  is adopted for zenith angles  $\leq 40^\circ$ , and it is assumed constant for the 400- to 700-nm interval of interest. The upwelling irradiance from the ocean above the sea surface (H(0,+)) is the sum of the diffuse component from beneath the surface  $(R_dH(0,-))$  and the surface component  $(\rho H(0,-))$ .

Cox and Munk (1954) have shown that for solar zenith angles less than 70°, Fresnel's law is valid in a Beaufort 4 wind ( $^{8}$  m sec $^{-1}$ ). As white caps and foam cover larger areas of the sea surface, however,  $\rho$  will be altered because these features are approximately Lambertian, nondispersive, and have an albedo

of 1; thus, they contribute uniform irradiance above the surface (f H(0,-)) where f is the fraction of the sea covered by these diffuse reflectors. Therefore:

$$H(0,+) = R_dH(0,-) + (\rho(1-f) + f) H(0,-).$$
 (4.2)

The computed spectrum of upwelling irradiance for solar zenith angles less than  $40^{\circ}$  as a function of f for the data in figure 2.2a is given in figure 4.1. To be consistent, the values of H(0,-) observed by Tyler and Smith (1970) in the Gulf Stream at  $25^{\circ}45^{\circ}N$  on 3 July 1967 are used.

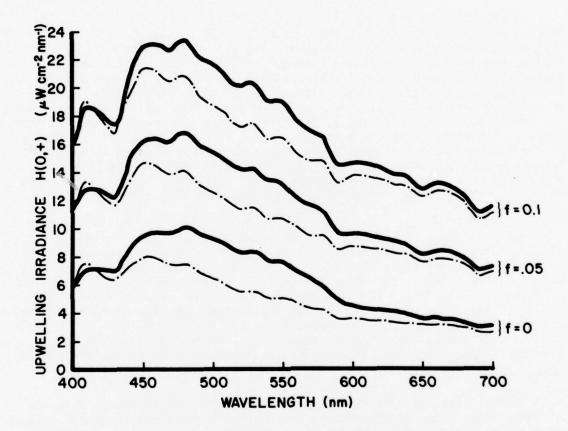


Figure 4.1 Theoretical spectra computed for three fractions of the sea surface covered with white caps, foam, or specular reflectors. Solid line uses the ratio of particle scattering to water-only scattering of 128; dashed line uses 32 for the ratio. Absorption coefficients used were 0.01 and 0.001 for the solid and dashed lines, respectively. This represents summer (low solar-zenith angle) conditions at the latitude of the Gulf of Mexico.

Upwelling irradiance values for f=0, 0.05, and 0.1 are given for the coastal water case (solid line) and the Gulf Stream (dashed line). Compare the spectrum where 10% of the sea is covered and the spectrum where no white caps or foam are present. Not only has the intensity changed, but the shape is also altered. The solar spectrum is fairly flat in the visible region: H(0,-) @ 550 nm  $\div$  H(0,-) @ 650 nm  $\approx$ 1.2. High sea states, which reflect non-selectively, will add relatively more long wavelength energy to the upwelling irradiance. Clark et al. (1970) have attempted to minimize these effects in the measurement of ocean spectra from aircraft by observing the ocean at Brewster's angle (directed away from the sun) through a polarizing filter. The degree to which these calculations effect their result is not known. For ERTS, the MSS views the earth at angles +5° from the nadir without polarizing filters. The sun's glitter affects the upwelling radiance (Strong, 1973), and this is a function of the solar declination. Similarly, sea-state effects on the upwelling spectra change the radiance in an MSS band.

In figure 4.2a, the irradiance is plotted as a function of f for the central wavelength of the ERTS MSS band 4 (500-600 nm) and band 5 (600-700 nm). The curves are linear as expected from (4.2) and are wavelength dependent. At 550 nm, the irradiance increases more quickly with f than at 650 nm. This is caused by the shape of the solar spectrum and the ratio discussed above. In figure 4.2b is plotted the irradiance ratio H(0,-) @ 550 nm  $\div H(0,-)$  650 @ nm as a function of f. The ratio decreases rapidly as the sea state builds, but then tends to level off. Further, the ratio is not the same for the two water types chosen here, which means that sea-state effects are not only a function of the fraction of white caps, but also the optical properties of the water itself. Unless the spot size of a remote sensor is small enough to exclude white caps, the effects of sea state will not only alter the interpretation of the  $\underline{\text{in}}$   $\underline{\text{situ}}$  optical properties of the water, but will dominate the spectral variability.

The linear dependence of upwelling irradiance as a function of the fraction of white caps (f) suggests that a simple correction scheme for seastate effects is possible (fig. 4.2a). At longer wavelengths (>700 nm), the absorption coefficient for water becomes very large, and the  $N_{\rm S}(\lambda)$  component of equation (2.1) is the dominant oceanic variable. At approximately 1000 nm in the reflected infrared, the absorption coefficient for water reaches a maximum and the transmittance of the atmosphere is also a maximum. If  $N_{\rm B}(\lambda)$  can be obtained or reduced to a standard value (e.g., Curran, 1972), then an absolute measure of N at 1000 nm provides a measure of f in a cloud-free atmosphere.

Several investigators have proposed using the radiant energy at a few wavelengths to infer concentrations of chlorophyll-a in multispectral scanner outputs (Szekielda, 1973), in differential radiometers (Arveson, 1972), from slopes in aircraft spectra (Clark et al., 1970), and in photographs (Baig and Yentsch, 1969). From the above discussion, it is seen that such ratios, differences, and slopes are strongly influenced by sea state; this factor was not considered in their work. The problem is further complicated because  $R_{\rm d}$  is also dependent on  $\omega_0$  and B (equation (2.5)), as will be discussed in the next section.

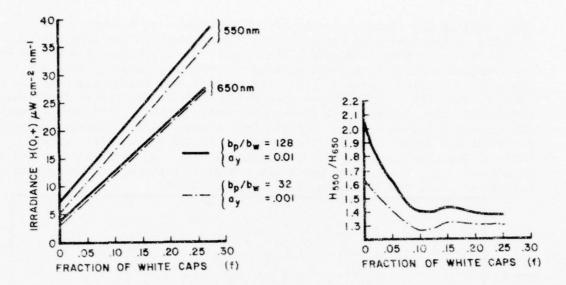


Figure 4.2a (left): Upwelling irradiance in the ERTS MSS-4 (550 nm) and MSS-5 (650 nm) intervals as a function of sea state for the two water types used in figure 4.1. Solid and dashed lines are as in other figures. Figure 4.1b(right): Irradiance ratio as a function of fraction of surface reflectors. The ratio is seen to be a function of both water type and sea state.

### 4.2 Spectroradiometer Observations

Optical properties of the ocean, as they relate to the upwelling spectrum, must be understood at the sea surface before ERTS data can be interpreted. Upwelling irradiance from 3 m above the surface given in figure 4.3 was observed using the same 4-m Ebert spectroradiometer used for the reflectance spectra in figure 2.2b. These observations were made during the time frame of figure 4.8 and represent the water types shown in that ERTS image. All spectra were carefully selected to represent approximately the same downwelling irradiance, sea state, sun angle, cloud cover, and absence of bottom influence. Specular reflection caused by waves was minimized by preselecting 10 spectra with similar shapes that did not contain anomalous random peaks. After digitizing the records, averages and standard deviations (o) were computed at 7-nm wavelength intervals; if values exceeded the average by lo, they were rejected and a new mean computed. Absolute values of the spectra are traced to NBS through the 2-m integrating sphere at NASA's Goddard Space Flight Center; reported values have ±3% error band (L. Blaine, personal communication).

The data in figure 4.3 can be used to interpret ocean color as measured by the multispectral scanner. The energy in an ERTS MSS band at the sea surface is

$$N(0,+) = \int_{0}^{\infty} \phi(\lambda)N(\lambda)d\lambda , \qquad (4.3)$$

where  $\phi(\lambda)$  is the filter function of the multispectral scanner; N is in units of watts cm<sup>-2</sup>sr<sup>-1</sup>and  $\phi$  is approximately a gate function for each MSS band  $(\phi(\text{MSS-5}) \approx 1 \text{ for } 600 \leq \lambda \leq 700$ , and 0 otherwise). The spectra in 4.3 are upwelling irradiance (H(0,+)) and are related to upwelling radiance (N(0,+)) by equation (2.2). Using equation (4.3), the spectra were integrated over the MSS-4 (500-600 nm), MSS-5 (600-700 nm), and MSS-6 (700-800 nm) filter functions to investigate the properties of these three water types as ERTS ground truth. The highest irradiance values for the Gulf Stream, coastal water, and plankton bloom all occur in MSS-4; the lowest is in MSS-6 with MSS-5 midway between. The plankton bloom is distinguished by having the highest irradiance in each channel. The coastal water has a higher irradiance in MSS-4 than the Gulf Stream, but the situation is reversed in MSS-5.

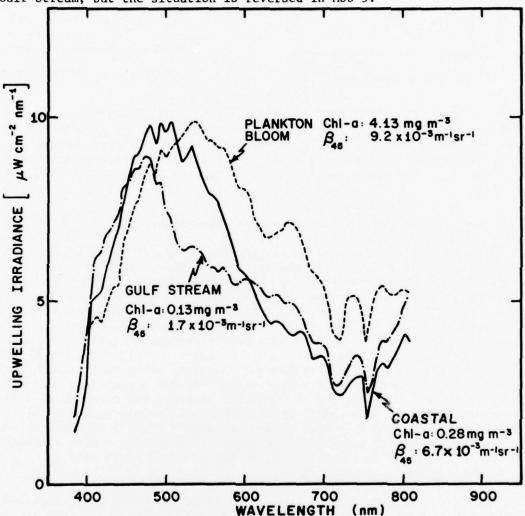


Figure 4.3 Observed upwelling spectral irradiance in the Gulf of Mexico, November 1972. The three spectra represent typical observations during the time series and show the shift of the dominant wavelength to larger values with increased surface chlorophyll-a. These spectra include the surface component  $N_{\rm S}$ .

In section 4.1, the effect of sea state on using ratios and differences was discussed. To test techniques of ratios, sums, and differences on comparable spectra, a series of numerical tests were made from the integrated irradiances. Combinations of all three channels for one water type were compared with the same combinations for the other water types. It was quite easy to differentiate on the basis of such calculations between the Gulf Stream waters and the coastal waters, and between the coastal waters and the plankton bloom; however, it was not possible to distinguish between the Gulf Stream and the plankton blooms. For example, MSS-4 ÷ MSS-5 is 1.4 for the Gulf Stream, 1.7 for the coastal water, and 1.4 for the plankton bloom. This suggests, as the theory implies (equation (2.5)), that even in the absence of sea-state changes, the ratio test (MSS-4 ÷ MSS-5) is not likely to be successful in specifying the chlorophyll-a concentration.

Multispectral identification and classification of scenes is well developed in agriculture and forestry. The technique consists of clustering radiances from known targets in n-dimensional histograms, where n is the number of wavelength increment bands. Unknown targets are then "identified" by comparing the radiances in these same n-channels with the statistics of known radiances. If a value falls within a given cluster, it is considered identified within certain error bounds which vary with the statistical spread of a cluster. The data from figure 4.3 were tested in this way for ERTS channels MSS-4, MSS-5, and MSS-6 in the same manner as described above. The location of the three water types in MSS-4, MSS-5, and MSS-6 Cartesian space is plotted in figure 4.4. The circle represents the upwelling radiance from the Gulf Stream, the triangle from the coastal water, and the square from the plankton bloom. Now it can be seen graphically why the ratio test failed: Both the Gulf Stream water and the plankton bloom water lie near the same diagonal in each two-dimensional space; however, when a vector is used to identify the water types, a clear distinction can be made. The length of the vector will depend on sea state, and this result must be used with caution. The more dimensions used, the closer the vectors are to representing the spectra (Baig and Yentsch, 1969). This is an example of how clustering can be used for automatic classification of water types in the ocean. It requires first that many spectra can be observed, that surface effects be accounted for, and that in situ properties be correlated.

Clark et al. (1970) noted that the slopes of their aircraft spectra correlate quite closely with chlorophyll concentrations. They did not specify the spectral region where the slopes were calculated. The spectra in figure 4.3 have peaks at 470 nm in the Gulf Stream and at 530 nm in the plankton bloom. From the discussion in section 2.2 on the effects of  $\omega$  and B on R, it would be fortuitous if these slopes represented changes in the chlorophyll only. There may, of course, be biogeographic regions where chlorophyll and spectra are canonically related (Duntley, 1972). However, since the data in figure 4.3 represent near-surface spectra, any ocean-color-multispectral scanner should have channels centered near 470 and 530 nm. The effect of the atmosphere (Hovis et al., 1974; Curran, 1972) is to alter markedly the upwelling radiance at satellite altitudes, particularly at shorter wavelengths (<500 nm). The fact remains that significant ocean information is contained between 470 and 530 nm, and these wavelengths must be considered along with a sea-state channel at 1000 nm.

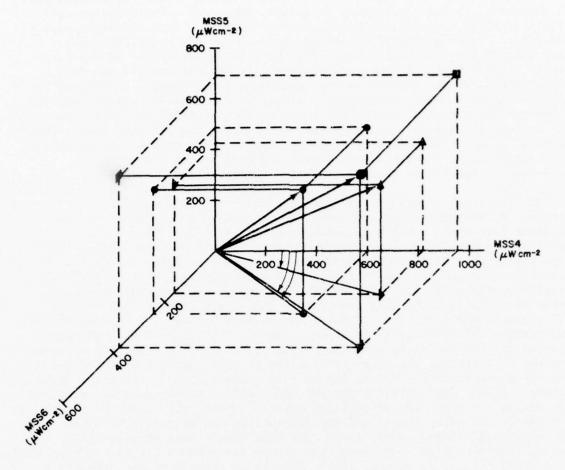


Figure 4.4 Three-dimensional clustering of the data in figure 4.3 when integrated over the filter of three MSS bands. The symbols represent the location in each of the three planes of the Gulf Stream (circle), coastal water (triangle), and the plankton bloom (square). A common location by vector can be given, with statistically derived bounds, to identify automatically a target.

The peak in the plankton bloom spectra at 675 nm (fig. 4.3) has been explained by Gordon (1974) as being caused by anomalous dispersion in the particles that causes scattering near the chlorophyll-a absorption band. The maximum in the absorption band occurs at 665 nm (equation (2.7)). The effect on the upwelling radiance is to cause the spectra to behave like the negative derivative of the absorption in the vicinity of 665 nm, i. e., a minimum in  $\rm R_d$  occurs at 655 nm and a maximum at 675. This suggests that two very narrow channels at 655 nm and at 675 nm in an ocean color sensor would be useful in identifying plankton blooms and determining whether the absorbing pigments are in the particles or dissolved in the water.

Probably the most efficient method of determining the concentration of the constituents in the ocean will be to compare theoretical and experimental spectra, adjusting the constituent concentrations in the theoretical spectra until agreement is found. This, of course, requires a basic understanding of the optical properties of the constituents which can be derived only from careful in situ and laboratory experiments. At the present time, much energy and money are being expended for optical methods to locate and study materials with nearly unknown optical properties suspended or dissolved in a medium with only poorly known optical properties. Lack of knowledge of the optical parameters affecting reflectance must be overcome before significant progress can be made.

### 4.3 ERTS Observations of the Gulf Loop Current

Several examples of ERTS observations of the current are given in figures 4.8 through 4.12. The location of each of these images is given in figure 4.5, which also includes pathlines of the 22°C isotherm at 100-m depth made during satellite transit. Significant variability exists in these two pathlines, only 36 days apart, which emphasizes the need for synopticity in oceanographic baseline measurements for remote sensing.

Diffuse reflectance from beneath the ocean is rarely more than 0.05 (cf., fig. 2.2). Reflectance from the ocean's surface, which is independent of this diffuse reflectance, has been shown to be comparable or even substantially larger depending on sea state. Reflectance from clouds and agricultural scenes, however, is sometimes an order of magnitude greater than from the ocean, even in the 500- to 600-nm wavelength region. For the NASA Data Processing Facility (NDPF) to produce an image for an average scene radiance, the ocean signal is compressed into the lowest few gray scales. This is clearly illustrated in figure 4.6, which is a scanline plot across the boundary of the Loop Current from the multispectral scanner. The large spikes in all four channels (MSS-4 upper) are clouds; there seems at first glance to be very little change in digital number (DN), which is proportional to radiant intensity, as a function of the sample number. Careful examination shows that the average value of the DN at samples greater than number 950 is slightly larger than those before this point. It will be shown that this marks the transition to higher radiances caused by increased sea state in the current.

To display graphically this small change over a two-dimensional region, computer enhancement is necessary. Techniques for ocean radiance levels have been studied by Maul, Charnell, and Qualset (1974), and an extension of their results will be used here. Evolution of the results to be discussed is shown in figure 4.7 a, b, c, and d. Figure 4.7 is the raw data from the original NDPF for MSS-5.

The ocean radiance from MSS-7 (800-1100 nm) is all constrained to  $0 \le DN \le 4$  (0-29 mW cm<sup>-2</sup>sr<sup>-1</sup>). The low radiances are caused by the very large values of the absorption coefficient of water at these wavelengths. Clouds and land (cf., fig. 4.6), however, have large near-infrared reflectance and are almost always above the DN range cited. This allows the computation of a binary mask wherein all DN>4 are set to 0 and all others are set equal to 1. The data matrix of an MSS band of interest when masked leaves only the ocean values for statistical analysis. Figure 4.7b is the mask computed for this purpose.

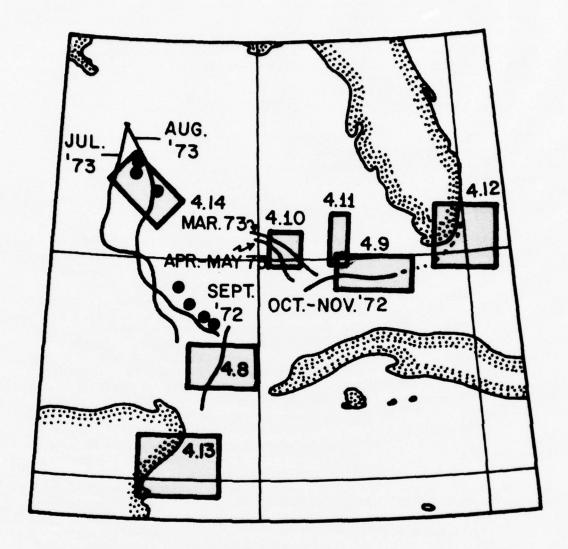


Figure 4.5 Location of observations for figures 4.8 through 4.14. The appropriate pathline for figure 4.8 is September 1972; for figure 4.9 is October-November 1972; for figure 4.10 is March 1973; for figures 4.11 and 4.12, there is no ship track; for figures 4.13 is August 1972; and for the Skylab photographs, figure 4.14, the pathlines are July and August 1973. Complete pathlines are given in figure 3.2.

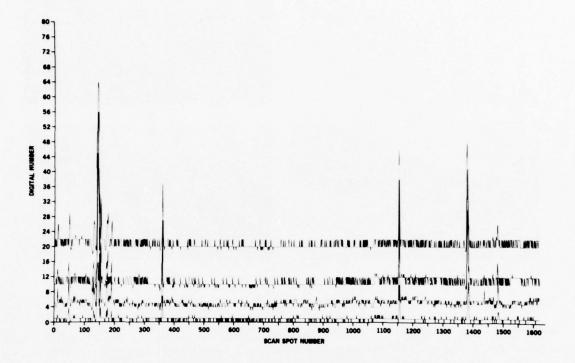


Figure 4.6 EFTS scanline plot across the Loop Current Front. Top scanline is MSS-4, next MSS-5, MSS-6, and MSS-7 on the bottom. The large energy spikes are clouds. At scan spot number 950, there is an increase in the average value of the digital number of 1 or 2; this marks the cyclonic edge of the current.

Cox and Munk (1954) have shown that the frequency distribution of ocean radiances is Gaussian to a very good approximation. Within the limits of resolution of the spacecraft data, histograms of masked MSS-4 or MSS-5 radiances are also approximately Gaussian, which is consistent with Cox and Munk's results. Gaussian properties will be used, but with the reservation that the coarse radiance quantization of ERTS over the ocean may depart from the continuous function especially at large standard deviations. The masked matrix is contrast-stretched by computing a stretch variable ( $\zeta$ ) from

$$\zeta = M \left[ \frac{(\overline{DN} + \kappa \sigma) - DN}{2\kappa \sigma} \right]^{n}, \qquad (4.4)$$

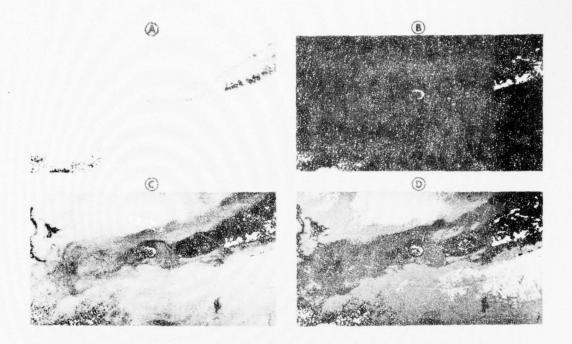


Figure 4.7a Raw data output of the NASA data-processing facility. The MSS-5 band is reproduced in the NOAA format which has an aspect ratio of 1.3 and thus is slightly distorted into the horizontal. b) Binary mask computed from simultaneous MSS-7 (reflected infrared) data. Land and clouds are set to zero; water features set to unity. c) Masking of 4.7a by 4.7b and contrast stretched according to 4.3; n=1, k=2. Compare with 4.7a for improvement in features in the ocean. d) Application of 19 x 19 Fourier filter to 4.7c. Filtering eliminates the banding in 4.7c, but reduces the spatial resolution from 100 to 1000 m.

where M is the maximum value allowed by the digital-to-analog output device,  $\overline{DN}$  is the average scene radiance, K is a constant, O is the standard deviation about  $\overline{DN}$ , and n is a constant. If it is desired to include 95% of the masked data, K=2; for 99%, K=3, etc. All values of  $\overline{DN}$   $\rightarrow DN$  + KO are set to  $\overline{DN}$  + KO, and similarly those values of  $\overline{DN}$   $\rightarrow N$  are clipped. The results of stretching the data in figure 4.7a are given in figure 4.7c. The range  $7 \le \overline{DN} \le 15$  was used here; significantly, more detail in the ocean features are clearly brought out by this technique as will be further discussed below.

Maul et al. (1974) also studied the power spectra of ERTS scanline data and were able to show that the banding in these images has significant energy at every six data samples. This is caused by the MSS design. They showed that the banding could be effectively eliminated by the use of a 19 x 19 Fourier filter which was 6 db down at 10 sample points and 90% effective at 14 and 6 sample points. Results of convolving that two-dimensional filter with the stretched matrix in figure 4.7a are given in figure 4.7d. The

filtered image contains spatial changes greater than 800 to 1000 m on the Earth's surface. Note the improvement in the removal of horizontal striping and the removal of high spatial variability. These filtered images are most effectively being exploited in the coastal zone, but are not used extensively in this study as it requires several hours of computer time to perform the convolution.

Equation (4.4) produces a negative image of the input digital image. Positive whole integers n further stretch the low radiance values, but this produces a nonlinear output and must be avoided when comparing images to ocean spectra. The graphic result of using this equation on the scanline data from which figure 4.6 was taken is given in figure 4.8.

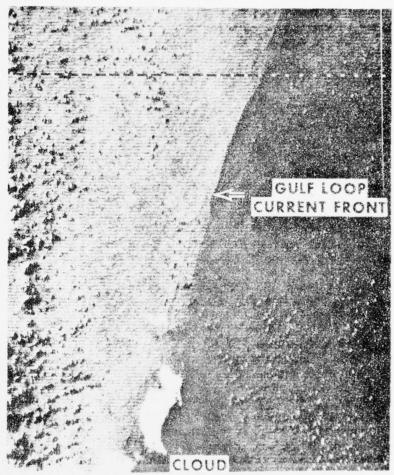


Figure 4.8 Negative print of computer-enhanced (9 <DN<13; n=1) MSS-5 image of the cyclonic boundary of the Gulf Loop Gurrent. Surface vessel track confirmed the location of the current to be the darker shade (higher radiance) region on the right-hand side of the image (ERTS ID 1065-15411). Scanline plot in figure 4.6 is taken along the dashed line in the middle of the scene. Horizontal distance across the image is 90 km.

Figure 4.8 is a negative print of the area due north of the Yucatan Straits using MSS-5 data. Computer enhancement in this image uses only five gray scales of the 128 levels available; all values below  $(DN - 2\sigma)$  are set to 127 and all above  $(DN + 2\sigma)$  are set to 0. The boundary between the resident gulf waters (left) and the current (right) is seen as a transition from light to dark tones, respectively. The exponent n was set equal to 1 for this experiment. Figure 4.9 is an enhancement of the Loop Current boundary in figure 4.7c, but which uses the MSS-4 data instead. In this negative image of the western Florida Keys, water from Florida Bay extends into the Straits of Florida and is entrained by the Florida Current. Comparing figures 4.9 and 4.7c, it is clear that more detail in the surface waters is seen in the MSS-4 image than in the MSS-5. MSS-4 can detect both absorption and scattering changes, whereas MSS-5 is essentially limited to scattering effects. The current boundary in both figures 4.8 and 4.9 was delineated by surface vessel tracks during the day of the satellite transit.

During the observations leading to figure 4.8, the winds were from the northeast at 12 to 14 m  $\sec^{-1}$ , whereas in figure 4.9, they were easterly at 3 to 5 m sec-1. When wind and waves run in opposition to a current, the waves quickly steepen, break, and generate white caps and foam on the surface. For weather conditions such as encountered during the trackline used to support figure 4.8, Ross and Cardone (1974) reported that as much as 10% of the sea surface will be covered with these diffuse reflectors. Shipboard records confirm this, but the sea state was much higher in the current than in the resident Gulf waters. The effect of these conditions on the upwelling irradiance was given in figure 4.1. Consider that the sea state in the current causes the f = 0.1 spectrum and that in the resident Gulf waters is given by the f = 0.05 spectrum labeled coastal water. In the MSS-5 bandpass, interval H(0,+) is larger in the current than in the coastal water; the high radiance values on the right-hand side of figure 4.8 come from the current. MSS-5 is more sensitive to small sea-state changes than MSS-4. MSS-5 then is a better choice for locating the Gulf Loop Current in the open sea because there the optical properties of the current and surrounding waters are not significantly different.

In the observations of figure 4.9, a different conclusion is drawn. Shipboard records show that the sea state was the same in both waters. Here the upwelling radiance is dominated by the  $R_{\rm d}$  H(0,-) component, and the color change allows detection of the current's boundary. Thus, it is seen that the current can be detected with opposite radiance distribution depending on the dominance of surface or subsurface variables. This can work against locating the current if both sources of energy, in and out of the current, add up to the same net radiance. This means that sea-state changes the spectrum of upwelling light from the ocean, and absolute values of radiance will vary with low level winds; conversely, sea state should be estimable from radiance where the spectra are known.

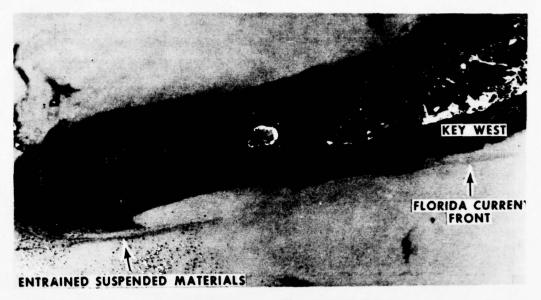


Figure 4.9 Negative print of computer-enhanced (12≤DN≤32; n=1) MSS-4 image of Marquesa Key and Key West (ERTS ID 1099-15293). Change in radiance southwest of Marquesa from dark to light coincides with the ship-located boundary between the higher intensity Florida Bay water and the lower intensity Gulf Stream. Bottom depth is in excess of 100 m at the cyclonic edge and does not contribute to the radiance. Horizontal distance across the image is 135 km.

Figures 4.10, 4.11, and 4.12 are important ERTS images obtained in this series for which either no vessel tracks are available or the image was obtained during the off 18-day transit. Figure 4.10 is an MSS-5 image of the current observed in the deep sea showing a double front. The fronts are approximately 10 km apart and can be seen to extend for 75 km from northwest to southeast. In this image, the boundaries appear to be made visible by two local areas of disturbed water which may represent two steps in the velocity shear profile as noted by Maul and Hansen (1972) in the Gulf Stream off Cape Hatteras. The radiance change here is quite small, one or two DN, as is the case with figure 4.8. It would be almost impossible to distinguish such streaks if there were any clouds present. Using MSS-7 to make cloud-free masks can lead to misinterpretation under these conditions because sea-state changes can sometimes be noticed in this channel. Usually sea-state values do not exceed DN>4 in MSS-7, and the condition is not serious; however, the user must be cognizant of the potential loss of ocean current information in an automatic masking scheme as outlined above.

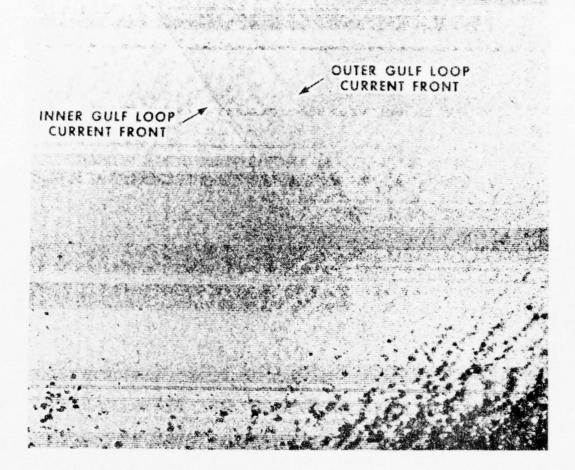


Figure 4.10 Negative print of computer-enhanced (10≤DN≤13; n=1) MSS-5 image (ERTS ID 1262-15355) of a double front in the Gulf Loop Current observed on 11 April 1973. This image was observed during the 18-day cycle when no ship track was obtained, but little translation of the indicator isotherm occurred between cruises. Horizontal distance across the image is 90 km.

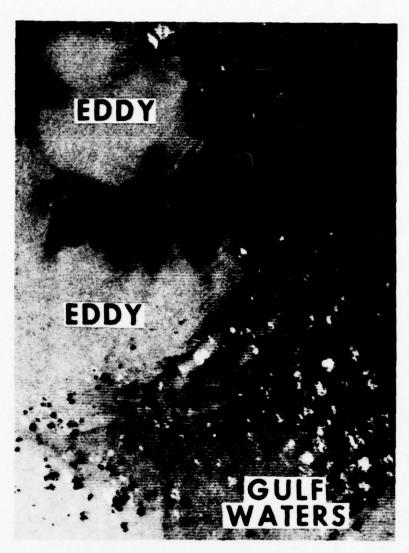


Figure 4.11 Negative print of computer enhanced (16 N 24; n=1) MSS-4 image (ERTS ID 1153-15292) of detached eddies on the west Florida shelf observed on 22 December 1972. Details of the boundary of these 20-km diameter Gulf Loop Current eddies show significant irregularity and nonsymmetry. Horizontal distance across the image is 45 km.

In figure 4.11, an MSS-4 image of two eddies on the west Florida Platform is shown. No vessel tracks are available to substantiate this conclusion; however, on the basis that these features are not visible in any other channel, it requires that the light areas on the negative print represent blue water. Here is another example (cf., Austin, 1971) of the interaction of this scale eddy with the coastal water. Austin noted that several eddies of this 20- to 50-km range were observed around the perimeter of the current in a survey in 1970. This is the first evidence that these features drift onto the shelf where they must exchange significant quantities of salt, heat, and momentum. Eddies such as these could interact to bring cyst stages of G.breve into the photic zone and contribute to the offshore initiation of a destructive plankton bloom.

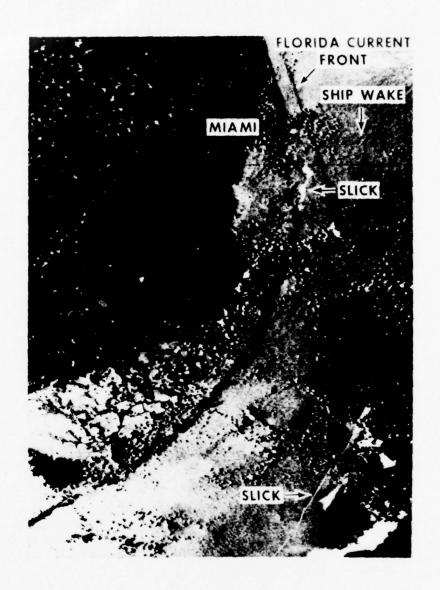


Figure 4.12 Negative print of computer-contrast-stretched (7≤DN≤15; n=2) ERTS image of South Florida (ERTS ID 1026-15230). The Florida Current can be seen as a line of dark lineation parallel to the coast; bottom is essentially invisible in the MSS-6 scene. A ship can be seen by its characteristic V-shaped wake just offshore of Miami Beach. Possibly the Virginia Key sewer outfall area can be observed by its low reflectance due to an organic slick. Horizontal distance across the image is 90 km.

An interpretation of coastal observations from ERTS is given in figure 4.12 which is a computer-enhanced MSS-6 negative image of southeastern Florida. The dark lineation parallelling the coast in the upper portion of the image is a zone of high reflection caused by locally increased  $N_{_{\mathbf{S}}}$  along the edge of the Florida Current. The increase in surface reflectance is probably caused by surface wave interaction with the cyclonic boundary and is not bottom influence. Another example of the dominance of Ns is the bright slick areas (low N) off the Virginia Key sewer treatment plant. This probably is caused by the dampening of the glitter, causing capillary waves in the oil film associated with the organic slick. The slick, which appears to have drifted south past the popular Key Biscayne beaches, offers an explanation of the narrow lineation offshore in the Straits of Florida. A passing oil tanker heading south which is pumping her bilges would cause a similar feature on the image. Note that the organic slicks observed here strongly affect the upwelling radiance, and this must also affect the ratios discussed in sections 4.1 and 4.2. The glitter pattern's nonuniformities further contribute to the complication in analyzing ERTS data for quantitative results.

# 4.4 Satellite Evidence of Fine-Scale Features in the Current

Cochrane (1965) noted that the surface velocity field of the Yucatan Current had double maxima. It was also noted by Pillsbury in 1890 in this area and by Stommel (1966, pp. 55-59) in other portions of the Gulf System. It does appear distinctly in Cochrane's geomagnetic-electrokinetograph profiles north of the Strait. Cochrane postulated that it occurs when the cyclonic edge of the Yucatan Current is found against the Mexican coast, and the main flow is bifurcated by Isla Cozumel; one branch passes between the island and the mainland, and the other branch passes to the east of this topographic wedge. He thus implied that the surface velocity profile may be caused by a turbulent vortex street downstream of Cozumel, which represents a disturbance in the current's vorticity field.

In this section, ERTS imagery and Skylab vertical photography are examined as evidence for this interpretation. In figure 4.5, a computer-enhanced MSS-5 image of the Yucatan-Cozumel area (fig. 4.13) and a Skylab photograph (fig. 4.14) in the central Gulf are located. The photograph and its interpretation are from a report by Maul  $\underline{\text{et al}}$ . (1974) and is rediscussed here in order to offer a unified explanation of the eddies observed therein.

Figure 4.13 is a negative print and thus dark tones represent areas of high radiance. The water outside the current is seen to be of lower radiance than that in the current, and once again the radiance is dominated by a higher sea state or different glitter pattern in the current. Here the edge of the current can be seen leaving the coast northwest of Cozumel. In the wake of the island is a spacecraft observation of an oceanic von Karman vortex street; this is clearly the oceanographic analog to similar observations in the atmosphere, taken by Gemini and Apollo astronauts of the cloud cover over the Guadeloupe Islands in the equatorial Pacific Ocean. Figure 4.13 was imaged on 21 August 1972. The August 1972 pathline was observed at this time, and the current's edge and the vortex street are ocean features.



Figure 4.13 Negative print (ERTS ID 1029-15413) of computer-contraststretched (8 \leq DN \leq 16; n=2) MSS-5 image of Yucatan and Cozumel, Mexico, observed on 21 August 1972. The Yucatan Current's cyclonic edge can be seen emerging from between the island and the mainland. In the lee of Cozumel is a vortex pattern which causes a disturbance in the surface velocity profile well downstream. Horizontal distance across image is 135 km.

Surface current velocities were determined by the geostrophic method from the hydrographic transect of Yucatan Strait on 21-22 August 1972; station location is given in figure 2.4. Station spacing was very nearly 18 km, and the north component of the surface speeds relative to 700 dB, from Yucatan to Cuba, were: 103, 145, 80, 119, 73, 88, 62, and 35 cm sec<sup>-1</sup>. The low value of 80 cm sec<sup>-1</sup>, bracketed by higher values of 145 and 119 cm sec<sup>-1</sup>, is in the middle of the vortex zone shown in figure 4.13. This cross correlation of hydrographic and satellite data is taken as evidence that the observed double maxima is caused by topographic-induced vortex generation, and it explains one type of fine-scale structure as eddies imbedded in the main flow of the Yucatan Current.



Figure 4.14 Portion of vertical photograph from Skylab showing mesoscale eddies (arrows) associated with the Gulf Loop Current. Relationship of these eddies to the current is given in figure 4.5. Film was high-resolution aerial color type SO-356 which is responsive in the 400- to 700-nm interval. Photograph is available from EROS Data Center, reference number SL3-22-124. Positive print.

Figure 4.14 shows a portion of a photograph taken vertically from Skylab at an altitide of 434 km at 1735 G.m.t. on 4 August 1973. Solar azimuth at this time was 175° and the zenith angle was 10°. The sun's glitter pattern, or sunglint, permits the observation of the eddies which are located by arrows in the figure. In figure 4.5, the centers of the three eddies in figure 4.14 are located by dots. Four other eddies of the same size range, approximately 12 to 32 km in diameter, were photographed several seconds later northeast of the Yucatan Peninsula; their centers are located by dots near 24°N, 80°W. The bright feature dominating the lower left of figure 4.14 is part of a large cloud region, the height of which may be estimated from its shadow to be 12,000 m. Lower clouds, however, are difficult to separate from ocean surface sunglint. The photographs were spaced so that 18% of the area appears in the adjacent photograph. This provides the parallax for a stereographic analysis

which insures that the eddies are indeed water surface features.

The specular point of the sun is outside the field of view, but surface waves spread the glitter pattern past the photograph's nadir point. During periods of light winds (2 to 4 m sec<sup>-1</sup> for these data), alternating slicks made visible by changes in reflectance can delimit the circulation pattern (Ewing, 1950). Reflectance differences are caused by slicks with suppressed capillary waves in which organic films are compacted because of lower surface tension under the film.

The most probable generation mechanisms of eddies are shear instability, topographic influence, or current meandering. Ocean eddies whose diameters are in the range 10 to 100 km are known to be quasigeostrophic and confined to the upper 100 to 200 m of the water column. Considering the size, shape, and position of the eddies, it seems reasonable to propose that they are associated with the horizontal velocity shear of the Gulf Loop Current (Lee, 1974) and appear to be instabilities at a surface of separation (Prandtl and Tietjens, 1957). According to this interpretation, the eddies are cyclonic; that is, the water on the right of figure 4.14 is moving toward the top of the photograph relative to that at the left.

Because the indicator isotherm has undergone a large eastward translation between July and August, exact relation of the eddies to the current is difficult to ascertain, however, the data suggest that these eddies may be in the main body of the current. The four eddies northeast of the Yucatan Peninsula are to the right of both indicator isotherms and within the current's characteristic width of 100 km. Hence, they appear to be embedded in the main flow near the current axis. This is in agreement with the observations taken I year earlier wherein it was observed that the fine-scale structure from the island is in midstream. These eddies, however, do not appear to be genetically the same as the vortex sheet eddies, which would make alternating vorticity downstream.

The possibility that the eddies in mid-Gulf are generated by Isla Cozumel cannot be dismissed based on these data. Photographic observations such as these are chance opportunities that may not capture the entire field of flow. If these eddies were shear instability features, then one could expect to find them in other areas of the stream as Stommel (1966) reported. If Cozumel was the only source of disturbance vorticity, then these eddies have been advected 600 km downstream and may be found many thousands farther. The latter seems unreasonable because of Cochrane's report that velocity profiles well upstream of Cozumel do not often exhibit these features. This may be dependent on the season of the year because the current does not always flow as close to the Mexican coast as it seems to in mid-summer.

#### 5. DISCUSSION

The first section of this chapter addresses the capability of ERTS itself, and ocean color data in general, to observe pathlines of the Gulf Loop Current. Several factors limit the capability of ERTS to reproduce the ship tracklines; the reasons for the shortcomings are analyzed, and suggestions are made on the proper temporal, spatial, and spectral requirements for accomplishing the task. The pathlines of the current obtained by the ships are then discussed as though they were satellite observations in order to investigate the usefulness of such data to physical oceanography. Finally, suggestions for future research are made.

# 5.1 Evaluation of Ocean Color Data for Locating the Gulf Loop Current

During the course of observing the pathlines given in figure 3.2, over 250 ERTS scenes (>1000 images) were received, studied, and compared to the research vessel data. Approximately 60% of the ERTS scenes received for the Gulf of Mexico were not usable because of atmospheric conditions. Weather records for Key West during 1972 show that cloud cover was  $\leq$  3/10, 39% of the time. The coincidence of these statistics suggests that when more than 3/10 of a scene is cloud-covered, interpretation of the data for ocean currents is impossible or inconclusive. The original ERTS data order placed an automatic rejection limit at 75% cloud cover. This appears to be too liberal, and significant processing and sorting time could have been saved if the upper limit were placed more conservatively at 40 to 50%.

Some images were disappointing because the sky was clear and yet there was no indication of the current, even though the surface observations indicated good Forel-color changes or sea-state changes. One explanation is to ascribe this to the gain settings on ERTS as being incorrect for the ocean. Incorrect gain settings also made distinguishing between thin clouds and subtle oceanic features impossible even with ground truth. This is perspicuous from the contrast-stretching (section 4.3) requirements; computer enhancement is necessary only because the dynamic range of ERTS was not set for the ocean. Hovis  $\underline{\text{et}}$   $\underline{\text{al}}$ . (1974) have studied gain settings in the development of an ocean color sensor. If that instrument is incorporated on NIMBUS G as planned, the Gulf Loop Current will be observed more frequently.

The chlorophyll-a data given in table 3.1 show that there are at least 3 months of the year when no surface color change can be expected because there was a lack of chlorophyll-a change. Austin's (1971) maps of indicator organisms support the deep-sea chlorophyll observations made during these trackings, in that lower levels of change are found in deep water; that is, the values reported herein should be considered upper limits and perhaps even influenced by the proximity of coastal waters, especially in the Yucatan Strait. This implies that there are times when no significant color signature of the current exists. These data indicate that the color signature is lost during the winter. This is the time of year when temperature signatures are useful. Thus, a combination of color and infrared sensing is potentially capable of locating the Gulf Loop Current throughout the seasons.

Several important ancillary sensors are thus required which would overcome some of the shortcomings discussed above. An infrared channel (10.5-12.5  $\mu$ m) is mandatory for identification of clouds in the absence of ocean thermal gradients, particularly when subtle color or sea-state changes occur. Stereographic cloud identification, which was so valuable in section 4.4, could also eliminate this problem. Cloud identification by stereographic means requires two scanners: one normal viewing and one with an angled view along the satellite trackline in order to duplicate the effect of overlapping photography.

The current was identified in 5% of the ERTS scenes which geographically coincided with the ship locations. ERTS reoccupies each suborbital track only once in 18 days and this has contributed to the sparsity of useful data. If ERTS obtained observations on a daily basis, then 5% data return would provide a useful observation every 20 days. This is entirely acceptable because, as the discussion in sections 1.2 and 3.2 indicate, the Gulf Loop Current was adequately located at 36-day intervals. This observation frequency, which satisfies needs in the eastern Gulf Of Mexico, is not a general statement of temporal requirements of the Gulf Stream System.

Temporal scales can best be discussed in light of a frequency spectrum. In figure 5.1, a kinetic energy spectrum of current meter records is shown. These data were collected by the Woods Hole Oceanographic Institution at site "D," which is located in deep water between the New England continental shelf and the Gulf Stream (Webster, 1967). Plotted on the upper abscissa is the period; the corresponding frequency in cycles per hour is plotted on the lower abscissa. The ordinate is in units of kinetic energy, cm² sec². Causality of the several peaks is labeled on the diagram.

The Nyquist sampling theorem requires that a random variable must be sampled at a frequency at least twice the maximum frequency at which significant energy is found. Energy at higher frequencies will be folded at the Nyquist and alias the spectrum unless it is initially removed by the sampling technique. The local sea and swell shown in figure 5.1 will not be observable in remotely sensed imagery unless very high spatial resolution (1 m for 1-sec waves) is used. A large scanspot is equivalent to a low pass filter which cuts off the local sea. The spectrum can be considered to have a spectral gap at about 40 hr separating the energetic fluctuations at tidal and midlatitude inertial periods from the rest of the continuum, higher frequencies not being observable due to scanspot size.

If a sampling scheme were chosen with daily observations, the spectrum would be folded about 48 hr and the semidiurnal energies would be aliased into the spectrum at 96 hr. In the open sea, the energy in the tidal periods is quite small compared to that in Gulf Stream meanders (periods of about 45 days, Hansen, 1970). Therefore, a daily observational schedule for the open ocean is not a significant compromise. As the coast is approached, however, this no longer is valid. Here the tidal currents have a great deal more energy, and the use of the spectral gap at less than 6 hr is required. Except for tides, the Nyquist criterion is probably not adequate for resolving a geophysical random variable, and one would like to sample at 3-hr intervals in order to define other semidiurnal processes.

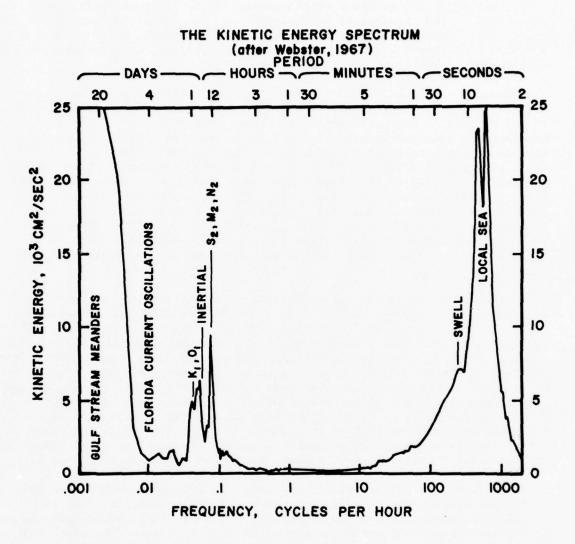


Figure 5.1 Kinetic energy spectrum of current meter records taken in water 2600-m deep at 39.3°N, 70°W by the Woods Hole Oceanographic Institution. The area under the spectral curve is kept proportional to total kinetic energy in this energy versus log frequency plot. Note that a displacement spectrum differs from this kinetic energy spectrum in that high frequency data would be much lower in amplitude.

As alluded to earlier, the spatial resolution can be used to limit what high frequency processes are observable. For example in deep water, swell with a period of 10 sec has a wavelength of 156 m. Since the radiance (N) in a scanspot is the integral of each element dN, the reflection pattern of sunlight, which varies with wave height within the scanspot, is lost. Most of the high frequency energy has periods less than 20 sec; to eliminate waves of that period, a spot size of 625 m is required.

A study of the effect of different spatial scales is given in figure 5.2. Figure 5.2a is an S190B Skylab photograph of the Straits of Florida showing a mass of Florida Bay water which has flowed through the pass just west of Marquesa Key into the strait. Figure 5.2b is an S190A Skylab photograph of the same feature taken on 8 January 1974. Spatial resolution of S190A is ~30 m and that of S190B is ~10 m. An ERTS image at the same time was not available; however, on 31 October 1972, an observation of a similar event occurred (fig 5.2c; see also fig. 4.9). ERTS has a scanspot size of approximately 80 m at the nadir. The ERTS resolution could be degraded by averaging the scanspot matrix into blocks of 2, 5, and 10. This corresponds to equivalent scanspot sizes of 160, 400, and 800 m for figures 5.2d, e, and f, respectively. All images in figure 5.2 are printed at the same scale.

Major features in the bottom topography are discernable up to 160-m resolution, but degrade rapidly after that. The shoreline of Marquesa Key loses its distinctiveness for mapping and identification purposes when the resolution is less than that in figure 5.2d. However, the major circulation feature in the sequence is still clear at 400-m resolution and somewhat less distinct at 800-m resolution. Thus, water mass features of this scale in the coastal zone are usefully detected with resolutions of about 400 m. Judging from other images (not shown) that show river plumes and waste dumping sites, the 400-m resolution is an appealing near upper limit. A spot size of this magnitude should be considered in light of the signal-to-noise requirements of an ocean color sensor which must have narrower optical spectral bandwith than ERTS and indeed may specify those bandwidths (see also section 4.2).

The above considerations were all made without acknowledging one fundamental assumption: The data flow was assumed to be continuous. This is an unrealistic assumption for any sensor in the 0.4- to 16-µm wavelength region of the electromagnetic spectrum because the normal state of the atmosphere is cloudy. To fill the gaps caused by the opaqueness of clouds, both temporal and spatial compositing is required. In midlatitudes, where atmospheric cyclonic waves have periods of about 5 days, variations in ocean color or temperature of not less than 10 days are then observable; this is adequate for Gulf Stream meanders and eddies. In the subtropics and tropics, the cloudiness is more nearly a diurnal event and higher frequencies can be detected such as Florida Current oscillations (periods of 4 to 6 days, Duing, 1973). Further, the subtropical clouds are typically 1 km in diameter and can be identified individually with a 400-m resolution scanspot; this is not the case in the higher latitudes where cloud cover is more extensive areally.

The spatial resolution requirements for ocean currents must then be broken down into what area is being studied and for what reason.

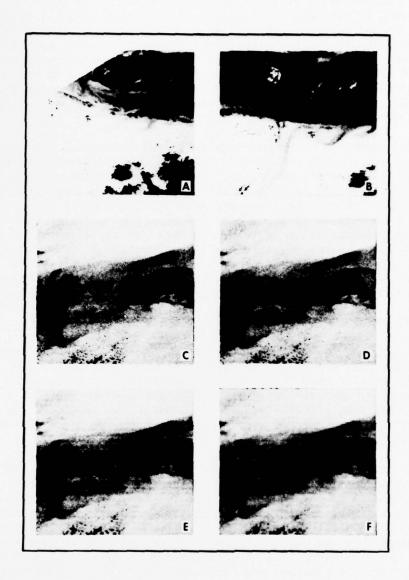


Figure 5.2 Negative prints of Marquesa Key in the Florida Keys showing water from Florida Bay to the north flowing into the straits. a) S190B black and white contrast-enhanced photograph. b) S190A color photograph, printed in black and white and contrast-enhanced. c) Original ERTS MSS-4 image, computer-contrast-stretched. d) ERTS image in (c) with data matrix blocked off in 2x2 units of original enhanced image. e) ERTS image in (c) with 5x5 blocking. f) ERTS image in (c) with 10x10 blocking. Photographs were taken by Skylab on 8 January 1974; ERTS images on 31 October 1972.

Certainly the 8-km resolution of the SMS-GOES infrared sensor or the NOAA scanning radiometer is adequate for location of the major features of the Gulf Stream. It is not adequate for studies of the fine-scale (10-15 km) eddies along the stream's cyclonic front or for Florida Current oscillations whose lateral extent may be of the order of 10 km. For such scale phenomenon, the NOAA-VHRR or Air Force DAPP data are spatially acceptable. On the other hand, ERTS data are more than adequate for the major coastal circulation features spatially, but temporally it is wholly inadequate because of its 18-day observation schedule.

In summary, there is a direct correlation between temporal and spatial requirements, and any sensing system must have the observational flexibility to accomplish the goal. Specifically, the following minimum requirements are noted: scanspot size for the open ocean and shelf areas not more than 10 km with periods not more than 24 hr; scanspot size for the coastal zone not more than 500 m with periods of about 3 hr; as an aside, scanspot size for internal wave observations not more than 25 m with periods of about 10 min and, for surface waves, 1-m resolution and 1-sec periods. ERTS data are spatially adequate for oceanography including certain internal wave observations, but they are not adequate temporally except for the utility of chance observations and to demonstrate the feasibility of sensing ocean color through the atmosphere.

# 5.2 Some Features of the Current Usefully Observed From Satellites

As discussed in the previous section, the ERTS data would be capable of providing adequate observations of the Gulf Loop Current if the orbital parameters of the vehicle were different. To assess the usefulness of a satellite time series, the pathlines of the 22°C isotherm at 100 m will be discussed as if they were remotely sensed data. Since the pathlines are about 15 km to the right of the cyclonic edge (facing downstream), they will be treated as if they were that edge for this analysis.

As shown in figure 4.13, both the direction of the current and the proximity to the Yucatan coast can be observed by remote sensing. Several investigators have related the behavior of the Yucatan Current and the Gulf Loop Current to the direction of flow through the Yucatan Strait: Simple dynamic models of the Gulf Loop Current such as those by Ichiye (1962) and Reid (1972) suggest that the penetration of the Yucatan Current into the Gulf depends on the flow direction. Molinari and Cochrane (1972) studied the influence of bottom topography and concluded that when the Yucatan Current is close to the coast, topography controls the flow through the conservation of potential vorticity.

The potential vorticity conserving model of Ichiye and Reid, in natural coordinates for a two-layer ocean with the lower layer at rest, is given by

$$\frac{KV - \frac{\partial V}{\partial n} + f}{D} = constant,$$

(5.1)

where K is curvature, V is velocity along a streamline,  $\hat{n}$  is the coordinate mormal to the velocity vector, positive to the left facing downstream, f is the Coriolis parameter, and D is the depth of the upper layer. In the pathlines given in section 3.2, D is a constant 100 m. If it is assumed that the velocity core is a streamline whose neighboring streamlines are nearly equidistant,  $\partial V/\partial n$  is also constant. For that case, Ichiye and Reid's work gives

$$V = \frac{1}{2} p^2 \beta , \qquad (5.2)$$

where p is the penetration of the streamline into the Gulf, and  $\beta$  is the meridional variation of f. To apply such a two-layer model to nature, the velocity in the upper layer is considered an average value. For the range of penetration distances observed in this work, 210 to 750 km, V would have to vary from 44 to 562 cm sec<sup>-1</sup> at Yucatan.

Reid was careful to point out that the model only holds in deep water, that is, north of Campeche Bank. A simple translation of the coordinates to account for this would make the lower velocity limits too small. If, however, the model is applied north of Campeche during those months when bottom topography controls the flow as far as 23°30'N (Molinari and Cochrane, 1972), and at the latitude of Cabo San Antonio at other times, then the velocity range is 44 to 303 cm sec<sup>-1</sup> (excluding August 1973). For the cyclonic turning from the Gulf into the Straits of Florida, velocities would have to be less than 50 cm sec<sup>-1</sup> to match the curvature. 44 to 50 cm sec<sup>-1</sup> is a reasonable value for the average surface value, but 303 cm sec<sup>-1</sup> is beyond the range of observations. These data suggest that a geostrophic deep-water potential vorticity-conserving model is not an adequate explanation.

During the February, March, April-May, June, and July 1973 cruises, the 22°C indicator closely follows the 100-m isobath from the Yucatan Strait almost to 24°N. Molinari and Cochrane used (5.1) to study the effect of topographic control; they assumed a homogeneous fluid with water depth D. From figure 3.2, it can be seen that the bottom topography of Campeche Bank does not control the current during August, September, October-November, and December 1972, or September 1973. The Yucatan Current is farther to the west during periods when surface velocities are highest, and these are also the months where the indicator hugs Campeche Bank. Thus, when the current is strongest, in spring and summer (Molinari and Cochrane did their analysis on data observed in May 1962, 1965, and 1966), and is farther to the west, the velocity near the bottom may be sufficient for equation (5.1) to describe the dynamics coarsely.

It is useful to compare pathlines of the 22°C isotherm with historical data averaged by months. Robinson's (1973) atlas clearly shows that the minimum penetration of the Loop occurs in March and April, whereas the maxima are in August and September. Whitaker's (1971) averages show that the minimum is in November and the maxima are in May and October. Leipper found minima in August 1965 and November 1965 and a maximum in August-October 1966. From figure 3.2, it is seen that the minimum here occurred in October-November and the maximum in July-August. This summary points out the high degree of

temporal variability in the Gulf Loop Current and emphasizes that the data obtained in this study are not to be considered as a final description of the cycle.

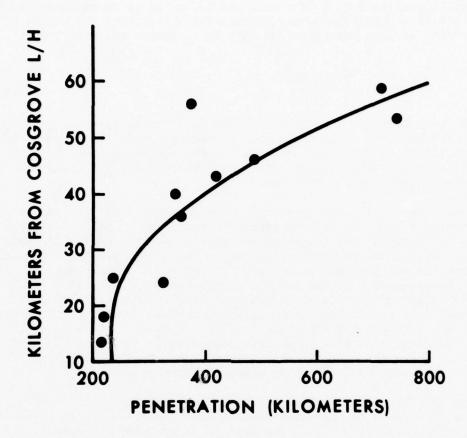


Figure 5.3 Distance that the 22°C isotherm at 100-m depth was found from Cosgrove Lighthouse (northern terminus of the Straits of Florida transects) versus distance from Cabo San Antonio to the northern penetration of the current into the Gulf of Mexico. The heavy line is the least-squares fit to the data. The point at 55 and 400 km represents a case where the indicator was near 100 m for three STD stations, but was chosen to be the first crossing from north to south for consistency.

One interesting kinematic result is summarized in figure 5.3. The northern terminus of the Florida-Cuba section was near Cosgrove Lighthouse. The horizontal distance between the navigation aid and the 22°C isotherm at 100-m depth is plotted against the northern extent of the indicator into the Gulf as measured from Cabo San Antonio. The solid line through the data is the second-degree least-squares polynomial. The farther north that the current penetrates into the Gulf, the farther south it was found in the Straits of Florida. This relationship eventually must break down. Topography is a limiting factor in causing this, since the current must be turned by the Cuban coast (see especially the July and August 1973 cruise tracks). Paskausky and Reid's (1972) numerical model also shows that the current flows close to Cuba when the penetration of the Loop Current is greatest. This suggests that topography limits the description of this current as an inertial flow and contributes to the apparent curvature of the data in figure 5.3. There are no analytic models of inertial currents that incorporate bottom topography against which these observations can be tested.

The salt and heat balance in the Gulf of Mexico is a problem to which satellite data may be applied. The volume of water necessary to make the Loop grow can be estimated from the length of the pathlines which can be measured from satellite images. Assuming a mean depth of 500 m. pathline measurements show that  $64,000~{\rm km}^3$  of resident Gulf water must be displaced by Yucatan water in the 6 months that the Loop grows. The excess transport of Yucatan water into the Gulf in this period averages  $4.1 \times 10^6~{\rm m}^3~{\rm sec}^{-1}$ . Continuity requires that this inflow must be balanced by a discharge as will be discussed below.

As an independent check on the above value, sea-level records were studied. Cochrane (1965) showed that there is a good correlation between the monthly sea-level difference between Habana and Progreso and the average ship drift in the western Yucatan Strait. Approximately the transport (T) difference between Yucatan and Florida should be reflected in the sea-level data. Marmer's (1954) mean monthly sea-level data, uncorrected for barometric differences, are used. The stations are Habana (1947-1950), Key West (1930-1948), and Progreso (1947-1950). Each of these stations show a characteristic rise in sea level to a maximum in September or October and a minimum in February or March in response to the annual steric cycle range of  $\pm$  15 cm. For a geostrophically balanced barotropic flow, the transport difference between the Habana-Progreso ( $T_H$ -K) is given by

$$T_{H}-P - T_{H} - K = \frac{gz}{f} (h_{K}-h_{P}) + C ,$$
 (5.3)

where g is gravity, z is depth,  $h_K$  is the monthly sea level at Key West,  $h_p$  is at Progreso, and  $C = (\overline{h}_K - \overline{h}_p) gz/f$ , where the overbars denote mean annual sea level. Progreso and Key West are on the same side of the current, and it is assumed that mean sea level along the coast is approximately the same; therefore C=0. During the period that the Loop is growing, the difference  $h_K - h_p = 4.88$  cm. The transport difference calculated from (5.3), assuming again the current to be 500 m deep, is  $3.8 \times 10^6$  m³sec<sup>-1</sup> during this period.

By two independent methods, it is shown that there must be an excess inflow of Yucatan water. Jacobs (1951) estimated that evaporation exceeds precipitation in the Gulf by 35 cm per year. This would account for only 0.02 x  $10^6~\rm x~m^3~sec^{-1}$  excess of inflow. Sea level in the Gulf does not rise 34.5 m in 6 months as implied by excess inflow, and Wennekens estimated very little Gulf of Mexico water exits the Straits of Florida. This implies that Hansen's (1972) and Schlitz's (1973) direct measurements of a net south drift at the bottom of the Yucatan Strait may have detected the major source of discharge. Schlitz's estimate of the southward transport through the Yucatan Strait, based on April 1970 data, is 4 x  $10^6~\rm m^3~sec^{-1}$  which is in excellent agreement with this discussion.

The area enclosed by the 22°C isotherm at 100-m depth along the line from Cosgrove Lighthouse to Habana, along the Cuban coast to Cabo San Antonio and across to Isla Contoy, was estimated using a polar planimeter from figure 3.2. The area enclosed by the Loop Current defines a volume of Yucatan water, and its annual cycle should be related to volume transports. As a first estimate, the transports are assumed proportional to current velocities through the Yucatan Strait, as estimated from Cochrane's ship drift studies. The comparative results are plotted in figure 5.4. The sharp decrease in area between August and September 1973 is due to the separation of the anticyclonic eddy discussed in section 3.2. A clear correlation exists between area and current velocities, with little phase lag between transport and the area covered by the current system. The numerical models of Wert and Reid (1972) and Paskausky and Reid (1972) attempted to relate the penetration of the Gulf Loop Current to changes in the vorticity distribution or velocity field of the Yucatan Current, but they kept the volume transport constant; Ichiye (1972) used changes in the Yucatan velocity in a rotating tank model, but did not relate the velocities to the penetration. There are no established relationships between velocity or vorticity fields in the Yucatan Current with transports, nor are there any models (except indirectly Reid (1972) or Ichiye (1962)) which use changes in transport to drive the circulation in the Gulf of Mexico.

If the difference in area between August and September 1973 in figure 5.4 is used as an estimate of the eddy size,  $89,000~\rm{km^2}$  of Yucatan water has been exchanged into the Gulf. A characteristic length scale for the eddy is its diameter (L). The Austausch coefficient is proportional to  $\rm L^2/t$  and, for a t of 1 year, this calculates to be a coefficient of  $\rm 3.6 \times 10^7~\rm cm^2~\rm sec^{-1}$ . Paskausky and Reid used 1 x  $\rm 10^6~\rm cm^2~\rm sec^{-1}$  in their barotropic model; Wert and Reid selected 5 x  $\rm 10^6~\rm cm^2~\rm sec^{-1}$  for the lateral friction coefficient in their baroclinic model. Ichiye (1972) chose parameters in a physical model that make the corresponding horizontal Austausch coefficient 1.8 x  $\rm 10^6~\rm cm^2~\rm sec^{-1}$ . These values are approximately an order of magnitude less than estimated from the eddy separation. It would be a useful theoretical problem to relate surface areas such as this to estimates of exchange coefficients and processes.

In summary, treating the time series as if it were satellite data has illustrated several useful applications to physical oceanography. Potential vorticity-conserving models, used for estimating penetration (5.2) and topo-

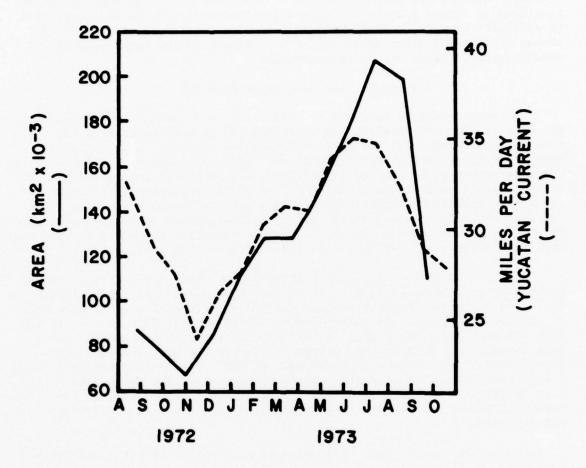


Figure 5.4 Annual cycle of surface area, enclosed by the 22°C isotherm in the Gulf and the Key West-Habana-Cabo San Antonio-Isla Contoy boundary, is the solid line. Dashed line is the annual cycle of surface velocities as estimated by Cochrane (1965) for the Yucatan Current from ship drift reports.

graphic control, are not adequate in explaining the data set obtained as part of this research (fig. 3.2). Comparisons with atlases and Leipper's (1970) sequence show that there is a great deal of variability in the current pattern; that variability could be investigated with continued satellite studies. The kinematic observation given in figure 5.3 suggests that a productive interplay between remote sensing and conventional oceanography is the usefulness of satellite data in "tuning" numerical models. Finally, estimates of the excess inflow of Yucatan water during Loop growth can be made by areal measurements of satellite-sensed coverage.

## 5.3 Suggestions for Future Research

The ship pathlines observed in this study were planned to give adequate ground truth for the satellite observations. Their contribution to the physical oceanography of the Gulf of Mexico has not been fully exploited. Figure 5.4 suggests that the cycle of the Gulf Loop Current is related to the changing transport of the Yucatan Current. The numerical models referred to in section 5.2 used changing distributions of the velocity field or the vorticity field in the Yucatan Strait as a varying boundary condition. The hydrographic data across this channel should be studied to determine if there is a relationship between transport, surface velocity, and vorticity and thus to specify the dominant driving mechanisms for the annual cycle.

As noted in section 5.2, the Gulf of Mexico has a net excess of evaporation over precipitation (E>P). It is for this reason that the basin is called the American Mediterranean. C.G.H. Rooth (personal communication) has raised the question of the salt balance problem for the Gulf since not only does E>P contribute to higher salinities, the separation of an anticyclonic eddy contains the core of the Subtropical Underwater must also add salt. Since there is no evidence that the Gulf of Mexico salinities are increasing, a Mediterranean-type circulation may be superimposed. The other possibility is that salinity in the Straits of Florida is slightly higher than in the Yucatan Strait. Estimates of the net salt flux may be possible from the hydrographic transect data.

During the January-June 1973 phase of this study, infrared and visible data from the NOAA-2 satellite scanning radiometer were archived. The ERTS visible data have been shown to have a Gaussian frequency distribution in section 4.3. An initial evaluation of the NOAA-2 visible data show that the distribution is positively skewed when clouds partially fill the scene. Skewness then is applicable as a test for determining the radiance range of visible data that are cloud-free. This allows a scanspot-by-scanspot test as to whether an infrared data point is cloud-free. The acceptable infrared data can then be corrected for atmospheric transmittance, using the technique proposed by Maul and Sidran (1973), and then mapped with consideration to objective analysis (Gandin, 1963).

During the course of this research, approximately 325 reflectance spectra were observed in the eastern Gulf of Mexico. This data set represents spectra from these waters, for which the chlorophyll-a concentration and volume-scattering function are known. Baig and Yentsch (1969) have shown that a suite of spectra can be represented by linear combination of their average and three

eigenvectors. Using a multiple forward-selection procedure, it is possible to extend Baig and Yentsch's results and specify several wavelengths (say three or four) needed to reconstruct a spectrum (S. Baig, personal communication). Thus, the specification of the most important wavelengths for an ocean color sensor, needed to reconstruct the spectrum, can be accomplished in an objective manner.

The study of climate is fast becoming an important and popular research topic. An important variable in climate modelling is the albedo of the Earth. The data in figure 4.8 and the discussion in section 4.1 on the effect of sea state on upwelling radiation show that the albedo of the sea changes with changing wind speed. Thus, a feedback mechanism in climate studies (that has not been addressed) is the air-sea interaction effect on climate. If the mean wind speed changes as the climate changes, the albedo of the Earth will also change, and this will cause a change in the radiation balance of the Earth in the visible region of the spectrum. The importance of this has not been assessed in the recent literature and could very profitably be studied by satellite techniques.

Finally, as noted in section 4.1, the most efficient means of analyzing spectra will probably be to compute best fits of theoretical spectra to observations. These spectra must then be related to the biological and optical aspects of the water under study. Phytoplankton samples have been obtained and sorted by Ednoff (1974) for many of the spectra. Thus, a catalog of spectra for the area can be initiated for which the theoretical parameters and observational variables are known. It is not until sufficient spectra with known relationships to the marine environment are available that spacecraft observations can be utilized to their full potential.

#### 6. CONCLUSION

This research has been primarily undertaken to evaluate the use of an ocean-color-sensing satellite (ERTS) for observing currents in the subtropics. The Gulf of Mexico was chosen as a test site because there the cyclonic boundary of the Gulf Loop Current cannot be detected by infrared techniques during the summer, and this current is the major circulation feature of the eastern Gulf. The ground-truth pathlines (fig. 6.1) provide measurements of the seasonality of several optical properties across the current as well as a proper history of the flow itself for comparison with satellite data and for basic oceanography.

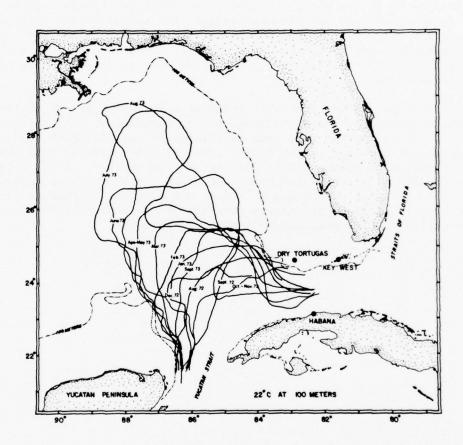


Figure 6.1 Compiliation of pathlines of the 22°C isotherm at 100-m depth from August 1972 through September 1973 (see also fig. 3.2). Where the indicator isotherm intersected the bottom topography, a dashed line is used to estimate its position from the other thermal data. Where the cruise started in 1 month and ended in another, both months are indicated. 100-m isobath is indicated by a dash-dot line and it represents very closely the shelf break and escarpment zone.

From the results of this study, it has been shown that:

- (1.) Using color-sensing satellites to detect the Gulf Loop Current (and other baroclinic flows) is feasible, but ERTS is not an ideal vehicle because of sensor gain settings, multispectral scanner channel wavelengths, and the 18-day revisit cycle (section 5.2).
- (2.) Currents can be detected by color sensing satellites in three ways: by a color change across the cyclonic boundary (changes in the optical properties of the water), by a change in sea state at that boundary (changes in surface albedo), and by changes in the glitter patterns which delimit circulation patterns (sections 4.3 and 4.4).
- (3.) Variations in chlorophyll-a concentrations and volume-scattering function throughout the year are such that there is not a significant permanent color signature of the cyclonic boundary at all times. This data set, however, suggests that a combination of visible and infrared remote sensing can potentially locate the Gulf Loop Current throughout the year (sections 3.1 and 4.3).
- (4.) Shipboard observations of upwelling spectral irradiance show that clustering techniques can differentiate between Gulf Stream water, coastal waters, and plankton blooms, but the ratio or difference of radiance methods gives ambiguous results. Important wavelengths identified for future ocean color sensors are: 470, 530, 655, 675, and 1000 nm (sections 4.1 and 4.2).
- (5.) Evidence for turbulence embedded in the core of the Gulf Loop Current is obtained from comparing velocity profiles across the Yucatan Strait with satellite imagery. Two sources of turbulence are tentatively identified: shear instability and topographic influence (section 4.4).
- (6.) The average separation between the satellite-sensed front of the Gulf Loop Current and the 22°C isotherm at 100 m or the 15°C isotherm at 200 m is approximately 15 km. Curvature effects have been shown to alter significantly the separation between the surface front and the indicator isotherms (sections 3.1 and 3.3).
- (7.) An unambiguous time series of the Gulf Loop Current based on ship observations shows that Leipper's (1970) proposition is correct in that there is an annual cycle of growth and decay, but that year-by-year variability in the patterns is significant. An anticyclonic eddy separation is shown to have occurred at least once each year in the last 5 years (section 3.3).

- (8.) The annual cycle of growth, eddy separation, and decay is in phase with the annual cycle of transport of the Gulf Stream System. During the period that the Gulf Loop Current is growing, resident Gulf of Mexico waters must be displaced; this requires that  $4 \times 10^6 \, \mathrm{m}^3 \, \mathrm{sec}^{-1}$  more Yucatan water enters the basin in the upper layers than leaves through the Straits of Florida (section 5.2).
- (9.) Radiance range of ERTS bandpass sensors for the ocean is estimated from the computer-enhanced images to be (cf. table 2.1):

MSS	Range	(m W	$cm^{-2}sr^{-1}$
4		0.15	- 0.75
5		0.05	- 0.35
6		0.05	- 0.25
7		0.05	- 0.40

Contrast-stretching is required to obtain useful oceanographic information from ERTS (section 4.3).

#### ACKNOWLEDGMENTS

The data in this time series were obtained by the R/V BELLOWS and the R/V VIRGINIA KEY and are a testimony to the dedication and seamanship of the crews of these 65-ft vessels, and particularly to their masters, F. Davis, G. Hood, and B. Neill. I received valuable assistance in data collection from M. Ednoff, G. Dingle, J. Holmes, C. Bernier, I. Velez, D. Mayer, J. Festa, B. Kolitz, E. Murphy, C. Thacker, and J. Hazelworth. Much of the data processing was ably assisted by R. Qualset, M. McCaslin, R. DeVivo, and I. Burden. Drafting and advice on figures and layout were done by R. Carrodus, D. Senn, and S. O'Brien; photography was by A. Ramsay.

I have had many fruitful discussions on these data with colleagues and friends from the Texas A & M University, the Florida State University, the Florida State University System Institute of Oceanography, the National Aeronautics and Space Administration, and the University of Miami as well as the Atlantic Oceanographic and Meteorological Laboratories. Particularly, I would like to acknowledge J. Cochrane, M. Ednoff, M. Rinkel, D. Norris, W. Johnson, A. Leetmaa, R. Molinari, F. Chew, and my mentors, H. Gordon, C. Rooth, D. Hansen, E. Corcoran, K. Hanson, and W. Duing.

This research was in part supported by contract GSFC-C0315 through the National Aeronautics and Space Administration's Earth Resources Program and the National Environment Satellite Service's Environmental Sciences Group. The author of this manuscript wrote the original proposal to NASA and was awarded the contract by NASA as principal investigator. Results reported herein are due to direct supervision by the principal investigator.

### 8. REFERENCES

- Anderson, E. R. (1954), Energy budget studies. In: <u>Water Loss Investigations</u>
  <u>Lake Hefner Studies</u>. U. S. Geological Survey Professional Papers 269,
  pp. 71-117.
- Arvesen, J. C. (1972), Airborne differential radiometer measurements of chlorophyll in water. Fourth Annual Earth Resources Review, Vol. IV. NASA MSC-05937, pp. 104-1 to 104-2.
- Austin, H. R. (1971), The characteristics and relationships between the calculated geostrophic current component and selected indicator organisms in the Gulf of Mexico Loop Current System. Ph. D. Dissertation, Florida State University, Department of Oceanography, Tallahasee, 369 pp.
- Baig, S. R., and C. S. Yentsch (1969), A photographic means of obtaining monochromatic spectra of marine algae. Appl. Opt., 8 (12), pp. 2566-2568.
- Beardsley, G. F., H. Pak, K. Carder, and B. Lundgren (1970), Light scattering and suspended particles in the eastern equatorial Pacific Ocean.

  J. Geophys. Res., 75 (15), pp. 2837-2845.
- Capurro, L. R. A., and J. L. Reid, Editors (1972), Contributions on the Physical Oceanography of the Gulf of Mexico. Gulf Publ., Houston, 288 pp.
- Chandrasekhar, S. (1960), Radiative Transfer. Dover, New York, 393 pp.
- Charnell, R. L., and G. A. Maul (1973), Oceanic observation of New York Bight by ERTS-1. Nature, 242 (5398), pp. 451-452.
- Chew, F. (1974), The turning process in meandering currents: A case study. J. Phys. Oceano., 4 (1), pp. 27-57.
- Clark, G. L., G. C. Ewing, and C. J. Lorensen (1970), Spectra of back-scattered light from the sea obtained from aircraft as a measurement of chlorophyll concentration. <u>Science</u>, <u>167</u>, pp. 1119-1121.
- Cochrane, J. D. (1965), The Yucatan Current. In: Annual Report, Project 286. Texas A & M University, Ref. 65-17 T, College Station, pp. 20-27.
- Corcoran, E. A., and J. E. Alexander (1963), Nutrient, chlorophyll, and primary production studies in the Florida Current. <u>Bull. Mar. Sci. Gulf and Carib.</u>, <u>13</u> (4), pp. 527-541.
- Corwin, T. L., and H. R. Richardson (1974), Preliminary Report to the
  Commandant of the Coast Guard on the Gulf of Mexico Cyanide Barrel Spill.
  Daniel H. Wagner Assoc., Paoli, Pa., 36 pp.

- Cox, C., and W. Munk (1954), Measurements of the roughness of the sea surface from photographs of the sun's glitter. J. Opt. Soc. Am., 44 (11), pp. 838-850.
- Curran, R. J. (1972), Ocean color datermination through a scattering atmosphere. Appl. Opt., 11 (8), pp. 1857-1866.
- Duing, W. (1973), Some evidence for long-period barotropic waves in the Florida Current. J. Phys. Oceano., 3 (3), pp. 343-346
- Duntley, S. Q. (1972), Detection of ocean chlorophyll from earth orbit.

  Fourth Annual Earth Resources Review, Vol. IV. NASA MSC-05937, pp. 102-1 to 102-25.
- Ednoff, M. E. (1974), Surface phytoplankton communities and their relationship to the Loop Current in the Gulf of Mexico. Master's Thesis, Florida State University, Department of Oceanography, Tallahassee, 187 pp.
- Ewing, G. (1950), Slicks, surface films, and internal waves. J. Mar. Res., IX, (3), pp. 161-187.
- Ford, W. L., J. R. Longard, and R. G. Banks (1952), On the nature, occurance and origin of cold low salinity water along the edge of the Gulf Stream Front. <u>Deep-Sea Res.</u>, 3, pp. 46-65.
- Fuglister, F. C. (1951), Annual variations in current speeds in the Gulf Stream. J. Mar. Res., 10, pp. 119-127.
- Fuglister. F. C., and A. D. Voorhis (1965), A new method of tracking the Gulf Stream. Limnol. Oceanogr., 10, pp. R115-R124.
- Galtsoff, P. S., Editor (1954), Gulf of Mexico--It's Origin, Waters, and Marine Life. Fishery Bulletin 89, Fish and Wildlife Service, 604 pp.
- Gandin, L. S. (1963), Objective Analysis of Meteorological Fields. National Technical Information Service, TT 65-50007, Springfield, Va., 242 pp.
- Gordon, H. R. (1973), A simple calculation of the diffuse reflectance of the ocean. Appl. Opt., 12, pp. 2804-2805.
- Gordon, H. R., O. B. Brown, and M. M. Jacobs (1974), Computed relationships between the inherent and apparent optical properties of a flat homogenous ocean. Submitted to Appl. Opt.
- Gordon, J. R. (1974), Spectral variations in the volume scattering function at large angles in natural waters. J. Opt. Soc., 64, (6), pp. 773-775.
- Gordon, H. R., and W. R. McCluney (1974), Estimation of the depth of sunlight penetration in the sea for remote sensing. Submitted to Appl. Opt.

- Hansen, D. V., and G. A. Maul (1970), A note on the use of sea surface temperature for observing ocean currents. Remote Sensing of Environ., 2, pp. 161-164.
- Hansen, D. V. (1970), Gulf Stream meanders between Cape Hatteras and the Grand Banks. <u>Deep-Sea Res., 17</u>, pp. 495-511.
- Hansen, D. V. (1972), Deep currents in the Yucatan Strait. EOS, Transactions, A.G.U., 53 (4), p. 392.
- Hanson, K. J. (1972), Remote sensing of the ocean. In: <u>Remote Sensing of the Troposphere</u> (V. G. Derr, Ed.). U.S. Govt. Print. Off., Washington, pp. 22-1 to 22-56.
- Hovis, W. A., M. L. Forman, and L. R. Blaine (1974), Detection of ocean color changes from high altitudes. <u>NASA GSFC X-652-73-371</u>, Greenbelt, Md., 25 pp.
- Ichiye, T. (1962), Circulation and water mass distribution in the Gulf of Mexico. Geofis. Inter., 2 (3), pp. 47-76.
- Ichiye, T. (1972), Experimental circulation modelling within the Gulf and the Caribbean. In: Contributions on the Physical Oceanography of the Gulf of Mexico. Gulf Publ., Houston, pp. 213-226.
- Jacobs, W. C. (1951), The energy exchange between sea and atmosphere and some of its consequences. <u>Bull.</u>, <u>Scripps Inst. Oceanogr.</u>, <u>6</u> (2), pp. 27-122.
- Jerlov, N. G. (1968), Optical Oceanography. Elsevier, New York, 194 pp.
- Kalle, K. (1938), Zum problem der Meeres wasserfarbe. Ann Hydrol. Marine Mitt., 66, pp. 1-13.
- Lee, T. N. (1974), Florida Current spin-off eddies. Submitted to <a href="Deep-Sea Res">Deep-Sea Res</a>.
- Leipper, D. F. (1970), A sequence of current patterns in the Gulf of Mexico. J. Geophys. Res., 75 (3), pp. 637-657.
- Leipper, D. F., and D. Volgenau (1970), Hurricane heat potential of the Gulf of Mexico. EOS, Transactions, A.G.U., 51 (4), p. 312.
- Lorenzen, C. J. (1971), Continuity in the distribution of surface chlorophyll. J. du Conseil Inter. Pour l'Exploration de la Mer, 34 (1), pp. 18-23.
- Mairs, R. L. (1970), Oceanographic interpretation of Apollo photographs. Photogrammetic Engr., pp. 1045-1058.
- Maul, G. A. (1973), Remote sensing of ocean currents using ERTS imagery.

  Symposium on Significant Results Obtained from the Earth Resources

  Technology Satellite--1. NASA SP-327, Vol. 1(B), pp. 1365-1375.

- Maul, G.A. (1974), A one year time series of the Gulf Loop Current. <u>EOS</u>, <u>Transactions</u>, <u>A.G.U.</u>, <u>56</u>(4), p. 283.
- Maul, G.A., and D.V. Hansen (1972), An observation of the Gulf Stream front structure by ship, aircraft, and satellite. Remote Sensing of Environ., 2, pp. 109-116.
- Maul, G.A., and M. Sidran (1973), Atmospheric effects on ocean surface temperature sensing from the NOAA satellite scanning radiometer.

  J. Geophys. Res., 78 (12), pp. 1909-1916.
- Maul, G.A., and H.R. Gordon (1974), Relationships between ERTS radiances and gradients across oceanic fronts. Third Earth Resources Technology Satellite-1 Symposium. NASA SP-351, Vol. 1(B), pp. 1279-1308.
- Maul, G.A., and R.L. Charnell, and R.H. Qualset (1974), Computer enhancement of ERTS-1 images for ocean radiances. Remote Sensing of Environ. (In press).
- Maul, G.A., D.R. Norris, and W.R. Johnson (1974), Satellite photography of eddies in the Gulf Loop Current. Geophys. Res. Ltrs. (In press).
- Molinari, R.L., and J.D. Cochrane (1972), The effect of topography on the Yucatan Current. In: <u>Contributions on the Physical Oceanography of the Gulf of Mexico</u>. Gulf Publ., Houston, pp. 149-155.
- Murphy, E., K. Steidinger, B. Roberts, J. Williams, and J. Jolley (1974), An explanation of the Florida East Coast Gymnodinium breve red tide, November 1972. <u>Limnol. Oceanogr</u>. (In press).
- NASA (1971), Earth Resources Technology Satellite Data Users Handbook. NASA Document No. 71SD4249.
- Neumann, G., and W. J. Pierson, Jr. (1966), <u>Principles of Physical</u> Oceanography. Prentice-Hall, Englewood Cliffs, N.J., 545 pp.
- Niiler, P.P., and W.S. Richardson, Jr. (1973), Seasonal variability of the Florida Current. <u>J. Mar. Res.</u>, <u>31</u> (3), pp. 144-167.
- Nowlin, W.D., Jr., and H.J. McLellan (1967), A characterization of the Gulf of Mexico waters. J. Mar. Res., 25 (1), pp. 29-59.
- Parker, C.E. (1972), Some direct observations of currents in the Gulf Stream. <u>Deep-Sea Res.</u>, <u>19</u> (12), pp. 879-893.
- Paskausky, D.F., and R.O. Reid (1972), A barotropic prognostic numerical circulation model. In:

  Oceanography of the Gulf of Mexico. Gulf Publ., Houston, pp. 163-176.
- Prandtl, L., and O.G. Tietjens (1957), <u>Fundamentals of Hydro- and Aeromechanics</u>. Dover, New York, pp. 221-223.

- Reid, R. O. (1972), A simple dynamical model of the Loop Current. In:

  <u>Contributions on the Physical Oceanography of the Gulf of Mexico.</u>

  <u>Gulf Publ.</u>, Houston, pp. 157-159.
- Robinson, M. K. (1973), Atlas of Monthly Mean Sea Surface and Subsurface

  Temperature and Depth of the Top of the Thermocline Gulf of Mexico
  and Caribbean Sea. Scripps Inst. Oceanogr. Reference 73-8,

  105 pp.
- Ross, D. B., and V. Cardone (1974), Observations of oceanic whitecaps and their relation to remote measurements of surface wind speed.

  J. Geophys. Res., 79, (3), pp. 444-452.
- Sauberer, F., and F. Ruttner (1941), <u>Die Strahlingsverhaltnisse der</u>
  Binnengewasser. Akademie Verlag, Berlin, 240 pp.
- Schlitz, R. J. (1973), Net total transport and net transport by water mass categories for Yucatan Channel based on data for April 1970. Ph.D. Dissertation, Texas A & M University, Department of Oceanography, College Station, 107 pp.
- Smith, R. E., Editor (1974), <u>Proceedings of Marine Environmental Implications</u>
  of Offshore Drilling Eastern Gulf of Mexico; 1974. Florida State University
  System Institute of Oceanography, St. Petersburg, 455 pp.
- Stommel, H. (1966), The Gulf Stream. Univ. of California, Berkeley, 248 pp.
- Strong, A. E. (1973), ERTS-1 anomalous dark patches. National Technical Information Service, NASA CR-1333115; E73-10747, Springfield, Va.
- Strickland, J. D. H., and T. R. Parsons (1968), A Practical Handbook of Seawater Analysis. Fisheries Research Board of Canada, Ottawa, 311 pp.
- Szekields, K. H. (1973), Distribution pattern of temperature and biomass in the upwelling area along the NW coast of Africa. In: Proceedings of the Fall Convention ASP-ASCM October 2-5, 1973, pp. 664-719.
- Tyler, J. E., and R. C. Smith (1970), <u>Measurements of Spectral Irradiance</u>
  Underwater. Gordon and Breach, New York, 103 pp.
- Uda, M. (1938), Researches on "Siome" or current rip in the seas and ocean. Geophys. Mag., 11 (4), pp. 307-372.
- von Arx, W. S., D. Bumpus, and W. S. Richardson (1955), On the fine structure of the Gulf Stream front. <u>Deep-Sea Res.</u>, <u>3</u>, pp. 46-65.
- Webster, F. (1967), A scheme for sampling deep-sea currents from moored buoys. Transactions, 2nd International Buoy Technology Symposium. Mar. Tech. Soc., Washington, pp. 419-431.

- Wert, R. T., and R. O. Reid (1972). A baroclinic prognostic numerical circulation model. In: Contributions on the Physical Oceanography of The Gulf of Mexico. Gulf Publ., Houston, pp. 177-209.
- Wennekens, M. P. (1959), Water mass properties of the Straits of Florida and related waters. <u>Bull. Mar. Sci. Gulf and Carib.</u>, <u>9</u> (1), pp. 1-52.
- Whitaker, R. E. (1971), Seasonal variations of steric and recorded sea level of the Gulf of Mexico. Master's Thesis, Texas A & M University, Department of Oceanography, College Station, 109 pp.
- Yentsch, C. S. (1960), The influence of phytoplankton pigment on the color of the sea. <u>Deep-Sea Res.</u>, 7, pp. 1-9.
- Yentsch, C. S. (1962), Measurement of visible light absorption by particulate matter in the ocean. Limnol. Oceanogr., 7 (2), pp. 207-217.

#### 9. APPENDIXES

#### APPENDIX A

In this section, several ERTS-1 images of the Gulf Stream System are summarized. Each of the selected images used in this report are located in figure A.1. Frame numbers 1, 2, 3, 4, and 5 were discussed in the body of the text and will not be repeated here. The selected images are from the area of concern as stated in the title; this does not mean that these were the only good images of the current. About 10% of the images received that passed the 60% cloud cutoff criterion actually had ocean current information. The rest were either in the wrong area or the current was not visible; the latter cause accounted for about 25% of the null information.

Figure A.2 was used by Maul and Gordon (1974) to study the capability of ERTS to determine the particle concentration. In that study, they showed that if

$$\frac{MSS-4}{MSS-5} = constant,$$
(A.1)

then

$$\nabla$$
 MSS-4 or-5  $\propto$   $\nabla$ b<sub>p</sub>/b<sub>W</sub> , (A.2)

which is in turn proportional to the gradient of the particle concentration. Along the scanline shown in figure A.2, the gradient in MSS-4 and MSS-5 has been computed using several filters; the correlation coefficient (r) has been computed for each filter pair as well. The results of using different low pass filters and filter lengths are summarized in figure A.3.

The general trend is that r increases with longer filter kernels and with lower pass filters. This means that the gradient on the Earth's surface with 8-km (100 sample low pass) spatial scale has greater coherence between bands. It is not certain as to why the small-scale correlation coefficient is so low. This area has significant amounts of coastal sediments which are rich in organics, and thus the Gelbstoff concentrations probably vary over a wide range.

In the images to follow, the interpretations given are based on the discussion in the text. Only one band is given in the appendix, but all were studied for interpretation. Clouds were identified in MSS-6 and MSS-7 and were optically masked out of the image before study, so that the data discussed are water phenomenon and not an atmospheric contribution. Water color shift from green to blue was made by studying whether the variation in MSS-4 disappeared in MSS-5; if so, the color of low radiance scanspots in MSS-4 must be bluer than the higher radiance data. Similarly sediments are not seen in MSS-7 or frequently even in MSS-6; clouds are always seen in all four channels. The images are presented for the general use of other marine scientists without discussion except for the figure captions.

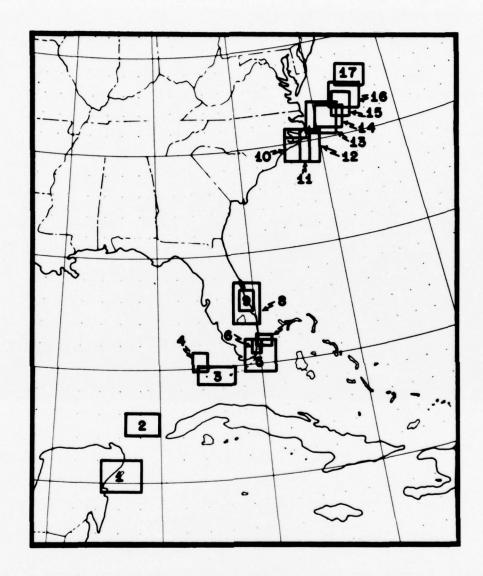


Figure A.1 Location map of selected images in appendix A. Images 1, 2, 3, 4, and 5 were discussed in the text and are not repeated here. Images 6-17 are labeled figures A.6-A.17: There is no figure A.5, and figures A.1 and A.4 are used for introductory discussion.

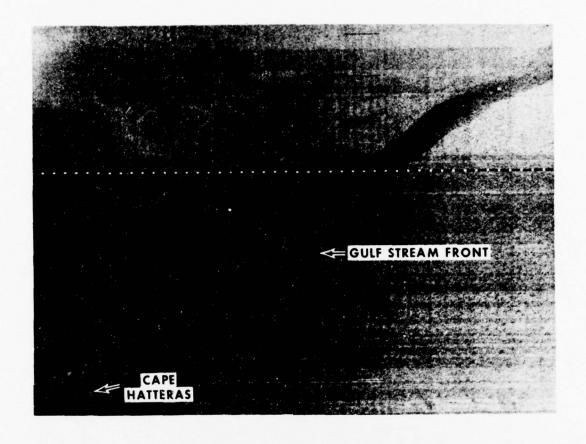


Figure A.2 Contrast-stretched (4\leq DN\leq12; n=2) negative MSS-5 image of the ocean area offshore of Cape Hatteras (ERTS ID 1132-15042), observed on 2 December 1972. The Gulf Stream can be seen as the bright area to the south of the entrained sediment from the coastal estuaries. The least-squares fit of (A.1) was done along the scanline north of the Cape and extending from nearshore, through the suspended sediment, and into the current. Extensions of this plume were observed for 150 km farther east on other ERTS images. Horizontal distance across the image is 135 km.

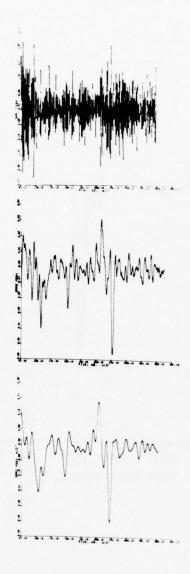


Figure A.3 Gradient of radiance received at the satellite in MSS-4 along the scanline shown in figure A.2. Scanspot numbers arbitrarily start at 1 which is just off the image in the previous figure and over the coast. Correlation coefficient (r) for the MSS-4, MSS-5 linear correlation is: upper - 10 sample low pass (199 element kernel), r=0.085; middle - 100 sample low pass (59 element kernel), r=0.398; lower - 100 sample low pass (159 element kernel), r=0.698. Compare with figure A.4 for 100 sample low pass using 199 elements in the filter kernel, where r=0.740.

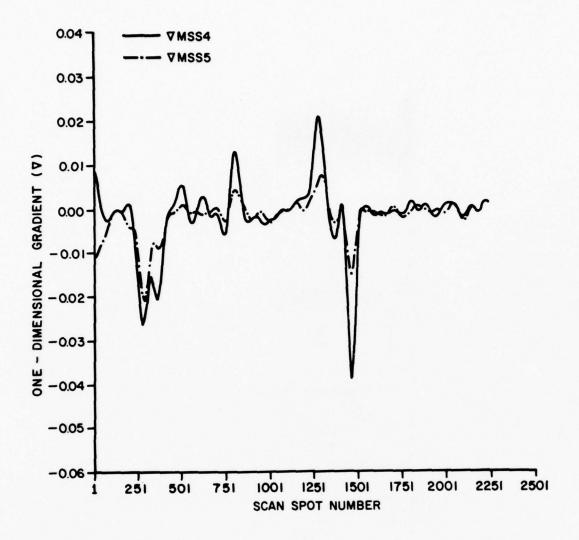


Figure A.4 Gradient of radiance in MSS-4 and MSS-5 along the scanline shown in figure A.2, using a 100 sample low pass filter (199 element kernel). The linear correlation coefficient (r) is 0.740 for this filter. These data suggest that  $\nabla$ MSS-4 or  $\nabla$ MSS-5 is a good estimate of the gradient of the particle concentration.

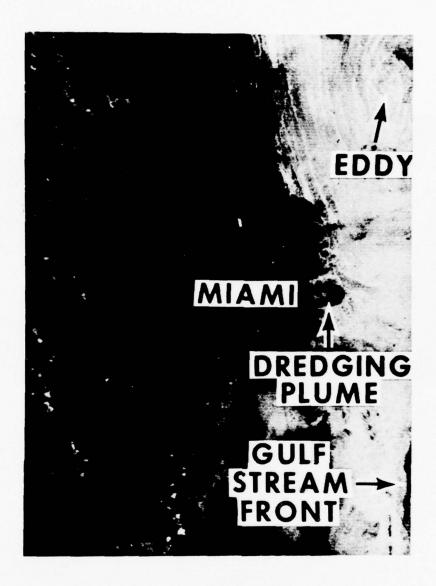


Figure A.6 Contrast-stretched (12<DN<21; n=1) negative MSS-5 image of Miami, Florida (ERTS ID 1350-15231), observed on 8 July 1973. Government Cut and the Miami harbor basin were being dredged when this image on the ebb tide was taken. The dredge spoil can be seen as a jet flowing out into the shelf where a cyclonic circulation is caused by the Longshore drift. A cyclonic eddy, either spinoff or shear-induced (Lee, 1974) by the Gulf Stream, is seen in the upper right due to changes in surface reflectance. The Gulf Stream front at the lower right is seen due to higher radiance in the current. Complications of nearshore currents can be deduced because of the offshore eddy, and the northern inlets have a southward inshore drift that has reversed or slackened near the dredging plume. Horizontal distance across the image is 45 km.



Figure A. 7 Contrast-stretched sequence of MSS-6 data off Miami Beach, Florida (ERTS ID 1026-15230), observed on 18 August 1972. Sequence shows the effect of varying the DN range and n in the contrast equation. a) Upper left: Raw data, positive print. b) Upper middle: 7≤DN≤15; n=1. c) Upper right: 7≤DN≤15; n=3. d) Lower left: 7≤DN≤11; n=1. e) Lower middle: 9≤DN≤13; n=1. f) Lower right: MSS-6 minus MSS-7, then 5≤DN≤13; n=3. Note that using powers of n brings out water details (cf. b & d). Water details in e are less distinct than in b which uses the statistically determined limits. Sea state only is observable in MSS-7, so MSS-6-MSS-7 should minimize the surface contribution as is shown in f. Horizontal distance across each image is 45 km.

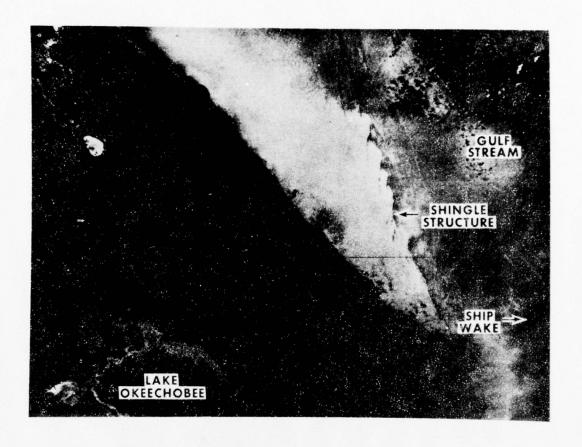


Figure A.8 Contrast-stretched (9≤DN≤17; n=1) negative MSS-5 image of the region offshore of Cape Canaveral, Florida (ERTS ID 1260-15233), observed on 9 April 1973. Fine-scale "shingle structure" (von Arx, Bumpus, and Richardson, 1955) can be seen along the cyclonic edge of the Gulf Stream. The shingel structure in this image is at least an order of magnitude less than the von Arx et al. description off the Carolinas. Wind streaks and a ship wake can be observed in the Gulf Stream which is leaving the coast at the lower right. Loss of water detail in Lake Okeechobee is caused by the contrast stretch limits and shows that the very high radiance from this water body is due to a turbidity about equal to the coastal inlet plume in the upper left. Horizontal distance across the image is 135 km.



Figure A.9 Contrast-stretched (8≤DN≤16; n=1) negative MSS-5 image of the Florida coast south of Cape Canaveral (ERTS ID 1206-15232), observed on 18 August 1972. Plumes of water from behind the barrier islands can be seen ebbing through the inlets. Complicated patterns of coastal sedimentation show a multifronted boundary between the nearshore water and the Gulf Stream. Changes in the radiance appear to be dominated by changes in suspended sediments. Horizontal distance across the image is 45 km.

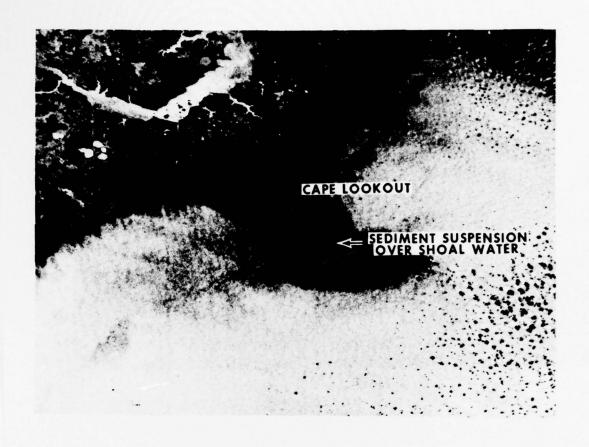


Figure A.10 Contrast-stretched (7≤DN≤15; n=2) negative MSS-5 image of Cape Lookout, North Carolina, (ERTS ID 1115-15152), observed on 14 November 1972. The shoals offshore of the promitory are shallow and keep sediments in suspension. By comparing the sediment pattern over such areas (cf., fig. A.11), an estimate of the bottom topography can be made and, conversely, the variability of the suspended load as well. There is no evidence of the Gulf Stream front in this image. Horizontal distance across the image is 135 km.

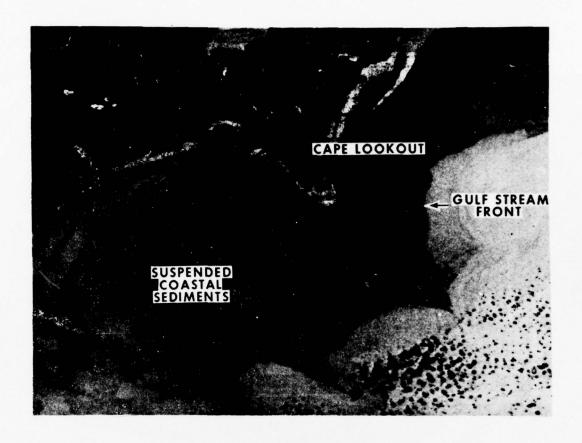


Figure A.11 Contrast-stretched (4\leqnameleq

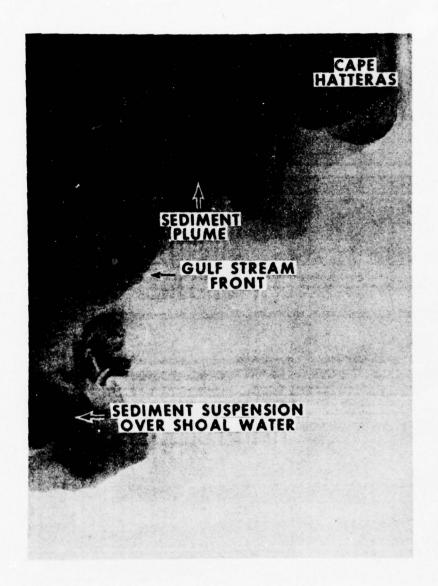


Figure A.12 Contrast-stretched (5≤DN≤13; n=2) negative MSS-5 image of the Cape Hatteras, North Carolina area (ERTS ID 1132-15094), observed on 1 December 1972. Mairs (1970) correlated the pulses in the Ocracoke Inlet sediment plume to several stages in the tide. The Cape Hatteras materials are transported from farther north, and an eddy has been observed in several ERTS images in the Hatteras region. Compare again the sediment suspension over Lookout Shoals with the scene in figures A.10 and A.11; detail changes are due to both different stretch limits as well as environmental conditions. Horizontal distance across the image is 90 km.



Figure A.13 Contrast-stretched (14≤DN≤22; n=2) negative MSS-4 image of an eddy over Diamond Shoals, North Carolina (ERTS ID 1186-15093), observed on 25 January 1973. A deep penetration of water from north of Cape Hatteras can be seen as part of the cyclonic eddy developing over the shoals. The Gulf Stream front appears to be well offshore of the eddy front. Meander scale in the Gulf Stream appears to be about 50 km with an amplitude of about 10 km. Details in the sediment suspension patterns support the notion of multiple fronts, probably tidally pumped and advected by alongshore current patterns. Streaks can be seen in the current at the lower right and may be internal wave activity. Horizontal distance across the inage is 90 km.

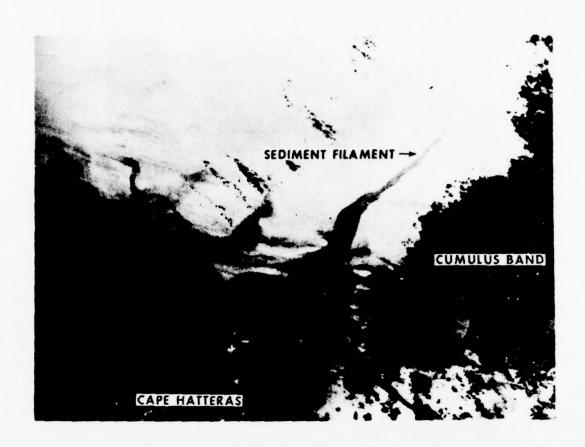


Figure A.14 Contrast-stretched (7≤DN≤15; n=2) negative MSS-5 image of a sediment filament in the offing of Cape Hatteras, North Carolina (ERTS ID 1222-15093), observed on 2 March 1973. The squaring in the stretch equation overaccentuates the low radiance features so that details at Cape Hatteras are lost; generally n≈1 is a better choice because it is linear with radiance for spectral comparison purposes. The sediment filament extends 120 km offshore and is probably material from Pamlico Sound as Ford, Longard, and Banks (1952) have suggested in their entrainment studies. Horizontal distance across the image is 135 km.

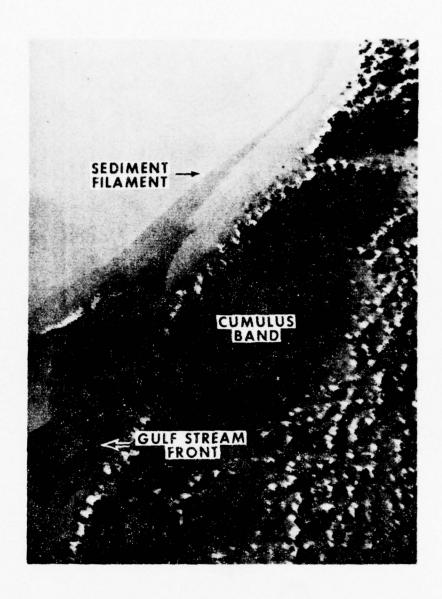


Figure A.15 Contrast-stretched (16≤DN≤24; n=3) negative MSS-4 image of the Gulf Stream in deep water off Cape Hatteras (ERTS ID 1221-15035), observed on 1 March 1973. Taken 1 day earlier than figure A.14, this plume is over 180 km long on this image and extends over 300 km from Cape Hatteras. The cumulus band is a frequent feature of the stream from space and is caused by the convection when cool dry continental air is heated by the stream. This feature follows the Gulf Stream front quite well as seen in the image and can be used as an ancillary feature for identification of the stream. Horizontal distance across the image is 90 km.

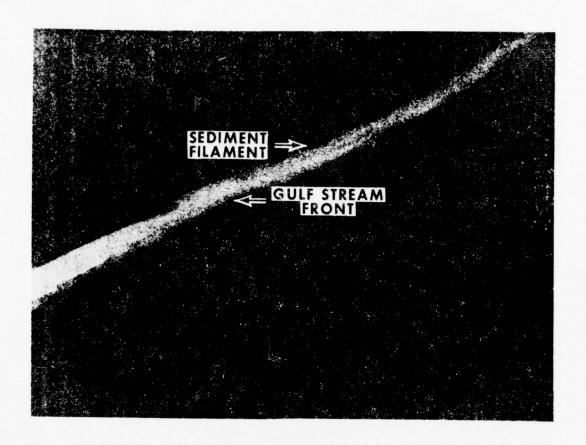


Figure A. 16 Contrast-stretched (12<DN<16; n=1) negative MSS-4 image of a sediment filament offshore of Cape Hatteras, North Carolina (ERTS ID 1149-15033), observed on 19 December 1972. This image was observed 17 days later than the data in figure A.2, but is an almost perfect extension of that sediment filament and about 270 km to sea. Note the DN limits have a range of only 5. The Gulf Stream waters are at the same intensity as the waters north of the sediment filament, and the stream is observable only because little small-scale mixing has occurred across the boundary. Horizontal distance across the image is 135 km.

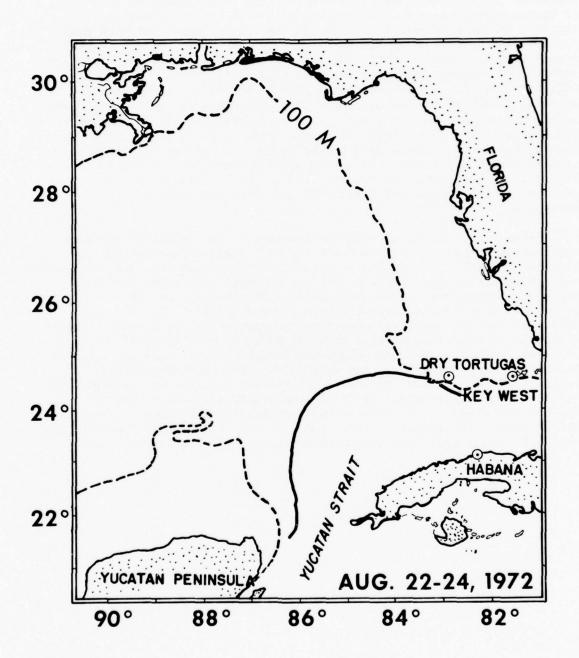


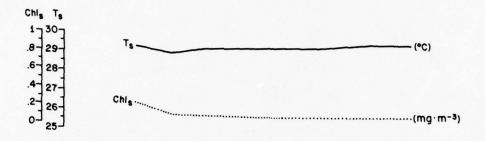
Figure A.17 Contrast-stretched (11≤DN≤15; n=1) negative MSS-5 image of the Gulf Stream off Delaware (ERTS ID 1257-15033), observed on 6 April 1973. The stream is observable in this case due to higher radiance caused by increased sea state in the flow. This image is 350 km northeast of Cape Hatteras. There is a hazard in using sea state only to identify the current because, even in MSS-7, a slight increase in radiance occurs which could be caused by high thin cirrus clouds. Horizontal distance across the image is 135 km.

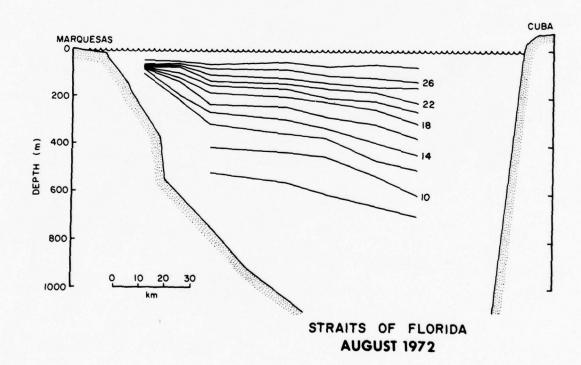
## APPENDIX B

Details of the time series presented in figure 3.2, and the cross-section from which table 3.1 was tabulated, are presented in this appendix. As described before, the solid line on the chart of the Gulf of Mexico represents the 22°C isotherm at 100 m. This stretch of the 22°C isotherm is presented first in the three figures for each cruise (except January 1973 which has two figures). The second figure is the transect of the Straits of Florida showing the surface values of temperature ( $T_s$ ,°C), volume-scattering function ( $\beta_s$ ) at 45° using a blue (436 nm) filter ( $m^{-1}$  sr<sup>-1</sup>), and chlorophyll-a (Chl<sub>s</sub>) observed by the method of Lorenzen (1966) at the surface ( $m_s$ ). Temperature and chlorophyll were continuous observations, whereas volume scattering was observed at each STD station. The third figure of each section is the transect data for the Yucatan Strait, in the same format as for the Straits of Florida. In general, seven STD stations at ~18 km spacing were taken in the Straits of Florida, and nine stations were required in the Yucatan Strait; the cross sections of the temperature field (°C) are given below the surface variables.

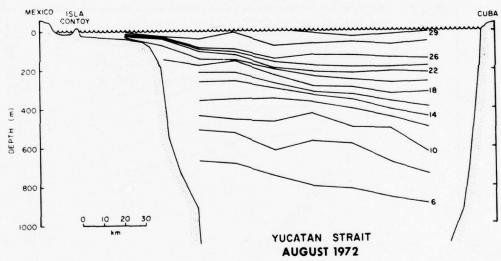
Dates on the charts showing the location of the indicator isotherm represent the time required to track the 22°C @ 100 m from Yucatan to Florida. In 1972, the cruises originated in St. Petersburg, and the Yucatan section (which required about 24 hr) was observed immediately preceeding the tracking; the Straits of Florida section also required about 24 hr and was done 1 day after the transect was completed. In January 1973, foul weather prevented observing the section in the Straits, however, a suborbital track section from 25°55'N, 84°40'W to 23°26'N, 85°20'W was observed. Chlorophyll-a and volume-scattering function were not observed because of equipment failure and rough seas. The remaining cruises originated in Miami, and the Straits of Florida section was observed prior to the tracking; approximately 24 hr were required to reach Cabo San Antonio from Habana. The Straits of Florida section is also a suborbital trackline that was occupied within a day or two of satellite transit. All standard hydrographic data presented herein are on file at NODC.

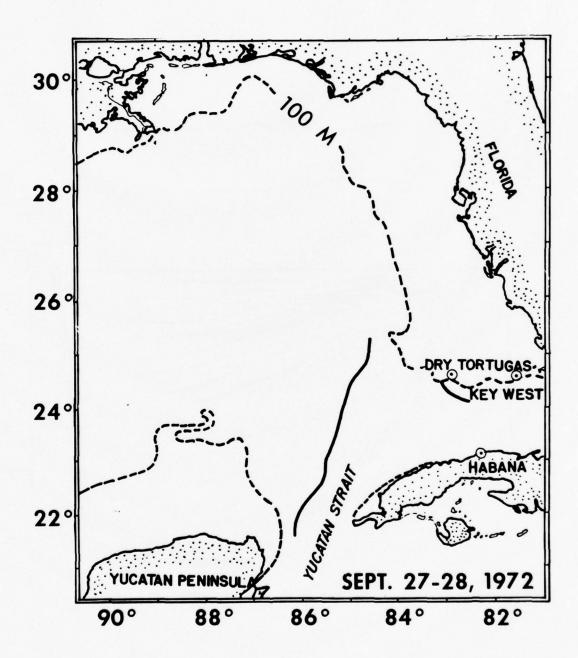


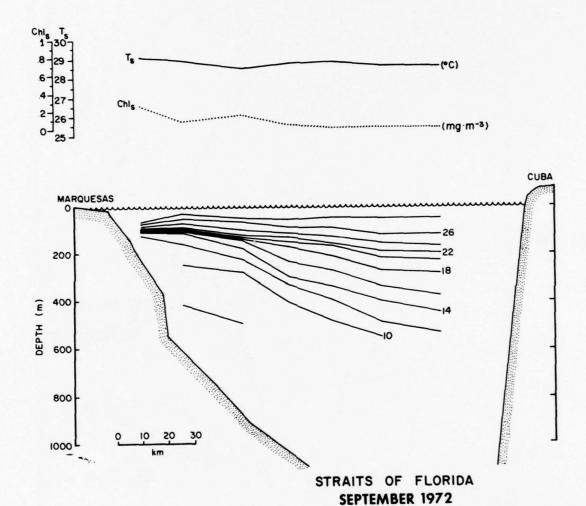


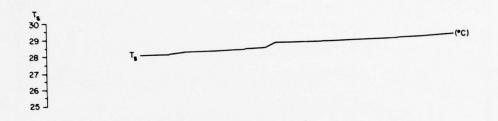


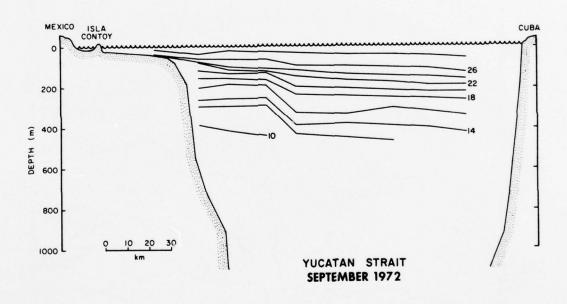


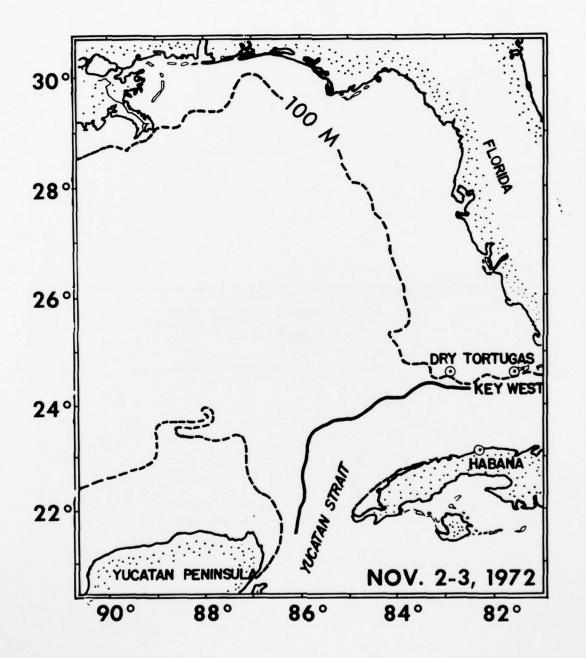


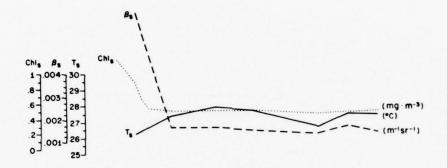


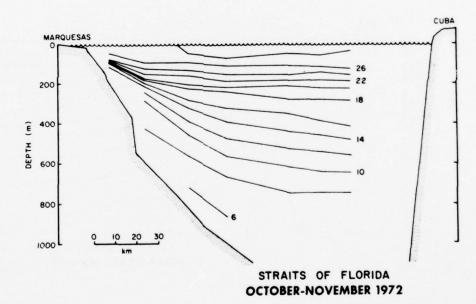


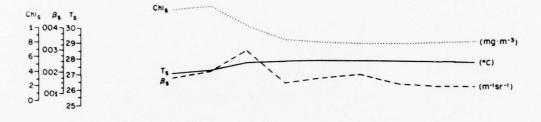


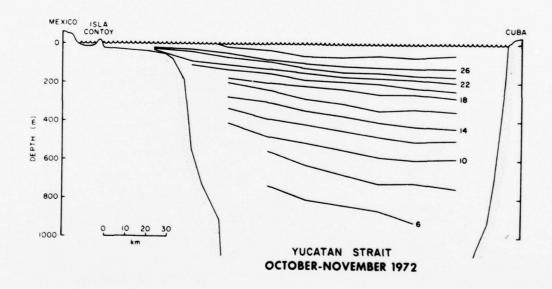


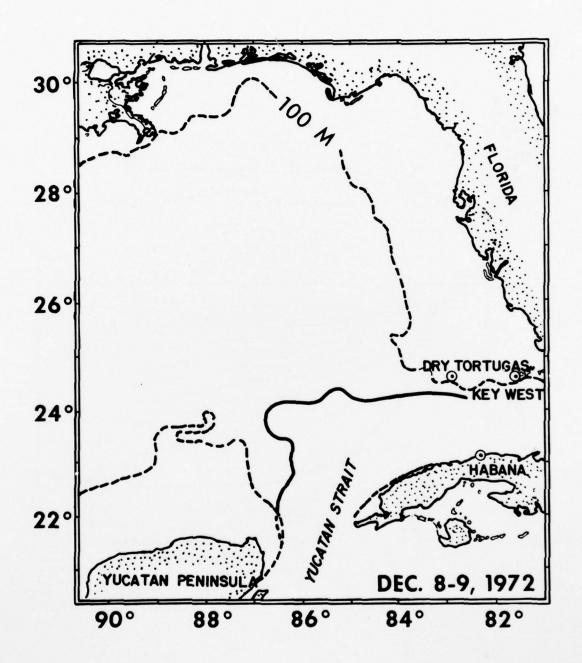




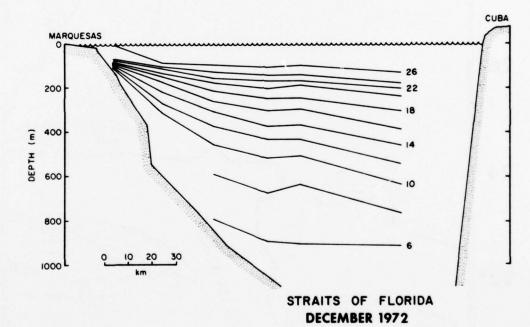


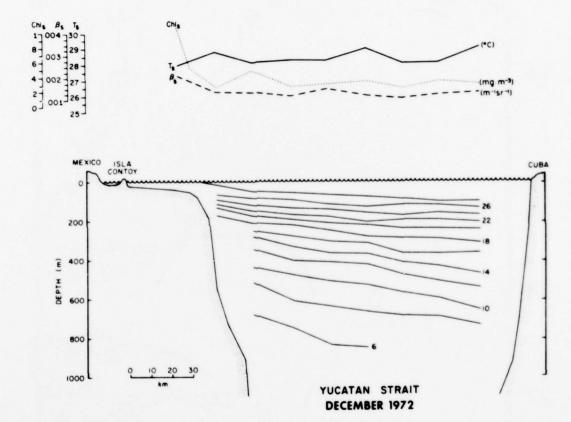


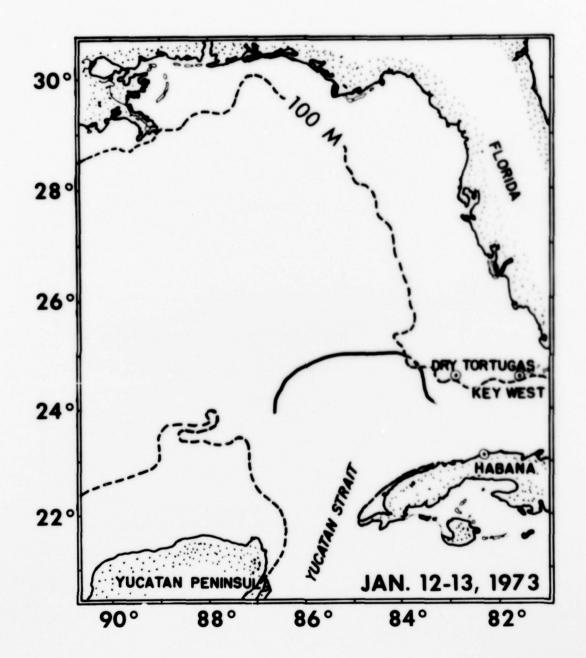


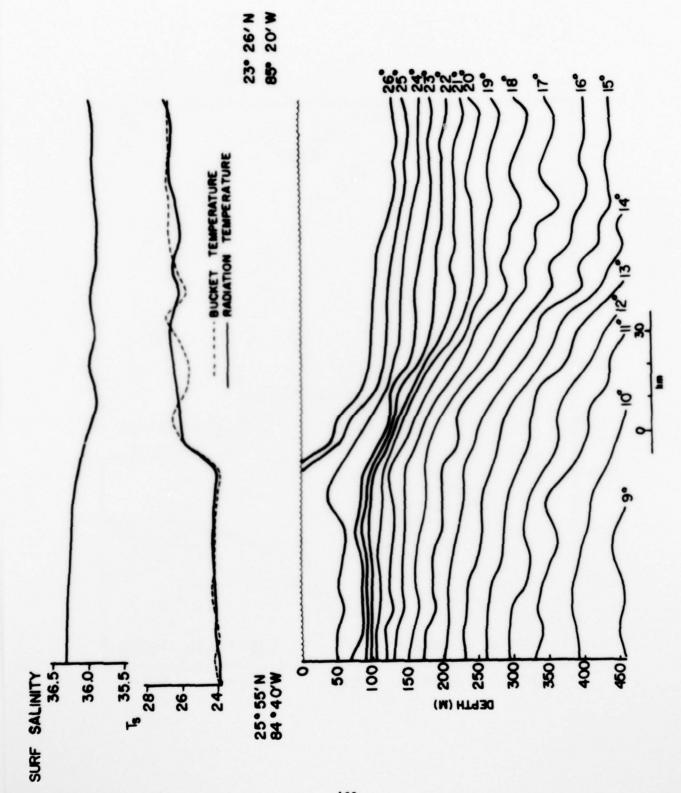


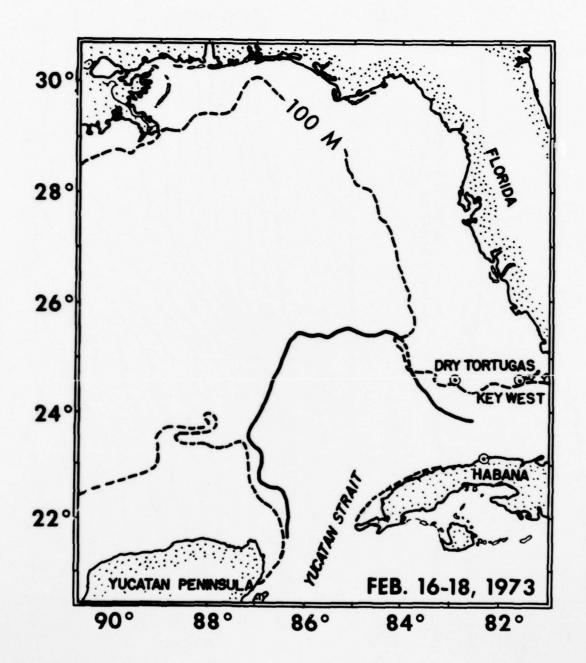


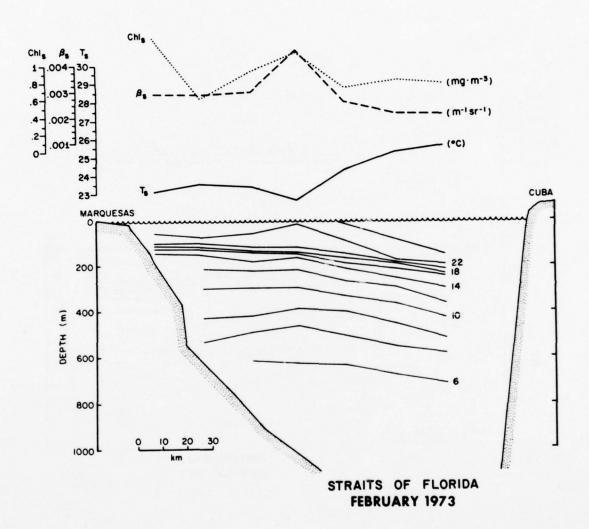


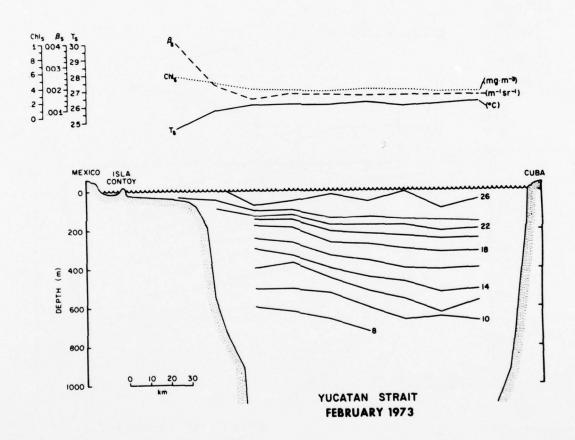


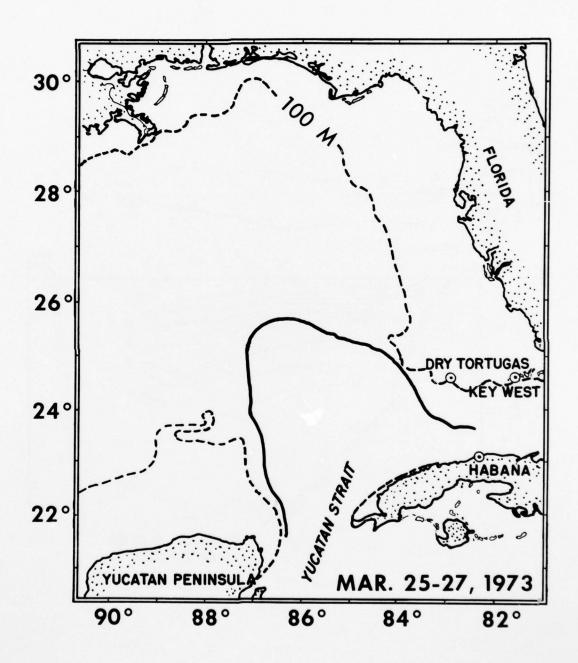


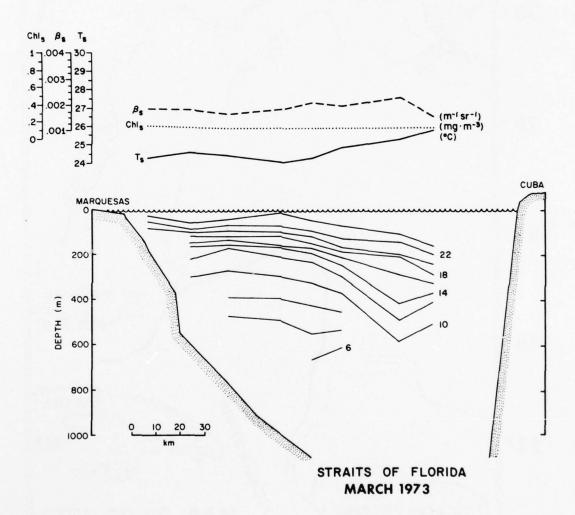


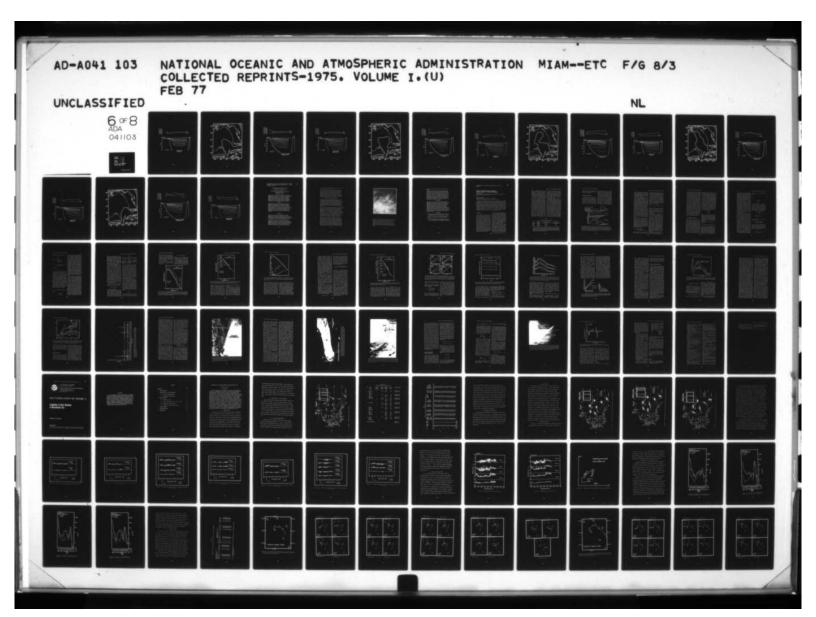


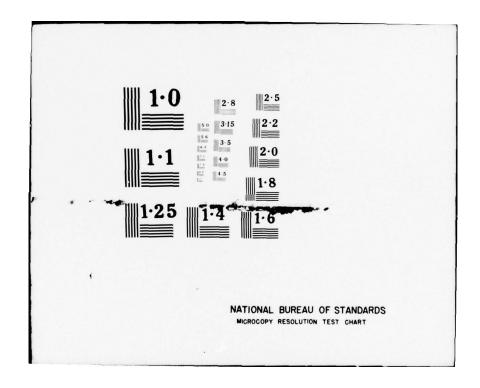


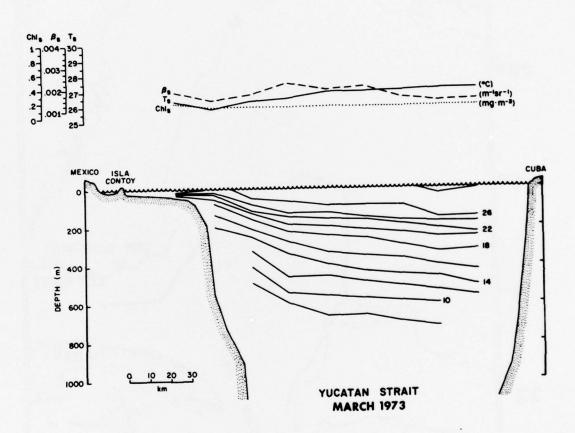


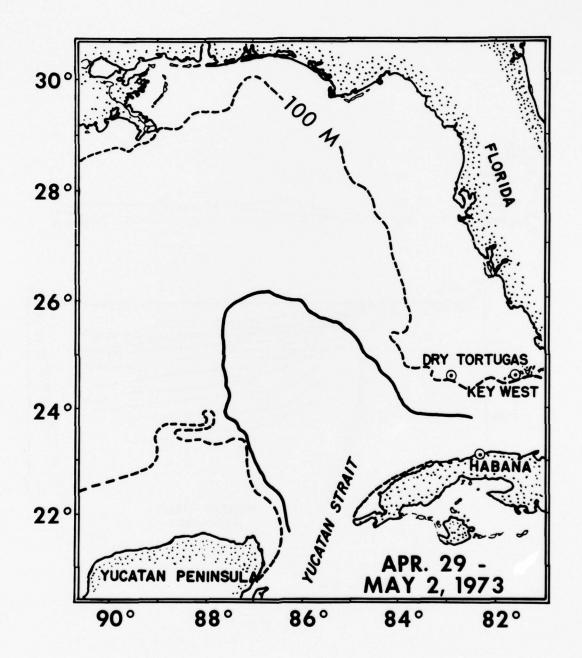


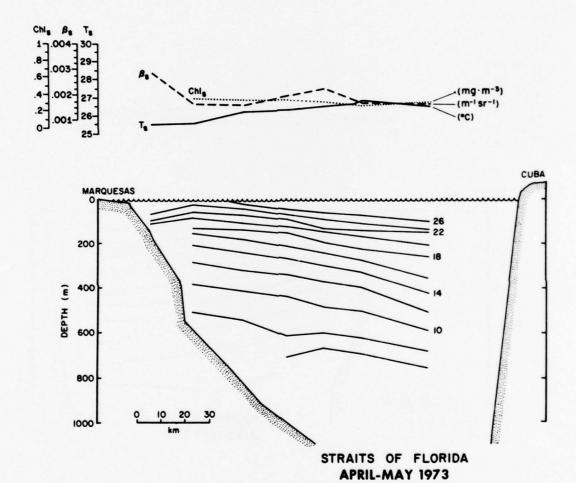


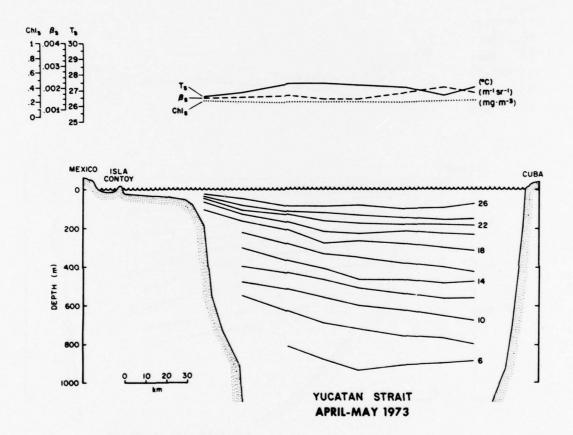


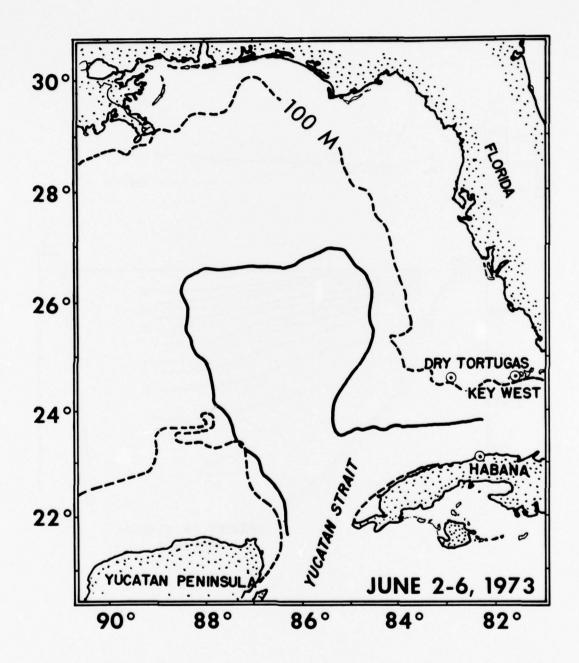




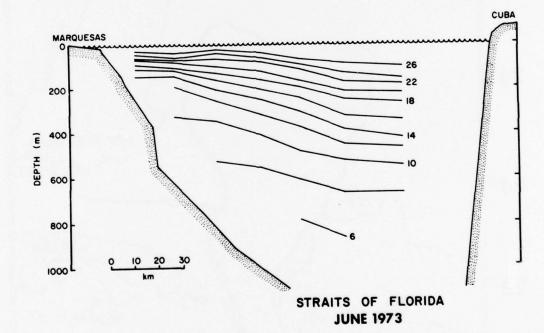


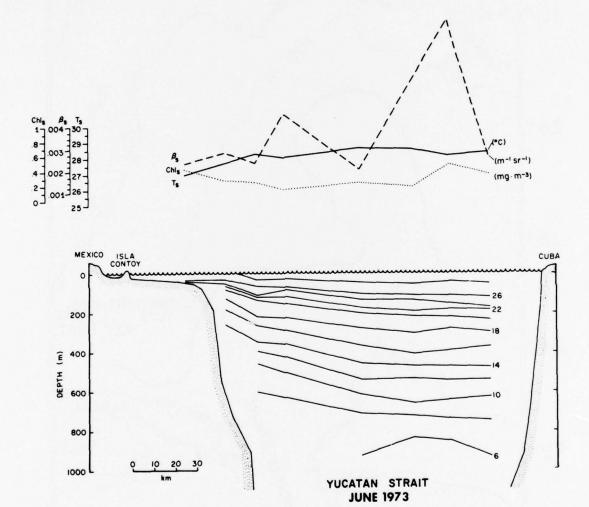


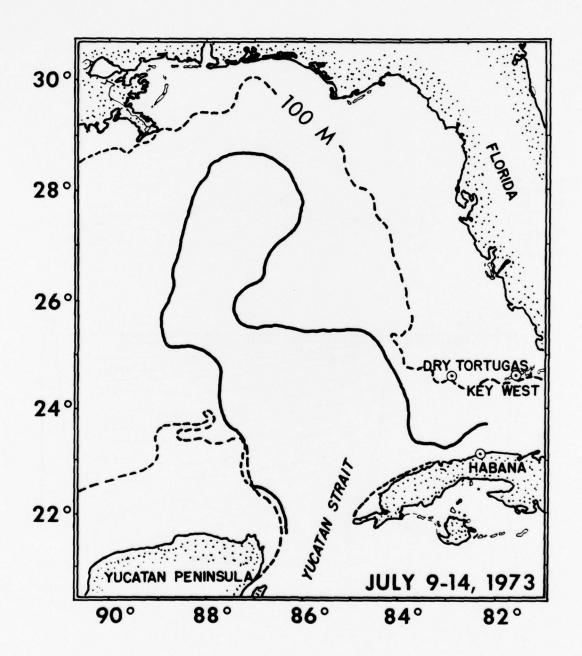




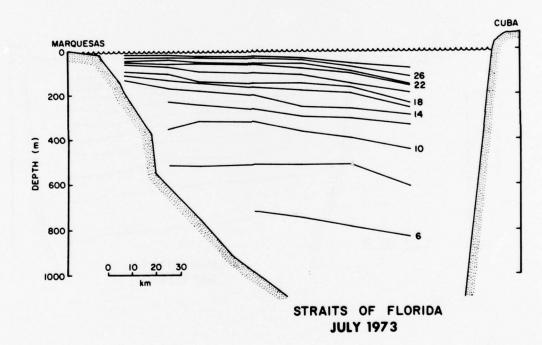


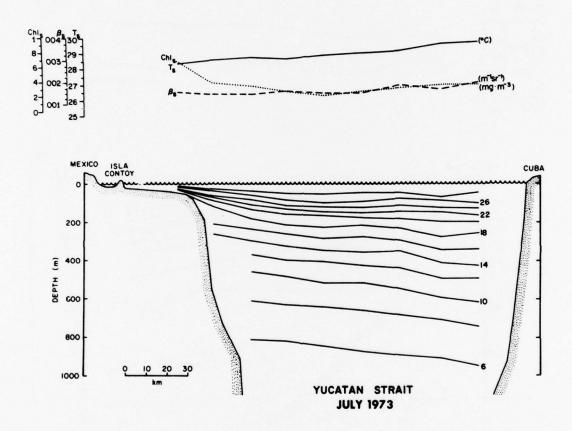


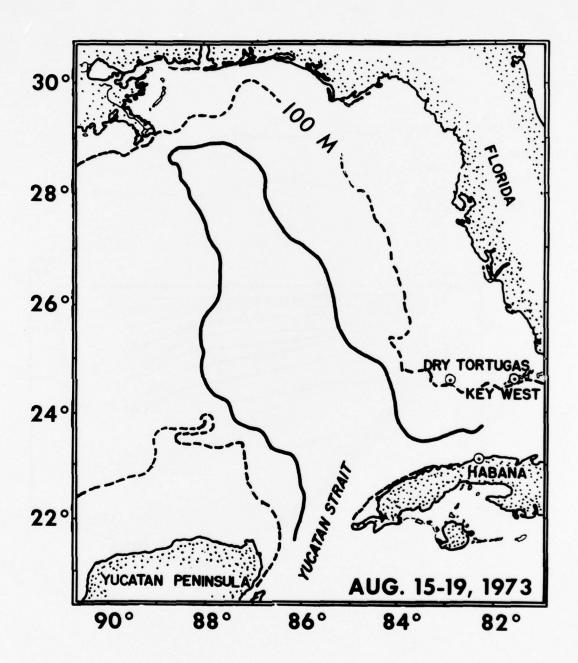




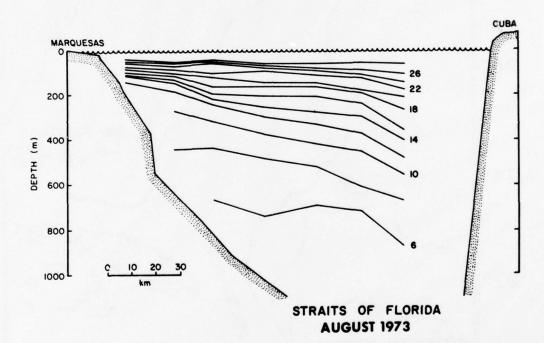


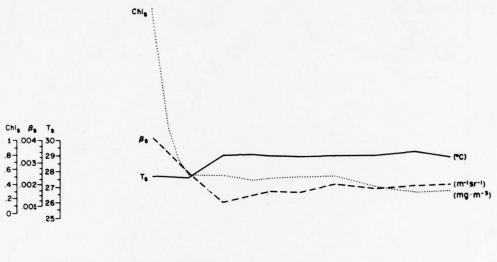


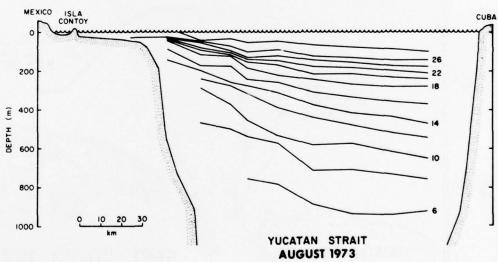


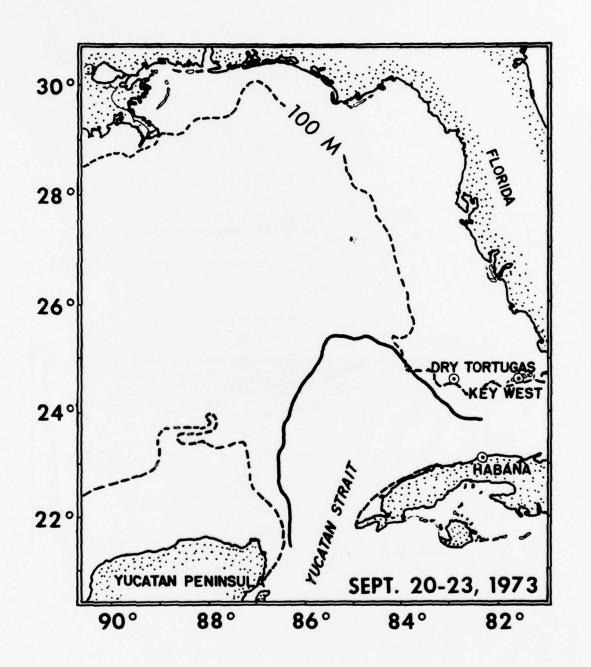


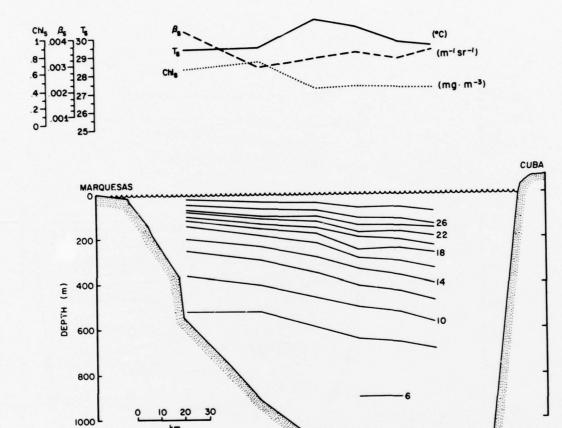






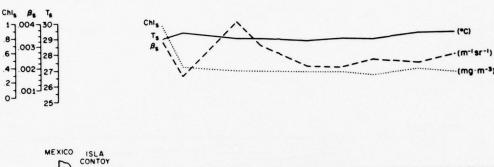


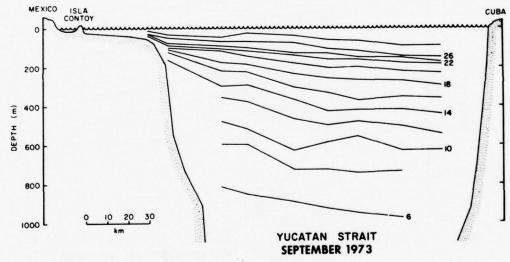




483

STRAITS OF FLORIDA SEPTEMBER 1973





A NEW TECHNIQUE FOR OBSERVING MID-LATITUDE OCEAN CURRENTS FROM SPACE

George A. Maul and Stephen R. Baig

National Oceanic and Atmospheric Administration 15 Rickenbacker Causeway Miami, Florida 33149

#### BIOGRAPHICAL SKETCH

George A. Maul is a research oceanographer in the Physical Oceanography Laboratory of NOAA's Atlantic Oceanographic and Meteorological Laboratories. Dr. Maul's current interests are the remote sensing, optical oceanography, and time dependent motion of the Gulf Stream System. Stephen R. Baig is the oceanographic laision officer of the Miami Satellite Field Station of NOAA's National Environmental Satellite Service. Dr. Baig is responsible for developing satellite services for oceanography and is interested in the application of photography to the marine sciences.

#### ABSTRACT

Infrared observations from the Synchronous Meteorological Satellite are used to locate the cyclonic edge of the Gulf Stream in the offing of the Middle Atlantic Bight. Film loops are made from the high resolution infrared scanner using observations every 30 minutes. For periods of one to three days, the stream's meanders can be considered quasi-stationary. The high velocity of clouds makes identification of the current possible because of the relative motion difference and is analogus to land identification. The technique requires only one channel of carefully gridded data and is free of atmospheric radiative transfer corrections necessary in other multi-channel compositing schemes.

#### INTRODUCTION

Variability in the ocean is the current focus of many research studies in physical oceanography. The Gulf Stream System in particular has been studied, with increasing attention being given to its temporal and spatial scales. The correlation of movements between the stream's meanders and the velocity field in the western Sargasso Sea is a subject of intense interest in the upcoming POLYMODE project.

Conventional tracking of the Gulf Stream's cyclonic edge (left-hand edge facing downstream) requires extensive commitments of research vessel time to obtain quasi-synoptic pathlines of the current. It has been repeatedly demonstrated that infrared sensing satellites are capable of providing occasional synoptic views of the cyclonic edge, but no sequence of pathlines has been constructed. This lack of satellite derived sequences is due to the difficulty of

an objective cloud discrimination technique in daily observations from polar orbiting vehicles.

In order to obtain a pathline from daily observations, two simultaneous channels of satellite information are required. The visible channel is used to identify clouds in the scene by their characteristically high radiance. Then, unless an areally clear day occurred, other days are required in a composite. Compositing usually is further complicated by the need to correct each clear day for the atmospheric attenuation (Maul, 1973) so that the data have a common base. The process is lengthy and requires considerable computer time to solve the radiative transfer equation, manipulate the data matrices, contour the final composite, and output the results.

#### APPLICATION OF GEOSYNCHRONOUS DATA

The Synchronous Meteorological Satellite (SMS-1) is the first geosynchronous vehicle to have an infrared channel in the scanner. Ground resolution is approximately the same as the high resolution scanning radiometer on the NOAA or NIMBUS satellites, 8 km at the nadir. SMS scans the earth every 30 minutes so that 48 images are made every day, day and night. Film loops are made from the individual images by photographing them in sequence after they are registered and gridded by Fujita's method (1969). These infrared film loops are then used to locate the Gulf Stream's cyclonic edge.

The Gulf Stream can be located because there is a temperature increase when crossing into the current across the cyclonic edge. This is a permanent feature of the stream north of Cape Hatteras. As the stream flows out to sea from the Carolina Capes, it meanders much like an exponentially growing sinusoid. The wavelength is typically 300 km, amplitude is 50 km, and phase speed approximately 8 cm sec 1 (Hansen, 1970). The low phase speed means that a meander will shift only 35 km in five days; five days is the average time between frontal passages in mid-latitudes, and thus is the time between periods of cloudiness. Therefore, for temporal scales up to five days, the Gulf Stream can be considered quasi-stationary and treated like land or any other permanent feature. Conversely, the stream can be used to assist in accurate gridding of the SMS data.

Infrared film loops are made for periods of from one to five days in order to locate the current. The loops are projected down onto a base map, and the steady cyclonic edge of the Gulf Stream is sketched as the cloud patterns quickly advect past. Locating the steady signal from the land and quasi-stationary current is very easy as is shown in the film loop (presented at the conference). Any one single frame would not accomplish the goal as well because it is not possible to distinguish between clouds and ocean with the same temperature. However, with the relative motion of clouds being two orders of magnitude faster than the phase speed of the current's meanders, the identification task is simple. Figure 1 is a still frame from SMS-1



Figure 1. Infrared image from SMS-1 of the western North Atlantic. Light tones represent cold temperatures in this 10.5-12.5 um band passed image. The warm (dark tone) Culf Stream can be followed from Florida to the offing of Cape Hatteras. Gridding along the Atlantic Coast is accurate enough to keep motion of the quasi-stationary stream's edge within one or two scanspots in the film loop (shown at the convention). The image in this figure and the film loop were produced by the Miami Satellite Field Services Station of the NOAA National Environmental Satellite Service.

showing the gridding, land, and current in the infrared channel.

Experience to date has shown that stream-edge pathlines can be made on a daily basis when cloud conditions permit. Daily motion of the meanders is less than the scan spot size of SMS so that no motion at all is detected. Longer loops over several days may show slight motion of the meanders, but the jitter in the film loop due to gridding is often-times more than the movements of the current. The film loops to date have been standard production-type NOAA products displaying a small sector of the ocean which has been enlarged. Contrast stretched images are known to bring out the ocean features; this will be an improvement over using the standard product. From the daily pathlines, a film loop of the meanders of the stream is easily made using existing photographic equipment.

#### CONCLUSIONS

Infrared film loops from an operational geosynchronous satellite have been used to locate the cyclonic edge of the Gulf Stream. The technique requires only one channel of spacecraft data; no extensive computer time, atmospheric transmittance corrections, or new display techniques are required. Pathline sequences of the major baroclinic flows in mid-latitudes are possible using only analog data, and can be easily accomplished by a technician. With further refinement of the operational technique, a Gulf Stream position map in near-real time could become part of the routine service of NOAA to the maritime community. Experience to date suggests that these pathlines can be made at intervals of three to five days. This is adequate for most requirements of ship routing, weather forcasting, and scientific investigation into the nature of the western boundary currents.

#### REFERENCES

- Fujita, T. (1969) Present Status of Cloud Velocity Computations from the ATS-1 and ATS-3 Satellites. Space Research IX, University of Chicago Press, pp. 557-570.
- Hansen, D. V. (1970) Gulf Stream Meanders between Cape Hatteras and the Grand Banks, <u>Deep Sea Research</u> Vol. 17, pp. 1 - 17.
- Maul, G. A. (1973) Infrared Sensing of Ocean Surface Temperature, in Advances in the Astronautical Sciences, F. S. Johnson (Ed.), A. A. S., Tarzana, Ca., pp. 451-464.

95

# On the Use of the Earth Resources Technology Satellite (LANDSAT-1) in Optical Oceanography

GEORGE A. MAUL

National Oceanic and Atmospheric Administration, Atlantic Oceanographic and Meteorological Laboratories, Physical Oceanography Laboratory, Miami, Florida 33149

and

## HOWARD R. GORDON

Department of Physics, Optical Physics Laboratory, University of Miami and Rosenstiel School of Marine and Atmospheric Science, Coral Gables, Florida 33124

Observations of the Gulf Stream System in the Gulf of Mexico were obtained in synchronization with LANDSAT-1. Computer enhanced images, which are necessary to extract useful oceanic information, show that the current can be observed by color (diffuse radiance) or sea state (specular radiance) effects associated with the cyclonic boundary even in the absence of a surface thermal signature. The color effect relates to the spectral variations in the optical properties of the water and its suspended particles, and is studied by radiative transfer theory. Significant oceanic parameters identified are: the probability of forward scattering, and the ratio of scattering to total attenuation. Several spectra of upwelling diffuse light are computed as a function of the concentration of particles and yellow substance. These calculations compare favorably with experimental measurements and show that the ratio of channels method gives ambiguous interpretative results. The results are used to discuss features in images where surface measurements were obtained and are extended to tentative explanation in others.

#### Introduction

The location of ocean currents by infrared radiometers in aircraft and satellites has been demonstrated, and is in fact operationally successful from aircraft over the Gulf Stream. The statistical correlation between the surface thermal signature of the Gulf Stream and the velocity core was studied and it was shown (Hansen and Maul, 1970) that north of Cape Hatteras, there is a thermal indication of the cyclonic edge (left hand side facing downstream in the northern hemisphere) at all seasons. Atlases, however (e.g., Robinson, 1973), show that major portions of the Gulf Stream system have no surface thermal gradients due to seasonal heating for as much as four months of the year.

The cyclonic edge of Gulf Stream type flows are frequently well-defined, and can often be observed by noting changes in temperature, salinity, color, and sea state (Stommel, 1966; Uda, 1938). Color changes imply that the optical properties of the ocean change in the vicinity of the cyclonic edge. If those optical properties are observable when the thermal signature is lost, a year-round remote sensing technique is potentially available.

Remote sensing of the ocean in the visible region of the spectrum is being explored for a variety of reasons. Maximum insolation at 475 nm provides a natural energy source for passive sensors. A minimum in the attenuation coefficient for water may allow a passive measurement of some oceanic properties as a function of depth. Variations in the

©American Elsevier Publishing Company, Inc., 1975

spectra of upwelling light at these wavelengths can be attributed to variations in pigment forming molecules such as in phytoplankton, and to variations in the concentration of scattering particles such as suspended sediments. Strongly baroclinic currents are potentially detectable by changes in the optical properties across their boundaries. Patterns of man's activities in and on the ocean have near surface manifestations that change the nature of upwelling visible radiance.

Discussions in the present paper use examples of the optical properties of the Gulf Stream System from the Yucatan Strait to Cape Hatteras as detected by the Earth Resources Technology Satellite (LANDSAT-1). This intense ocean current transports vast amounts of thermal and kinetic energy through the eastern Gulf of Mexico and up the southeast coast of the United States. Temporal and spatial variability in the flow and its optical and biological changes were studied as part of a one-year (August 1972-September 1973) ground truth time-series in which a

research vessel followed the anticyclonic turning from Yucatan to the Florida Straits (Maul, 1975; Ednoff, 1974). Analysis of the simultaneous ship/satellite observations obtained in the eastern Gulf of Mexico every 36 days are extended to discuss data from other regions of the Gulf Stream.

LANDSAT-1 is a polar orbiting research and development satellite originally designed to return seven channels of data; one instrument failed (channels 1-3) early in the mission. The ground swath is 185 kilometers wide and the revisit time is 18 days. The sensors of the multispectral scanner are in the visible and near infrared (reflected infrared) region. Pertinent details of the multispectral scanner (MSS) are given in Table 1. The satellite does not receive any information from the blue portion of the spectrum (400-500 nm). In the discussion to follow, it will be seen that this is a severe limitation for oceanography, since most of the spectral information observed at the sea surface is contained in this spectral interval. Atmospheric

TABLE 1

Multrispectral Scanner Specifications<sup>a</sup>

Band	Bandpass (nm)	Nominal radiance response $(mW cm^{-2} sr^{-1})$	Digital steps (quantized onboard)
MSS-4	500-600	0-2.48	128
MSS-5	600-700	0-2.00	128
MSS-6	700-800	0-1.76	128
MSS-7	800-1100	0-4.60	64

<sup>&</sup>lt;sup>a</sup>The Earth Resources Technology Satellite's multispectral scanner is quantized onboard and the data relayed in a digital bit stream. An oscillating mirror system reflects upwelling radiation into six detectors for each channel so that six scanlines of the earth are observed simultaneously. Energy for each quantum step can be estimated by assuming a linear relationship over the 128 (64) steps (NASA, 1971).

effects will not be addressed in great detail since this was recently done by Curran (1972) and others.

# Hydrographic Background

Prior to the launch of LANDSAT-1, a field experiement was performed to confirm that the satellite had the capability to observe the ocean color changes associated with the Gulf Stream and to determine surface vessel measurements required to obtain satisfactory ground

truth. The location of the cyclonic boundary of the current was obtained by tracking the 22°C isotherm at 100 meters depth using expendable bathythermographs. The pathline of this isotherm was shown by Leipper (1970) to be an effective means of tracking the velocity core of the current, and Maul (1975) showed that the average horizontal separation between the indicator isotherm and the cyclonic edge is 14.4 km. Figure 1 is a south-north section through the cyclonic front of the Gulf Loop Current near Dry Tortugas. These

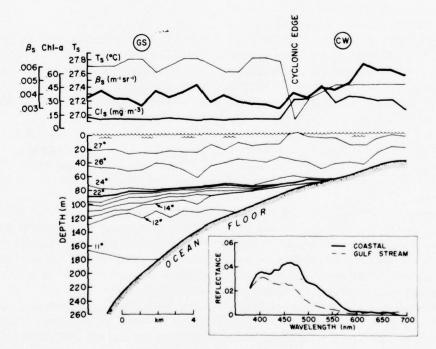


FIG. 1. South to North (left to right) across section of the Gulf Stream's cyclonic boundary. Isotherms in the thermal cross section are in degrees Celsius. The cyclonic edge marks not only where temperature, scattering, and chlorophyll values change, but also salinity, current velocity, and frequently sea state. Inset are reflectance spectra, one taken in the Gulf Stream (GS), the other taken in the coastal water (CW). Mixed layer depth suggests that the optical properties that affect spectra are homogeneous for at least 20 meters.

data were collected during a joint ship/aircraft experiment on 27-28 June 1972, and are representative of the variability in temperature, scattering, chlorophyll-a concentration, and spectra.

The surface temperature field  $(T_s)$ shows a marked decrease near the current's edge. This thermal signature completely disappears for three or four months when summer insolation makes these waters isothermal, thus rendering infrared techniques useless. The subsurface thermal field reflects early summer conditions: mixed layer depth of approximately 20 meters, gentle slope of the warmer isotherms (i.e., 22°C), and steeper slope of cooler isotherms (i.e., 15°C) when going toward the current core; the core of the current is further offshore (to the left) than this section shows. Details of the boundary between the east flowing current (out of the plane of the page) and the coastal waters are emphasized to demonstrate the need to use visible techniques for remote sensing in tropical and subtropical waters.

Surface profiles of chlorophyll-a concentration (Chl-a) and the volume scattering function at  $45^{\circ}$  ( $\beta_s(45^{\circ})$ ) made during the transect are shown along with the thermal signature. Light scattering measurements were made during the experiment using a Brice-Phoenix light scattering photometer and a blue (436 nm) filter; the volume scattering function was calculated using

$$\beta(45^\circ) = \frac{aTD}{h\pi} \cdot \frac{D(45^\circ)}{D(0^\circ)} \cdot \tau \sin 45^\circ,$$

where a is the ratio of the working standard diffuser to the reference stan-

dard diffuser, TD is the transmittance of the reference standard diffuser, h is the dimension of the irradiated element, D is the deflection of the galvonometer and  $\tau$  is the transmittance of the neutral density filters. Chlorophyll-a measurements were made  $in\ vitro$  on a fluorometer calibrated with pure chlorophyll-a. The calibrations were checked on a spectrophotomer, and calculations were made using the SCOR/UNESCO (Strickland and Parsons, 1968) equation:

CHI-
$$a = 11.64 E_{663} - (2.16 E_{645} + 0.10 E_{630}),$$

where E is the extinction (defined as the logarithim of the reciprocal of transmittance) and subscripts are the applicable wavelength in nanometers. These techniques are used for all values reported herein.

The profiles in Fig. 1 demonstrate that the general level of scattering is 0.7 X  $10^{-3} \text{ m}^{-1} \text{ sr}^{-1}$  (18%) more in the coastal water than in the current. Similarly the chlorophyll-a concentration is 0.2 mg  $m^{-3}$  (100%) more in the coastal water. This is the general situation observed in these transects, especially near the coast. However, many times there was no distinct change of these indicators of optical properties across the cyclonic edges, and there were incidences where scattering from an isolated sample was higher in the current. The slight peak in Chl-a just before reaching the edge is a common feature (Lorenzen, 1971), which was related by Maul (1973) to the accumulation mechanism of the edge of these currents.

Spectra of upwelling irradiance at 1 meter depth and downwelling irradiance

from the sun and sky 3 meters above the water surface were made during the ship/aircraft experiment. Reflectance ratios (uncorrected for the immersion effect) are graphed as an inset on Fig. 1. Approximate locations of these observations in the Gulf Stream (GS) and coastal waters (CW) are indicated on the top of the figure. The reflectance in coastal waters is generally higher than in the current, and the wavelength of maximum reflectance is shifted to higher values. This is in agreement with the expected spectral behavior (to be discussed below) and is supported by color aerial photographs taken concurrently; a distinct discontinuity in color from the green of the coastal water to the blue of the Gulf Stream occurred at the point labeled cyclonic edge in Fig. 1. These spectra show that there are significant differences in the upwelling radiance in both the MSS-4 and MSS-5 bandpasses, and thus it appeared useful to attempt a year-long ship/satellite experiment.

# Some Theoretical Considerations

At this point it is useful to consider in detail the processes contributing to the radiance spectrum  $N(\lambda)$  at the position of the satellite. Solar radiation incident at the top of the atmosphere is absorbed and scattered in the atmosphere. Some radiation is scattered back into space without striking the ocean, contributing a radiance  $N_a(\lambda)$  at the satellite. The rest (which is not absorbed) will interact with the ocean. This interaction can yield upwelling radiance above the ocean in three ways: (1) specular reflection from the surface or glitter, (2) diffuse

reflection from foam (bubbles) on or just beneath the ocean surface, and (3) the diffuse reflection from water molecules and suspended particles in the water. Of these, the first two phenomena are closely related in that they depend on the sea state, while the third source of radiance is essentially independent of sea state. The specular reflectance from the rough ocean surface can be computed by the methods of Cox and Munk (1954) in terms of the wind speed and incident radiance distribution. The diffuse reflectance from white caps can be approximately accounted for by assuming they are "white", Lambertian, and have an albedo of 1 so that they contribute uniform upwelling radiance just above the surface given by

$$\frac{H_0(\lambda)f}{\pi}$$
,

where f is the fraction of the scene covered by the white caps and  $H_0(\lambda)$  the irradiance incident on the sea surface. The third source of radiance, that from beneath the surface, is the most difficult to compute and will be discussed in detail below.

The radiance at the satellite can be written as

$$N(\lambda) = N_a(\lambda) + \gamma(\lambda) N_s(\lambda) + \alpha(\lambda) N_d(\lambda), (1)$$

where  $N_s(\lambda)$  is the contribution at the surface due to reflection from the surface and whitecaps,  $N_d(\lambda)$  is the diffuse radiance just above the surface due to photons that have penetrated the ocean,  $\alpha(\lambda)$  and  $\gamma(\lambda)$  are atmospheric transmittance factors for  $N_d(\lambda)$  and  $N_s(\lambda)$ .  $\alpha(\lambda)$  and  $\gamma(\lambda)$  are in general not equal

since the radiance distribution (variation with angle) of  $N_s(\lambda)$  and  $N_d(\lambda)$  are different. It is possible for photons to be reflected from the surface, backscatter from the atmosphere into the ocean, and scatter back into the atmosphere. Photons that do this are considered to be a part of  $N_d(\lambda)$ . It should be stressed at this point that  $N_d(\lambda)$  in the above equation is the only source of radiance that contains information about conditions beneath the sea surface such as the concentration and composition of suspended particles and dissolved organic material. A thorough understanding of the dependence of  $N_d(\lambda)$  on the basic optical properties of the water and its constituents is required in order to obtain quantitative information about the constituents of the ocean from measurements of  $N_d(\lambda)$ .

Assume that the radiance distribution incident on the sea surface is given, and that the radiance is transmitted from the ocean to the satellite in a known manner given by  $\alpha(\lambda)$  and  $\gamma(\lambda)$  in Eq. (1). This reduces the problem to that of taking a known downwelling radiance distribution just above the sea surface, and computing the distribution (just above the surface) of the upwelling radiance. As mentioned above, radiant energy interacting with the ocean can be absorbed by water, suspended particles, and dissolved organic material commonly called yellow substance (Gelbstoff; Kalle, 1938) with absorption coefficients  $a_w$ ,  $a_p$ ,  $a_y$ , respectively, and scattered by the water and particles with scattering coefficients  $b_w$  and  $b_p$  (scattering by the yellow substance appears to be negligible). The total attenuation

coefficient, c, for these interactions is given by

$$c = c_w + c_p + c_v, \tag{2}$$

where

$$c_w = a_w + b_w,$$

$$c_p = a_p + b_p,$$

$$c_v = a_v$$
(3)

are the beam attenuation coefficients of the water, particles, and yellow substance. The scattering is further characterized by the phase function,  $P(\Theta)$ , which relates to the intensity of radiation,  $dJ(\Theta)$ , singly scattered from a small sample volume, dv, when illuminated by an incidence irradiance,  $H_0$ , through

$$P(\Theta) = \frac{dJ(\Theta)}{H_0 dv b} ,$$

$$2\pi \int_0^{\pi} P(\Theta) \sin\Theta d\Theta = 1.$$
(4)

The total phase function for water and particle scattering is

$$P(\Theta) = \frac{(b_w P_w(\Theta) + b_p P_p(\Theta))}{(b_w + b_p)},$$

where  $P_{\rm w}$  and  $P_{\rm p}$  are the phase functions due to water only and particles only, respectively. It is convenient to further define the forward (F) and backward (B)single scattering probabilities by

$$B \equiv 1 - F ,$$

$$F \equiv 2\pi \int_{0}^{\pi/2} P(\Theta) \sin \Theta d\Theta ,$$
(5)

and the single scattering albedo by

$$\omega_0 \equiv \frac{b}{c}$$
. (6)

Hence it is clear that

$$B = \frac{(b_p B_p + b_w B_w)}{(b_p + b_w)} , (7$$

$$\omega_0 = \frac{(b_w + b_p)}{(a_w + a_p + a_y + b_p + b_w)}, \quad (8)$$

and in general,

$$0 \le \omega_0 \le 1$$
.

It should be noted that all of the above quantities depend on wavelength ( $\lambda$ ).

The transfer of radiation in the ocean is governed by the radiative transfer equation, which has been discussed in detail by Chandrasekhar (1960) and Preisendorfer (1965). Gordon and Brown (1973) have computed the diffuse reflectance (upwelling irradiance  $\div$  incident irradiance) just above a flat, homogenous ocean as a function of its optical properties by a Monte Carlo technique. Using a combination of the parameters that arise naturally from Gordon's (1973) scattering model, Gordon, Brown, and Jacobs (1975) show that the diffuse reflectance  $[R_d(\lambda)]$  can be written

$$R_d(\lambda) = 0.179x + 0.0510x^2 + 0.1710x^3$$
, (9)

where

$$x \equiv \frac{B\omega_0}{[1-\omega_0 F]} \ .$$

 $R_d(\lambda)$  is, to first order, independent of the distribution of the incident irradiance. It should be emphasized that the above equation does not include the irradiance specularly reflected from the sea surface or the bottom, i.e.,  $R_d(\lambda)$  is the contribution to the reflectance from photons that penetrate the surface and are multiply scattered back into the atmosphere. Preliminary computations (Gordon and Brown, unpublished) indicate that Eq. (9) is also valid for a moderately rough surface. The radiance distribution above the sea surface (due to photons scattered out of the ocean) is only weakly dependent on  $\omega_0$ , and thus the radiance at any viewing angle will, in first order, vary with  $\omega_0(\lambda)$  and  $B(\lambda)$  in the same fashion as  $R_d(\lambda)$ . Hence, it is sufficient to study the influence of the optical properties of the ocean on  $R_d(\lambda)$ alone.

Equation (9) shows that the important oceanic parameters are  $\omega_0(\lambda)$  and  $B(\lambda)$ , and so the observed reflectance spectrum,  $R_d(\lambda)$ , can be explained entirely through a knowledge of  $\omega_0(\lambda)$  and  $B(\lambda)$ . Conversely, under optimum conditions only  $\omega_0(\lambda)$  or  $B(\lambda)$  can be deduced from  $R_d(\lambda)$  and then only if one of these quantities is already known. The situation appears quite depressing when it is realized that  $\omega_0(\lambda)$  is only imperfectly known even for pure water and to our knowledge there are no measurements of  $B_p(\lambda)$  and  $\omega_0(\lambda)$  for various kinds of suspended particles. Hence at the present time it is difficult to interpret  $\omega_0(\lambda)$  and  $B(\lambda)$  even if both could be extracted from  $R_d(\lambda)$  measurements. This underscores the necessity of laboratory experimentation to determine these optical properties for various ocean constituents such as marine phytoplankton, and suspended mineral particles, for adequate interpretation of oceanic "color". If the optical properties of the constituents are known, then it is theoretically possible to determine their concentrations through observations of  $R_d(\lambda)$  as is discussed in several examples below.

A particularly simple problem of interpretation, that of determining the concentration of suspended material in the absence and presence of yellow substance, is now examined. The particles are assumed to be nonabsorbing, and their scattering coefficient is assumed to be independent of wavelength [cases where  $b_p = (\text{const}) \lambda^{-n}$  with  $n \le 1$  have also been investigated and yield results not dramatically different from the n = 0case]. These calculations will not apply at all to locations with particles containing absorbing pigments such as phytoplankton in the water, because Mueller (1973) and Gordon (1974) have shown that scattering from such particles varies strongly with wavelength near the pigment absorption bands.

In order to use Eq. (9),  $B(\lambda)$  and  $\omega_0(\lambda)$  in Eqs. (7) and (8) must be determined. For water,  $B_w = 0.5$  and

$$b_w = 0.00154 (530 \text{ nm/}\lambda)^4,$$
 (10)

is taken from Jerlov (1968).

To find  $B_p$ , Petzold's (1972) measurements of  $P(\Theta)$  from the Tongue of the Ocean (TOTO), San Diego Harbor (SDH), and Off Shore California (OSC) at 530 nm have been used. Assuming the above for  $b_w(\lambda)$  and  $B_w(\lambda)$ , the contribution from water is subtracted yielding

TABLE 2

Derived Values of  $B_D$  for the Indicated Locations

тото	SDH	OSC
0.01899 (.59)	0.01869 (.82)	0.01089 (.59)
0.02436 (.25)	0.01950 (.83)	0.00989 (.55)
0.02044 (.26)	0.01718 (.91)	

the  $B_p$  values listed in Table 2 ( $\omega_0(\lambda)$  is given in the parenthesis). From Table 2 it is clear that  $B_p$  not only varies considerably from one location to another, but also varies considerably for a single region. This is unfortunate because for small  $\omega_0(\lambda)$ ,  $R_d(\lambda)$  is directly proportional to  $\omega_0 \cdot B$ , and  $\omega_0(\lambda)$ , and  $B(\lambda)$  are then equally important in determining  $R_d(\lambda)$  for these cases. It will be assumed that Table 2 gives the range of variation of  $B_p$  to be expected in natural waters, however, this may not be the case. Furthermore  $B_p$  is assumed to be independent of wavelength.

For a given  $b_p(\lambda)$ ,  $a(\lambda)$  must be known in order to compute  $\omega_0(\lambda)$ . To find this  $a_w(\lambda)$  is needed, which unfortunately has not been determined experimentally for pure water or clear ocean water. Tyler and Smith (1970), however, have measured K(z,-) (the downwelling irradiance attenuation coefficient) for the clear waters of Crater Lake, Oregon. Since Preisendorfer (1961) has shown that (under conditions found in Crater Lake)

$$a(z) \leq K(z, -), \tag{11}$$

if it is assumed  $a_w(\lambda) = K_{\lambda}(z, -)$  for z = 10 meters the depth at which the smallest  $K_{\lambda}(z, -)$  values are found, then the

resulting  $a_w(\lambda)$  values will represent an upper limit to the spectral absorption coefficient of clear natural waters. Because of this the  $K_{\lambda}(z,-)$  data of Tyler and Smith have been smoothed and used for  $a_w(\lambda)$  in this paper.

Since  $a_p$  is taken to be zero, only  $a_y(\lambda)$  remains to be considered. This is taken from Jerlov (1968) and is parameterized by

$$a_y(\lambda) = a_y e^{0.0145(530-\lambda)}$$
,

where  $\lambda$  is in nm. Reasonably high concentrations of yellow substance in the open ocean have  $a_y \approx 5 \times 10^{-3} \text{ m}^{-1}$  (i.e., near Galapagos Islands), however,  $a_y$  can be much larger in coastal regions.

The reader should note that the above model differs significantly from those given in an earlier report (Maul and

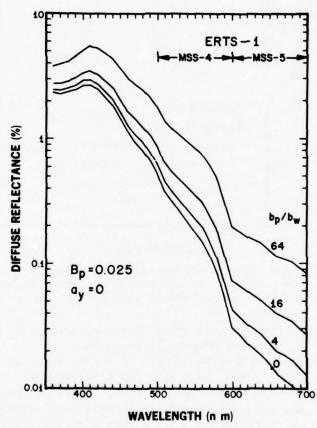


FIG. 2. Log-lin plot of computed diffuse reflectance spectrum for the fraction of back scattered light = 0.025, the yellow substance absorption coefficient = 0, and for various values of the ratio of the particle scattering coefficient to the water scattering coefficient. Note that the spectrum changes shape in a wavelength dependent fashion; a similar result occurs if sea state changes are included in upwelling radiance spectrum (see Fig. 8).

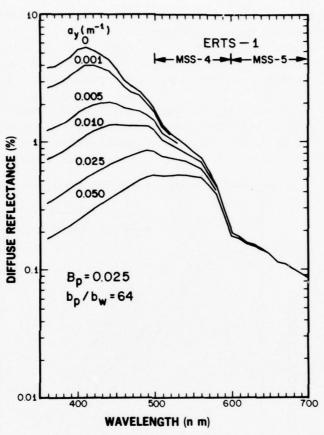


FIG. 3. Computed diffuse reflectance spectrum for the portion of backscattered light = 0.025 and the particle to water scattering coefficient ratio = 64 for varying values of yellow substance absorption. The LANDSAT-1 MSS-4 and MSS-5 bandpass response is labeled at the top.

Gordon, 1973). The difference arises from the fact that herein an upper limit to  $a_w(\lambda)$  is determined from Eq. (11), while in the previous work, the  $a_w(\lambda)$  estimates of Tyler, Smith and Wilson (1972) were used. For consistancy this required the use of filtered sea water data for  $b_w(\lambda)$  rather than the actual Rayleigh scattering coefficient given by Eq. (10). As discussed below, the present model results in better quantitative

agreement between the calculations and observation.

Using the above and Eq. (9),  $R_d(\lambda)$  has been computed as a function of  $b_p/b_w$  at 530 nm (proportional to the concentration of suspended particles) for values of  $B_p$  and  $a_y(\lambda)$  which it is felt covers the range of these variables found in nature. Figure 2 shows  $R_d(\lambda)$  for  $B_p = 0.025$  and  $a_y = 0$  as a function of  $b_p/b_w$ . These spectra have the same general

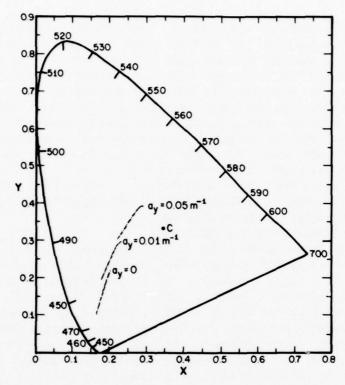


FIG. 4. Chromaticity diagram with the data used in Figs. 2 and 3 (and others) plotted for a fraction of backscattered light = 0.025; the scattering ratios are 4 (lower left), 8, 16, 32, 64, 128, 256, 512, and 1024 (upper right) for each of the three values of the absorption coefficient due to yellow substance.

shape as those observed by Tyler and Smith just beneath the surface in Crater Lake, and when the transmittance loss through the water surface is taken into account, the  $b_p/b_w=64$  curve is in rough quantitative agreement with the Crater Lake observations. It should be noted that, since the  $a_w(\lambda)$  being used is certainly too large in the blue portions of the spectrum, the reflectance there will be somewhat larger than shown in the figure for a given  $b_p/b_w$ . Note that increasing the concentration of sus-

pended material increases  $R_d(\lambda)$  at all wavelengths, however, the effect is most dramatic in the red. Figure 3 shows the influence of yellow substance on the reflectance for  $B_p = 0.025$  with  $b_p/b_w = 64$ . Clearly the main influence of  $a_y(\lambda)$  is to depress the blue region of the reflectance spectrum while leaving the red portion of the spectrum unchanged.

To provide an objective measure of the visual effects produced by varying concentrations of suspended particles and yellow substance, in Fig. 4 the chromaticity coordinates of  $R_d(\lambda)$  for  $a_v$ = 0, 0.01 and  $0.05 \text{ m}^{-1}$  on the C.I.E. chromaticity diagram (Committee on Colorimetry, 1953) are presented. As  $b_p/b_w$  or  $a_v(\lambda)$  is increased the dominant wavelength in the ocean color increases while the spectral purity decreases, i.e., increasing the concentration of particles that scatter light independently of wavelength (white scatterers) does not, as one might expect, move the chromaticity coordinates directly toward the white point (C), but rather shifts the dominant wavelength toward the green as well as decreasing the purity. It is interesting to note that the ocean reflection spectra for such a wide range of water properties  $(b_p = 0 \text{ and } a_y = 0)$ through  $b_p = 1.6 \text{ m}^{-1}$  and  $a_v = 0.05$ m<sup>-1</sup>), when represented on the chromaticity diagram, produce a sequence of colors that fall on a near straight line from (x,y) = (0.15, 0.10) to (0.30, 0.40). On the basis of Figs. 2 through 4 it is clear that the spectrum of diffusely reflected light from the ocean contains significant information concerning the concentration of suspended material and yellow substance.

Now turn briefly to the question of the depth of water over which this information can be retrieved. Gordon and McCluney (1974) have treated this problem in detail; they show that for a homogeneous ocean, the depth above which 90% of the diffusely reflected irradiance originates  $(Z_{90})$ , is the depth at which the downwelling irradiance falls to 1/e of its value at the surface, or

$$Z_{90}(\lambda) = 1/K_d(\lambda) , \qquad (12)$$

where  $K_d(\lambda)$  is the irradiance attenuation coefficient (this is the attenuation coefficient for diffuse light in the sea and should not be confused with the beam attenuation coefficient c). Gordon, et al. (1975) have found that if the incident irradiance on the sea surface is in the form of a collimated beam making an angle  $\Theta_0$  with the zenith,

$$K_d = c (1.0016 - 0.9959\omega_0 F + 0.1089\omega_0^2 F^2 - 0.1527\omega_0^3 F^3)/\cos\Theta_0'(13)$$

where  $\sin\Theta_0' = 0.75 \sin\Theta_0$ . If the incident irradiance is completely diffuse, Eq. (13) is still valid if  $1/\cos\Theta_0$  is taken to be 1.197. Equation (13) can be used to compute  $K_d(\lambda)$  as long as  $\omega_0(\lambda) \leq 0.95$ , and hence can be combined with Eq. (12) to give  $Z_{90}(\lambda)$ .  $Z_{90}(\lambda)$  has been computed for the cases discussed above, and it is found that for  $0 \le b_p/b_w \le 100$ ,  $Z_{90}(\lambda)$  is nearly independent of  $b_p/b_w$  for a given  $a_v(\lambda)$ .  $Z_{90}(\lambda)$  does however, depend very strongly on  $a_v(\lambda)$  and this is shown in Fig. 5. The main influence of  $a_v(\lambda)$  on  $Z_{9,0}(\lambda)$  is to decrease the penetration depth strongly in the blue while again leaving  $Z_{9,0}(\lambda)$  in the red unchanged. Since  $F = 1 - B \approx 1$ , Fig. 5 is essentially independent of  $B_p$ , so the penetration depth is roughly independent of the concentration and properties of the particles (assuming they do not absorb radiation). For small  $a_v(\lambda)$ , the maximum  $Z_{9,0}(\lambda)$  is of the order of 50 to 60 meters, so this is the maximum depth to which information concerning the ocean properties can be obtained through measurement of  $R_d(\lambda)$ .

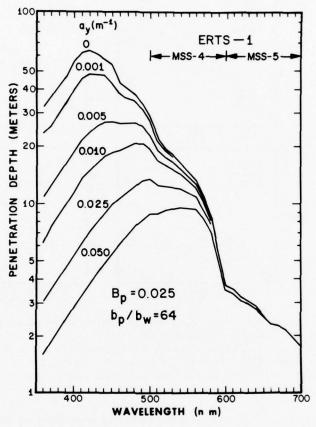


FIG. 5. Penetration depth  $(Z_{90})$  as a function of wavelength for  $B_p = 0.025$ ,  $b_p/b_w = 64$  and for  $0 \le a_y \le 0.050$ . Note that the penetration depth in MSS-5 is essentially independent of yellow substance, however, MSS-4 is significantly affected.

In order to apply these results to LANDSAT-1,  $R_d(\lambda)$  must be integrated over the MSS channels of interest (4 and 5). Figure 6 shows the mean reflectance ( $\bar{R}_d$ ) averaged over MSS-4 and MSS-5 as a function of  $b_p/b_w$  for various values of  $B_p$  and  $a_y(\lambda)$ . It is evident that  $\bar{R}_d$  depends nearly linearly on  $b_p/b_w$  with the actual relationship between  $\bar{R}_d$  and  $b_p/b_w$  strongly dependent on  $B_p$  and

 $a_y(\lambda)$ . The dependence on  $B_p$  is very important because it shows that  $\bar{R}_d$  cannot be quantitatively interpreted in the absence of information concerning the scattering particles. Likewise it is seen that variations in the concentration of yellow substances could be misinterpreted as variations in particle concentrations in MSS-4. However,  $\bar{R}_d$  for MSS-5 is for all practical purposes independent

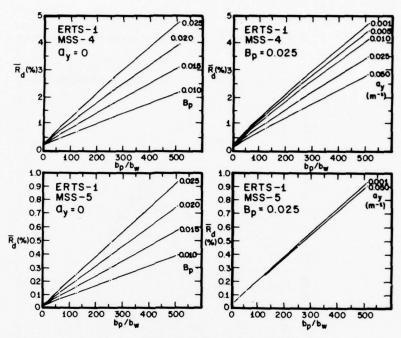


FIG. 6. Computed average reflectance for the MSS-4 filter (upper panels) and the MSS-5 filter (lower panels) as a function of the ratio of particle scattering coefficient to the water scattering coefficient. Lefthand panels show the effect of varying the fraction of forward scattered light and the righthand panels show the effect of varying the concentration of yellow substance on the upper curve of the lefthand panels. Note the linearity depends on both  $a_y$  and  $B_p$  for MSS-4, but only on  $B_p$  for MSS-5.

of  $a_y(\lambda)$ , and in this respect, it is the best channel to try and observe variations in  $b_p/b_w$ .

Figure 7 shows the mean penetration depth averaged over the LANDSAT-1 channels according to

$$\bar{Z}_{90} = \frac{\int_{\lambda_1}^{\lambda_2} Z_{90}(\lambda) R_d(\lambda) d\lambda}{\int_{\lambda_1}^{\lambda_2} R_d(\lambda) d\lambda}$$
(14)

for the case where  $B_p=0.025$  (remember  $Z_{90}(\lambda)$  is nearly independent of  $B_p$ ). Clearly  $Z_{90}$  is only a weak function of the

concentration of particles in both channels, however, it depends very strongly on  $a_y(\lambda)$  in MSS-4. For the open ocean, Fig. 7 indicates penetration depths of the order of 15 to 18 meters for MSS-4 and about 3 meters for MSS-5. Hence even though MSS-5 is the better channel for observation of  $b_p/b_w$  (because of its independence of  $a_y(\lambda)$ ), the variations in  $b_p/b_w$  that can be observed are only those that take place in the upper 2-3 meters. It should be emphasized again that the above discussion refers only to the case of no phytoplankton (chlorophyll).

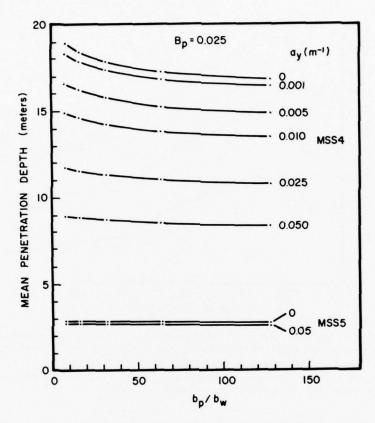


FIG. 7. Mean penetration depth vs the ratio of particle scattering coefficients to water scattering coefficient, averaged over the MSS-4 and MSS-5 filter functions. Backscattering fraction is 0.025; absorption coefficient for yellow substances is varied from 0 to 0.050 in each channel.

Equation (1) identified three components to the radiation received by a satellite: diffuse radiation from beneath the sea, atmospheric radiation, which is mostly scattered light, and the radiation reflected from the sea surface itself. Because the surface component to N can dominate the scene (i.e., sunglint), attention is now turned to investigating sea state effects on upwelling spectral irradiance.

Let  $\rho(\Theta)$  be the Fresnel reflectance

from a calm surface where again  $\Theta$  is the zenith angle (angle of incidence). Then the total reflectance ( $\rho$ ) from the ocean's surface, in the absence of foam, white caps, and glitter, is given by

$$\rho = \frac{\int_0^{2\pi} \int_0^{\pi/2} \rho(\Theta) N_0 \sin\Theta \cos\Theta d\Theta d\psi}{\int_0^{2\pi} \int_0^{\pi/2} N_0 \sin\Theta \cos\Theta d\Theta d\psi} , (15)$$

where the integration is over  $2\pi$  Steridians  $(\Theta, \psi)$ . Even though  $N_0(\lambda)$  is

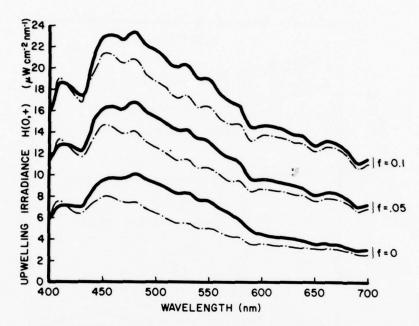


FIG. 8. Theoretical spectra computed for three fractions of the sea surface covered with white caps, foam, or specular reflectors. Solid line uses the ratio of particle scattering to water only scattering of 128; dashed line uses 32 for the ratio. Yellow substance absorption coefficients used were 0.01 and 0.001 for the solid and dashed lines, respectively. This represents summer (low solar zenith angle) conditions at the latitude of the Gulf of Mexico.

strongly dependent on wavelength, Sauberer and Ruttner (1941) have shown that for zenith angles less than  $40^{\circ}$ ,  $\rho$  is essentially nondispersive. Therefore, Anderson's (1954) value of  $\rho = 0.03$  is adopted for zenith angles  $<40^{\circ}$ , and it is assumed constant for the 400-700 nm interval of interest. The upwelling irradiance from the ocean above the sea surface (H(0,+)) is the sum of the diffuse component from beneath the surface  $(R_d H(0,-))$ , and the surface component  $(\rho H(0,-))$ .

Cox and Munk (1954) have shown that for solar zenith angles less than 70°, Fresnel's law is valid in a Beaufort 4

wind ( $\sim$ 8 m sec<sup>-1</sup>). As white caps and foam cover larger areas of the sea surface, however,  $\rho$  will be altered because these features are approximately Lambertian, nondispersive, and have an albedo of 1. Thus, they contribute uniform irradiance above the surface (f·H(0,-)) where, as before, f is the fraction of the sea covered by these diffuse reflectors. Therefore

$$H(0,+) = R_d H(0,-) + (\rho(1-f) + f)H(0,-).$$
 (16)

The computed spectrum of upwelling irradiance for solar zenith angles less than  $40^{\circ}$  as a function of f is given in

Fig. 8. Values of H(0,-) observed by Tyler and Smith (1970) in the Gulf Stream at 25° 45′N on 3 July 1967 are used in Eq. (16). The dashed lines are for values of  $b_p/b_w = 32$ ,  $a_y = 0.001$  and are representative of Gulf Stream waters. The solid lines use  $b_p/b_w = 128$ ,  $a_y = 0.01$  and are representative of coastal waters (compare the f=0 case with the insert to Fig. 1).  $B_p = 0.025$  for these calculations (cf. Fig. 2 and 3.).

Consider the spectrum where 10% of the sea is covered, and the spectrum where no white caps or foam are present. Not only has the intensity changed but the shape is also altered. The solar spectrum is fairly flat in the visible region: H(0,-) @ 550 nm  $\div H(0,-)$  @ 650 nm  $\approx 1.2$ . High sea states, which reflect nonselectively, will add relatively more long wavelength energy to the upwelling irradiance. Clark, Ewing, and Lorenzen (1970) have attempted to minimize

these effects in the measurement of ocean spectra from aircraft by observing the ocean at Brewster's angle (directed away from the sun) through a polarizing filter. The degree to which these calculations affect their results is not known. For LANDSAT-1, the MSS views the earth at angles ±5° from the nadir without polarizing filters. The sun's glitter affects the upwelling radiance (Strong, 1973), and this is a function of the solar declination. Similarly other sea state effects on the upwelling spectra change the radiance in an MSS band.

In Fig. 9(a) the irradiance is plotted as a function of f for the central wavelength of the MSS-4 and MSS-5. The curves are linear as expected from Eq. (16) and are wavelength dependent. At 550 nm the irradiance increases more quickly with f than at 650 nm. This is due to the shape of the solar spectrum and the ratio discussed above. In Fig.

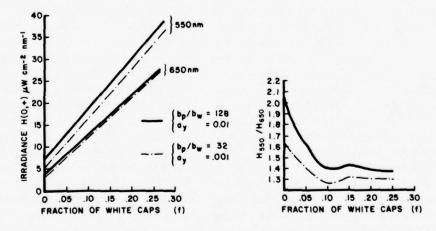


FIG. 9. (a) Upwelling irradiance in the LANDSAT-1 MSS-4 (550 nm) and MSS-5 (650 nm) intervals as a function of sea state for the two water types used in Fig. 4.1. Solid and dashed lines are as in other figures. (b) Irradiance ratio as a function of fraction of surface reflectors. The ratio is seen to be a function of both water type and sea state.

9(b) is plotted the irradiance ratio H(0,-) @ 550 nm ÷ H(0,-) 650 @ nm as a function of f. The ratio decreases rapidly as the sea state builds, but then tends to level off. Further, the ratio is not the same for the two water types chosen here, which means that sea state effects are not only a function of the fraction of white caps, but also the optical properties of the water itself. Unless the spot size of a remote sensor is small enough to discriminate white caps, the effects of sea state will not only alter the interpretation of the in situ optical properties of the water, but will dominate the spectral variability.

The linear dependence of upwelling irradiance as a function of the fraction of white caps (f) suggests that a simple correction scheme for sea state effects is possible (Fig. 9(a)). At longer wavelengths (>700 nm) the absorption coefficient for water becomes very large, and the  $N_s(\lambda)$  component of Eq. (1) is the dominant oceanic variable. At approximately 1000 nm, in the reflected infrared, the absorption coefficient for water reaches a maximum, and the transmittance of the atmosphere is also a maximum. If  $N_a(\lambda)$  can be obtained, or reduced to a standard value (e.g., Curran, 1972), then an absolute measure of N at 1000 nm provides a measure of f in a cloud-free atmosphere.

Several investigators have proposed using the radiant energy at a few wavelengths to infer concentrations of chlorophyll-a in multispectral scanner outputs (Szekielda, 1973), in differential radiometers (Arveson, 1972), from slopes in aircraft spectra (Clark et al.), and in photographs (Baig and Yentsch, 1969).

From the above discussion it is seen that such ratios, differences, and slopes are strongly influenced by sea state; this factor was not considered in their work.

### **Spectroradiometer Observations**

Optical properties of the ocean as they relate to the upwelling spectrum at the sea surface must be understood before LANDSAT-1 data can be interpreted. Upwelling irradiance from 3 meters above the surface given in Fig. 10 was observed using the same 1/4 meter Ebert spectroradiometer used for the reflectance spectra in Fig. 1. These observations were made during the time frame of Fig. 14 and represent the water types shown in that image. All spectra were carefully selected to represent approximately the same downwelling irradiance, sea state, sun angle, cloud cover, and absence of bottom influence. Specular reflection due to waves was minimized by preselecting ten spectra with similar shapes that did not contain anomalous random peaks. From digitized records, averages and standard deviations  $(\sigma)$ were computed at 7 nm wavelength intervals; if values exceeded the average by lo, they were rejected and a new mean computed. Absolute values of the spectra are traced to NBS through the 2-meter integrating sphere at NASA's Goddard Space Flight Center; reported values have a ±3% error band (L. Blaine, personal communication).

The data in Fig. 10 can be used to interpret ocean color as measured by the multispectral scanner. The energy in an MSS band at the sea surface is

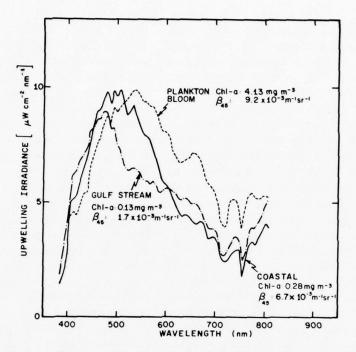


FIG. 10. Observed upwelling spectral irradiance in the Gulf of Mexico, November 1972. The three spectra represent typical observations during the time series, and show the shift of the dominant wavelength to larger values with increasing surface chlorophyll-a. These spectra include the surface component  $N_{5}$ .

$$N(0,+) = \int_0^\infty \phi(\lambda) \left[ N_s(\lambda) + N_d(\lambda) \right] d\lambda, \quad (17)$$

where  $\phi(\lambda)$  is the filter function of the multispectral scanner; N is in units of watts cm<sup>-2</sup> sr<sup>-1</sup>, and  $\phi$  is approximately a gate function for each MSS band  $(\phi(MSS-5)\approx 1$  for  $600 \leq \lambda \leq 700$ , and 0 otherwise). The spectra in Fig. 10 are upwelling irradiance (H(0,+)) and are related to upwelling radiance (N(0,+)); Eq. 17)

$$N_d \propto R_d(0,-) \cdot H(0,-) = H(0,+).$$
 (18)

Using Eq. (17), the spectra were inte-

grated over the MSS-4, MSS-5, and MSS-6 filter functions in order to investigate the properties of these three water types as LANDSAT-1 ground truth. The highest irradiance values for the Gulf Stream, coastal water, and plankton bloom all occur in MSS-4; the lowest is in MSS-6 with MSS-5 midway between. The plankton bloom is distinguished by having the highest irradiance in each channel. The coastal water has a higher irradiance in MSS-4 than the Gulf Stream, but the situation is reversed in MSS-5.

In the preceding section, the effect of sea state on ratios and differences was

discussed. To test techniques of ratios, sums, and differences on comparable spectra, a series of numerical tests were made from the integrated irradiances. Combinations of all three channels for one water type were compared with the same combinations for the other water types. It was quite easy to differentiate on the basis of such calculations between the Gulf Stream waters and the coastal waters, and between the coastal waters and the plankton bloom, however, it was not possible to distinguish between the Gulf Stream and the plankton bloom. For example, MSS-4  $\div$  MSS-5 is 1.4 for the Gulf Stream, 1.7 for the coastal water, and 1.4 for the plankton bloom. This suggests, as the theory implies (Eq. (9)), that even in the absence of sea state changes, the ratio test (MSS-4 ÷ MSS-5) is not likely to be successful in specifying the chlorophyll-a concentration.

Clark et al., noted that the slopes of their aircraft spectra correlate quite closely with chlorophyll concentrations. They did not specify the spectral region where the slopes were calculated. The spectra in Fig. 10 have peaks at 470 nm in the Gulf Stream and at 530 nm in the plankton bloom. From the theoretical discussion on the effects of  $\omega_0(\lambda)$  and  $B(\lambda)$  on  $R_d(\lambda)$ , it would be fortuitous if these slopes represented changes in the chlorophyll only. There may of course, be biogeographic regions where chlorophyll and spectra are canonically related (Duntley, 1972). However, since the data in Fig. 10 represent near-surface spectra, an ocean color multispectral scanner should have channels centered near 470 and 530 nm. The effect of the atmosphere (Hovis, Foreman and Blaine, 1974; Curran, 1972) is to markedly alter the upwelling radiance at satellite altitudes, particularly at shorter wavelengths (<500 nm). The fact remains that significant ocean information is contained between 470 and 530 nm, and these wavelengths must be considered along with a sea state channel at 1000 nm.

The peak in the plankton bloom spectra at 675 nm (Fig. 10) has been explained by Gordon (1974) as being caused by anomalous dispersion in the particles, which cause scattering near the chlorophyll-a absorption band. The maximum in the absorption band occurs at 665 nm. The effect on the upwelling radiance is to cause the spectra to behave like the negative derivative of the absorption in the vicinity of 665 nm, i.e., a minimum in  $R_d(\lambda)$  occurs at 655 nm, and a maximum at 675 nm. This suggests that two very narrow channels at 655 nm and at 675 nm in an ocean color sensor would be useful in identifying plankton blooms and determining whether the absorbing pigments are in the particles or dissolved in the water.

Probably the most efficient method of determining the concentration of the constituents in the ocean will be to compare theoretical and experimental spectra, adjusting the constituent concentrations in the theoretical spectra until agreement is found. This of course requires a basic understanding of the optical properties of the constituents, which can be derived only from careful in situ and laboratory experiments. At the present time much energy and money are being expended for optical methods to locate and study materials with nearly unknown optical properties

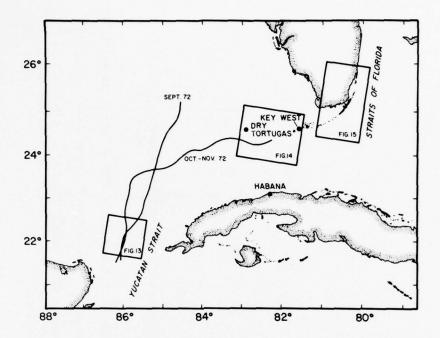


FIG. 11. Location of the LANDSAT-1 images in Fig. 13, 14 and 15 are superimposed on a map of the southeastern Gulf of Mexico. The pathlines are the location of the 22° C isotherm at 100 meters depth for September 27-28, 1972 and November 2-3, 1972. These cruises were made at 36 day intervals, in synchronization with every other ERTS transect (after Maul, 1975).

only poorly known optical properties. Lack of knowledge of the optical parameters affecting reflectance must be be made.

# Satellite Observations

Several examples of LANDSAT-1 observations of the Gulf Stream system are given in Figs. 13, 14, and 15. The location of each of these images is given in Fig. 11, which also includes pathlines of the 22°C isotherm at 100 meters

suspended or dissolved in a medium with depth made during satellite transit. As noted before, this isotherm is generally  $\sim 14 (1\sigma = \pm 10)$  kilometers to the left (facing upstream) of the cyclonic edge, overcome before significant progress can but has significant variability about this mean value due to surface winds, curvature in the current, and current speed. It is seen that significant variability exists in these pathlines, only 36 days apart, which emphasizes the need for synopicity in oceanographic baseline measurements for remote sensing.

> Diffuse reflectance from beneath the ocean is rarely more than 0.05 (cf., inset to Fig. 1). Reflectance from the ocean's surface, which is independent of this



FIG. 12. LANDSAT-1 scanline plot across the loop current front. Top scanline is MSS-4, next MSS-5, MSS-6, and MSS-7 on the bottom. The large energy spikes are clouds. At scan spot number 950 there is an increase in the average value of the digital number of 1 or 2; this marks the cyclonic edge of the current.

diffuse reflectance, has been shown to be comparable or even substantially larger depending on sea state. Reflectance from clouds and agricultural scenes however, is sometimes an order of magnitude greater than from the ocean, even in the 500-600 nm wavelength region. In order for the NASA Data Processing Facility to produce an image for an average scene radiance, the ocean signal is compressed into the lowest few gray scales. This is clearly illustrated in Fig. 12 which is a scanline plot across the boundary of the Loop Current from the multispectral scanner. The large spikes in all four channels are clouds; there seems at first glance to be very little change in digital number (DN), which is proportional to radiant intensity, as a function of the sample number. However, careful examination shows that the average value of the DN at samples greater than the number 950 is slightly larger than those before this point. It will be shown that this marks the transition to higher radiances caused by increased sea state in the current.

In order to graphically display this small change over a two-dimensional region, computer enhancement is necessary. Techniques for ocean radiance levels have been studied by Maul, Charnell, and Qualset (1974), and an extension of their results will be used here. The technique discussed here is a modification that allows automatic selection of the *DN* range for a given ocean scene.

The ocean radiance from MSS-7 (800-1100 nm) is all constrained to  $0 \le DN \le (0-0.29 \text{ mW cm}^{-2} \text{ sr}^{-1})$ . The low radiances are caused by the very large values of the absorption coefficient of

water at these wavelengths. Clouds (cf. Fig. 12) and land however, have large near infrared reflectance and are almost always above the DN range cited. This allows the computation of a binary mask wherein all DN < 4 in MSS-7 are set to 1 and all others are set equal to 0. The data matrix of an MSS band of interest when masked, leaves only the ocean values for statistical analysis.

Cox and Munk (1954) have shown that the frequency distribution of ocean radiances is Gaussian to a very good approximation. Within the limits of resolution of the spacecraft data, histograms of masked MSS-4 or MSS-5 radiances are also approximately Gaussian, which is consistent with the results of Cox and Munk. Gaussian properties will be used, but with the reservation that the coarse radiance quantization of LANDSAT-1 over the ocean departs from the continuous function, especially at large standard deviations. The masked matrix is contrast stretched by computing a stretch variable (ζ) from

$$\zeta = M \left[ \frac{(\overline{DN} + \kappa \sigma) - DN}{2\kappa \sigma} \right]^n, \quad (19)$$

where M is the maximum value allowed by the digital to analog output device,  $\overline{DN}$  is the average scene radiance,  $\kappa$  is a constant,  $\sigma$  is the standard deviation about  $\overline{DN}$ , and n is a constant. If it is desired to include 95% of the masked data,  $\kappa$  =2; for 99%  $\kappa$  =3, etc. All values of  $\overline{DN} > (\overline{DN} + \kappa\sigma)$  are set to  $(\overline{DN} + \kappa\sigma)$  and similarly those values of  $DN < (\overline{DN} - \kappa\sigma)$  are clipped. Equation (19) produces a negative image of the input digital image. Positive whole integers n further stretch the low radiance

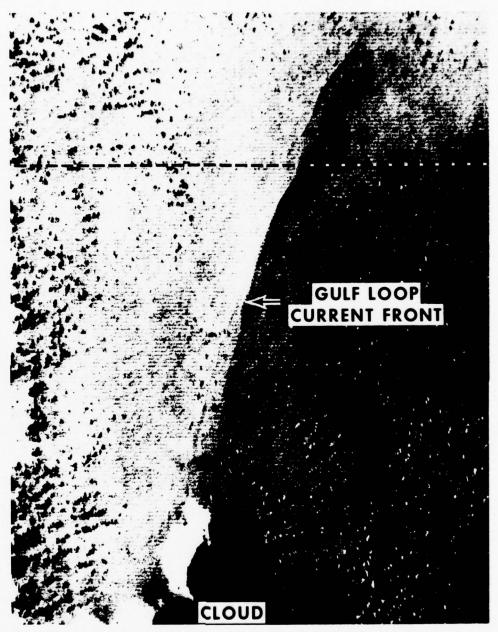


FIG. 13. Negative print of computer enhanced  $(9 \le DN \le 13; n=1)$  MSS-5 image of the cyclonic boundary of the Gulf Loop Current. Surface vessel track confirmed the location of the current to be the darker shade (higher radiance) region on the righthand side of the image (ERTS ID 1065-15411). Scanline plot in Fig. 12 is taken along the dashed line in the middle of the scene. Horizontal distance across the image is 90 kilometers.

values, but this produces a nonlinear output and must be avoided when comparing images to ocean spectra. The graphic result of using this equation on the scanline data from which Fig. 12 was taken is given in Fig. 13.

Figure 13 is a negative print of the area due north of the Yucatan Strait using MSS-5 data. Computer enhancement in this image uses only five grey scales of the 128 levels available; all values below  $(\overline{DN} - 2\sigma)$  are set to 127 and all above  $(\overline{DN} + 2\sigma)$  are set to 0. The boundary between the resident Gulf waters (left) and the current (right) is seen as a transition from light to dark tones, respectively. The exponent n was set equal to 1 for this experiment. Figure 14 is an enhancement of the Loop Current boundary located in Fig. 11, which uses MSS-4 data. In this negative image of the western Florida Keys, water from Florida Bay extends into the Florida Straits and is entrained by the Florida Current. MSS-4 can detect both absorption and scattering changes whereas MSS-5 is essentially limited to scattering effects as shown theoretically in Figs. 2 and 3. The current boundary in both Figs. 13 and 14 was delineated by surface vessel tracks during the day of the satellite transit.

In the time period of Fig. 13, the winds were from the northeast at 12-14 m/sec, whereas in Fig. 14 they were easterly at 3-5 m/sec. When wind and waves run in opposition to a current, the waves quickly steepen, break and generate white caps and foam on the surface. For weather conditions such as encountered during the trackline used to support Fig. 13, Ross and Cardone

(1974) report that as much as 10% of the sea surface will be covered with these diffuse reflectors. Shipboard records confirm this, but the sea state was much higher in the current than in the resident Gulf waters. The effect of these conditions on the upwelling irradiance was given in Fig. 8. Consider that the sea state in the current causes the f = 0.1spectrum and that in the resident Gulf waters is given by the f = 0.05 spectrum labeled coastal water. In the MSS-5 bandpass interval, H(0,+) is larger in the current than in the coastal water; the high radiance values on the right hand side of Fig. 13 come from the current. MSS-5 is more sensitive to small sea state changes than MSS-4. MSS-5, therefore, is a better choice for locating the Gulf Loop Current in the open sea, because there the optical properties of the current and surrounding waters are not significantly different (Maul, 1975).

In the observations of Fig. 14, a different conclusion is drawn. Shipboard records show that the sea state was the same in both waters. Here the upwelling radiance is dominated by the  $R_d H(0,-)$  component, and the color change allows detection of the current's boundary. Thus, it is seen that the current can be detected with opposite radiance distribution depending on the dominance of surface or subsurface variables. This can work against locating the current if both sources of energy, in and out of the current, add up to the same net radiance.

An interpretation of coastal observations from LANDSAT-1 is given in Fig. 15, which is a computer enhanced MSS-6 negative image of southeastern Florida. The dark lineation paralleling



FIG. 14. Negative print of computer enchanced  $(12 \leqslant DN \leqslant 32; n=1)$  MSS-4 image of Marquesa Key and Key West (ERTS ID 1099-15293). Change in radiance southwest of Marquesa from dark to light coincides with the ship located boundary between the higher radiance Florida Bay water and the lower radiance Gulf Stream. Bottom depth is in excess of 100 meters at the cyclonic edge, and does not contribute to the radiance. Horizontal distance across the image is 135 kilometers.

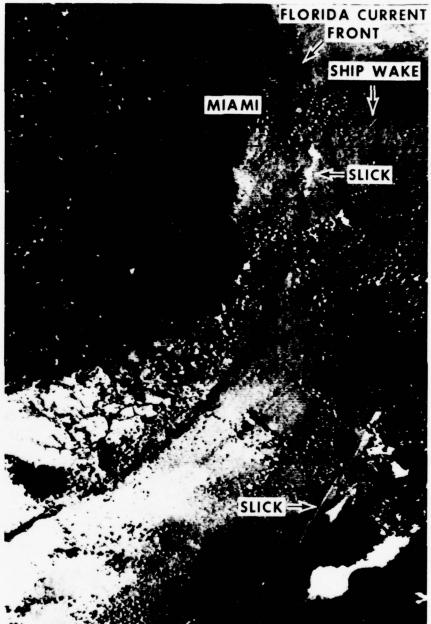


FIG. 15. Negative print of computer contrast stretched  $(7 \le DN \le 15; n=2)$  LANDSAT-1 image of South Florida (ERTS ID 1026-15230). The Florida Current can be seen as a line of dark lineation parallel to the coast; bottom is essentially invisible in this MSS-6 scene. A ship can be seen by its characteristic V-shaped wake just offshore of Miami Beach. Possibly the Virginia Key sewer outfall area can be observed by its low reflectance due to an organic slick. Horizontal distance across the image is 90 kilometers.

the coast in the upper portion of the image is a zone of high reflection caused by locally increased  $N_s$  along the edge of the Florida Current. The increase in surface reflectance is probably caused by surface wave interaction with the cyclonic boundary and is not bottom influence. Another example of the dominance of  $N_s$  is the bright slick areas (low N) off the Virginia Key sewer treatment plant. This probably is caused by the dampening of the glitter causing capillary waves in the oil film (Stumpf and Strong, 1974) associated with the organic slick. The slick, which appears to have drifted south past the popular Key Biscayne beaches, offers an explanation of the narrow lineation offshore in the Florida Straits: a passing ship heading south that is pumping her bilges would cause a similar feature on the image. Note that the organic slicks observed here strongly affect the upwelling radiance and this must also affect the ratios discussed earlier. The glitter pattern's non-uniformities further contribute to the complication in analyzing these data for quantitative results.

# Estimation of Suspended Particle Concentrations

The cyclonic boundary has been shown to be a region where the volume scattering function changes, which implies that suspended particle concentration also changes. This suggests that the ratio of scattering due to particles to that of water also changes, and attention is now turned to the problem of estimating  $b_p/b_w$  or some related quantity

from satellite observations. Since the above theoretical calculations are only for the case of negligible phytoplankton (chlorophyll) concentrations, criteria must be found from which to choose the LANDSAT-1 channels that will satisfy this constraint. Also unless only MSS-5 is used, it is expected that yellow substance is important especially in coastal regions where river runoff, etc. may be considerable. Furthermore, there is the additional problem that the reflectance depends on  $B_p$ , which is also unknown, as well as  $b_p/b_w$ . A method is now developed that partially overcomes some of these problems. Considering the radiances observed in MSS-4 and MSS-5, approximately

$$N_4 = \alpha_4 N_{d4} + \gamma_4 N_{s4} + N_{a4} ,$$

$$N_5 = \alpha_5 N_{d5} + \gamma_5 N_{s5} + N_{a5} ,$$
(20)

where  $\alpha_i$  and  $\gamma_i$  (i = 4, 5) are the fractions of  $N_{di}$  and  $N_{si}$  (measured at the sea surface) that reach the sensor. It is assumed that  $\alpha_i$  and  $\gamma_i$  are constant over a LANDSAT-1 frame (if they vary in a known way, their influence is easily accounted for and will not be discussed further). Now from the theory (see again Fig. 6)

$$N_{d4} = k_4 \frac{b_p}{b_w},$$

$$N_{d5} = k_5 \frac{b_p}{b_w},$$
(21)

where  $k_4$  and  $k_5$  are essentially independent of  $b_p/b_w$ , but dependent directly on  $B_p$ . Taking the horizontal gradient,  $\nabla H$ , of Eq. (20) using Eq. (21),

$$\nabla_{H} N_{i} = k_{i} \alpha_{i} \nabla_{H} \left( \frac{b_{p}}{b_{w}} \right) + \gamma_{i} \nabla_{H} N_{si} ; \qquad (22)$$

since  $N_{ai}$  is nearly constant over a frame  $\nabla_H N_{ai} = 0$ . The last term in Eq. 22,  $\nabla_H N_{si}$ , is the horizontal gradient of the reflected radiance from the sea surface. This is nearly zero everywhere except where the sea state changes dramatically with horizontal distance (for example in Figs. 13 and 15). Nearly everywhere on the frame  $\nabla_H N_{si} = 0$ , so

$$\frac{\nabla_H N_4}{\nabla_H N_5} = \frac{k_4 \alpha_4}{k_5 \alpha_5} \tag{23}$$

Again  $\alpha_4/\alpha_5$  is constant (or slowly varying) over the scene. Thus, almost everywhere in the frame, variations in  $\nabla_H N_4 / \nabla_H N_5$  are the result of variations in  $k_4/k_5$ . Now if  $B_p$  is constant, or if the "mean"  $B_p$  is constant in each wavelength band, this would imply that only the concentration of scattering particles varies over the frame, i.e., not the nature of particles or their size distribution. In this case,  $k_4/k_5$  would be constant. Essentially k4/k5 will vary if the nature or size distribution of the particles varies over the frame  $(B_n)$ changes), or if the yellow substance concentration varies considerably over the frame, which would force  $k_4$  to vary independently of  $k_5$ . If it is found that

$$\frac{\nabla_H N_4}{\nabla_H N_5} = \text{Constant}, \tag{24}$$

it is reasonable to expect that only the particle concentration changes over the frame. In this case

$$\nabla_H N_4$$
 or  $\nabla_H N_5 \sim \nabla_H$  (particle concentration). (25)

These relations should also apply to scenes containing phytoplankton if they are the dominant scatterers; for mixtures of phytoplankton and suspended white particles, one would expect Eq. 24 to be violated over a scene if the relative concentrations vary drastically. To reiterate, if Eq. (24) holds, probably only the particle concentration varies over the frame, and Eq. (25) can be used to measure the gradient of its concentration. Since  $B_p$  is unknown, the actual concentration is indeterminate without ground truth to better than a factor of two, since this is the assumed uncertainity in  $B_p$ .

Equation (25) was applied to MSS-4 and MSS-5 in Fig. 16. This computer enhanced negative image of the Cape Hatteras region shows what appears to be large gradients in suspended sediment. The Gulf Stream apparently has entrained particles from Raleigh Bay and is carrying them out to sea. Along the scanline shown in Fig. 16.

$$\frac{\partial}{\partial x} \left[ N_4 \right] = g \, \frac{\partial}{\partial x} \left[ N_5 \right] + h \tag{26}$$

has been computed.

The least squares value for g is 0.38, for h is 0.00, and the linear correlation coefficient, r, is 0.74. The coefficient of determination,  $r^2$ , which is the ratio of the explained variation from the mean (by the least squares line) to the total variation, is 55%. Physically this means that this image may be useful for determining particle concentrations but

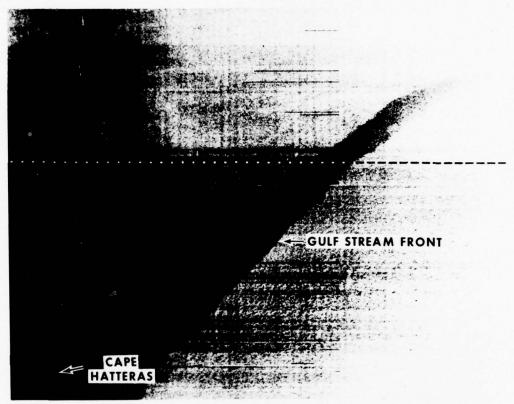


FIG. 16. Contrast stretched ( $4 \le DN \le 12$ ; n=2) negative image of the ocean area offshore of Cape Hatteras (ERTS ID 1132-15042). The Gulf Stream can be seen as the bright area to the south of the entrained sediment from the coastal estuaries. The least squares fit of Eq. (26) was done along the scanline north of the Cape and extending from nearshore, through the suspended sediment and into the current. Extensions of this plume were observed for 150 kilometers further east on other LANDSAT-1 images. Horizontal distance across the image is 135 kilometers.

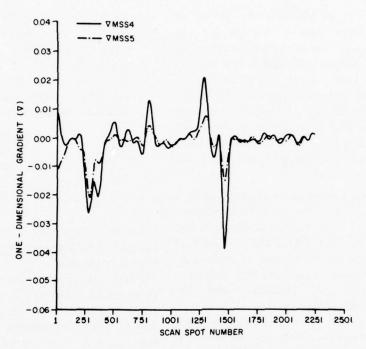


FIG. 17. Gradient of radiance received at the satellite in MSS-4 and MSS-5 along the ocean line shown on Fig. 16. Scan spot numbers arbitrarily start at 1, which is just off the image in the previous figure and over the coast.

 $B_p$ ,  $\omega_0$  (i.e.,  $a_y$ ), or  $b_p/b_w$  may be changing. The extent to which this holds true in natural waters is unknown; this will be extensively tested in the New York Bight area where turbidity measurements are being made by NOAA vessels concurrent with LANDSAT-1 and 2 transits (cf. Maul, et. al., 1974).

Figure 17 is a plot of the horizontal gradient from MSS-4 and MSS-5 along the scanline marked in Fig. 16, and least square analyzed by Eq. (26). The data have been filtered with a low-pass Lanczos kernel, 6 db down at 100 scan spots. As an example of the need to filter these data, consider again the raw scan line plot in Fig. 12, when the

derivative is taken, the high wave number variability dominates, and little useful information can be extracted.

Samples 1-100 or so are on land, but the remainder are over water. MSS-4 appears to follow MSS-5 quite well in the ocean area, even though the coefficient of determination is low. The gradient in MSS-5 is larger than in MSS-4. This is caused by loss of contrast in MSS-4 due to atmospheric scattering and is the reason many ocean investigators using LANDSAT-1 data prefer MSS-5.

#### Conclusions

This research has been primarily

undertaken to evaluate the use of an ocean color sensing satellite for observing currents in the subtropics. The Gulf of Mexico was chosen as a test site because there, the cyclonic boundary of the Gulf Stream System cannot be detected by infrared techniques during the summer, and this current is the major circulation feature of the eastern Gulf.

From the results of this study, it has been shown that:

- 1. Using ocean color sensing satellites to detect the Gulf Loop Current (and other baroclinic flows) is feasible, but LANDSAT-1 is not an ideal vehicle because of sensor gain settings, multispectral scanner wavelength channels, and the 18-day revisit cycle.
- 2. Currents can be detected by color sensing satellites in two ways: a color change across the cyclonic boundary (changes in the optical properties of the water), and a change in sea state at that boundary (changes in surface albedo). That is, the current boundary can be detected by changes in the surface reflectance,  $N_s$ , as well as the diffuse reflectance,  $N_d$ , from below the surface;  $N_d$ , however, is dependent on both  $B(\lambda)$  and  $\omega_0(\lambda)$ , and thus the spectral interpretation of the ocean color requires surface truth measurements for meaningful results.
- 3. Particle concentrations, which can delineate currents, can be estimated in MSS-5 if the ratio  $\nabla_H N_4 / \nabla_H N_5$  is reasonably constant over a scene. MSS-4 is strongly influenced by yellow sub-

stance, and particle estimation based on these data are invalid in many coastal zones.

4. Radiance range of LANDSAT-1 bandpass sensors for the ocean, is estimated from the computer enhanced images to be

MSS	Range (mW cm $^{-2}$ sr $^{-1}$ )
4	0.15-0.75
5	0.05-0.35
6	0.05-0.25
7	0.05-0.40

Contrast stretching is required to obtain useful information for ocean current boundary location.

Finally it must be emphasized that these results are invalid if bottom reflection is encountered. In very turbid waters, where the penetration depth of light is small, these techniques may be extended into very shallow waters. These turbid, shallow regions are frequently rich in yellow substance however, and extreme caution must be exercised in inferring suspended particle concentration.

We wish to acknowledge the assistance of R. L. Charnell and R. M. Qualset for many fruitful discussions and computer programming. This work was in part supported by NASA contract S-70246-AG.

#### References

Anderson, E. R. (1954), Energy Budget Studies, in Water Loss Investigations: Lake Hefner Studies, U.S. Geological Survey Professional Papers 269, pp 71-117. Arvesen, J. C. (1972), Fourth Annual Earth Resources Review, Vol. IV, NASA MSC-05937, pp 104-1 to 104-2.

Baig, S. R., and C. S. Yentsch (1969), Appl. Opt. 8(12), 2566-2568.

Chandrasekhar, S. (1960), Radiative transfer, Dover, New York, 393 pp.

Clark, G. L., G. C. Ewing, and C. J. Lorensen (1970), *Science* 167, 1119-1121.

Committee on Colorimetry of the Optical Society of America (1953), *The Science of Color*, Optical Society of America, Washington, D.C.

Cox, C., and W. Munk (1954), J. Opt. Soc. Am. 44(11), 838-850.

Curran, R. J. (1972), Appl. Opt. 11 (8), 1857-1866.

Duntley, S. Q. (1972), Fourth Annual Earth Resources Review, Vol. IV, NASA MSC-05937, pp 102-1 to 102-25.

Ednoff, M. E. (1974), Surface phytoplankton communities and their relationship to the Loop Current in the Gulf of Mexico, Master's thesis, Florida State University, Department of Oceanography, Tallahassee, 187 pgs.

Gordon, H. R. (1973), Appl. Opt. 12, 2804-2805.

Gordon, H. R., and O. B. Brown (1973), Appl. Opt. 12, 1549-1551.

Gordon, H. R. (1974), J. Opt. Soc. 64 (6), 773-775.

Gordon, H. R., and W. R. McCluney (1974), *Appl. Opt.* **14**, 413-416.

Gordon, H. R., O. B. Brown, and M. M. Jacobs (1975), Appl. Opt. 14, 417-427.

Hansen, D. V., and G. A. Maul (1970), Remote Sensing of Environment 2, 161-164.

Hovis, W. A., M. L. Forman, and L. R. Blaine (1974), Detection of ocean color changes from high altitudes, NASA GSFC X -652-73-371, Greenbelt, Md., 25 pp.

Jerlov, N. G. Optical Oceanography, Elsevier, New York, 194 pgs.

Kalle, K. (1938), Ann Hydrol. Marine Mitt. 66, 1-13.

Leipper, D. F. (1970), J.G.R. 75 (3), 637-657. Lorenzen, C. J. (1971), J. du Conseil Int'l Pour l'Exploration de la Mer 34, (1), 18-23.

Maul, G. A. (1973), Symposium on Significant Results Obtained from the Earth Resources *Technology Satellite-1*, NASA SP-327, Vol. 1 (B), pp 1365-1375.

Maul, G. A., and H. R. Gordon (1973), Proceedings, Third ERTS-1 Symposium, Vol. 1 (B), NASA SP-351, pp. 1279-1308.

Maul, G. A. (1975), An Evaluation of the Use of the Earth Resources Technology Satellite for Observing Current Boundaries in the Gulf Stream System, NOAA Technical Report (in press).

Maul, G. A., R. L. Charnell, and R. H. Qualset (1974), Remote Sensing of Environment 3 (4), 237-252.

Mueller, J. L. (1973), PhD. Dissertation Oregon State University, Corvalis, Oregon, 239 numbered leaves.

NASA (1971), Earth Resources Technology Satellite Data Users Handbook, NASA Document No. 71SD4249.

Petzold, T. J. (1972), Volume Scattering Functions for Selected Ocean Waters, Scripps Institution of Oceanography, Visibility Laboratory SIO Ref. 72-28, 82 pgs.

Preisendorfer, R. W. (1961), *Monogrs. I.U.G.G.* (10), 11-30.

Preisendorfer, R. W. (1965), Radiative Transfer on Discrete Spaces, Pergamon, New York, 462 pgs.

Robinson, M. K. (1973), Atlas of Monthly Mean Sea Surface and Subsurface Temperature and Depth of the Top of the Thermocline Gulf of Mexico and Caribbean Sea, Scripps Institution of Oceanography References 73-8, 105 pgs.

Ross, D. B., and V. Cardone (1974), J. Geophys. Res 79 (3), 444-452.

Sauberer, F., and F. Ruttner (1941), Akademie Verlag, Berlin, 240 pgs.

Stommel, H. (1966), The Gulf Stream, California, pp 62-65.

Strong, A. E. (1973), ERTS-1 anomalous dark patches, National Technical Information Service, NASA CR-1333115; E73-10747, Springfield, Va.

Strickland, J. D. H., and T. R. Parsons (1968), A Practical Handbook of Seawater Analysis, Fisheries Research Board of Canada, Ottawa, 311 pgs.

Stumpf, H. G., and A. E. Strong (1974), Remote Sensing of Environment 3 (1), 87-90. Szekielda, K.-H. (1973), Proceedings of the Fall Convention ASP-ASCM October 2-5, 1973, pp 664-719.

Tyler, J. E., and R. C. Smith (1970), Measurements of Spectral Irradiance Underwater, Gordon and Breach, New York, 103 pgs.

Tyler, J. E., R. C. Smith, and W. H. Wilson, Jr. (1972), J. Opt. Soc. 62 (1), 83-91. Uda, M. (1938), Geophysical Magazine 11 (4), 307-372.

Received 2 May 1975; revised 19 May 1975

Reprinted from: NOAA Technical Report ERL 328-AOML 17, 46 p.



U.S. DEPARTMENT OF COMMERCE Frederick B. Dent, Secretary

NATIONAL OCEANIC AND ATMOSPHERIC ADMINISTRATION
Robert M. White, Administrator
ENVIRONMENTAL RESEARCH LABORATORIES
Wilmot N. Hess, Director

# NOAA TECHNICAL REPORT ERL 328-AOML 17

# **Examination** of Water Movement in Massachusetts Bay

DENNIS A. MAYER

BOULDER, COLO.
January 1975

# DISCLAIMER

The Environmental Research Laboratories do not approve, recommend, or endorse any proprietary product or proprietary material mentioned in this publication. No reference shall be made to the Environmental Research Laboratories or to this publication furnished by the Environmental Research Laboratories in any advertising or sales promotion which would indicate or imply that the Environmental Research Laboratories approve, recommend, or endorse any proprietary product or proprietary material mentioned herein, or which has as its purpose an intent to cause directly or indirectly the advertised product to be used or purchased because of this Environmental Research Laboratories publication.

# CONTENTS

			Page
ABS	STRACT		0
1.	INTRO	DUCTION	1
2.	DESCR	IPTION OF THE EXPERIMENT	2
	2.1	Eulerian Measurements	2
	2.2	Lagrangian Measurements	6
3.	MEAN	MOTIONS	7
	3.1	Direction Data	7
	3.2	Vector Time Series of 40-Hr Lp Data	11
	3.3	Temperature Time Series	19
	3.4	Spectra of Current Meter Data	23
4.	DROGU	E TRACKS	28
5.	ACKNO	WLEDGMENTS	45
6.	REFER	ENCES	46

## EXAMINATION OF WATER MOVEMENT IN MASSACHUSETTS BAY

## Dennis A. Mayer

#### ABSTRACT

NOMES (New England Offshore Mining and Environmental Study) was conducted by the National Oceanic and Atmospheric Administration (NOAA) and the State of Massachusetts to determine what impact offshore mining of sand and gravel would have on the chemistry and biology of Massachusetts Bay. Specifically, the physical oceanography part of the study was intended to predict how material, in this case the dredge plume fines (d<100 m), would be dispersed. Water movement in Massachusetts Bay is characterized by great spatial and temporal variability. During the month that current meter and drogue measurements were taken, the major feature of the variability was the existence of a strong north-south current shear zone. The mean motions near shore (≈10 km) were predominantly northward; and in less than 10 km to the east, the motions were mostly southward. A prediction, therefore, of how material would be dispersed if it were introduced in the water column would depend largely on where and when it was introduced. In addition, a comparison of drogue and current meter data points out the hazards of depending exclusively on either Lagrangian or Eulerian measurements in describing how material would be dispersed in Massachusetts Bay.

#### 1. INTRODUCTION

NOMES was conducted by NOAA and the State of Massachusetts to determine what impact offshore mining of sand and gravel would have on the chemistry and biology of Massachusetts Bay. Specifically, the physical oceanography part of the study was intended to predict how the dredge plume fines (d<100 m) would be dispersed. A four-pronged assault was launched on the problem in May 1973; on May 24th and 25th, eight current meter stations with a total of 28 current meters were deployed by EG&G and the Atlantic Oceanographic

and Meteorological Laboratories (AOML). These remained in place until June 25th. Of the 28 current meters deployed, 21 produced full record lengths. The last three phases began on June 11th when four drogues were launched in conjunction with a water-tracing study. The drogues were tracked for 3 days, and the water-tracing study continued for 7 additional days. This report is devoted to the current meter and drogue data.

#### 2. DESCRIPTION OF THE EXPERIMENT

Eight current meter stations were deployed on May 24th and 25th for 1 month. Of the 28 current meters, 10 were Aanderaa and 18 were photogeodynes deployed by EG&G (Magas, 1973). Current meter stations are shown in figure 1. Table 1 provides the necessary mooring data such as sensor depths for each of the stations. No data were recorded from station 3. All current meters that returned useful records are indicated in table 1; those that did not are excluded. Wind data were obtained from the Boston Lightship located near station A.

#### 2.1 Eulerian Measurements

The data sets were divided into three levels: upper, middle, and lower measurements; 1, 2, and 3, respectively. These three levels are indicated in table 2; statistics are also given. The statistics tabulated include monthly mean velocity components (the larger ones are plotted in fig. 1)

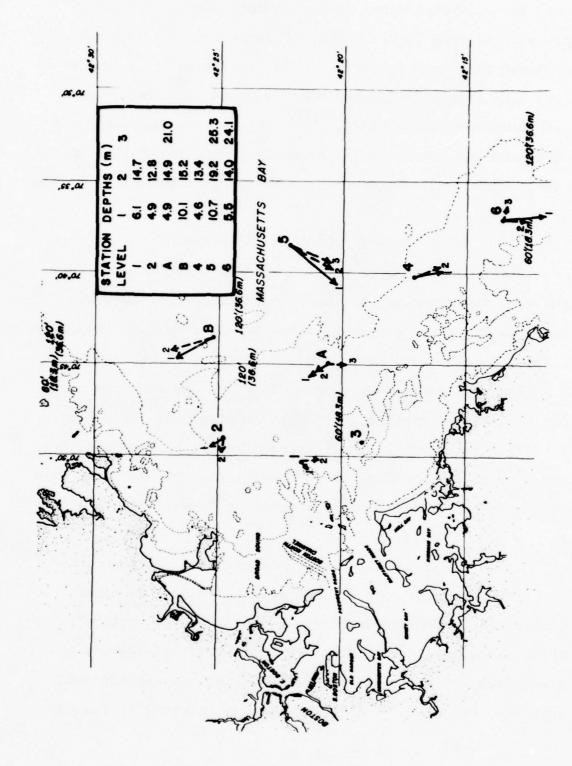


Figure 1. Monthly mean current vectors.

Table 1. Current Meter Mooring Data

Sta	* *	Number	Station		Meter	Coordinates
	of	of	depth	depths	number	
	sensor	meters	(m)	(m)		
1	Film	2	19.8	6.1	11	42°21.6'N
	Record-			14.7	12	70°50.3'W
	ing					
	Geodyne					
2	Film	3	33.2	4.9	21	42°24.8'N
	Record-			12.8	22	70.49.0'W
	ing			25.9	23	
	Geodyne					
A	Aanderaa	1	29.9	4.9	A1	42°20.6'N
		3	25.0	8.5	A 2	70°44.9'W
				14.9	A3	
				21.0	A4	
В	Aanderaa	2	49.4	10.1	B1	42°25.2'N
				15.2	B 2	70°43.6'W
		2	47.8	18.0	В3	
				31.7	В4	
4	Film	3	34.2	4.6	41	42°17.1'N
	Record-			13.4	42	70°40.2'W
	ing			26.8	43	
	Geodyne					
5	Film	5	71.4	10.7	51	42°22.1'N
	Record-			19.2	52	70°38.5'W
	ing			25.3	53	
	Geodyne			32.3	54	
				50.6	55	
6	Film	3	31.4	5.5	61	42°13.6'N
	Record-			14.0	62	70°36.9'W
	ing			24.1	63	
	Geodyne					
W1	nd Lightship					Next to
						station A

Table 2.

Sta.

			Stat	Statistics of	40-Hr Low-	← and High-rassed		Time Series		
Sta.	Meter	Level	Record length	cm/s mean	cm/s mean	HPV h1gh-	LPV low-	Squared	Ratio of HPV	Ratio of total
			number	north	east	passed	passed		to	variance
			points	nent	nent	ance	ance		vari-	mean
			Δt=1.0 hr						ance	
-	۵11	1	605	-0.84	-0.80	183.4	80.7	1.4	0.69	195.6
	۵12	7	592	-2.51	0.35	92.4	17.6	6.4	0.84	17.1
7	17	-1	586	1.87	-1.33	120.7	57.0	5.3	0.68	33.7
	22	7	286	0.42	-1.92	186.1	31.9	3.9	0.85	55.9
	*23	3	303	-3.42	7.30	80.1	11.3	65.0	0.88	1.4
4	VI VI	-	615	2.70	-2.03	125.0	106.0	11.4	0.54	20.3
	A2	-	615	3.42	-3.19	232.3	8.62	21.9	0.74	14.3
	A3	7	611	1.76	-1.52	154.4	46.2	5.4	0.77	37.2
	A4	3	611	-2.45	0.05	116.3	7.4	0.9	0.94	20.6
B	B1	-	615	5.04	-2.89	116.5	42.9	33.8	0.73	4.7
ı	B2	7	615	5.56	-1.27	42.6	43.7	34.1	0.49	2.5
	B3	7	611	4.43	-1.17	90.1	23.7	21.0	0.79	5.4
	B4	3	611	1.79	-0.48	85.0	9.4	3.4	0.90	27.8
4	41	-1	592	-3.48	96.0	228.0	156.2	13.0	0.59	30.0
	42	7	592	-3.47	1.42	188.6	94.6	14.0	0.67	21.0
	*43	9	158	5.98	0.12	266.6	26.2	35.8	0.91	8.2
2	51	-	592	-6.12	-5.52	171.0	106.0	67.9	0.62	4.1
	52	7	592	-6.12	-3.47	97.5	50.7	49.5	99.0	3.0
	53	3	592	-5.49	-2.33	68.4	42.0	35.6	0.62	3,1
	24	6	009	-5.97	-3.67	182.6	108.0	49.1	0.63	5.9
	Δ55	e	605	-3.22	-0.42	76.7	42.5	10.5	0.64	11.35
9	61	1	594	-5.49	0.74	172.8	148.9	30.7	0.54	10.5
	*62	7	535	-3.13	0.13	224.4	120.1	8.6	0.65	35.2
	63	3	594	-0.60	1.75	104.3	23.5	3.4	0.82	37.4
٥		too long.								
	Record too									

and the high-passed variance, low-passed variance, and squared mean. The data sets were partitioned into low and high frequency bands. Forty hours was selected as the period separating low and high frequency processes; thus, 40-hr hp data contain all high frequency events such as inertial and tidal frequencies, and 40-hr lp data contain all events with periods greater than 2 days or those usually associated with synoptic meteorological events. The variances computed are the sum of the squares of the variances of the velocity components for each time series—40 hr lp and 40-hr hp. In addition, the ratio of high-passed variance (HPV) to total variance and the ratio of total variance to the squared mean are also given. The latter ratio is of particular interest in analyzing the dispersion of materials.

# 2.2 Lagrangian Measurements

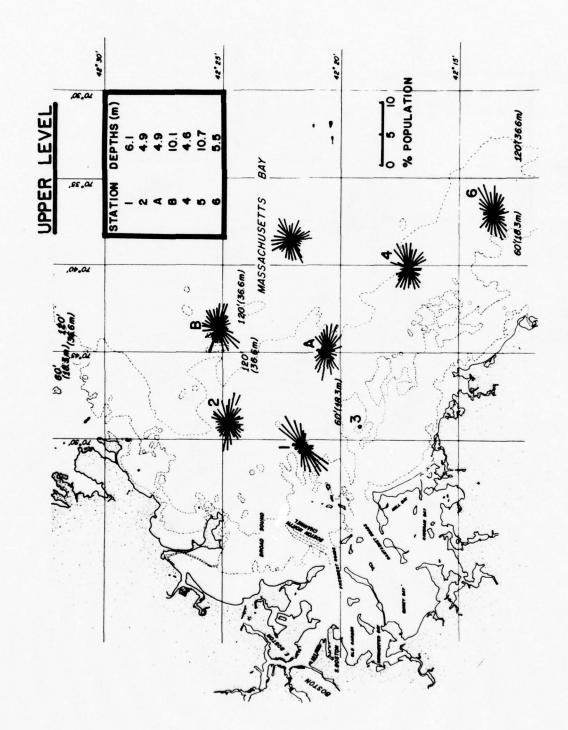
Three drogues were deployed, beginning at 1100 on June 11th and tracked for over 2 days. The drogues were developed by the R. M. Parsons Laboratory at Massachusetts Institute of Technology (MIT). Only the 7- and 12-m drogue data were used for comparison with the current meter data because not enough data from the stations at the lower level (3) were available. The 7- and 12-m drogues correspond to levels 1 and 2, respectively.

#### 3. MEAN MOTIONS

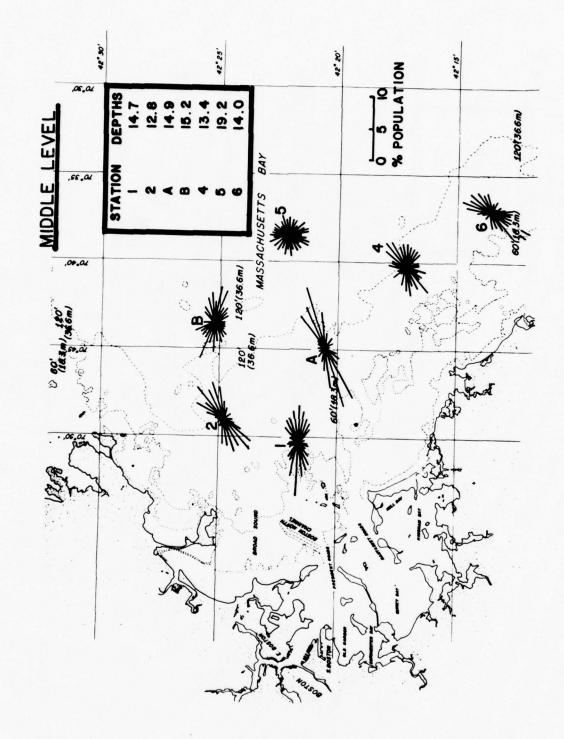
The larger mean current vectors at various levels for all the stations are shown in figure 1. These means should be interpreted with caution as they reflect an average of about a month. With only this much data and such great variability, these means are probably not well determined and would fluctuate from month to month. To show how variable the motions are, we can look at the ratio of the total variance to the mean squared (table 2). This quantity varies from about 3 to 200. Data from station 1 show almost zero mean with a very large variance. Station 5, on the other hand, shows small values ranging from 3 to about 11. This shows that a consistently large mean flow existed for the duration of the experiment for station 5. The flow at all levels for station 5 is consistently to the southwest, whereas most other means appear to parallel the isobaths. At every other station, the flow seems to be influenced by the boundaries. An interesting feature of the vertical structure is seen in the record for the near bottom meter (A4) at station A. Here the current is to the south, whereas the upper three sensors at station A show a mean northerly flow.

#### 3.1 Direction Data

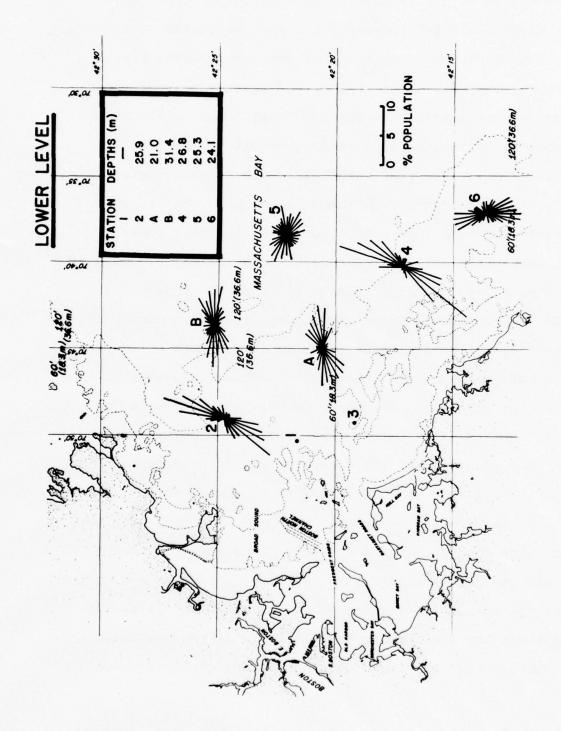
Histograms in polar form summarize the direction data for the 40-hr hp time series for all three levels in figures 2 to



Current roses of percent population for upper level meters. Figure 2.



Current roses of percent population for middle level meters. Figure 3.



Current roses of percent population for lower level meters. Figure 4.

The histograms display the preferred directions of the water motion as the frequency distribution of currents, partitioned into 10° increments, where the length of each line represents the percentage of the total record length occupying that direction segment. Frequency distributions change significantly with depth. Level 1 has fairly homogeneous distributions of currents, except for station 1. Levels 2 and 3 show that materials would be transported in a preferred southwest and northeast direction. Of course, there is no phase information contained in these roses. This means that material introduced into the water column at the same place, but at different times in the tidal cycle, could be transported in completely opposite directions; and if the spatial variation of currents is as great as it is in Massachusetts Bay, then a slug of material could move in almost any direction, depending on the time it was introduced into the water column. This will be brought up again when an explanation of the drogue tracks is presented.

3.2 Vector Time Series of 40-Hr Lp Data

The low frequency content of the data is best displayed as a stick diagram. These are shown in figures 5 through 11 for all stations, and the time interval is every 6 hr. Here it can be seen that stations 4, 5, and 6 differ distinctly from the other stations in that the flow is predominantly southward. Also the low frequency motions of these three

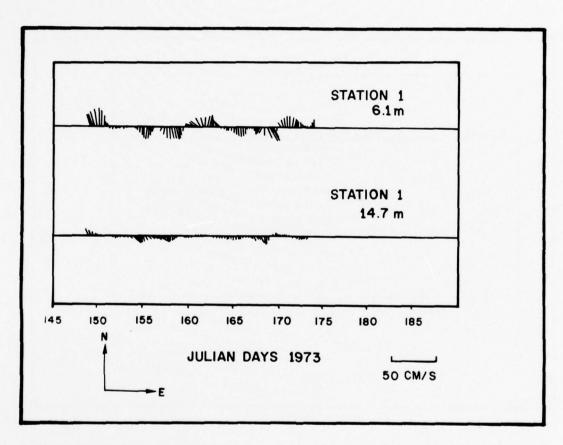


Figure 5. Vector time series of 40-hr lp data for station 1 ( $\Delta t = 6 \text{ hr}$ ).

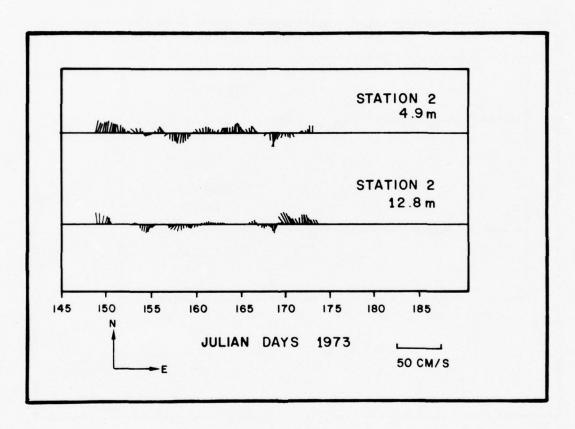


Figure 6. Vector time series of 40-hr lp data for station 2 ( $\Delta t = 6 \ hr$ ).

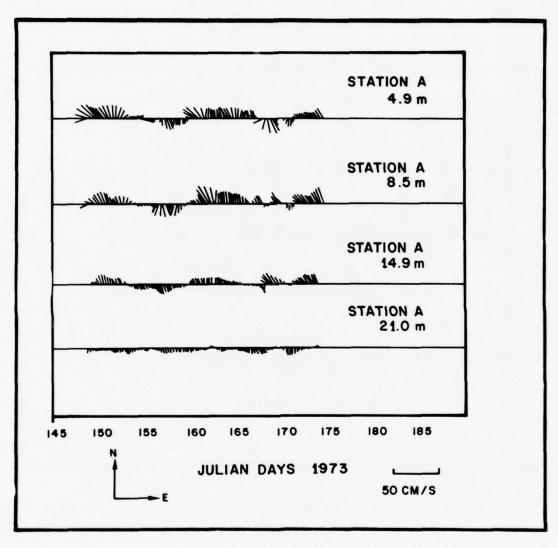


Figure 7. Vector time series of 40-hr lp data for station A ( $\Delta t = 6 \text{ hr}$ ).

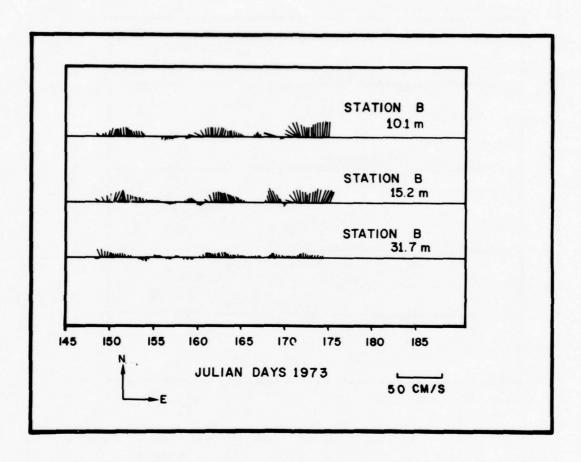


Figure 8. Vector time series of 40-hr lp data for station B ( $\Delta t = 6 \text{ hr}$ ).

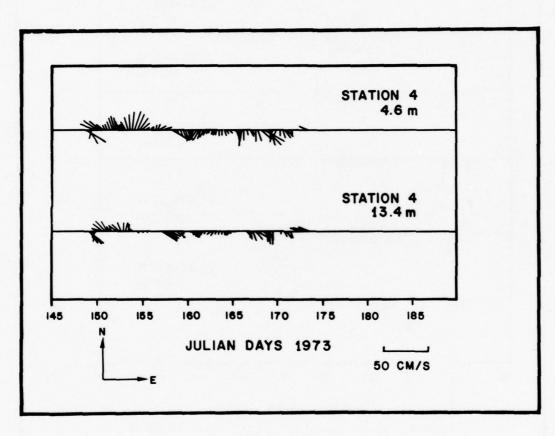


Figure 9. Vector time series of 40-hr lp data for station 4 ( $\Delta t = 6 \text{ hr}$ ).

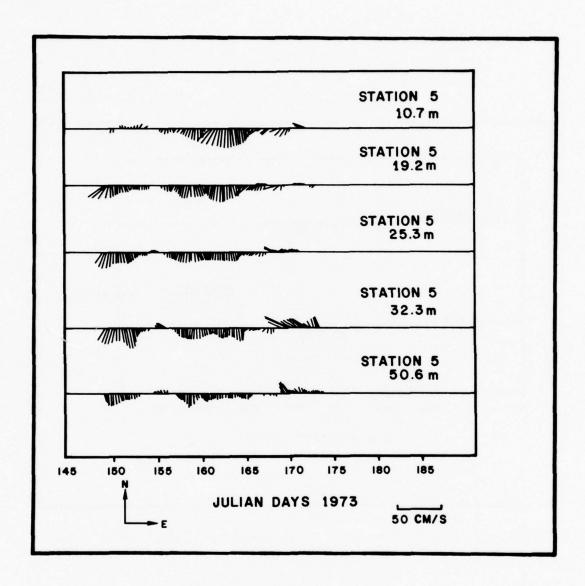


Figure 10. Vector time series of 40-hr lp data for station 5 ( $\Delta t = 6 \text{ hr}$ ).

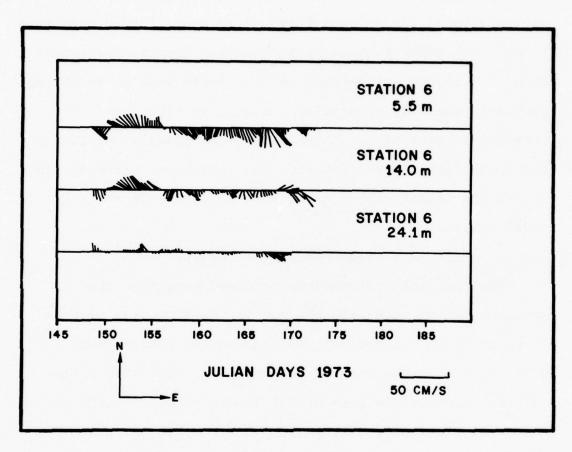


Figure 11. Vector time series of 40-hr lp data for station 6 ( $\Delta t = 6 \text{ hr}$ ).

stations appear to be as much as 180° out of phase with stations 1, 2, A, and B for more than one-half the record length. The flow at the 21-m sensor at station A is also southward. It is apparent that there is a great spatial variability in the current field, with scale length less than 10 km. The major feature of this variability is the existence of a strong north-south current shear zone where strong northerly currents at station A change to strong southerly currents at station 5. This feature can greatly complicate any comparison between Eulerian and Lagrangian measurements, unless the Lagrangian water-tracing is done over several tidal cycles.

# 3.3 Temperature Time Series

The only temperature data obtained were from the

Aanderaa meters at stations A and B. Here the raw temperature data (fig. 12 and 13) show decreasing fluctuations

with depth as expected, and both stations also show a significant temperature jump at all levels except for the 31.7-m

sensor at station B. The jump begins roughly on Julian Day

168 or June 17, 1973. The increase in temperature at all

levels above 20 m is roughly 5°C. This does not appear to be associated with any meteorological events because the progressive vector diagram in figure 14 of the wind, as observed by the lightship, shows nothing unusual occurring on that date. What may be significant, however, is that, from figures 5

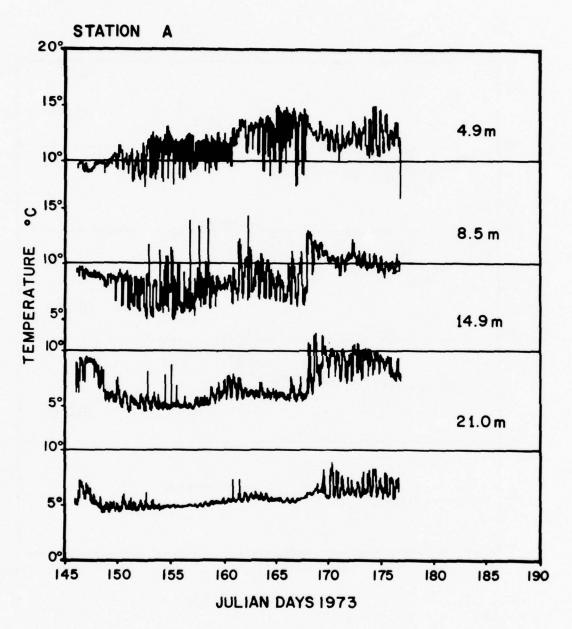


Figure 12. Temperature data from station A.

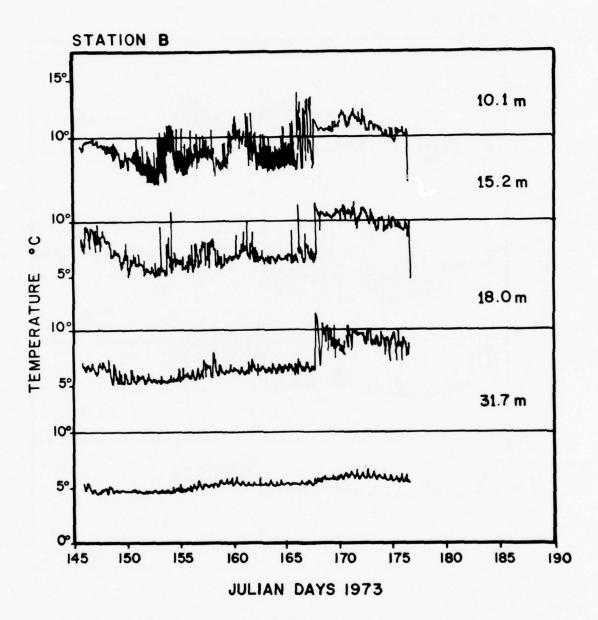


Figure 13. Temperature data from station B.

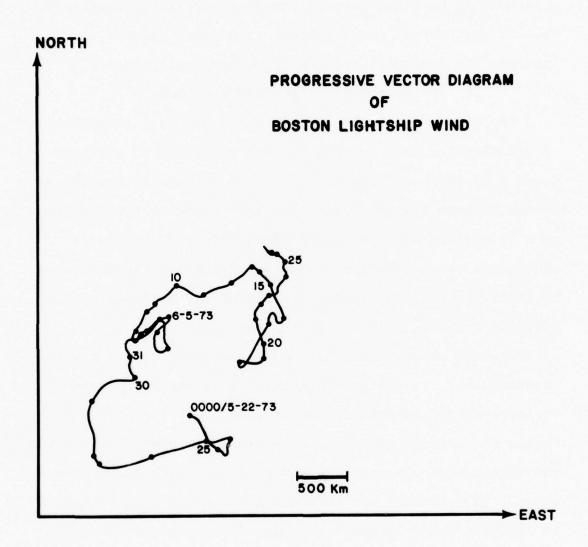


Figure 14. Progressive vector diagram of Boston Lightship wind.

through 11, stations 4 and 6 show unusually strong southerly flow, station 5 shows strong westerly flow, and station A has some unusual vertical current structure, that is, southerly flow at the surface and a variable structure below. This may indicate the transport onshore of warmer oceanic water.

# 3.4 Spectra of Current Meter Data

Comparison of spectra of the north and east components of velocity for mean surface and bottom meters at stations 5 and A is shown in figures 15 through 18. These spectra were chosen because station 5 with its low ratios of total variance to squared mean is, except for station B, unlike the other data sets. Station A, however, with its higher values of this ratio is more characteristic of the stations west of stations 5 and B, at least in its energetics.

Spectra of station A data are characteristic of spectra at stations 2, 4, and 6. This means that the low-passed variance decreased regularly with depth, but the high frequency variance sometimes increases with depth, reflecting the rather vigorous inertial and tidal activity nearer the shore. This feature can be seen in the spectra of station A in figures 15 and 16 where the high frequency portion of the spectra for the upper and lower sensors is quite close in magnitude. Station S, on the other hand, shows that both low and high frequency variance decrease fairly uniformly with depth. This can be seen in table 2 by looking at the ratio

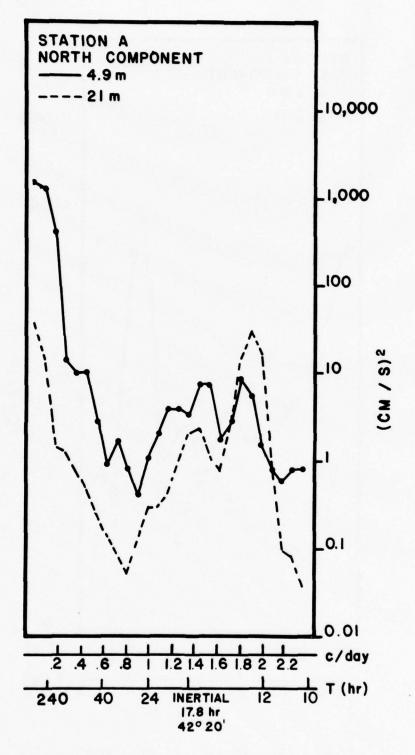


Figure 15. Spectra of north component of current for station A at 4.9 and 21 m.

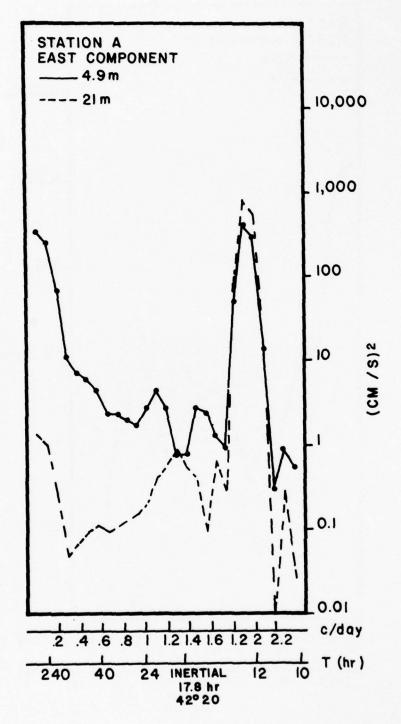


Figure 16. Spectra of east component of current for station A at 4.9 and 21 m.

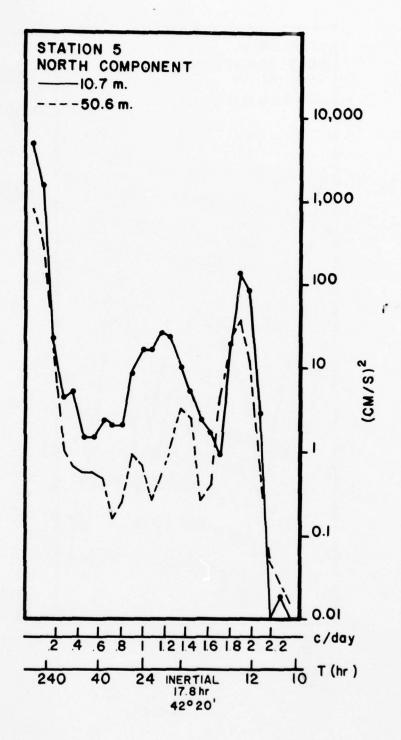


Figure 17. Spectra of north component of current for station 5 at 10.7 and 50.6 m.

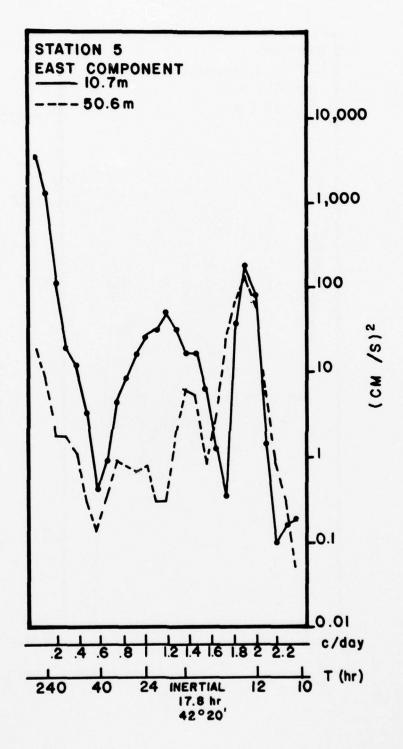


Figure 18. Spectra of east component of current for station 5 at 10.7 and 50.6 m.

of HPV to the total variance for stations A and 5. These characteristics of station 5 data are not clearly duplicated by any of the other stations. However, the total variance decreases with depth in most cases. This can be seen by the much lower energy in the spectra of the deeper sensors in figures 17 and 18. Thus, it seems that any material introduced in the water column beyond stations 5 and B would be dispersed in the water column increasingly by the lower frequencies than would be the case nearer the shore.

#### 4. DROGUE TRACKS

The tracks of the 7- and 12-m drogues are shown in figure 19 and 20. Each point on the track is an observation taken at a specific time. The observation numbers and associated times are listed in table 3. The locations of all current meters are also shown. Following figures 19 and 20 are sequences of current vector fields for each drogue observation. There are 19 for drogue 1 and 29 for drogue 2. Each drogue position and associated vector field show the actual drogue position at the observed time in relation to all the other drogue positions. The current vector fields were constructed from 3-hr 1p data that include both low and high frequencies.

By looking at each drogue observation, it can be seen that the drogue movement is not inconsistent with the current vectors; in fact, it is quite clear that the 12-m drogue in figures 20-1 through 20-29 is in phase with the vector at

Table 3.

Times of Drogue Observations for the 7- and 12-m Drogues

Drogue number 1 (7 m), beginning 6-11-73	, (1		_	Drogue number 2 (12 m), beginning 6-11-73	(12 m),			
	OBS#	Time	0BS#	Time	OBS#	Time	0BS#	Time
	11	0200	7	1100	11	0100	21	1800
_	7	0300	7	1200	12	0200	22	2100
_	3	0200	3	1300	13	0300	23	2300
	14	0090	4	1400	14	0200	24	0000
7	5	1000	2	1600	15	0090	25	0100
_	9	1100	9	1700	16	0060	56	0200
_	1	1300	7	2000	17	1100	27	0300
	18	1400	80	2100	18	1300	28	0400
	19	1600	6	2300	19	1500	29	0090
			10	0000	20	1700		

All times have been rounded off to the nearest hour to correspond with hourly current meter data. Note:

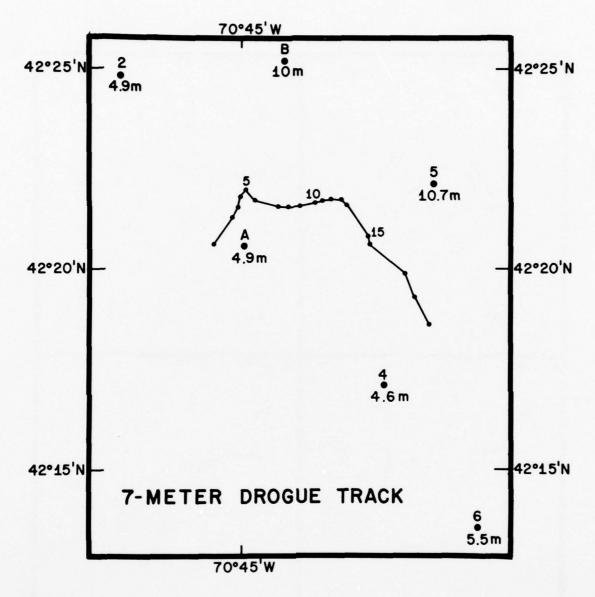


Figure 19. Seven-m drogue track from 1100, June 11, to 1600, June 12; 19-1 through 19-19 are current vectors at the time of drogue position observations.

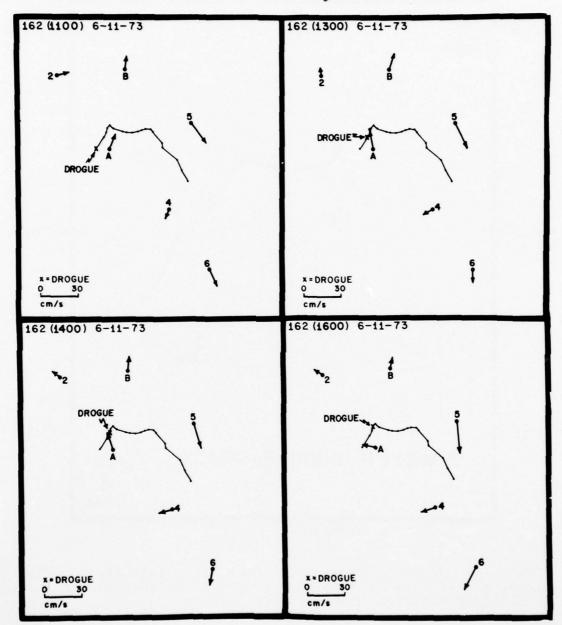


Figure 19-3.

Figure 19-4.

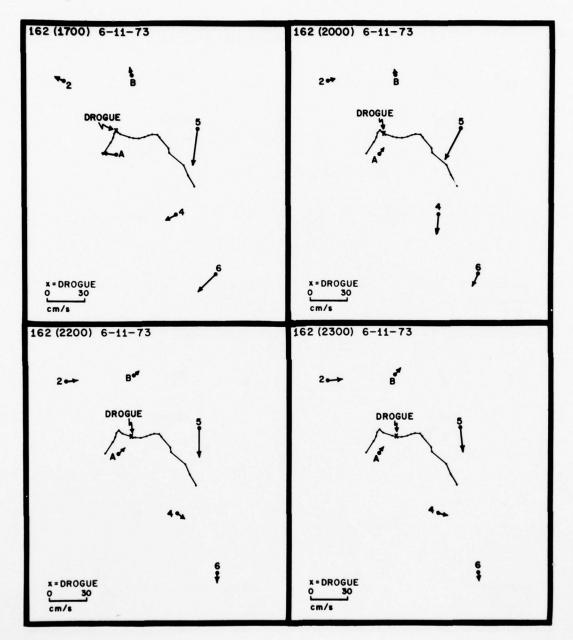


Figure 19-7.

Figure 19-8.

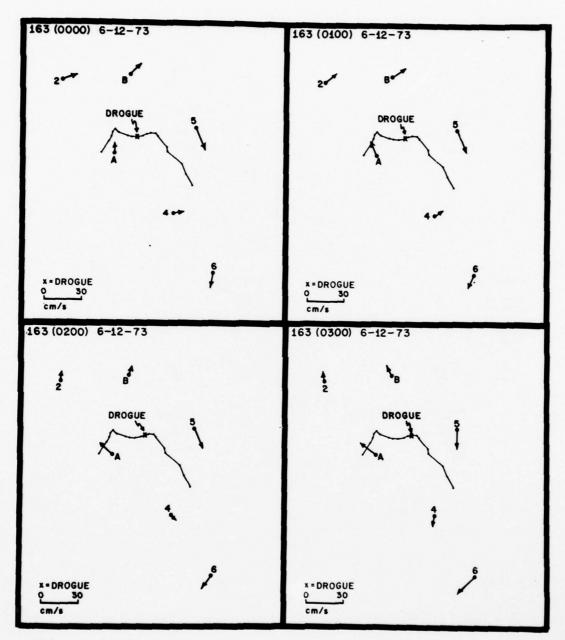


Figure 19-11.

Figure 19-12.

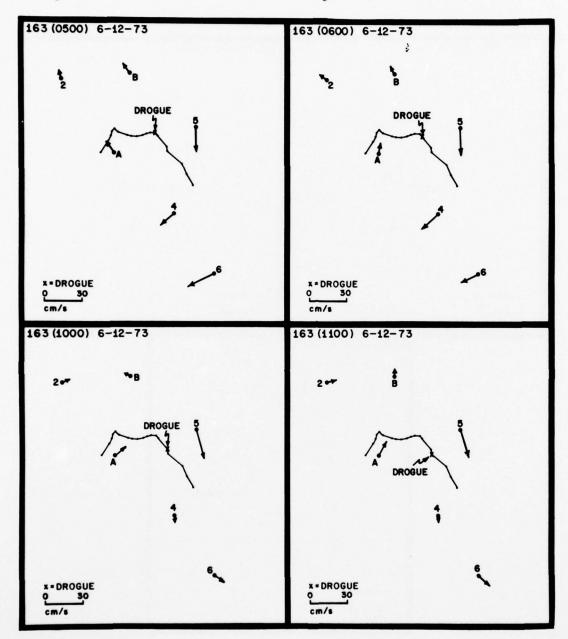


Figure 19-15.

Figure 19-16.

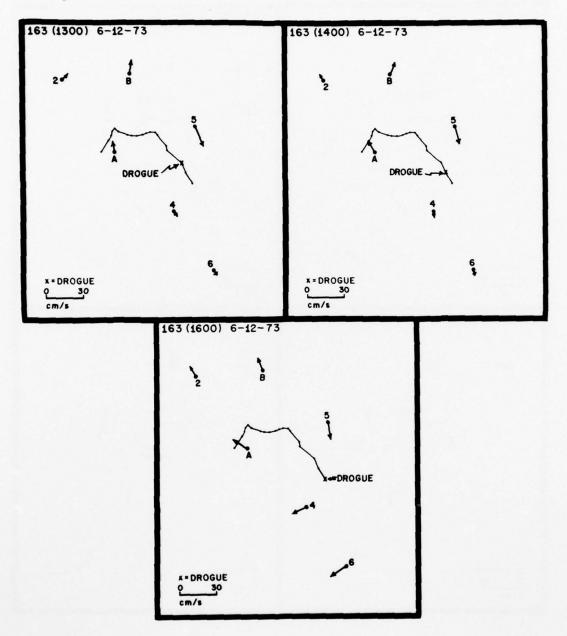


Figure 19-19.

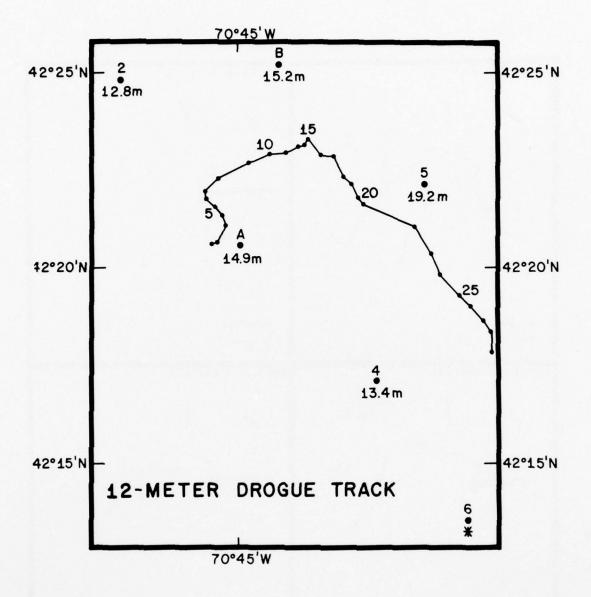
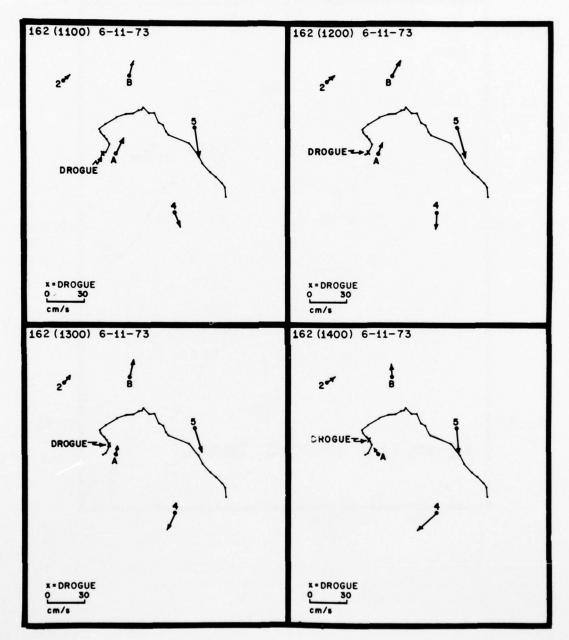


Figure 20. Twelve-m drogue track from 1100, June 11, to 0600, June 13; 20-1 through 20-29 are current vectors at the time of drogue position observation.



rigure 20-3.

Figure 20-4.

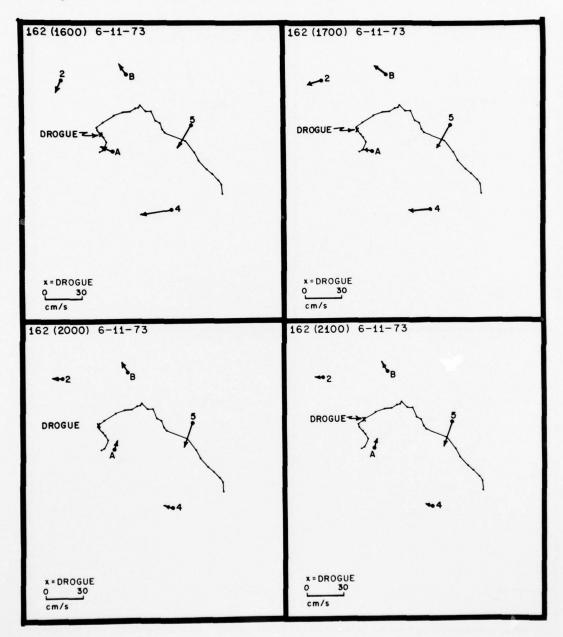


Figure 20-7.

Figure 20-8.

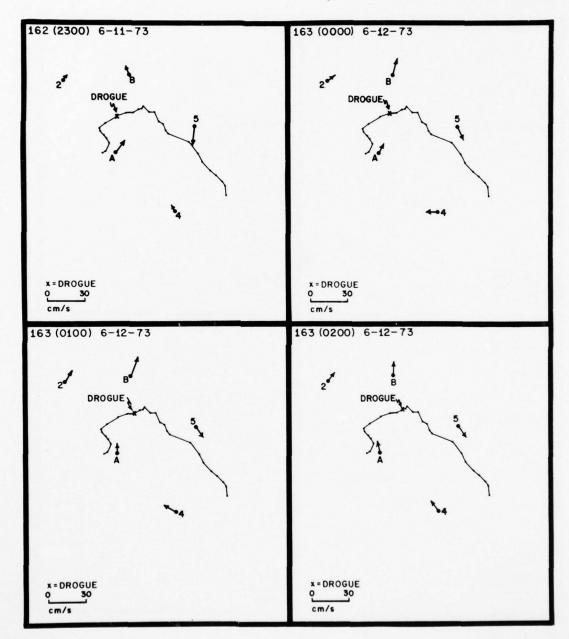
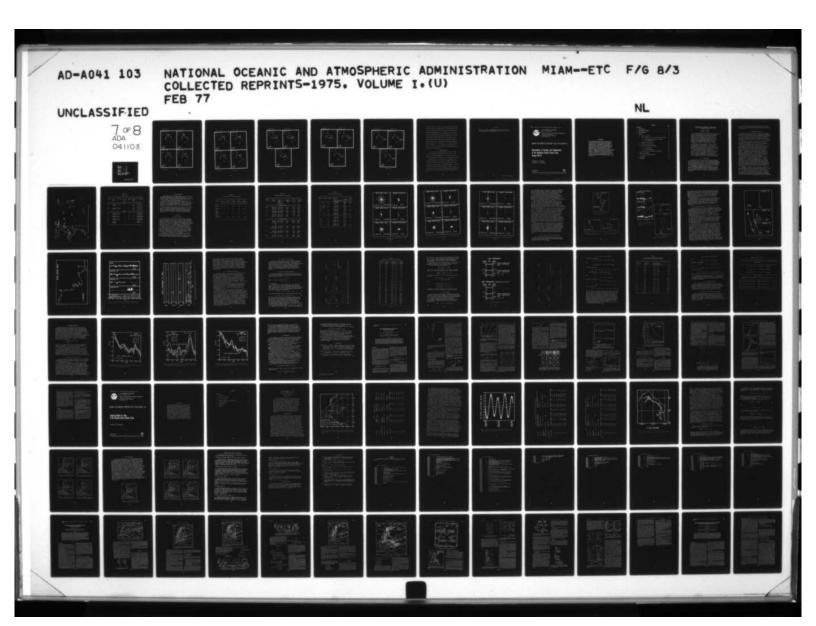
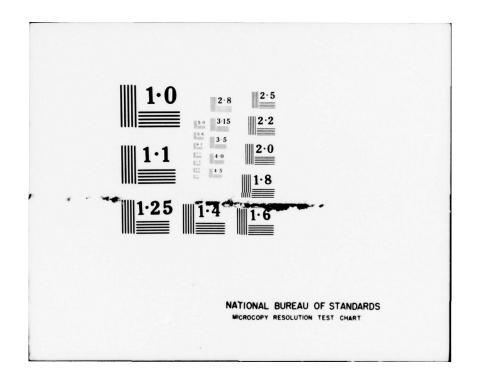


Figure 20-11.

Figure 20-12.





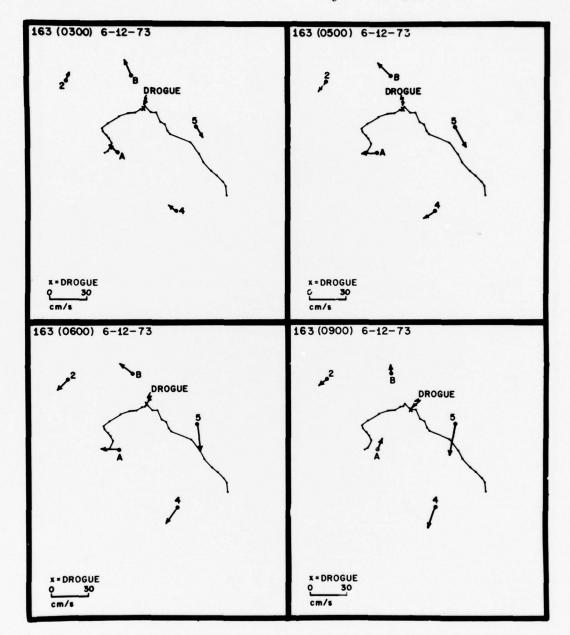


Figure 20-15.

Figure 20-16.

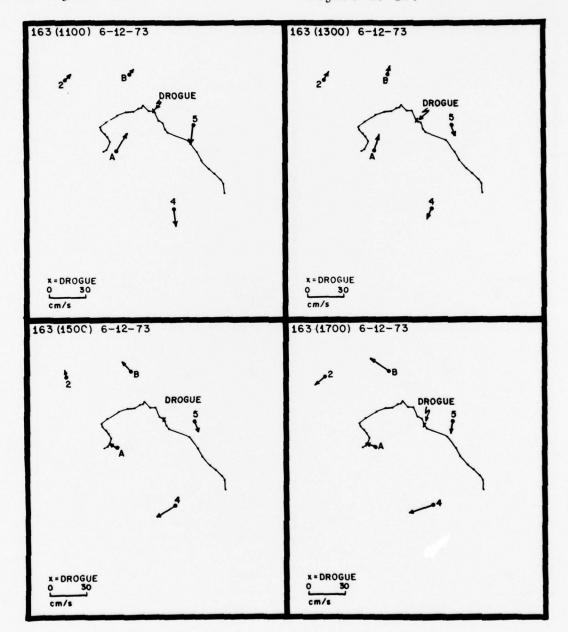


Figure 20-19.

Figure 20-20.

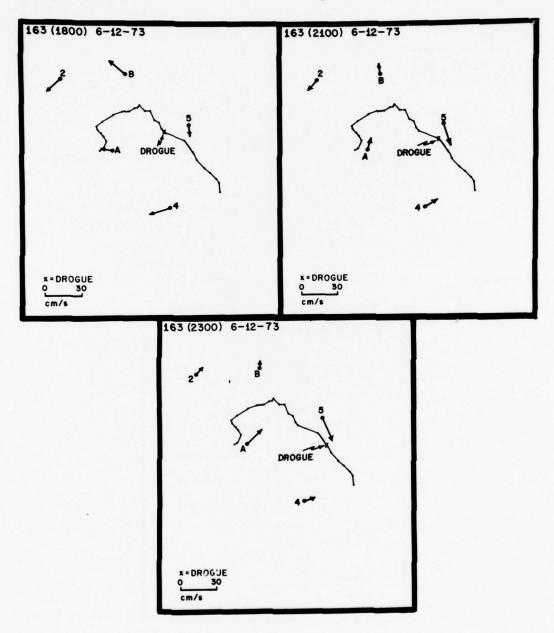


Figure 20-23.

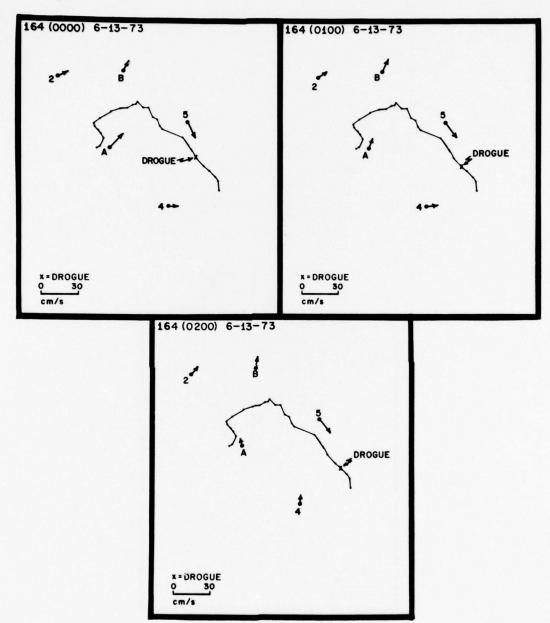


Figure 20-26.

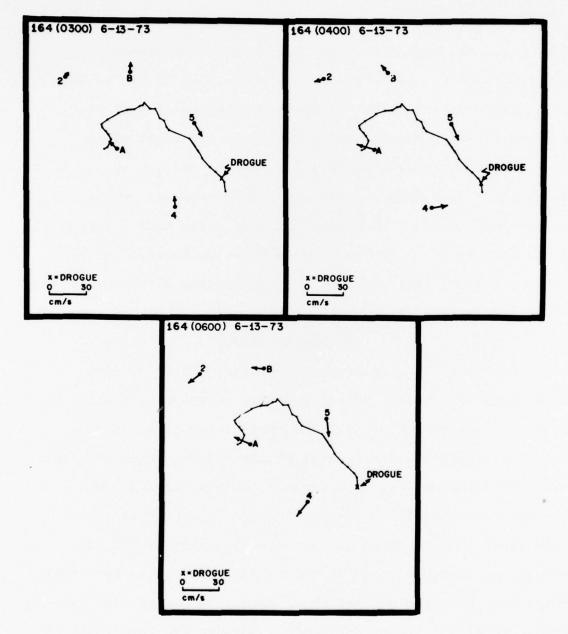


Figure 20-29.

station A while it is near A. As the drogue advances along the track from 20-1 through 20-14, it fluctuates east and then west and then east again in phase with the fixed-point (Eulerian) measurements at A. Ultimately, both drogues wound up much farther offshore and travelling to the south. This happened because of the spatial inhomogeneity of the current field in Massachusetts Bay. The east-west tidal motion transported the drogues far enough east through a sharp shear zone into a southerly flowing current regime where they remained. Conceivably, this could have occurred quite differently. If the drogues had been deployed at a different time, they probably would have gone much farther north before turning south.

#### 5. ACKNOWLEDGMENTS

The Physical Oceanography Laboratory (PhOL) of AOML thanks the Commanding Officer and crew of the U.S. Coast Guard buoy tender Whiteheath for their valuable assistance during deployment and retrieval of the current meter moorings.

Appreciation is also expressed to Alan Herman, PhOL Systems Programmer, for translating the EG&G current meter data types, and to the R.M. Parsons Laboratory at MIT for providing the drogue data in a convenient format to facilitate comparison with the current meter data. Thanks is also extended to Rich Boehmer, State of Massachusetts, Department of Water Resources, for furnishing the Boston Lightship wind data.

# 6. REFERENCES

Magas, A. P. (1973): Oceanographic Report: NOMES Project
Massachusetts Bay, Massachusetts, for NOAA by EG&G Environmental Equipment Division, Waltham, Mass.



U.S. DEPARTMENT OF COMMERCE Rogers C. B. Morton, Secretary

NATIONAL OCEANIC AND ATMOSPHERIC ADMINISTRATION
Robert M. White, Administrator
ENVIRONMENTAL RESEARCH LABORATORIES
Wilmot N. Hess, Director

# NOAA TECHNICAL REPORT ERL 346-AOML 21

# Observations of Currents and Temperatures in the Southeast Florida Coastal Zone During 1971-72

DENNIS A. MAYER DONALD V. HANSEN

BOULDER, COLO.

June 1975



572

#### DISCLAIMER

The NOAA Environmental Research Laboratories do not approve, recommend, or endorse any proprietary product or proprietary material mentioned in this publication. No reference shall be made to the NOAA Environmental Research Laboratories, or to this publication furnished by the NOAA Environmental Research Laboratories, in any advertising or sales promotion which would indicate or imply that the NOAA Environmental Research Laboratories approve, recommend, or endorse any proprietary product or proprietary material mentioned herein, or which has as its purpose an intent to cause directly or indirectly the advertised product to be used or purchased because of this NOAA Environmental Research Laboratories publication.

$\alpha$	N		NTT	יכי
	11/4	P.	IV I	

		CONTENTS	Page
ABS	TRACT		1
1.	INTRO	DDUCTION	1
2.	MEASI	JREMENT PROGRAM	2
3.	DATA	REDUCTION	5
4.	RESU	LTS	5
	4.1	Water Movements	5
		4.1.1 Current Shear of Stations O(1) and A(1)	12
		4.1.2 Low Frequency Motions at Stations V1, V2, and V3	15
	4.2	Temperature Variations	20
	4.3	Spectra of Time Series	21
	4.4	Fluxes of Heat and Momentum	21
		4.4.1 Heat Fluxes	24
		4.4.2 Momentum Fluxes	29
	4.5	Limitations of Divergence Calculations	29
5.	SPEC	TRAL ESTIMATES	31
	5.1	Stability and Stationarity	31
6.	CONC	LUSIONS	35
7	PFFF	PENCES	36

### OBSERVATIONS OF CURRENTS AND TEMPERATURES IN THE SOUTHEAST FLORIDA COASTAL ZONE DURING 1971-72

Dennis A. Mayer Donald V. Hansen

The long, narrow, and shallow (less than 20 m) shelf region of Southeast Florida is distinctly different from the deeper offshore water where the dominant motions are those of the Florida Current. The shallow water is primarily wind driven, but also subject to tidal motions near tidal inlets. A basic problem in determining South Florida coastal processes is that the major dynamics and, hence, the major exchange mechanisms contain so much energy at low frequency that at least 4 months of data are required for computation of reliable statistics.

In long current measurement records, the net northward motion is nearly zero. In the winter, the temperature of coastal water is less than the temperature of offshore water by about  $\frac{1}{2}$  C/km. This positive east-west gradient of temperature is caused by the frequently occurring cold fronts which pass over South Florida regularly in the winter.

The momentum flux that had the most spatial variation and, hence, whose divergence was also the largest, was the low frequency covariance between the north and east components of current where its sign actually changed from -26 to 20 cm<sup>2</sup>/sec<sup>2</sup> over a distance of only 2 km. The resulting divergence, or Reynolds stress, was of order 10-4) cm/sec2.

#### 1. INTRODUCTION

A description of Southeast Florida coastal processes, particularly the fluxes of material and momentum, depends on understanding the role that three major forcing mechanisms play in driving coastal waters. These have been identified as tidal inlet effects, proximity of the Florida Current, and wind effects. Together they combine to produce complex shelf water motions, especially near inlets.

Understanding exchange processes of shallow coastal waters is aided by identifying the more important fluxes and the frequency bands wherein most of their energy lies. This establishes terms in the material budget equations and the dynamical equations needed to describe the coastal

processes.

The fluxes of heat and momentum computed using temperature and velocity measurements as observed in the coastal waters off southeast Florida during 1971 and 1972 are described in this report.

## 2. MEASUREMENT PROGRAM

Locations of current meter and wind sensor installations are shown on the chart in figure 1. Coordinates, depths, and all relevant data associated with each sensor are outlined in table 1. The measurement program consisted of two phases.

During Phase I, an attempt was made to evaluate the performance of different sensors and different types of mooring for sampling currents in the surface-wave-influenced open coastal zone and to obtain some useful data at stations O(1) and A(1).

Phase II was designed to provide more detailed measurements of coastal processes at stations V1, V2, and V3. All stations, except for 0(1), were taut-wire moorings using the Aanderaa Model 4 Meter. Station 0(1) was a tripod

supporting two ODESSA sensors (Goodheart, 1966).

Originally designed for relatively calm estuaries, ODESSA sensors have two features which detract from their utility for open coastal current measurements. Unless they are mounted on tripods to remove mooring motion, the small direction vane, in combination with low data sample rate, produces such noisy data as to be almost useless. In addition, they do not record internally but rather transmit data through an electromechanical cable (another problem source) to a surface buoy that houses a battery pack and data tapes. This, along with their weight and bulk, requires a costly investment in time and effort for the amount of useful data obtained.

ODESSA sensors were deployed at station O(1) in February 1971 as a part of the comparison of sensors; two Aanderaa meters on a taut wire were installed at A(1) in April 1971. Each station produced less than 2 weeks of useful data. Station O(1) had severe fouling problems after about 10 days, and the meters on A(1) were needed for another project. The fouling problems turned out to be much more severe than anticipated. In the shallow water (less than 20 m) off Southeast Florida, the current meters must be cleaned once a week unless protective coatings are applied. In Phase II, by far, the most extensive data

were collected.

In Phase II, Aanderaa meters were used exclusively, and the problem of fouling was eliminated by frequent cleaning. Data were collected for 11.8 weeks (82.3 days) at V1, for 6.8 weeks (47.9 days) at V2, and 2.7 weeks (19.0 days) at V3. With the better quality data obtained in Phase II, it was possible to calculate fluxes of heat and momentum and spectra of the more important parameters. In addition, vector time series of winds and currents show qualitatively the importance of wind as a forcing mechanism for shallow water.

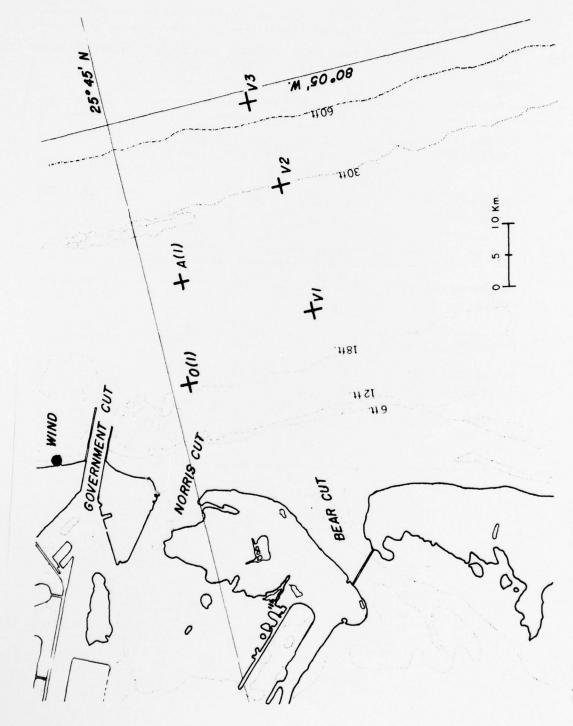


Figure 1. Location of current meter and wind sensor installation.

Table 1. Sensor Data

Station	Type of sensor	Mooring	No. of sensors	Depth (m)	Sensor depth (m)	Coordinates
			1971			
0(1)	ODESSA (TICUS)	Tripod	2	5.5	1.7 and 4.1	25 <sup>°</sup> 44'54''N 80 <sup>°</sup> 07'30''W
A(1)	Aanderaa Model 4	Taut wire	2	8.2	2.7 and	25 <sup>0</sup> 44'45"N
			1972		4.9	80 <sup>0</sup> 06'34''W
V1	Aanderaa Model 4	Taut wire	1	6.1	3.7	25 <sup>0</sup> 43'43''N 80 <sup>0</sup> 07'06''W
V2	Aanderaa Model 4	Taut wire	1	11.0	6.1	25 <sup>0</sup> 43'43''N 80 <sup>0</sup> 05'44''W
V3	Aanderaa Model 4	Taut wire	1	38.1	12.2	25 <sup>0</sup> 43'50''N 80 <sup>0</sup> 05'05''W
Wind	Weather Service F420C		1			25 <sup>0</sup> 46' N 80 <sup>0</sup> 08' W

#### DATA REDUCTION

Specifications of the digital filters used in analyzing the various time series are summarized in table 2a. All pertinent information for the raw time series and the various filtered series, such as start time, record length, and sample interval, is contained in table 2b.

Before computations were performed on any of the time series, all raw data were filtered and resampled at 1-hr intervals. For the 6-min sample rate at O(1), and the 10-min sample rate at all Aanderaa stations, a 3-hr low pass was applied. The resultant series of hourly values were then used in the computations of 40-hr low- and high-passed time series.

For the more extensive data set of Phase II, statistics of the 3-hr and 40-hr low-passed data from stations V1, V2, and V3 for current components and temperature are given in table 2c together with their 70-percent confidence limits. These are fluctuation bounds within which an observation would be found 70 percent of the time for that particular data set.

#### 4. RESULTS

#### 4.1 Water Movements

The statistics of the time series in table 2c indicate that at all stations there is a net mean westward (shoreward) current component that diminishes eastward. The northward mean flow component has a somewhat peculiar structure, being northward at V3 and V1, as expected if coupling to the northwardflowing Florida Current is important, but surprisingly southward at V2. For the same time period as V2, V1 also shows a mean southward flow. The most probable explanation of this result is that it is due to undersampling of the lowfrequency-dominated currents, even in a 6-week sampling period.

Except in the proximity of tidal inlets, the coastal waters of Southeast Florida are driven primarily by the wind and the Florida Current. In addition, the coastal processes can be partitioned into high and low frequency bands. High frequency is defined as all events having periods of less

than 40 hr, and conversely for low frequency.

Histograms, in polar form, of the Phase II data were constructed for the 3- and 40-hr low-passed data and for the 40-hr high-passed data in figures 2a, 2b, and 2c. These show the frequency distribution of currents partitioned into 10° increments, where the length of each is proportional

Table 2a.

Specifications of Digital Filters

Decibels	3-hi low	pass	5-hr low pass	20-hr low pass	40-hr low pass	40-hr high pass
Hours (6 db)	2.5	2.9	5	16.7	37	37
Hours (20 db)	2	2	4	14	30	48
Filter length (#of points)	53	79	15	79	127	127
Sample interval At (min)	10	6	60	60	60	60

Table 2b.
Relevant Data for Time Series

Station	Type of filter	Start Julian Day (hr) Eastern Std. Time	Sample interval (\Delta t)	Number of points	Record length (hr)
		Phase I	971		
0(1)	Raw data 3-hr LP 20-hr LP	57 (13.6) 58 (0.0) 60 (0.0)	6 min 1 hr 6 hr	2617 248 27	261.6 247 156
A(1)	Raw data 3-hr LP 20-hr LP	110 (16.67) 110 (21.0) 113 (0.0)	10 min 1 hr 6 hr	1955 318 38	325.7 317 222
Wind	5-hr LP 20-hr LP 20-hr LP	58 ( 0.0) 60 ( 0.0) 113 ( 0.0)	1 hr 6 hr 6 hr	248 27 38	247 156 222
		Phase II	1972		
V1	Raw data 3-hr LP 40-hr LP and HP	48 ( 9.83) 49 ( 0.0 ) 52 ( 0.0 )	10 min 1 hr 1 hr	11855 1958 1823	1975.7 1957 1822
V2	Raw data 3-hr LP 40-hr LP and HP	47 (13.83) 49 (0.0) 52 (0.0)	10 min 1 hr 1 hr	6904 1111 976	1150.7 1110 975
V3	Raw data 3-hr LP 40-hr LP and HP	95 (13.83) 96 (0.0) 99 (0.0)	10 min 1 hr 1 hr	2729 441 306	454 .8 440 305
Wind	5-hr LP 40-hr LP	49 ( 0.0 ) 52 ( 0.0 )	1 hr 1 hr	1958 1823	195 <b>7</b> 1822

Table 2c.
Statistics of Time Series

Filter	Station	Parameter	Mean and 70% confidence cm/sec and	limits OC	σ Standard deviation	Number of points
	V1	v <sub>1</sub> u <sub>1</sub> t <sub>1</sub>	$\begin{array}{c} 2.73 \pm .43 \\ -2.10 \pm .29 \\ 24.35 \pm .03 \end{array}$		19.09 12.69 1.42	1958
low pass	First 1111 hr of V1	$v_1$ $u_1$ $t_1$	-0.41±.60 -2.25±.40 23.54±.03		20.41 13.43 1.01	1111
3-hr 10	V2	$\begin{array}{c} \mathtt{v}_2 \\ \mathtt{u}_2 \\ \mathtt{t}_2 \end{array}$	-1.60±.52 -1.80±.29 23.76±.02		17.46 9.80 0.64	1111
	V3	V <sub>3</sub> u <sub>3</sub> t <sub>3</sub>	43.80±1.4 -1.18±.23 24.61±.02		29.69 4.73 0.51	441
pass	V1	$\begin{array}{c} v_1 \\ u_1 \\ t_1 \end{array}$	3.27±.37 -2.23±.08 24.34±.57		15.64 3.33 1.37	1823
low	V2	V <sub>2</sub> u <sub>2</sub> t <sub>2</sub>	-0.063 ±.46 -1.87 ±.12 23.79 ±.01		14.22 3.77 0.60	976
40-hr	V3	V <sub>3</sub> u <sub>3</sub> t <sub>3</sub>	35.86 ±1.4 -0.83 ±.09 24.50 ±.03		25.07 1.60 0.44	306

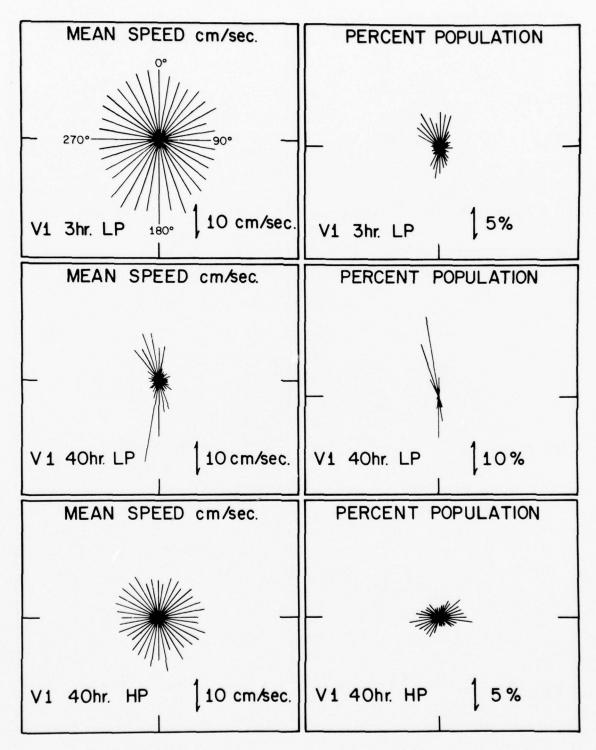


Figure 2a. 3- and 40-hr low-passed and 40-hr high-passed data at station V1.

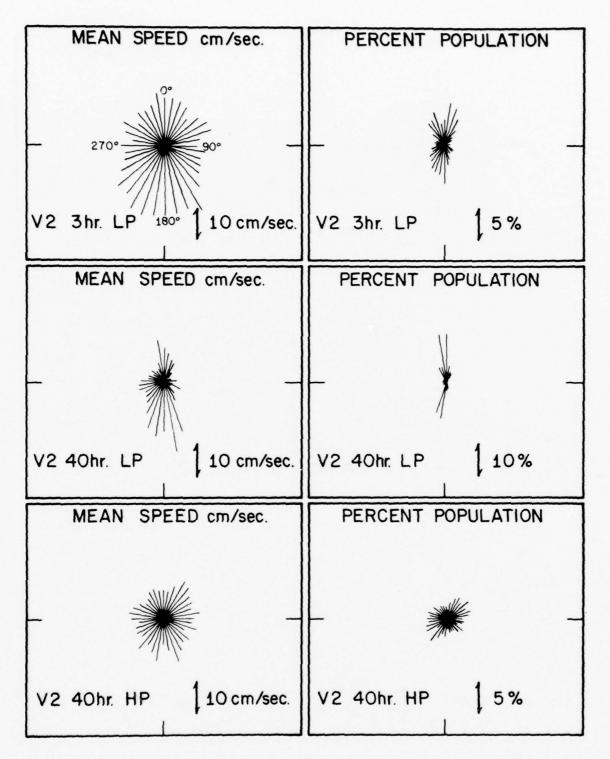


Figure 2b. 3- and 40-hr low-passed and 40-hr high-passed data at station V2.

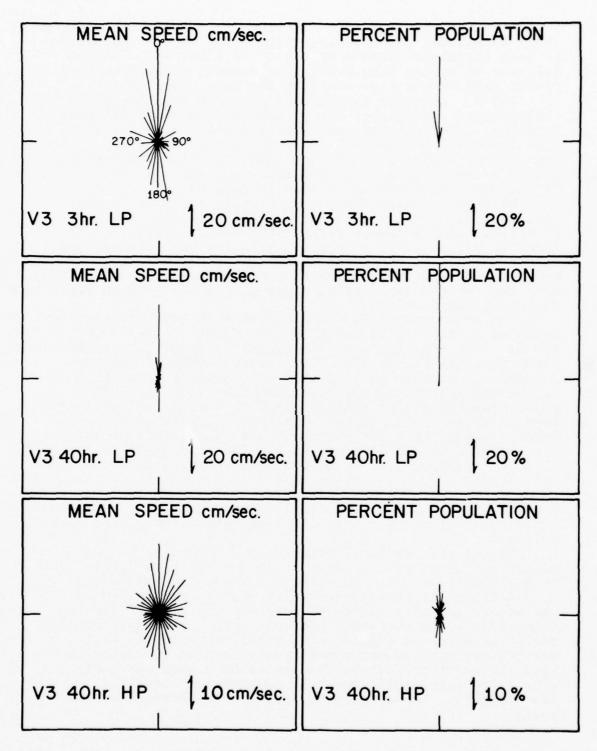


Figure 2c. 3- and 40-hr low-passed and 40-hr high-passed data at station V3.

to the mean speed  $(X_m)$ . In addition, the percent population  $(X_{np})$  is plotted for each increment.  $X_{np}$  is the population of each increment divided by the total population, or the fraction of record length that the current directions were within each of the increments at the mean speed  $X_m$ .

The current-rose (histogram) plots of the low and high frequency processes for V1 and V2 show quite different behavior. The 3-hr low-passed data combine both low and high frequency processes. This combination masks the features of the motions in each band. By plotting separately the 40-hr low- and high-passed data, however, different features

of the water motions can be seen in each band.

Most of the high frequency activity at Vl is in the east-west direction, since this station was situated near an inlet. A more evenly distributed set of directions is found at V2, since it is about a mile farther offshore and more removed from the inlet effects. At V3, however, mostly north-south fluctuations were observed. Low frequency behavior, on the other hand, shows mostly north-south variations for all three stations.

The net movement past a fixed site is conveniently shown by means of a Progressive Vector Diagram (PVD), see figures 3a, 3b, and 3c. The importance of the wind as a driving mechanism is shown in these PVD's. The close relationship of currents to winds at station O(1) is even more clearly shown by a vector time series of currents and winds (fig. 4). rapid response of the shallow water to a classical weather frontal system resulting in an abrupt reversal of the water movement is clearly shown. Such a reversal occurs between days 63 and 65, and, within the resolution of the data, there appears to be no phase lag between the wind and the currents. The 20-hr low pass filter removes the energetic inlet effects from the PVD (see fig. 3c). Wind fluctuations in figure 3b contain mostly low frequencies; thus, one would naturally expect only low frequency wind-induced water motions.

During the period of observations for A(1), the wind record contained mostly daily variations with no significant frontal activity (fig. 5). Again a 20-hr low pass filter was used for all three vector diagrams to exclude semi-daily variations and to present more clearly any diurnal fluctuations induced by the wind. The wind has a good deal of daily variation which is typical in Southeast Florida in April, yet the currents do not consistently respond to the daily wind fluctuations. There appears to be a mean northerly wind drift with small reversals occurring on days 117, 120, and 121. These could be caused by a Florida Current event.

# 4.1.1 Current Shear of Stations O(1) and A (1)

Not enough data were collected at these stations to establish a clear and consistent velocity profile. However, reasonable velocity shears and ratios (speed of upper meter divided by speed of lower meter)

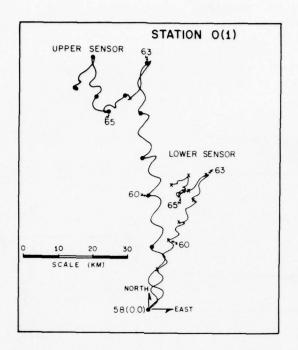


Figure 3a. 3-hr low-passed PVD of station 0(1).

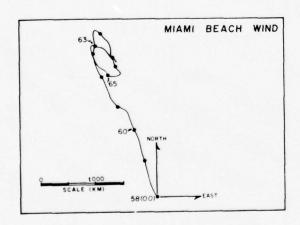
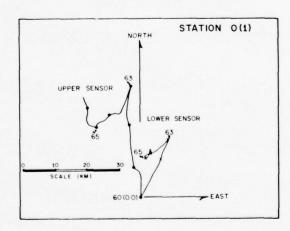


Figure 3b. 5-hr low-passed PVD Figure 3c. 20-hr low-passed of Miami Beach, Fla., wind. PVD of station 0(1).



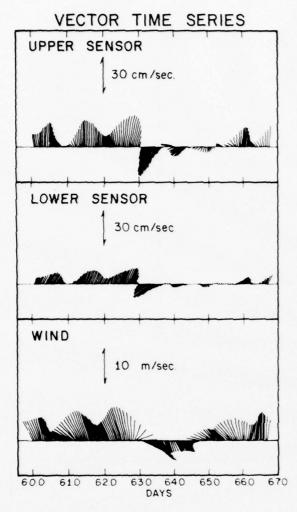


Figure 4. Vector time series of 20-hr low-passed wind and current components from station 0(1).

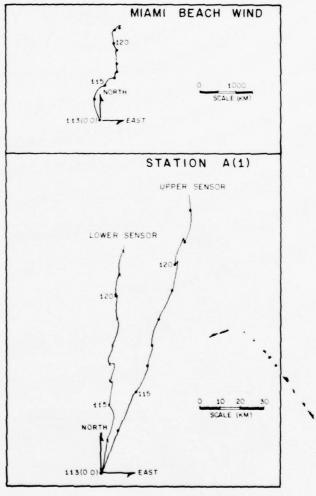


Figure 5. 20-hr low-passed PVD of station A(1).

were computed from the data. The gradients apply to those that would be found approximately at mid-depth and varied between  $(10)^{-2}$  and  $5(10)^{-2}$  (sec<sup>-1</sup>) for 0(1). For A(1), the gradient was  $(10)^{-2}$  (sec<sup>-1</sup>). Velocity ratios fluctuated between 1.9 and 2.8 for 0(1). For A(1), the ratio was 1.2. These computations were based on four time intervals for 0(1) and one for A(1) where the set of the current was reasonably constant.

The degree of vertical variability was investigated by computing correlation coefficients which are the normalized covariances between the velocity components of the upper and lower sensors. These coefficients were very close to 0.90 for each of the components at A(1) and O(1). This implies, therefore, that a single point measurement, near mid-depth, is representative of motions throughout the water column.

## 4.1.2 Low Frequency Motions at Stations V1, V2, and V3

Figures 6a and 6b contain PVD's assembled from the 40-hr low-passed data for V1, V2, and V3 and the Miami Beach wind. These display the motions of the low frequency or slowly varying coastal processes. The most notable aspect of the long period processes represented by the PVD's in figure 6 is that the shallow shelf water monitored by V1 and V2 appears to be quite sensitive to low frequency wind forcing. This is indicated as well in the 40-hr low-passed vector time series plots and plots of the north components of wind and currents in figures 7a and 7b.

The major low frequency features can be seen in figure 6. From days 52 to 92, the coastal water movements were parallel to the coast and oscillated with a period of about 20 days with little net movement. This corresponds quite closely to the variation of the wind. From days 92 to 115, the wind was directed much more to the north, and the current at VI showed similar behavior.

The shorter time scale features (several days) reflect both wind and Florida Current mechanisms. In figures 6 and 7, one can see that wind events were centered about the following days: 66, 69, 80, 92, and 100. On these days, the coastal waters reversed approximately in phase with the wind direction. Mixed processes occurred over the time spans, days 52 to 54, 100 to 102, and 115 to 118. Here, except for day 100, the phase between wind and currents is not clear. In each case, the change in current direction leads the wind. It is also notable that direction changes at VI lead those at V2, and east-west displacement is smaller at V1 than at V2. Because V3 is located near the shelf break, it is more strongly influenced by modulations of the western edge of the Florida Current which probably dominates wind-induced variability at that location. The mean direction at V3 is northward with occasional excursions southward, as is clearly shown in the histograms of currents at V3 (fig. 2) where almost 80 percent of the observations for V3 show current moving north and about 5 percent show currents moving south. Two of these

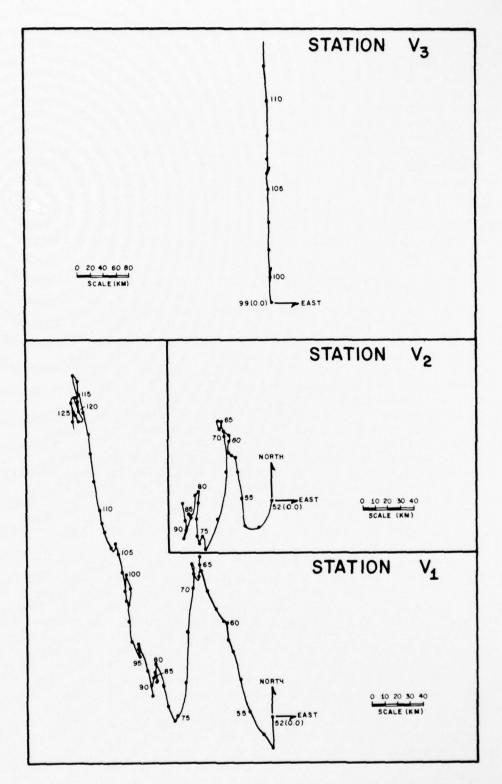


Figure 6a. 40-hr low-passed PVD's of stations V1, V2, and V3.

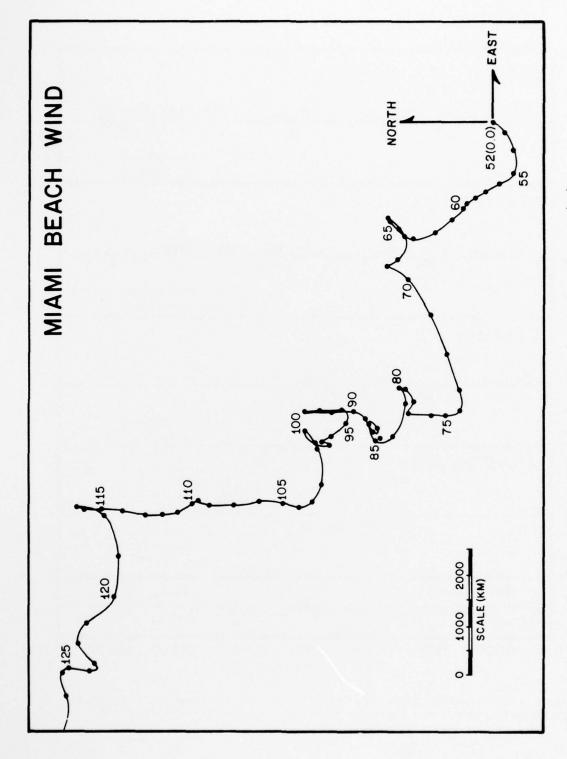


Figure 6b. 40-hr low-passed PVD of the Miami Beach, Fla., wind.

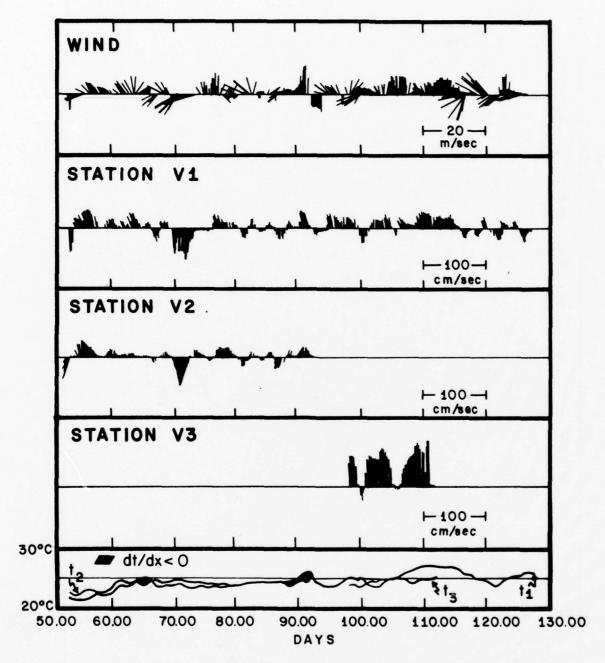


Figure 7a. Vector time series of 40-hr low-passed wind and currents with temperature from stations V1, V2, and V3.

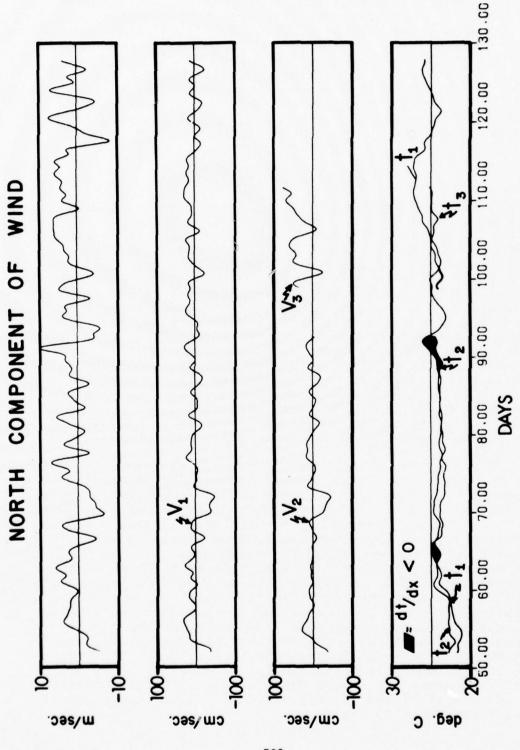


Figure 7b. 40-hr low-passed time series plots of north components of wind and currents with temperature from stations VI, V2, and V3.

southward flow events were recorded at V3 while the meter was operating (see fig. 6 and 7). These southward flow events resemble Florida Current spinoff eddies as observed by Lee (1973). Florida Current processes are clearly shown when the wind is not changing direction. This occurs around days 57, 60, and 106. On day 101, the Florida Current was apparently reinforcing the southward movement of the shelf water induced by the wind. On day 106, a small reversal occurred at V3, and the coastal waters responded accordingly. On days 57 and 60, although there are no data from V3, the Florida Current must have varied, as the wind did not change direction on these days.

## 4.2 Temperature Variations

Distinctive temperature variations are associated with the long period motions. Time series plots in figure 7 of 40-hr low-passed data show the north components of wind, currents, and temperatures  $(t_1, t_2, t_3)$  at each station. The temperature of the coastal water at this time of year is generally lower than near-surface temperatures in the Florida Current, hence temperature gradients are positive to the east, that is, dt/dx > 0. This was the case during the time period when stations V1 and V2 were sampled, except for two events that produced negative gradients. These negative gradients are noted in figure 7.

At VI, there are five temperature drops associated with weather frontal activity and accompanying flow reversals or generally southerly flow. The first temperature minimum occurs on about day 54. The next temperature events cover days 66 to 68, 92 to 95, 100 to 102, and 115 to 121, all time spans of from 2 to 7 days over which the temperature dropped from  $1^{\circ}$  to  $5^{\circ}$  C.

Temperature at V2 does not seem to fluctuate as strongly as at V1, but it does rise abruptly on day 59, probably because of a Florida Current event bringing warm water onshore. Just before the first two of the above five temperature events,  $t_1 > t_2$  or dt/dx < 0 (see fig. 7). Very few data were collected at station V3, but there are two Florida Current events (or perhaps Florida Current spinoff eddies) noted. On day 101, there was a temperature minimum for t3 associated with the maximum southerly flow. This increased to a maximum on approximately day 105 at the same time that the flow was a maximum to the north. Similarly, for the next reversal of V3, beginning on day 106 there was a temperature minimum, but it lagged the flow reversal by about a day. The northerly flow, however, was again accompanied by an increase in temperature. The temperature at station V3 is not directly comparable to that at V1 and V2 because the sensor depth is significantly greater than sensors at VI and V2, and vertical temperature gradients can be strong in this region.

## 4.3 Spectra of Time Series

Spectra of current components and temperature and the spectra for wind are plotted in figure 8. Here can be seen the rationale for the partition between low and high frequency processes at 40 hr or 0.6 c/day. The strong semidiurnal signal (inlet effects) for the east components of current is clearly seen as well as the fairly distinct diurnal signal for the temperature (diurnal heating) and wind (sea breeze). The broad band of energy in the low frequency range for the north components or current and wind is also evident.

## 4.4 Fluxes of Heat and Momentum

The data from Phase II have been used to evaluate the fluxes of heat and momentum. Here heat is used as an example. It is convenient to represent the time series in terms of three important time scales as

$$W = \langle W \rangle + \overline{W} + W',$$

where W = (u, v) for velocity, and

$$t = \langle t \rangle + \overline{t} + t'$$

for temperature.

The symbol <> is a time average over the record length; thus <w> is the mean for the record length  $W_m$ . The overbarred terms,  $\overline{W}$  and  $\overline{t}$ , are 40-hr low-passed data minus the mean and represent the slowly varying or low frequency processes. Terms like W' and t' are 40-hr high-passed data and represent the rapidly varying or high frequency processes. Heat flux over the record length is expressed as

$$\langle Wt \rangle = \langle W \rangle \langle t \rangle + \langle \overline{Wt} \rangle + \langle W't' \rangle$$
, (1a)

and the momentum flux over the record length is expressed as

$$\langle W | W \rangle = \langle W \rangle \langle W \rangle + \langle \overline{W} | \overline{W} \rangle + W'W'.$$
 (1b)

The terms <WW> are usually called Reynolds stresses. The units of the heat flux terms in equation (la) are heat flow per unit area. Its divergence is proportional to the sum of heat storage rate per unit volume and vertical flux. Similarly, the terms in equation (lb) are proportional to the transport of momentum. Statistics of the time series and flux series are tabulated in tables 2 and 3 with the fluctuation bounds around the means that correspond to approximately 70-percent confidence limits.

The cross-terms involving  $\langle W' t \rangle$  and  $\langle \overline{W} t' \rangle$  are conventionally regarded as contributing only an insignificant amount to

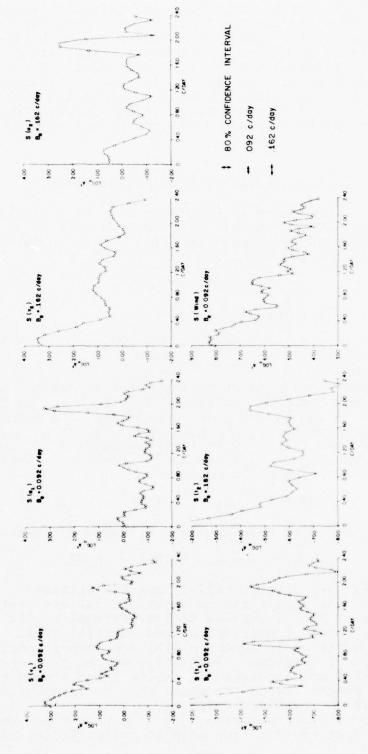


Figure 8. Spectra of north and east components of currents from stations VI and V2, spectra of temperature from VI and V2, and spectra of north component of wind.

 $\label{eq:Table 3.} \mbox{Statistics of Heat and Momentum Flux Time Series}$ 

Parameter	Length of series	Mean and 70% confidence limits		Standard deviation
$\bar{v}_1 \bar{t}_1$	976	-1.04 ±	0.57	17.92
$\overline{u}_1 \overline{t}_1$	976	0. <b>89</b> ±	0.17	5.26
$\overline{v}_2 \overline{t}_2$	976	-2.46 ±	0.33	10.37
$\overline{u}_2 \overline{t}_2$	976	0. <b>91</b> ±	0.12	3.80
$\overline{v}_1 \overline{t}_1$	1823	2.95 ±	0.54	23.06
$\overline{u}_1  \overline{t}_1$	1823	0.75 ±	0.14	5.75
v¦t¦	976	-0.25 ±	0.12	3 . 68
u¦ t¦	976	-1.01 ±	0.14	4.45
v' t'	976	21 ±	0.07	2.26
u't'	976	0.12 ±	0.07	2 .04
v¦t¦	1823	-0.18 ±	0.07	3.11
u¦t¦	1823	-0.61 ±	0.09	3 .72
$\overline{v}_1 \overline{v}_1$	976	299.43 ±	15.60	487 .33
$\overline{u}_1\overline{u}_1$	976	-26.15 ±	2.00	62 .51
$\overline{u}_1\overline{u}_1$	976	11.69 ±	0.62	19.27
$\overline{v}_2\overline{v}_2$	976	202.26 ±	11.97	373.83
$\overline{u}_2\overline{u}_2$	976	19.61 ±	2.53	79 .11
$\overline{u}_2\overline{u}_2$	976	14.18 ±	0.98	30 .75
$\overline{v}_1\overline{v}_1$	1823	244.56 ±	9.50	405 . 55
$\overline{t}_1\overline{u}_1$	1823	-26.16 ±	1.29	55 .18
$\overline{i}_1\overline{u}_1$	1823	11.11 ±	0.44	18 .84
v'v'i	976	106.49 ±	6.25	195.12
viui	976	14.74 ±	5.27	164.62
ı'u'	976	172.85 ±	8.19	255.72
v'2 v'2	976	84.14 ±	6.10	190.42
'¿u'2	976	15.52 ±	3.87	120.89
ı'u'z	976	80.01 ±	4.37	136.66
'iv'i	1823	97.34 ±	4.28	182.82
'iui	1823	9.42 ±	3.45	147.34
ı'u'	1823	149.07 ±	5.36	229.00

flux balances because of low correlation, and on this basis were neglected. Their evaluation is also possible for these data, and indeed they are found to be small. however, their large variances produce confidence limits troublesomely large compared to the mean fluxes of the high frequency terms < W't' > .

For components of the flux divergences, it was possible to compute only east-west derivatives, since the current meters were oriented in an east-west direction.

The east-west divergence component is

$$\frac{\partial P}{\partial X} + \frac{P}{h} \frac{\partial h}{\partial X} = \frac{1}{h} \nabla_{\mathbf{X}}.$$
 (Ph),

where P is the flux density and h is the depth. For these calculations, the above derivatives can be approximated by

$$\frac{P_2 - P_1}{\Delta X} + \frac{P_2 + P_1}{2} \quad (3 \times 10^{-6}).$$

The following divergences of heat and momentum have been computed

where

$$<(u-u_m)(t-t_m)> = <\overline{u} \ \overline{t}> + < u't'>$$
 $<(v-v_m)(u-u_m)> = <\overline{v} \ \overline{u}> + < v'u'>$ 
 $<(u-u_m)(u-u_m)> = <\overline{u} \ \overline{u}> + < u'u'>$ .

A schematic of the more important flux terms that result in the most significant divergences is given in figure 9.

#### 4.4.1 Heat Fluxes

During the months of November through April, measurable temperature gradients exist between the Florida Current and the coastal waters, making temperature an indicator for inshore water and heat flux a potential measure of coastal exchange rates. Heat flux spectra are shown in figure 10.

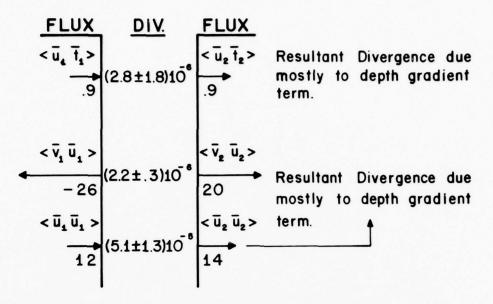
rates. Heat flux spectra are shown in figure 10.

In general, slowly varying processes transport heat offshore, and the high frequency processes transport heat shoreward. Integrated values for the long period processes are

$$\langle \overline{u}_1 \overline{t}_1 \rangle = 0.89 \pm 0.17 \, (^{\circ}C \, \text{cm/sec})$$

and

## LOW FREQUENCY



## HIGH FREQUENCY (Excluding tidal inlet effects.)

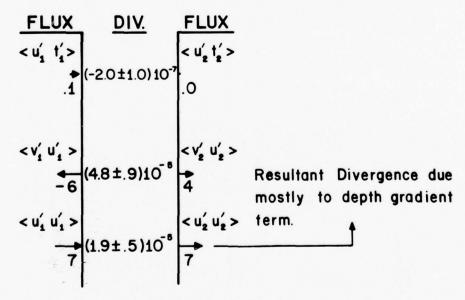


Figure 9. Schematic of the more important flux and divergence terms.

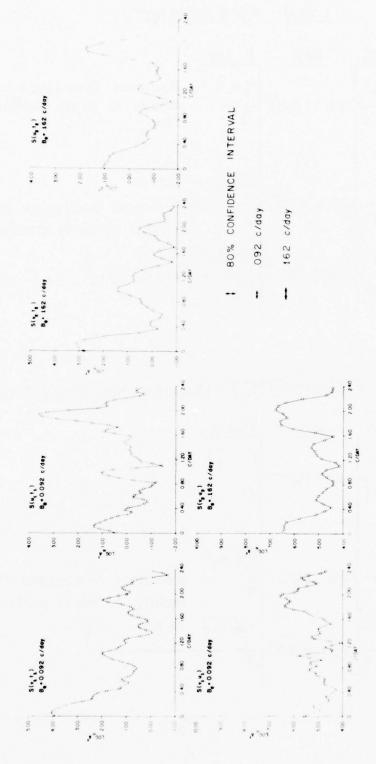


Figure 10. Spectra of north and east components of heat flux from stations VI and V2 and spectra of momentum flux from VI and V2.

$$\langle \overline{u}_2 \overline{t}_2 \rangle = 0.91 \pm 0.12$$
 (°C cm/sec),

yielding a divergence of

$$\frac{\partial}{\partial \mathbf{x}}$$
 ( $\langle \overline{\mathbf{u}} \ \overline{\mathsf{t}} \rangle$ )  $^{\circ}$  (0.01 ± 0.15) (10)<sup>-5</sup> (°C/sec)

and

$$\langle \overline{u} \ \overline{t} \rangle \frac{1}{h} \frac{\partial h}{\partial x} \approx (0.27 \pm 0.04) (10)^{-5} (^{O}C/sec),$$

with the total being

$$\frac{1}{h} \nabla_{\mathbf{x}} \cdot (\langle \overline{\mathbf{u}} \ \overline{\mathbf{t}} \rangle \ h) \sim (0.28 \pm 0.18) (10)^{-5} (^{\circ}\text{C/sec}). (2)$$

High frequency heat transports show that

$$\langle u_1't_1' \rangle = -1.01 \pm 0.14 (^{\circ}C \text{ cm/sec})$$

and

$$\langle u_2^{\dagger} t_2^{\dagger} \rangle = 0.12 \pm 0.07 \, (^{\circ}C \, cm/sec),$$

yielding a divergence of

$$\frac{\partial}{\partial x}$$
 ( )% (0.56 ± 0.11) (10)<sup>-5</sup> (°C/sec)

and

$$\langle u't' \rangle \frac{1}{h} \frac{\partial h}{\partial x} \sim (-0.14 \pm 0.03) (10)^{-5} (^{\circ}C/\text{sec}),$$

with the total being

$$\frac{1}{h} \nabla_{\mathbf{x}} \cdot (\langle u't' \rangle h) \approx (0.42 \pm 0.14) (10)^{-5} (^{\circ}C/sec)$$
 (3)

This divergence (3) was calculated without removing the tidal currents. This is especially significant near tidal inlets, and, of course, stations V1 and V2 are directly east of the Bear Cut inlet. An estimate of the importance of flux terms for areas where there are no inlets, the more typical coastal area, can be obtained by applying a 20-hr low pass filter to the 40-hr high-passed series and then forming the fluxes and calculating the statistics of these product series. This has been done for the momentum fluxes as well, and the results are tabulated in table 4. This bandpassing admits processes whose periods lie between 20 and 30 hr, thereby excluding the major semidiurnal tidal effects.

Recalculating equation (3) from the statistics in table 4,

the high frequency transports are

The state of the s

Table 4.

Fluxes with Semi-Daily Fluctuations Removed Before Forming Product Series

Parameter	Length of series	Mean and 70% confidence limits	σ
v <sub>i</sub> t <sub>1</sub>	889	0.02 ± 0.03	1.01
u <sub>1</sub> t <sub>1</sub>	889	0.08 ± 0.01	0.35
$v_2t_2$	889	-0.06 ± 0.02	0.61
u <sub>2</sub> t <sub>2</sub>	889	0.01 ± 0.01	0.29
v <sub>1</sub> t <sub>1</sub>	1736	-0.06 ± 0.02	0.99
u <sub>1</sub> t <sub>1</sub>	1736	0.05 ± 0.01	0.46
v <sub>1</sub> v <sub>1</sub>	889	37.75 ± 2.32	69.31
$v_1 u_1$	889	-5.88 ± 0.66	19.59
$u_1u_1$	889	$7.30 \pm 0.33$	9.95
$v_2 v_2$	889	24.39 ± 1.91	56.91
$v_2u_2$	889	4.25 ± 0.73	21.66
$u_2 u_2$	889	6.86 ± 0.42	12.64
$v_1 v_1$	1736	36.95 ± 1.64	68.34
$v_1u_1$	1736	-7.82 ± 0.65	27.13
$\mathbf{u}_1\mathbf{u}_1$	1736	8.84 ± 0.38	15.79

$$\langle u_1't_1' \rangle = 0.08 \pm 0.01 (^{\circ}C \text{ cm/sec})$$

and

$$\langle u_2't_2' \rangle = 0.01 \pm 0.01 (^{\circ}C \text{ cm/sec}),$$

yielding a divergence of

$$\frac{\partial}{\partial x}$$
 () % (-0.03 ± 0.01) (10)<sup>-5</sup> (°C/sec)

and

$$\langle u't' \rangle \frac{1}{h} \frac{\partial h}{\partial x}$$
 (0.01 ± 0.00) (10)  $^{-5}$  (°C/sec),

with the total being

$$\frac{1}{h} \nabla_{x} \cdot (\langle u't' \rangle h) = (-0.02 \pm 0.01) (10)^{-5} (^{\circ}C/sec),$$

which is more than an order of magnitude smaller than equation (3).

The longshore heat transport consists of a fairly stationary southward high frequency component and a nonstationary long period component. The latter result is consistent with the rather wide band forcing of the coastal waters by the wind and the Florida Current.

## 4.4.2 Momentum Fluxes

For the momentum fluxes tabulated in tables 3 and 4, two major features can be identified, one with the slowly varying processes and the other with the high frequency terms. Spectra of momentum fluxes are shown in figure 10. The contribution of slowly varying processes to the cross terms  $\langle \overline{V} \ \overline{U} \rangle$  has great spatial variation. Table 5 and figure 9 summarize the most important flux and divergence terms.

## 4.5 Limitations of Divergence Calculations

Since the means summarized in table 2 are unstable, though they were computed from record lengths of  $l^{\frac{1}{2}}$  to 3 months, the flux calculations of heat and momentum and hence their divergences are suspect. Stable statistics of Southeast Florida coastal processes require record lengths of at least 4 months. The summary of divergence calculations in table 5, however, does hint at the most important terms for the diffusion of heat and momentum.

Table 5

Summary of Flux Divergences

-	_
Low	frequency

$$\frac{1}{h} \nabla_{\mathbf{x}} \cdot (\langle \overline{\mathbf{u}} \ \overline{\mathbf{t}} \rangle \mathbf{h}) \quad (2.8 \pm 1.8) \quad (10)^{-6} \quad (^{\circ}\text{C/sec})$$

$$\frac{1}{h} \nabla_{\mathbf{x}} \cdot (\langle \overline{\mathbf{u}} \ \overline{\mathbf{u}} \rangle \mathbf{h}) \quad (2.2 \pm 0.3) \quad (10)^{-4} \quad (\text{cm/sec}^2)$$

$$\frac{1}{h} \nabla_{\mathbf{x}} \cdot (\langle \overline{\mathbf{u}} \ \overline{\mathbf{u}} \rangle \mathbf{h}) \quad (5.1 \pm 1.3) \quad (10)^{-5} \quad (\text{cm/sec}^2)$$

## High frequency

$$\frac{1}{h} \nabla_{\mathbf{x}} \cdot (\langle \mathbf{u't'} \rangle h) = (4.2 \pm 1.4) (10)^{-6} \qquad (^{\circ}\text{C/sec}) (-2.0 \pm 1.0) (10)^{-7} \qquad (^{\circ}\text{C/sec})$$

$$\frac{1}{h} \nabla_{\mathbf{x}} \cdot (\langle \mathbf{v'u'} \rangle h) = (4.9 \pm 5.9) (10)^{-5} \qquad (\text{cm/sec}^2) (4.8 \pm 0.9) (10)^{-5} \qquad (\text{cm/sec}^2)$$

$$\frac{1}{h} \nabla_{\mathbf{x}} \cdot (\langle \mathbf{u'u'} \rangle h) = (8.4 \pm 0.8) (10)^{-4} \qquad (\text{cm/sec}^2) (1.9 \pm 0.5) (10)^{-5} \qquad (\text{cm/sec}^2)$$

## 5. SPECTRAL ESTIMATES

Spectra with  $15^{\circ}$  of freedom and a Tukey lag window were calculated for all the parameters, including heat and momentum fluxes (Jenkins and Watts, 1969). If n represents the number of degrees of freedom, T the record length, and M the number of lags, then n = 2BT, where the effective bandwidth Be for a Tukey lag window is 1.33 (1/M) or 2.67 (1/2M), almost three times the resolution frequency 1/2M, and almost three times the effective bandwidth of a rectangular window. The variance for each spectral estimate is reduced by 86.5 percent compared with the variance of the sample spectrum. In other words, the variance of the spectral estimates is only 13.5 percent of the variance of the sample spectrum which is just a simple Fourier transform. A sample spectral component  $X_{\rm D}$  is defined as

 $X_{n} = \left| \frac{1}{T} \int_{-T/2}^{T/2} x(t) e^{-2\pi f t} dt \right| ,$ 

where  $X_n$  is the amplitude of the nth frequency component of the time series x(t). The variance ratio for a Tukey lag window is 0.75 (M/T)., and with 15° of freedom, M/T = 0.18 and the variance ratio (0.75) x (0.18) = 0.135.

With 15° of freedom, fluctuation bounds or a confidence interval, within which each of the spectral estimates will lie with a certain probability, may be defined. For each of the spectral plots, this confidence interval was chosen as 80 percent and its limits are shown on each of the plots in figures 8 and 10 with the effective bandwidth  $B_{\rm e}$ . The ordinates of all the spectral plots are  $\log_{10}$  (amplitude squared), making the confidence interval for each of the estimates constant.

## 5.1 Stability and Stationarity

The stability of the spectra may be evaluated by comparing estimates with different degrees of freedom, and the question of stationarity may be addressed by looking at a time history of the spectral estimates.

The question of stationarity was approached by taking the north component of current at station V1, together with the east-west heat flux at V1, and the north component of wind, and breaking the series up into five chunks or segments of 1024 points or hours for each. Each chunk was a data block shifted 240 hours from the previous block, except for the last chunk which represented less than a 240-hr shift. Thus, for each parameter, five spectra were computed, each of which was about 77-percent redundant, or contained an overlap of 77 percent of the points of the previous chunk. The amount of redundancy involved here produced gradual changes in the spectral estimates. These are shown in figures 11a, 11b, and 11c where five spectra were computed for the north component of current, east-west heat flux at V1, and the north component of

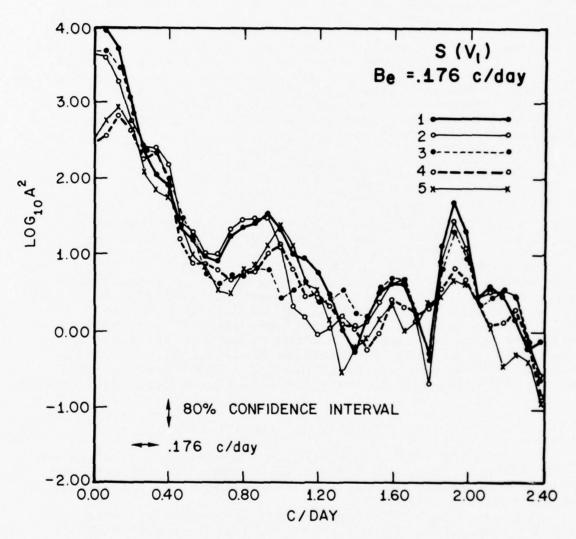


Figure 11a. Spectra of north component of current at station V1 for record lengths of 1024 hours. Each record length overlaps its adjacent record length by 77%.

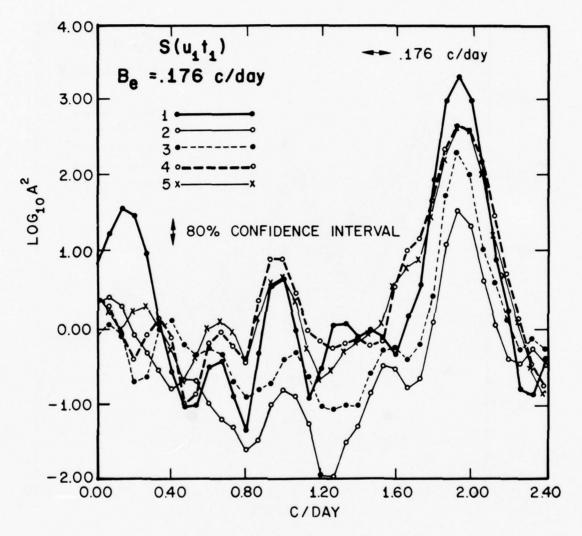


Figure 11b. Spectra of east-west heat flux at station V1 for five record lengths of 1024 hours. Each record length over-laps its adjacent record length by 77%.

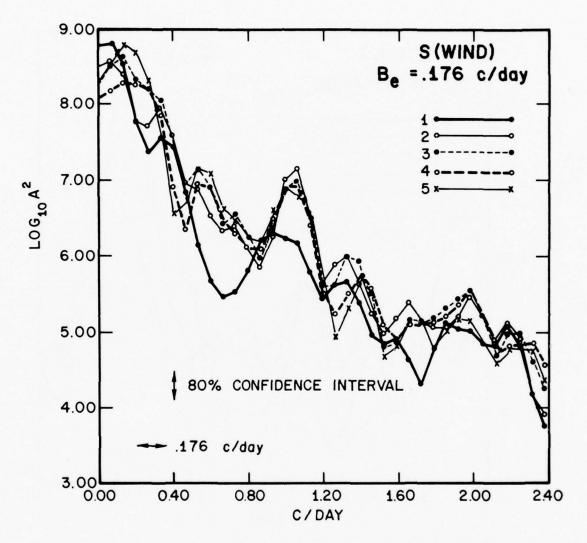


Figure 11c. Spectra of north component of wind for five record lengths of 1024 hours. Each record length overlaps its adjacent record length by 77%.

wind. The spectra computed in figures 8 and 10 represent a synthesis of the nonstationary features in figure 11.

The overall tendency of the spectra is for the energy to shift about in the low frequency part of the spectrum. This can be seen for all three parameters, the north component of current at VI, the east-west heat flux, and the wind. In some instances, the daily variations appear to be partially masked by the low frequency part of the spectrum except for the wind which has a fairly distinct and stationary diurnal peak.

## 6. CONCLUSIONS

The histograms of direction from all three stations show a clearly defined north-south fluctuation for the low frequency motions. The high frequency motions tend to flatten out the distribution of low frequency directions. This is caused by the east-west tidal current movements associated with the proximity of coastal inlets to these stations.

Shallow water motions (less than 20 m) tend to be driven largely by the wind for low frequency forcing (periods

longer than several days) with negligible lag.

In shallow water the mean vertical velocity shear near mid-depth is on the order of  $10^{-2}$  to  $5 \ (10)^{-2}$  sec<sup>-1</sup>, and data suggest that single point measurements characterize water column motions since linear correlations between components of upper and lower sensors were very near 0.9.

Motions with periods of 10 days or less can be attributed

to both the Florida Current and the wind forcing.

Temperature can be used as a tracer of coastal water during the winter and early spring where, on the average, the temperature gradient is positive to the east. This appears to be caused by frequently occurring cold fronts (every 1 to 2 weeks) that lower the temperature of the shallow shelf water. Occasionally, however, the temperature gradient will change sign (see fig. 7) when too few cold front events of sufficient intensity occur, allowing a rise in the temperature of the inshore waters even in winter.

Near the shelf break (station V3), there appears to be a temperature drop associated with southerly flow for the

two southerly flow events recorded at station V3.

The dominant east-west divergences of heat flux are associated with the slowly varying processes, that is,

$$\frac{1}{h} \nabla_{\mathbf{x}} \cdot (\langle \overline{\mathbf{u}} \ \overline{\mathbf{t}} \rangle \mathbf{h}) \sim 0(3(10)^{-6}), {}^{\mathsf{O}}\mathsf{C/sec};$$

with the tidal inlet effects removed, the divergence of the high frequency  $\operatorname{term}$ 

$$\frac{1}{h} \nabla_{\mathbf{x}} \cdot (\langle \mathbf{u}' \mathbf{t}' \rangle h) \sqrt{0} (2(10)^{-7}), {}^{0}C/\text{sec}$$

is an order of magnitude smaller. This suggests that the scale length for spatial variation of east-west heat flux is larger than the distance between V1 and V2.

The dominant momentum flux divergence is at low frequency.

$$\frac{1}{h} \nabla_{\mathbf{x}} \cdot (\langle \overline{\mathbf{v}} \ \overline{\mathbf{u}} \rangle h) \sim 0(2(10)^{-4}) \text{ cm/sec}^2.$$

The remaining divergences of  $<\overline{u}$   $\overline{u}>$ , <v'u'>, and <u'u'> vary between  $2(10)^{-5}$  and  $5(10)^{-5}$ , where <v'u'> and <u'u'> are the fluxes with the tidal effects removed; thus, it seems that the shallow water shelf dynamics are controlled mainly by the low frequency heat and momentum exchange.

The major problem in computing the statistics of South Florida coastal processes is one of adequate sampling or sufficient record length. It is estimated that at least 4 months of record are needed for stability of the computations.

Spectra of the data show basically nonstationary low frequency forcing of the shelf water by the wind and the Florida Current.

## 7. REFERENCES

- Goodheart, A. J. (1966): ODESSA, presented at the World Meteorology Organization Technical Conference on Automatic Weather Systems, Sept. 1966, Geneva, Switzerland, TCAWS/Doc. 28 (8.VII.1966); also in (1968): ODESSA, small buoys with big voices, Special Report: Instrumentation, Ocean Industry 3(10):55-59.
- Jenkins, G. M., and D. G. Watts (1969): Spectral Analysis and Its Application, San Francisco, Holden-Day, 525 pp.
- Lee, T. N. (1973): "Florida Current Spin-Off Eddies," Ph.D Dissertation, Florida State University, Tallahassee, 92 pp.

## Barotropic Rossby Waves in a Zonal Current: Effects of Lateral Viscosity<sup>1</sup>

HAROLD O. MOFJELD

Atlantic Oceanographic and Meteorological Laboratories, NOAA, Miami, Fla. 33149

MAURICE RATTRAY, JR.

Department of Oceanography, University of Washington, Seattle, 98105 (Manuscript received 21 December 1973, in revised form 11 February 1975)

#### ABSTRACT

The behavior of a barotropic Rossby wave in a zonal current is studied theoretically using a beta-plane ocean of constant depth in which the current depends only on latitude. The wave may be reflected or absorbed, depending on whether the relative frequency as detected in the moving water increases or decreases, respectively, as the wave penetrates into the current. An eastward-flowing current can reflect a Rossby wave with little transfer of zonal momentum or energy to the current, even in the presence of lateral viscosity. It does transfer meridional momentum. A westward-flowing current can absorb a Rossby wave, receiving all the wave momentum and much of its energy. Near the absorption velocity there is a balance between viscous diffusion and advection of vorticity, and relative accelerations are insignificant.

#### 1. Introduction

The behavior of Rossby waves in a mean flow is of interest in both atmospheric science and oceanography. A large literature has evolved to explain time-dependent motions and their effect on the mean circulation in terms of these waves. In this paper, we will focus on a limited aspect of this problem: the behavior of barotropic Rossby waves in a barotropic zonal current when lateral viscosity is present. We will show that Rossby waves which propagate into a sufficiently strong zonal current are either reflected or absorbed by the current and that the fate of the waves depends on whether the relative or Doppler-shifted frequency of the waves increases or decreases as the waves encounter larger current speeds.

For simplicity, the model concerns a homogeneous ocean of constant depth on a beta-plane, covered by a rigid lid. The wave motion is then governed by conservation of potential vorticity. When we average this equation over a period and then subtract the mean from the total, we obtain the vorticity equation for waves

$$\left(\frac{\partial}{\partial t} + U \frac{\partial}{\partial x}\right) \zeta + (\beta - U^{\prime\prime}) v = A_H \nabla_H^2 \zeta. \tag{1}$$

The equation states that, at any instant, there is a balance between the time rate of change of the wave vorticity  $\zeta = \partial v/\partial x - \partial u/\partial y$ , as seen by water moving with the zonal current, the advection of mean vorticity by the meridional wave velocity v, and the lateral diffusion of wave vorticity caused by lateral viscosity. Since none of the coefficients in (1) depends explicitly on time t or on the zonal coordinate x, the wave motion may be decomposed into individual waves, each with a particular frequency  $\omega$  and zonal wavenumber  $k_x$ . The model which we have chosen is barotropic and using continuity we may define a streamfunction  $\psi$ , for which  $u = -\partial \psi/\partial y$  and  $v = \partial \psi/\partial x$ . A given wave may be expressed in terms of

$$\psi = \Psi(y) \exp[i(k_x x - \omega t)], \tag{2}$$

for which the meridional dependence  $\Psi(y)$  satisfies the ordinary differential equation

$$A_H \Psi^{\prime\prime\prime\prime} + (i\sigma - 2k_z^2 A_H) \Psi^{\prime\prime} + \left[ik_x (U^{\prime\prime} - \beta) - i\sigma k_z^2 + k_x^4 A_H\right] \Psi = 0, \quad (3)$$

where primes denote differentiation. The relative frequency,  $\sigma = \omega - k_x U$ , determines the behavior of the Rossby wave in the current. It is the relative frequency of the wave as seen by water moving with the current U.

In Fig. 1, a Rossby wave is shown propagating toward zonal current; that is, the group velocity  $\mathbf{C}_{\sigma}$ , indicating the direction of energy propagation (Longuet-Higgins, 1964), is into the current. In still water U=0, and without viscosity, the wave satisfies the classical dispersion relation for Rossby waves given below and

<sup>&</sup>lt;sup>1</sup> Contribution No. 850 of the Department of Oceanography, University of Washington. This work was supported by the National Science Foundation under Grant GA 30745X.

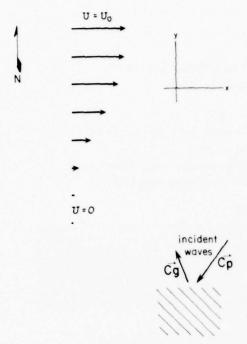


Fig. 1. Schematic diagram of a Rossby wave propagating into a zonal current which is independent of longitude. While the wave's phase velocity  $C_p$  is away from the current, the group velocity  $C_q$  carries the wave energy into the current.

illustrated in Fig. 2:

$$\omega = \frac{-\beta k_x}{k_x^2 + k_y^2}.\tag{4}$$

When lateral viscosity is present, the wave is damped as it propagates although the energy loss per wavelength is small when  $A_H$  is small. The current is also subject to viscosity which, through the diffusion of vorticity, causes the current to spread as well as dissipate. We use sufficiently small values of  $A_H$  in this paper that the time scales of the current are large compared with the wave period.

#### 2. Numerical techniques

In all the examples of Rossby waves in a current shown in this paper, the solutions are obtained by numerically integrating ordinary differential equations. All variables are first non-dimensionalized with the length scale  $k^{-1}$ , where  $k = (k_x^2 + k_y^2)^{\frac{1}{2}}$  is the wavenumber of the incident Rossby wave, and with the time scale  $k/\beta$ .

Without viscosity, the Rossby waves are governed by the ordinary, second-order differential equation

$$\Psi^{\prime\prime} + \left[\frac{k_x}{\sigma}(U^{\prime\prime} - \beta) - k_x^2\right]\Psi = 0, \tag{5}$$

where  $\sigma = \omega - k_x U$  and U'' are functions of the meri-

dional coordinate y. The current profile U(y) consists of a constant current region  $U=U_0$ , a shear zone of width  $y_0$ , and region of still water U=0 as shown in Fig. 1. The current within the shear is a fifth-order polynomial which fits U, U' and U'' continuously between the two constant current regions.

The boundary conditions needed to complete the problem are that  $\Psi$  and  $\Psi'$  in the  $U_{\theta}$  region and the still region be equal to the analytic solution of (5) which represents the incident wave and waves which decay away from the shear zone. Functions  $\Psi$  and  $\Psi'$  were found for the shear zone by integrating (5) numerically using Milne's method, as discussed by Scarborough (1966). The solution was then renormalized so that the streamfunction of the incident wave had unit magnitude; all dynamic variables were computed from  $\Psi$  and  $\Psi'$ 

With lateral viscosity, the motion is governed by the fourth-order, ordinary differential equation (3). Viscous dissipation attenuates Rossby waves as they propagate. Outside the shear zone, the governing equation may be solved analytically; we keep those solutions corresponding to the incident wave in still water and solutions which decay away from the shear zone. These solutions include not only Rossby waves, modified by viscosity, but also viscous boundary layers, modified by the beta effect. Our choice of solutions insures that the incident wave comes from still water toward the shear zone and that the response of the current radiates away from that zone.

These analytic solutions were extended into the shear zone by integrating (3) numerically using a Runge-Kutta scheme given by Collatz (1966). These solutions were matched at the center of the shear zone,  $y = y_0/2$ , by solving a complex matrix equation so that  $\Psi$ ,  $\Psi'$  and  $\Psi'''$  are continuous throughout the region of interest. All dynamic variables are then computed from  $\Psi$  and its derivatives.

## Reflection of Rossby waves by an eastwardflowing current

When a Rossby wave propagates from either the north or the south into an eastward-flowing current,

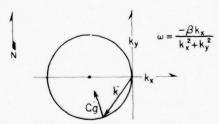


Fig. 2. In an inviscid, beta-plane ocean covered by a rigid lid, Rossby waves outside the region of currents satisfy the dispersion relation given above. All waves with the same angular frequency have wavenumbers lying on a circle of radius  $\beta/2\omega$  whose center is at  $(0, -\beta/2\omega)$ . The direction of the group velocity  $\mathbf{C}_{q}$  is from the tip of the wavenumber vector toward the center of the circle.

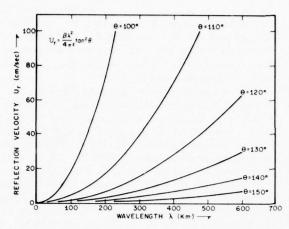


Fig. 3. The velocity  $U_r$  at which Rossby waves propagating into an eastward-flowing current would be reflected. The curves show the dependence of  $U_r$  on the wavenumber  $\lambda$  and the angle  $\theta$  between the wavenumber vector and due east, assuming  $\beta = 2.3 \times 10^{-13} \, \mathrm{S}^{-1} \, \mathrm{cm}^{-1}$ .

its relative frequency increases. For a given current system,  $\sigma$  may become so large that the wave is reflected by the current. In this section, we will consider the basic mechanism by which reflection occurs and give examples with and without lateral viscosity.

A useful way to begin the discussion is to consider waves whose wavelengths are small compared with the horizontal scale of the current. Neglecting viscosity for the moment, we apply the WKB approximation in which a Rossby wave is locally a plane wave whose amplitude and wavenumber change slowly as the wave propagates. Taking the form

$$\psi = a \exp[i(k_x x + k_y y - \omega t)] \tag{6}$$

for the streamfunction, the inviscid equation (5) becomes a dispersion relation which gives the meridional wavenumber

$$k_y = \pm \left[ \frac{k_x}{\sigma} (U^{\prime\prime} - \beta) - k_x^2 \right]$$
 (7)

as a function of relative frequency  $\sigma$ . The  $(\pm)$  sign in (7) indicates that there are two waves which, as we will see later, correspond to the incident and reflected waves.

As the wave propagates into an eastward-flowing current (U>0), the first term  $[(k_x/\sigma)(U''-\beta)]$  inside the brackets of (7) becomes smaller as  $\sigma=\omega-k_xU$  increases. There is a reflection velocity  $U_\tau$  at a latitude  $L_\tau$ , where  $k_y$  goes to zero. For larger currents,  $U>U_\tau$ ,  $k_y$  is imaginary so that the wave decays exponentially in latitude; the wave has become evanescent.

An eastward-flowing current causes a Rossby wave to refract. As wave energy approaches the reflection latitude  $L_r$ , the group velocity of the wave becomes zonal. The wave continues to refract back toward the still

water outside the current. Near  $L_\tau$ , wave motion and pressure fluctuations induce periodic motions in the current where  $U>U_\tau$ . The latter decay in latitude away from  $L_\tau$ . Currents narrow relative to the decay distance are "leaky" and a transmitted wave propagates away from the current on the far side (the "tunnel effect"). The wave near and in an eastward-flowing current consists of an interference pattern between the incident and reflected waves where  $U<U_\tau$  and a zonally periodic boundary layer decaying away from  $U_\tau$  toward larger current speeds. The total pattern propagates westward with the zonal phase velocity of the wave.

In the discussion thus far, we have not explicitly mentioned the role of the relative vorticity gradient U''. It acts to modify the reflection velocity  $U_\tau$  and the waveform, but essentially does not change the reflection process. The relative vorticity gradient may become comparable with  $\beta$  is the western boundary currents like the Gulf Stream. There is then the possibility of barotropic instabilities for which  $\beta < U''$  is a necessary condition (see Lipps, 1965). In the discussion to follow, we assume that  $U'' < \beta$  to consider waves which may give energy or momentum to the current as opposed to waves which extract energy and momentum from the current.

Solving (7) for the reflection velocity and expressing  $k_x$  in terms of the wavelength  $\lambda$  and angle  $\theta$  of the wavenumber vector with respect to east, we obtain the reflection velocity as a function of the wavelength and the orientation of the Rossby wave before it enters

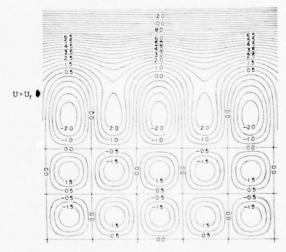


FIG. 4. Streamlines of the interference pattern between an incident Rossby wave and its reflected wave, superimposed on the eastward-flowing current which caused the reflection. In this example, the lateral viscosity is identically zero. As time proceeds, the pattern moves westward with the zonal phase velocity of the waves. The group velocities in this example are meridional. There is no exchange of energy between the waves and the current, and the wave is perfectly reflected.

the current. Neglecting U'', we obtain

$$U_r = \frac{\beta \lambda^2}{4\pi^2} \tan^2 \theta. \tag{8}$$

In Fig. 3, the distance a Rossby wave penetrates into a current, as expressed by  $U_r$ , depends strongly on both the initial wavelength and orientation. Waves with long wavelengths or whose wavenumbers are nearly meridional propagate farthest (that is, to largest values of  $U_r$ ) into the current.

An example of a Rossby wave being reflected by a current is shown in Fig. 4. What we see is an interference pattern of the incident and reflected waves, superimposed on the eastward-flowing current. The figure shows the streamline pattern at one instant in time; as time proceeds, the pattern would move westward with the zonal phase velocity  $\omega/k_z$  of the Rossby waves.

The incident and reflected waves in Fig. 4 have equal amplitudes. This is consistent with the finding of Bretherton and Garrett (1968) that waves in a shearing, inviscid fluid conserve wave action, the ratio of the energy flux to the relative or "intrinsic" frequency  $\sigma$ . Outside the current, the reflected wave, for which the frequency  $\sigma = \omega$ , is equal to frequency of the incident wave; and its energy flux is equal to the energy flux of the incident wave. Since the magnitudes of the group velocities for the two waves are equal, their amplitudes must be equal.

Without viscosity, the Rossby wave is reflected without transferring zonal momentum to the current, as can be seen from the symmetry of the streamlines in Fig. 4. During a wave period the meridional velocity advects as much zonal momentum into the current as it advects back out again; the zonal Reynolds stress  $-\overline{uv}$  is identically zero. The wave does exert a meridional force through  $-(\overline{v^2})'$ , which is positive and hence tends to increase the shear of the current.

When lateral viscosity is included in the theoretical model, we find that the reflection process is only slightly modified. In Fig. 5, the streamfunction pattern for a reflection wave in a viscous ocean strongly resembles the pattern for the inviscid case (Fig. 4). The reflection process is therefore basically inviscid with viscosity acting to modify but not completely alter the dynamics. Viscosity allows the transfer of zonal momentum and energy between the wave and current, but the exchange is not greatly different from the inviscid case, as we see by comparing the energy transfer terms in Fig. 6 with similar terms in Fig. 11, corresponding to absorption of a wave.

## Absorption of Rossby waves by a westwardflowing current

If a Rossby wave propagates from either the north or the south into a westward-flowing current (U<0), its relative frequency  $\sigma$  decreases, and the wave may encounter a region where  $\sigma$  goes to zero. Relative accelerations, proportional to  $\sigma$ , no longer play a significant role in the wave dynamics. Assuming that lateral viscosity is present, a balance is then maintained between the wave advection of mean vorticity and the diffusion of wave vorticity.

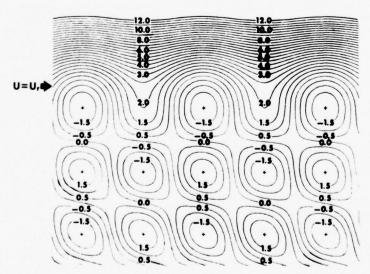


Fig. 5. Streamline pattern due to reflection of a Rossby wave when lateral viscosity is present  $\left[ (k^3/\beta) A_H = 0.025 \right]$ . The pattern is similar to the inviscid case (Fig. 4) indicating that the reflection process is basically inviscid. The differences between the figures arise because the incident and reflected waves are damped by viscosity as they propagate.

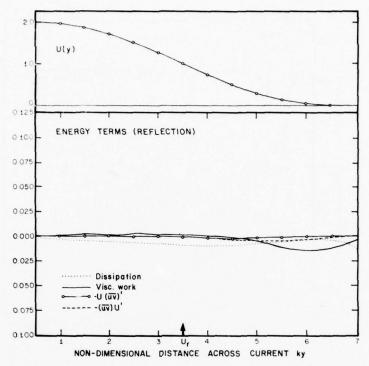


Fig. 6. Profiles of the energy terms corresponding to the example in Fig. 5 of the reflection of a Rossby wave by an eastward-flowing current. Little energy is transferred between the wave and the current during reflection compared with absorption of a wave (Fig. 11).

This is a different balance than occurs with a solid boundary present because the two "viscous" solutions are small everywhere and the viscosity-modified "inviscid" wave solutions dominate. As shown by Reid (1965) and Lakin (personal communication), there are four solutions to Eq. (3),  $\Psi_1$ ,  $\Psi_2$ ,  $\Psi_3$  and  $\Psi_4$ , in which  $\Psi_{1,2}$  are essentially inviscid while  $\Psi_{3,4}$  are essentially viscous and would not occur in an inviscid fluid. With sufficiently small viscosity each can be expanded

$$\Psi = \sum_{i=0}^{\infty} \epsilon^{i} \overline{\Psi}^{(i)}, \qquad (9)$$

with

$$\epsilon = (iA_H k_x^2 / U_a')^{\frac{1}{2}}, \quad |\epsilon| \ll |. \tag{10}$$

Near the critical layer we take

$$\sigma = \frac{d\sigma}{dy}\bigg|_{y=y_a} (y-y_a) = -k_x U_a'(y-y_a), \qquad (11)$$

and

$$\eta = k_x (y - y_a) / \epsilon. \tag{12}$$

Substituting then into (3) and collecting terms, the two lowest order equations are

$$\left(\frac{d^2}{d\eta^2} + \eta\right) \frac{d^2 \Psi^{(0)}}{d\eta^2} = 0,\tag{13}$$

$$\left(\frac{d^2}{d\eta^2} + \eta\right) \frac{d^2 \bar{\Psi}^{(1)}}{d\eta^2} = -\frac{U_a''}{k_x U_a'} \left[\frac{1}{2} \eta^2 \frac{d^2}{d\eta^2} - \frac{U_a'' - \beta}{U_a''}\right] \bar{\Psi}^{(0)}. \quad (14)$$

The zero-order "viscous" solutions are double integrals of the Airy functions and as stated above are small. The zero-order "inviscid" solutions are

$$\Psi_1 = \epsilon \eta = k_x (y - y_a), \tag{15}$$

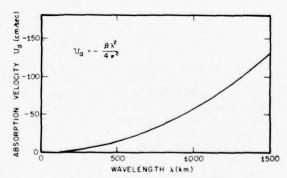


Fig. 7. The absorption velocity  $U_a$  (negative toward the west) of a westward-flowing current at which a Rossby wave of wavelength  $\lambda$  is absorbed; it is equal to the zonal phase velocity  $\omega/k_x$  of the wave. Note that  $U_a$  is independent of the direction of propagation, although waves coming from different directions have in general different periods.

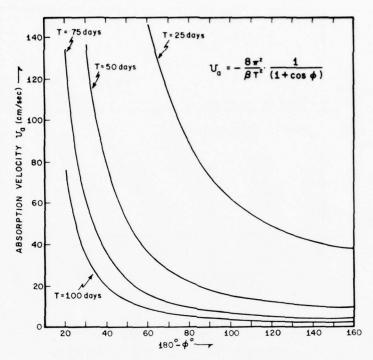


Fig. 8. The absorption velocity as a function of the wave period T and the angle  $\phi$  between the group velocity  $C_{\sigma}$  and due east. For a given wave period,  $U_{\sigma}$  becomes increasingly larger as the wave energy propagates more westward  $(\phi \to 0)$ .

the leading term in  $\Psi_1$ , and

$$\Psi_2 = 1, \tag{16}$$

the leading term in the regular part of  $\Psi_2$  ( $\Psi_2$  has a singularity as  $y=y_a$  in the inviscid case). Since these terms satisfy the zero-order equation trivially, the balance of forces is determined from the first-order equations, and at  $\eta=0$  the only remaining terms are

$$\frac{d^4}{d\eta^4} \overline{\Psi}_2^{(1)} = \frac{U_{a''} - \beta}{k_x U_{a'}} \overline{\Psi}_2^{(0)} = \frac{U_{a''} - \beta}{k_x U_{a'}},\tag{17}$$

which represents a balance between the advection of mean vorticity and the diffusion of wave vorticity. The wave is absorbed within the region, giving its momentum to the current. The wave energy goes partially into work done on the current, and the rest is dissipated by viscosity.

The absorption velocity  $U_a$ , often called the critical velocity, is equal to the zonal phase velocity  $\omega/k_x$  of the Rossby wave in still water. Writing the absorption velocity in terms of the wavelength  $\lambda$  in still water, we find from (4) that the absorption velocity

$$U_a = -\frac{\beta \lambda^2}{4\pi^2} \tag{18}$$

is independent of the direction of propagation;  $U_a$  is plotted in Fig. 7 as a function of wavelength. All waves absorbed at a given current velocity had the same wavelength in still water, although they could have come from different source regions.

Since Rossby waves are anisotropic, waves having the same wavelength but different orientations have, in general, different periods. Letting  $\phi$  be the angle between the group velocity  $\mathbf{C}_{\varphi}$  and due east, the absorption velocity may be expressed as a function of  $\phi$  and the wave period T:

$$U_a = -\frac{8\pi^2}{\beta T^2 (1 + \cos\phi)}.\tag{19}$$

This is plotted in Fig. 8. We see from the figure that for a given period, the waves have smallest absorption velocities when the wave energy is propagating nearly eastward. Waves whose group velocities are nearly westward have large absorption velocities and would probably not be absorbed. Actually, around  $\phi=0$ , the rigid lid assumption breaks down. As shown by Rattray (1964) for a beta-plane ocean with a free surface, gravity modifies the dispersion relation, preventing k from going to zero and thus constraining  $U_a$  to finite but large values.

An example of a Rossby wave being absorbed by a westward-flowing current is shown in Fig. 9. The tech-

nique for solving the viscous problem is given in the section on numerical techniques. The wave, which is partially damped by viscosity as it propagates into the current, is absorbed around the absorption velocity  $U_a$ . A viscous boundary layer extends the wave influence into stronger current. Contrary to an inviscid model, the meridional wavenumber  $k_y$  does not become infinite at  $\sigma=0$ ; nor does the wave amplitude increase without bound. Our results agree with those of Bennett and Young (1971) who studied Rossby waves subject to linear friction and initial transients.

In Fig. 9 we see the streamline pattern at one instant. As time proceeds, the wave pattern moves westward with the zonal phase velocity  $\omega/k_x$ . The pattern moves more rapidly westward than water in the current for which  $|U| < |U_a|$ ; where  $|U| > |U_a|$ , the water overtakes the wave pattern. The phase propagation outside the current gives the illusion that the Rossby wave is radiating from the current. However, the group velocity, indicating the direction of energy propagation, is into the current.

The momentum transferred from the Rossby wave to the current may be seen qualitatively in Fig. 9. Since the wave is attenuated within the current, decreasing amplitude of the meridional wave velocity produces a meridional force  $-(\overline{v^2})'$ , exerted away from still water. The wave also exerts a zonal force  $-(\overline{uv})'$  in the direction of the current. Using the same argument

presented by Starr (1968) to describe momentum transfer by Gulf Stream meanders, the skewed pattern of streamlines near  $U=U_a$  in Fig. 9 allows the meridional wave velocity v to carry more zonal momentum into the current than it returns. Details of the Reynolds stresses  $\overline{-uv}$  and  $\overline{-v^2}$  and their dependence on lateral viscosity are shown in Fig. 10. The zonal force exerted by the wave does work on the current; this work and the viscous dissipation of the wave are shown in Fig. 11. We see that Rossby waves propagating into a westward-flowing current can sharpen the shear and accelerate the current.

## 5. Discussion

Let us consider a large gyre of oceanic dimensions and explore the behavior of Rossby waves, generated in the gyre's quiescent center, as they propagate into the anticyclonic current system. Waves whose group velocities carry the waves toward the equator are absorbed by the westward-flowing current. Waves, whose group velocities carry them into the eastward-flowing, high-latitude current, are reflected and propagate back toward the equator; they are also absorbed by the westward-flowing current.

The analysis thus far has not included non-zonal currents, such as the poleward-flowing, western boundary currents or equatorward-flowing drift on the

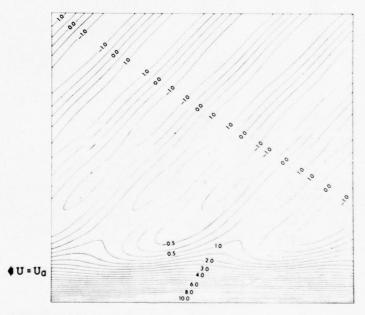
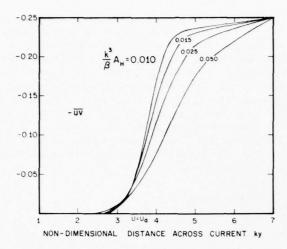


Fig. 9. The absorption of a Rossby wave by a westward-flowing current. The wave, incident from the top of the figure, propagates into the current; it is absorbed near the absorption velocity  $U_{\sigma}$  in a region whose width depends on the lateral viscosity. In this example,  $(k^2/3)A_H = 0.025$  and the width of the shear zone within the current is  $ky_0 = 7.0$ . The asymmetry of the streamlines within the current indicates that the Rossby wave is giving up zonal momentum to the current.



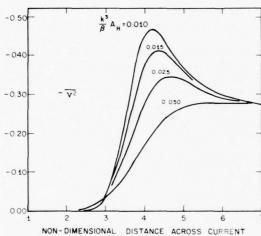


FIG. 10. The Reynolds stresses -uv and  $-v^2$  for a Rossby wave being absorbed by a westward-flowing current, the same wave illustrated in Fig. 9. The curves indicate the dependence of these stresses on lateral viscosity. The behavior of waves with non-meridional group velocities is similar to that shown here.

eastern part of gyres. It seems clear though that the fate of the Rossby waves depends on the relative frequency  $\sigma = \omega - \mathbf{k} \cdot \mathbf{U}$ . If  $\sigma$  increases and  $|\mathbf{k} \cdot \mathbf{U}|$  becomes sufficiently large, the waves will be reflected. If, on the other hand,  $\sigma$  decreases to zero, the waves will be absorbed and give all their momentum and some of their energy to the current. In general, whether the waves are reflected or absorbed, they exert a force on the water within the current system, tending to push the water out away from the center of the gyre. This force is a generalization of the meridional force  $-(v^2)'$  and is in the direction of maximum attenuation of the waves within a given current. Since longer wavelength waves have smaller wavenumbers, those waves penetrate furthest into the currents, and they may reach the

continental slope, where they are reflected back into the gyre, usually with a different wavelength.

While we have used lateral viscosity in this paper, Bennett and Young (1971) chose a linear friction to study the behavior of barotropic Rossby waves in a mean flow. Instead of the diffusion term on the right-hand side of the vorticity equation (1), linear friction creates a loss term  $-\alpha\zeta$ , which is proportional to the vorticity. We may attribute this loss to the bottom Ekman layer. Similarly, the linear momentum of the waves is lost to the fluid through bottom drag. There is, then, an essential difference between lateral viscosity which couples laterally adjacent water parcels and linear friction which couples a given water parcel to the bottom Ekman layer.

A barotropic Rossby wave is subject to both lateral viscosity and spindown by the bottom Ekman layer. As we generalize the homogeneous model to a more realistic model in which the ocean is stratified, the vertical density gradient may suppress Ekman suction. Stratification decouples barotropic motions from the bottom, and viscous processes are then dominated by lateral viscosity.

Dickinson (1970) and Bennett and Young (1971) also considered the development of Rossby waves in a mean flow as they propagate into an initially steady flow. They find that the time scale for development of a stationary wave pattern is so long compared with the time scale of seasonally fluctuating winds that the atmosphere is

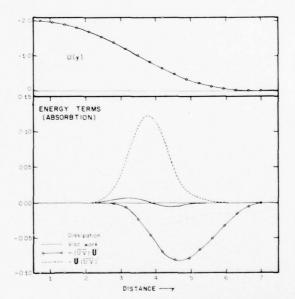


Fig. 11. Profiles of the energy terms corresponding to the example of absorption of a Rossby wave by a westward-flowing current given in Figs. 9 and 10. The term -(uv)U' appears in the energy equation, giving the rate at which energy is added or removed from the wave by the current. The term -U(uv)' is the rate at which work is done on the current by the wave.

always in a transient state. There are important currents in the oceans, such as the Somali Current, which have seasonal time scales, and the results of the above papers are of particular interest in studying these currents. Most major current systems in the ocean are far steadier than the major wind systems in the atmosphere. We may expect for these currents that a Rossby wave could become fully developed and that the results of the present paper would then apply.

The real oceans do not, of course, have a constant depth, and, as shown by Rhines (1969), bottom topography can trap Rossby waves. The oceans are also not covered by a rigid lid and the combined role of gravity and the beta-effect can cause equatorial trapping of waves. Both these effects may constrain Rossby waves to particular regions where the waves are either absorbed by currents or dissipated by friction. If the waves are absorbed by currents the absorption process should resemble that described in this paper.

#### 6. Summary

When a Rossby wave propagates into a zonal current, its behavior is determined by the relative or intrinsic frequency as seen by water moving with the current. If the frequency becomes sufficiently large, the wave will be reflected by the current. The wave then exerts a meridional force on the water; even with lateral viscosity, most of the zonal momentum and energy of the waves propagates away with the reflected wave. If the relative frequency decreases to zero, the Rossby wave is completely absorbed, giving up all of its momentum and much of its energy to the current. In the absorption region, the dynamic balance is between

wave advection of vorticity and the diffusion of wave vorticity caused by lateral viscosity.

Acknowledgments. The authors wish to thank F. P. Bretherton for discussions on the pitfalls of non-zonal currents in the theory of waves in currents. The authors also wish to thank F. A. Lee for his suggestions on numerical techniques.

#### REFERENCES

- Bennett, John R., and John A. Young, 1971: The influence of latitudinal wind shear upon large-scale wave propagation into the tropics. Mon. Wea. Rev., 99, 202-214.
- Bretherton, Francis P., and Christopher J. R. Garrett, 1968: Wave trains in inhomogenous moving media. Proc. Roy. Soc. London, A302, 529-554.
- Collatz, Lothar, 1966: Numerical Treatment of Differential Equations, 3rd ed. (Grundlehren der Mathematischen Wissenschaften, Vol. 60), Springer-Verlag.
- Dickinson, Robert E., 1970: Development of a Rossby wave critical level. J. Atmos. Sci., 27, 627-633.
- Lipps, Frank B., 1965: The stability of an asymmetric zonal current in the atmosphere. J. Fluid Mech., 21, 225-239.
- Longuet-Higgins, and Michael S., 1964: On group velocity and energy flux in planetary wave motions. Deep Sea Res., 11, 35-42.
- Rattray Jr., Maurice, 1964: Time-dependent motion in an ocean:
  A unified two-layer, beta-plane approximation. Studies on
  Oceanography, Hidaka Commemoration Volume, The University of Washington Press, 19-29.
- Reid, William H., 1965: The stability of parallel flows. Basic Developments in Fluid Dynamics, Vol. 1, Maurice Holt, Ed., 249-307.
- Rhines, Peter B., 1969: Slow oscillations in an ocean of varying depth, Part I: Abrupt topography. J. Fluid Mech., 37, 161-190.
- Scarborough, James B., 1966: Numerical Mathematical Analysis. 6th ed., The Johns Hopkins University Press, 600 pp.
- Starr, Victor P., 1968: Physics of Negative Viscosity Phenomena. McGraw-Hill, 256 pp.

22 Reprinted from: NOAA Technical Report ERL 340-AOML 19, 24 p.



U.S. DEPARTMENT OF COMMERCE Rogers C. B. Morton, Secretary

NATIONAL OCEANIC AND ATMOSPHERIC ADMINISTRATION
Robert M. White, Administrator
ENVIRONMENTAL RESEARCH LABORATORIES

Wilmot N. Hess, Director

# NOAA TECHNICAL REPORT ERL 340-AOML 19

# **Empirical Model for Tides in the Western North Atlantic Ocean**

HAROLD O. MOFJELD

BOULDER, COLO.
October 1975



## DISCLAIMER

The NOAA Environmental Research Laboratories do not approve, recommend, or endorse any proprietary product or proprietary material mentioned in this publication. No reference shall be made to the NOAA Environmental Research Laboratories, or to this publication furnished by the NOAA Environmental Research Laboratories, in any advertising or sales promotion which would indicate or imply that the NOAA Environmental Research Laboratories approve, recommend, or endorse any proprietary product or proprietary material mentioned herein, or which has as its purpose an intent to cause directly or indirectly the advertised product to be used or purchased because of this NOAA Environmental Research Laboratories publication.

## CONTENTS

		Page
ABST	TRACT	. 1
1.	INTRODUCTION	1
2.	FUNDAMENTAL FORMULAS	9
3.	USE OF THE MODEL	12
4.	COMPUTER SUBROUTINES AND FUNCTIONS	14
5.	ACKNOWLEDGMENTS	15
6.	REFERENCES	16
7.	APPENDIX	17

# EMPIRICAL MODEL FOR TIDES IN THE WESTERN NORTH ATLANTIC OCEAN

Harold O. Mofjeld

#### ABSTRACT

This report describes an empirical tide model for the western North Atlantic ocean which predicts the semi-daily and daily tides relative to mean sea level. The model interpolates harmonic constants from three reference stations on a Mercator projection to obtain constants at a given location, from which the tides are then computed. The geographic region over which the model predicts tides within a standard deviation of 5 cm was determined through a comparison with data from test tide stations. A set of FORTRAN subroutines and their use are described, allowing a user to implement the model. Minor modifications of two subroutines are required to extend the period of the model 1973-1978 to either earlier or later periods.

#### 1. INTRODUCTION

This tide model, developed by the author under NASA Contract Number 369-07-01-17-53, is designed to provide seasurface displacement information for tides in the western North Atlantic Ocean. The model is a set of computer subroutines which compute the tidal displacement from mean sea level, given the coordinates of the desired location and the desired date and time. It can be used to generate a time series at a given location, the geographical distribution of tidal height at a given instant, and/or the tidal height under a satellite as it passes over the model area. The model was developed in support of the GEOS-III satellite program to measure tides from space; the model area corresponds to part of the calibration area for this satellite.

The tidal displacement is computed from a set of harmonic constants which have been obtained by linear interpolation on a Mercator projection of harmonic constants at three reference stations. The latter constants were found through analysis of actual pressure or sea level observations. Figure 1 shows the western North Atlantic Ocean reference and test stations and a cross-hatched area indicating where the model is applicable as estimated from an accuracy criterion applied at test stations. Table 1 lists the locations of the reference stations, the periods over which the observations were made, the analysis method, literature references, and harmonic constants.

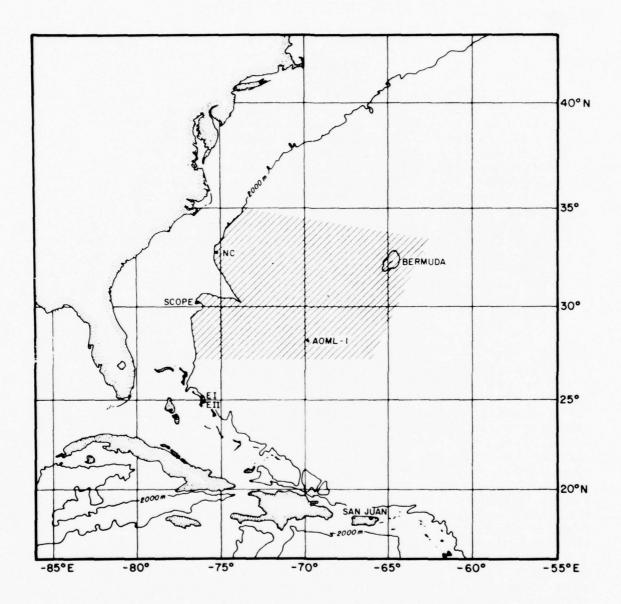


Figure 1. GEOS-III calibration area in the western Atlantic with reference and test stations and the geographical extent of the GEOS-III tide model as defined by the cross-hatched region.

Table 1. Reference Stations

Location	Bermuda 32°24N,	-64042E	MODE/AOML-1 28 <sup>0</sup> 08N, -69 <sup>0</sup> 45E	-1.69°45E	SCOPE 30 <sup>2</sup> 26N, -76 <sup>o</sup> 25E	76 <sup>0</sup> 25E
Gage type	Shore gage	3e	Bottom pressure gage	essure	Bottom pressure	essure
Observation period	1950-1951,	,,,	11 Mar 29 June 1973	1973	18 Sept. 1973 20 Mar. 1974	1973 - 974
Type of analysis	Response method	method	Response method	method	Response method	method
References	Zetler et al. $(1975)$	$(\frac{1}{5})^{\frac{1}{a_1}}$ .	Zetler et al. (1975)	$(5)^{\frac{a}{1}}$ .	Pearson (1975)	
Constituents	Amplitude Phase	Phase	Amplitude Phase	Phase (06)	Amplitude	Phase
$M_2$	0.356	358.3	0.345	9.0	0.434	357.6
N <sub>2</sub>	0.082	337.7	0.080	339.8	0.106	335.7
52	0.081	24.2	0.071	30.8	0.082	23.1
K2	0.021	22.7	0.019	28.0	0.018	(21.6)
K <sub>1</sub>	990.0	187.0	0.077	194.7	960.0	189.8
0,1	0.053	192.1	0.061	197.6	0.073	194.
$^{P}_{1}$	0.020	187.8	0.024	195.2	0.032	189.8
Q <sub>1</sub>	0.011	186.6	0.013	193.3	0.014	183.8

The accuracy of the model depends on several factors: How accurately the harmonic constants have been determined at the reference stations, how well the interpolation scheme follows the actual distribution of harmonic constants, and whether the limited number of harmonic constants used in the model adequately describe the tides. The goal of the model is to provide tidal displacements above mean sea level within  $\pm 5$  cm standard deviation in the area shown in figure 1. Eight harmonic constants have been selected for the model: four daily constituents,  $K_1$ ,  $O_1$ ,  $P_1$ ,  $O_1$ ; and four semi-daily constituents,  $V_2$ ,  $V_2$ ,  $V_3$ ,  $V_4$ . These eight constituents contain almost all the energy in the daily and semi-daily tidal frequency bands.

Lower frequency, minor daily and semi-daily, and higher frequency sea-level fluctuations are not included in the model. A discussion of the excluded fluctuations and their behavior in the western Atlantic can be found in Zetler et al. (1975), and Brown et al. (1975). The observations at the reference stations are measurements of either bottom pressure or sea level. Such measurements do not include displacements of the sea surface caused by the vertical motion of the bottom; the model therefore

does not contain earth tides.

A comparison of tidal heights as obtained from observations at the MODE/AOML-1 station with predictions of the model is shown in figure 2. The standard deviation of model from the observations for the duration of the AOML-1 record is 3.0 cm. The observations have been filtered to remove fluctuations

at frequencies lower than tidal bands.

The area within which the model should meet the +5 cm accuracy criterion was obtained through a study of tidal distributions for the Atlantic Ocean as given by Dietrich (1963) and through a comparison of harmonic stations at tide stations other than the reference stations. There is good agreement at the NC (North Carolina) station. The model's predictions should therefore be accurate as far north as 35°N, near the continental shelf.

The discrepancies at Eleuthera Island and Puerto Rico stations define the southern limit of the model as shown in figure 1. The differences in harmonic constants between the model and these latter stations, as given in table 2, result from changes in the tidal regime between the western and equatorial Atlantic Oceans and from more localized influences of tidal regimes behind the islands, extending through the passes between the islands. A clear example of variations in tides near passes can be seen in table 2 by comparing the two Eleuthera Island stations shown in figure 3. The tidal regime on the Bahama Banks influences the tides at both stations; Eleuthera I, to a greater extent with smaller tidal amplitudes and later phases, than Eleuthera II, which is farther from island passes. Neither station can be considered representative of the open

Through studies such as Redfield (1958), it is clear that, on the continental shelves, tidal amplitudes and phases change over distances which are short compared with distances over which amplitudes and phases vary in the western Atlantic

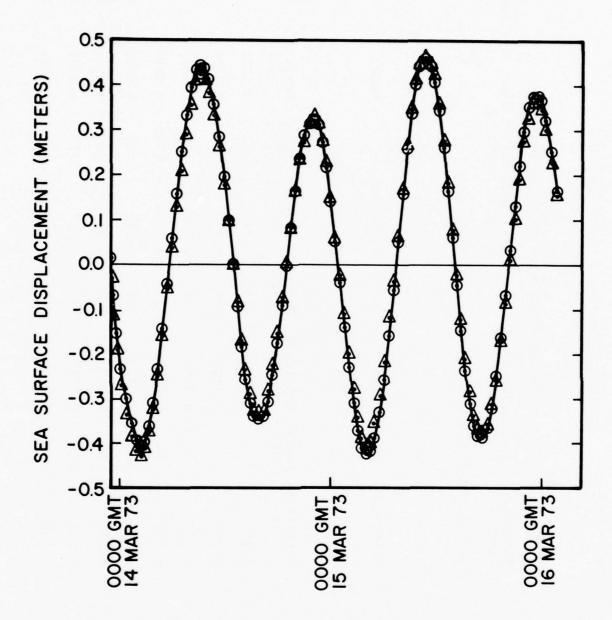


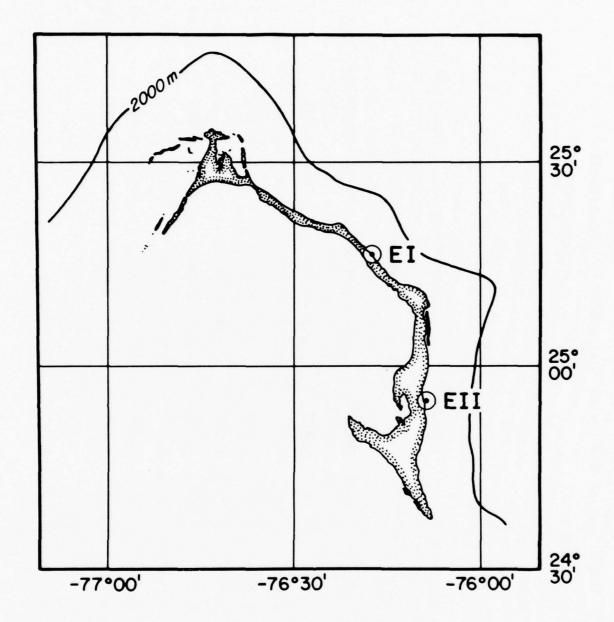
Figure 2. Comparison of observed and predicted sea-surface displacements at the MODE/AOML-1 reference station (28 08N, -69 45E) for the interval 18-21 Mar. 1973.

Table 2. Comparison of Model with Test Stations

	.7 01001		arraon or n	7000	comparison of mour with 103t oracions	CHOTA		
Location	North Carolina Station 32041.5'N, -75037.5'E	olina St , -75°37	ation 1		San Juan, 18 <sup>0</sup> 29'N, -	Puerto   66 <sup>0</sup> 07'E	San Juan, Puerto Rico, Station 18 <sup>0</sup> 29'N, -66 <sup>0</sup> 07'E	uo
Gage type	Bottom pressure		gage		Shore gage			
Observation period	9 July - 6 Aug. 1972	5 Aug. 1	972		1899; 191 1/2-day duration	1/2-day	duration	
Type of analysis	Harmonic		Model		Harmonic		Mode1	
Reference	Mofjeld, 1972	2761			USC&GS, 1942	4.2		
Constituents	Amplitude (m)	Phase (OG)	Amplitude (m)	Phase (0G)	Amplitude (m)	Phase (0G)	Amplitude (m)	Phase
M2	0.481	356	0.4574	356	0.149	18	0.2021	16
N <sub>2</sub>	0.093	339	0.1123	334	0.034	4	0.0409	7
S <sub>2</sub>	0.072	27	0.0891	20	0.021	39	0.0518	65
K2	(0.020)	(27)	0.0193	17	(0.000)	(38)	0.0187	54
K <sub>1</sub>	0.101	185	0.0955	186	0.082	228	0.0680	216
01	0.077	192	0.0721	192	0.073	227	0.0551	211
$P_1$	(0.033)	(185)	0.0320	187	0.027	228	0.0191	220
Q1	(0.015)	(185)	0.0135	179	0.015	227	0.0154	213

Comparison of Model with Test Stations -- (Continued) Table 2.

Location	Eleuthera I (25 <sup>0</sup> 16.1'N,		-76 <sup>0</sup> 17.2'E)		Eleuthera II (24 <sup>o</sup> 55.8'N, -76 <sup>o</sup> 09.2'E)	11 -7600	9.2'E)	
Gage type	Shore gage				Shore gage			
Observation period	1-29 Sept. 1974	1974			1946; 369-day duration	day dur	ation	
Type of analysis	Harmonic		Mode1		Harmonic		Model	
Reference	Carrier (1975)	(375)			Goodman (1975)	975)		
Constituent	Amplitude (m)	Phase (°G)	Amplitude (m)	Phase (°G)	Amplitude (m)	Phase (OG)	Amplitude (m)	Phase (OG)
M <sub>2</sub>	0.344	6.7	0.367	1.2	0.321	20.3	0.361	1.5
$N_2$	960.0	346.7	0.087	339.7	0.071	0.3	0.080	340.1
$S_2$	0.058	29.5	0.067	34.2	0.052	48.3	990.0	35.2
K <sub>2</sub>	0.016	29.5	0.016	34.8	0.013	39.0	0.016	35.8
$\kappa_1$	0.076	213.8	0.093	197.5	0.084	209.0	0.093	198.0
$s_1$	0.061	204.8	0.072	199.8	0.065	212.3	0.072	200.2
$^{P}_{1}$	0.025	213.8	0.030	197.2	0.026	213.8	0.030	197.8
$Q_1$	0.012	20.3	0.015	194.3	0.013	209.3	0.015	195.0



## • TIDE STATIONS

Figure 3. Tide stations Eleuthera I and Eleuthera II located in the Bahamas near passes between Eleuthera and adjacent islands.

Ocean. The GEOS-III tide model is based on harmonic constants from the open ocean and is applicable only where the tidal amplitude and phase variations have oceanic rather than shelf spatial scales. The model should be used seaward of the 2000-m depth contour. If extrapolated into shallower water, the model will underestimate the tidal amplitudes. The discrepancy increas-

es rapidly shoreward of the 200-m depth contour.

While it is traditional in tidal prediction calculations to fix the node factors at a single set of values for time series up to 1 year in duration, the model computes the instantaneous node factors for each time. The more accurate procedure is used for two reasons: First, the operational period of the GEOS-III satellite coincides with a period in which the node factors are changing rapidly, and hence the fixed factors are likely to differ significantly from the correct values; and second, variable node factors allow direct comparisons between results of the model and observations obtained several years before the launch date of the satellite. The additional computer time required to compute the node factors is not significant.

Because of assumptions used in establishing the time base of the model and because of assumptions made about the functional dependence of the node factors on time, the model should be used only within the time period 1973-1978. Extending this period requires simple modifications of subroutines TIME and

NODE.

In the open ocean the sea surface is fluctuating about a time-independent mean because of several processes of which ocean tides produce some of the largest displacements. In the GEOS-III calibration area, tidal displacements amount to about ±0.5 m. Other processes such as time-dependent currents, atmospherically induced, low frequency waves, seasonal heating and cooling (steric anomaly), and earth tides may produce displacements of perhaps ±0.1 m. The region of the Gulf Stream in the calibration area is subject to meanders of the current which can produce sea surface fluctuations as large as 1 m. If the altimeter of the GEOS-III is found to have sufficient resolution, these processes must be included in any analysis scheme to remove and/or study time-dependent sea surface fluctuations in the altimetry data.

#### 2. FUNDAMENTAL FORMULAS

The sea surface displacement at a given time and location is computed using the expression

$$h = \sum_{i=1}^{8} f_i A_i \cos (\sigma_i t - \tau_i) , \qquad (1)$$

where  $f_i$ ,  $A_i$ ,  $\sigma_i$ , and  $\zeta_i$  are the node factor, amplitude, frequency, and phase lag of the i-th tidal constitutent and t is the time relative to 0000 GMT 1 March 1975. The frequencies of the eight principal constituents are obtained from Schureman (1941); all other quantities are computed by the model.

The node lactors  $f_i$  are computed from cubic polynomials, derived from Stirling's interpolation formula applied to values for the middle of each year 1973-1977, as found in Schureman (1941),

$$f_i = a_i + b_i u + c_i u^2 + d_i u^3$$
, (2)

where  $a_i$ ,  $b_i$ ,  $c_i$ , and  $d_i$  are coefficients, and u = t- $t_o$ , and  $t_o$  being the time lag in hours from the start time of the model to 0000 GMT 1 July 1975.

The amplitudes  $A_i$  and phase lags  $\zeta_i$  are computed from the complex harmonic constants  $H_i$  =  $H_i$ ,  $H_i$ ,

$$A_{i} = \left(H_{i}^{'} + H_{i}^{'}\right)^{1/2},$$
 (3)

and

$$\zeta_{i} = \arctan \left( H''_{i} / H'_{i} \right) .$$
 (4)

The complex harmonic constants are computed at a given location by the linear polynomial

$$H_{i} = (H_{i,1}) \times + (H_{i,2}) \times + H_{i,3}$$
 (5)

where  $H_{i,1}$ ,  $H_{i,2}$ , and  $H_{i,3}$  are coefficients and x and y are the zonal and meridional Mercator coordinates, corresponding to the latitude  $\theta$  and east longitude  $\lambda$  of the location, measured westward as a negative quantity from 0°E:

$$x = \pi \lambda$$
 (6)

and

$$y = 1n$$
 {tan ( 45° +  $\theta/2$  )} . (7)

The coefficients  $H_{i,j}$  are found by fitting equation (5) to complex harmonic constants (Greenwich phase adjusted to 0000 GMT 1 March 1975) at three reference stations, using the Mercator coordinates. Contour maps of the real and imaginary parts of the complex harmonic constants for M2 and K1 are shown in figure 4.

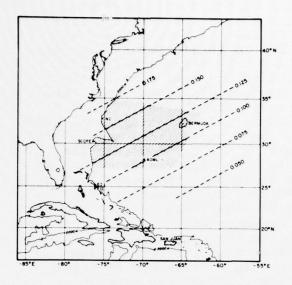


Figure 4a. Real part of the M<sub>2</sub> complex harmonic constant.

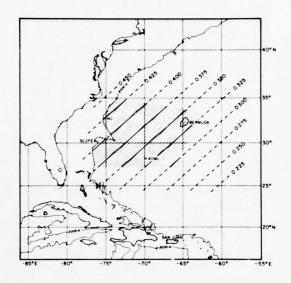


Figure 4b. Imaginary part of the  $M_2$  complex harmonic constant.

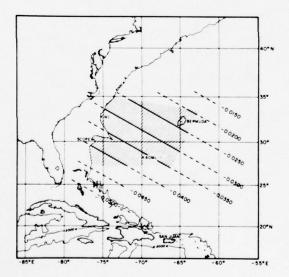


Figure 4c. Real part of the K<sub>1</sub> complex harmonic constant.

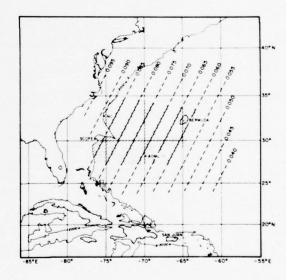


Figure 4d. Imaginary part of the K<sub>1</sub> complex harmonic constant.

## 3. USE OF THE MODEL

A straightforward application of the model would be to call TIME first to obtain the time T from the date and time in Greenwich Mean Time and then to call TIDE with T and the latitude THETA and longitude LAMBDA to obtain the sea surface displacement at that time and place. By repeating the TIDE call at different locations but using the same time T, the spatial distribution of the sea surface displacement at that instant can be obtained for the calibration area. Figure 5 gives contour maps of sea level during a semi-daily tidal cycle, using this procedure to generate the distributions over a grid at successive times. Contour maps of sea level within the model area are shown in figure 5 at 3-hr intervals, beginning 0000 GMT 1 March 1975. The maps illustrate the distribution of tidal deviation from mean sea level during a semi-daily tidal cycle. For a satellite passing over the calibration area in a time period which is short compared with the tidal periods, the displacement under the satellite may be obtained by fixing T and computing the displacements at a series of locations under the trajectory. Time series can be obtained by using the entry point TIDE1 in subroutine TIDE, as was done to generate the time series in figure 3. TIDE must be called once to establish the harmonic constants at the desired location, after which TIDE1 may be called in a DØ loop to generate the time series.

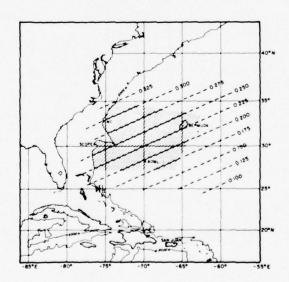
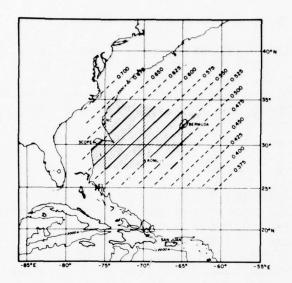


Figure 5a. Sea surface displacement at 0000 GMT 1 Mar. 1975.



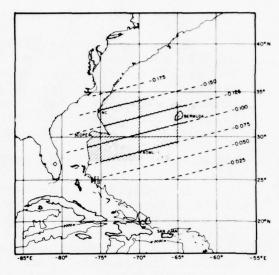


Figure 5b. Sea surface displace- Figure 5c. Sea surface displace-ment at 0300 GMT 1 Mar. 1975. ment at 0600 GMT 1 Mar. 1975.

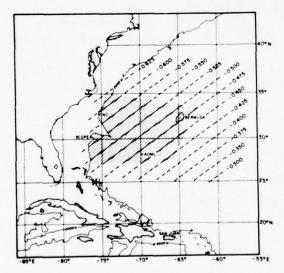
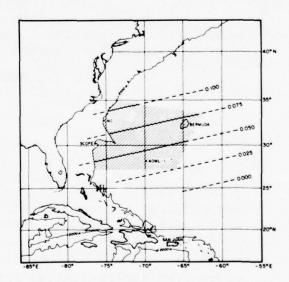


Figure 5d. Sea surface displace- Figure 5e. Sea surface displace-ment at 0900 GMT 1 Mar. 1975. ment at 1200 GMT 1 Mar. 1975.



## 4. COMPUTER SUBROUTINES AND FUNCTIONS

Following are descriptions of the subroutines and functions which comprise the tide model:

SUBROUTINE TIME (YEAR, MONTH, DAY, HOUR, MINUTE, SECOND, T)

Given the date in YEAR, MONTH (floating-point variable), and DAY and the time in HOUR, MINUTE (floating-point variable), and SECOND in Greenwich Mean Time, TIME computes the time elapsed in hours T since 0000 GMT 1 March 1975. This subroutine accounts for only 1 leap year 1976 and is valid only for the period 1 March 1972 - 29 February 1980.

Example: CALL TIME (1975.0, 3.0, 1.0, 0.0, 0.0, 0.000, T)

SUBROUTINE TIDE (THETA, LAMBDA, T, HEIGHT)

As input data, the user provides TIDE with the latitude THETA and east longitude LAMBDA (floating-point variable given as a negative quantity, measured westward from 0°E), both in degrees, and the elapsed-time T in hours since 0000 GMT 1 March 1975 as obtained from TIME. TIDE then returns the sea surface displacement from the time mean in meters at that location and time.

Example: CALL TIDE (28.00, -69.40, T, HEIGHT)

ENTRY TIDE1 (T, HEIGHT)

This entry point in TIDE is used to produce time series at a given location whose harmonic constants need not be recomputed at each time step. TIDE must be called at least once to establish the harmonic constants after which TIDE1 may be used.

Example: CALL TIDE1 (TO+FLOAT (IT), HEIGHT) where IT is the

Example: CALL TIDE1 (TO+FLOAT (IT), HEIGHT) where IT is the index of a DØ loop and TO is the initial start time of the series.

### SUBROUTINE CONST (H)

CØNST contains the harmonic constants at the reference stations and equilibrium-phase information relative to 0000 GMT 1 March 1975. When called by TIDE, CØNST returns a complex array H(I,J) of coefficients that is used in subroutine AMPL to compute the harmonic constants at a given location. CØNST need be called only once. Example: CALL CØNST (H)

SUBROUTINE LØCATE (THETA, LAMBDA, X, Y)

Using the latitude THETA in degrees and the east longitude LAMBDA (floating-point) in degrees, LØCATE returns the zonal and meridonal Mercator coordinates X and Y, respectively, where the origin is assumed to be  $0^{\rm O}N$ ,  $0^{\rm O}E$ . This subroutine

neglects the earth's eccentricity in the computations of Y. Example: CALL LØCATE (28.00, -69.40, X, Y)

SUBROUTINE AMPL (X, Y, H, A, Z)

From the Mercator coordinates X and Y, obtained from LØCATE, and the coefficient array H, obtained from CØNST, AMPL uses a linear interpolation scheme to compute the amplitudes A and phases Z, relative to 0000 GMT 1 March 1975, of the eight tidal constituents M2, N2, S2, K2, K1, O1, P1, and Q1. Example: CALL AMPL (X, Y, H, A, Z)

SUBROUTINE NØDE (T, F)

Given the time T, NØDE returns an array F(I) of node factors which adjust the amplitudes of the harmonic constants for their 8.7 and 19-yr cycles. Example: CALL NØDE (-2000.0,F)

FUNCTION SUM (F, A, Z, T)

Using the node factors F, the amplitudes A and phases Z of the eight principal tidal constituents and the time T, SUM computes the sea surface displacements caused by water tides in meters.

Example: HEIGHT = SUM (F, A, Z, T)

## 5. ACKNOWLEDGMENTS

The author would like to thank Lt. Carl Pearson (NOAA) for the use of the harmonic constants from the SCOPE reference station and Ms. Nancy Targett for her help in testing the model and preparing the examples. The author would also like to thank Mr. Bernard Zetler and Dr. Myrl Hendershott for their comments on the model and on the manuscript.

## 6. REFERENCES

- Brown, W., W. Munk, F. Snodgrass, H. Mofjeld, and B. Zetler (1975): MODE bottom experiment, <u>Journal of Physical Oceanography</u>, 5: 75-85.
- Carrier, D. (1975): Private communication.
- Dietrich, G. (1963): General Oceanography, Interscience, New York, 588 pp.
- Goodman, L. R. (1975): Private communication.
- Mofjeld, H. (1972): Tides across the continental shelves, In preparation.
- Pearson, C. (1975): Tides off the U. S. southeast coast, In preparation.
- Redfield, A. C. (1958): The influence of the continental shelf on the tides of the Atlantic coast of the United States, <u>Journal of Marine Research</u>, 17: 432-448.
- Schureman, P. (1941): Manual of Harmonic Analysis and Prediction of Tides,  $\overline{U}$ . S. Government Printing Office, Washington,  $\overline{317}$  pp.
- U. S. Coast and Geodetic Survey (1942): <u>Tidal Harmonic Constants</u>; <u>Atlantic Ocean</u>, <u>Including Arctic and Antarctic Regions</u>, TH-1, U. S. Government Printing Office, Washington, 137 pp.
- Zetler, B., W. Munk, H. Mofjeld, W. Brown, and F. Dormer (1975): MODE tides, <u>Journal of Physical Oceanography</u>, 5:430-441.

#### 7. APPENDIX

Listings of the model's FORTRAN subroutines are given below:

## @ FLI TIME . 1 . 750326 . 40045

```
SUBPOUTINE TIME ( YEAR, MONTH, DAY, HOUR, MINUTE, SECOND, T )
000001
000002
                              GEOS-C TIDE MODEL.
SUPPOUTINE TO COMPUTE TIME T IN HOURS
000003
                     C
000004
                             T = 0 AT 000UZ 1 MARCH 75
SUBROUTINE WRITTEN BY H. MOFJELD, NOAA/AOML, MIAMI, FLA. 33149
000005
                     C
000106
                     C
000107
                     C
                             SUBMOUTINE REVISED 6 FEB 75
000108
                     C
                             PEAL MONTH, MINUTE DIMENSION AM( 12 ) DATA AM / 31.0, 24.0, 31.0, 30.0, 31.0, 31.0, 31.0, 30.0,
000009
000010
000011
000012
                            1 31.0, 30.0, 31.0 /
000013
                     C
                             TY = 8760.0 * ( YEAR - 1975.0 )
IF( YEAR - 1976.0 ) 10.8.9
IF( MONTH - 2.0 ) 10.10.9
TY = 1Y + 24.0
000014
000015
000116
                             MAX = IFIX( MONTH - 0.999 )
TM = 0.0
000018
                      17
000019
                             1F( MAX .EQ. U ) 90 TO 2
000020
000121
000055
                             TM = 1M + 24.0 + AM( 1 )
000123
                     C
                            T = TY + TM + 24." * DAY + HOUR + MINUTE / 60.0 + SECOND / 3600.0
1 - 1440.0
000124
                       2
000125
000126
                       5
                              RETURN
UUUn27
                             END
     2. LIST TIME
```

#### @ ELI TIDE . 1 . 750326 . 40046

```
100000
                                  SUBROUTINE TIDE ( THETA, LAMBRA, T. HEIGHT )
000102
                         C
000003
                         000000
                                   GEOS-C TIDE MODEL FOR THE CALIBRATION AREA
                                  SEA SURFACE HEIGHT COMPUTED FROM LATITUDE THETA, EAST LONGITUDE LAMBDA, AND TIME T IN HOURS FROM 0,0002 1 MARCH 75
SUBROUTINE TIME IS CALLED BEFORE TIDE
SUBROUTINE WRITTEN BY H. MOFJELD, NOAA/AOML, MIAMI, FLA. 33149
SUBROUTINE REVISED 6 FEB 75
000004
000006
000007
800000
000009
                                  REAL LAMBDA
000010
                                  COMPLEX H( 3.8 )
000011
                                  DIMENSION A( 8 ). Z( 8 ). F( 8 )
000012
                         C
000013
                                   INITIAL SET-UP OF HARMONIC CONSTANTS
000014
                         C
                                 IF( ITAG - 5 ) 10.20.10

CALL COMST( H )

PHINT 1. ( ( I.J., H(I.J.).J=1.8), I=1.3 )

FORMAT( 4H H( , I', 1H., II, 4H ) =, 2F10.5 )
000015
000116
                          17
000017
000018
                          1
000119
                                  11AG = 5
000020
                          20
                                  CONTINUE
000021
                         C
000022
                                  CALL LOCATE ( THETA, LAMBIDA, Y, Y )
                         C
000123
                                  CALL AMPL( X, Y, H, A, Z )
000024
000025
                         C
000026
                                  ENTRY TIDEL ( T. HFIGHT )
                                  CALL NODE ( T. F )
HEIGHT = SUM( F. A. Z. T )
000027
000028
000029
                         C
000030
                                  RE LUPN
000031
                                 END
     3. LIST CONST
```

#### W ELI CONST.1,750326, 40048

```
UUUNNI
                             SUBHOUTINE CONST( H )
000002
                     C
000003
                              GEOS-C TIDE MODEL SUPROUTINE TO COMPUTE THE COMPLEX COEFS FOR SUBROUTINE AMPL
                     C
000104
                     C
000005
                     C
                             STAPT TIME ODUOZ 1 MARCH 75
000006
                     C
                              THE COMPLEX HARMONIC CONSTANTS ARE ASSUMED TO LIE ON PLANES
000007
                             RETWEEN REFERENCE STATIONS
000008
                              ORDER OF CONSTITUENTS MZ. NZ. SZ. KZ. K1. 01. P1. Q1
000009
                     C
                              LONGITUDES FAST FROM GREENWICH
                             SUBROUTINE WRITTEN BY H. MOFJELD, NOAA/AOML, MIAMI, FLA. 33149
SUBROUTINE REVISED 6 FEB 75
000010
                     C
000011
000012
                     C
                             REAL L1, L2, L3
UUUn14
                             COMPLEX H( 3,8 ), H1( 8 ), H2( 8 ), H3( A ), CEXP
000015
                             DIMENSION A1( 8 ) . A2( 8 ) . A3( 8) . P1( 8 ) . P2( 8 ) . P3( 8 ) .
000016
                            1V( A )
000017
                     C
                             SCOPE BOTTOM STATION ( REF. C. PEARSON, DEEP-SEA TIDE ORSERVATIONS OFF THE SOUTHEASTERN UNITED STATES, IN PREPARATION )
000018
                     C
000019
000120
000021
                            PATA T1, L1 / 30.43, -76.42/
1 A1 / 0.434, U.106, 0.082, 0.018, 0.096, 0.0/3, 0.032, 0.014 /
2 P1 / 357.6, 335./, 25.1, 21.6, 189.8, 194.3, 189.8, 183.8 /
000122
000123
000024
                     C
000025
                             PERMIDA ISLAND STATION ( REF. ZETLER ET AL, MODE TIDES, JPO,
000026
                             THE PRESS 1
000027
                     C
                            DATA T2, L2 / 32.4, -64.7 /
1 A2 / 0.356, 0.042, 0.081, 0.022, 0.066, 0.053, 0.020, 0.011 /
2 P2 / 358.3, 337.7, 24.2, 22./, 187.0, 192.1, 187.8, 186.6 /
000128
000129
0.000030
000031
UUUn32
                             MODE ACML-1 ROTTOM STATION ( HEF. IRID. )
000033
                     C
                            DATA T3, L3 / 28,14, -69,75 / 1 A3 / 0.345, 0.084, 0.071, 0.019, 0.077, 0.061, 0.024, 0.013 / 2 P3 / 0.6, 339,8, 30.8, 29,9, 194.7, 197.6, 195.2, 193.3 /
000034
000035
000036
UU0037
UUU0138
                             FOULLIBRIUM PHASES RELATIVE TO 0000 GMT 1 MAR 75
000039
000140
                            1 V / 287.3, 244.5, 0.0, 332.1, 76.4, 206.8, 291.9, 164.0 / 2 PI / 1.7453293E-2 /
000041
000042
000143
                     C
000144
                              no 10 I = 1.8
                              H1( I ) = A1(1) + CEXP( CMPLX( 0.0, PI*( P1(1)-V(1) ) )
000045
000046
                              H2(1) = A2(1) + CFXP( CMPLX( U.O. PI + ( P2(1)-V(1) ) ) )
                             P3( ) = A3(1) + CEXP( CMPLY( 0.0+ PI + ( P3(1)-V(1) ) )
000147
                       10
000148
                      C
000049
                              CALL LOCATE( 11, L1, X1, Y1 )
000050
                             CALL LOCATE ( 12, L2, X2, Y2 )
CALL LOCATE ( 13, L3, X3, Y3 )
000051
000052
000153
                              DET = X1+( Y2-Y3 ) + X2+( Y3-Y1 ) + X3+( Y1 - Y2 )
000054
```

```
H(1+1) = H1(1)*( Y2-Y3) + H2(1)*( Y3-Y1 ) + H3(1)*( Y1-Y2 )

H(2+1) = H1(1)*( X3-X2 ) + H2(1)*( X1-X3 ) + H3(1)*( X2-X1 )

H(5+1) = H1(1)* ( X2*Y3-X3*Y2 ) + H2(1)*( X5*Y1-X1*Y3 )

1 + H3(1) * ( X1*Y2-X2*Y1 )
000155
000056
000057
000058
000059
                                 C
                                              H(1,I) = H(1,I) / DET
H(2,I) = H(2,I) / DET
H(3,I) = H(3,I) / DET
000061
                                  50
000162
000063
                                              RETURN
000064
                                              FNU
000065
        4. LIST LOCATE
```

## @ ELI LOCATE, 1.750327, 44721

```
SUBROUTINE LOCATE( THETA, LAWRUA, X, Y )

GEOS-C TIDE MODEL

SUBROUTINE TO COMPUTE MERCATOR COORDINATES FROM LAT AND LONG
ONIGIN AT 0 N 0 E

SUBROUTINE WRITTEN BY H. MOFJELD, NOAA/AOML, MIAMI, FLA. 3314
SUBPOUTINE REVISED 25 MAR 75
000001
000002
                                 000000
000003
000004
000005
000006
000107
                                              PFAL LAMRDA
DATA PI, E / 1.7453293E-2, 8.1819494E-2 /
X = P1 * LAMRDA
Y1 = TAN( PI*( 45. + IMETA/2. ) )
800000
000009
000011
                                               Y=ALOG(Y1)
000012
                                  C
C
000013
000014
                                               RETURN
000015
                                               END
000116
        5. LIST AMPL
```

#### @ ELI AMPL, 1, 750326, 40049

```
000001
                                              SUBROUTINE AMPL( X. Y. H. A. Z )
000002
                                  000000
                                              GEOS-C TIDE MODEL SURROUTINE TO COMPUTE THE AMPLITUDES A AND GREENWICH PHASES Z SUBPOUTINE WRITTEN BY H. MOFJELD, NOAA/AOML, MIAMI, FLA. 33149 SUBPOUTINE REVISED 6 FEB 75
000n03
000n04
000n05
000006
000107
                                              COMPLEX H( 3.8 ), HC
DIMENSION Z( 8 ), A( 8 )
DATA R / 1.7453294E-2 /
800000
000009
000110
000011
                                  C
000n12
000n13
000n14
000n15
                                              TO 10 I = 1,R

HC = H(1.I) * X + H(2.I) * Y + H(3.I)

A( I ) = CABS( HC )

Z( I) = ATAN2( AIMAG( HC ), REAL( HC ) ) / R
                                  c 10
000n16
000n17
                                              PETURN
000018
                                              END
       6. LIST NODE
```

```
SUBROUTINE NODE ( T. F )
000101
000002
UUUnn3
                                                    GEOS-C TIDE MODEL
                                                   GF05-C TIDE MODEL
SUBMOUTINE TO ADDIIST AMPLITUDES FOR NODE FACTORS USING STIRLINGS
INTERPOLATION FORMULA ON DATA FROM TABLE 14 OF P. SCHUREMAN,
MANUAL OF HARMONIC ANALYSIS AND PREDICTION OF TIDES, DEPT. OF
COMMERCE SPECIAL MUBL. NO. 98, 1941.
OMDER OF CONSTITUENTS M2, N2, S2, K2, K1, O1, P1, 01
SUBMOUTINE WRITTEN BY H. MOFJELD / NOAA/ AOML/ MIAMI, FLA.
AULIAN 75
000104
000005
000106
UU0107
80000
000009
000010
                                                      30 JAN 75
00011
000012
                                                    DIMENSION F( 8 )
                                                    " = ( T-2920.0 ) / 8760.0
r(1) = 1.020 + ( 0.0107 + ( -0.0015 - 1.7E-4 * U ) * U ) * U
000113
000014
                                                   F(1) = 1,020 + ( 0,0107 + ( -0.0015 - 1,724 + 0 ) * 0 ) * 0

F(2) = F(1)

F(3) = 1.000

F(4) = 0.871 + ( -0.0777 + ( 0.0095 + 0.0012 * U ) * U ) * U ) * U

F(5) = 0.951 + ( -0.0585 + ( 6.0025 + 0.0017 * U ) * U ) * U

F(6) = 0.920 + ( -0.0619 + ( 0.0035 + 0.0014 * U ) * U ) * U

F(7) = 1.000
000015
000016
000017
000018
000019
บบบาวก
000021
                                                    F(8) = F(6)
000022
UUUn23
                                                    PETURN
000124
                                                    FNO
         7. LIST SUM
```

#### ₩ ELI SUM, 1.750326, 40051

```
000001
                                                         FUNCTION SUM( F. 4, Z, T )
                                                        FUNCTION SUM( F, A, Z, T )
GEOS-C TIDE MODEL
FUNCTION TO COMPUTE THE SEA SURFACE DISPLACEMENT FROM
HAPMONIC CONSTANTS AND TIME
ORDER OF CONSTITUENTS M2, N2, S2, K2, K1, U1, P1, Q1
CUBROUTINE WRITTEN BY H. MOFJELD, NOAM/AOML, MIAMI, FLA. 33149
SUBMOUTINE REVISED 6 FEB 75
000002
UUUnn3
000104
000005
000006
000007
                                          C
                                                      Olmension A( 8 ), Z( 8 ), S( 8 ), F( 8 )
OATA 5 / 28.984104, 28.459730, 30.0, 30.082137,
1 15.041069, 13.943056, 14.958931, 13.398661 /
2 R / 1.7453293E-2 /
SUM = 0.0
000009
000010
000011
000012
UUUn13
                                                       SUM = 0.0

00 100 N = 1.8

P = S(N) * T - Z(^1)

TF( IIG .NE. 25 ) PRINT 1. P

FORMAT( 16H PHASE FOR M2 = . F20.5 // )

IIG = 25

SUM = SUM + F(N)**(N) * COS( R*P )

RETURN
000014
000115
000116
000018
000019
000020
000021
                                                         FND
```

END CUR LCC 1102-0038 L8

## A Comparison of Observed and Numerically Simulated Circulation in the Cayman Sea

#### ROBERT L. MOLINARI

Atlantic Oceanographic and Meteorological Laboratories, NOAA, Miami, Fla. 33149 (Manuscript received 24 October 1973, in revised form 12 May 1974)

#### ABSTRACT

An observational and numerical study of the circulation in the Cayman Sea is presented. Data taken in three different years suggest a common February to May circulation pattern. A well-developed current crosses 85W south of the Cayman Ridge. An anticyclonic eddy in the central basin appears to be a common feature of this season's circulation. Finally, the data from these cruises consistently portray significant accelerations occurring in the vicinity of Cozumel Island where the flow merges with the Yucatan Current. A different pattern is inferred from data collected in July and August. The north component of the flow over the western edge of the Cayman Ridge appears to determine the type of flow regime observed.

The numerical model is based upon predictive equations for the vorticities in a two-layer ocean on a betaplane, and includes topographic, advective and friction effects. The model is driven by lateral input boundary conditions derived from an April-May 1968 observational study. The baroclinic western boundary current of the numerical model develops in response to eastern input boundary conditions, while the barotropic current is constrained to intensify and flow along the continental slopes.

#### 1. Introduction

The western Caribbean Sea Basin is shown schematically in Fig. 1. Historically, this area also has been called the Cayman Sea, although it is comprised of both the Cayman Basin and the Yucatan Basin. In the present study, the term Cayman Sea will be used to denote the western Caribbean Sea, just north of Honduras and west of 83W longitude.

Cochrane (1971) has discussed the April-May circulation of the Cayman Sea and the Yucatan Strait. The data consistently portray a flow regime dominated by an anticyclonic loop in the central basin, and a strong Yucatan Current on the western boundary. Cochrane considers bottom topography to be an important factor in determining the flow pattern.

The Yucatan Current has been described as a western boundary current similar in dynamics to the Gulf Stream (Cochrane, 1969). Saylor (1963), applying a variation of the Charney-Morgan inertial model, concluded that the conservation of potential vorticity could explain the formation of the Yucatan Current. However, Ahrens (1965), in an analysis of available hydrographic data, found that potential vorticity was not conserved along the Current and attributed the gain of cyclonic vorticity to frictional effects.

A marked association between the highest surface velocities of the Yucatan Current and a relatively constant depth has been noted in the vicinity of the Yucatan Channel by Cochrane (1966). Molinari and Cochrane (1972), assuming the conservation of potential vorticity and using observed data for initial conditions,

calculated paths of the current core which were similar to observed paths from the Yucatan Strait to 23°30′N. At 23°30′N the Current separates from the Campeche Bank and enters the Gulf of Mexico Basin.

The present investigation is an attempt to study the circulation patterns of the Cayman Basin, and the dynamics of the formation of the Yucatan Current. In particular, the western boundary character of and the effect of topography upon the flow are considered. Observations available from various cruises in the area are analyzed to identify important features of the Cayman Sea current pattern. Finally, a predictive numerical model of the circulation is used in an attempt to ascertain the important dynamical parameters affecting the flow.

## 2. Circulation deduced from available data

In order to specify the boundary conditions which will be required in the two-layer numerical model, and to describe the observed baroclinic flow, an Equivalent Baroclinic Height (EBH) parameter is introduced. The EBH is derived, as illustrated in Fig. 2, by equating the area under an observed  $\sigma_t$ -depth curve to the area under an equivalent two-layer  $\sigma_t$ -depth curve. The observed  $\sigma_t$ -depth area is calculated by numerically integrating from the surface to a level of small density gradients ( $\sigma_t$ =27.75). The EBH is then obtained by dividing this area by an average density difference ( $\Delta \sigma_t$ =2.5×10<sup>-3</sup>). Fofonoff (1962) qualitatively defines the baroclinic flow component in an analogous manner.

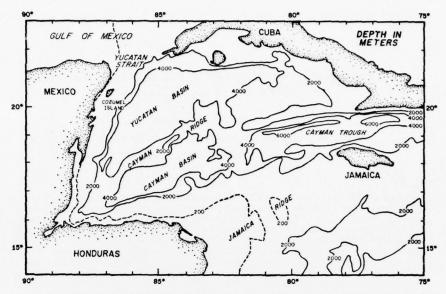


Fig. 1. The Cayman Sea (western Caribbean Sea), and its major topographic features.

The observational data taken during the spring of 1933, 1961 and 1968 all suggest a similar circulation pattern. March 1961 and April–May 1968 EBH data given in Figs. 3 and 4, respectively, show the dominant features of the flow.

During both years the major portion of the flow through the Yucatan Strait crossed 85W as an intense coherent current south of the Cayman Ridge. The current had a predominantly westerly drift at this longitude. In 1968, a closed eddy was centered at approximately 85°30′W, 19°30′N (Fig. 3). The 1961 data do not permit closure of the contours but they do indicate a similar circular pattern centered to the east of the 1968 feature (Fig. 4). During both years the western intensification convergence of the isopleths occurs at the vicinity of and north of Cozumel Island.

The April-May 1933 and February 1961 data, although sparse, present further evidence for a common spring circulation pattern. Since neither field can be contoured, only the EBH values and the direction of the EBH computed velocity are given for the February

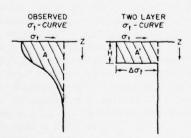


Fig. 2. Schematic diagram illustrating the Equivalent Baroclinic Height (EBH) parameter H.

1961 data on Fig. 3, and for the 1933 data on Fig. 4. The EBH values of the 1933 field closely correspond to those of the 1968 field, suggesting a similar inflow south of the Cayman Ridge and a similar position and intensity for the eddy. The February 1961 data depict a corresponding but shallower baroclinic field than given by the late March 1961 data.

The geostrophic volume transport per unit width per unit time of the baroclinic component is defined by the relation

$$T \approx \frac{g\epsilon}{2f} (H^2 - H_0^2), \tag{1}$$

where g is the acceleration of gravity,  $\epsilon$  the relative density anomaly  $(2.5 \times 10^{-3})$ , f the Coriolis parameter, H the value of EBH, and  $H_0$  the value of EBH contour at the coastal boundary. Longitudinal sections of transport are given in Fig. 5 and zonal sections in Fig. 6.

The longitudinal sections of Fig. 5a are very similar in that between 20 and  $30 \times 10^6$  m<sup>3</sup> s<sup>-1</sup> entered the basin south of the Cayman Ridge. The spike in the April–May 1933 data at 17°30′ (Fig. 5a) is apparently a function of the shallow depth at the station, and the flow regime it suggests is questionable. The March 1956 data shown in Fig. 5b represent the available information for this period, and possess the same property of intense flow south of the Cayman Ridge. Finally the March–April 1961 and May 1968 transport curves of Fig. 5c are further evidence for the similarity of circulation patterns during these periods.

Zonal cross sections of geostrophic transport for March-April 1961 and for May 1968 (Fig. 6) depict the western intensification process. The distances are

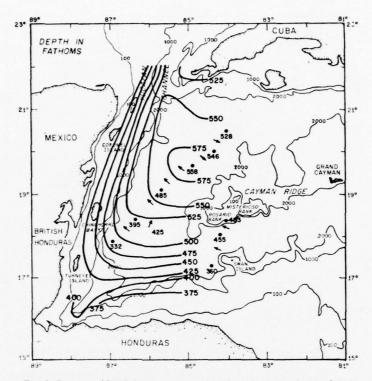


Fig. 3. Contours of EBH, in meters, determined from data taken in March 1961. Also shown are EBH values and directions of geostrophic flow computed from data collected in February 1961.

calculated from the  $H_0$  contour. In both Figs. 6a and 6b the northerly flow is fully developed by 18°30′N. North of 18°30′N the increase in slope of the transport curves is a measure of western intensification. Both years have countercurrents indicated on the Cuban side of the Yucatan Strait.

A different circulation pattern can be inferred from data taken in August 1970 and July 1971. The data were expendable bathythermograph (XBT) profiles and thus EBH's could not be computed. Comparing the equivalent baroclinic heights with the corresponding T-z curves of various cruises indicates that, throughout the basin, the depth of the 11°C isotherm can be used as a first approximation of the EBH.

A map of the August 1970 11°C isothermal surface is given in Fig. 7, and the July 1971 surface in Fig. 8. July 1971 drifting buoy trajectories (Fig. 9) presented by Molinari and Starr (1972) suggest surface currents similar to those indicated by the temperature distribution of Fig. 8.

The major part of the 1970 current entering across the 85°30′W meridian is at a more northerly latitude than either the 1961 or 1968 currents (Figs. 3 and 4). In addition, the 1970 flow has a more northerly component at 85°30′W than indicated by the 1961 or 1968 data. Both the August 1970 and July 1971 figures

(Figs. 7 and 8) suggest a considerable portion of the total flow through the Strait has joined the boundary current at more northerly latitudes than during the February to May cases.

#### 3. The numerical model

### a. Model formulation

The numerical model is essentially that of Wert and Reid (1972). The major assumptions and constraints of their formulation are that:

- 1) A two-layer ocean, each layer incompressible and with uniform density, is located on a beta-plane.
- An influx of mass through an open boundary drives the upper layer, and an interlayer stress drives the lower layer.
- All other driving forces, including wind and tidal effects are neglected.
- 4) Topography is allowed only in the lower layer.

Lateral and bottom friction as well as advection of momentum and of vorticity are allowed in the system.

In the following expressions, the east and north directions are represented by the x and y axes respectively Primed terms are lower layer variables, and unprimed terms are upper layer variables. The two-

(4)

(5)

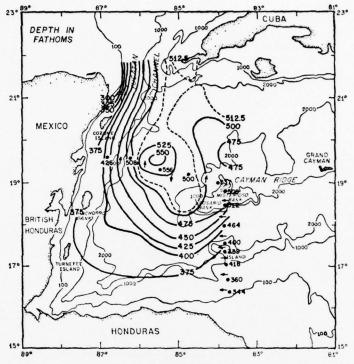


Fig. 4. Contours of EBH, in meters, determined from data taken in April-May 1968. Also shown are EBH values and directions of geostrophic flow computed from data collected in April-May 1933.

dimensional fluid velocity is represented by the vector  $\mathbf{v} = u\mathbf{i} + v\mathbf{j}$ . The H's are layer thicknesses, and D the undisturbed water depth. The frictional coefficients are lateral friction K, interlayer friction  $\sigma$ , and bottom friction  $\sigma'$ . With these symbols and the above assumptions, the vertically integrated equations of motion and the continuity equations can be written as

d bottom e assumption and 
$$= \sigma \left( \frac{\mathbf{v} - \mathbf{v}'}{H'} \right) - \frac{\sigma' \mathbf{v}'}{H'} + K \nabla^2 \mathbf{v}', \quad (3)$$

$$\frac{\partial H}{\partial t} + \nabla \cdot (H \mathbf{v}) = 0, \quad (4)$$

 $\frac{\partial \mathbf{v}'}{\partial t} + (\mathbf{v}' \cdot \nabla)\mathbf{v}' + f\mathbf{k} \times \mathbf{v}' + g\nabla \left(\frac{\rho}{\rho'}H + H' - D\right)$ 

$$\frac{\partial \mathbf{v}}{\partial t} + (\mathbf{v} \cdot \nabla)\mathbf{v} + f\mathbf{k} \times \mathbf{v} + g\nabla(H + H' - D)$$

= 
$$-\sigma\left(\frac{\mathbf{v}-\mathbf{v}'}{H}\right) + K\nabla^2\mathbf{v}$$
, (2)  $\frac{\partial H'}{\partial t} + \nabla \cdot (H'\mathbf{v}') + 0$ .

Fig. 5. Geostrophic baroclinic transports computed from Eq. (1) at 84W, 84°30'W and 85-86W. Panel (a) also includes the smoothed version of the April 1968 curve used to drive the numerical models.

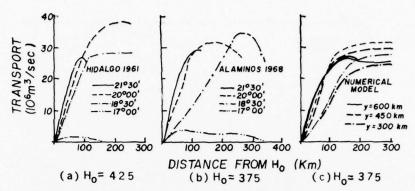


Fig. 6. Geostrophic baroclinic transports computed from Eq. (1) for March 1961, April–May 1968 and for the numerical model. The thicker lines of panel (c) were computed from the results of the non-topographic model, and the thinner lines from the topographic model.

A vorticity equation for each layer is formed from these equations. Prediction equations for H and H' are obtained from the vorticity equation by making the geostrophic approximation in each layer. The geostrophic constraint eliminates internal gravity waves. Moreover, the use of a rigid-lid condition on the sea surface (H+H'-D), independent of t) eliminates surface gravity waves.

The prediction equations for the baroclinic and barotropic modes, with

$$B \equiv \frac{\rho}{\rho'} H + H' - D,\tag{6}$$

$$\epsilon \equiv \frac{\rho' - \rho}{\rho'},\tag{7}$$

are respectively

$$\epsilon \nabla^{2} \frac{\partial H}{\partial t} + \epsilon H J \left[ H, \frac{\zeta + f}{H} \right] + H J \left[ B, \frac{\zeta + f}{H} \right] \\
- H' J \left[ B, \frac{\zeta' + f}{H'} \right] - \frac{f}{g} \frac{\partial H}{\partial t} \left[ \frac{\zeta + f}{H} + \frac{\zeta' + f}{H'} \right] \\
= \frac{f}{g} \left[ K \nabla^{2} (\zeta - \zeta') - \sigma(\zeta - \zeta') \left( \frac{1}{H} + \frac{1}{H'} \right) + \frac{\sigma' \zeta'}{H'} \right] \quad (8)$$

and

$$\nabla^{2} \frac{\partial B}{\partial t} + H'J \left[ B, \frac{\zeta' + f}{H'} \right] + \frac{f}{g} \left( \frac{\zeta' + f}{H} \right) \frac{\partial H}{\partial t}$$

$$= \frac{f}{g} \left[ \sigma \frac{(\zeta - \zeta')}{H'} - \frac{\sigma' \zeta'}{H'} + K \nabla^{2} \zeta' \right]. \quad (9)$$

The relative vortices are given by

$$\zeta = \zeta' + \frac{g\epsilon}{f} \nabla^2 H \tag{10}$$

and

$$\zeta' = \frac{g}{f} \nabla^2 B. \tag{11}$$

The Jacobians are used in the form

$$J(A,B) = \frac{\partial}{\partial y} \left( B \frac{\partial A}{\partial x} \right) - \frac{\partial}{\partial x} \left( A \frac{\partial A}{\partial y} \right), \tag{12}$$

for reasons discussed below.

The finite-difference analogues of Eqs. (8) and (9) were taken as those given by Wert and Reid (1972). In summary, centered difference forms are used for the time and space derivatives. The nonlinear instabilities caused by the advective terms are suppressed by the use of the form of the Jacobian given in Eq. (12) (Arakawa, 1966). The DuFort-Frankel scheme (Smith, 1965) was used to represent the lateral diffusion of vorticity because of its stable properties.

#### b. Boundary conditions

The basin used in the numerical model is shown schematically in Fig. 10. The model basin is rectangular with an east-west dimension of 300 km, and a north-south dimension of 600 km. The Yucatan Strait is modelled as 180 km wide.

Fig. 10 also gives the bottom topography of the model basin. The Cayman Ridge and its associated Banks are not modelled. To insure that the bottom topography is confined to the lower layer, the shallowest depth is 700 m. The continental slopes closely approximate those found in the Cayman Basin, and a Yucatan Channel sill depth of 1800 m in the model approximates the actual sill depth. In the lower left hand corner of Fig. 10 is given a portion of the space grid; the space increment  $\Delta x = \Delta y = \Delta s = 10$  km.

Mass inflow and outflow are allowed through the eastern boundary and the Yucatan Strait. Solid impermeable boundaries in the model basin exist along

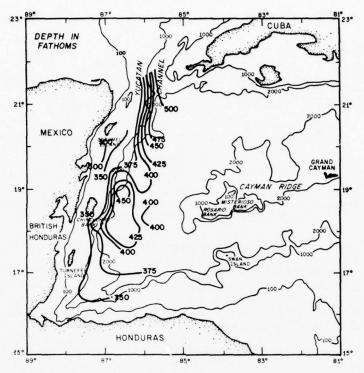


Fig. 7. The distribution of the depth, in meters, of the 11°C isotherm for August 1970.

the southern and western boundaries, and along that portion of the northern boundary to the east of the Yucatan Channel.

A schematic grid, shown in Fig. 11, will be used to demonstrate the boundary conditions applied to the various models. The inclusion of lateral friction requires two boundary conditions on all boundaries. To satisfy these conditions a fictitious boundary one space increment beyond the perimeter (the dots in Fig. 11) is introduced.

Two types of eastern boundary conditions are used to drive the interior baroclinic flow. In the first model this flow component is assumed normal to the open boundaries. If  $x=i\Delta s$  and  $y=j\Delta s$  on the numerical grid, then this boundary condition is given on the schematic grid as

$$H(7,j) = H(5,j)$$
.

Furthermore the values of H(6,j) are given as an initial condition and held constant throughout the time integration. The following conditions are applied along the solid walls to satisfy the no-slip condition:

$$H(i,2) = H(2,j)$$
  
 $H(i,1) = H(i,3)$   
 $H(1,j) = H(3,j)$   
 $H(6,11) = H(5,11) \neq H(i,2)$   
 $H(i,12) = H(i,10)$ .

Prediction of H(2,11) and H(3,11) at the Yucatan Strait requires the determination of  $\zeta(2,12)$  and  $\zeta(3,12)$ . The method of Wert and Reid is followed in that  $\zeta$  is determined from upstream conditions. For currents flowing out of the basin,  $\zeta$  is determined by advecting potential vorticity; and for currents flowing into the basin,  $\zeta$  is arbitrarily set outside the grid (Wert and Reid, 1972, p. 183).

A second model considers non-normal flow at the eastern forcing boundary. Again, H(6,j) is both specified and constant with time. The assumption of non-normal flow requires that

$$H(7,j) = H(5,j) - \alpha(6,j)[H(6,j+1) - H(6,j-1)],$$

where

$$\alpha(6,j) = \tan^{-1} \left[ \frac{v(6,j)}{u(6,j)} \right]$$

is given at t=0 and independent of time. The conditions along the solid boundaries and at the Yucatan Strait are identical to those of the preceding model.

The barotropic flow parameter B is a predicted variable at both the eastern and Yucatan Channel openings. This component is constrained to flow normal to the openings by the application of the conditions used in determining H at these grid points. The solid

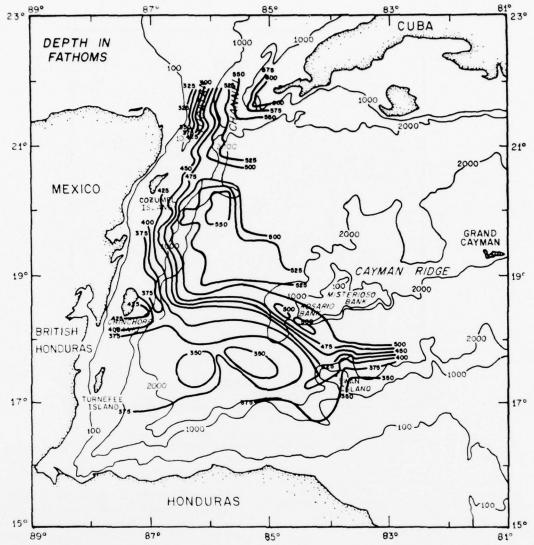


Fig. 8. The distribution of the depth, in meters, of the 11°C isotherm for July 1971.

boundary constraints are

$$B(i,2) = B(2,j) = B(5,11) = B(6,11) = 0,$$
  
 $B(i,1) = B(i,3),$   
 $B(1,j) = B(3,j),$   
 $B(i,12) = B(i,10).$ 

## c. Numerical procedure

The following procedure of Wert and Reid can be applied to the numerical equations to obtain interior values of H and B, if H and  $\alpha$  are specified at the eastern forcing boundary: At the initial time step the upper layer flow is assumed to be irrotational and geostrophic, and the lower layer at rest. The relaxation

of  $\nabla^2 H$  provides the upper layer thickness at t=0, and and a one-step Euler forward time integration of the equations gives the H field at the second time step.

The numerical analogue to (8) is then solved by a Gauss-Siedel over-relaxation scheme (Smith, 1965) to obtain successive values of H. The lower layer is kept at rest during these iterations by specifying B=0. The effects of initial transients are reduced by this technique (Wert and Reid, 1972).

The baroclinic calculations were continued until the changes in upper layer thicknesses were no longer significant. At that time the barotropic flow was initiated with the introduction of the numerical analogue to (9). The same procedure used to obtain upper layer thickness was followed successively to solve (8) for values of B.

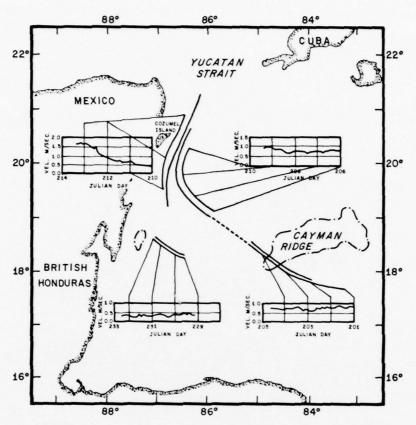


Fig. 9. Approximate drifting buoy tracklines obtained in July and August 1971.

Also given are the velocities of the surface drifters.

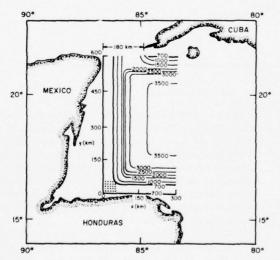


Fig. 10. The numerical model basin and its associated bottom topography, depth in meters, superimposed on a chart of the Cayman Sea. A portion of the numerical grid, with a 10 km spatial interval, is given in the lower left-hand corner of the model basin.

## 4. Application of the numerical model

The results of several applications of the numerical model are presented. Two of the numerical integrations consider only flow in the upper layer, while a third case allows flow in both layers. A complete parametric study involving the frictional coefficients was not conducted. However, one test was made to assess the effect of lateral friction on a steady flow regime. The results of this model are presented in the following discussion.

## a. Comparison of frictional and frictionless model results

Fig. 12 gives the upper layer thicknesses determined from the frictionless inertial model of Saylor (dashed lines) and the present inertial frictional model (solid lines). In both cases the depth of the 10°C isotherm along 84°30′W during March 1958 was used to specify the geostrophic mass influx at the eastern boundary. Also, the flow is normal to the eastern boundary in both incidents.

The inertial-frictional model was spun up to nearly steady state in 600 time steps ( $\Delta t = 2 \text{ h}$ ) using a lateral frictional coefficient of 500 m<sup>2</sup> s<sup>-1</sup>. The lower layer was

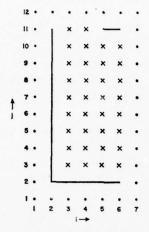


Fig. 11. A reduced version of the numerical grid used in the explanation of the boundary conditions.

kept at rest in this test. It should be noted that in the inertial model H can vary along the western solid boundary, but is a constant in the frictional case.

Viscous spreading of the boundary current at lower latitudes is evident in Fig. 12. This feature is characteristic of inertial-friction models [as noted first by Munk (1950)] in which the effect of friction is to retard the formation of the boundary current. Also, the inertial-frictional boundary current is less intense and has a more easterly core location than the purely inertial current.

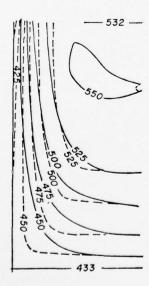


Fig. 12. Steady-state results from the present inertial-frictional model (solid lines) after a 1200 h numerical integration and the rictionless-inertial model of Saylor (dashed lines).

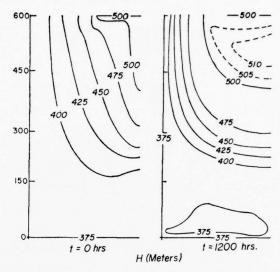


Fig. 13. The upper layer height (H), in meters, for the case of normal flow at the eastern input boundary, at t=0 h (left panel), and t=1200 h (right panel).

## b. Baroclinic flow regime specifying normal flow at the eastern boundary

The mass influx required to drive the normal flow model is taken as a smoothed version of the equivalent baroclinic transport curve at 84W obtained during April–May 1968 (Fig. 5a). As the data along 84W do not extend to the Cuban coast, the values of the EBH at the western tip of Cuba are used to complete this section. The Laplacian flow pattern obtained from this influx is given in the left panel of Fig. 13. The only intensification in the flow is at the Yucatan Strait, where this constriction causes increased outward velocities at both sides.

Using the Laplacian field of Fig. 13 as the initial field of flow, the model was allowed to run for 1200 h (600 iterations) while the lower layer remained at rest. The time step and frictional coefficient were identical to the previous example. The 600th iteration (1200 h) upper layer height field is given in the right panel of Fig. 13.

The baroclinic spin-up process was essentially complete after 600 h with small, non-systematic changes occurring throughout the next 600 h. The convergence of the *H* lines as they approach the Yucatan Channel represents the western boundary intensification process. The maximum velocity of the flow has increased from 0.6 m s<sup>-1</sup> at the eastern boundary to 0.8 m s<sup>-1</sup> at the Yucatan Strait. Fig. 14 shows a plot of the north component of velocity at various latitudes, and indicates that the major accelerations have occurred by 450 km.

Fig. 15 gives the relative vorticity at two latitudes, and at the eastern opening. The maximum relative vorticity at the eastern opening is approximately one-

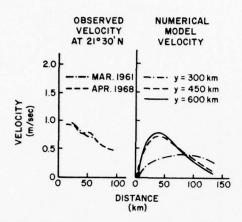


Fig. 14. Cross-stream geostrophic velocity profiles at the Yucatan Strait determined from observation (left panel) and numerical model (right panel).

quarter of the mean planetary vorticity. However, as the flow turns north and accelerates along the western boundary the cyclonic vorticity increases dramatically.

As the northward flowing current accelerates, the area under the relative vorticity curve increases. Cyclonic vorticity is being diffused into the current as a result of frictional boundary effects. Thus, the cyclonic vorticity flank of the boundary current can be considered to represent the frictional boundary layer. At the Yucatan Strait, the frictional boundary layer is only 30 km wide.

The intense northerly flow which was present at the western tip of Cuba in the Laplacian field at t=0 has vanished, and been replaced by a countercurrent. The southerly flow appears in response to the eastward flow at the forcing boundary. In the extreme southern basin, a closed cyclonic gyre has developed.

## c. Barotropic flow regime specifying normal flow at the eastern boundary

At the 600th iteration, two barotropic models were initiated, one with bottom topography in the lower layer and one without. In both cases the interlayer stress coefficient  $\sigma$  was taken as  $1\times 10^{-3}$  cm s<sup>-1</sup> and the bottom stress coefficient  $\sigma'$  as  $50\times 10^{-3}$  cm s<sup>-1</sup>. The barotropic flow components of both models at 1800 and 2400 h are given in Fig. 16. Although neither model attained a steady state, it was necessary to limit both time integrations to 600 additional 2 h steps.

The effect of topography on the barotropic regime is to confine and intensify the flow along the isobaths. While the core of the non-topographic barotropic current coincides with the core of the forcing upper layer flow, the core of the topographic current is along the continental slope. Because of the shallow sill depth at the Yucatan Channel, much of the barotropic regime is forced to the east instead of flowing out of the basin to the north.

During these 1200 h, the changes occurring in the upper layer thicknesses of both the cases are small. The more intense and systematic changes occur in the topographic model along the core of the barotropic flow. However, the maximum changes are of the order of meters, which do not significantly affect the velocity distributions.

## d. Baroclinic flow regime specifying non-normal flow at the eastern boundary

To determine the effect of varying the boundary conditions the numerical model was rerun with the model inflow angles approximating the inflow angles observed during April-May 1968. Fig. 17 gives the upper layer height field at  $t\!=\!500\,\mathrm{h}$  (less panel) and at  $t\!=\!1000\,\mathrm{h}$  (right panel). No significant upper layer height changes occurred after 1000 h.

At t=500 h the numerical field closely approximates the observed field as given in Fig. 4. As the time integration continues the circulation about the closed eddy in the interior of the basin becomes less intense.

#### 5. Discussion

The dynamical processes active in the basin can be inferred from a comparison of the numerical and observational circulation regimes. For instance, the baroclinic western intensification of the model and observed flows appears similar. The largest acceleration occurs close to the Yucatan Strait in both cases, an

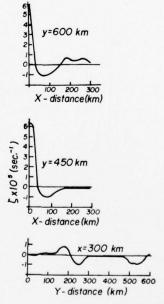


Fig. 15. The upper layer relative vorticity at t = 1200 h, for the upper panel, latitude y = 600 km (Yucatan Strait); middle panel, latitude y = 450 km; and lower panel, longitude x = 300 km (eastern input boundary).

observational feature previously noted by Cochrane (1971). The model baroclinic velocity profile at the Strait approximates the observed profile both in the speed and position of the current axis (Fig. 14).

This similarity of velocity profiles suggests that the frictional boundary layer in the actual basin is also very narrow. The observed velocity curves of Fig. 14 indicate that the cyclonic flank of the current is very close to the coastline. Molinari and Starr (1972) indicate that the relative speeds of their surface drifters (Fig. 9) in the vicinity of the Strait also suggest a narrow cyclonic boundary layer.

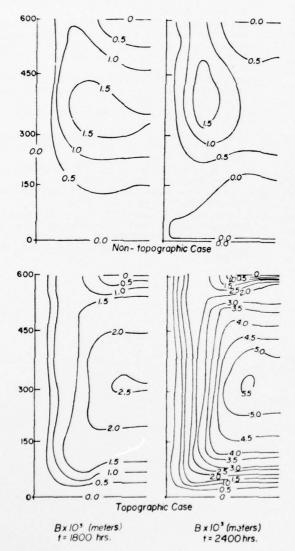


Fig. 16. The barotropic height (B), in meters, for the topographic case (lower panels) and non-topographic case (upper panels), at the time steps  $t=1800\,\mathrm{h}$  (left panels), and  $t=2400\,\mathrm{h}$  (right panels).

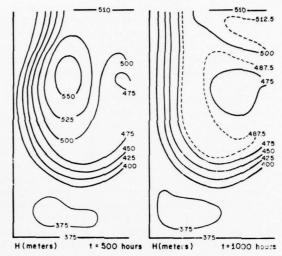


Fig. 17. The upper layer height (H), in meters, for the case of non-normal flow at the eastern input boundary, at t=500 h (left panel), and t=1000 h (right panel).

The upper layer changes noted after the initiation of the lower layer motion do not significantly affect the western boundary current, suggesting that topography is not an important factor in the baroclinic intensification. The beta-effect and advection as indicated in the Charney-Morgan inertial theories are sufficient to account for the baroclinic accelerations.

In contrast, the model barotropic component is very dependent on topographic influences. Once initiated, barotropic intensification does not occur in the vicinity of the Strait but rather along the continental slopes of the boundaries. This suggests that topography rather than the beta-effect is the prime mechanism responsible for the barotropic boundary current. The observed topographic trapping of the current (Cochrane, 1966; Molinari and Cochrane, 1972) and the model trapping of the barotropic mode of the flow suggest that, particularly at shallow depths, the barotropic component can contribute significantly to the current. However, the magnitude of this barotropic component is sensitive to changes of  $\sigma$  or  $\sigma'$ .

The influence of Cuba on the intensification process can be obtained from consideration of the flow through the Strait. Both the model and the observed data have countercurrents present at the western tip of Cuba. This separation of the main northerly flow and the island suggests that the western intensification of the Yucatan Current is dynamically independent of Cuba.

Wert and Reid varied the input at the Yucatan Strait seasonally to obtain a one-year prediction of the circulation in the Gulf of Mexico. The lack of sufficient data to realistically specify an annual variation of mass influx at 84W precludes the possibility of conducting a similar study for the Cayman Sea at the present time.

An indication of the variations occurring in the Cayman Sea circulation can be discerned from the data analysis. The July-August circulation is characterized by a more northerly development of the boundary current than occurs in the spring. This can result in a cyclonic flow pattern in the southern basin in July (Fig. 8).

The differences in the flow patterns appear to be a function of the northern component of the flow as it crosses the western Cayman Ridge. As mentioned previously the summer pattern exhibits a more northerly flow at 85W than is found in the spring. Since the angle of the flow across the Ridge is determined by conditions upstream, the cause of the variability cannot be ascertained from the data considered in this paper.

However, the data presented are consistent with other studies of the variability of the circulation pattern in this region. Perlroth (1968) conducted a compilation of bathythermographs taken in the Caribbean Sea in which he catalogued the records for two 2-month seasons. His winter results indicate less of a northerly component at 85W than do his summer results.

Acknowledgments. The contributions to this study by R. O. Reid are gratefully acknowledged. The author also wishes to express his appreciation to Mr. J. D. Cochrane for the use of his data, and to Dr. D. Fahlquist for permitting the collection of XBT data on his August 1970 cruise. This work was supported by the National Science Foundation under Grant GA-20569 to the Texas A & M University Research Foundation, and under International Decade of Ocean Exploration Grant AG-253.

### REFERENCES

- Ahrens, J., 1965: Potential vorticity in the thermocline of the Yucatan Current. Masters thesis, Texas A&M University, 44 pp.
- Arakawa, J., 1966: Computational design of a long-term numerical integration of the equations of fluid motion: Two-dimensional incompressible flow—Part 1. J. Comput. Phys., 1, 119-143.
- Cochran, J. D., 1966: The Yucatan Current. Rept., Dept. of Oceanography, Texas A&M University, Ref. 66-23-T, 14-25.
- —, 1969. The currents and water masses of the eastern Gulf of Mexico and western Caribbean. Rept., Dept. of Oceanography, Texas A&M University, Ref. 69-0-T, 29-31.
- -, 1971: Current observations in Yucatan Strait. Trans. Amer Geophys. Union, 52, 254 (Abstract).
- Fofonoff, N., 1962: Dynamics of ocean currents. The Sea, Vol. 1. Interscience, 323-396.
- Molinari, R. L., and J. D. Cochrane 1972: The effect of topography on the Yucatan Current. Contributions Phys. Oceanogr. Gulf of Mexico, Texas A&M University Oceanog. Studies, Vol. 2, L. R. A. Capurro and J. L. Reid, Eds., Gulf Publ. Co., 149-155.
- —, and R. B. Starr, 1972: Lagrangian current and hydrographic measurements in the Western Caribbean Sea. Trans. Amer. Geophys. Union, 53, 392 (Abstract).
- Munk, W. H., 1950: On the wind-driven ocean circulation. J. Meteor., 1, 79-93.
- Perlroth, I., 1968: Distribution of mass in the near surface waters of the Caribbean. Natl. Oceanog. Data Center, Progress Report No. P-72, 15 pp.
- Saylor, J. H., 1963: Inertial currents in the Caribbean Sea. Masters thesis, Texas A&M University, 48 pp.
- Smith, G. D., 1965: Numerical Solution of Partial Differential Equations. Oxford University Press, 179 pp.
- Wert, R. T., and R. O. Reid, 1972: A baroclinic prognostic numerical circulation model. Contributions Phys. Oceanogr. Gulf of Mexico, Texas A&M Univ. Oceanogr. Studies, Vol. 2, L. R. A. Capurro and J. L. Reid, Eds., Gulf Publ. Co., 177-209.

## Calculations of Differential Kinematic Properties from Lagrangian Observations in the Western Caribbean Sea

#### R. MOLINARI

Atlantic Oceanographic & Meteorological Laboratories, NOAA, Miami, Fla. 33149

#### A. D. KIRWAN, JR.

Department of Oceanography, Texas A&M University, College Station 77843 (Manuscript received 12 December 1974, in revised form 4 March 1975)

#### ABSTRACT

Observations of the motions of drifter clusters were made in the western Caribbean Sea during the summer of 1971. By two independent analyses of the relative motions of a cluster, two time series of horizontal divergence, vorticity, shear deformation rate, and normal deformation rate are developed. The results of the two approaches are very similar. The time series for these differential kinematic properties are fairly smooth when the drifters were moving in the Yucatan Current. Otherwise, the time series are ragged with frequent changes in sign. It is speculated that the raggedness is due to small values of the shear rates relative to random observational errors or small-scale turbulent processes. The records of the differential kinematic properties are used to evaluate the stretching and material derivative terms of the vorticity equation. Calculations indicate that potential vorticity is conserved along trajectories in the Yucatan Current.

#### 1. Introduction

The differential kinematic properties (DKP) of fluid flow, divergence, vorticity, shearing deformation rate, and stretching deformation rate are important elements in describing ocean current kinematics and dynamics. Divergence, for example, is a diagnostic of vertical motion. Vorticity can be related to external excitation functions of circulation such as wind stress and bottom topography. The deformations are important in the evolution of oceanic frontal zones. In brief, the DKP are important in describing mesoscale processes. Kirwan (1975) has given physical interpretations of these quantities and discussed their significance in oceanography.

Measurements of DKP are well established in meteorology (see Pettersen, 1953), but few observations of these terms have been made for the ocean. Usually, oceanographers have used Lagrangian observations either to obtain trajectory and velocity data for the large-scale currents or information on the small-scale turbulent characteristics of local regions. However, Reed (1971) has computed horizontal divergence and relative vorticity in the Alaskan Stream from drifter data, and Chew and Berberian (1971) and Chew (1974) have used similar data to compute values of some of the DKP in the Florida Current.

Lagrangian measurements are planned in the near future as components of many large-scale studies. The most obvious use of such data would be to map largescale circulation features. However, it may also be possible by analysis of the differential motions in drifter clusters to calculate the DKP. The emphasis of this paper is on an investigation of the capabilities and limitations of two techniques for computing DKP from observations of the differential motions of drifter clusters. Consequently, the discussion of the results is limited to a brief summary of the kinematics of the region from which the data were obtained. Reports being prepared for publication will focus on the dynamic interpretation of these drifter data and concurrent hydrographic data.

#### 2. Experimental and data reduction procedures

The Lagrangian observations used here were obtained during an experiment conducted in the western Caribbean Sea in the summer of 1971. A typical drifter used in this study was composed of a small surface buoy supporting a radar transponder. The buoy, most of which was submerged, was saucer-shaped, 1.83 m in diameter and 0.91 m thick. The radar transponder was on a pole 1.83 m long and 20.32 cm in diameter. Each buoy was drogued at 40 m by a 10.67 m parachute. The data collection technique is summarized by Molinari (1973).

A satellite navigation system was used as the primary control for positioning the vessel. This system provided on the average a fix every 1.5 h. Omega fixes and buoy positions relative to the ship were obtained at 15 min intervals. Errors in buoy position are introduced by

spurious satellite and radar fixes, as well as by the imprecision of the two systems.

Edited satellite fixes (Molinari, 1973) were used to calibrate the Omega fixes. Simultaneous satellite and Omega ship positions, a total of 234 values, were compared, and the Omega values were on the average 1.4 ( $\pm 1.4$ ) km to the east and 0.8 ( $\pm 1.8$ ) km to the south of the satellite values. These values were added to all the Omega coordinates to obtain the accepted positions.

The standard deviations of buoy positions include errors introduced by both the satellite and Omega systems; however, the largest errors probably are introduced by Omega. Taking Omega fixes as accurate to within  $\pm 1.5$  km radius and a typical velocity as 0.75 m s<sup>-1</sup>, it is seen that the error in position measurement may be greater than the displacement between the 15 min fixes. In fact, it could take perhaps an hour for a drifter to move outside its initial position error circle.

Because of the large uncertainty in the 15 min positions, we did not feel the data contained any reliable information on motions whose time and space scales were less than 2 h and 2 km respectively. Preliminary analysis indicated that even for periods greater than 6 h, the position data were dominated by random effects.

The randomness was surpressed by the following procedure. First, five consecutive 15 min fixes were averaged to produce smooth hourly positions. A running second-degree polynomial was then fitted to 13 consecutive hourly positions. Evaluation of the polynomial at its midpoint yielded the positions used in the analysis. As the lag on the running average was 2 h, this procedure produced positions every 2 h for each leg. Drifter velocities were determined by both centered finite differences and spline functions with nearly the same results. The running polynomial and the centered differences constitute a low-pass filter which surpresses energy at periods less than 12 h with essentially no phase shift.

Kirwan et al. (1975) have investigated the effects of wind and current on surface drifters. Using their analysis for the drifter configuration used in this experiment, it was found that a 10 m s<sup>-1</sup> wind, the highest observed, could cause a 5% error in the estimate of the true current, assuming no vertical shear between the surface and 40 m. The wind effect was not considered in reducing the data from this experiment.

## 3. Calculation of differential kinematic properties

There are a number of techniques discussed in elementary dynamic meteorology texts for evaluating divergence and vorticity. Many of these approaches utilize synoptic charts, a product not readily available in oceanography. Here, two approaches are compared which require only observations from clusters of three or more drifters.

#### a. Method I: Least squares

Consider a test ocean region of small but finite size wherein the velocity at any point is adequately represented by the linear terms in a Taylor's expansion about the center of mass of the parcel. For a cluster of n drifters located within the parcel, the expansion yields for the ith drifter:

$$U_{i} = U + g_{i} + [(D+N)X_{i}]/2 + [(S-\zeta)Y_{i}]/2$$

$$V_{i} = V + h_{i} + [(S+\zeta)X_{i}]/2 + [(D-N)Y_{i}]/2$$

$$i = 1, \dots, n. \quad (1)$$

The U and V are the components of the velocity of the center of mass of the parcel; the coordinates with respect to the cluster center of mass of drifter i are  $X_i$  and  $Y_i$ ; and  $g_i$  and  $h_i$  represent the sum of the higher order nonlinear terms in the expansion. From the experimental standpoint, these terms would include measurement errors and, perhaps, random turbulent motion. Also, in these equations, we have written the velocity gradients across the parcel in terms of the elementary kinematic modes:

$$D = \frac{\partial U}{\partial X} + \frac{\partial V}{\partial Y} \quad \text{(divergence)}$$

$$\zeta = \frac{\partial V}{\partial X} - \frac{\partial U}{\partial Y} \quad \text{(vorticity)}$$

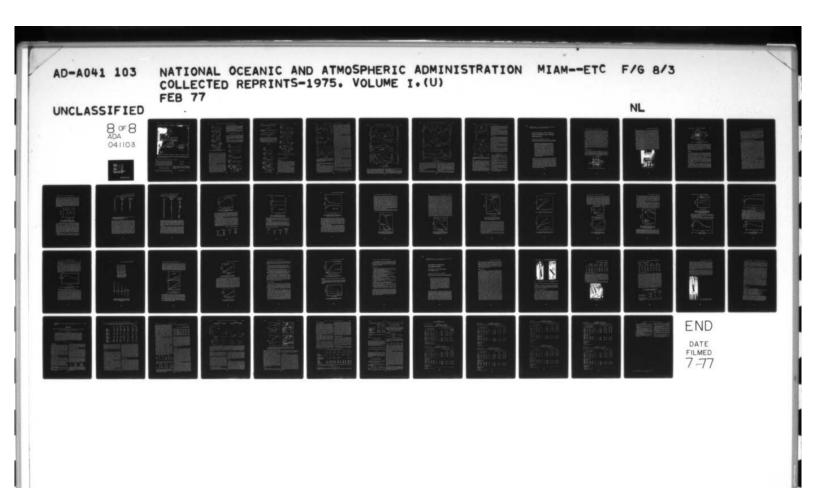
$$S = \frac{\partial V}{\partial X} + \frac{\partial U}{\partial Y} \quad \text{(shearing deformation rate)}$$

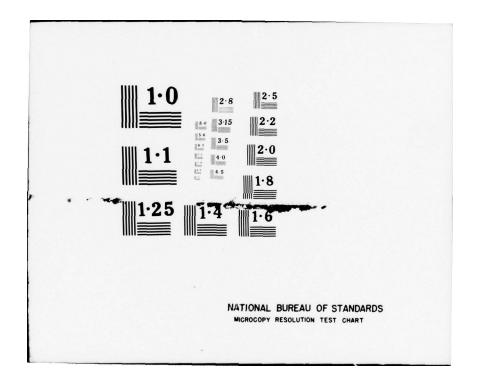
$$N = \frac{\partial U}{\partial X} - \frac{\partial V}{\partial Y} \quad \text{(stretching deformation rate)}$$

The horizontal divergence D is a measure of the parcel area change without change of orientation or shape. The vorticity is  $\zeta$  and is a measure of the orientation change without area or shape change of the parcel. Shape changes without change of area or orientation are given by S and N respectively. The former is for the shape change produced by differential motions of the boundaries parallel to the boundary, while the latter is for motions normal to the boundaries.

R. O. Reid (personal communication) has provided us with a physical interpretation of the model equations. An individual drifter's velocity is given by the mean translatory velocity of the parcel, plus a velocity induced by the rotation, divergence, and distortion of the parcel, plus a random or turbulent velocity. The mean parcel velocity is attributed to large-scale (relative to cluster size) motions, the induced velocity to cluster-scale motions, and the random component to the small-scale turbulent field. The scale of these latter motions is less than that of the cluster. Okubo and Ebbesmeyer (1975) have also suggested this interpretation.

The basic observation in a drifter study is the position vector for each float for a series of times. This position vector will generally be referred to a fixed geographic origin. For simplicity, it will be assumed here that the drifters are all at the same depth. In practice this may not be the case, and unless vertical





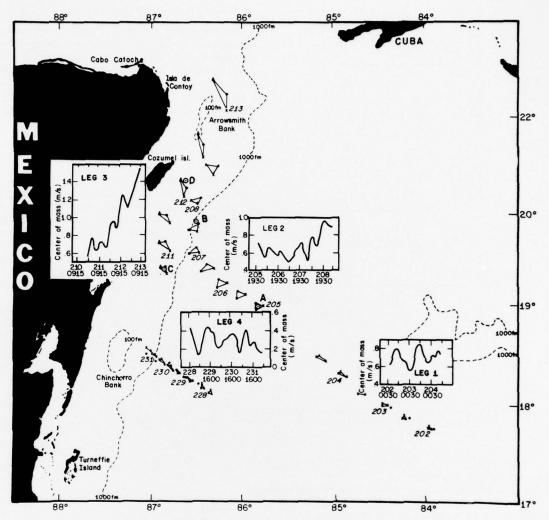


Fig. 1. Diagram of the drifter trajectories, including speeds for legs 1 through 4. The four legs were occupied in chronological order. The times are in Julian Day/Hour. The intervals (A, B) and (C, D) refer to the part of trajectory over which potential vorticity was conserved (See Fig. 9).

shear is accounted for, serious biasing of the data will occur.

The series of components of the horizontal position vectors for drifter i is denoted by  $\alpha_i$  and  $\beta_i$ . From this it is easy to calculate the position vector with respect to the center of mass. For each successive time interval  $\Delta t$ , the velocities [the left-hand side of (1)] can be calculated from spline functions or finite differences such as

$$U_{i}(t) = \left[\alpha_{i}(t+\Delta t) - \alpha_{i}(t-\Delta t)\right]/2\Delta t$$

$$V_{i}(t) = \left[\beta_{i}(t+\Delta t) - \beta_{i}(t-\Delta t)\right]/2\Delta t$$
(2)

Here U and V, the average velocity components or the velocity of the center of mass at any time t, are

calculated from

$$U = \left(\sum_{i=1}^{n} U_{i}\right)/n$$

$$V = \left(\sum_{i=1}^{n} V_{i}\right)/n$$
(3)

The g and h functions and D, N, S and  $\zeta$  can be computed by noting that at each time, the total kinetic energy per unit mass of the cluster due to small-scale turbulence is

$$KE = \sum_{i=1}^{n} [g_{i}^{2} + h_{i}^{2}]/2.$$
 (4)

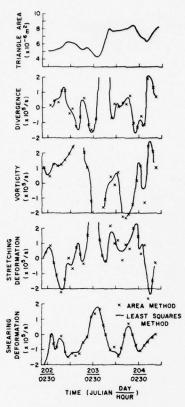


Fig. 2. The triangle areas and the differential kinematic properties computed for the buoy triads of leg 1.

Substituting (1) into (4) shows that the kinetic energy density depends upon D, S, N and  $\zeta$ . These four parameters can be estimated by selecting values which give a minimum for the kinetic energy function. The g and h functions can then be determined from (1).

As this method is a least-squares approach, there is no difficulty in extending it to large numbers of drifters. In fact, the statistical confidence in the values of the kinematic parameters increases with the number of drifters. The minimum number of drifters that can be used to determine D, S, N and  $\zeta$  is three. In this case, the least-squares procedure reduces to four algebraic equations for four unknowns. The g and h functions are then identically zero.

Two points should be made about this approach. First, statistical theory can be applied to questions regarding sampling variability, confidence limits on the coefficients, analysis of variance, and biased data. Second, the approach generates time series of turbulent velocities. It is then possible to form direct estimates of turbulent stresses and to compare these with parametric representations of the non-advective fluxes of turbulent momentum. Okubo and Ebbesmeyer (1975) have discussed these two points in some detail.

### b. Method II: Area rate of change

Saucier (1955) discusses a method for computing atmospheric divergence, vorticity, stretching and shearing deformation. The method requires wind observations from closely spaced stations. However, it is readily adapted to ocean drifter data.

Horizontal divergence can be expressed as the fractional time rate of change of the horizontal area A of a parcel, i.e.,

$$(\partial U/\partial X + \partial V/\partial Y) = A^{-1} dA/dt.$$
 (5)

For a triad of drifters, A is readily evaluated at each time step by calculating the position vector cross product of two of the drifters with respect to the third. From the time series of A's, a multitude of numerical techniques are available to estimate the time rate of change.

As shown by Saucier (1955), vorticity, shearing and stretching deformation can be evaluated by selected rotations of the velocity vectors of the three drifters.

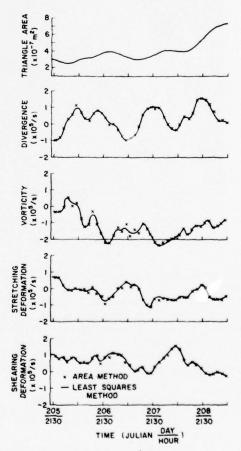


Fig. 3. As in Fig. 2 except for leg 2.

For example, a 90° clockwise rotation transforms

$$\left. \begin{array}{l} U \rightarrow -V' \\ V \rightarrow .U' \end{array} \right\}.$$

Substituting this into the divergence expression in (5), it is seen that

$$(\partial V/\partial X - \partial U/\partial Y) \rightarrow (\partial U'/\partial X + \partial V'/\partial Y).$$
 (6)

The right-hand side of (6) is recognized as

$$(1/A')dA'/dt$$
,

where A' is the area enclosed by the triangle whose vertices are formed by the rotated velocity vectors. The time rate of change is evaluated by taking the difference between this area and the area enclosed by the drifter triad at the previous time step.

By a similar analysis it is seen that the transformation

$$U \to U'' \\ V \to -V''$$

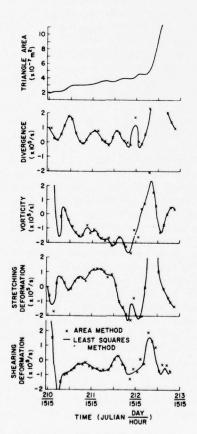


Fig. 4. As in Fig. 2 except for leg 3.

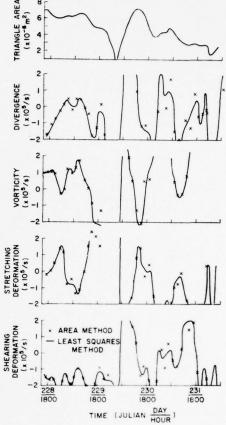


Fig. 5. As in Fig. 2 except for leg 4.

yields the stretching deformation. Finally, the rotation

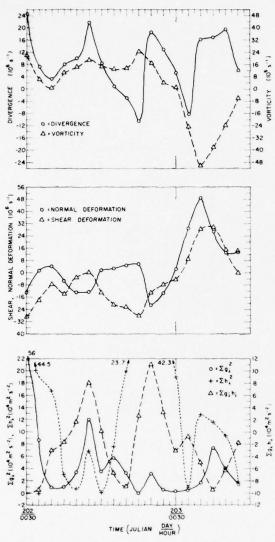
$$U \rightarrow V'''$$

produces the shearing deformation.

### 4. Results

The data reported on here were obtained from four distinct flow regimes. Fig. 1 summarizes the trajectories and speeds of the drifter cluster center of mass for each of the four legs. During legs 1 and 4, the accelerations and trajectory curvature were small compared with legs 2 and 3. During the latter two mentioned legs, the drifters entered the Yucatan Current.

Figs. 2, 3, 4 and 5 show the triangle area, divergence, relative vorticity, and the shearing and stretching deformation rates for the four legs as calculated by the two methods previously outlined. As can be seen, there is little difference between the values of the DKP calculated by the two different procedures. Note, however, that the DKP time series obtained for legs 2 and



 $F_{1G}$ . 6. Differential kinematic properties  $\Sigma g_1^2$ ,  $\Sigma h_1^2$  and  $\Sigma g_1h_i$  for leg 1 as calculated from observations of four drifters. When comparing Figs. 6, 7 and 8 with Figs. 2, 4 and 5, respectively, note that the scale for the differential kinematic properties in the first set of figures is ten times greater.

3 are smoother than those computed for legs 1 and 4. In the latter cases, the series are ragged with frequent sign changes.

There are two explanations for the differences in smoothness of the DKP time series. One is random errors in the measurements. The triad areas of legs 1 and 4 are an order of magnitude smaller than the areas of legs 2 and 3. If the statistics of the observational errors are the same for all legs, the smaller areas will introduce a larger error into the DKP estimates.

The other explanation has been pointed out to us by R. O. Reid (personal communication). He has shown

that the DKP will exhibit frequent sign changes if the drifters were responding to an energetic small-scale random or turbulent motion field. If the turbulent motions are more important in the relative motion of cluster elements than velocity gradient effects, then for a large number of drifters, the g and h functions are the dominant terms on the right-hand side of (1). However, for three drifters, the g and h functions are identically zero, and any turbulence appears as errors in the DKP estimates. If more than three drifters are present, then estimates of the DKP should be considerably improved. Okubo and Ebbesmeyer (1975) suggest that at least six are required.

During parts of legs 1, 3 and 4, there were four drifters deployed. Data from these legs can thus be used to demonstrate the effect of the number of drifters on estimates of the DKP. The time series for the DKP along with  $\Sigma g_i^2$ ,  $\Sigma h_i^2$  and  $\Sigma g_i h_i$  are shown in Figs. 6, 7 and 8. For legs 1 and 4, it is seen from comparison of Figs. 2 with 6, and Figs. 5 with 8 that calculations of DKP which use four drifters are much smoother than those which utilize just three. We interpret this to mean that the additional drifters provide better estimates of the DKP for these legs. On the other hand, it is seen from Figs. 4 and 7 that for leg 3, there is virtually no difference between the calculations for DKP using three or four drifters. Apparently for this leg, the estimates of the DKP obtained from three drifters were valid and not significantly affected by measurement error or small-scale motions.

As there were only four drifters for these legs, there is little confidence in the estimates of the turbulent statistics,  $\Sigma g_i^2$ ,  $\Sigma h_i^2$  and  $\Sigma g_i h_i$ . The ragged character during legs 1 and 4 (Figs. 6 and 8) probably reflects the poor estimates. These statistics were considerably smoother during leg 3 (Fig. 7) which suggests that the order of magnitude for this leg is correct. It is also seen that for all three legs, the time average of  $\Sigma g_i h_i$  was nearly zero. This implies that there was little flux of X-directed momentum in the Y direction, and vice versa, when viewed from a coordinate system moving with the mean velocity.

It is possible from Figs. 1 and 7 to assess the relative roles of the mesoscale and turbulent velocities for producing neighbor separations for leg 3. From Fig. 4 a characteristic length of the cluster is found to be  $5\times10^3$  m. From Fig. 7 characteristic values of the gradients and the rms values of  $g_i$  and  $h_i$  can be obtained at selected times. Inserting these values into (1), it is found that the ratio of mesoscale velocity to turbulent velocity ranges from 0.85 to 2.5. Calculations for the other two legs yield a much greater range of ratios.

As an example of the use of the DKP, consider a simple dynamical model of conservation of potential vorticity for the Yucatan Current. This relation is

$$d(\zeta + f)/dt + (\zeta + f)D = \text{residual}, \tag{7}$$

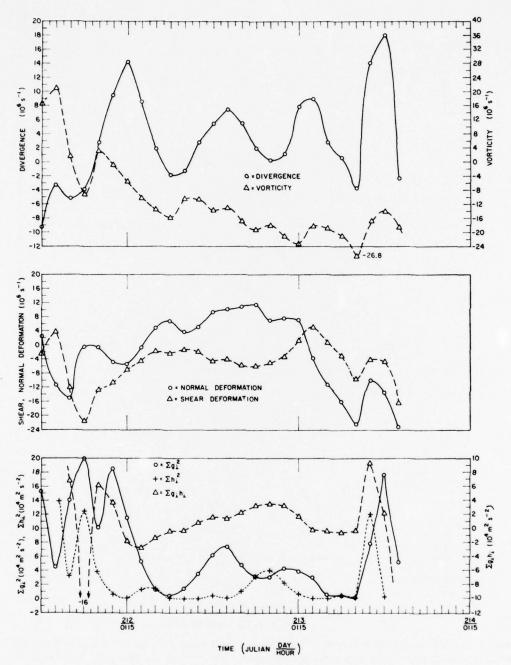


Fig. 7. As in Fig. 6 except for leg 3.

where f is the Coriolis parameter, and residual includes all factors which tend to upset the potential vorticity balance, as well as errors in measurement. In order to examine the balance of terms in (7), the vorticity, divergence and Coriolis parameter were smoothed by a three-point running average to obtain values every 6 h.

Then the averaged values were substituted into a centered difference form of (7).

The evaluations of the two terms in (7) for legs 2 and 3 are given in Fig. 9. From this it is seen that the two terms on the left-hand side of (7) tend to be out of phase. The residual is of the order of magnitude of

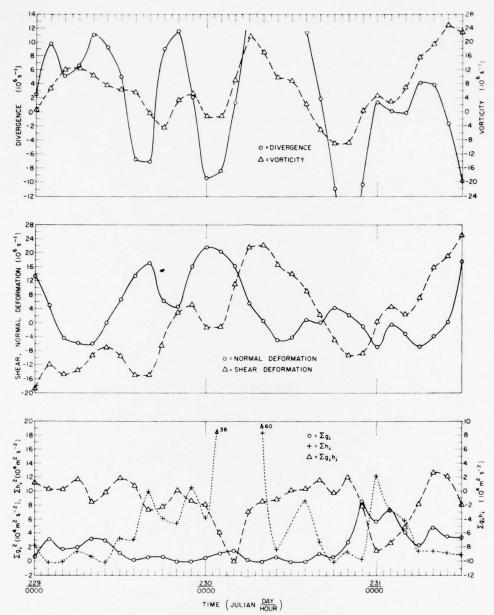


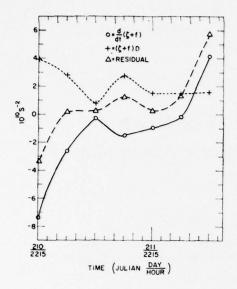
Fig. 8. As in Fig. 6 except for leg 4.

these terms but is typically smaller. The potential vorticity in both legs thus is approximately conserved from intervals A to B for leg 2 and C to D for leg 3 (refer to Fig. 1). At point B, two of the drifters passed over a seamount with a consequent decrease in water depth to less than 300 m. Beyond point D, one drifter passed over Arrowsmith Bank while the other two remained in deeper water.

#### 5. Discussion

The observations and calculations presented here provide quantitative data on the magnitude for the velocities and the DKP of the Yucatan Current and the western Caribbean. It was found that the shear and normal deformations were the same order of magnitude as the vorticity and of the order of  $10^{-5}$  s<sup>-1</sup> or smaller. The horizontal divergence also was of this magnitude. Similar values for the divergence were reported by Chew and Berberian (1971) and Reed (1971). Finally, it was found that trajectories in the vicinity of the Yucatan Current axis approximately conserve potential vorticity.

We feel that these results have significance beyond a contribution to the description of the regional oceanog-



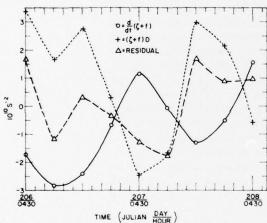


Fig. 9. Material derivative, stretching and residual terms for potential vorticity equation for legs 2 and 3. The time intervals are for the portions of the trajectories shown in Fig. 1 by (A, B) and (C, D).

raphy of the Caribbean. First, two procedures have been developed for calculating the DKP. In regions where the horizontal velocity gradients are significant, the two methods give comparable results. The calculation of the DKP thus fills the gap, noted in the Introduction, between the use of Lagrangian data to infer characteristics of large-scale circulation features and small-scale turbulent processes in the ocean.

Second, the observations reported here show that the DKP can make a considerable contribution to drifter separations. For example, if the DKP had been ignored, and the separation of pairs of drifters had been attributed solely to the neighbor or turbulent diffusivity,

then one would infer that the Yucatan Current was highly turbulent. This may be the case, but it would appear from our results that mesoscale phenomena are at least as equally important in this current for producing neighbor separations.

Finally, we have demonstrated that it is possible to infer the material derivative and stretching terms of the vorticity equation from Lagrangian measurements. This means that by combining Lagrangian measurements with synoptic pictures of the field of mass, it should be possible to test dynamical concepts of strong current regimes.

Acknowledgments. The contributions of the officers and crew of the NOAA ship Researcher during the data collection phase of this study are gratefully acknowledged. Support for this portion of the study was provided in part by the Office of the International Decade of Ocean Exploration of the National Science Foundation, Grant AG-253, to the Atlantic Oceanographic and Meteorological Laboratories.

Support for A. D. Kirwan, Jr., has been provided by the Ocean Sciences and Technology Division of the Office of Naval Research and the Office of the International Decade of Ocean Exploration of the National Science Foundation.

We are especially grateful to R. O. Reid for making available to us some preliminary results of a theoretical analysis of drifter motions in a random turbulent field and to A. Okubo and C. Ebbesmeyer for a copy of their manuscript. Finally, we wish to acknowledge valuable criticisms provided by R. Bernstein.

### REFERENCES

- Chew, F., 1974: The turning process in meandering currents: A case study. J. Phys. Oceanogr., 4, 27-57.
- —, and G. A. Berberian, 1971: A determination of horizontal divergence in the Gulf Stream off Cape Lookout. J. Phys. Oceanogr., 1, 39-44.
- Kirwan, A. D., Jr., 1975: Notes on oceanic velocity shears. (Submitted for publication).
- —, G. McNally, M. S. Chang and R. Molinari, 1975: The effect of wind and surface currents on drifters. J. Phys. Oceanogr., 5, 361-368.
- Molinari, R., 1973: Data from the Lagrangian current measurement project conducted aboard the NOAA ship Researcher during CICAR survey month 1. NOAA Tech. Memo. ERL AOML-19, 81 pp.
- Okubo, A., and C. C. Ebbesmeyer, 1975: Determination of vorticity, divergence, and deformation rates from analysis of drogue observations. (Submitted to *Deep Sea Res.*).
- Pettersen, S., 1953: On the relation between vorticity, deformation and divergence and the configuration of the pressure field. *Tellus* 5, 231-237.
- Reed, R. K., 1971: An observation of divergence in the Alaskan Stream. J. Phys. Oceanogr., 1, 282-283.
- Saucier, W. J., 1955: Principles of Meteorological Analysis. The University of Chicago Press, 438 pp.

Reprinted from: Advances in Chemistry Series, Number 147, Analytical Methods in Oceanography, 56-81.

# Direct Determination of Trace Metals in Seawater by Flameless Atomic Absorption Spectrophotometry

DOUGLAS A. SEGAR and ADRIANA Y. CANTILLO

National Oceanic and Atmospheric Administration, Atlantic Oceanographic and Meteorological Laboratories, 15 Rickenbacker Causeway, Miami, Fla. 33149

Flameless atom reservoir atomic absorption spectrophotometry, because of its extremely high sensitivity, has found many applications in trace metal analysis of seawater, marine organisms, and sediments. Direct analysis of seawater for trace metals was not possible with early atomizer designs because of matrix interferences. A new generation of atomizer reduces these interferences and has been tested for its utility in direct analysis of seawater. All elements so far investigated—iron, manganese, copper, and cadmium—can be rapidly, simply, and precisely determined in their normal range of concentrations in seawater. Several precautions are necessary to obtain accurate results, as matrix composition, injection volume, atomizer conditions, and changes in graphite atomizer tube characteristics all affect the sensitivity of analysis.

The marine chemistry of trace transition metals is not well understood, despite many years of intense interest and research activity. The comparative lack of success of most investigations of marine geochemical cycles of transition elements undoubtedly arises largely from the inadequate analytical techniques used to determine elemental concentrations, particularly concentrations of metals dissolved in seawater. Not only are the historically preferred techniques inaccurate (1), but also their length and difficulty normally preclude the analysis of sufficient samples to describe adequately environmental variations. Unless these variations, both in time and space, can be adequately described, little can be learned about marine geochemical processes.

Trace metal concentrations in seawater are so low that contamination of the sample and loss of metal to container walls are critical problems in any analytical technique. These problems are particularly severe when the water sample must undergo extensive chemical treatment prior to the determination step. Most available techniques require such a chemical step or steps, because of their inadequate sensitivity and/or inability to determine the metal in the presence of the other sea water salts. Even those neutron activation procedures established for analysis of elements in seawater usually require a preactivation concentration step (2).

Recently, flameless atomization techniques have been developed for atomic spectroscory, particularly for atomic absorption. Absolute sensitivities of atomic absorption using these flameless atomizers are, for most elements, comparable with or better than those attainable by any other technique. Additionally, unlike most other techniques the atomic absorption method is relatively free from interferences by other components of the sample matrix. Therefore, flameless atomic absorption holds great promise for direct analysis of trace metals in seawater and other environmental samples. This paper reports the successful application of a new design of commercial atomizer to direct analysis of several metals in seawater.

#### Flameless Atomizers

Flameless atomic absorption spectrophotometry is essentially very simple. A substrate upon which the sample matrix can be deposited is placed in or immediately adjacent to the spectrophotometer light beam, and a means of heating this substrate rapidly to 800°–3500°C is provided. Electrical resistance is usually the heating method used. The substrate

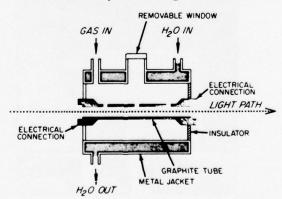


Figure 1. Cross section of HGA-2000 atomizer head

itself has been made from various materials, and a large number of atomizer designs have been used. Two substrates-graphite and tantalum -appear to be best suited to routine use, and two basic atomizer designs -the open rod or West type and the closed furnace or Massman typehave been used (3). Of the two basic designs, the closed furnace appears to be preferable for routine analysis of most samples (3) because it does not require as stringent optical alignment as open filament types, generally can accept larger sample volume, and shows fewer inter-element interferences because of the smaller temperature gradient observed within the atomization zone. One such atomizer, the Perkin Elmer HGA-70 (later designated the HGA-2000) with a modified power supply, has been extensively evaluated for use in marine chemical analysis (4-11). One of the major disadvantages of this atomizer was the physical arrangement which allowed the cooling, condensing atom gas cloud to remain in the optical path of the spectrophotometer while it was swept laterally out of the atomizer (Figure 1). This led to nonspecific absorption or scattering attenuation of the light beam, thereby preventing the analysis of high solid content matrices such as seawater (4). This attenuation was so great that it prevented the use of a background correction system, such as that based on the deuterium arc lamp (12). Recently, a new heated graphite atomizer has been designed, the Perkin Elmer HGA-2100 (Figure 2), which alleviates this problem by modifying the

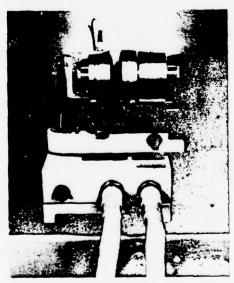


Figure 2. HGA-2100 atomizer head

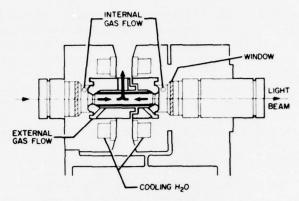


Figure 3. Cross section of HGA-2100 atomizer head showing gas flow

gas flow within the heated graphite tube to remove the hot atom cloud from the light beam before the atom cloud is significantly cooled. The purge gas enters the atomizer tube at each end and exits through the sample introduction port at its center (Figure 3). A second inert gas supply is provided outside the atomizer tube to prevent its oxidation. The atomizer can accept up to  $50~\mu l$ . of solution and be heated in three different temperature steps up to about  $3000^{\circ}C$ .

#### Equipment

A Perkin Elmer model 503 atomic absorption spectrophotometer, equipped with Perkin Elmer HGA-2100 heated graphite atomizer (Figure 2), a deuterium arc background corrector (12), and a strip chart recorder, was used. The HGA-2100 graphite furnace was purged with argon. Hollow cathode lamps were used except for cadmium for which an electrodeless discharge lamp (Perkin Elmer) was used.

The reported temperature settings for the graphite furnace were read from the HGA-2100 power supply readout and are approximate. These temperatures are based upon the applied voltage across the atomizer terminals. All absorbances were obtained from peak heights read from either the strip chart or the digital peak height reader of the Perkin Elmer 503.

The measurement of peak areas rather than peak heights would undoubtedly eliminate or reduce some of the matrix effects on sensitivity reported below (13). However, the integration mode of the Perkin Elmer 503 does not provide true peak area integration, but instead provides signal averages for a preset time subsequent to initiation of the atomiza-

tion step. Because of the adverse signal-to-noise relationship caused by this procedure, the detection limits obtained with the integration mode are not as good as those obtained by peak height measurement. A fast response integrator programmed to the output peaks would ur Joubtedly enhance the analysis of complex samples such as seawater.

All standards were prepared by dilution of Alfa Inorganics Ventron primary standard solutions using acidified filtered surface Gulf Stream seawater (salinity ca. 36%) or distilled water. Sample injections were made with Eppendorf microliter pipets with disposable plastic tips.

#### Preliminary Assessment of Seawater Analysis

The preliminary assessment of the behavior of seawater in the HGA-2100 was carried out in conjunction with the Perkin Elmer Co. Some of these results have been published elsewhere (14). The HGA-2100 gave rise to considerably smaller background absorbances than the HGA-2000 during atomization of sodium chloride solutions and measurement of the absorbance at the copper wavelength (324.7 nm). The charring temperature used was low enough so that no salt was volatilized before atomization. Plots of the molecular absorbance of sodium chloride vapor produced by the two atomizers as a function of concentration are shown in Figure 4. A 10 µl. aliquot of 35% seawater will contain 350 µg of total salt. From Figure 4 it can be seen that for a sample containing this quantity of sodium chloride, the background signal with the HGA-2000 is more than one absorbance unit while with the HGA-2100 it is about 0.1 absorbance -a value more readily correctable by means such as the deuterium arc background corrector (12). Even the reduced background absorbance afforded by the HGA-2100 is larger than desirable, particularly when analyzing samples having metal concentrations close to the detection limits of flameless atomic absorption. This condition is encountered for many elements in unpolluted seawater (Table I), and it is, therefore, necessary to use the selective volatilization technique where possible (15) to further reduce background interference.

Trace elements in seawater can be divided into two somewhat arbitrary groups according to their relative volatilities. The first group, including elements such as V, Co, Ni, Cu, Mn, Fe, Cr, and Mo is not volatilized at temperatures sufficient to volatilize the alkali chlorides. The second group consists of elements whose salts have volatilities similar to or greater than the alkali chlorides, including cadmium, zinc, lead, and gold. Selective volatilization can be used to remove the bulk of seawater salts prior to atomization of the low volatility elements but not the volatile elements (4). Elements which have been determined by flameless atomic absorption using the heated graphite atomizer are listed

in Table I as being volatile or involatile. The division between the two groups is not well defined by observation, and some elements may fall into the other group when atomization from a seawater matrix is attempted as opposed to atomization of the simple salts. Table I shows approximate detection limits obtainable for various elements in simple aqueous solution. In addition, the approximate concentrations of the elements in unpolluted seawater are listed. A comparison reveals that, if detection limits comparable with those in distilled water can be obtained in seawater and if matrix effects can be compensated or eliminated, a number of elements could be determined by direct injection of seawater into the HGA-2100.

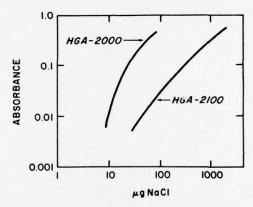


Figure 4. Absorbance of sodium chloride at 324.7 nm without background correction using the HGA-2000 and the HGA-2100 atomizers

An evaluation of direct analysis of seawater by the HGA-2100 was carried out for three elements with lower volatilities than the alkali metal chlorides (copper, iron, and manganese) and one element with higher volatility (cadmium). Analysis of seawater for each of these elements proved to be possible and sufficiently sensitive. However, a number of variables affect the analysis. These variables, in addition to the atomic absorption spectrophotometer settings, include the purge gas flow rate through the atomizer, the ashing temperature and time, the atomization temperature, the salinity of the sample, the volume of injection, and the changing surface properties of the graphite tube. To optimize the analytical sensitivity and precision, the effect of each of these variables was investigated.

Purge Gas Flow Rate. The purge gas flow rate can be adjusted up to about 220 ml of argon per minute. Normally the flow rate of the argon

Table I. Trace Elements in Seawater and Detection Limits

	Volatile Elements	
	Approximate	Approximate
	Detection	Seawater
Element	Limit*	Concentration b
Ag	0.1	0.1
As	1	2.3
Au	0.5	0.005 °
Bi	0.2	0.02
Cd	0.04	0.05
Hg	220	0.05°
In	16	0.0001
Pb	1	0.03 °
Sb	5	0.01
Se	60	0.45
Sn	60	0.01
Te	600	
Tl	3	0.01
Zn	0.02	5

\*Detection limit in  $\mu g/l$ . for a 50- $\mu$ l. injection. Detection limit taken to be equal to sensitivity listed by Perkin Elmer Corp. (21).

\*From Riley and Chester (17)  $\mu g/l$ . for salinity = 35%.

Considerable variations known to occur.

gas is maintained as low as possible (about 50 ml/min) to maximize the residence time of atoms in the atomizer and, therefore, the peak atoms population and the analytical sensitivity. To obtain maximum sensitivities, the internal gas flow may even be switched off for a few seconds during the atomization step (16). Higher flow rates lead to generally lower sensitivities and are, therefore, undesirable. However, low flow rates will retard flushing of the cooling atom cloud from the furnace. When determining elements in a high salt content matrix, this significantly increases background absorption. Consequently, either the compensation ability of the deuterium arc background corrector is exceeded, or the reproducibility and precision of the analysis are reduced because of noise introduced by imperfect correction of large background signals. Thus, it was found that a flow rate of about 150 ml/min was optimal for manganese and copper analysis. Despite removal of the major seawater salts by ashing before atomization, sufficient matrix material remains to pro-

#### of Flameless Atomic Absorption Spectrophotometry

Involatile Elements

Involatile Elements			
	Approximate Detection	Approximate Seawater	
Element	Limit*	Concentration b	
Al	3	5 °	
Ba	6	30 °	
Be	0.7	0.0006	
Co	2	0.08°	
Cr	0.5	0.6°	
Cs	2	0.5	
Cu	1	3 °	
Dy	15	0.0009	
Er	35	0.0009	
Eu	800	0.0001	
Fe	0.5	3°	
Ga	50	0.03	
Ir	60		
Li	1	180	
Mn	0.2	2°	
Mo		10	
Ni	3	2	
Pd	2 3 3 2 1	_	
Pt	2	<u> </u>	
Rb	ī	120	
Rh	4	0.01	
Si	3	1000°	
Sr	4	8500	
Ti	40	1	
v	7	1.5	

duce significant background signals during atomization at low flow rates. Although sensitivity for manganese and copper is somewhat less at the chosen flow rate than at lower values, the difference is small and compensated for by improved reproducibility. For iron analysis, where a higher ashing temperature may be used and, therefore, more matrix material removed before atomization, the optimum flow rate is about 100 ml/min.

When atomizing cadmium from seawater, the atomic absorption signal is followed by a spurious non-atomic signal from the major salts (see Figure 22). The analysis depends upon the temporal separation of these two signals. At high gas flow rates, cadmium is swept out of the light beam before the spurious signal is generated. At lower rates, the sensitivity of the analysis is improved as the residence time of cadmium atoms in the light beam is increased. However, this increased residence time reduces the separation between the atomic and spurious peaks,

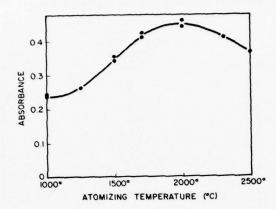


Figure 5. Effect of atomization temperature on the absorbance of 5 µl. of a 10-ppb spike of cadmium in seawater

causing overlap and interference. The optimum gas flow rate is, therefore, about 70 ml/min. It is possible that the limiting factor in resolution of the cadmium and matrix signals is the relatively slow response time of conventional atomic absorption spectrophotometer readout electronics. If this is the case, then use of a faster readout system and lower gas flow should improve sensitivity.

Atomization Temperature and Time. The maximum temperature of the heated graphite tube during the atomization step and the rate at which this temperature is achieved determines the rate of volatilization and atomization of the sample and, therefore, the peak atom population and sensitivity. For involatile elements, the peak height sensitivity increases with increasing temperature until a plateau is reached. The optimum atomization temperature is then the lowest temperature at which maximum sensitivity is obtained. For some volatile elements, the peak absorbance may reach a maximum with increasing temperature and

Table II. Optimum Conditions for

Element	Ashing Temp. (°C)	Ashing Time (sec)	Atomization Temp. (°C)
Cd	400	10	1500
Cu	600	25	2500
Fe	1250	25	2500
Mn	1100	25	2400

<sup>\*</sup> Rotameter reading HGA-2100.

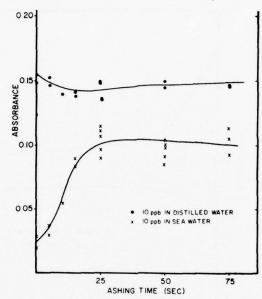


Figure 6. Effect of ashing time on the absorbance of 40  $\mu$ l. of a 10-ppb spike of manganese in distilled water and seawater (ashing temperature = 600°C)

may then decrease with further temperature increase (Figure 5). The optimum atomization temperatures for seawater analysis were found to be essentially the same as those for dilute aqueous metal salts and are listed in Table II.

The atomization time is set at the shortest time necessary for complete removal of the analysis element from the atomizer. Generally, a time is selected which continues atomization for a period after the peak signal is observed, corresponding to about twice the peak width at half height at the highest concentration to be determined. This ensures that

## Seawater Analysis by Direct Injection

Atomization Time (sec)	Gas Flow	Usual Sample Vol. (µl.)	Approximate Detection Limits (µg/kg)
7	40	10	0.01
7	80	50	0.5
7	60	20	0.4
7	80	20	0.3

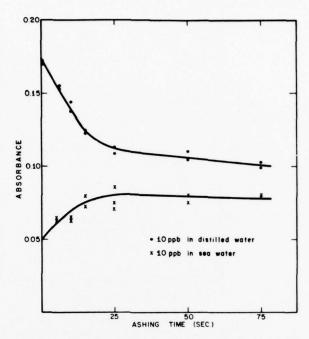


Figure 7. Effect of ashing time on the absorbance of 40 µl. of a 10-ppb spike of manganese in distilled water and seawater (ashing temperature = 1100°C)

memory effects are eliminated and permits examination of the analytical baseline immediately after the absorption signal while the atomizer is still at the atomization temperature. For some elements, particularly those whose analytical lines are of longer wavelength, there is a small but significant baseline shift caused by black body emission from the incandescent atomizer tube. This shift may be minimized by careful alignment of the optical train but still must be corrected for when low concentrations are determined.

Ashing Temperature and Time. The intermediate temperature heating cycle of the heated graphite atomizer, referred to here as the ashing cycle, removes as much of the matrix as possible without significant loss of the analyte. For involatile elements a significant proportion of seawater salts can be removed by this means before the atomization step. The choice of ashing temperature and time is made to obtain the optimum balance of sensitivity and reproducibility. At too low an ashing temperature or too short an ashing time the incomplete removal of the matrix

salts and the consequent inability of the deuterium arc background corrector to compensate precisely for nonspecific absorption will reduce the reproducibility. Too high an ashing temperature will lead to significant loss of analyte metal from the atomizer before atomization and consequently a loss of analytical sensitivity. The effect of ashing time on manganese analysis in seawater is illustrated in Figures 6 and 7. At an ashing temperature of 600°C, little loss of manganese from the atomizer occurs even for long ashing times. However, the reproducibility of the analysis for seawater is extremely poor even at long ashing times (Figure 6). At an ashing temperature of 1100°C, although significant loss of manganese occurs from a distilled water matrix, the reproducibility of the analysis in seawater is much improved while the sensitivity is reduced by only about 25% (Figure 7). Optimum ashing times required at each temperature are similar. Little change in either reproducibility or sensitivity occurs with increasing time above 25 sec.

The effect of ashing temperature upon the analysis of iron, manganese, and copper is illustrated in Figures 8, 9, and 10, respectively.

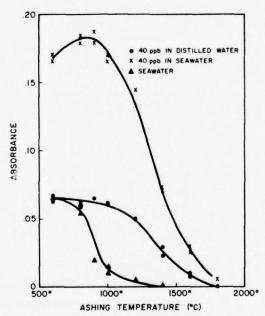


Figure 8. Effect of ashing temperature on the absorbance of 20-µl, injections of a 40-ppb spike of iron in distilled water and seawater and of unspiked seawater (Fe < 0.5 ppb)

When introduced in chloride salt solution in distilled water, the response to changes in ashing temperature is, in each instance, relatively simple. The analytical sensitivity falls off at temperatures above 500°C, as increasing amounts of metal are lost from the atomizer during the ashing cycle. When the salts are introduced in natural seawater, observed sensitivity changes are more complex. As with distilled water, sensitivity drops above a critical temperature, which is different for each element, because of loss of the element from the atomizer during ashing. However, below this temperature, the sensitivity drops instead of leveling off as with simple solutions. The cause of this sensitivity loss is unknown, although it must be caused by either lowered instrument response arising from large nonspecific absorption and considerably decreased light level reaching the photomultiplier or, more likely, chemical interference by the major seawater salts. Such chemical interference might be caused by suppression of dissociation of molecular species of the analyte element in the molecule and atom cloud by the presence of large quantities of more easily dissociable salts. This would be analogous to the suppression of ionization, achieved for many elements in flames or arcs by the addition of large quantities of easily ionizable elements. Sodium chloride at a concentration of 3.5 g/l. has a larger suppression effect than seawater with a total salt content of 3.5 g/l. The effect is thus not simply determined by the total quantity of elements in the sample but is also dependent upon the composition of the matrix. The complexity of the

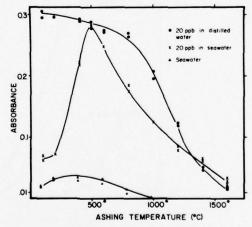


Figure 9. Effect of ashing temperature on the absorbance of 40-µl. injections of 20-ppb spike of manganese in distilled water and seawater and of unspiked seawater (Mn < 1 ppb)

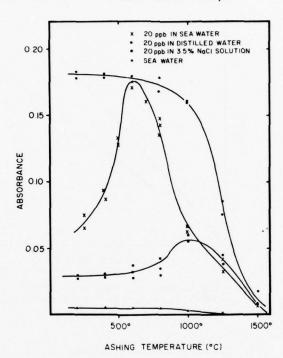


Figure 10. Effect of ashing temperature on the absorbance of 40- $\mu$ l. injections of a 20-ppb spike of copper in distilled water, seawater, 3.5% sodium chloride solution, and of unspiked seawater (Cu < 0.5 ppb)

atomization phenomenon from a complicated matrix is further illustrated by the observation that, although the managanese and copper sensitivities are suppressed in seawater as compared with simple chloride solutions regardless of ashing temperature, the sensitivity for iron is considerably enhanced in seawater. Too little is known about the chemistry of atomic vapor clouds, such as are generated in the heated graphite atomizer, to enable more than speculation upon the cause of enhancement or suppression. However, the matrix clearly must affect such vital parameters as the chemical form of the analysis element deposited in the solid state after drying in the atomizer and the volatilization and dissociation of these compounds. Considerably more research, both experimental and theoretical, is called for in this area.

Injection Volume. The volume of sample injected into the HGA-2100 may be up to 100  $\mu$ l., but usually is between 10 and 50  $\mu$ l. The

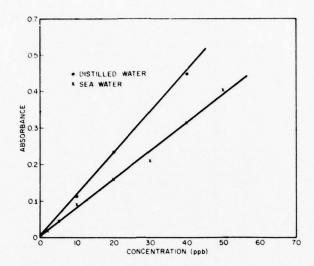


Figure 11. · Calibration for manganese (0–50 ppb) in seawater and distilled water (injection volume = 40  $\mu$ l.)

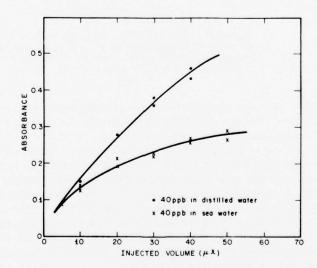


Figure 12. Calibration for manganese (40 ppb) in seawater and distilled water (injection volume = 10–50  $\mu$ l.)

injection volume affects analytical sensitivity both with simple salt solutions and with seawater. Figures 11 and 12 both show calibration curves for manganese in distilled and seawater. Figure 11 shows linear calibrations obtained by injecting different concentrations of manganese in identical volumes of sample. Figure 12 was obtained by injection of different volumes of a single concentration of manganese in both distilled and seawater. As the injection volume increases, the peak height drops, in each instance leading to curvature of the calibration. With distilled water injections, this curvature is probably caused by a change in the volatilization rate of manganese because of its wider distribution on the

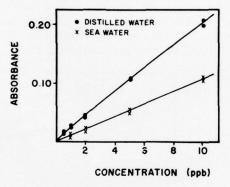


Figure 13. Calibration for cadmium (0–10 ppb) in seawater and distilled water (injection volume =  $5 \mu l$ .)

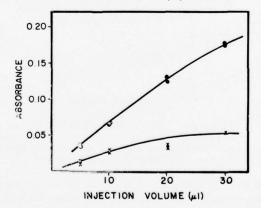


Figure 14. Calibration for cadmium (0.5 ppb) in seawater and distilled water (injection volume = 5-30  $\mu$ l.)

floor of the graphite tube, which is not uniformly heated. Atomization does not take place simultaneously at all points in the tube, which leads to a broader, smaller, output signal. In seawater, the curvature is much greater, and the large quantity of salt must have an additional effect at larger injection volumes. Similar calibrations were obtained for other elements. Figures 13 and 14 show the corresponding calibration for the volatile element cadmium.

In order to show the effect of total salt quantity in the atomizer, a series of injections were made for cadmium and manganese analysis with different volumes of solution but with the same total quantity of the analysis metal present per injection. Three series of injections were made—in distilled water, in seawater, and in seawater diluted to maintain the total salt quantity per injection constant. The results are shown in Figures 15 and 16 for manganese and cadmium, respectively. It is

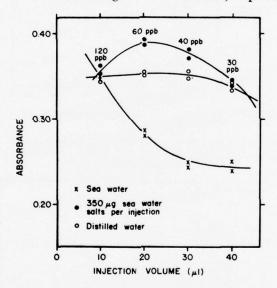


Figure 15. Effect of injection volume on the absorbance of 1.2 ng of manganese in distilled water with 350 ng of seawater dissolved salts per injection and in seawater of 35% salinity

apparent that the injection volume alone has only a small effect on the sensitivity, although some sensitivity loss occurs with increasing volume of distilled water. The effect of increased total salt content in the atomizer is to reduce the sensitivity in each case, presumably because of a suppression of dissociation or similar phenomenon. The effect of maintaining

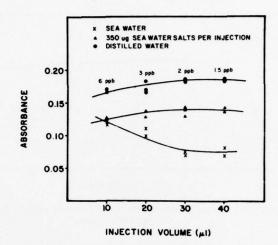


Figure 16. Effect of injection volume on the absorbance of 60 ng of cadmium in distilled water with 350 ng of seawater dissolved salts per injection and in seawater of 35‰ salinity

constant salt quantity and constant metal quantity while varying the injection volume is complex but resembles to some extent the effect of salinity (see Figures 17 and 20).

Although at this time the sensitivity variations seen when changing injection volume with saline samples cannot be explained, it is clear that

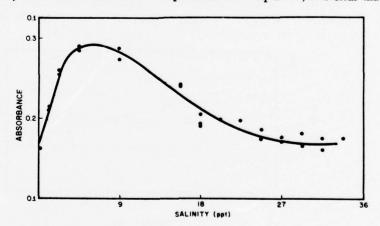


Figure 17. Effect of salinity on the absorbance of 40 µl. of 20 ppb manganese in seawater

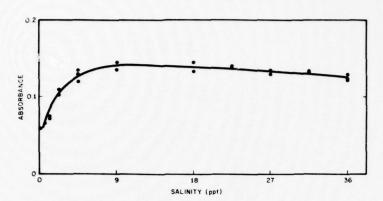


Figure 18. Effect of salinity on the absorbance of 20  $\mu$ l. of 40 ppb of iron in seawater

for accurate results all samples and standards must be injected in the same volumes and with the same salinity.

Salinity. The sensitivity of the analysis for each of the elements investigated depends on the salinity of the sample (Figures 17-20). Sensitivities for iron and manganese are both enhanced at low salinities, compared with distilled water standards, and in each instance sensitivity falls off at higher salinities. The effect of salinity on copper and cadmium analysis is more complex (Figures 19 and 20). A large drop in sensitivity occurs from distilled water to low salinities. At higher salinities, the sensitivity increases again and then drops slowly. As has already been stated, it is not possible to explain variations of sensitivity with salinity

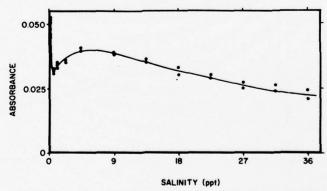


Figure 19. Effect of salinity on the absorbance of 40 µl. of 20 ppb of copper in seawater

because of the lack of knowledge of the chemistry of hot atomic and molecular clouds.

The maximum rate of change in sensitivity for each element takes place at salinities near those of fresh waters; therefore, such samples should always be analyzed by standard additions. This is also necessary because of the variability of major ion compositions of natural fresh water, which may be expected to affect sensitivity, along with changes in the total salt content. Fortunately, small changes of salt content near the values of salinity found in the open sea have very little effect on the analytical sensitivity for any of the metals studied. Trace metal analysis of seawater may, therefore, be performed using standard additions on selected samples only.

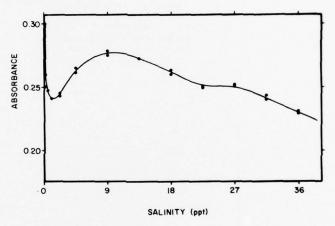


Figure 20. Effect of salinity on the absorbance of 10 μl. of 20 ppb of cadmium in scawater

#### Seawater Analysis, Analytical Conditions, and Procedure

Analytical conditions adopted for analysis of iron, manganese, cadmium, and copper in seawater are summarized in Table II. Output peaks obtained are illustrated in Figure 21 for copper and Figure 22 for cadmium. For copper and other refractory elements, spurious signals generated by atomizing seawater salts at the ashing temperature are not recorded since the recorder is switched on automatically immediately prior to the atomization step. However, immediately following the atomic absorption peak for cadmium, the atomized major salts produce strong scattering and molecular absorption which reduces the light intensity passing through the atomizer almost to zero. This leads to spurious signals on the recorder which at first are negative, then positive, and

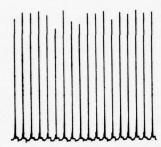


Figure 21. Reproducibility of analysis of copper in seawater, 50 µl. injections of a 40-ppb spiked sample of 35% salinity (recorder scale expansion, 2×; chart speed, 5 mm/min)

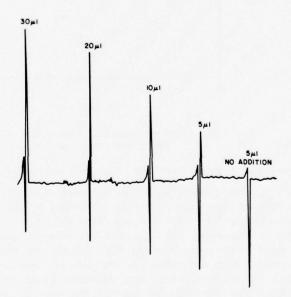


Figure 22. Recorder signal for cadmium analysis in seawater and seawater spiked with 0.5 ppb of cadmium (recorder scale expansion, 5×; chart speed, 160 mm/min)

then return to the baseline during the atomization cycle (Figure 22). These spurious peaks may be ignored and do not affect the analytical signal as long as the electrodeless discharge lamp and deuterium arc lamp beams are well aligned and intensity matched. Examination of the response at a nonabsorbing line close to the analytical line shows that the cadmium peak precedes, and is unaffected by, the scattering signal. Calibration curves for iron, copper, cadmium, and manganese are shown in Figures 23, 24, 25, and 11 respectively. From these calibrations, it can

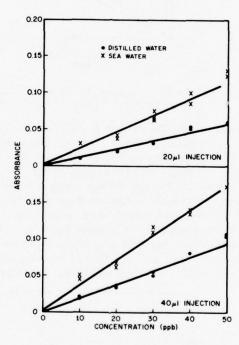


Figure 23. Calibration for iron (0-40 ppb) in seawater and distilled water

be seen that analysis of samples of seawaters with concentrations of these elements within the normal range (17) is possible with acceptable precision. Precision is estimated to be better than  $\pm 10\%$  above about 0.1 ppb cadmium and above about 2 ppb for the other elements. The 18 successive injections of 40 ppb of copper in seawater shown in Figure 21 have a standard deviation of  $\pm 4\%$ . The analytical procedure is, therefore, very simple. Analytical conditions are set, and an appropriate volume of acidified seawater in injected.

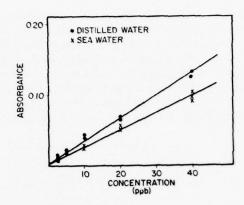


Figure 24. Calibration for copper (0-40 ppb) in seawater and distilled water (50-µl. injection)

A number of precautions must be observed to obtain accurate data. These are necessitated primarily by variability in graphite tubes and degradation of these tubes during use. No two tubes have precisely the same surface properties and, for example, variations of sensitivity with salinity (Figures 17 through 20) are completely reproducible only in form and not in absolute magnitude from tube to tube. In addition, sensitivity declines slowly with tube use as the tube surface is degraded. Fortunately the sensitivity loss is linear for at least the early part of a graphite tube life (Figures 26 and 27) and can be easily calibrated. Loss of sensitivity increases rapidly and reproducibility decreases dramatically at the end of the tubes useful life. Tubes are discarded before

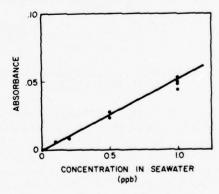


Figure 25. Calibration for cadmium (0-1 ppb) in seawater (5-µl. injection)

this rapid deterioration begins. Tube lifetimes vary slightly from one to another, but vary more with changes in sample matrix, and analytical conditions. The following steps are, therefore, adopted to ensure accurate results.

- 1. Each sample is injected at least twice or until replication of output peaks is better than a desired precision level (usually  $\pm 10\%$ ).
- 2. A series of standards of various concentrations, spiked into one of the seawater samples, is run to establish a calibration curve with each new tube.
- 3. An intermediate concentration standard is reanalyzed after approximately every 20 injections, to calibrate sensitivity drift.
- 4. Samples are grouped within salinity ranges covering no more than 5‰ (smaller for low salinity samples). Spiked standards are prepared in representative seawater samples from each of these ranges.
  - 5. Sample and standard injection volumes are always the same.

Direct injection analysis for iron, manganese, copper, and cadmium has been successfully performed on more than 500 samples of seawater taken in the New York Bight as part of the National Oceanic and Atmospheric Administration's (NOAA) Marine Ecosystem Analysis (MESA) Program. Although the instrumental analysis is tedious, no problems have been incurred in this routine process. Approximately 50–100 samples may be analyzed for one element in a day.

#### Future Developments

The four elements investigated here are by no means the only elements which may be directly determined in seawater. Preliminary investigations for other elements, including As, Pb, Zn, Si, and Al, are encouraging and will be pursued further. In addition, for those elements that cannot be directly determined, pre-concentration may be carried out before analysis, although this is usually tedious and may lead to contamination error (6).

Biological tissues and sediments may be analyzed for many trace elements by flameless atomic absorption after dissolution (6, 7). The reduced background signal observed with the new HGA-2100, compared with its predecessors, suggests that direct analysis for many of these elements may now be possible in these matrices. The sample may be introduced either directly as solids (18) or, more easily, as homogeneous suspensions after ultrasonic dispersion in water or solubilizing media (19). Perhaps the most exciting future prospect for the flameless atomizer in chemical oceanography is its use as a high sensitivity specific detector for gas and eventually liquid chromatography (20). Such instruments may provide the means for determining metallo-organics such as the

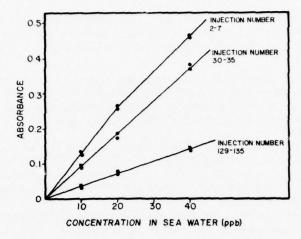


Figure 26. Change of calibration for manganese (10-40 ppb) in seawater with graphite tube use

alkylated lead, mercury, and cadmium compounds in environmental samples.

Analysis of seawater for zinc, chromium, and nickel has been carried out successfully by the techniques outlined in this paper. Approximate detection limits are 0.05 ppb for zinc, 0.5 ppb for chromium, and 3.0 ppb for nickel.

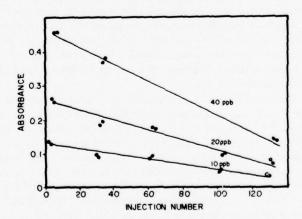


Figure 27. Linearity of calibration drift for manganese (10-40 ppb) in seawater with graphite tube use

The strength of compression used to hold the graphite tube in place in the HGA-2100 atomizer head critically affects the tube life. Optimization of this parameter has resulted in considerably slower sensitivity degradation than shown in Figures 26 and 27. The sensitivity degradation is nevertheless linear as shown.

#### Literature Cited

- Brewer, P. G., Spencer, D. W., "Technical Report, Woods Hole Oceanographic Institute" (1970) 70-62.
   Goldberg, E. D., "Marine Pollution Monitoring: Strategies for a National Program," NOAA, Washington, D. C., 1972.
   Kirll Sight (1971) 96 (1976) 600

3. Kirkbright, G. F., Analyst (1971) 96 (1146), 609.

- 4. Segar, D. A., Gonzalez, J. G., Anal. Chim. Acta (1972) 58, 7.
  5. Segar, D. A., Proc. 3rd Int. At. Absorp. Fluores. Spectrom. Cong., Oct., 1971, Paris, France (1973) 523

6. Segar, D. A., Int. J. Environ. Anal. Chem. (1973) 3, 107.

7. Segar, D. A., Gilio, J. L., Int. J. Environ. Anal. Chem. (1973) 2, 291. 8. Paus, P. E., At. Absorpt. Newsl. (1971) 10, 69.

- 9. Paus, P. E., Z. Anal. Chem. (1973) 264, 118
- Muzzarelli, R. A. A., Rocchetti, R., Anal. Chim. Acta (1973) 64, 371.
   Robinson, J. W., Wolcott, D. K., Slevin, P. J., Hindman, G. D., Anal. Chim. Acta (1973) 66, 13.

- Kahn, H. L., Manning, D. L., Am. Lab. (1972) 4, 51.
   L'vov, B. V., "Atomic Absorption Spectrochemical Analysis," p. 324, American Elsevier, New York, 1970.
- 14. Ediger, R. D., Peterson, G. E., Kerber, J. D., At. Absorp. News. (1974) 13, 61.

- Segar, D. A., Gonzalez, J. G., At. Absorp. Newsl. (1971) 10, 94.
   Kahn, H. L., Slavin, S., At. Absorp. Newsl. (1971) 10, 125.
   Riley, J. P., Chester, R., "Introduction to Marine Chemistry," Academic, London and New York, 1971.
- 18. Kerber, J. D., Koch, A., Peterson, G. E., At. Absorp. Newsl. (1973) 12, 104. 19. Segar, D. A., Abstracts 4th Int. Conf. At. Spectros., Toronto, Canada, 1973.

Segar, D. A., Anal. Lett. (1974) 7, 89.
 Perkin Elmer Corporation, "Analytical Methods for Atomic Absorption Spectroscopy Using the HGA Graphite Furnace," Perkin Elmer, Conn.,

RECEIVED January 13, 1975. Support for this research has come primarily from National Oceanic and Atmospheric Administration's (NOAA) Marine Ecosystem Analysis (MESA) New York Bight Program with some support from NSF grant GA 33003. The Environmental Research Laboratories of the National Oceanic and Atmospheric Administration does not approve, recommend, or endorse any product; and the results reported in this document shall not be used in advertising or sales promotion or in any manner to indicate, either implicitly or explicitly, endorsement by the United States Government of any specific product or manufacturer.

Reprinted from: Advances in Chemistry Series, Number 147, Analytical Methods in Oceanography, 9-15.

# Trace Metal Contamination by Oceanographic Samplers

A Comparison of Various Niskin Samplers and a Pumping System

DOUGLAS A. SEGAR and GEORGE A. BERBERIAN

National Oceanic and Atmospheric Administration, Atlantic Oceanographic and Meteorological Laboratories, 15 Rickenbacker Causeway, Miami, Fla. 33149

Simultaneous collections were made of water and suspended sediments by an Inter-Ocean pump sampling system, Niskin bottles with internal rubber closures, Niskin bottles with Teflon-coated coil springs, and newly designed Niskin bottles without internal closures. The samples were examined for contamination, particularly of trace metals. All the sampling systems led to some metal contamination of the samples except the new Niskin bottles. However, each system was found acceptable for nutrient analysis. Because of its novel closure, the newly designed Niskin bottle is convenient for suspended material analysis. Samples may be filtered directly from the sampling bottle without contacting the atmosphere.

The analysis of seawater for trace components, particularly metals, is a notoriously difficult task. Sophisticated and expensive analytical instruments are used, and many difficulties are incurred in the procedure. Considerable efforts have been expended on analytical problems (1, 2) and problems of sample contamination from storage bottles and reagents used for analysis (3). However, little attention has been paid to the problem of sample contamination during the process of obtaining the seawater sample from the ocean. Solving the analysis problems is of little use if uncontaminated samples cannot be obtained. In a separate paper in this volume, a new analytical technique is described, which

eliminates the worst of the analytical problems for several elements (4). These new methods were developed for use in the National Oceanic and Atmospheric Administration's (NOAA) Marine Ecosystem Analysis (MESA) Project and for studies of water column chemistry over midocean ridges. This paper describes a parallel effort to test sampling systems for trace metal contamination and to develop a sampling procedure which minimizes contamination.

## Sampling Systems

Two basically different systems, pumps and sampling bottles, are used to obtain seawater samples. Bottles such as the Nansen, Niskin, National Institute of Oceanography (NIO), and Van Dorn samplers have been used extensively throughout the world ocean. Pumping systems have been used less frequently, usually only in shallow water and when large volume samples or continuous profiles are required. A review of the literature reveals that little has been published regarding contamination of samples from sampling bottles. Cooper (5), in reviewing the problems of seawater sampling, pointed out that contamination, particularly from metal and rubber components of the samplers, was a serious problem. Subsequently, sampling bottles made from polyvinyl chloride (PVC) were almost universally adopted for trace metal analysis. Unfortunately, the standard versions of such sampling bottles all use either rubber end caps or rubber "springs" inside the bottle as a closure mechanism. The most widely used sampler, the Niskin bottle, has silicone internal rubber closures that pass through the sampler and remain in contact with the sample after the bottle is closed. Such silicone rubber is reported to give off considerable quantities of zinc to solution. In addition, the rubber, particularly when new, gives off large quantities of particles to the water sample during the closing process (6). To solve this problem many researchers adopted a Teflon-coated stainless steel coil spring to replace the rubber. Unfortunately, no investigation of the contamination generated from this spring has been reported. However, Teflon is known to be porous, particularly in thin coatings or films, and the coatings themselves tend to crack with even very limited use.

Faced with these sampler problems, a new design of PVC Niskin bottle was constructed which eliminated the internal closures (7). This bottle (Figures 1 and 2) is designed to be closed from the outside. The top and bottom plugs are both loaded at the top of the bottle before lowering. Upon triggering, the bottom plug free falls within the bottle until it closes the bottom end of the bottle by resting on an O-ring seal. The top plug is pulled into place by three tensioned latex rubber bands outside the bottle and then locked in place by three spring-loaded cams.

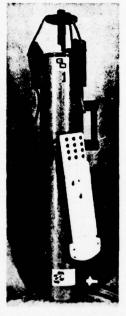




Figure 1. Top drop Niskin bottle Figure 2. Top drop Niskin bottle closed

The sample thus comes in contact only with PVC during its time in the sampler.

The pump sampling system used in this study was an Inter-Ocean OSEAS system (7) which features a submersible, multi-stage axial flow pump. All metal parts of this system are Teflon coated so that samples may be collected for trace metal analysis.

# Comparisons of Sampling Systems

Upon acquisition of the Inter-Ocean pump sampling system, a series of seawater samples was collected from New York Bight at 10 m depth simultaneously with the pump and with Niskin 10-l. samplers with internal rubber closures. The samples were filtered through  $0.4\mu$  Nucleopore filters. One aliquot was frozen for subsequent analysis of nitrate, nitrite, phosphate, and silicate by standard automated techniques. A second aliquot was acidified to pH 1 with silica-distilled, concentrated nitric acid and was subsequently analyzed by flameless atom reservoir atomic absorption spectrophotometry, both by direct injection (4) and after extraction of the metal pyrollidine dithiocarbamates with methyl isobutyl

Table I. Comparison of Pump and

		phate at/l)		rate at/l)		trite at/l)	Silicate $(\mu g \ at/l)$	
Station	Pump	Niskin	Pump	Niskin	Pump	Niskin	$\overline{Pump}$	Niskin
S								
6	0.70	0.69	3.0	2.9	0.21	0.26	< 0.2	< 0.2
8	1.2	1.4	7.8	9.6	0.94	1.1	5.2	6.3
12	0.64	0.58	2.6	2.2	0.14	0.10	0.2	< 0.2
13	0.92	0.76	3.1	3.0	0.30	0.30	< 0.2	< 0.2
22	0.78	0.74	3.5	3.5	0.50	0.51	0.2	0.2
25	0.63	0.64	2.6	2.5	0.28	0.28	0.5	0.4

a Niskin bottle with internal closures

ketone (9). The results of these analyses are shown in Table I. It is readily apparent either that no nutrient contamination or loss occurs with either sampling system or that any contamination or loss is identical in each system. This second possibility is unlikely because of the considerable differences in the two systems. The same conclusion—that neither sampler contaminates the sample—may be reached for manganese. However, for copper, to a lesser extent for nickel, and possibly for iron, the pump system contaminated the sample.

In light of the above data, use of the pump system was discontinued, and a Niskin Rosette sampler (Figure 3) was used to perform a com-

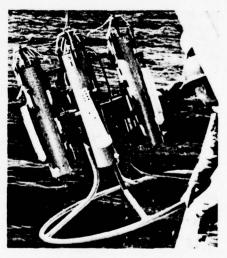


Figure 3. Rosette sampler with 10-l. top drop bottles

# Niskin Bottle" and Collected Samples

	$Nickel \ (\mu g/kg)$		$Manganese \ (\mu g/kg)$		$Iron \ (\mu g/kg)$		$per \ kg)$
Pump	Niskin	Pump	Niskin	Pump	Niskin	Pump	Niskin
4.7	4.6	6.1	5.9	110	115	17.4	3.8
2.8	2.0	3.5	1.6	412	131	17.6	2.3
2.4	1.9	0.57	0.59	43	32	15.3	1.4
1.4	0.7	0.62	0.62	22	19	13.1	1.2
1.4	1.0	0.68	0.72	37	37	13.7	1.3
0.7	0.4	0.51	0.49	69	55	11.3	0.59
0.9	0.7	0.58	0.60	24	23	11.7	0.66

<sup>&</sup>lt;sup>b</sup> Average of duplicate samples

parison among three Niskin bottles-one with rubber internal closures, a second with an internal Teflon-coated coil spring, and a newly designed "top drop" bottle with no internal closures. Samples were collected with these three samplers simultaneously at 10 m depth at a station several miles off the New Jersey and Long Island shores. Immediately upon recovery, duplicate aliquots of water were drawn from each of the bottles, filtered through a 0.4  $\mu$  Nuclepore filter, and acidified to pH 1 with silicadistilled nitric acid. The Niskin bottles containing the remainder of the samples were then allowed to stand for 3 hr in the ship's laboratory when a second set of duplicate aliquots was withdrawn, filtered, and acidified. The samples were analyzed for iron and zinc by direct injection flameless atomic absorption spectrophotometry (4). The results are presented in Table II. The analytical precision for these analyses is better than  $\pm 10\%$ as determined from multiple analyses of replicate samples. As was expected from previous experience, the internal rubber closure bottle clearly contaminates the sample with zinc. Unexpectedly, however, it also con-

Table II. Comparisons of Samples Collected by Three Designs of Niskin Bottle

	Top Drop	Silicone Rubber Spring	Teflon- Coated Coil Spring
Drawn immediately Drawn after 3 hr in bottle	Iron (μg/kg) α 23 20	55 33	28 23
Drawn immediately Drawn after 3 hr in bottle	Zinc $(\mu g/kg)^a$ 1.3 1.1	6.2 6.6	1.6 2.7

<sup>&</sup>lt;sup>a</sup> Each number represents the average of multiple analyses (more than three) of each of duplicate samples.

taminates the sample with iron. Possibly, this iron is in the form of very fine particles which pass through the Nuclepore filter. This hypothesis is supported by the much larger drop in iron concentration with time in this than in both of the other bottles. This drop in "dissolved" iron concentrations is probably caused by agglomeration of colloids which become large enough to be retained by the filter. Newly formed colloidal-sized iron-containing particles generated from the rubber springs would be expected to agglomerate at a faster rate than the already aged material present naturally.

The use of a coil spring, whose new Teflon coat was not visibly damaged, contaminates the sample with small but significant amounts of both dissolved iron and zinc. Of particular interest, is the increase in zinc concentrations with time in all but the top drop bottle. Apparently, zinc continues to "dissolve" from the coil spring and possibly the rubber after closure, suggesting that deep ocean samples may be more contami-

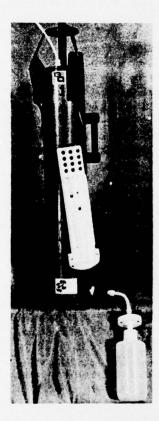


Figure 4. Top drop Niskin bottle with snap-on pressure fittings for filtration

nated than shallow samples because of the longer residence time of water in the bottle. The loss of zinc over the 3-hr period in the top drop bottle is small and only marginally significant compared with the analytical error. If the loss is real, then it may indicate that some zinc is associated with an actively precipitating phase such as that apparently removing the iron.

The top drop bottle is superior to other available bottles with respect to its lack of, or at least minimized, sample contamination for some trace metals. The top drop bottle has the additional advantage that it may be internally pressurized, permitting the seawater sample to be filtered without transfer to another container. This minimizes the risk of contamination of the water and particularly of the filter by the ship's atmosphere or other extraneous sources. A snap-on fitting has been developed so that a filter head containing a filter, preloaded in a dust-free atmosphere, may be attached to the petcock of the top drop bottle. A gas-tight nylon fitting is installed on the top drop in place of the air vent of normal Niskin samplers. A supply of filtered inert gas at excess pressures up to 1 atm is then coupled to this fitting and the water sample filtered without ever contacting the ambient atmosphere (Figure 4).

Top drop bottles were successfully and routinely operated on a Rosette system and on normal hydrowires during several cruises of the MESA New York Bight Project. Loading and handling of the bottles is minimally more difficult than for the older designs. They may, therefore, be used without difficulty in place of the older design for collection of samples for other than trace metal analysis. The use of such bottles for trace metal or suspended particulate chemistry would appear to be indicated.

## Literature Cited

Brewer, P. G., Spencer, D. W., unpublished data.
Goldberg, E. D., "Marine Pollution Monitoring: Strategies for a National Program," p. 203, NOAA, Washington, D.C., 1972.

Robertson, D. E., Anal. Chem. (1968) 40, 1067 Segar, D. A., Cantillo, A. Y., ADVAN. CHEM. SER. (1975) 147, 56.

- Cooper, L. H. N., J. Mar. Res. (1958) 17, 128. Bader, H., University of Miami, personal communication, 1972.
- Niskin, S. J., Segar, D. A., Betzer, P. R., in press. Sigalove, J. J., Pearlman, M. D., Undersea Technol. (1972) 24.

9. Segar, D. A., Int. J. Environ. Anal. Chem. (1973) 3, 107.

RECEIVED January 13, 1975. This research was carried out as part of the National Oceanic and Atmospheric Administration (NOAA) Marine Ecosystem Analysis (MESA) New York Bight Project. The Environmental Research Laboratories of NOAA do not approve, recommend, or endorse any product, and the results reported in this document shall not be used in advertising or sales promotion or in any manner to indicate either implicit or explicit endorsement by the U. S. Government of any specific product or manufacturer.

## MODE Tides1

Bernard Zetler,<sup>2</sup> Walter Munk,<sup>2</sup> Harold Mofjeld,<sup>3</sup> Wendell Brown<sup>2</sup> and Florence Dormer<sup>2</sup>
(Manuscript received 6 October 1974, in revised form 14 January 1975)

#### ABSTRACT

IGPP and AOML bottom pressure measurements at four MODE stations constitute a unique set of deep-sea tidal measurements (although deployed for other purposes). A response analysis relative to a Bermuda reference has been optimized with regard to the number of complex weights and the makeup of gravitational and radiational inputs. Duplicate instrumentation on EDIE capsule gave 32.067, 2.5°; 32.074, 2.6° for M2 amplitude (cm) and Greenwich epoch, thus attesting the reality of measured small station differences (order 1 cm, 1°). M2 tidal currents (calculated from the M2 surface and bottom slopes) have u and v speeds of 0.5 and 0.8 cm s<sup>-1</sup>, respectively, in rough agreement (both amplitude and phase) with preliminary estimates from current measurements. M2 and K1 tides are in accord with some existing cotidal and co-range charts. M3 tides are a fraction of equilibrium magnitude, whereas M4, M5 and M6 (typically 0.07, 0.05, 0.03 cm) vastly exceed equilibrium values. Presumably these overtides are generated by nonlinear coupling in the world's shallow basins, from where they radiate into the global oceans to attain a level where radiative and dissipative processes are somehow balanced.

#### 1. Introduction

Measurements of bottom pressure during the MODE (Mid-Ocean Dynamics Experiment) experiment, March to July 1973, were for the purpose of studying mesoscale eddies, and accordingly the emphasis was on periods longer and length scales much shorter than those typical of tides. In fact, one premise underlying the experiment was that the "tidal noise" could be effectively eliminated from the records (Brown et al., 1975). In accomplishing this mission, we have performed a unique experiment of simultaneous deep-sea tide measurements. Information concerning instrumentation and experimental procedures has been described separately (Snodgrass et al., 1975).

## 2. Bermuda reference

The response method (Munk and Cartwright, 1966) was used, following the procedure by Cartwright et al. (1969) for the analysis of relatively short deep-sea records. This involves a two-step analysis: (i) the transfer functions of a reference station relative to the tidal potential, and (ii) the transfer functions of the deep-sea records relative to the reference station.

The 1950-60 tide record at Bermuda was used to derive the transfer functions relative to the input potentials; these transfer functions subsequently served

as a basis of a Bermuda tide prediction for the MODE period. Table A (Appendix) shows the results of a combined analysis of three 355-day series equally spaced in a period of lunar perigee (8.85 Julian years).

## 3. MODE transfer functions

Transfer functions and harmonic constants for the seven deep-sea data series<sup>5</sup> are given in Tables B to H. Table 1 is a summary of principal constituents for the five series exceeding one month (thus excluding MERT and EDIE-MARCH). The transfer functions are based on two complex weights (0, -2 days) for diurnal constituents, and three complex weights  $(0, \pm 2 \text{ days})$  for semidiurnal constituents (see below). "Grav+rad" and "grav only" refer to separate analyses with regard to the nongravitational (radiational) solar effects; we

<sup>&</sup>lt;sup>4</sup> After all of the MODE tide analyses were completed, a small error was found in the analysis of the diurnal tides at Bermuda. Inasmuch as the variation was used consistently in arriving at both the Bermuda harmonic constants and the Bermuda prediction for the MODE period, the accuracy of the MODE tide analyses is not affected. For the record, Table A values and corrected values (in parentheses) are as follows:

	H (cm)	G (deg)		
$Q_1$ :	1.13 (1.13)	188.2 (186.6)		
O <sub>1</sub> :	5.30 (5.30)	192.0 (192.1)		
$P_1$ :	2.02 (2.01)	187.7 (187.8)		
K1:	6.56 (6.55)	187.1 (187.0)		

<sup>&</sup>lt;sup>8</sup> IGPP (Institute of Geophysics and Planetary Physics, University of California, San Diego) sea-floor pressure series are named REIKO-MAY, MERT, EDIE-MARCH, EDIE-MAY P1, and EDIE-MAY P2. AOML (Atlantic Oceanographic and Meteorological Laboratories, Miami, Fla.) series are named AOML1 and AOML3.

<sup>&</sup>lt;sup>1</sup> MODE Contribution No. 16.

<sup>&</sup>lt;sup>2</sup> Institute of Geophysics and Planetary Physics, Scripps Institution of Oceanography, University of California, La Jolla 92037.

<sup>&</sup>lt;sup>3</sup> Atlantic Oceanographic and Meteorological Laboratories, NOAA, Miami, Fla. 33149.

Table 1. Admittances and tidal constants: R is amplitude ratio,  $\phi$  station lead (deg) relative to Bermuda, H amplitude (cm), and G Greenwich epoch (deg). The frequency (cycles per day) is given at the head of each column.

				Grav+rad			Grav only	
		O <sub>1</sub> 0.930	K <sub>1</sub> 1.003	(N <sub>2</sub> ) 1.895	M <sub>2</sub> 1.932	(S <sub>2</sub> ) 2.000	M <sub>2</sub> 1.932	(S <sub>2</sub> ) 2.000
	AOML3	1.142	1.138	0.956	0.943	0.877	0.943	0.752
	AOML1	1.156	1.180	0.983	0.967	0.877	0.967	0.764
R	REIKO	1.174	1.187	1.003	0.970	0.838	0.969	0.706
	EDIE-MAY P1	1.172	1.196	0.921	0.9000	0.787	0.900	0.666
	EDIE-MAY P2	1.180	1.184	0.920	0.9002	0.782	0.900	0.663
	AOML3	-4.9	-6.8	0.2	-0.6	- 7.3	-0.6	- 9.1
	AOML1	-5.6	-7.6	-2.1	-2.3	- 6.6	-2.3	- 8.2
φ	REIKO	-4.0	-7.4	-1.4	-2.4	- 8.5	-2.4	-12.6
	EDIE-MAY P1	-7.9	-10.3	-3.8	-4.2	-10.3	-4.1	-13.5
	EDIE-MAY P2	-8.0	-10.2	-4.0	-4.3	-10.1	-4.3	-13.3
	AOML3	6.05	7.47	7.82	33.60	7.09	33.60	6.08
	AOML1	6.13	7.74	8.04	34.45	7.08	34.45	6.17
H	REIKO	6.22	7.79	8.20	34.57	6.77	34.53	5.70
	EDIE-MAY P1	6.21	7.84	7.54	32.067	6.35	32.07	5.38
	EDIE-MAY P2	6.25	7.77	7.53	32.074	6.32	32.07	5.36
	AOML3	196.9	193.9	337.5	358.9	31.5	358.9	33.3
	AOML1	197.6	194.7	339.8	0.6	30.8	0.6	32.4
G	REIKO	196.0	194.5	339.1	0.7	32.7	0.7	36.8
N.G.W.	EDIE-MAY P1	199.9	197.4	341.5	2.5	34.5	2.4	37.7
	EDIE-MAY P2	200.0	197.3	341.7	2.6	34.3	2.6	37.5

prefer the grav+rad values. In the past, the choice of the number of weights and the treatment of radiational tides have been subjective. On the basis of MODE and other recent measurements, Zetler and Munk (1975) have established some criteria. Here we shall give a brief review of how the selection was made.

# a. Weights

In the response analysis, the measured series is approximated (in the least-square sense) as a weighted sum of the reference series for various leads or lags. For example, a single complex weight (1+0i) for zero lag corresponds to identical series; 0+2i corresponds to a measured series in quadrature with the reference series and of twice its amplitude. The vertical lines (solid and dashed) in the bottom left corner of Fig. 1 show a diurnal amplitude ratio of 1.18 and phase lag of 8° of EDIE-MAY P1 relative to Bermuda, obtained for a single (complex) weight.

Munk and Cartwright (1966) recommend lag intervals of 2 days. For two complex weights (lags 0, 2 days) the admittance is now a smoothly varying function of frequency: e.g., the amplitude ratio and phase lag are somewhat larger at higher frequency for the diurnals (see also O<sub>1</sub> and K<sub>1</sub> in Table 1). For additional weights, the admittances become increasingly more wiggly, in part (one surmises) as a result of the noise content. The trick is to terminate when one's credo on the smoothness of oceanic admittances is violated.

To obtain objective criteria, the series was divided into sections A and B. The top left panel gives the variance in the residual of section A predicted from an analysis of A and B, respectively. For self-prediction (A residuals from A weights) one expects, and finds, that the residuals diminish with increasing number of weights. However, after three weights, the improvement is slow and one suspects that the analysis is responding more to noise than to signal. At approximately that point one expects, and finds, that A residuals from B weights should deteriorate. The results are similar for B residuals, except that the overall residual is lower. On this basis the decision was made to stop at two weights. For the semidiurnal tides the "turning point" is a bit later, hence the decision to stop at three weights. The decisions are in general accord with the wiggliness of the admittances, taking into account also the resemblance between admittances from A and B residuals.

# b. Radiational tides

Radiational tides are periodic variations in sea level primarily related to meteorological changes such as the semi-daily cycle in barometric pressure and daily land and sea breezes. These cyclical variations match the frequencies of solar (not lunar) gravitational tidal constituents. Cartwright (1966) and Zetler (1971) found the average ratio of radiational amplitude to gravitational amplitude at the  $S_2$  frequency to be about 0.17.

The bandwidths of the radiational tides are much narrower than those of the gravitational tides, essentially covering tidal lines separated by cycles per year (cpy) rather than cycles per month (cpm). Furthermore, the relative amplitudes within the 1 cpm range

are quite different for gravitational and radiational tides. In particular, equilibrium K2/S2 (grav) is 0.27, whereas the rad ratio is 0.09. A response analysis for a sufficiently long record (as the 10-year Bermuda record) satisfactorily resolves these different bandwidths and amplitude relationships, and the gravitational admittances across tidal bands are expected to be smooth. Inasmuch as traditional tidal analysis for any length of series and response analysis for short series cannot distinguish between gravitational and radiational contributions to a constituent, but instead solve for their vectorial sum, discontinuities in admittances at the S<sub>2</sub> frequency are inevitable. In fact, Zetler (1971) used these discontinuities as a simple means of calculating the radiational S2 from harmonic constants computed by traditional analysis,

Gravitational and radiational weights were resolved for the Bermuda record and separate gravitational and radiational predictions were prepared for the MODE period. Given these reference predictions for Bermuda, there are three options for analyzing the MODE data: (i) compute gravitational and radiational admittances separately in a combined analysis; (ii) use the gravitational predictions only; and (iii) sum the gravitational and radiational predictions for each species and use the summed complex predicted series as reference.

All three methods were tried. For the first case, it quickly became evident that a much longer deep-sea series was required (probably 10 years) to separate gravitational and radiational contributions. An unstable matrix in solving for the weights resulted in some absurd results (such as a predominance of radiational tides). An extrapolation was made from the (lunar) N<sub>2</sub> and M<sub>2</sub> frequencies to the (solar) S<sub>2</sub> frequency to determine the extent of the discontinuity at the latter frequency, using both the second and third options with EDIE-MAY P1 (Table 1):

	N <sub>1</sub>	M <sub>2</sub>	S <sub>2</sub>				
Fre- quency (cpd)	1.895	1.932	Extra- polated	2.000 Grav + rad	Grav		
R \$\phi\$	0.92 -3.8°	0.90 -4.2°	0.86 -4.9°	0.79 -10.3°	0.67 -13.5°		

<sup>6</sup> Only the gravitational admittances are listed in Table A. The gravitational and radiational constants and their sums are as follows:

Gravitational		Radia	ational	Sum		
H (cm)	G (deg)	H (cm)	G (deg)	H (cm)	G (deg)	
2.16	187.7	0.15	5.9	2.01	187.8	
6.70	187.0	0.15	5.9	6.55	187.0	
9.26	21.7	1.24	185.3	8.08	24.2	
2.31	21.9	0.11	185.3	2.21	22.7	
	H (cm) 2.16 6.70 9.26	H G (deg) 2.16 187.7 6.70 187.0 9.26 21.7	H G H (cm) (deg) (cm) 2.16 187.7 0.15 6.70 187.0 0.15 9.26 21.7 1.24	H G H G (cm) (deg) (cm) (deg) 2.16 187.7 0.15 5.9 6.70 187.0 0.15 5.9 9.26 21.7 1.24 185.3	H         G         H         G         H           (cm)         (deg)         (cm)         (deg)         (cm)           2.16         187.7         0.15         5.9         2.01           6.70         187.0         0.15         5.9         6.55           9.26         21.7         1.24         185.3         8.08	

In a comparison of the Bermuda harmonic constants with those obtained for a different period by traditional harmonic analysis (IHB Spec. Publ. No. 26, Sheet 600), the discrepancies in amplitude are less than 4%, in epoch less than 2°.

TABLE 2. Ratio of residual to recorded variance.

			Station		
	AOML3	AOML1	REIKO	EDIE- MAY PI	EDIE- MAY P2
Total (0 to 1	2 cpd)				
grav+rad	0.00931	0.01338	0.00483	0.00680	0.00948
grav only	0.00937	0.01340	0.00485	0.00680	0.00949
Diurnal (1 cp	od±4½ cpi	m)			
grav+rad	0.00207	0.00212	0.00051	0.00107	0.00135
grav only	0.00206	0.00192	0.00054	0.00105	0.00136
Semi diurnal	(2 cpd±4	cpm)			
grav+rad	0.00066	0.00051	0.00014	0.00020	0.00021
grav only	0.00068	0.00056	0.00019	0.00022	0.00024

The discontinuity is smaller for the grav+rad option. Furthermore, residual variances for grav+rad are generally somewhat smaller than for grav only (Table 2). The better results with the grav+rad option indicate a common origin for Bermuda and MODE radiational tides, with a similar relation to the gravitational tides. We would expect the grav only procedure to be superior if Bermuda radiational tides were the result of (i) local effects such as diurnal winds from island heating, or (ii) inverted barometer response to atmospheric pressure (absent from bottom pressure readings). Evidently this is not the case.

#### c. Admittance

Inasmuch as the transducers for EDIE P1 and P2 were only 10 cm apart, a comparison of the two records is a measure of reproducibility of results (Snodgrass et al., 1975). For  $M_2$  the admittances differ by only  $2\times10^{-4}$  in amplitude and 0.1° in phase. For the four diurnal tidal constituents listed, the amplitude discrepancy is always less than 1% (the largest being 0.07 cm for  $K_1$ ) and the phases all agree within 0.1°.

Changes between constituents within each species (relative to Bermuda) are smooth. We find that for O<sub>1</sub> and K<sub>1</sub> relative amplitudes at any one station are within 2%, relative phases within 3°; for N<sub>2</sub> and M<sub>2</sub> the values are 3% and 1°. Yet, the Bermuda reference (Table A) shows marked variation across the semi-diurnal band, possibly the result of a free mode. The evidence is for a resonance of large areal extent, rather than highly localized.

The satisfactory agreement at one site assures us of the reality of the small difference between REIKO near the central mooring (28°00′N, 69°40′W) and EDIE-MAY about 150 km to the south-southeast, a small separation when reckoned in tidal dimensions. (The locations of all bottom pressure sensors are shown in Fig. 2). The reasonable fit between the harmonic constants for REIKO and AOML1, roughly 20 km apart near the central mooring, encourages us to discuss jointly results from the IGPP and AOML data. Nevertheless, even though there is no obvious calibration

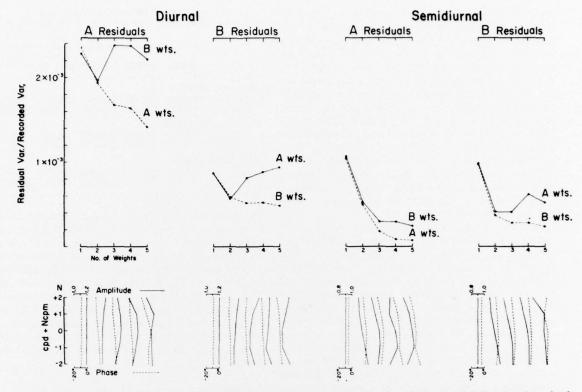


Fig. 1. Analysis of variance for EDIE-MAY P1. The left upper panel gives the ratio of residual to recorded diurnal variance for the first 29 days (record A), with prediction weights based on the A record (self-prediction) and B record (last 29 days), respectively. The remaining upper panel gives the B residuals and corresponding semidiurnal ratios. In each case the dashed lines refer to "self-predictions," the solid lines to future (B residuals from A weights) or past (A residuals from B weights) predictions, respectively. The lower panels give the corresponding amplitude ratios (solid) and phase lags (dashed) relative to Bermuda reference, as a function of frequency (1 cpd $\pm$ 0, 1, 2 cpm for diurnals, 2 cpd $\pm$ 0, 1, 2 cpm for semidiurnals), for 1, 2, ..., 5 complex weights. With increasing number of weights the self-prediction residuals (but not necessarily those for the future predictions) diminish, and the admittances become increasingly wiggly.

difference between the IGPP and AOML gauges, it seems prudent to use the REIKO, EDIE capsules for comparison between central mooring with the area to the south and the AOML1, AOML3 capsules for comparison between central mooring with the area to the east.

Station differences are consistent for different constituents within each species. At the central mooring the semidiurnal tides are about 8% larger and 2° earlier than at EDIE; the diurnal tides are about equal in amplitude and 3°-4° earlier than at EDIE. Comparing the AOML data, at the central mooring the semidiurnal tides are about 2% larger and 2° later than at AOML3; the diurnal tides slightly smaller and earlier at AOML3. These comparisons imply that both the 1 and 2 cpd tides progress from the northeast, arriving first at AOML3, then the central mooring, and finally at EDIE.

#### 4. Comparison with cotidal charts

There is a general impression that the state-of-the-art in preparing cotidal and co-range charts leaves much to be desired; certainly there are considerable variations between published charts. Most charts deal with only the largest tidal constituent, M<sub>2</sub>, sometimes labeling the chart as applying to semidiurnal tides. Similarly, if a chart is designated "diurnal tides," ordinarily it refers to the K<sub>1</sub> constituent. Fig. 2 is a comparison of Dietrich's (1944) charts for M<sub>2</sub> and K<sub>1</sub> with our long series, AOML1 and 3, REIKO, and EDIE-MAY P1 and P2.

## a. M2 tides

Dotted lines show our inference of Dietrich's 0h15m and 0h30m cotidal lines. All four MODE stations and Bermuda lie between 0h and 0h15m lines (solar hours, not component hours), so their Greenwich epochs should be between 0° and 7.2°. The indicated Bermuda epoch (from our analysis) is 358.3° (IHB sheet 600 gives 0°). Dietrich's 0h line would need only small displacements to fit the Bermuda values. AOML1, EDIE and REIKO fit Dietrich's chart and are relatively consistent; AOML3 is roughly 3° (6 min in time) early

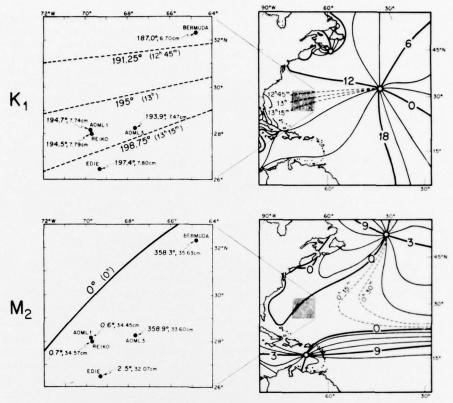


Fig. 2. Right panels show Dietrich's (1944) cotidal lines in the North Atlantic for  $K_1$  and  $M_2$  tides, respectively. Values are in solar hours, with dashed curves designating our interpolation. The MODE area falls within the shaded square which is shown on an enlarged scale in the left panels, for comparison with the results at MODE stations ( $\bullet$ ).

relative to the other MODE epochs and to the Dietrich configuration. Dietrich does not show co-range lines and the M<sub>2</sub> cotidal lines are too complex in this region to infer readily whether the M<sub>2</sub> amplitudes are consistent with distance from an amphidrome.

Although the Tiron et al. (1967) M<sub>2</sub> cotidal chart has the XII<sup>h</sup> (same as 0<sup>h</sup>) in a similar position and orientation as Dietrich's, one would interpret his progression in time in the MODE area to be to the northwest, contrary to Dietrich's chart and to the values for three MODE stations. The orientation of the Tiron et al. XII<sup>h</sup> line would call for the AOML3 epoch to be between the epochs of EDIE and the central mooring stations (REIKO and AOML1); thus, on this chart, too, the AOML3 epoch seems to be slightly low (early). The orientation and progression of the Tiron et al. co-range lines call for the largest MODE amplitude at the central mooring, as is found to be the case. AOML3 amplitude conforms in that its value falls between those for EDIE and the central mooring.

## b. Ki tides

All stations are roughly 2°-3° early relative to the cotidal lines, yet they are consistent in that they pro-

gress toward the south-southeast with spacing matching that of the inferred cotidal lines. As expected, amplitudes increase with distance from the amphidrome.

# c. Baroclinic noise

In making detailed comparisons with cotidal charts it should be recognized that the measurements contain a baroclinic contribution of roughly 1% amplitude, 1° in phase. The characteristic wavelength of the baroclinic tides is 100 km, and at separations of several hundred kilometers the baroclinic contribution to the measured vector sum will differ almost randomly from station to station. This effect exceeds the instrumental noise. If we may assume that barotropic and baroclinic tidal currents are of the same order (Section 6), then the pressure gradients and associated surface slopes are of the same order, 10-2 cm km-1 for M2. To obtain baroclinic surface amplitudes we multiply by  $\lambda/2\pi$ , with  $\lambda = 160$  km for the gravest baroclinic mode. This gives a near-bottom baroclinic amplitude of 0.3 cm, and for a random orientation the phase shift is by roughly 10. If there had been surface measurements, the baroclinic contribution would have been several times larger.

## 5. Tides of higher order

The high reproducibility of the principal tidal constituents encouraged us to analyze MODE pressures for the relatively small components of higher order. These are derived by the response method, using the equilibrium potential  $G_3^3$  as reference function for  $M_3$ , and the nonlinear input functions  $G_2^2G_2^2$ ,  $G_2^1G_2^2G_2^2$ ,  $G_2^2G_2^2G_2^2$ (rather than  $G_4^4$ ,  $G_5^5$ ,  $G_6^6$ ) for M<sub>4</sub>, M<sub>5</sub>, M<sub>6</sub>, for the reasons stated below. For comparison, Table 3 includes the principal diurnal and semidiurnal tides, equilibrium amplitudes, and some Bermuda estimates. The amplitudes for the higher-order tides at MODE stations correspond to total species energy and therefore are somewhat higher than comparable values for the specific constituents.

M<sub>3</sub> amplitudes at MODE stations and Bermuda are within a factor of 2, and phases lie within one octant. There is nothing extraordinary about this result other than the satisfaction of detecting a 1 mm constituent in deep-sea records. Amplitudes are somewhat less than the equilibrium value, about the same ratio as for the diurnals.

M<sub>4</sub>, M<sub>5</sub>, M<sub>6</sub> amplitudes are tiny (typically 0.7, 0.5, 0.3 mm) yet very much larger than the equilibrium values  $(3 \times 10^{-2}, 4 \times 10^{-4}, 3 \times 10^{-6} \text{ mm})$ . One's first inclination is to attribute these results to experimental noise. We note that IHB values are generally high, perhaps because they include the noise continuum, whereas other estimates reflect only the coherent signal. AOML3 amplitudes are generally higher. Yet in spite of these inconsistencies we believe the estimates for the higher-order harmonics to be significant, for the reason that phases are not randomly distributed, especially if one allows for the fact that distances between stations are no longer negligible as compared to wavelengths.

There is then the question as to why the M<sub>4</sub>, M<sub>5</sub>, M<sub>6</sub> amplitudes are so much larger than equilibrium amplitudes. Garrett and Munk (1971) (see also Gallagher and Munk, 1971) have suggested that quadratic and higher-order interactions in the world's shallow basins produce multiple frequencies which leak into the global oceans and attain an equilibrium level for which radiative and dissipative processes are somehow balanced. For these reasons the response method was used with double and triple products of the appropriate semidiurnal and diurnal tide potentials as input functions.

## 6. Inferred tidal currents

Tidal measurements at two points determine the tidal variations in the average pressure gradient between these points, and impose some conditions on the tidal currents. The tidal displacement of the seafloor (and bottom pressure gauge) must here be taken into account (Munk et al., 1970). We use §8 and §B for the radial (upward) displacement, relative to the center of the Earth, of the sea surface and bottom, respectively;  $\zeta = \xi^{8} - \xi^{B}$  is the surface displacement relative to the sea bottom, as observed.

The gravitational forces of the Moon and Sun are conveniently expressed in terms of the equilibrium

TABLE 3. Amplitudes and Greenwich epochs of higher-order tides.

	K	1	N	12	M	3	M <sub>4</sub>		M <sub>6</sub>		M <sub>6</sub>	
	H (cm)	G (deg)	H (cm)	G (deg)	H (cm)	G (deg)	H (cm)	G (deg)	H (cm)	G (deg)	H (cm)	G (deg
Equilibrium												
Normalized*	36.9	-	63.2		0.76	-	1.1×10 <sup>-2</sup>	-	1.5×10-4	-	1.5×10-6	-
At MODE latitude 28°N	11.8	Annes.	19.0	-	0.22	-	$3.0 \times 10^{-3}$	-	3.7×10 <sup>-6</sup>	-	3.4×10 <sup>-7</sup>	
Bermuda												
St. George (IHB p. 600)	6.4	189	35.5	000	0.15	40	0.40	232	_		0.18	83
Wunsch (1972)**		_		-	0.13	74	0.16	260	-	-	-	_
Garrett and Munk (1971)		-	36.2	-	-	-	0.18		-		0.08	-
MODE***												
AOML3	7.5	194	33.6	359	0.078	69	0.134	354	0.58	321	0.031	255
AOML1	7.7	195	34.5	001	0.155	36	0.065	330	0.021	277	0.003	102
REIKO	7.8	195	34.6	001	0.155	38	0.074	278	0.033	262	0.021	125
EDIE-MAY PI	7.8	197	32.1	003	0.136	40	0.077	271	0.050	302	0.032	19
EDIE-MAY P2	7.8	197	32.1	003	0.104	55	0.074	253	0.045	295	0.019	59

Using the normalization by Munk and Cartwright (1966). K<sub>1</sub>, M<sub>2</sub> and M<sub>3</sub> are from Cartwright and Taylor (1971); M<sub>6</sub>, M<sub>5</sub> and M<sub>6</sub> are from a computer-generated potential. Latitude factors are

$$(-1)^m \left[\frac{2n+1}{4\pi}\right]^{\frac{1}{2}} \left[\frac{(n-m)!}{(n+m)!}\right]^{\frac{1}{2}} p_n^m \left(\cos\theta\right)$$

where  $\theta = 90^{\circ}$  - latitude.

<sup>\*\*</sup>Some values have been modified in accordance with a recent personal communication.
\*\*\*M<sub>3</sub>, M<sub>4</sub>, M<sub>5</sub> M<sub>6</sub> are derived fro a total species energy. Epochs for M<sub>4</sub>, M<sub>5</sub>, M<sub>6</sub> are for the summed tides within the appropriate cpd bands.

TABLE 4. Computed and measured tidal currents.\*

	u comp	onent	a comf	onent
	Speed (cm s <sup>-1</sup> )	G (deg)	Speed (cm s <sup>-1</sup> )	G (deg)
From pressure gradients [Eq. (4)]	0.49	110	0.80	258
Hendry central mooring				
Measured	0.30	72	0.31	233
Barotropic (0)	0.60	110	0.55	328
Baroclinic (1)	0.37	306	0.64	184
(2)	0.37	218	0.36	108
Hendry average, all depths and moorings	0.49	106	0.38	299

<sup>\*</sup> Values in parentheses are modes obtained by a mode decomposition.

response

$$\begin{cases}
\xi_{\epsilon}^{\mathbf{B}} = (1+k)U/g, & \xi_{\epsilon}^{\mathbf{B}} = hU/g \\
\xi_{\epsilon} = \xi_{\epsilon}^{\mathbf{B}} - \xi_{\epsilon}^{\mathbf{B}} = (1+k-h)U/g
\end{cases}$$
(1)

of surface, bottom and surface relative to bottom, respectively, and this essentially defines Love numbers k, h (k allows for the self-attraction of the tidal bulge). The procedure does not allow for non-equilibrium self-attraction and loading (Hendershott, 1973).

The equations of motion in the center-of-earth system are

$$\partial_t u - fv = g \partial_x (\hat{\xi}^S - \hat{\xi}^S), \quad \partial_t v + fu = g \partial_u (\hat{\xi}^S - \hat{\xi}^S), \quad (2)$$

where  $f = 2\Omega \cos\theta$  is the Coriolis parameter. We now set

$$\hat{\xi}^{B} = \hat{\xi}^{B}, \tag{3}$$

thus assuming that the bottom distortion (unlike the surface) can be adequately represented by the equilibrium configuration. It follows that  $\zeta_{\epsilon}^{S} - \hat{\xi}^{S} = \zeta_{\epsilon} - \zeta_{\epsilon}$ . For harmonic oscillations  $\exp(-i\omega t)$ , Eqs. (2) can be written in the bottom-of-the-sea system (observation coordinates) as

$$\begin{bmatrix} u \\ v \end{bmatrix} = \frac{g}{f^2 - \omega^2} \begin{bmatrix} -i\omega\partial_x + f\partial_y \\ -f\partial_z - i\omega\partial_y \end{bmatrix} (\zeta_e - \zeta). \tag{4}$$

Let the real part of  $\zeta_m = A_m \exp -i(\omega t - G_m)$  designate the tidal elevation at station m, and

$$\zeta_{mn} = (A_n e^{iG_n} - A_m e^{iG_m})e^{-i\omega t} = A_{mn} e^{iG_{mn}}e^{-i\omega t}$$

the station difference between m and n. For  $M_2$ , we have the following:

The average tidal gradient over the MODE area has

been obtained from the station differences according to

$$\zeta_{13} = L_{13}(\partial_{x}\zeta \cos\phi_{13} + \partial_{y}\zeta \sin\phi_{13})$$

$$\zeta_{ER} = L_{ER}(\partial_{x}\zeta \cos\phi_{ER} + \partial_{y}\zeta \sin\phi_{ER})$$
(5)

with  $L_{13}$ = 218 km,  $L_{ER}$ = 171 km,  $\phi_{13}$ = 3°,  $\phi_{ER}$ = 102° designating the appropriate station separations and bearings for AOML1 and 3, REIKO and EDIE. The corresponding equilibrium gradients derived from

$$U/g = (24.39 \text{ cm}) \sin^2\theta \exp[-i(\omega t + 2\lambda)]$$

are as follows:

$$\frac{\partial_{x} \zeta_{e} = R^{-1}(1+k-h)(2\times24.39)}{\times \sin\theta \exp[-i(\omega t + 2\lambda + \pi/2)]}, \quad (6)$$

$$\times \sin2\theta \exp[-i(\omega t + 2\lambda + \pi)]$$

where  $k = 0.2\overline{9}$ , h = 0.59 are the Love numbers,  $\theta = 62^{\circ}$  is colatitude,  $\lambda = -70^{\circ}$  is east longitude, and R the equatorial radius of the earth. The numerical values from (5) and (6) are

 $\rm M_2$  tidal currents were then computed from (4), using  $f=6.8\times 10^{-5}~\rm s^{-1}$ . Listed with them in Table 4 are some analyses of current records by Ross Hendry, MIT: (i) the measured near-bottom currents; (ii) the contributions to near-bottom currents from various modes, using a mode decomposition of current profiles at the central mooring; (iii) an average over all depths and for many moorings.

In principle, the currents computed from (4) are to be interpreted as the total tidal current (barotropic plus baroclinic) at the depth of the array. The difficulty is that the spacing between stations (~200 km), though small compared to the barotropic wavelength, is comparable to the baroclinic wavelength ( $\lambda = 160$  km for mode 1), so that the baroclinic contributions are substantially reduced in an average taken between stations. We may then look for a first-order agreement between the computed values and the barotropic component (whether derived from mode separation or by averaging), and this is roughly what is found. But the baroclinic contributions at a given point are comparable to the barotropic contribution, as has long been known, and for a detailed comparison it would be necessary to resolve the baroclinic cotidal field by closely spaced stations.

Acknowledgments. This work was supported by the Office of Naval Research (Contract N00014-69-A-0200-6008) and the National Science Foundation (Grant NSF-GX-29052). We have received helpful comments by Ross Hendry and Carl Wunsch.

## APPENDIX

## Results of MODE Tide Measurements

#### TABLE A.

Station: Bermuda standard tide gauge

32°24′N, 64°42′W

Station: Bermuda standard tide gauge  $52^{\circ}24^{\circ}3, 64^{\circ}4^{\circ}24$  First series starts 1950 May 21 (441652-450171)† Second series starts 1953 May 2 (467500-476019) Combined solution using meaned matrices Third series starts 1956 April 14 (493372-501891) Reference: Gravitational and radiational potentials:  $G_2^1(0, \pm 2, \pm 4), G_2^2(0, \pm 2, \pm 4), G_3^2(0), G_3^2(0), R_1^1(0), R_2^2(0)$ 

0

		+ /C+++!/D	of arona)			Princip	al harmonic	constituent	s	
Admittances‡ (Station/Reference)  Intervals 1 cpm (0.0366011 cpd)							Stat	ion		ce (gravi- al only)
Frequency (cpd)	Real	Imaginary	R	φ* (deg)		Frequency (cpd)	// (cm)	G <sup>♠</sup> (deg)	H (cm)	G* (deg)
0.8929346	0.2221	-0.0316	0.2244	-8.1	$(Q_1)$	0.8932441	1.13	188.2**	5.02	0
0.9295357	0.1976	-0.0421	0.2020	-12.0	$O_1$	0.9295357	5.30	192.0**	26.22	0
0.9661368	0.1820	-0.0250	0.1837	-7.8						
					$(\mathbf{P_1})$	0.9972621	2.02**	187.7	12.21	0
1.0027379	0.1823	-0.0214	0.1835	-6.7	Kı	1.0027379	6.56**	187.1**	36.88	0

0.1956	-0.0433	0.2003	-12.5					
0.6266	0.3772	0.7314	31.0					
0.6259	0.2589	0.6773	22.5	$(N_2)$	1.8959820	8.18	337.7	12.10
0.5636	0.0169	0.5369	1.7	$M_2$	1.9322736	35.63	358.3	63.19
0.4340	-0.1248	0.4516	-16.0					
				$(S_2)$	2.0000000	8.08	24.2	29.40
0.2677	-0.1078	0.2885	-21.9	K <sub>2</sub>	2.0054758	2.21	22.7	8.00
	0.6266 0.6259 0.5636 0.4340	0.6266     0.3772       0.6259     0.2589       0.5636     0.0169       0.4340     -0.1248	0.6266         0.3772         0.7314           0.6259         0.2589         0.6773           0.5636         0.0169         0.5369           0.4340         -0.1248         0.4516	0.6266     0.3772     0.7314     31.0       0.6259     0.2589     0.6773     22.5       0.5636     0.0169     0.5369     1.7       0.4340     -0.1248     0.4516     -16.0	0.6266 0.3772 0.7314 31.0 0.6259 0.2589 0.6773 22.5 (N <sub>2</sub> ) 0.5636 0.0169 0.5369 1.7 M <sub>2</sub> 0.4340 -0.1248 0.4516 -16.0 (S <sub>2</sub> )	$ \begin{array}{cccccccccccccccccccccccccccccccccccc$	$ \begin{array}{cccccccccccccccccccccccccccccccccccc$	$ \begin{array}{cccccccccccccccccccccccccccccccccccc$

<sup>†</sup> Greenwich hours since 1900 January 1, 0h.

## TABLE B.

Station: REIKO-MAY Pressure

1 June-5 July 1973 27°58.2′N, 69°40.4′W

(643496 to 644368 Greenwich hours since 1900 January 1 0h) Reference: Bermuda summed complex prediction:  $G_2^1+G_3^1+R_1^1+R_2^1\ (0,-2),\ G_2^2+G_3^2+R_2^2\ (0,\pm 2)$ 

A	dmittances	st (Station/R	eference)			Princi	pal harmoni	c constituer	nts	
1	intervals 1	cpm (0.03660	011 cpd)				Sta	tion	Ref	erence
Frequency (cpd)	Real	Imaginary	R	φ* (deg)		Frequency (cpd)	H (cm)	G* (deg)	H (cm)	G* (deg)
0.8929346	1.1459	-0.0560	1.1473	-2.8	(Q <sub>1</sub> )	0.8932441	1.30	191.0	1.13	188.2
0.9295357	1.1713	-0.0823	1.1742	-4.0	$O_1$	0.9295357	6.22	196.0	5.30	192.0
0.9661368	1.1824	-0.1172	1.1882	-5.7						
					(P <sub>1</sub> )	0.9972621	2.40	194.9	2.02	187.7
1.0027379	1.1768	-0.1533	1.1868	-7.4	K <sub>1</sub>	1.0027379	7.79	194.5	6.56	187.1
1.0393390	1.1558	-0.1832	1.1702	-9.0						
Recorded va	ariance: 85	.3 cm²								
Residual va Ratio: 0.000		43 cm <sup>2</sup>								
1.8590714	0.9946	-0.0372	0.9953	-2.1						
1.8956725	1.0025	-0.0252	1.0028	-1.4	(N <sub>2</sub> )	1.8959820	8.20	339.1	8.18	337.7
1.9322736	0.9693	-0.0400	0.9702	-2.4	M,	1.9322736	34.57	0.7	35.63	358.3
1.9688747	0.9020	-0.0787	0.9055	-5.0						
					(S2)	2.0000000	6.77	32.7	8.08	24.2
2.0054758	0.8145	-0.1331	0.8253	-9.3	K <sub>2</sub>	2.0054758	1.82	32.0	2.21	22.7
Recorded v	ariance: 67	4 cm²								
Residual va		The Market								
Ratio: 0.000										

<sup>†</sup> Dimensionless.

<sup>‡</sup> Dimensionless. • G is Greenwich epoch,  $\phi$  is station lead.

<sup>••</sup> Small corrections for those values listed in the text.

<sup>•</sup> G is Greenwich epoch,  $\phi$  is station lead.

TABLE C.

Station: MERT-Pressure

17 March-1 April 1973 27°59.3'N, 69°40.3'W

(641741 to 642089 Greenwich hours since 1900 January 1 0<sup>k</sup>) Reference: Bermuda summed complex prediction:  $G_2^1 + G_3^1 + R_1^1 + R_2^1$  (0, -2),  $G_2^2 + G_3^2 + R_2^2$  (0, -2)

A	dmittance	s† (Station/R	eference)	nts						
1	Intervals 1 cpm (0.0366011 cpd)						Sta	tion	Ref	erence
Frequency (cpd)	Real	Imaginary	R	φ <sup>•</sup> (deg)		Frequency (cpd)	H (cm)	<i>G</i> * (deg)	H (cm)	G* (deg
0.8929346	1.3560	-0.1951	1.3699	-8.2	(Q <sub>1</sub> )	0.8932441	1.55	196.4	1.13	188.2
0.9295357	1.2718	-0.2041	1.2881	-9.1	$O_1$	0.9295357	6.83	201.1	5.30	192.0
0.9661368	1.1924	-0.1747	1.2051	-8.3						
					$(\mathbf{P_i})$	0.9972621	2.32	193.9	2.02	187.7
1.0027379	1.1342	-0.1132	1.1399	-5.7	K <sub>1</sub>	1.0027379	7.48	192.8	6.56	187.1
1.0393390	1.1094	-0.0323	1.1099	-1.7						
Recorded va	ariance: 34	.0 cm <sup>2</sup>								
Residual va Ratio: 0.008		02 cm²								
1.8590714	0.9496	0.0889	0.9537	5.3						
1.8956725	0.9647	0.0361	0.9654	2.1	$(N_2)$	1.8959820	7.90	335.6	8.18	337.7
1.9322736	0.9549	-0.0178	0.9550	-1.1	M:	1.9322736	34.03	359.4	35.63	358.3
1.9688747	0.9221	-0.0618	0.9241	-3.8						
					(S <sub>2</sub> )	2.0000000	7.15	29.7	8.08	24.2
2.0054758	0.8732	-0.0867	0.8775	-5.7	K:	2.0054758	1.94	28.4	2.21	22.
Recorded va	ariance: 47	1 cm <sup>2</sup>								
Residual va	riance: 0.2	63 cm <sup>2</sup>								
Ratio: 0.000	056									

Station: EDIE-March Pressure

20 March-9 April 1973 26°36.9'N, 69°19.0'W

(641810 to 642282 Greenwich hours since 1900 January 1 0<sup>k</sup>) Reference: Bermuda summed complex prediction:  $G_2^1+G_3^1+R_1^1+R_2^1$  (0, -2),  $G_2^2+G_3^2+R_2^2$  (0, -2)

A	dmittance	st (Station/R	cference)			Princi	ipal harmon	ic constitue	nts	
1	Intervals 1	cpm (0.03666	011 cpd)				Sta	ition	Rei	ference
Frequency (cpd)	Real	Imaginary	R	φ* (deģ)		Frequency (cpd)	H (cm)	G <sup>●</sup> (deg)	H (cm)	G• (deg
0.8929346	1.0705	-0.1095	10.761	-5.8	(Q <sub>1</sub> )	0.8932441	1.22	194.0	1,13	188.2
0.9295357	1.1343	-0.1430	1.1433	-7.2	Oı	0.9295357	6.06	199.2	5.30	192.0
0.9661368	1.1766	-0.2014	1.1938	-9.7						
					$(\mathbf{P_i})$	0.9972621	2.46	200.1	2.02	187.
1.0027379	1.1886	-0.2724	1.2195	-12.9	K <sub>1</sub>	1.0027379	8.00	200.0	6.56	187.1
1.0393390	1.1679	-0.3415	1.2167	-16.3						
Recorded va	ariance: 54	.2 cm²								
Residual va Ratio: 0.00		98 cm²								
1.8590714	0.8566	0.0725	0.8597	4.8						
1.8956725	0.8797	0.0254	0.8800	1.7	(N <sub>2</sub> )	1.8959820	7.20	336.1	8.18	337.7
1.9322736	0.8794	-0.0270	0.8798	-1.8	M <sub>2</sub>	1.9322736	31.35	0.1	35.63	358.3
1.9688747	0.8559	-0.0738	0.8591	-4.9						10.5.505
					(S2)	2.0000000	6.69	31.3	8.08	24.2
2.0054758	0.8140	-0.1054	0.8208	-7.4	K <sub>2</sub>	2.0054758	1.81	30.1	2.21	22.7
Recorded v	ariance: 51	8 cm²								
Residual va										
Ratio: 0.000										

<sup>†</sup> Dimensionless. • G is Greenwich epoch,  $\phi$  is station lead.

<sup>†</sup> Dimensionless. • G is Greenwich epoch,  $\phi$  is station lead.

TABLE E.

A	dmittance	st (Station R	eference)			Princi	pal harmon	ic constituer	nts	
1	ntervals 1	cpm (0.03660	011 cpd)				Sta	tion	Refe	erence
Frequency (cpd)	Real	Imaginary	ĸ	φ* (deg)		Frequency (cpd)	H (cm)	G* (deg)	// (cm)	G* (deg)
0.8929346	1.1378	-0.1465	1.1472	-7.3	$(Q_1)$	0.8932441	1.30	195.5	1.13	188.2
0.9295357	1.1609	-0.1621	1.1722	-7.9	O <sub>1</sub>	0.9295357	6.21	199.9	5.30	192.0
0.9661368	1.1748	-0.1864	1.1894	-9.0						
					$(\mathbf{P_t})$	0.9972621	2.41	197.8	2.02	187.7
1.0027379	1.1764	-0.2142	1.1957	-10.3	K <sub>1</sub>	1.0627379	7.84	197.4	6.56	187.1
1.0393390	1.1654	-0.2399	1.1899	-11.6						
Recorded va	riance: 76	.0 cm <sup>2</sup>								
Residual va Ratio: 0,001		82 cm <sup>2</sup>								
1.8590714	0.9013	-0.0845	0.9053	-5.4						
1.8956725	0.9192	-0.0608	0.9213	-3.8	$(N_2)$	1.8959820	7.54	341.5	8.18	337.7
1.9322736	0.8976	-0.0652	0.9000	-4.2	M:	1.9322736	32.07	2.5	35.63	358.3
1.9688747	0.8410	-0.0968	0.8465	-6.6						
					(S2)	2.0000000	6.35	34.5	8.08	24.2
2.0054758	0.7611	-0.1490	0.7755	-11.1	K <sub>2</sub>	2.0054758	1.71	33.8	2.21	22.7
Recorded va	triance : 55	6 cm <sup>2</sup>								
Residual va	riance: 0.1	09 cm <sup>2</sup>								
Ratio: 0.000	20									

<sup>†</sup> Dimensionless.

TABLE F.

Station: EDIE-May P2

12 May-9 July 1973 26°27.8'N 69°19.6'W

 $(643072\ \text{to}\ 644468\ \text{Greenwich hours since}\ 1900\ \text{January}\ 1\ 0^{\text{h}}$  Reference: Bermuda summed complex prediction:  $G_2^1+G_3^1+R_1^1+R_2^1\ (0,\ -2),\ G_2^2+G_3^2+R_2^2\ (0,\ \pm 2)$ 

.\	dmittances	f (Station Re	eference)			Princi	pal harmoni	c constituer	its	
1	ntervals 1	cpm (0.03660	011 cpd)				Sta	tion	Refe	rence
Frequency (cpd)	Real	Imaginary	R	φ* (deg)		Frequency (cpd)	11 (cm)	G* (deg)	II (cm)	G• (deg
0.8929346	1.1543	-0.1456	1.1635	-7.2	$(Q_1)$	0.8932441	1.31	195.4	1.13	188.2
0.9295357	1.1681	-0.1644	1.1796	-8.0	O <sub>1</sub>	0.9295357	6.25	200.0	5.30	192.0
0.9661368	1.1721	-0.1872	1.1870	-9.1						
					$(\mathbf{P_i})$	0.9972621	2.39	197.7	2.02	187.3
1.0027379	1.1656	-0.2095	1.1843	-10.2	K <sub>1</sub>	1.0027379	7.77	197.3	6.56	187.
1.0393390	1.1498	-0.2266	1.1720	-11.1						
Recorded va	riance : 75	5 cm <sup>2</sup>								
Residual va	riance: 0.1	02 cm <sup>2</sup>								
Ratio: 0.00	13									
1.8590714	0.8971	-0.0861	0.9012	-5.5						
1.8956725	0.9182	-0.0638	0.9204	-4.0	(N <sub>2</sub> )	1.8959820	7.53	341.7	8.18	337.
1.9322736	0.8977	-0.0677	0.9002	-4.3	M:	1.9322736	32.07	2.6	35.63	358.
1.9688747	0.8399	-0.0969	0.8454	-6.6						
					(S2)	2.0000000	6.32	34.3	8.08	24.
2.0054758	0.7568	-0.1454	0.7707	-10.9	K <sub>2</sub>	2.0054758	1.70	33.6	2.21	22.
Recorded va	ariance: 55	6 cm <sup>2</sup>								
Residual va										
Ratio: 0.000										

<sup>\*</sup> G is Greenwich epoch,  $\phi$  is station lead.

<sup>†</sup> Dimensionless. • G is Greenwich epoch,  $\phi$  is station lead.

TABLE G.

A	dmittance	s† (Station/R	eference)		Principal harmonic constituents					
1	ntervals 1	cpm (0.03660	011 cpd)				Sta	tion	Ref	erence
Frequency (cpd)	Real	Imaginary	R	φ* (deg)		Frequency (cpd)	II (cm)	G <sup>♠</sup> (deg)	H (cm)	G* (deg)
0.8929346	1.1282	-0.1014	1.1327	-5.1	(Q <sub>1</sub> )	0.8932441	1.28	193.3	1.13	188.2
0.9295357	1.1502	-0.1127	1.1557	-5.6	Ot	0.9295357	6.13	197.6	5.30	192.0
0.9661368	1.1650	-0.1326	1.1725	-6.5						
					$(\mathbf{P_1})$	0.9972621	2.38	195.2	2.02	187.7
1.0027379	1.1693	-0.1569	1.1798	-7.6	K <sub>1</sub>	1.0027379	7.74	194.7	6.56	187.1
1.0393390	1.1625	-0.1807	1.1764	-8.8						
Recorded va	ariance: 54	9 cm²								
Residual va										
Ratio: 0.002	21									
1.8590714	0.9678	-0.0589	0.9695	-3.5						
1.8956725	0.9824	-0.0366	0.9831	-2.1	(N2)	1.8959820	8.04	339.8	8.18	337.7
1.9322736	0.9663	-0.0386	0.9670	-2.3	M:	1.9322736	34.45	0.6	35.63	358.3
1.9688747	0.9228	-0.0645	0.9251	- 4.0						
					$(S_2)$	2.0000000	7.08	30.8	8.08	24.
2.0054758	0.8610	-0.1088	0.8679	-7.2	K <sub>2</sub>	2.0054758	1.92	29.9	2.21	22.
Recorded va	ariance: 60	99 cm²								
Residual va	riance: 0.3	10 cm <sup>2</sup>								
Ratio: 0.000	051									

TABLE H.

A	dmittance	s† (Station/R	eference)			Princi	pal harmoni	c constituer	nts	
	intervals 1	cpm (0.03660	011 cpd)				Sta	tion	Ref	erence
Frequency (cpd)	Real	Imaginary	R	φ* (deg)		Frequency (cpd)	// (cm)	G* (deg)	H (cm)	G* (deg)
0.8929346	1.1281	-0.0812	1.1310	-4.1	(Q <sub>1</sub> )	0.8932441	1.28	192.3	1.13	188.2
0.9295357	1.1372	-0.0980	1.1414	-4.9	Oi	0.9295357	6.05	196.9	5.30	192.0
0.9661368	1.1379	-0.1171	1.1440	-5.9						
					$(\mathbf{P_1})$	0.9972621	2.30	194.4	2.02	187.7
1.0027379	1.1301	-0.1346	1.1381	-6.8	K <sub>1</sub>	1.0027379	7.47	193.9	6.56	187.
1.0393390	1.1153	-0.1467	1.1250	-7.5						
Recorded va Residual va Ratio: 0,002	riance: 0.1									
1.8590714	0.9454	-0.0213	0.9457	-1.3						
1.8956725	0.9557	0.0024	0.9557	0.1	(N <sub>2</sub> )	1.8959820	7.82	337.5	8.18	337.7
1.9322736	0.9428	-0.0092	0.9429	-0.6	M <sub>2</sub>	1.9322736	33.60	358.9	35.63	358.
1.9688747	0.9095	-0.0540	0.9111	-3.4						
					(S <sub>2</sub> )	2.0000000	7.09	31.5	8.08	24.3
2.0054758	0.8626	-0.1225	0.8712	-8.1	K <sub>2</sub>	2.0054758	1.93	30.8	2.21	22.7
Recorded va Residual va Ratio: 0.000	riance: 0,4									

<sup>†</sup> Dimensionless. 
• G is Greenwich epoch,  $\phi$  is station lead.

<sup>†</sup> Dimensionless. 
• G is Greenwich epoch,  $\phi$  is station lead.

#### REFERENCES

- Brown, W., W. Munk, F. Snodgrass, H. Mofjeld and B. Zetler, 1975: MODE bottom experiment. J. Phys. Oceanogr., 5, 75-85.
- Cartwright, D. E., 1968: A unified analysis of tides and surges round north and east Britain. Phil. Trans. Roy. Soc. London, A263, 1-55.
- ---, W. Munk and B. Zetler, 1969: Pelagic tidal measurements. Trans. Amer. Geophys. Union, 50, 472-477.
- —, and R. J. Tayler, 1971: New Computations of the tidegenerating potential. *Geophys. J. Roy. Astron. Soc.*, 23, 45-74. Dietrich, G., 1944: Die Schwingungssysteme der halb-und
- Dietrich, G., 1944: Die Schwingungssysteme der halb-und eintägigen Tiden in den Ozeanen. Veröffentl. Inst. Meereskunde Univ. Berlin, A41, 7-68.
- Gallagher, B. S., and W. H. Munk, 1971: Tides in shallow water: Spectroscopy *Tellus*, 23, 346-363.
- Garrett, C. J. R., and W. H. Munk, 1971: The age of the tide and the "Q" of the oceans. Deep-Sea Res., 18, 493-503.
- Hendershott, M. C., 1973: Ocean tides. Trans. Amer. Geophys. Union, 54, 76-86.

- Munk, W. H. and D. E. Cartwright, 1966: Tidal spectroscopy and prediction. Phil. Trans. Roy. Soc. London, A259, 533-581.
- —, F. E. Snodgrass and M. Wimbush, 1970: Tides off shore— Transition from California coastal to deep-sea waters. Geophys. Fluid Dyn., 1, 161-235.
- Snodgrass, F., W. Brown and W. Munk, 1975: MODE: IGPP measurements of bottom pressure and temperature. J. Phys. Oceanogr., 5, 63-74.
- Tiron, K. D., Y. Sergeev and A. Michurin, 1967: Tidal charts for the Pacific, Atlantic and Indian Oceans. Vestnik Leningrad Univ., 24, 123-135.
- Wunsch, C., 1972: Bermuda sea level in relation to tides, weather, and baroclinic fluctuations. Rev. Geophys. Space Phys., 10, 1-49.
- Zetler, B. D., 1971: Radiational ocean tides along the coasts of the United States. J. Phys. Oceanogr., 1, 34-38.
- ---, and W. H. Munk, 1975: The optimum wiggliness of tidal admittances. J. Marine Res. (in press).